Nuclear Physics B121 (1977) 514–530


# THE $\pi\pi$ AND $K\bar{K}$ AMPLITUDES, THE S* AND THE QUARK STRUCTURE OF $0^{++}$ RESONANCES

A.D. MARTIN, E.N. OZMUTLU and E.J. SQUIRES
*University of Durham, England*

Received 26 July 1976
(Revised 19 January 1977)

The nature of mesons in the $0^{++}$ nonet is studied. In particular we discuss the parametrization of the $I = 0$ S wave in terms of the S* and possible $\epsilon$ mesons. The S* parameters are determined by fitting to $\pi^- p \to \pi^+$ and $K^- K^+$ production data. In particular we find $(g^{S^*}_{KK}/g^{S^*}_{\pi\pi})^2 = 4.0 \pm 0.6$.

## 1. Introduction

Recent high statistics experiments have provided much new information on the $0^{++}$ meson nonet. The $I = 1$ member, $\delta(970)$, is seen as a peak in the $\pi\eta$ spectrum just below the $\bar{K}K$ threshold and also as a threshold enhancement in the $K^- K^0$ spectrum (see ref. [1] for recent data and references to earlier observations). The broad $\kappa$ resonance is seen as the rise through 90° of the, approximately elastic, $I = \frac{1}{2}$ $K\pi$ S wave in the region of 1200 MeV [2]. The structure in the $\pi\pi$ S wave at the KK threshold [3] is attributable to an $I = 0$ S* resonance, and it has been argued [4] that there is in addition a broad $\epsilon$ resonance in the $I = 0$ $\pi\pi$ S wave whose mass ($m_\epsilon \sim 1300$ MeV) is consistent with the Gell-Mann-Okubo mass formula for the ($\delta$, $\kappa$, $\epsilon$, S*) nonet.

In the $L$ excitation quark model the $0^{++}$ mesons are an $L = 1$ nonet. Apart from the $L = 0$ ground state $0^{-+}$ and $1^{--}$ nonets, the only other nonet for which all the members are observed is the $L = 1$, $2^{++}$ nonet. The nature and symmetry properties of the $0^{++}$ nonet are therefore of considerable importance, particularly as many decay channels are experimentally accessible: $\epsilon$, S* $\to \pi\pi$, KK, $\eta\eta$; $\delta \to \pi\eta$, KK and $\kappa \to K\pi$, $K\eta$. The fact that both the S* and $\delta$ resonance poles occur just below the KK threshold increases the difficulty of obtaining reliable couplings. For the S* there is the additional complication of the large ($\epsilon$) background.

The main purpose of this paper is to perform a coupled channel ($\pi\pi$, KK) analysis of the $\pi^- p \to \pi^- \pi^+ n$ and $\pi^- p \to K^- K^+ n$ data in the region of the KK threshold, and thereby to obtain a reasonable description of the S*, $\epsilon$ effect in the $I = 0$ S wave. The most satisfactory procedure [4] that has been used to describe these overlapping

resonances is to parametrize the Jost function (denoted by $d(s)$ in sect. 2 below). In ref. [4] this is done by writing $d(s)$ as the product of an S* contribution and an $\epsilon$ contribution (essentially model IV of our sect. 4). Such a parametrization is hard to interpret from the dynamical viewpoint, and so we consider several alternatives for $d(s)$ motivated by different possible structures of the resonances and see to what extent the data can distinguish between them. This should help illuminate the nature of low-energy resonances.

There is no doubt that one of the most important questions of elementary particle theory is whether the low-energy mesons, for example, are predominantly qq composites as in the simple quark model or whether some, or all, are predominantly meson-meson $\sim$ qqqq states, as in the old 'bootstrap' type models. It could, of course, be the case that they are 'mixed' so that neither extreme is realistic [5]. If the mesons are qq states then in a many-channel model which ignores the quark channels they would have to be inserted as CDD poles. This is obvious and well known if the quarks are real particles whose non-appearance is due to their large mass. If the quarks are permanently confined (as in the MIT bag model, for example ref. [6]) they will never enter into an $S$-matrix description so their bound states should again appear as elementary particles, i.e. require CDD poles. However, because we have no real understanding of confinement theories, it may be possible to take a contrary view here; see Gustafson et al. [7].

In the work on baryon resonances by the above group [7], who explicitly calculate the left-hand cuts, it is claimed that the low-energy states are meson-baryon composites and that no CDD poles are required. Except for the proviso noted above, this appears to rule out the possibility that those baryons are 3q states as in the simple quark model.

Even within a particular realisation of the quark model this problem is not solved. For instance in the MIT bag model of mesons, in addition to the qq states there are qqqq states with similar masses and indeed the suggestion has been made [8] that the $0^+$ mesons considered in this note are of such a type.

It is worth noting that the same problem occurs in the study of the pomeron. In one scheme [9] the non-planar diagrams (the cylinder, etc. of the topological expansion) simply renormalise the f upwards to make a pomeron, whereas in the other (generally referred to as the Harari-Freund scheme, also a property of the dual model) the cylinder itself has a new singularity so that in addition to the (qq) f, etc. there is a ($qq\bar{q}\bar{q}$) pomeron.

The plan of this paper is as follows. In sect. 2 we briefly recall the analytic structure of the $S$ matrix in the two-channel situation and in sect. 3 we consider the parametrization of the $\delta$ resonance. In sect. 4 we study the more interesting case of the description of the $I = 0$ S wave in the region of the $K\bar{K}$ threshold. We consider three parametrizations which appear to arise naturally in: (I) a model with a $\pi\pi$ state ($\epsilon$) and a $K\bar{K}$ state (S*) together with a coupling between them, (II) a model with a $\pi\pi$ state ($\epsilon$) and a $q\bar{q}$ state (S*) with no significant force in the KK channel, and (III) a model with no significant forces in the $\pi\pi$ and KK channels and two

states ($\epsilon$, S*) in the qq channels. In a sense that will be made explicit in sect. 5 the results of the analysis of the data appear to rule out III and to favour II over I.

In sect. 5 we describe the coupled channel ($\pi\pi$, K$\bar{\text{K}}$) analysis of the $\pi^- p \to \pi^- \pi^+ n$ and $\pi^- p \to K^- K^+ n$ in the region of the K$\bar{\text{K}}$ threshold. We analyse the data in terms of S, P, D partial waves of the produced di-meson system. We study various parametrizations of the $I = 0$ S wave, including those mentioned above, and determine the S* resonance parameters. In particular, the (sheet II) resonance pole is found to be well determined and independent of the parametrization of the S wave. A discussion of the results is given in sect. 6, together with comments on the status of SU(3) for the $0^{++}$ nonet and our conclusions.

## 2. The *S*-matrix

Consider a two-channel situation, for example $\pi\pi$ and KK, and denote the thresholds as $s_1 = 4m_1^2$ and $s_2 = 4m_2^2$, with channel momenta $k_i = \frac{1}{2}(s - s_i)^{1/2}$. The elements of the $S$ matrix, $S_{ij}$, have right-hand cuts in the $s$ plane starting at $s_1$ and $s_2$. As we are only interested in the S wave we omit the subscript $I$ from $\boldsymbol{S}$. We refer to the physical sheet as sheet I; the physical amplitudes are evaluated on the upper side of the right-hand cuts on this sheet. We can define sheets II, III and IV by continuing analytically through the cuts as shown in fig. 1, where, for clarity, we have shown the cuts displaced just below the real axis. Sheets I, II, III, IV correspond to (Im $k_1$, Im $k_2$) = ++, −+, −−, +−, respectively.

A convenient way to guarantee the singularity structure and unitarity properties of $\boldsymbol{S}$ is to introduce [10] a real analytic function $d(s) \equiv d(k_1, k_2)$ with square root branch points at $k_1 = 0$ and $k_2 = 0$. Then if we put

$$S_{11} = \frac{d^{\text{II}}(s)}{d^{\text{I}}(s)} = \frac{d(-k_1, k_2)}{d(k_1, k_2)}, \tag{1}$$

$$S_{22} = \frac{d^{\text{IV}}(s)}{d^{\text{I}}(s)} = \frac{d(k_1, -k_2)}{d(k_1, k_2)}, \tag{2}$$

$$S_{11}S_{22} - S_{12}^2 = \frac{d^{\text{III}}(s)}{d^{\text{I}}(s)} = \frac{d(-k_1, -k_2)}{d(k_1, k_2)}, \tag{3}$$

we find that $\boldsymbol{S}$ has the correct analytic structure and is unitary * in the physical region. This method is easily generalised to many channels [10]. The poles of the $S$ matrix are caused by the zeros of $d^{\text{I}}(s) \equiv d(s)$.

We will use the multichannel $\boldsymbol{N}$ over $\boldsymbol{D}$ method and write the S-wave amplitude

$$\boldsymbol{T} = \boldsymbol{N}\boldsymbol{D}^{-1},$$

* This requires also that $|d(-k_1, k_2)| \leq |d(k_1, k_2)|$.

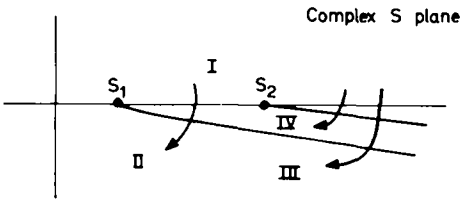


Fig. 1. The sheets reached from the physical sheet, sheet I, by continuing through the right-hand cuts. The cuts are displaced just below real axis for clarity.

where $N$ has the left-hand cuts and $D$ the right-hand cuts. We normalise $T$ so that

$$\text{Im } T = T^* \rho T , \tag{4}$$

$$\rho_{ij} = \theta(s - s_i) k_i \delta_{ij} , \tag{5}$$

hence

$$\text{Im } D = -D\rho N . \tag{6}$$

The real analytic function $d(s)$, introduced above, can be taken to be det $D(s)$. On the physical sheet $d(s)$ does not have the left-hand cuts of $S$.

### 3. The ò resonance

We first apply this formalism to the simple case of a single two-channel resonance: the $I = 1$ S-wave $\delta$ resonance in the $\pi\eta$ and $K\bar{K}$ channels. We consider the parametrization of this resonance supposing it to be (a) a meson-meson state (we call this exchange model *) and (b) a $q\bar{q}$ state (the quark model).

*(a) Exchange model.* In this model we assume that the $\pi\eta$ and $K\bar{K}$ exchange forces are responsible for the $\delta$ meson. In particular, suppose that forces in the $K\bar{K}$ channel are predominantly responsible for the $\delta$, then we may parametrize $D_{22}$ by a linear function of $s$ and the other elements by constants. We add the threshold terms multiplied by constants. This approximation gives

$$D = \begin{bmatrix} 1 & A - iBk_1 \\ C - iDk_2 & s_R - s - iEk_2 \end{bmatrix} \tag{7}$$

in the resonance region, where $A, B, C, D, E$ and $s_R$ are real parameters. The corresponding $N$ is given by

$$N = \begin{bmatrix} 0 & B \\ D & E \end{bmatrix} , \tag{8}$$

* This is not an ideal name but we follow Gustafson et al. [7] who, like us, were unable to think of a better one.

and the symmetry condition $T_{12} = T_{21}$ requires

$$D = 0 , \qquad B = EC . \tag{9}$$

We therefore obtain

$$d(s) = \det D = m^2 - s - im\Gamma_1 - im\Gamma_2 , \tag{10}$$

with

$$m^2 = s_R - AC , \qquad m\Gamma_1 = EC^2 k_1 , \qquad m\Gamma_2 = Ek_2 . \tag{11}$$

This form of $d(s)$ is the two-channel Breit-Wigner formula.

Note that the form of $d(s)$ would not be different if we put the 'uncoupled' δ in the ππ channel rather than in KK channel. However, if we tried a linear form in both $D_{11}$ and $D_{22}$ (as in model I for the S*, ε in the next section), the fit would require $s_{R1}$ or $s_{R2}$ to be large, so that $d(s)$ would reduce essentially * to form of eq. (10). This is because the data indicate there is no S-wave 'background' to the δ resonance.

*(b) Quark model.* In this model we assume that the meson-meson forces are weak except *via* the quark channel, MM → qq → MM. In this case we have

$$D = \begin{bmatrix} 1 & 0 & A - iBk_1 \\ 0 & 1 & C - iDk_2 \\ E & F & s_R - s \end{bmatrix} , \tag{12}$$

where the elements in the third row are real, since we are interested in a region well below the qq threshold. It is straightforward to show that $d(s) = \det D$ is once again of the form of eq. (10).

Thus we see that the two models for the δ are indistinguishable and both lead to the Breit-Wigner formula

$$T_{ij} = \frac{mg_i g_j}{d(s)} , \tag{13}$$

where $d(s)$ is given by eq. (10) and $\Gamma_i = k_i g_i^2$. This expression for $T_{ij}$ has poles on sheet III and on sheet II (or sheet IV). We can get an idea about the location of the poles if we ignore the $s$ dependence of the $\Gamma_i$. Of course, this is not a reasonable approximation when the poles occur near threshold and so in practice we must solve exactly. However for the purpose of discussion we take $\Gamma_i = \bar{\Gamma}_i \equiv \Gamma_i(m)$. Then the pole nearest the physical region on sheet III is at

$$s = m^2 - im(\bar{\Gamma}_1 + \bar{\Gamma}_2) , \tag{14}$$

* The amplitudes are unchanged if $d(s)$ is multiplied by a real constant.

and that on sheet II (or, if $\Gamma_2 > \Gamma_1$, sheet IV) is at

$$s = m^2 \quad im(\bar{\Gamma}_1 - \bar{\Gamma}_2) . \tag{15}$$

There are also the more distant complex conjugate poles. When the resonance occurs well above both thresholds only the sheet III pole is important. However the $\delta$ resonance occurs just below the KK threshold and the 'nearby' sheet II pole is manifest in the $\pi\eta$ mass spectrum.

The $\pi\eta$ mass spectrum has been fitted [1] by this two-channel Breit-Wigner formula with the coupling constant ratio $g^2_{\pi\eta}/g^2_{K\bar{K}}$ fixed at the SU(3) value of $\frac{2}{3}$. The parameters of the $\delta$ were found to be

$$m = 974 \pm 9 \text{ MeV} , \qquad \Gamma_{\pi\eta} = 72 \pm 51 \text{ MeV} . \tag{16}$$

These values give a $K^0K^-$ mass spectrum which is in good agreement with the data, when allowance is made for incoherent background effects [1].

Flatté [11] has shown several other Breit-Wigner fits to these $\pi\eta$ and $K^0K^-$ mass spectra and concludes that the data can be fitted almost as well by larger partial widths, $\bar{\Gamma}_{\pi\eta} \sim 300$ MeV. Even with large partial widths the sheet II pole can occur close to the real axis. However, the fall-off of the $\delta$ contribution to the KK mass spectrum is a crucial indicator of the sheet III pole position. Although the statistics are low, the $K^0K^-$ spectrum [1] above 1060 MeV suggests that the sheet III pole is closer to the real axis than is permitted by Flatté [11].

For completeness we mention an alternative description of a resonance occurring just below the second threshold, which is based on a constant inverse $K$-matrix and which has been frequently discussed in the literature [12]. In our notation this parametrization is

$$\boldsymbol{D} = \begin{bmatrix} \alpha - ik_1 & \gamma \\ \gamma & \beta - ik_2 \end{bmatrix} , \tag{17}$$

and therefore $\mathcal{N}$ is the unit matrix. For $\beta$ small and negative this leads to a sheet II pole just below the (second) $K\bar{K}$ threshold ($k_2 = i|k_2|$) at

$$|k_2| = -\beta + \gamma^2/(\alpha - ik_1) . \tag{18}$$

This pole manifests itself as a resonance in channel 1, which may be called a $K\bar{K}$ bound state resonance. It is easy to show that such a resonance is effectively described by two of the parameters, the third being associated with a background contribution. There is no nearby sheet III pole in this parametrization and so the resonant amplitude $T_{12}$ dies away more slowly ($\sim 1/k_2$) than in the Breit-Wigner description in contradiction with the indications of the data.

## 4. Parametrization of the S* and ε

Like the $\delta$, the S* resonance occurs just below the $K\bar{K}$ threshold and the sheet II pole is manifest in the structure of the $\pi\pi$ spectrum. However in this case the de-

scription is complicated by the presence of a large, possibly resonant ($\epsilon$), background in the $I = 0$ S wave. We discuss possible parametrizations of this partial wave in the $\pi\pi$, $K\bar{K}$ channels in the region of the KK threshold *.

*(I) Exchange model.* In this model we assume that the amplitudes are dominated by forces in the $\pi\pi$ and KK channels, together with a coupling between them. We parametrise the diagonal elements of $D$ by linear functions of $s$ and the off-diagonal elements by constants. We add the appropriate threshold terms multiplied by arbitrary constants. Thus,

$$D = \begin{bmatrix} s_\epsilon - s - i\gamma_1 k_1 & A - iBk_1 \\ C - iDk_2 & s_R - s - i\gamma_2 k_2 \end{bmatrix}, \tag{19}$$

which corresponds to an $N$ given by

$$N = \begin{bmatrix} \gamma_1 & B \\ D & \gamma_2 \end{bmatrix}. \tag{20}$$

We calculate $T = ND^{-1}$ and impose the condition that $T_{12} = T_{21}$. This yields

$$B = D, \qquad C = [\gamma_1 A - B(s_\epsilon - s_R)]/\gamma_2 . \tag{21}$$

Thus, for det $D$ we have the 6-parameter form

$$d(s) \equiv \det D = (s_\epsilon - s - i\gamma_1 k_1)(s_R - s - i\gamma_2 k_2) - \frac{1}{\gamma_2}(A - iBk_1)(\gamma_1 A - B(s_\epsilon - s_R) - i\gamma_2 Bk_2) . \tag{22}$$

In the limit in which the $\pi\pi \to$ KK coupling is ignored this model permits a resonance in $\pi\pi$ and one in KK. The former, which we identify with the $\epsilon$, gives the background to the S* state in the $K\bar{K}$ channel.

*(II) Mixed model.* Here we permit an $\epsilon$ background in the $\pi\pi$ state as before, but we do not include any forces in the $\pi\pi \to K\bar{K}$ or $K\bar{K} \to KK$ amplitudes. Instead we include a qq channel in which there is a bound state. Thus

$$D = \begin{bmatrix} s_\epsilon - s - i\gamma_1 k_1 & 0 & A - iBk_1 \\ 0 & 1 & C - iDk_2 \\ E & F & s_3 - s \end{bmatrix}. \tag{23}$$

We have ignored the threshold terms in the $q\bar{q}$ channel since we assume that these are sufficiently distant not to affect the results.

* Here we neglect the $K^+K^-$ and $K^0\bar{K}^0$ mass difference. When detailed threshold mass spectra are available, it will be interesting to study this effect.

When we impose $T_{12} = T_{21}$ we find

$$B = 0\,, \qquad D = -\gamma_1 AF/E\,. \tag{24}$$

We can therefore write

$$d(s) \equiv \det D = (s_\epsilon - s - i\gamma_1 k_1)(s_R - s - i\gamma_2 k_2) - AE\,, \tag{25}$$

which has five effective parameters ($s_\epsilon, s_R$ ($\equiv s_3 - CF$), $\gamma_1, \gamma_2$ ($\equiv \gamma_1 AF^2/E$), $AE$).

We see that this model is identical to model I except that it has the additional restriction that $B$ of model I is zero.

*(III) Quark model.* Here we ignore all forces in the meson channels and we treat the $\pi\pi \to q\bar{q}$ coupling to lowest significant order. It is convenient to include two $q\bar{q}$ channels (e.g. a $\underline{1}$ and $\underline{8}$ of SU(3)) and parametrize each as a linear function of $s$. Thus we put

$$D = \begin{pmatrix} 1 & 0 & A + iBk_1 & C + iDk_1 \\ 0 & 1 & E + iFk_2 & G + iHk_2 \\ I & J & s_3 - s & Y \\ K & L & X & s_4 - s \end{pmatrix}. \tag{26}$$

Provided we do not go beyond second order off-diagonal terms, we obtain

$$d(s) \equiv \det D = (s^2 + as + b + ik_1(c + ds) + ik_2(e + fs))\,, \tag{27}$$

where $a, b, c, d, e, f$ are six real constants. Although they both have six parameters, (27) and (22) are different. In particular (27) does not allow any term of the form $(ik_1)(ik_2)$.

In sect. 5 we analyse $\pi^- p \to \pi^- \pi^+ n$, $K\bar{K}n$ data in an attempt to distinguish between the above parametrizations. We also compare with the description obtained by the following parametrizations used in earlier analyses [4,13,14].

*(IV) Breit-Wigner and background.* In our notation this description means that the $S$ matrix is given by eqs. (1)- (3) with the factorizing form [4]

$$d(s) = d^R(s) d^B(s)\,, \tag{28}$$

where $d^R$ is a two-channel Breit-Wigner form for the S* resonance,

$$d^R(s) = s_R - s - i\gamma_1 k_1 - i\gamma_2 k_2\,, \tag{29}$$

and $d^B$ is the background to the resonance. We take

$$d^B(s) = e^{-ik_1\phi_B}\,, \tag{30}$$

that is we assume a background phase, $\delta_B \equiv k_1\phi_B$, only in the $\pi\pi$ channel. The de-

tails of the fit are found to be independent of the parametrization of $\delta_B$ provided it approximates 90° in the S* region. We choose to parametrize $\delta_B$ in terms of a broad ππ resonance.

*(V) Constant inverse K matrix.* In this description the $S$ matrix is calculated using

$$d(s) = (\alpha - ik_1)(\beta - ik_2) - \gamma^2 , \tag{31}$$

see eq. (17), where $\alpha, \beta, \gamma$ are the elements of the $K^{-1}$ or $M$ matrix and are real. If $\alpha, \beta, \gamma$ are taken to be constant we can get a 3-parameter description of a resonance and background. For example,

$$S_{11} = \left(\frac{ik_2 + \kappa_R^*}{ik_2 + \kappa_R}\right)\left(\frac{\alpha + ik_1}{\alpha - ik_1}\right), \tag{32}$$

where $\kappa_R$ is the value of $|k_2|$ given in eq. (18). This expression for $S_{11}$ is in the form of resonance (sheet II pole) multiplied by background, where $\delta_B \sim 90°$ provided $|\alpha| \ll k_1$.

## 5. Analysis of data in the S* region

In order to study the properties of the S* we performed a coupled channel analysis by fitting ππ and $K\bar{K}$ production amplitudes direct to $\pi^- p \to \pi^- \pi^+ n$ and $\pi^- p \to K^- K^+ n$ data. For each reaction we describe the observed moments $\langle Y_M^J \rangle$, with $J \leqslant 2, M \leqslant 1$, of the produced di-meson system in terms of S, P and D waves.

For $\pi^- p \to \pi^- \pi^+ n$ we used the $t$-channel moments obtained by the CERN-Munich collaboration [15] (see fig. 2). We fitted to data (with $-t < 0.15$ GeV$^2$) in 20 MeV bins through the range $0.8 < M_{\pi\pi} < 1.2$ GeV using the 'Ochs-Wagner' method [16,17]. That is, the $\pi N \to \pi\pi N$ amplitudes, $L_{\lambda^+}$, for producing a ππ system of spin $L$, helicity λ by ± exchange naturality, are assumed to satisfy (i) $|L_{1+}| = |L_{1-}|$, (ii) $L_{\lambda^+} = 0$ for $\lambda > 1$, (iii) $L_{1-}/L_0 = \sqrt{L(L+1)}/C$ where $C$ is real. We parametrized $C$ as a quadratic function of $M_{\pi\pi}$. The observed moments, with $J \leqslant 2$, are then expressed in terms of $L_0$, with $L = 0, 1, 2$, and $C(M_{\pi\pi})$.

For $\pi^- p \to K^- K^+ n$ we used the $t$-channel moments obtained at 6 GeV/$c$ by the Argonne EMS group [18] ($-t < 0.08$ GeV$^2$) and at 18.4 GeV/$c$ by the CERN-Munich collaboration [19] ($-t < 0.2$ GeV$^2$). The exchange mechanisms are more complicated in this reaction and to study the $M_{K\bar{K}}$ dependence it is desirable to consider data extrapolated to the π exchange pole. Such a cross-section extrapolation has been done by the CERN-Munich group [19] and so we have normalized all the observed moments to these values. The moments obtained in this way are shown in fig. 3, and are analysed in terms of amplitudes by the 'Ochs-Wagner' method for $M_{K\bar{K}} < 1.15$ GeV.

The observable ππ and $K\bar{K}$ moments are expressed [15–17] in terms of the production amplitudes $L_0(\pi\pi)$ and $L_0(\pi^-\pi^+ \to K^-K^+)$ for $L = 0, 1, 2$, which, in turn,

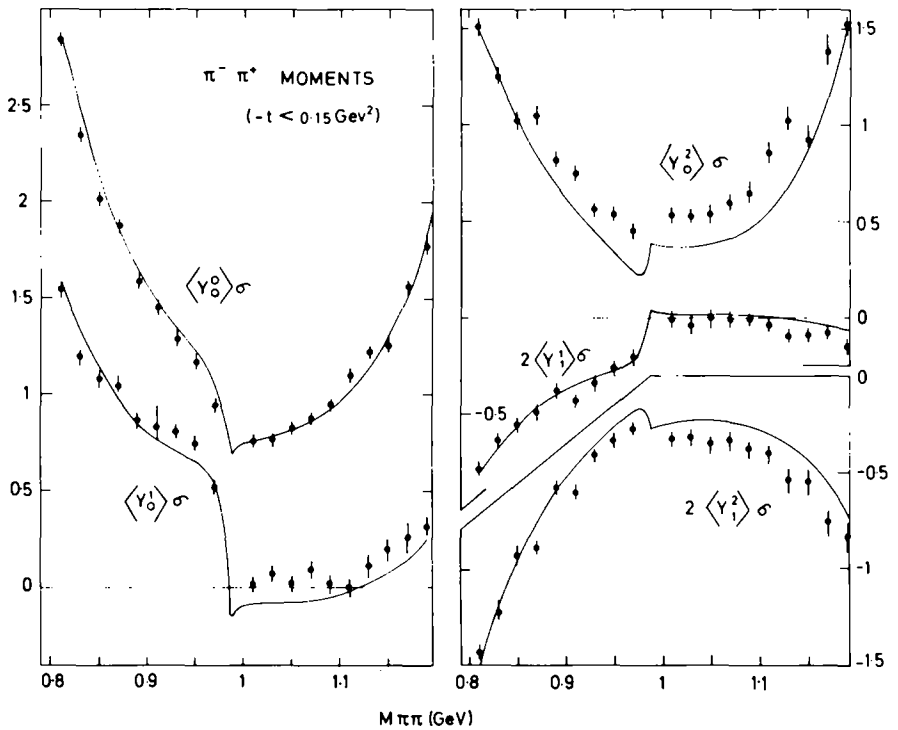


Fig. 2. The mass spectra of the unnormalized $t$ channel $\pi\pi$ moments in the region $0.8 < M_{\pi\pi} < 1.2$ GeV. The data were obtained in the CERN-Munich 17.2 GeV/$c$ $\pi^- p \to \pi^- \pi^+ n$ experiment [15] and correspond to $-t < 0.15$ GeV$^2$. The curves are the fit using model I.

are given in terms of the S, P, D coupled channel ($\pi\pi$, KK) partial wave amplitudes. We investigated the $I = 0$ S wave parametrizations discussed in sect. 4 by fitting to the data keeping the other partial waves fixed. For the $I = 2$ $\pi\pi$ S wave we input the values of $\delta_S^2$ used in ref. [17] (for example $\delta_S^2 = 22.4°$ at $M_{\pi\pi} = 1$ GeV). For the P and D waves * we used $\rho$ and f resonant forms with the relative $\pi\pi/K\bar{K}$ couplings fixed at their SU(3) values.

The curves on figs. 2 and 3 correspond to the best fit † obtained using the model I parametrization, eq. (22). The parameters obtained are

$$s_R = 0.94 \pm 0.08\,, \qquad \gamma_2 = 0.94 \pm 0.03\,,$$

$$s_\epsilon = 1.4^{+0.9}_{-0.6}\,, \qquad \gamma_1 = 9^{+10}_{-5}\,,$$

$$A = -0.22 \pm 0.42\,, \qquad B = 0.06 \pm 0.55\,, \tag{33}$$

* The small contribution to $\pi\pi$ production from the g resonance tail was also included.

† To allow for the excess of $\pi\pi$, as compared to $K\bar{K}$, production data, we reduced the contribution to $\chi^2$ from the fit to the $\pi\pi$ data by a factor of 4.

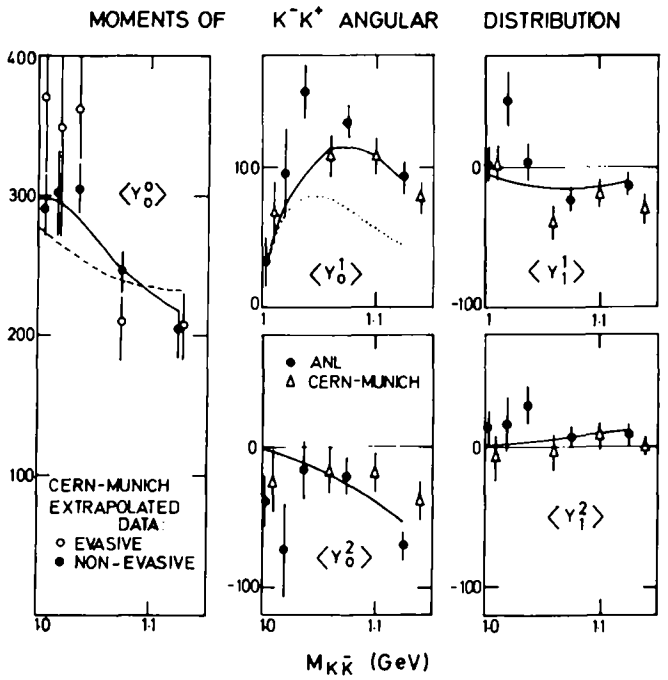


Fig. 3. The $t$ channel moments of the $K^-K^+$ angular distribution in the reaction $\pi^- p \to K^- K^+ n$. The data for $\langle Y_0^0 \rangle$ are obtained by the CERN-Munich collaboration by extrapolating the cross section to the $\pi$ exchange pole (see fig. 6 and ref. [19]). All the other moments shown are normalized to these (non-evasive) extrapolated values. The curves correspond to the fit of model I (the dotted line for $\langle Y_0^1 \rangle$ is obtained if the $\rho$ phase is input). The dashed line for $\langle Y_0^0 \rangle$ is the fit using the constant $K$ matrix, model V.

in units of GeV. There are systematic discrepancies in the description of some of the $\pi\pi$ moments which may be due to using fixed Breit-Wigner forms to describe the tails of the $\rho$ and f resonances. Similar systematic misfits in this region were also found [16] in the CERN-Munich phase-shift analysis based on resonance parametrizations. It is interesting to note that if the fit is compared to preliminary Argonne 4 and 6 GeV/$c$ $\pi^- p \to \pi^- \pi^+ n$ data [20] that these discrepancies are reduced *. In the fit we allowed the P wave phase $\delta_P(\pi\pi \to K\bar{K})$ to be free. We found that it was in agreement with that predicted by the tail of the $\rho$ resonance just above the KK threshold, but by $M_{K\bar{K}} = 1.1$ needed to be some 30° larger. If $\delta_P(\pi\pi \to K\bar{K})$ is assumed to be given by the $\rho$ tail, and the other parameters left unchanged, then the dotted curve is obtained for $\langle Y_0^1 \rangle$ for $K\bar{K}$ production, see fig. 3.

The values of four of the six parameters of model I, eq. (33), are poorly deter-

* In particular the ANL data show evidence for the structure indicated for $\langle Y_0^2 \rangle$ at the $K\bar{K}$ threshold.

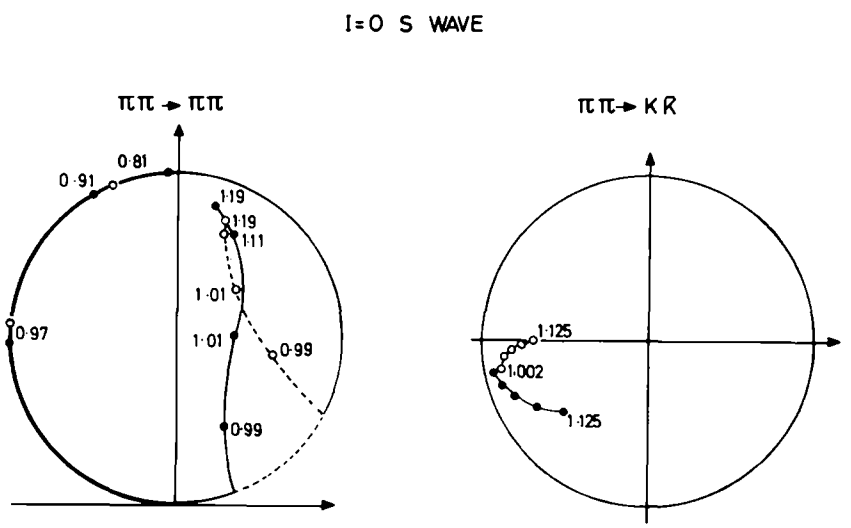


Fig. 4. Argand plots of $k_1 T_{11}$ and $(k_1 k_2)^{1/2} T_{12}$, respectively. The continuous curves, with the mass marked in GeV, are the S wave amplitudes obtained in the fit using model I. Models II and IV give essentially the same amplitudes. The dashed line corresponds to model V. The unmarked points for $\pi\pi \to K\bar{K}$ correspond to $M_{K\bar{K}} = 1.02$, 1.0375, 1.075 GeV respectively.

mined and suggest that the $I = 0$ S wave is over-parametrized. $s_\epsilon$ is badly determined because $\gamma_1$ is large and the parameters are strongly correlated. As expected from the values of $B$ in eq. (33), model II, which has this $B = 0$, gives essentially the same fit. Moreover model IV, eq. (28), with four effective parameters $s_R = m(S^*)^2$, $\gamma_1 = g^2_{\pi\pi}$, $\gamma_2 = g^2_{K\bar{K}}$ and $\delta_B$ * also gives an essentially identical fit, with

$$m(S^*) = 0.978 \pm 0.005\,, \qquad \gamma_1 = 0.199 \pm 0.014\,,$$
$$\delta_B(1\text{ GeV}) = 86.5^\circ\,, \qquad \gamma_2 = 0.792 \pm 0.099\,, \tag{34}$$

in units of GeV.

That such different parametrizations are likely to lead to similar fits can be demonstrated as follows. Since the background phase, $\delta_B$, in model IV is approximately 90° we have

$$d(s) \simeq -i(k_1)(s_R - s - i\gamma_1 k_1 - i\gamma_2 k_2)\,. \tag{35}$$

The introduction of the slowly varying factor $(k_1)$ is irrelevant to the fit, but is required by unitarity. On the other hand for model II the values of the parameters are such that

$$d(s) \simeq -i\gamma_1' k_1 (s_R - s \quad i\gamma_2' k_2) \quad C'\,. \tag{36}$$

* In practice $\delta_B$ was parametrized in terms of a broad elastic $\pi\pi$ resonance. The best values were $m(\epsilon) = 1.1$, $g^\epsilon_{\pi\pi} = 3.7$ with very large, strongly correlated errors.

Table 1
The S* pole positions and couplings

| Model | Sheet II pole (GeV) | Sheet III pole (GeV) | $(g^{S^*}_{KK}/g^{S^*}_{\pi\pi})^2$ |
|---|---|---|---|
| I Exchange | 0.997 − *i* 0.017 (±0.002) (±0.002) | 0.837 − *i* 0.148 (±0.013) (±0.008) | 4.0 |
| II Mixed | 0.996 − *i* 0.017 (±0.002) (±0.001) | 0.835 − *i* 0.146 (±0.008) (±0.005) | 3.9 |
| IV Breit-Wigner | 0.996 − *i* 0.016 (±0.003) (±0.002) | 0.876 − *i* 0.077 (±0.010) (±0.008) | 4.0 |
| V Constant $K^{-1}$ matrix | 0.988 − *i* 0.012 (±0.003) (±0.002) | | (8.7) |

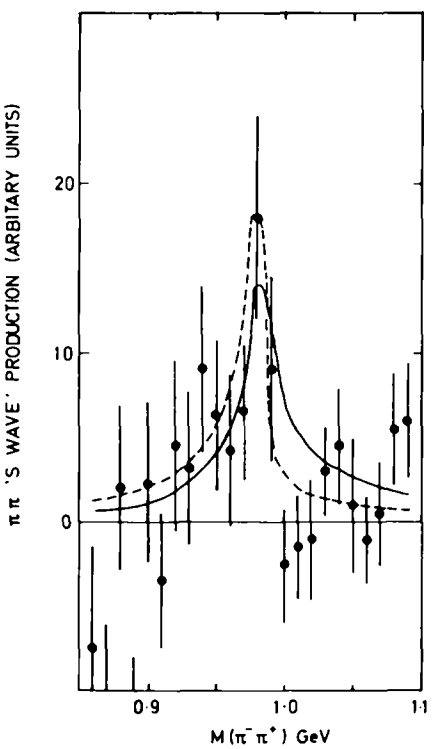


Fig. 5. The $\pi^-\pi^+$ mass distribution observed in $K^-p \to \pi^-\pi^+(\Lambda, \Sigma^0)$ in the S* region with the background and $\rho$ resonance events subtracted [21]. The continuous curve corresponds to the prediction for model I (II, IV) and the dashed curve to that for model V. The curves are proportional to $k_1 M_{\pi\pi}|T_{12}|^2$ and are unnormalized.

To the extent that $k_1$ is constant over the region of interest, the parametrizations can be seen to be equivalent: $\gamma_2 = \gamma_2'$, $\gamma_1 = C'/k_1^2\gamma_1'$.

We find that model III, eq. (27), is ruled out by the data since it is unable to reproduce the necessary background in the $\pi\pi$ channel. Also the constant inverse $K$ matrix, model V, is unable to give a satisfactory fit to the data. The best fit, using eq. (31), has

$$\alpha = 0.095\,, \qquad \beta = 0.045\,, \quad \gamma = 0.163 \tag{37}$$

in units of GeV, but leads to the behaviour of $\langle Y_0^0 \rangle$ for $K\bar{K}$ production shown by the dashed line in fig. 3. There is only a nearby sheet II pole, and the absence of a nearby sheet III pole does not allow $\langle Y_0^0 \rangle$ to decrease rapidly enough with increasing $M_{K\bar{K}}$ [4,14].

The $I = 0$ S wave amplitudes obtained in the fits are shown in the Argand plots of fig. 4. There is no ambiguity in the sign of the S wave amplitude $T_{12}$ since the interference with the resonance tail contributions is compatible with the $K\bar{K}$ production data provided $g^{S^*}_{K\bar{K}}/g^{S^*}_{\pi\pi}$ is positive [4]. In table 1 we show the S* pole positions corresponding to the various parametrizations. We notice that the sheet II pole position is very stable to changes of the parametrization. We also give the ratio of the S* coupling to the two channels, defined as $|T_{22}/T_{11}|$ at the sheet II pole position.

The S* is also evident in the $\pi\pi$ spectrum observed in the reaction $K^- p \to \pi^-\pi^+(\Lambda, \Sigma^0)$ [21]. The data, with the $\rho^0$ tail subtracted [21], are shown in fig. 5 together with our predictions for the shape of the spectrum.

## 6. Discussion and conclusion

We have proposed a form of parametrization of the coupled channel ($\pi\pi$, $K\bar{K}$) $I = 0$ S wave which allows for the presence of overlapping S* and $\epsilon$ resonances and which permits an investigation of the nature of these mesons. We found that model III, which we called the quark model, is not able to fit the $\pi^+\pi^-$ and $K^+K^-$ production data. This does not mean, of course, that the S* and $\epsilon$ are not predominantly $q\bar{q}$ states, but it does mean that such a description is not simple and that forces in the meson sector are also important. There has to be a significant admixture of meson-meson ($qq\bar{q}\bar{q}$) states in the wave functions. Of course it is not obvious that this makes these resonances any different from the better known ones such as the $\rho$, since, for example, the observed coupling of the $\rho$ to $\pi\pi$ inevitably mixes a ($qq\bar{q}\bar{q}$) component into its wave function. However, the necessity for such a component has not previously been required experimentally.

Models I and II give satisfactory fits to the data. In the fit with model I a particular parameter turns out to be essentially zero, a fact which is predicted by model II. This gives some evidence in support of model II. However this evidence is very weak as indicated by the errors in (33). The fact that an equivalent fit can be obtained with the four effective parameters of model IV indicates that the S wave is over-pa-

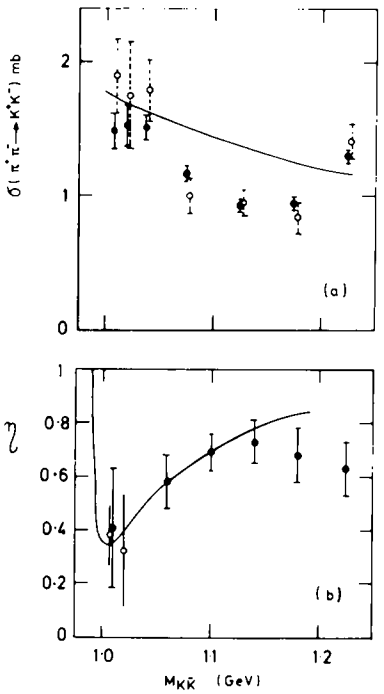


Fig. 6. (a) The $\pi^-\pi^+ \to K^- K^+$ cross section obtained by the CERN-Munich collaboration [19] by extrapolating their 18.4 GeV/$c$ $\pi^- p \to K^- K^+ n$ data to the $\pi$ exchange pole. The open (closed) points correspond to evasive (non-evasive) extrapolation. The curve is the S wave unitarity limit. (b) The S wave inelasticity, $|S_{11}| = \eta$, obtained from an S, P, D partial-wave analysis of $\pi^- p \to K^- K^+ n$ data [19] normalized to the cross section obtained by the non-evasive extrapolation. The two open points for $\eta$ are the values obtained assuming only the S wave contributes to the $\pi^-\pi^+ \to K^-K^+$ cross section. The curve corresponds to the model I (II, IV) parametrization.

rametrized in models I and II. Since four S wave parameters suffice to describe the structure of the data in the S* region (three of which are associated with the S*) we are unable to determine meaningful parameters for the $\epsilon$.

Recent $\pi^- p \to K^0_S K^0_S n$ data [22], which contain only even-$L$ $\pi\pi \to K\bar{K}$ partial waves, show evidence for a large S wave under the f resonance. A detailed study of this effect will require a partial wave analysis of data extrapolated to the $\pi$ exchange pole. Of the recent experiments, the only extrapolated values presently available are those given in the upper part of fig. 6, which shows the $\pi^+\pi^- \to K^+K^-$ cross section obtained by the CERN-Munich collaboration [19] by extrapolation of their $\pi^- p \to K^- K^+ n$ data. We performed an S, P, D wave analysis of the $K^+K^-$ moments [19] for $-t < 0.2$ GeV$^2$ and calculated the S wave contribution * to the cross sec-

* We show the solution with the larger $|S|$ as required by a study of the $K^0_S K^0_S$ production data [22].

tion. The results are shown in the lower part of fig. 6. The curve corresponds to the model I (II, IV) S wave parametrization. The data indicate that there exists some additional S wave effect for $M_{K\bar{K}} \gtrsim 1.2$ GeV.

If the large S wave under the f resonance is associated with the $\epsilon$ then it is at variance with our expectations for SU(3) for the $0^{++}$ nonet. The SU(3) couplings for the decay of the $0^{++}$ mesons into two pseudoscalars are given in terms of $g_1, g_8$ and $\theta_S$, the $\epsilon$ - S* mixing angle, in ref. [4]. Note that we define $\Gamma_i = k_i g_i^2$ whereas in ref. [4] $\Gamma_i$ is essentially $2k_i g_i^2$. Using the $\delta$ width to determine * $g_8$, and using the S* couplings found above, we obtain

$$g_8 = 0.76 \pm 0.2\,, \qquad g_1 = 1.17 \pm 0.2\,, \qquad \theta_S = 68^\circ \pm 15^\circ\,.$$

The $\epsilon$ – S* mixing in the $0^{++}$ nonet is far from ideal [4]. If we use the above values, then SU(3) predicts a broad $\epsilon$ resonance in the $\pi\pi$ channel with a very small coupling to the KK channel.

Cerrada et al. [23] have recently discussed $\pi\pi$ and $K\bar{K}$ scattering in the S* region using a different parametrization. They claim that they do not require any nearby resonances. However it is clear that they do not fit the $\pi\pi \to K\bar{K}$ cross section near threshold as shown in our fig. 6 (compare $\eta$ of their fig. 1). These data are crucial in determining the S* parameters. The claim, that the $KK \to K\bar{K}$ left-hand cut is important, is incorrect since it does not contribute to either $T_{11}$ or $|T_{12}|^2$. In fact this can be seen explicitly using their parametrization: putting $\gamma_{ab} \equiv 0$ in their eq. (8) is found not to affect the results in the S* region.

In summary, we have determined the properties of the S* resonance using $\pi^+\pi^-$ and $K^+K^-$ production data below 1.2 GeV, but are unable to say much about the possible $\epsilon$ state in this mass region. The behaviour of the $K\bar{K}$ production data just above threshold are invaluable in determining the S* parameters. Similarly the $(K\bar{K})^{\pm}$ spectra will be crucial for studying the $\delta$. We note that recent $K\bar{K}$ production experiments are finding interesting S wave structure in the region of the f resonance. The high statistics data [24] on the line-reversed reactions $\pi^- p \to K^- K^+ n$ and $\pi^+ n \to K^- K^+ p$ will be invaluable for investigating exchange mechanisms, S* - $\delta$ interference and for establishing whether the S wave structure under the f is associated with the $\pi\pi \to K\bar{K}$ channel.

It is a pleasure to thank Drs. P. Estabrooks, D. Morgan, M.R. Pennington, J.L. Petersen and T. Shimada for helpful discussions, and for their interest in this work, and to thank Drs. N.M. Cason, E. Lorenz, A.J. Pawlicki and A.B. Wicklund for communicating and discussing the results of their experiments prior to publication. One of us (E.N.O.) thanks the Turkish Government for financial support.

* The value of $g_8$ is constrained to be compatible [4] with the behaviour of the $K\pi$ $I = \frac{1}{2}$ S wave phase.

## References

[1] J.B. Gay et al., Physics Letters 63B (1976) 220.
[2] T.G. Trippe et al., P.D.G. tables, Rev. Mod. Phys. 48 suppl. (1976) no. 2.
P. Estabrooks et al., contrib. to 18th Int. Conf. on high-energy physics, Tbilisi, 1976.
[3] S.M. Flatté et al., Phys. Letters 38B (1972) 232;
G. Grayer et al., Nucl. Phys. B75 (1974) 189.
[4] D. Morgan, Phys. Letters 51B (1974) 71; New directions in hadron spectroscopy, eds. S.L. Kramer and E.L. Berger, ANL report, p. 45.
[5] E.J. Squires and P.J.S. Watson, Ann. of Phys. 41 (1967) 409.
[6] A. Chodos et al., Phys. Rev. 9 (1974) 3471.
[7] G. Gustafson et al., Nordita preprint 76/5.
[8] R.L. Jaffe and K. Johnson, Phys. Letters 60B (1975) 201.
[9] C. Rosenzweig and G. Chew, Phys. Letters 58 B (1975) 93;
C. Schmid and C. Sorensen, Nucl. Phys. B96 (1975) 209;
H. Lee, Phys. Rev. Letters 30 (1973) 719;
G. Veneziano, Phys. Letters 43B (1973) 413.
[10] K.J. Le Couteur, Proc. Roy. Soc. A256 (1960) 115;
R.G. Newton, J. Math. Phys. 2 (1961) 188;
R. Blankenbecler, Strong interactions and high energy physics, ed. R.G. Moorhouse (1964) p. 411;
M. Kato, Ann. of Phys. 31 (1965) 130.
[11] S.M. Flatté, Phys. Letters 63B (1976) 228.
[12] R.H. Dalitz, Rev. Mod. Phys. 33 (1961) 471;
W.R. Frazer and A.W. Hendry, Phys. Rev. 134 (1964) B1307.
[13] S.D. Protopopescu et al., Phys. Rev. D7 (1973) 1279;
G. Grayer et al., Proc. Tallahassee Conf. AIP Conf. Proc. 13 (1973) 117.
[14] Y. Fujii and M. Fukugita, Nucl. Phys. B85 (1975) 179.
[15] G. Grayer et al., Nucl. Phys. B75 (1974) 189.
[16] W. Ochs, Thesis, University of Munich (1973);
B. Hyams et al., Nucl. Phys. B64 (1973) 134.
[17] P. Estabrooks and A.D. Martin, Nucl. Phys. B79 (1974) 301; B95 (1975) 322.
[18] A.J. Pawlicki et al., Phys. Rev. D12 (1975) 631.
[19] G. Hentschel, Thesis, University of Munich (1976);
E. Lorenz, private communication.
[20] A.B. Wicklund et al., private communication.
[21] G.W. Brandenburg et al., Nucl. Phys. B104 (1976) 413.
[22] N.M. Cason et al., Phys. Rev. Letters 36 (1976) 1485;
W. Wetzel et al., Nucl. Phys. B115 (1976) 208.
[23] M. Cerrada et al., Phys. Letters 62B (1976) 353.
[24] A.J. Pawlicki et al., Phys. Rev. Letters 37 (1976) 971.

# A STUDY OF ISOSPIN 1 MESON STATES USING 10 GeV/$c$ $K^-K^0$ PRODUCTION DATA

A.D. MARTIN and E.N. OZMUTLU
*University of Durham, Durham City, UK*

R. BALDI, T. BÖHRINGER, P.A. DORSAZ, V. HUNGERBÜHLER [1], M.N. KIENZLE-FOCACCI, M. MARTIN, A. MERMOUD, C. NEF and P. SIEGRIST
*University of Geneva, Switzerland*

Received 1 February 1978

We perform an amplitude analysis of 10 GeV/$c$ $\pi^-p \to K^-K^0_S p$ data as a function of $K^-K^0$ mass from threshold up to 2 GeV. We find that the $A_2$ and g resonances are produced dominantly by natural and unnatural parity exchange, respectively and we determine their resonance parameters. We present further evidence for the $I = 1, 4^+$ state $A_2^*(1900)$, in particular by isolating interference effects. The structure of S-wave $K^-K^0$ production suggests an $I = 1, 0^+$ state just below 1300 MeV of width about 250 MeV.

The high statistics data for the reaction $\pi^-p \to K^-K^0p$ allow a study of the meson spectrum that is more selective than that for $K^+K^-$ production. The $K^-K^0$ channel has isospin 1 and is thus only accessible to even spin states of odd $G$-parity (such as the $\delta(0^+)$, $A_2(2^+)$) and to odd spin states of even $G$-parity (such as the $g(3^-)$). The data that are available on $K^-K^0_S$ production therefore complement the information available [‡1] from the high statistics $K^+K^-$, $K^0_SK^0_S$, $\pi^+\pi^-$ and $\pi^0\pi^0$ production data.

The even and odd $G$-parity $K^-K^0$ states are produced by different exchange mechanisms. The allowed natural and unnatural parity exchanges (denoted by NPE and UPE) are shown in table 1. From studies of the SU(3)-related reactions $KN \to (K\pi)N$ we expect isoscalar NPE (pomeron, f, and $\omega$ exchange) and isovector UPE to be dominant [3]. The possibility of pomeron exchange (P) means that at high energies even-$L$ $K^-K^0$ states should be more copiously produced than those with odd $L$.

Here we analyse the 10 GeV/$c$ $\pi^-p \to K^-K^0_S p$ data obtained using the University of Geneva two-arm spectrometer [4]. We use the moments $\mathrm{Re}\langle Y_J^M \rangle$, of the $K^-$ angular distribution in the $t$-channel $K^-K^0$ helicity frame in 50 MeV intervals over the mass range $1 < M(K^-K^0) < 2$ GeV, integrated over the $t$ interval $0.07 < -t < 1$ (GeV/$c$)$^2$. Only the $J \leqslant 8, M \leqslant 2$ moments are found to be significantly different from zero [‡2], and these are determined by the constrained linear fit described in the preceding letter [5]. The resulting mass spectra are shown in fig. 1. These may be compared with the moments, shown in ref. [5], obtained from the same data by a maximum likelihood

Table 1
Allowed exchanges for spin-$L$ $K^-K^0$ production.

| | $L$ even | $L$ odd |
|---|---|---|
| NPE | P, f, $\rho$ | $\omega$, $A_2$ |
| UPE | B, Z [a] | $\pi$, $A_1$ |

[a] Z is used to denote the possible $2^{--}$ exchange trajectory.

[1] Present address: CERN, Geneva, Switzerland.

[‡1] Recent reviews are given, for example, by Petersen [1] and Cohen [2].

[‡2] In the mass region of the $A_2$ resonance there is evidence for a small, but non-zero, $\langle Y_4^3 \rangle$ signal; we discuss the implication of this below.

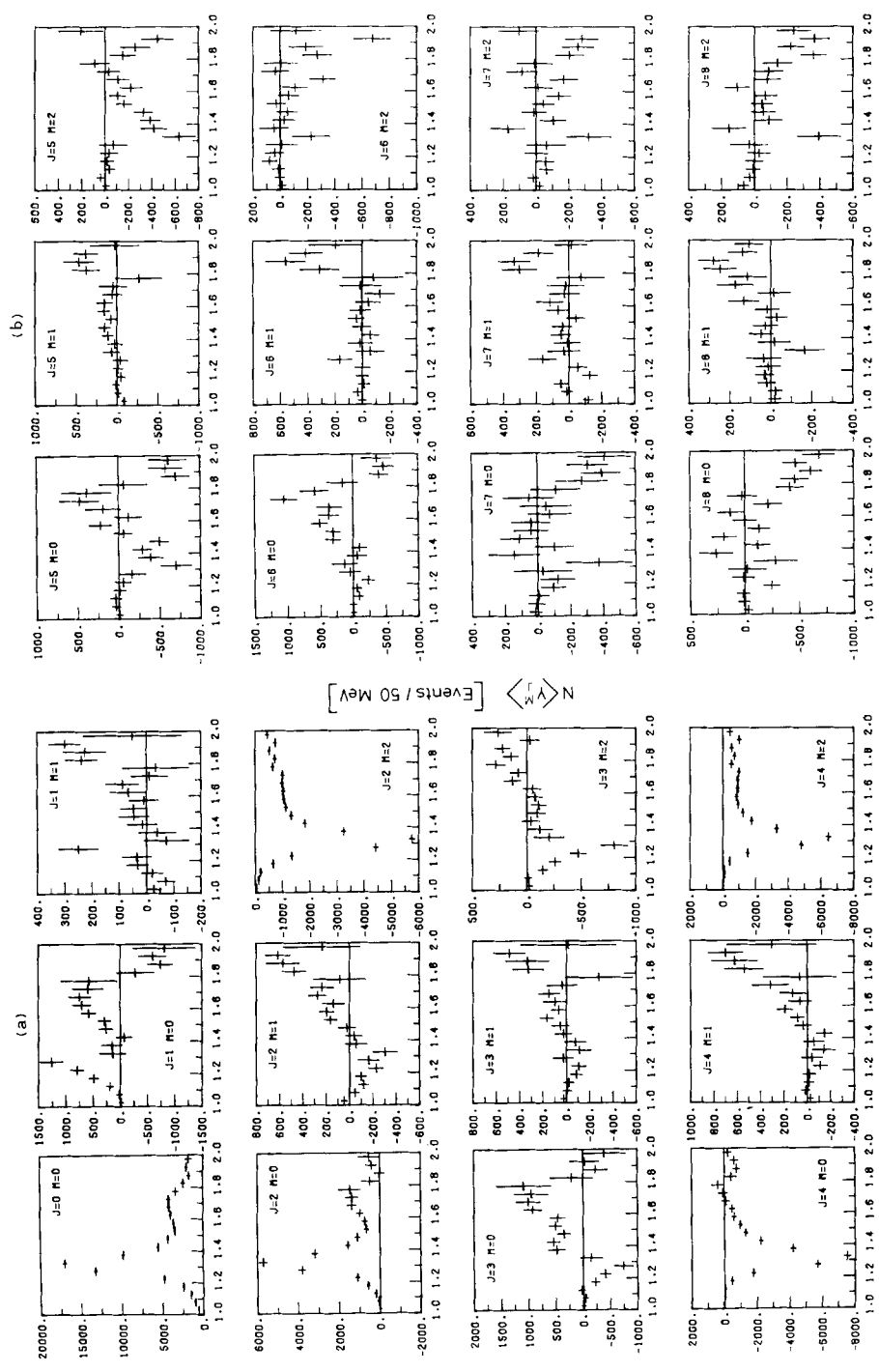


Fig. 1. The mass spectra of the $t$-channel acceptance corrected moments for 10 GeV/$c$ $\pi^- p \to K^- K^0 p$ data, after allowance for the observed $K^0 \to K^0_S \to \pi^+\pi^-$ decay. The data are integrated over the $t$ interval $0.07 < -t < 1$ (GeV/$c$)$^2$. The sensitivity of the data is 7671 corrected events per $\mu$b.

method, but integrated over a somewhat smaller $t$ interval.

The moments can be expressed [6] as the sum of bilinear products of amplitudes, $L_{\lambda\pm}$, describing, to leading order in the energy, the production of a $K^-K^0$ system of spin $L$, helicity $\lambda$ by NPE and UPE, respectively. In terms of the helicity amplitudes $H_{L\lambda}$, we have $L_{\lambda\pm} \equiv [H_{L\lambda} \pm (-1)^{\lambda+1} H_{L,-\lambda}]/\sqrt{2}$ for $\lambda \neq 0$; and $L_0 \equiv H_{L0}$, that is only UPE for $\lambda = 0$. We will use the abbreviated notation $L_\pm \equiv L_{1\pm}$. A summation over helicity flip and non-flip at the nucleon vertex is implicit in each bilinear product, that is $|L|^2 = |L_f|^2 + |L_{nf}|^2$. The interference terms can be written in the form

$$\mathrm{Re}(L'L^*) = |L'| \cdot |L| (\xi \cos\phi)_{L'L},$$

where $\xi$ is the degree of nucleon spin coherence ($0 \leqslant \xi \leqslant 1$) and $\phi$ is the relative phase between amplitudes $L$ and $L'$. We note that the observed moments do not contain interference terms between NPE and UPE amplitudes. That is, terms of the form $\mathrm{Re}(L'_{\lambda'+} L^*_{\lambda-})$ do not occur.

The number of observed moments is insufficient to determine the magnitudes and phases of all the amplitudes $L_{\lambda\pm}$. Fortunately, for a given $L$, not all ($t$-channel) helicity components are important. The study of the $t$ structure in the $A_2$ and g resonance regions [7] (as well as the amplitude structure in the SU(3)-related reactions [3] $K^\pm p \to (K\pi)^\pm p$) shows that the dominant NPE amplitudes are $L_+$, and that UPE proceeds mainly via $L_0$. This can also be inferred directly from the observed $t$-channel moments as a function of mass (fig. 1); we see that the $\langle Y_J^{0,2} \rangle$ moments are, in general, larger than those with $M = 1$.

For other related dimeson production processes (such as $\pi^+\pi^-$ [8], $K^-\pi^+$ [9], $K^+K^-$ [10], $K^0\pi^+$ [3], $\bar{K}^0\pi^-$ [3]), it is found that the $t$-channel moments with $M > 2$ are compatible with zero, indicating that the amplitudes with $\lambda \geqslant 2$ can be neglected. However, for $\pi^- p \to (K^-K^0)p$ in the $A_2$ mass region a definite signal is found [7] in the $\langle Y_4^3 \rangle$ $t$-channel moment. Owing to the dominance of $D_+$ in this mass region, this signal can be attributed to $D_+ D_{2+}$ interference. In fact an amplitude analysis [7] of $A_2$ production as a function of $t$ shows that $|D_{2+}| \sim 0.1 |D_+|$, on an average over the relevant $t$ range. We therefore conclude that the $L'_+ L^*_{2+}$ interference terms will, in general, contribute to the $M = 1$ moments at least as strongly as the $L'_0 L^*_-$ interference terms. The data are unable to determine both $L_-$ and $L_{2+}$. However, these small amplitudes only contribute quadratically to the $M = 0$ and 2 moments and so it should be reliable to use these moments to determine the more dominant $L_0$ and $L_+$ amplitudes.

For these reasons we use the $M = 0$ and 2 $t$-channel moments with $J \leqslant 8$ (fig. 1) to determine the magnitudes and relative phases of the amplitudes in the NPE sector ($P_+, D_+, F_+, G_+$) and in the UPE sector ($S_0, P_0, D_0, F_0, G_0$) as a function of the produced $K^-K^0$ mass in the range $1 < M < 2$ GeV. For example, for each mass bin above 1.8 GeV, where amplitudes up to $L = 4$ are required, we use 16 moments to determine 9 amplitude magnitudes and 7 relative phases. In principle, this assumes that, within each sector, the amplitudes have a common coherence factor $\xi$. There is no certainty that this is correct. However, in practice, at a given mass, often only one interference term is important within each sector, and then the data give a reliable determination of the corresponding spin-phase coherence [‡3] $\xi \cos\phi$. For example, in the $A_2$ mass region the data determine $\xi \cos\phi$ for $S_0 D_0$ and $P_+ D_+$ interference.

Even then the amplitude determination is not unique The data determine only $(\cos\phi)_{LL'}$, and not the relative phases $\phi_{LL'}$, and so there remain discrete ambiguities. At each $K^-K^0$ mass $M$ we obtain all possible solutions by using a similar technique to that proposed by Gersten [11] and Barrelet [12]. We write the amplitudes, describing $\pi^- p \to K^-K^0 p$ by UPE and NPE, in the form

$$A(\mathrm{UPE}) = a(M) \prod_{i=1}^{\mathcal{L}} (z - z_i),$$

$$A(\mathrm{NPE}) = a'(M) \sin\phi \sin\theta \prod_{i=1}^{\mathcal{L}-1} (z - z'_i),$$

with $z = \cos\theta$, where $\theta$ and $\phi$ are the angles specifying the direction of the $K^-$ in the ($t$-channel) $K^-K^0$ rest frame. $\mathcal{L}$ is the maximum value of $L$ included in the partial wave decomposition of $A$(UPE) and $A$(NPE) into the $L_0$ and $L_+$ amplitudes, respectively. The "Barrelet" zeros, $z_i(M)$ and $z'_i(M)$ are complex. The ambiguities arise because the data do not determine

[‡3] The value represents the spin-phase coherence averaged over the $t$ interval of the data, $0.07 < -t < 1$ (GeV/$c$)$^2$.

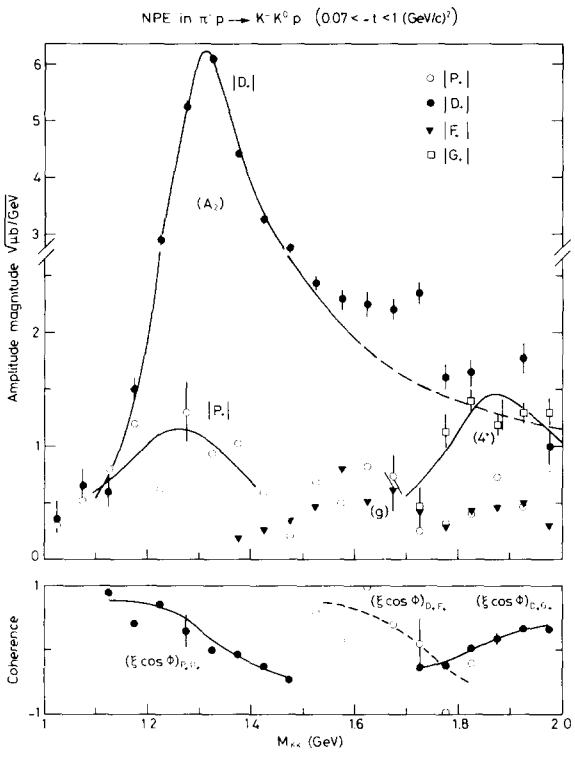


Fig. 2. The ($t$-channel) amplitudes describing $K^-K^0$ production by NPE obtained by analysing the moments of fig. 1. Representative errors are shown. The curves through the $L \geqslant 2$ amplitudes correspond to the Breit–Wigner resonant fits of table 2. Only the coherences between significant amplitudes are shown.

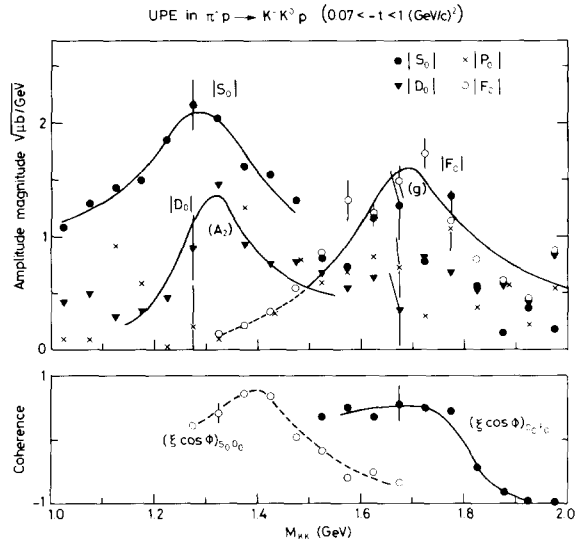


Fig. 3. Same as fig. 2, but for UPE $K^-K^0$ production.

the signs of Im $z_i$ or Im $z_i'$. Thus there is a $2\mathcal{L}$-fold ambiguity within the UPE sector and a $2^{\mathcal{L}-1}$-fold ambiguity with the NPE sector. From a given solution we generate the other solutions by first determining the $z_i$ ($z_i'$) and then making substitutions $z_i \to z_i^*$ ($z_i' \to z_i'^*$) for the various combinations of the zeros.

We find that the amplitude $G_0$, describing $L = 4$ $K^-K^0$ production by UPE, is compatible with zero. This can be anticipated by inspection of the $J = 8$, $M = 0, 2$ moments. In the results presented below we have therefore set $G_0 \equiv 0$. For $K^-K^0$ masses below 1.7 GeV we fix $G_+$ to be given by the tail of a spin 4 resonance and fit only moments with $J \leqslant 7$. For $K^-K^0$ masses below 1.5 GeV we fix the $L = 3$ amplitudes, $F_0$ and $F_+$, to be given by the tail of the g resonance and fit only moments with $J \leqslant 5$. The resonance forms are normalized to fit the amplitude determinations in the higher mass bins.

We tabulate all the allowed solutions in each mass bin. In the majority of mass bins these solutions give an essentially exact description of the data. In all but the mass bin about 1.325 GeV (see the data fluctuations in fig. 1) and those above 1.85 GeV the fits have an acceptable $\chi^2$. In figs. 2 and 3 we present the solution that is selected at each mass by requiring

(i) the dominance of $S_0$ just above the $K^-K^0$ threshold. ($P_0$ and higher waves are suppressed by factors of $(q_{K\bar{K}})^L$),

(ii) the continuity of Im $z_i$ and Im $z_i'$ as a function of the $K^-K^0$ mass,

(iii) amplitude behaviour consistent with the presence of the $A_2$ and g resonances.

Leading resonant waves are essentially unchanged in magnitude by Barrelet transformations and the third criterion is mainly helpful off resonance. The first two criteria eliminate an alternative solution with $P_0$ similar in magnitude and structure to that shown for $S_0$ below 1.4 GeV (see fig. 3) and with $S_0$ smaller and structureless.

From the results, we see that the $A_2$ resonance is dominantly produced by NPE, whereas g resonance production proceeds mainly by UPE. This is consistent with the exchange expectations of table 1. The curves shown through the $A_2$ and g amplitudes correspond to Breit–Wigner fits and lead to the resonance production cross sections given in table 2.

Table 2
$A_2$ and g resonance parameters and cross sections [a].

| Quantity fitted | | Mass interval fitted (GeV) | Mass (MeV) | Width (MeV) | $\sigma$ [b] ($\mu$b) |
|---|---|---|---|---|---|
| $A_2$ | Mass spectrum | 1.0–2.0 | 1316 ± 1 | 104 ± 2 | 5.00 ± 0.04 |
| | $\lvert D_+\rvert^2$ | 1.15–1.45 | 1318 ± 1 | 113 ± 4 | 4.62 ± 0.06 |
| | $\lvert D_0\rvert^2$ | | | | 0.20 ± 0.06 |
| g | Mass spectrum | 1.0–2.0 | 1697 ± 4 | 177 ± 11 | 0.93 ± 0.06 |
| | $\lvert F_+\rvert^2$ | | | | 0.08 ± 0.03 |
| | $\lvert F_0\rvert^2$ | 1.50–1.95 | 1698 ± 12 | 199 ± 40 | 0.51 ± 0.06 |

[a] All errors are statistical only. The systematic error of the mass scale is 4 MeV (st. dev.) and the uncertainty of the cross-section normalization 8%. The interaction radius in the centrifugal barrier factor of the Breit–Wigner shape is taken to be $R = 3.5$ GeV$^{-1}$.
[b] $\sigma$ is the production cross section times the branching ratio for decay into $K^0K^-$, corrected for the unseen $K^0$ decays. The cross section is calculated in the $t$ interval $0.07 < -t < 1.0$ (GeV/$c$)$^2$, and mass interval $1.2 < M < 1.4$ GeV and $1.55 < M < 1.85$ GeV for the $A_2$ and g, respectively.

Above 1.8 GeV we see the emergence of $L = 4$ $K^-K^0$ production. Unfortunately, the data do not allow reliable partial-wave analysis above 2 GeV so as to establish a resonance shape for $G_+$. However, support for resonance identification comes from the behaviour of the $D_+G_+$ interference contribution. This is the dominant interference term in this mass range and, moreover, both $L = 2$ and $L = 4$ $K^-K^0$ states have similar production mechanisms. The behaviour of $(\xi\cos\phi)_{D_+G_+}$ should therefore reproduce $\cos(\delta_2 - \delta_4)$, where $\delta_L$ are the $I = 1$ $K\bar{K}$ phases. Assuming $\delta_2$ is given by the tail of the $A_2$, we see that the behaviour of $\xi\cos\phi$, as a function of mass, gives further confirmation of the spin 4 resonance of mass $M \sim 1.9$ GeV reported in the preceding letter [5].

Another new and surprising feature of the results is the importance of S-wave $K^-K^0$ production in the $A_2$ mass region. The $0^{++}$ states are an outstanding problem in meson spectroscopy, and this result has crucial implications. It is true that lower partial waves are, in general, less constrained than leading waves, and moreover that $S_0$ is dominated by $D_+$. However, another place where such structure should manifest itself is in $K^+K^-$ and $K^0_SK^0_S$ production. There the problem is not the dominance of NPE, but the separation of $I = 0$ and $I = 1$ $K\bar{K}$ effects. We recall that the S-wave spectrum obtained from $K^+K^-$ and $K^0_SK^0_S$ production data [10,13] do in fact show, besides the $S^*$ threshold enhancement, a significant bump at 1.3 GeV. This bump was originally attributed to a state in the $I = 1$ $K\bar{K}$ channel [13], but a more recent analysis [2] favours an $I = 0$ assignment. However, the present analysis shows a clear S-wave structure just below 1300 MeV in the $I = 1$ $K\bar{K}$ channel. Such information on the $K^-K^0$ channel will be invaluable in separating $I = 0$ and $I = 1$ effects in $K^+K^-$ and $K^0_SK^0_S$ production data.

We thank the British Science Research Council and the Fonds National Suisse for support of this work. One of us (E.N.O.) thanks the Turkish Government for financial support.

[1] J.L. Petersen, The $\pi\pi$ interaction, CERN 77-04 (1977).
[2] D. Cohen, $K\bar{K}$ amplitude analyses, ANL-HEP-CP-77-37, Proc. 5th Experimental meson spectroscopy Conf. (Boston, 1977), to be published.
[3] R. Baldi et al., Phys. Lett. 70B (1977) 377;
A.D. Martin et al., Amplitude and natural-parity-exchange analysis of $K^\pm p \to (K\pi)^\pm p$ data at 10 GeV/$c$, submitted to Nucl. Phys. B;
P. Estabrooks et al., SLAC-PUB-2011 (1977).
[4] R. Baldi et al., Systematic study of $K\pi$ production in the reaction $K^\pm p \to K^0_S\pi^\pm p$: technique and measurements at 10 GeV/$c$, submitted to Nucl. Phys. B.
[5] R. Baldi et al., preceding letter.
[6] A.D. Martin and C. Michael, Nucl. Phys. B84 (1975) 83.
[7] A.D. Martin et al., A study of $A_2$ and g resonance production in $\pi^-p \to K^-K^0p$, to be submitted to Nucl. Phys. B.
[8] G. Grayer et al., Nucl. Phys. B75 (1974) 189.
[9] P. Estabrooks et al., Phys. Lett. 60B (1976) 473.
[10] A.J. Pawlicki et al., Phys. Rev. D15 (1977) 3196.
[11] A. Gersten, Nucl. Phys. B12 (1969) 537.
[12] E. Barrelet, Nuovo Cimento 8A (1972) 331.
[13] N.M. Cason et al., Phys. Rev. Lett. 36 (1976) 1485.

Nuclear Physics B140 (1978) 158–178


# A STUDY OF $A_2$ AND g RESONANCE PRODUCTION IN $\pi^- p \to K^- K^0 p$

A.D. MARTIN and E.N. OZMUTLU
*Department of Physics, University of Durham, UK*

R. BALDI, T. BÖHRINGER, P.A. DORSAZ, V. HUNGERBÜHLER *,
M.N. KIENZLE-FOCACCI, M. MARTIN, A. MERMOUD, C. NEF and
P. SIEGRIST
*University of Geneva, Switzerland*

Received 3 April 1978

We present the results and the analysis of a high-statistics experiment to study $A_2$ and g production in the reaction $\pi^- p \to K^- K^0_S p$ at 10 GeV/$c$. In each resonance region we perform a moment analysis of the data, and from the moments we determine the production amplitudes as a function of $t$. We find $A_2$ production proceeds dominantly by natural-parity (pomeron and f) exchange. We compare $A_2$ and diffractive $K^*(1420)$ production. We find g production proceeds by $\pi$ and $\omega$ exchange; we determine the $g \to K\bar{K}$ branching ratio.

## 1. Introduction

We study the reaction $\pi^- p \to K^- K^0_S p$ at 10 GeV/$c$ using the University of Geneva two-arm spectrometer [1]. We collected 40 000 such events. We determine the moments of the $K^-$ angular distribution, and from these the production amplitudes, as a function of $t$, in the $A_2$ and in the g resonance regions. The information we obtain for $\pi^- p \to A_2^- p$ is complementary to that obtained for the reactions $K^\pm p \to K^*(1420)^\pm p$ by the same apparatus at the same energy [2,3]. A study of this set of diffractive processes is invaluable in determining properties of pomeron exchange and in attempts to unravel the pomeron- and f-exchange contributions. Recent studies can be found elsewhere [4,5]. On the other hand, g production is non-diffractive and proceeds *via* $\pi$ and $\omega$ exchange. We shall see that the difference between $A_2$ and g production is strikingly evident in the data, and in the structure of the underlying amplitudes. The prominence of $\pi$ exchange in g production allows the determination of the product of the $\pi\pi$ and $K\bar{K}$ branching ratios of the g resonance.

* Present address: CERN, Geneva, Switzerland.

The organization of the paper is as follows. In sect. 2 we present the moments as a function of $t$, firstly, in the $A_2$ mass region, and, secondly, in the g mass region. The allowed exchanges for $A_2$ and g production are given in sect. 3, together with the definition of the amplitudes we use to describe $\pi^- p \to K^- K^0 p$ production. Sect. 4 describes the determination of the amplitudes in the $A_2$ mass region; and in sect. 5 we compare $A_2$ and $K^*(1420)$ production and discuss the implications for pomeron and f exchange. In sect. 6 we perform the amplitude analysis in the g resonance region; this is complicated by the presence of non-negligible $L = 4$ $K^- K^0$ production [6,7]. In sect. 7 we study the interference between the resonant $L = 3$ and $L = 2,4$ natural parity exchange (NPE) amplitudes in the g mass region. We find that g production by NPE is consistent with $\omega$-exchange expectations, and we estimate the $g \to K\bar{K}$ branching ratio by relating the $\omega$-exchange contributions for g and $\rho$ production. In sect. 8 we study the $\pi$-exchange contribution to g production. We extrapolate to the $\pi$ exchange pole and calculate the $g \to K\bar{K}$ branching ratio. We summarize our results in sect. 9.

## 2. Data selection and moment analysis in the $A_2$ and g regions

We have measured the reaction $\pi^- p \to K_S^0 K^- p$ with a seen $K_S^0 \to \pi^+ \pi^-$ decay using the University of Geneva two-arm spectrometer. The apparatus consisted of:

(i) a beam spectrometer to measure direction, momentum, and mass of the incident particle;

(ii) a proton arm at large angle (38° to 70° in the laboratory), to measure direction and momentum of slow recoil protons in the range of momentum transfer $0.07 < -t < 1.0$ $(\mathrm{GeV}/c)^2$, using multiwire proportional chambers (MWPCs) (6 planes) and a high-precision time-of-flight system;

(iii) a forward arm, consisting of MWPCs (8 planes), to record the directions of forward emitted charged particles within a large solid angle (0.3 sr). There is no magnetic momentum analysis.

A detailed description of the spectrometer can be found in ref. [1].

Channel identification is done first by requiring a second vertex at least 30 mm downstream from the $\pi p$ vertex to select the $K_S^0 \to \pi^+ \pi^-$ candidates. Events of the correct topology are then processed by a kinematical 2C-fit, and accepted if $P(\chi^2) > 5\%$. Finally we require $M_{K^- p} > 1.9$ GeV to eliminate $Y^*$ contributions and their kinematical reflections at high $K_S^0 K^-$ mass.

The quality of the data sample can be checked by estimating the background under the unfitted $K^0$ mass peak, or independently, by inspecting the shape of the $P(\chi^2)$ distribution. In both cases, we find a background of 4%.

Fig. 1 shows the $K_S^0 K^-$ mass spectrum of the final sample of 40 000 events, and illustrates the dominance of $A_2$ and g production in this mass region. The sensitivity of the data, corrected for unseen $K^0$ decays, is

$$N/\sigma(\pi^- p \to K^0 K^- p) = 7670 \pm 600 \text{ weighted events}/\mu\text{b} .$$

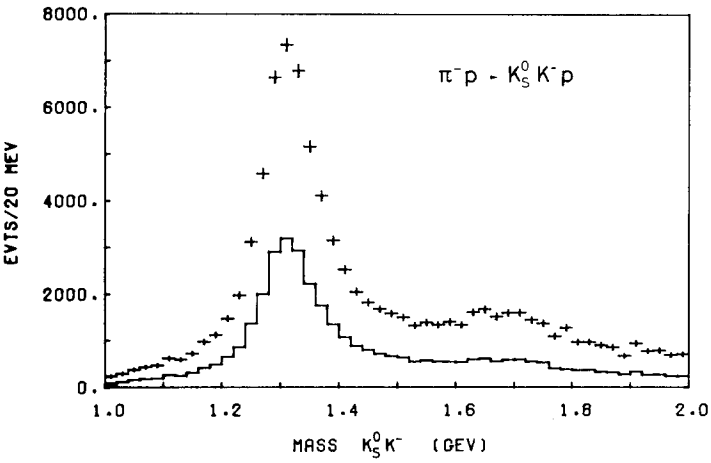


Fig. 1. $K^0_S K^-$ effective-mass spectrum, for $0.07 \leqslant |t| \leqslant 1.0$ $(\mathrm{GeV}/c)^2$. The spectrum is shown before (histogram) and after (points with error bars) acceptance correction. A constant factor of 5.8 due to the azimuthal aperture of the proton detector is not included in the correction.

Our cross-section normalization is in very good agreement with other $A_2^- \to K^0 K^-$ production data [8].

We have calculated the moments of the angular distribution of the $K^-$ in the $t$-channel helicity frame of the $K^0 K^-$ system. We have corrected for geometrical acceptance of the spectrometer, efficiencies, and absorption and decay of incident and outgoing particles, using the linear method described in ref. [1]. Fig. 2 shows the unnormalized moments $N\langle Y_J^M \rangle$ in the $A_2$ mass region ($1.2 < M < 1.4$ GeV) as a function of $t$, as obtained by fitting the terms $J \leqslant 4$ and $M \leqslant 4$. The normalization of the spherical harmonics is such that $\langle Y_0^0 \rangle = 1$.

Fig. 3 shows the momenta in the g mass region ($1.55 < M < 1.85$ GeV), resulting from a fit of the terms $J \leqslant 8$ and $M \leqslant 2$.

## 3. Amplitudes and allowed exchanges in $\pi^- p \to K^- K^0 p$

To extract the $\pi^- p \to K^- K^0_S p$ amplitudes from the experimental moments it is convenient to use combinations of helicity amplitudes with definite asymptotic exchange naturality. The moments can be expressed [9] as the sum of bilinear products of these amplitudes $L_{\lambda\pm}$, where $L_{\lambda\pm}$ describe, to leading order in the energy, the production of a $K^- K^0_S$ system of spin $L$, helicity $\lambda$ by natural and unnatural parity exchange, respectively. In terms of the helicity amplitudes, $H_{L\lambda}$,

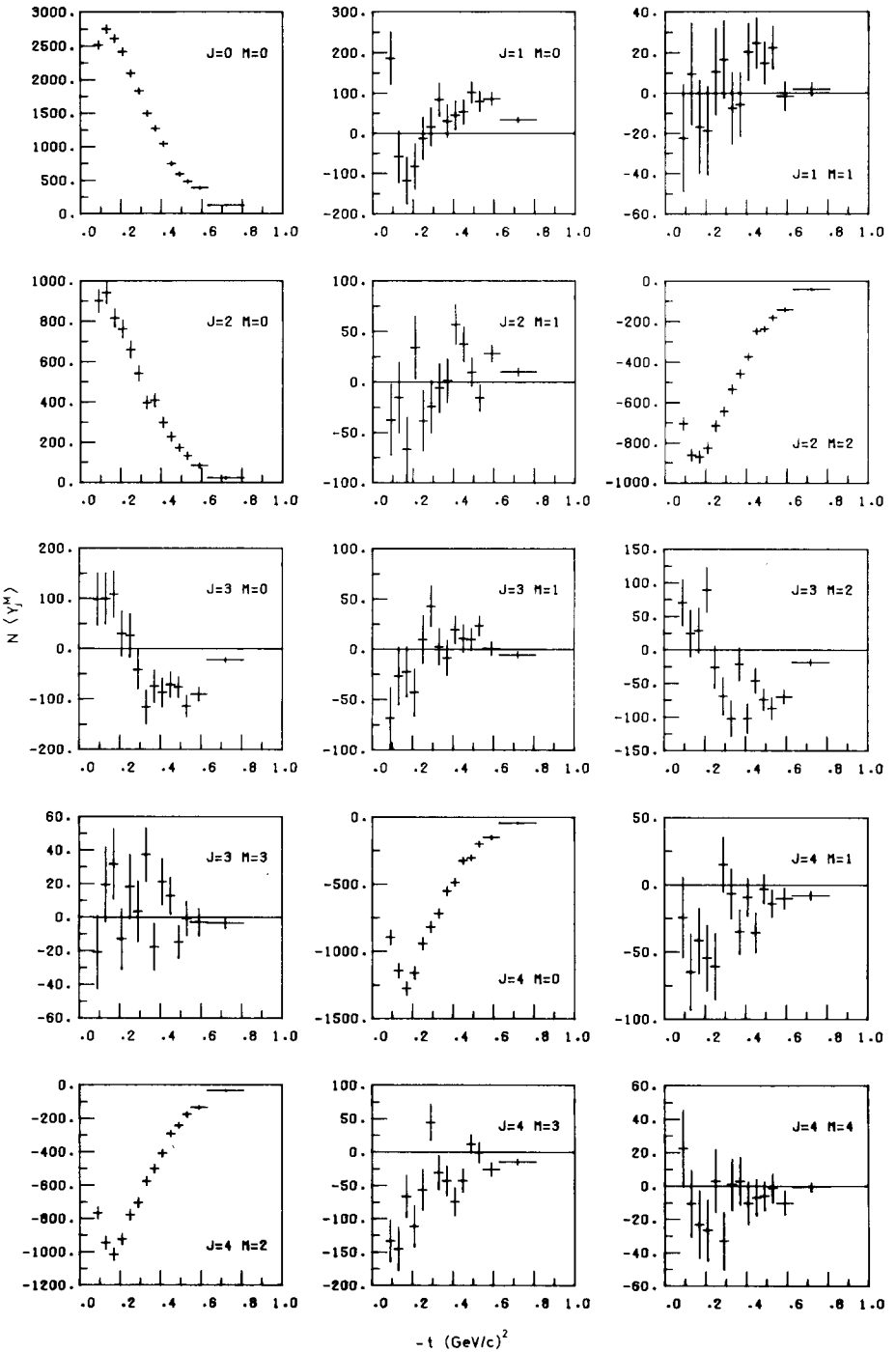


Fig. 2. Corrected spherical harmonic moments of the angular distribution of the $K^-$, in the $t$-channel helicity rest frame of the produced $K^-K^0$ system, as a function of $t$ in the $A_2$ mass region, $1.2 < M(K^-K^0) < 1.4$ GeV. The data are for $\pi^-p \to K^-K^0p$ at 10 GeV/$c$.

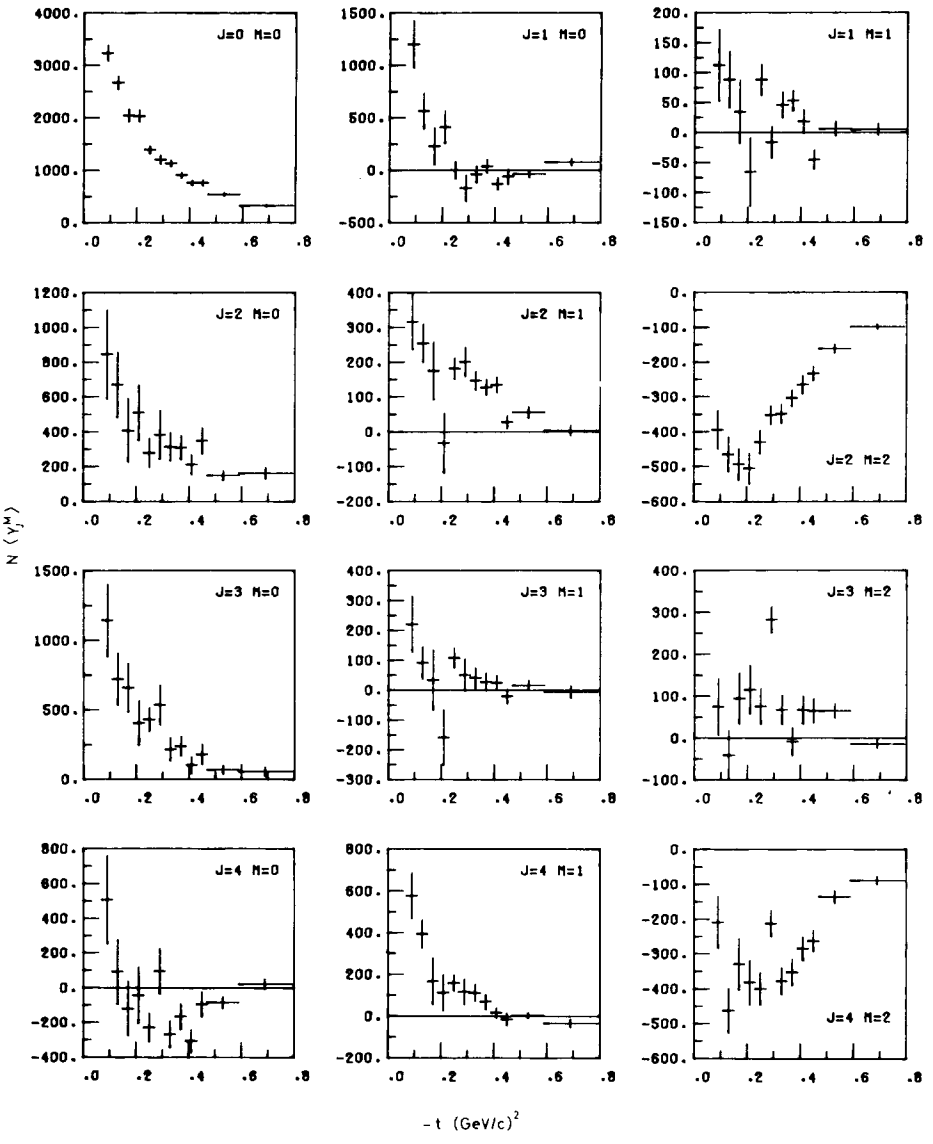


a

Fig. 3. As for fig. 2, but in the g-mass region $1.55 < M(\mathrm{K^-K^0}) < 1.85$ GeV.

we have

$$L_{\lambda\pm} \equiv \sqrt{\tfrac{1}{2}}\,[H_{L\lambda} \pm (-1)^{\lambda+1} H_{L,-\lambda}]\,, \qquad \lambda \neq 0\,, \tag{1}$$

$$L_0 \equiv H_{L0}\,,$$

That is only UPE occurs for $\lambda = 0$. We will use the abbreviated notation $L_\pm \equiv L_{1\pm}$.

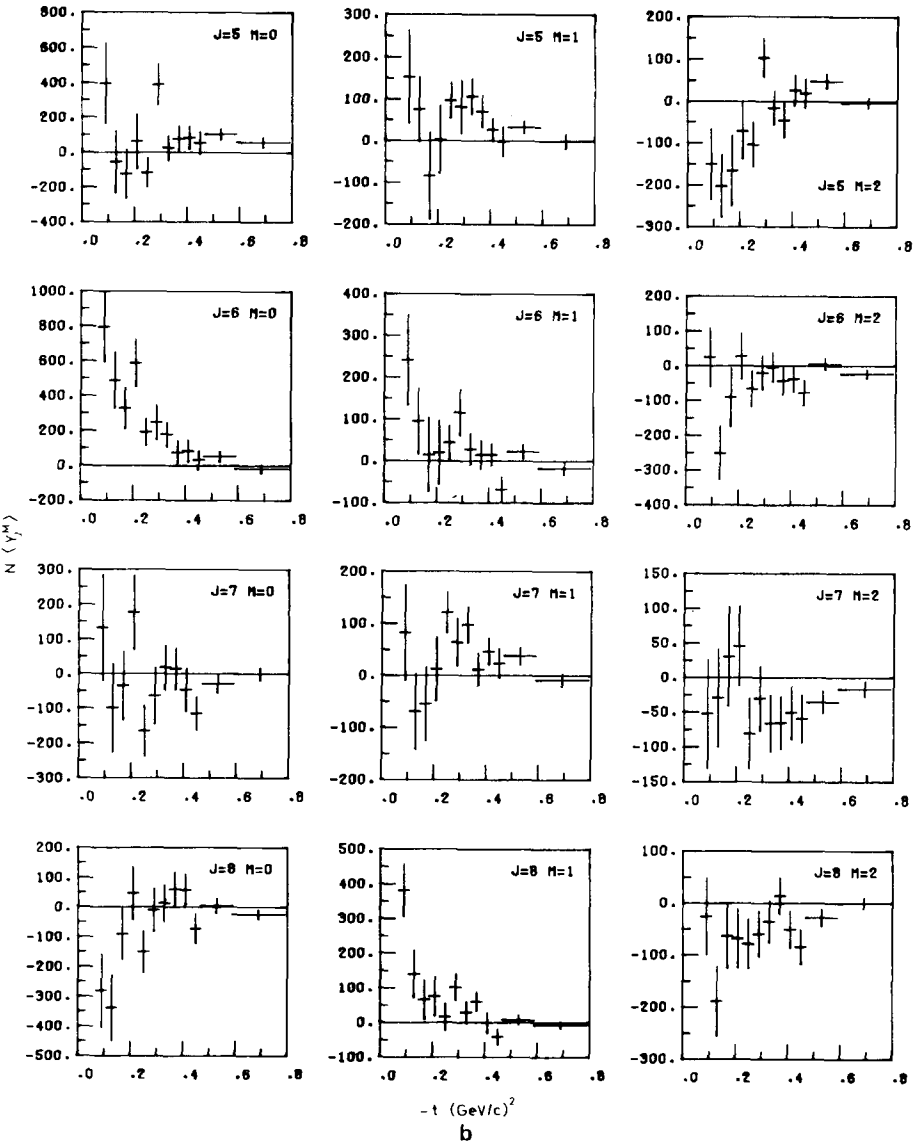


Fig. 3 (continued).

The amplitudes are normalized so that their moduli squared give the contribution to $d\sigma/dt$, that is

$$\frac{d\sigma}{dt} = |S_0|^2 + |P_0|^2 + |P_+|^2 + \dots . \tag{2}$$

A summation over helicity flip and non-flip at the nucleon vertex is implicit in each bilinear product, that is

$$|L|^2 = |L_f|^2 + |L_{nf}|^2 .$$

The interference terms can be rewritten in the form

$$\mathrm{Re}(L'L^*) = |L'||L|(\xi \cos\phi)_{L'L} , \tag{3}$$

where $\xi$ is the degree of nucleon spin coherence ($0 \leqslant \xi \leqslant 1$) and $\phi$ is the relative phase between amplitudes $L$ and $L'$. We note that the expressions for the observed moments do not contain interference terms between NPE and UPE amplitudes.

The observed moments, $\langle Y_J^M \rangle$ of figs. 2 and 3, show immediately that the production mechanisms are different in the $A_2$ and g mass regions. In the spin-2 $A_2$ mass region we observe strong negative $\langle Y_4^0 \rangle$ and $\langle Y_4^2 \rangle$ moments, whereas in the spin-3 g mass region we have a positive signal in $\langle Y_6^0 \rangle$ and a weaker negative signal in $\langle Y_6^2 \rangle$. Retaining only the $\lambda \leqslant 1$, spin-$L$ resonant amplitudes, these moments are

$$\langle Y_{2L}^0 \rangle = C_1|L_0|^2 - C_2(|L_-|^2 + |L_+|^2) ,$$

$$\langle Y_{2L}^2 \rangle = C_3(|L_-|^2 - |L_+|^2) ,$$

where $C_i$ are positive known coefficients. This implies that $A_2$ production is dominated by NPE ($D_+$), whereas g production proceeds mainly *via* UPE ($F_0$), and to a lesser extent *via* NPE ($F_+$). We also notice from the $J = 8$ moments that the $L = 4$ NPE amplitude ($G_+$) cannot be neglected in the g-resonance region.

The difference between g and $A_2$ production is due to the restrictions of $G$-parity at the meson vertex. For the production of a $K^-K^0$ system of spin $L$ the allowed exchanges are given in table 1.

From a study of the SU(3)-related reactions $K^\pm p \to K^{*\pm} p$ we expect isoscalar NPE and isovector UPE to be dominant. The pomeron (IP), $\omega$, and f exchanges contribute dominantly to overall single helicity-flip amplitudes, which vanish as $\sqrt{-t'}$ in the forward direction. For UPE, $\pi$ and B couple to overall helicity-flip amplitudes, whereas $A_1$ and Z quantum number exchange couple to overall non-flip amplitudes. Z is used to denote the possible $2^{--}$ exchange-degenerate partner of the $A_1$. The $\pi$-exchange pole is extremely close to the physical region so $\pi$

Table 1
Allowed exchanges in $\pi^- p \to K^- K^0 p$ for the production of a spin-$L$ $K^-K^0$ system

| | $L$ even (e.g. $A_2$) | $L$ odd (e.g. g) |
|---|---|---|
| NPE | IP, f, $\rho$ | $\omega$, $A_2$ |
| UPE | B(Z) | $\pi(A_1)$ |

domiantes $A_1$ exchange in the forward scattering region. The relative strength of the amplitudes with the quantum numbers of B and Z exchange are not so well known. There is evidence [10,11] from related reactions to suggest that non-flip Z exchange is larger for $-t \lesssim 0.2$ GeV$^2$, while B exchange dominates for $-t \gtrsim 0.2$ GeV$^2$.

The effects manifest in the data indicate that $A_2$ production proceeds dominantly by pomeron and f exchange, and that g production is due to $\pi$, and to a lesser extent $\omega$, exchange.

## 4. Amplitude analysis in the $A_2$ mass region

The $t$-structure of the observed $K^-K^0$ $t$-channel moments in the $A_2$ mass region, $1.2 < M < 1.4$ GeV, is shown in fig. 2. The explicit relations between the moments and the production amplitudes $L_+$, $L_0$ and $L_-$ are given in table 2. The five largest moments $\langle Y^0_{4,2,0}\rangle$, $\langle Y^2_{4,2}\rangle$ shown the dominance of the NPE amplitude $D_+$, and indicate that all other amplitudes will be much less reliably determined. The non-zero $\langle Y^3_4\rangle$ moment is attributable to interference of $D_+$ with the helicity-two NPE amplitude $D_{2+}$. The structure of $\langle Y^{0,2}_3\rangle$ can be accounted for by $P_+D_+$ interference and shows no evidence for a $P_0D_0$ effect. The UPE amplitudes are much harder to isolate. The moments $\langle Y^1_4\rangle$ and $\langle Y^1_2\rangle$, taken together with $\langle Y^3_4\rangle$, imply small $D_0D_-$ interference, but a larger $S_0D_-$ contribution. There is no evidence of either a $P_0$ or $P_-$ effect, except possibly $S_0P_0$ interference in the first $t$ bin of $\langle Y^0_1\rangle$.

As a result of these observations, we performed an amplitude analysis of the $J \leqslant 4, M \leqslant 4$ moments in the $A_2$ mass region in terms of the magnitudes and coherences of the NPE amplitudes $D_+$, $D_{2+}$, $P_+$, and of the UPE amplitudes $D_0$, $D_-$, $S_0$. Neglect of $P_0$ and $P_-$ means the moments $\langle Y^1_{3,1}\rangle$ are not included in the analysis, and as $\langle Y^3_3\rangle$ is also compatible with zero we do not determine the $P_+D_{2+}$ coherence. Moreover, the data cannot determine reliably the individual coherences in the weak UPE sector. We therefore assume nucleon spin-coherence and, motivated by $\pi$-B exchange degeneracy, $(\cos\phi)_{D_0D_-} = -1$.

The results are shown in fig. 4. We see the expected dominance of the NPE aplitude $D_+$. The clear $\langle Y^3_4\rangle$ signal is described by a $D_{2+}$ contribution of approximately 10% the magnitude of $D_+$. The suppression of the UPE D-wave amplitudes (associated with B and Z exchange) is to be compared with their relatively stronger $\pi$-exchange structure in $K^\pm p \to K^*(1420)^\pm p$ (see fig. 4 of ref. [2]).

We may compare the values of $|D_0|$ of fig. 4 with those obtained from charge-exchange (CEX) $A^0_2$ production. Data are available for $\pi^+n \to A^0_2p$ at 4 GeV/$c$ [12], and for $\pi^-p \to A^0_2n$ at 12 and 15 GeV/$c$ [13]. We interpolated the measured $t$-channel partial cross sections $\rho^D_{00}\, d\sigma/dt$ using the form $p_L^{2-2\alpha}$ with $\alpha(t) = -0.2 + 0.8\,t$. To convert to $|D_0|^2$ we included a 4.7% $A_2 \to K\bar{K}$ branching ratio [14], we multiplied by $\frac{1}{2}$ due to isospin, and corrected to a $1.2 < M < 1.4$ GeV mass interval. The

Table 2
The unnormalized moments $\sqrt{4\pi}N\langle Y_J^M\rangle$ in terms of the amplitudes $L_0$, $L_-$, and $L_+$, defined in the text [a)]

$$\sqrt{4\pi}N\langle Y_0^0\rangle = S_0^2 + P_0^2 + P_-^2 + P_+^2 + D_0^2 + D_-^2 + D_+^2 + F_0^2 + F_-^2 + F_+^2 + G_0^2 + G_-^2 + G_+^2$$

$$\sqrt{4\pi}N\langle Y_1^0\rangle = 2S_0P_0 + 1.789P_0D_0 + 1.549(P_-D_- + P_+D_+) + 1.757D_0F_0 + 1.650(D_-F_- + D_+F_+) + 1.746F_0G_0 + 1.690(F_-G_- + F_+G_+)$$

$$\sqrt{4\pi}N\langle Y_1^1\rangle = 1.414S_0P_- + 1.096P_0D_- - 0.633P_-D_0 + 1.581D_0F_- - 0.717D_-F_0 + 0.976F_0G_- - 0.756 F_-G_0$$

$$\sqrt{4\pi}N\langle Y_2^0\rangle = 0.894P_0^2 - 0.447(P_-^2 + P_+^2) + 0.639D_0^2 - 0.319(D_-^2 + D_+^2) + 0.596F_0^2 - 0.447(F_-^2 + F_+^2) + 0.581G_0^2 + 0.494(G_-^2 + G_+^2) + 2S_0D_0 + 1.757P_0F_0 + 1.714D_0G_0 + 1.451(P_-F_- + P_+F_+) + 1.565(D_-G_- + D_+G_+)$$

$$\sqrt{4\pi}N\langle Y_2^1\rangle = 1.414S_0D_- + 1.096P_0P_- + 1.171P_0F_- - 0.717P_-F_0 + 0.452D_0P_- + 1.107D_0G_- - 0.808P_-G_0 + 0.298F_0F_- + 0.225 G_0G_-$$

$$\sqrt{4\pi}N\langle Y_2^2\rangle = 0.548(P_-^2 - P_+^2) + 0.391(D_-^2 - D_+^2) + 0.365(F_-^2 - F_+^2) + 0.350(G_-^2 - G_+^2) - 0.293(P_-F_- - P_+F_+) - 0.319(D_-G_- - D_+G_+)$$

$$\sqrt{4\pi}N\langle Y_3^0\rangle = 2S_0F_0 + 1.757P_0D_0 + 1.746P_0G_0 - 1.914(P_-D_- + P_+D_+) + 1.383(P_-G_- + P_+G_+) + 1.193D_0F_0 + 0.422(D_-F_- + D_+F_+) + 1.091F_0G_0 + 0.704(F_-G_- + F_+G_+)$$

$$\sqrt{4\pi}N\langle Y_3^1\rangle = 1.414S_0F_- + 1.171P_0D_- + 1.011P_-D_0 + 1.193P_0G_- - 0.756P_-G_0 + 0.633D_0F_- - 0.298D_-F_0 + 0.498F_0G_- + 0.129F_-G_0$$

$$\sqrt{4\pi}N\langle Y_3^2\rangle = 0.926(P_-D_- - P_+D_+) - 0.578(P_-G_- - P_+G_+) + 0.578(D_-F_- - D_+F_+) + 0.514(F_-G_- - G_+F_+)$$

$$\sqrt{4\pi}N\langle Y_4^0\rangle = 0.857D_0^2 - 0.571(D_-^2 + D_+^2) + 0.516F_0^2 + 0.091(F_-^2 + F_+^2) + 0.486G_0^2 + 0.243(G_-^2 + G_+^2) + 2S_0G_0 + 1.746P_0F_0 - 1.069(P_-F_- + P_+F_+) + 1.162D_0G_0 + 0.518(P_-G_- + P_+G_+)$$

$$\sqrt{4\pi}N\langle Y_4^1\rangle = 1.414S_0G_- + 1.196P_0F_- + 0.976P_-F_0 + 1.107D_0D_- + 0.698D_0G_- + 0.225D_-G_0 + 0.498F_0F_- + 0.543 G_0G_-$$

$$\sqrt{4\pi}N\langle Y_4^2\rangle = 0.845(P_-F_- - P_+F_+) + 0.452(D_-^2 - D_+^2) + 0.455(D_-G_- - D_+G_+) + 0.288(F_-^2 - F_+^2) + 0.256(G_-^2 - G_+^2)$$

$$\sqrt{4\pi}N\langle Y_5^0\rangle = 1.741P_0G_0 - 1.101(P_-G_- + P_+G_+) + 1.699D_0F_0 - 1.201(D_-F_- + D_+F_+) + 1.052F_0G_0 + 0.008(F_-G_- + F_+G_+)$$

$$\sqrt{4\pi}N\langle Y_5^1\rangle = 1.206P_0G_- + 0.953P_-G_0 + 1.140D_0F_- + 1.075D_-F_0 + 0.577F_0G_- + 0.431 F_-G_0$$

$$\sqrt{4\pi}N\langle Y_5^2\rangle = 0.798(P_-G_- - P_+G_+) + 0.871(D_-F_- - D_+F_+) + 0.525(F_-G_- - F_+G_+)$$

$$\sqrt{4\pi}N\langle Y_6^0\rangle = 1.691D_0G_0 - 1.235(D_-G_- + D_+G_+) + 0.841F_0^2 - 0.630(F_-^2 + F_+^2) + 0.504G_0^2 - 0.025(G_-^2 + G_+^2)$$

$$\sqrt{4\pi}N\langle Y_6^1\rangle = 1.155D_0G_- + 1.055D_-G_0 + 1.112F_0F_- + 0.517G_0G_-$$

$$\sqrt{4\pi}N\langle Y_6^2\rangle = 0.844(D_-G_- - D_+G_+) + 0.431(F_-^2 - F_+^2) + 0.258(G_-^2 - G_+^2)$$

$$\sqrt{4\pi}N\langle Y_7^0\rangle = 1.672F_0G_0 - 1.295(F_-G_- + F_+G_+)$$

$$\sqrt{4\pi}N\langle Y_7^1\rangle = 1.131F_0G_- + 1.095F_-G_0$$

$$\sqrt{4\pi}N\langle Y_7^2\rangle = 0.848(F_-G_- - F_+G_+)$$

$$\sqrt{4\pi}N\langle Y_8^0\rangle = 0.851G_0^2 - 0.605(G_-^2 + G_+^2)$$

$$\sqrt{4\pi}N\langle Y_8^1\rangle = 1.115G_0G_-$$

$$\sqrt{4\pi}N\langle Y_8^2\rangle = 0.421(G_-^2 - G_+^2)$$

We use the abbreviated notation $LL' \equiv \mathrm{Re}(L^*L')$. A summation over helicity flip and non-flip at the nucleon vertex is implicit in each bilinear product, that is $\mathrm{Re}(L^*L') = \mathrm{Re}(L_f^*L_f' + L_{nf}^*L_{nf}')$.

a) These coefficients have been checked with those calculated by W. Männer. We thank him for providing a table for comparison.

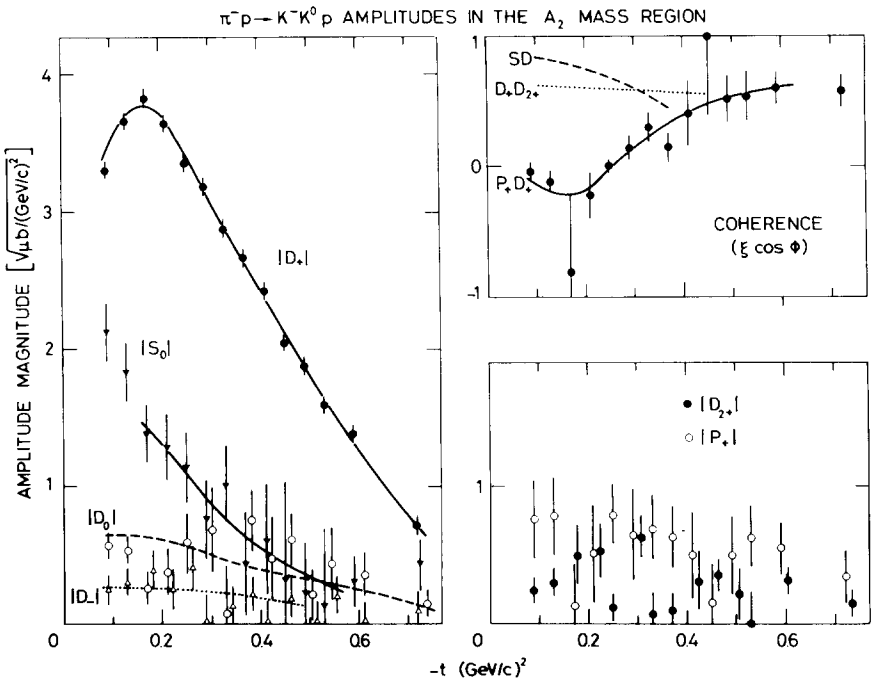


Fig. 4. The 10 GeV/$c$ $\pi^-p \to K^-K^0p$ amplitudes in the $A_2$ mass region, $1.2 < M(K^-K^0) < 1.4$ GeV. The curve for $|D_0|$ shows the prediction obtained from CEX $A_2^0$ production. The coherences of $SD_0$ and $-SD_-$ are assumed equal, and are denoted by $SD$. The $SD$ and $D_+D_{2+}$ coherences are not well determined and the curves only indicate the trend of the results.

values obtained for $|D_0|$ at $p_L = 10$ GeV/$c$ are indicated by the dashed line in fig. 4. The agreement between $|D_0|$ obtained from CEX and non-CEX reactions means that there is no evidence for isoscalar UPE in $\pi^-p \to A_2^-p$.

An interesting feature of our analysis is the importance of S-wave $K^-K^0$ production in the $A_2$ mass region (see fig. 4). In general, it is difficult to extract lower partial waves, and to study the reliability of this determination of $S_0$ we repeated the analysis with $P_0$ included, together with $P_- \equiv -0.5\,P_0$, but with $S_0$ omitted. The description of the moments was again reasonable, though not quite as good as that with $S_0$ included and $P_0$ omitted. Essentially the only change in the amplitude components shown in fig. 4 is that $|S_0| \to |P_0|$ and, of course, no $SD$ interference. The same ambiguity was present in the analysis of the moments as a function of the $K^-K^0$ mass [7]. There we argued, from the expected dominance of $S_0$ (rather than $P_0$) just above threshold and from the continuity of the solution as a function of mass, that the solution with the large $S_0$ in the $A_2$ region was favoured. There are other indicators that this is the physical solution. Firstly, by comparing $\pi$ and $\omega$ exchange for $Kp \to K^*(890)p$, and by comparing the P-wave background in the g

region (see below), there are indications that $|P_0| \lesssim |P_+|$. Secondly, by comparing $K^+K^-$ and $K^0_SK^0_S$ production data [15] (in particular the equality of the $\langle Y^0_2 \rangle$ moments) it has been noted that the P-wave $\pi$-exchange amplitude is small in our mass range. Quantitatively we find this $P_0$ cannot account for the required UPE contribution needed in $K^-K^0$ production. For these reasons we favour the $K^-K^0$ amplitude solution with the relatively large $S_0$ and a small $P_0$ contribution. Even if the two most forward points shown for $|S_0|$ are overestimated, owing to the omission of a possible $P_0$ contribution which peaks at small $t$ ($\pi$ exchange) and to large acceptance corrections, the $t$ structure still implies a strong non-flip component (Z exchange) in $S_0$ at small $t$. The analysis of the data as a function of the produced $K^-K^0$ mass showed an S-wave enhancement in this mass range [7]. This coincided with the bump previously seen in $K^+K^-$ and $K^0_SK^0_S$ production [15] and suggests that it should be attributed partly to $I = 1$, and not solely to $I = 0$, S-wave $K\bar{K}$ production. The importance of the non-flip exchange component for $I = 1$ S-wave production considerably complicates the extraction of $\pi\pi \to K\bar{K}$ partial waves from $K\bar{K}$ production data, particularly the determination of the $I = 0$ S-wave.

## 5. The relation between $A_2$ and $K^*(1420)$ diffractive production

$A_2$ production by NPE in the process $\pi^-p \to A_2^-p$ proceeds *via* pomeron and f exchange. We may write the dominant amplitude

$$D_+(A_2) = I\!P + f\,. \tag{4}$$

This contribution to the differential cross section for $A_2$ production, $|D_+(A_2)|^2$, is shown in fig. 5. It is obtained from $D_+(K^-K^0)$ of fig. 4 after correcting for (i) the unseen $A_2$ decay modes (using an $A_2 \to K\bar{K}$ branching ratio of 4.7%), and (ii) for the finite mass interval (1.2–1.4 GeV) using an $A_2$ Breit-Wigner form.

This may be compared with $K^*(1420)$ production isolated from the related $K^\pm p \to K^0\pi^\pm p$ reactions. High-statistics data for these latter processes have been taken, with the same spectrometer, at the same beam energy. These data were analysed [2] to determine the $K^0\pi^\pm$ production amplitudes in the mass region $1.34 < M < 1.5$ GeV and $K^*(1420)$ production was also found to proceed dominantly *via* the NPE amplitudes $D_+(K^{*\pm})$. The differential cross sections for $K^*(1420)$ production, or more precisely $|D_+|^2$, are also plotted in fig. 5, after correction for the unseen * $K^*(1420)$ decay modes and for the finite mass bin. The crossover at $-t = 0.3$ $(\mathrm{GeV}/c)^2$ has been interpreted in terms of the pomeron-, f- and $\omega$-exchange contributions [3]:

$$D_+(K^{*\pm}) = \gamma I\!P + \beta(f \mp \omega)\,,$$

where the coefficients $\gamma$ and $\beta$ are introduced since we have used $I\!P$ and $f$ to denote

* We include a factor of $\frac{3}{2}$ to allow for $K^* \to K^\pm\pi^0$ and use a $K^* \to K\pi$ branching ratio of 56.1%.

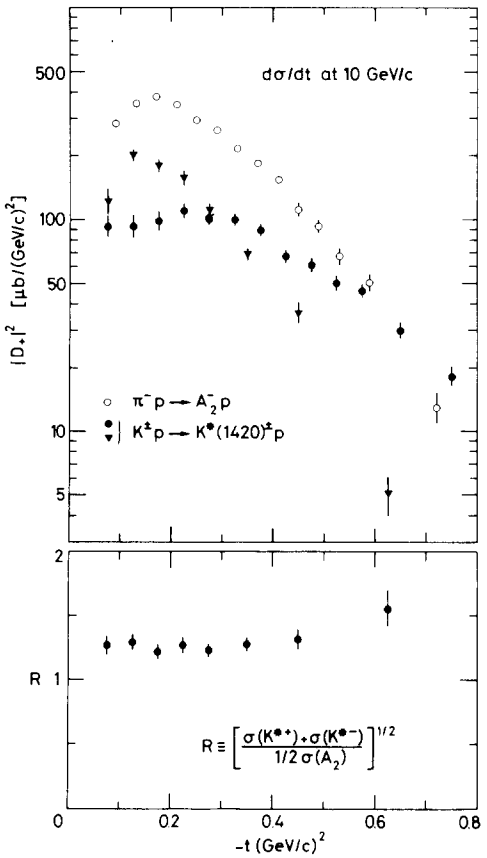


Fig. 5. The NPE cross sections $|D_+|^2$, for $\pi^- p \to A_2^- p$ and $K^\pm p \to K^*(1420)^\pm p$ at 10 GeV/$c$. The cross sections are corrected for the unseen decay modes and for the tails of the Breit-Wigner distributions outside the fitted mass intervals. This latter correction is a factor 1.23 and 1.27 for the $A_2$ and $K^*(1420)$ mass intervals, respectively. The ratio $R$ is discussed in sect. 5.

the exchange contributions for $A_2$ production, see eq. (4).

Here we wish to compare pomeron and f exchange in $A_2$ and $K^*(1420)$ production. Before confronting the data, it is informative to anticipate values of the coefficients $\gamma$ and $\beta$. From SU(3) invariance and magic f, f′ mixing we expect $\beta = \frac{1}{2}$. To estimate the relative coupling $\gamma$ of the pomeron, we may use the f, f′ dominated pomeron hypothesis [16]. According to this scheme [4,5]

$$\gamma = \tfrac{1}{2}(1 + r), \qquad \text{with} \qquad r(t) = \frac{\alpha_P - \alpha_f}{\alpha_P - \alpha_{f'}}, \tag{6}$$

where $\alpha_i(t)$ are the usual trajectory functions. In the symmetry limit $r = 1$ and the

pomeron is an SU(3) singlet. The departure of $r$ from 1 represents the effect of SU(3) mass breaking.

To facilitate the comparison of $A_2$ and $K^*(1420)$ production we plot, in fig. 5, the ratio

$$R \equiv \left[\frac{\sigma(K^{*+}) + \sigma(K^{*-})}{\frac{1}{2}\sigma(A_2)}\right]^{1/2}, \tag{7}$$

*versus* $t$, where we have used the differential cross sections, $\sigma \equiv d\sigma/dt\,|D_+|^2$, shown in the upper part of the figure. We have used the sum of $K^{*+}$ and $K^{*-}$ cross sections to remove the interference contributions between the even (IP, f) and odd ($\omega$) $G$-parity exchanges. If we assume $|\omega|^2$ is small compared to $|IP + f|^2$, then $R$ is an indicator of the relative strength of the pomeron and f contributions. If the processes are dominated by pomeron exchange than we expect $R \simeq 1 + r$, whereas if f exchange is dominant we expect $R \simeq 1$.

From fig. 5 we see that $R = 1.25 \pm 0.03$ for $-t < 0.4$ (GeV/$c$)$^2$. Assuming that $r(t) \simeq 0.5$ at $-t = 0.2$ (GeV/$c$)$^2$, and that the relative pomeron-f phase is 60°, this value of $R$ implies that the pomeron relative to f-exchange contribution is 1:1 in $\pi^- p \to A_2^- p$, and is 1.5:1 in $Kp \to K^*(1420)p$ at 10 GeV/$c$.

Before closing this section it is appropriate to comment on the observed $P_+D_+$ coherence in the $A_2$ region (*cf.* Fig. 4). This gives information on the behaviour of the relative phase $\phi_{PD} = \delta_D + \theta_D - \delta_P - \theta_P$, where $\theta$ and $\delta$ are the appropriate $K^-K^0$ production and decay phases, respectively. If we assume that the production phases $\theta_P$ and $\theta_D$ are in accordance with Regge expectations this would give information on $\delta_P$ in the $A_2$ region. However, the $P_+D_+$ coherence observed for the related $K^*(1420)$ reactions indicated anomalous behaviour for $\theta_P$ in the $K^*(1420)^{\pm}$ region; see, in particular, fig. 12 of ref. [3] *. We therefore cannot obtain a reliable estimate of $\delta_P$.

## 6. Amplitude analysis in the g resonance region

The $t$ structure of the moments of the $K^-K^0$ angular distribution in the g mass region, $1.55 < M < 1.85$ GeV, is shown in fig. 3. Clearly the data do not allow a full amplitude determination (*cf.* table 2). We use the $t$-channel moments $\langle Y_J^M \rangle$ with $J \leqslant 8$, $M = 0, 2$ to determine the magnitudes and coherences of the NPE amplitudes $L_+$, and of the UPE amplitudes $L_0$, with $L \leqslant 4$. We are led to this simplification by the results in the $A_2$ mass region. From the $A_2$ analysis we expect that $L_+L'_{2+}$ interference terms will contribute to the $M = 1$ moments at least as strongly as $L_0L'_-$ interference terms. The data are unable to determine

* Here $\theta_P$ denotes the P-wave $K^-K^0$ production phase; it corresponds to the phase of the odd-signatured $K^*$ production amplitude of fig. 12c of ref. [3].

both $L_-$ and $L_{2+}$. However, these small amplitudes only contribute quadratically to the $M = 0, 2$ moments and so it should be reliable to use these moments to determine the more dominant $L_0$ and $L_+$ amplitudes.

As mentioned before, the $J = 6, M = 0$ and 2 moments show that g resonance production proceeds mainly by UPE ($F_0$), and to a much lesser extent by NPE ($F_+$). The dominance of the $\langle Y_4^2 \rangle$ and $\langle Y_2^2 \rangle$ moments, as compared with the other $M = 2$ moments, indicates a very strong $D_+$ component in the g region. Moreover, the $J = 8$ moments suggests that $L = 4$ $K^-K^0$ production by NPE exchange ($G_+$) must be included in this mass interval. The presence of sizeable $D_+$ and $G_+$ amplitudes make the determination of $|F_+|$ very difficult. The difficulty is apparent from the expression for the $J = 6, M = 2$ moment:

$$\langle Y_6^2 \rangle = -0.431\,|F_+|^2 - 0.258|G_+|^2 - 0.844\ \mathrm{Re}(D_+G_+^*)\,.$$

The "background" waves, $D_+$ and $G_+$, are associated with pomeron exchange and are therefore enhanced relative to the ($\omega$-exchange) resonant amplitude $F_+$. On the other hand, since $P_+$, $D_+$, and $G_+$ are expected to be nucleon spin coherent, the data give valuable information on the relative phases of these amplitudes.

There is no evidence for the $L = 4$ UPE amplitude $G_0$, either from fig. 3 or from the moments as a function of the produced $K^-K^0$ mass [7]. This is in agreement with the exchange expectations of table 1. We therefore set $G_0 = 0$, and for $J \geqslant 7$ include only moments with $M = 2$ in the analysis *.

In each $t$ interval we use the $J \leqslant 8, M = 0, 2$ moments to determine the magnitudes and relative phases of the amplitudes within the NPE sector ($P_+, D_+, F_+, G_+$) and within the UPE sector ($S_0, P_0, D_0, F_0$). For each $t$ interval all the solutions are enumerated using the Barrelet zero technique [17] and the solution selected to correspond with that obtained as a function of mass in the g region [7]. The ambiguity is essentially only in the lower partial waves; in particular for the $S$, $P$, and $D_0$ amplitudes. We note also that the analysis assumes, within each sector, that the amplitudes have a common coherence factor $\xi$. Within the UPE sector there is no reason why this should be correct and so only the dominant UPE coherence, $\xi \cos\phi$, may be meaningful. $F_0$ is the dominant UPE amplitude and the other UPE quantities are much less reliably determined. To sum up, we note that the analysis should be reliable and unambiguous for ($D_+, F_+, G_+$) and $F_0$.

The results for the g production amplitudes and the background D- and G-waves, together with their respective coherences, are shown in fig. 6. The lower partial waves are, in general, not so well determined and depend on the Barrelet solution that is selected [7]. For our solution the magnitudes of $S_0$, $P_0$, $P_+$ are approximately 1.0, 0.6, 0.7 $\sqrt{\mu b}$/GeV, respectively, at $-t = 0.15$ (GeV/$c$)$^2$, and 0.3, 0.1, 0.2 $\sqrt{\mu b}$/GeV at $-t = 0.5$ (GeV/$c$)$^2$. The coherence of $S_0F_0$ is positive for all $t$, that of $P_0F_0$ is $\approx -0.4$ for $-t < 0.3$ (GeV/$c$)$^2$ and that of $P_+D_+$ is negative for all $t$.

* The data for the $\langle Y_8^2 \rangle$ moment were smoothed at $-t = 0.13$, 0.38, and 0.45 (GeV/$c$)$^2$.

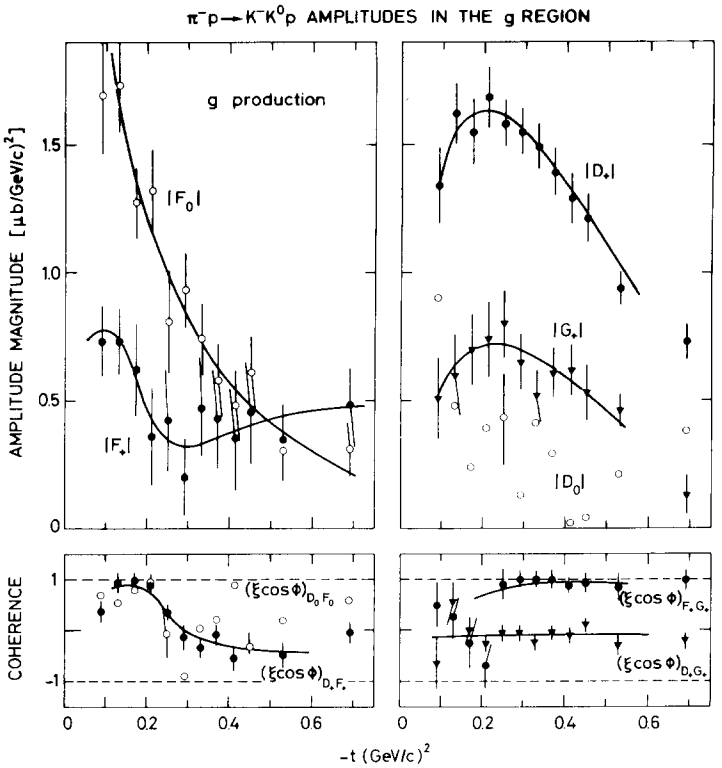


Fig. 6. The 10 GeV/$c$ $\pi^-p \to K^-K^0p$ amplitudes in the g mass region, $1.55 < M(K^-K^0) < 1.85$ GeV, obtained from the data of fig. 3. The extreme fluctuations seen in the $3 \leqslant J \leqslant 5$ moments at $-t = 0.29$ (GeV/$c$)$^2$ were removed before amplitude analysis. Only representative errors are shown for $|D_0|$ and the $D_0F_0$ coherence.

The difference of odd-$L$ and even-$L$ $K^-K^0$ production mechanisms is strikingly evident in fig. 6. For UPE, the g production amplitude $F_0$ ($\pi$ exchange) dominates the background $D_0$ amplitude (B, Z exchange). On the other hand, for NPE, g production proceeds *via* $F_+$ ($\omega$ exchange) which is smaller than, and of different $t$ structure from the even-$L$ background $D_+$ and $G_+$ amplitudes (pomeron, f exchange). The expected single helicity flip character of the NPE amplitudes is clearly apparent for $D_+$ and $G_+$.

## 7. g production by NPE: ω exchange

Although the presence of the relatively large $D_+$ and $G_+$ background waves complicate the determination of $|F_+|$ they do yield valuable phase information. To inter-

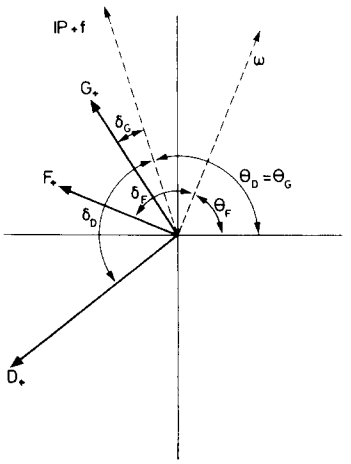


Fig. 7. An Argand plot of the phases of the NPE amplitudes, $D_+$, $F_+$, $G_+$, in the g resonance region. $\theta$ and $\delta$ are the $K^-K^0$ production and decay phases, respectively. The sketch is for $-t \approx 0.1$ (GeV/$c$)$^2$; for $-t \approx 0.5$ (GeV/$c$)$^2$, $F_+$ is rotated clockwise by about 90°. The observed coherences (*cf.* fig. 6) favour $\delta_D \approx 110°$.

pret the observed behaviour of the NPE coherences ($D_+F_+$, $F_+G_+$, $D_+G_+$), shown in fig. 6, we write the relative phase of each amplitude pair in the form

$$\phi_{LL'} \equiv \theta_L + \delta_L - \theta_{L'} - \delta_{L'} ,$$

where $\theta$ are production phases and $\delta$ decay phases of the $K^-K^0$ system. Both $D_+$ and $G_+$ arise from pomeron and f exchange. We therefore expect their production phases, $\theta_D \simeq \theta_G$, to be increasing relatively slowly from just above 90° as $-t$ increases from $t = 0$. Now in the g resonance region we are above the $A_2(1310)$, $2^+$ resonance ($\delta_D$ approximately 120–160°) and below the $A_2^*(1900)$, $4^+$ resonance [6,7] ($\delta_G$ approximately 20°). Moreover, for the resonant $F^+$ amplitude we have $\delta_F \simeq 90°$ and, assuming it is produced by $\omega$ exchange, we expect, up to a sign, $\theta_F$ to change from about 50–60° at $t = 0$, to 0° at $-t \sim 0.4$ (GeV/$c$)$^2$ where Im $\omega$ changes sign *. This latter cross over is generally associated with the $\omega$ nonsense-wrong-signature-zero at $\alpha_\omega = 0$ arising in the exchange-degenerate picture. The rapid phase change associated with $\omega$ exchange is manifest in the behaviour of $\xi \cos \phi$ for $D_+F_+$. The observed NPE coherences (*cf.* fig. 6) lead to the phases shown in the Argand plot of fig. 7, which appear consistent with the above expectations. However SU(3) and exchange degeneracy require the exchanges for $\pi^- p \to (K^-K^0)\, p$ to be $\mathbb{P}$ + f and $-\omega$. That is the above values of $\theta_F$ should be increased by $\pi$, in disagreement with

* This expectation is based on an analysis of $K^*$ production [3]; there we found an $\omega$ contribution somewhat modified from the exchange-degenerate form, $1 - \exp(-i\pi\alpha)$.

the sign of the observed $D_+F_+$ coherence.

$$\frac{d\sigma_\omega(\rho)}{dt} \equiv \tfrac{1}{2}(\rho_{11} + \rho_{1-1})\left[\frac{d\sigma}{dt}(\pi^+ p \to \rho^+ p) + \frac{d\sigma}{dt}(\pi^- p \to \rho^- p) - \frac{d\sigma}{dt}(\pi^- p \to \rho^0 n)\right] \tag{8}$$

Following Hoyer et al. [18] we apply finite-mass sum rules and two-component duality to relate the $\omega$-exchange contributions to these resonance-production reactions at a given energy:

$$\frac{d\sigma_\omega(\rho)/dt}{d\sigma_\omega(g)/dt} \simeq \left(\frac{m_\rho^2}{m_g^2}\right)^{-2\alpha_\omega(t)} . \tag{9}$$

From our results for $|F_+|$ (see fig. 6) we can estimate g production by $\omega$ exchange at 10 GeV/$c$, provided we are given the $g \to K\bar{K}$ branching ratio,

$$\frac{d\sigma_\omega(g)}{dt} = |F_+|^2/[BR(g \to K\bar{K})] . \tag{10}$$

Taking $\alpha_\omega = 0.4 + 0.9t$ in eq. (9), we then calculate $d\sigma_\omega(\rho)/dt$. In fig. 8 we compare our prediction with 6 GeV/$c$ $\rho$ production data [9], after allowing for the different beam momenta using the usual $p_L^{2-2\alpha_\omega}$ dependence. The curves, shown for two dif-

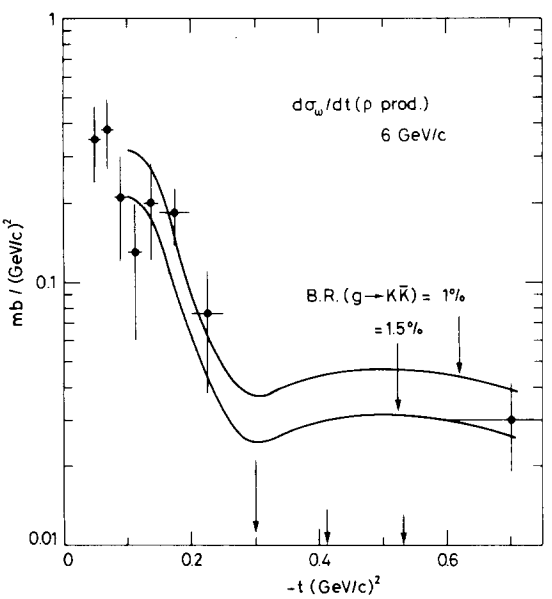


Fig. 8. Data for $\rho$ production by $\omega$ exchange at 6 GeV/$c$, taken from ref. [19]. The curves are the finite-mass sum-rule predictions, obtained from the g production amplitude $F_+$ of fig. 6, for two different values of the $g \to K\bar{K}$ branching ratio. The arrows at the bottom of the figure indicate data points off scale.

ferent $g \to K\bar{K}$ branching ratios, result from the curve through $|F_+|$ on fig. 6. The comparison, which is most relevant * for $0.1 < -t < 0.2$ (GeV/$c$)$^2$, favours a branching ratio

$$\frac{\gamma(g \to KK)}{\gamma(g \to \text{all})} \simeq 0.015 . \tag{11}$$

The 16 GeV/$c$ data for isospin-zero NPE $\rho$ production [20] have larger errors, but a similar comparison yields compatible results.

## 8. g production by UPE: $\pi$ exchange

The structure of $|F_0|$ of fig. 6 is indicative of $\pi$ exchange, and the values may be extrapolated to the $\pi$ pole ($t = \mu^2$) to give a more direct determination of the $g \to K\bar{K}$ branching ratio than that we obtain from $|F_+|$. To do this we use the Chew-Low form

$$\frac{d\sigma}{dt} = \frac{1}{m_N^2 p_L^2} \frac{g^2}{4\pi} \left( \frac{-te^{b(t-\mu^2)}}{(t-\mu^2)^2} \right) (2L+1) \int \frac{M^2}{q_\pi} |f_L|^2 \, dM , \tag{12}$$

with $L = 3$, where $M$ is the produced $K^-K^0$ mass, $q_\pi^2 = \frac{1}{4}M^2 - \mu^2$, and

$$f_L = \frac{M_R \sqrt{\Gamma_\pi \Gamma_K}}{M_R^2 - M^2 - iM_R\Gamma} .$$

We integrate over the experimental mass bin, 1.55–1.85 GeV. The total width of the g resonance is $\Gamma = \Gamma_\pi + \Gamma_K + \Gamma_0$, where

$$\Gamma_i(M) = \gamma_i \left( \frac{q_i}{q_i^R} \right)^7 \frac{D(q_i^R R)}{D(q_i R)} ,$$

with a barrier factor $D(z) = 225 + 45z^2 + 6z^4 + z^6$ and interaction radius $R = 3.5$ GeV$^{-1}$. We take the mass and width of the g resonance to be $M_R = 1.69$ GeV, $\gamma = 0.18$ GeV; and the momentum of the other decay channels, in addition to the $\pi\pi$ and $K\bar{K}$ channels, to be represented by $q_0 = q_K$. We fit $|F_0|^2$ to eq. (12) with $(\gamma_\pi \gamma_K)$ and the slope $b$ as free parameters. The fit ** is shown by the curve through $|F_0|$ on fig. 6 and corresponds to

$$\sqrt{\gamma_K \gamma_\pi}/\gamma = 0.056 \pm 0.017 ,$$

$$b = 4.5 \pm 1.1 \text{ GeV}^{-2} .$$

* Recall that the amplitude analysis for $0.2 < -t < 0.5$ (GeV/$c$)$^2$ revealed a relatively large $G_+$ contribution, which made the extraction of $F_+$ particularly difficult. It is therefore not surprising that the anticipated dip in $d\sigma_\omega(g)/dt$ is very shallow.

** We omit the first point owing to the large acceptance corrections in the near forward direction.

If we take the particle table [14] values of the $\pi\pi$ branching ratio, $\gamma_\pi/\gamma = 24 \pm 1\%$, then we find the $g \to \bar{K}K$ branching ratio is

$$\gamma_K/\gamma = 1.3 \pm 0.4\% .$$

This determination is in agreement with the independent estimation, $\gamma_K/\gamma \sim 1.5\%$, which we obtained in sect. 7 from the NPE amplitude $F_+$.

The above numbers yield a ratio of the $K\bar{K}$ and $\pi\pi$ decay modes of the g resonance of

$$\gamma_K/\gamma_\pi = 0.056 \pm 0.017 .$$

This is to be compared with the SU(3) value

$$\frac{\gamma_K}{\gamma_\pi} = \frac{1}{2}\left(\frac{q_K^R}{q_\pi^R}\right)^7 = 0.13 .$$

Note that SU(3) comparisons are better satisfied without including barrier factors [21]. To agree with SU(3) we would have had to input $\gamma_\pi/\gamma = 16\%$, which would have led to $\gamma_K/\gamma = 2\%$.

## 9. Conclusions

Here we summarize the main results of our study of $A_2$ and g production by the reaction $\pi^- p \to K^- K^0 p$ at 10 GeV/$c$.

### *9.1. The $A_2$ mass region*

(i) We find $A_2$ production proceeds dominantly by NPE. The $t$-channel $D_+$ amplitude is dominant, but a non-zero $\langle Y_4^3 \rangle$ signal leads to a $D_{2+}$ contribution which is, on the average, 10% of $|D_+|$.

(ii) The UPE amplitude $D_0$ is consistent in magnitude and $t$ structure with that found in CEX $A_2^0$ production, and lends support to the assumption that UPE is dominantly isovector in $\pi^- p \to A_2^- p$.

(iii) S-wave $K^- K^0$ production is important in the $A_2$ region, the $t$ structure implying a strong non-flip component at small $t$ (Z exchange). Combined with the $K^- K^0$ analysis as a function of mass [7], and with $K^+ K^-$ — and $K_S^0 K_S^0$ production data [15], this suggests the existence of an $I = 1, 0^+$ state under the $A_2$.

(iv) There is relatively little P-wave $K^- K^0$ production, although the $P_+ D_+$ coherence is well determined.

(v) $A_2$ and $K^*(1420)^\pm$ production are related using the f, f′ dominated scheme for the pomeron. We estimate the pomeron relative to f exchange and find, for example, at $-t \approx 0.2\ (\mathrm{GeV}/c)^2$ at ratio 1:1 in $\pi^- p \to A_2^- p$ at 10 GeV/$c$.

*9.2. The g mass region*

(i) We find g production proceeds dominantly by UPE ($\pi$ exchange).

(ii) We extrapolate to the $\pi$-exchange pole and find $\sqrt{\gamma_\pi \gamma_K}/\gamma = 5.6 \pm 1.7\%$, where $\gamma_\pi/\gamma$ and $\gamma_K/\gamma$ are the $\pi\pi$ and $K\bar{K}$ branching ratios, respectively, of the g. Taking $\gamma_\pi/\gamma = 24\%$ this gives $\gamma_K/\gamma = 1.3 \pm 0.4\%$.

(iii) The resonant NPE amplitude $F_+$ is reasonably consistent with $\omega$ exchange. It is, however, poorly determined, because g production by NPE ($\omega$ exchange) is masked by the production of $L = 2$ and $L = 4$ $K^-K^0$ systems, which can proceed by pomeron and f exchange.

(iv) Finite-mass sum rules and duality allow a comparison of the NPE amplitude $F_+$ with $\rho$-production data. This hypothesis leads to an estimate of the $g \to K\bar{K}$ branching ratio of $\gamma_K/\gamma \approx 1.5\%$.

Finally, we note that at higher energies $\pi^- p \to K^- K^0 p$ will be dominated by even-$L$ $K^-K^0$ production by NPE. Information about the odd-$L$ states will be obtained mainly through interference with the even-$L$ production amplitudes. The study of the reactions $\pi^\pm p \to K^\pm K_S^0 p$ and $K^\pm p \to K_S^0 \pi^\pm p$ at SPS energies will, when combined with $\pi N$ and KN elastic-scattering data, provide a powerful probe of the properties of the pomeron.

We thank P. Collins, A. Irving and T. Shimada for discussions during the course of this work. We are grateful to the Fonds National Suisse and the British Science Research Council for support. One of us (E.N.O.) thanks the Turkish Government for financial support.

## References

[1] R. Baldi et al., Nucl. Phys. B134 (1978) 365.
[2] R. Baldi et al., Phys. Lett 70B (1977) 377.
[3] A.D. Martin et al., Nucl. Phys. B134 (1978) 392.
[4] A.C. Irving, Nucl. Phys. B121 (1977) 176.
[5] P.D.B. Collins, F.D. Gault and A.D.M. Wright, J. of Phys. G4 (1978) 471.
[6] R. Baldi et al., Observation of a spin-4, isospin-1, meson resonance, Jan. 1978, Phys. Lett., submitted.
[7] A.D. Martin et al., A study of isospin-1 meson states using 10 GeV/$c$ $K^-K^0$ production data, Jan. 1978, Phys. Lett., submitted.
[8] CERN-Munich (MPI) Collaboration, H. Dietl, private communication.
[9] A.D. Martin and C. Michael, Nucl. Phys. B84 (1975) 83.
[10] A.C. Irving, Nucl. Phys. B105 (1976) 491.
[11] A.C. Irving and R.P. Worden, Phys. Reports 34 (1977) 119.
[12] M.J. Emms et al., Phys. Lett. 58B (1975) 117.
[13] M.J. Corden et al., Rutherford Lab. preprint RL-77-079/A (Sept. 1977).
[14] Particle Data Group, Rev. Mod. Phys. 48 (1976) S1.

[15] A.J. Pawlicki et al., Phys. Rev. D15 (1977) 3196;
N.M. Cason et al., Phys. Rev. Lett. 36 (1976) 1485;
D. Cohen, ANL-HEP-CP-77-37, *in* Proc. 5th Experimental Meson Spectroscopy Conf., Boston, 1977, to be published.
[16] R. Carlitz, M.B. Green and A. Zee, Phys. Rev. Lett. 26 (1971) 1515; Phys. Rev. D4 (1971) 3439;
P.G.O. Freund, H. Jones and R.J. Rivers, Phys. Lett. 36B (1971) 89.
[17] S. Gersten, Nucl. Phys. B12 (1969) 537;
E. Barrelet, Nuovo Cim. 8A (1972) 331.
[18] P. Hoyer, R.G. Roberts and D.P. Roy, Nucl. Phys. B56 (1973) 173.
[19] H.A. Gordon, K.-W. Lai and J.M. Scarr, Phys. Rev. D8 (1973) 779.
[20] J. Bartsch et al., Nucl. Phys. B46 (1972) 46.
[21] N.P. Samios, M. Goldberg and B.T. Meadows, Rev. Mod. Phys. 46 (1974) 1.

Nuclear Physics B158 (1979) 520–545


# ANALYSES OF $\bar{K}K$ PRODUCTION AND SCALAR MESONS

A.D. MARTIN and E.N. OZMUTLU
*Department of Physics, University of Durham, UK*

Received 7 May 1979

The high-statistics data for the various $K^-K^+$, $K^0_SK^0_S$, $K^-K^0_S$ production reactions are analysed. In particular we study both the isospin-zero and isospin-one $K\bar{K}$ S-wave in the mass region from threshold through the observed structure at 1300 MeV. The implications for the scalar mesons are discussed. We also determine branching ratios, and study interference of the produced f, f′ and $A_2$ resonances.

## 1. Introduction

High-statistics data now exist for the following $K\bar{K}$ production processes [1–5]

$$\pi^-p\to K^-K^+n\,,\qquad \pi^-p\to K^0_SK^0_Sn\,,$$
$$\pi^+n\to K^-K^+p\,,\qquad \pi^-p\to K^-K^0_Sp\,.$$

These are valuable for particle spectroscopy. The $K\bar{K}$ channel can have states $J^{PC}=0^{++}$, $1^{--}$, $2^{++}$, ... of both isospin $I=0$ and 1. The subset with $J+I$ even can be produced by pion exchange, and so can be also studied in $\pi\pi$ production. The S-wave ($0^{++}$) is sizable, and shows interesting structure, throughout the mass region from the $K\bar{K}$ threshold to 1.5 GeV.

$J^{PC}=0^{++}$ mesons are of unusual importance; however, they continue to be a centre of controversy [6–12], both theoretically and phenomenologically. The reasons are clear. In the quark–gluon approach we expect a rich spectrum of $0^{++}$ states below 1.5 GeV. In addition to the conventional P-wave $q\bar{q}$ nonet, it has been proposed [12] that there could be a low-lying $qq\bar{q}\bar{q}$ nonet. A third possibility for $0^{++}$ mesons are states built entirely from gluons [13]. On the phenomenological side the identification of $0^{++}$ mesons is far from easy. This is true despite their strong coupling to the readily accessible $0^-0^-$ channels, such as $\pi\pi$, $K\bar{K}$, $\pi K$. The resonances either appear very broad, or near the $K\bar{K}$ threshold, or hidden under the leading peripheral $2^{++}$ states. In each case they are prone to ambiguity.

Here we use the observed $K\bar{K}$ angular distributions to carry out partial-wave analyses, paying particular attention to the production mechanisms of the $K\bar{K}$ system. After defining, in sect. 2, the production amplitudes that we shall use, we begin (sect. 3) by re-analysing $\pi^-p\to K^-K^0p$ data [4, 5]. This reaction is valuable in

that only $I=1$ $K\bar{K}$ states are allowed, but suffers from the disadvantage that it is dominated by natural parity exchange (NPE). Our motivation here is to show that the data do contain an unnatural parity exchange (UPE) component and to isolate the amount of S-wave $K^-K^0$ production.

In sects. 4, 5 we analyse $K^-K^+$ production data. These charge-exchange reactions are dominated by UPE. First we study the $K\bar{K}$ D-wave in the f, $A_2$ and f' mass region, determining resonance branching ratios and studying interference effects. Then in sect. 5 we perform various partial-wave analyses of the $K^-K^+$ data, and compare with the ANL analysis [14]. For $K^-K^+$ both $I=0$ and $I=1$ S-wave production are allowed. We find that even with data for the four $K\bar{K}$ processes the isospin assignment of the S-wave structure at 1300 MeV is confused.

Finally, in sect. 6, the information on the $\pi\pi\to K\bar{K}$ S-wave is combined with that for the elastic $\pi\pi\to\pi\pi$ channel and a coupled-channel analysis is performed. The implications for the scalar mesons are discussed. In sect. 7 we present our conclusions.

## 2. The $\pi N\to K\bar{K}N$ amplitudes

To analyse the data for the various $\pi N\to K\bar{K}N$ reactions we use the amplitudes

$$L_{\lambda\pm}=\sqrt{\tfrac{1}{2}}(H_{L\lambda}\pm(-1)^{\lambda+1}H_{L,-\lambda}), \tag{1}$$

for $\lambda\neq 0$, and $L_0\equiv H_{L0}$ for $\lambda=0$, where $H_{L\lambda}$ are $t$-channel helicity amplitudes describing the production of a $K\bar{K}$ system of angular momentum $L$ and helicity $\lambda$. To leading order in the incident energy, $L_{\lambda\pm}$ correspond to $K\bar{K}$ production by natural and unnatural parity exchange (NPE, UPE) respectively; $\lambda=0$ production proceeds *via* UPE alone. We will use the abbreviated notation $L_\pm\equiv L_{1\pm}$.

The moments of the $K\bar{K}$ angular distribution can be expressed [5] as a sum of bilinear products of the form $\mathrm{Re}(L'_\lambda L^*_\lambda)$. A sum over helicity flip and non-flip at the nucleon vertex is implicit in each product*, for example

$$\mathrm{Re}\,(L'_\lambda L^*_\lambda)=\mathrm{Re}(L'_{++;\lambda}L^*_{++;\lambda}+L'_{+-;\lambda}L^*_{+-;\lambda}). \tag{2}$$

The observed moments do not contain interference terms between NPE and UPE amplitudes. That is, terms of the form $\mathrm{Re}\,(L'_{\lambda+}L^*_{\lambda-})$ do not occur.

We normalize the $\pi N\to K\bar{K}N$ amplitudes so that their moduli squared give the contribution to $\mathrm{d}\sigma/\mathrm{d}t\,\mathrm{d}M$, where $M$ is the mass of the $K\bar{K}$ system. Thus the $\pi$ exchange contribution may be written in the form

$$L_0=N(2L+1)C_L f^I_L(\pi\pi\to K\bar{K}), \tag{3}$$

with

$$N^2=\frac{2}{m_N^2 p_L^2}\left(\frac{g^2}{4\pi}\right)\frac{(-t)}{(t-\mu^2)^2}\,\mathrm{e}^{2b(t-\mu^2)}\frac{M^2}{q_\pi}, \tag{4}$$

* The available data for $\pi N\to K\bar{K}N$ is for unpolarized initial and final nucleons.

where $m_N$, $\mu$, $M$ are the nucleon, pion, $K\bar{K}$ masses respectively; $(g^2/4\pi) = 14.6$, $p_L$ is the pion laboratory momentum and $q_\pi^2 = \frac{1}{4}M^2 - \mu^2$. The $\pi\pi \to K\bar{K}$ partial-wave amplitudes, $f_{12} \equiv f(\pi\pi \to K\bar{K})$, are normalized such that

$$f_{12} = \tfrac{1}{2}\sqrt{1-\eta^2}\, e^{i(\delta_1+\delta_2)}, \tag{5}$$

where assuming only two channels ($\pi\pi$, $K\bar{K}$ with $k = 1, 2$)

$$f_{kk} = \frac{1}{2i}(\eta\, e^{2i\delta_k} - 1). \tag{6}$$

For simplicity the labels, $I$, $L$ are omitted from $f_{ik}$, $\eta$, $\delta_i$. Due to Bose statistics, $\pi$ exchange can produce only even-$L$ isospin-zero, or odd-$L$ isospin-one, $K\bar{K}$ systems. Further only $I = 1$ states occur in $\pi^- p \to K^- K^0 p$ and only even-$L$ states occur in $\pi^- p \to K_S^0 K_S^0 n$. For $\pi^- p \to K^- K^+ n$ the isospin coefficients in eq. (3) are

$$C_L = \begin{cases} \sqrt{\frac{1}{3}}, & \text{for even } L, \\ \sqrt{\frac{1}{2}}, & \text{for odd } L. \end{cases} \tag{7}$$

For $\pi^- p \to K^- K^0 p$ we have $C_L = \sqrt{\frac{1}{2}}$, odd $L$ only, and for $\pi^- p \to K_S^0 K_S^0 n$ we have $C_L = \sqrt{\frac{1}{6}}$, even $L$ only.

For resonant $K\bar{K}$ production we factor the $\pi N \to K\bar{K}N$ amplitude into a term describing the production of the resonance, $A_\lambda(t)$, which contains the $t$ dependence, and a term describing the decay into the $K\bar{K}$ channel which contains the $M$ dependence. For example, the production of an $A_2$ ($I = 1$) resonance of helicity $\lambda$ is described by

$$D_\lambda^{(I=1)} = A_\lambda(t) B(M), \tag{8}$$

where we expect $A_\lambda(t)$ to be of the form appropriate to, say B, $\rho$, or f exchange (depending on $\lambda$ and the charge configuration), and the decay factor to have a Breit–Wigner resonance form

$$B(M) = \frac{M(m_R \Gamma_R^{K\bar{K}})^{1/2}}{m_R^2 - M^2 - i m_R \Gamma_R}, \tag{9}$$

where the widths, $\Gamma_R$, are $M$-dependent

$$\Gamma_R = \sum_i \Gamma_R^i(M) = \sum_i \Gamma_R^i(m_R) \left(\frac{q_i}{q_i^R}\right)^{2L+1} \frac{D_L(q_i^R R)}{D_L(q_i R)}, \tag{10}$$

where $q_i^R$ is the value of the decay channel momentum, $q_i$, at the resonant mass $m_R$. For a spin $L = 2$ resonance we take the barrier penetration factor to be $D_2(x) = x^4 + 3x^2 + 9$, and the radius to be $R = 3.5\ \text{GeV}^{-1}$.

## 3. $\bar{K}K^0$ production

Information on the $I=1$ $K^-K^0$ channel has come from the analysis of the 10 GeV/$c$ $\pi^-p\to K^-K^0p$ data obtained by the University of Geneva spectrometer group [4, 5]. The NPE amplitudes are dominant and are well determined by the data, but the UPE amplitudes are harder to extract unambiguously. In the original analyses [4, 5] some simplifying assumptions were made, and of the two solutions in the UPE sector, the one with the sizable S-wave structure in the 1300 MeV $K^-K^0$ mass region was favoured over a solution with $P_0 > S_0$. In view of the spectroscopic implications of this result, we repeat these analyses with a more complete amplitude determination in the UPE sector, paying particular attention to the $S_0-P_0$ ambiguity.

We first reanalyse the $\pi^-p\to K^-K^0p$ data in the $A_2$ mass region ($1.2<M<1.4$ GeV) as a function of $t$, the momentum transfer at the nucleon vertex. Here we perform a $t$-dependent analysis rather than fitting the moments in each $t$ bin independently. We parametrize the amplitudes in terms of Regge forms (as described in appendix A of ref. [15]), though any suitably flexible form would suffice. We describe $D_+$, $D_{2+}$ in terms of pomeron and f exchange, and $P_+$ by $\omega$ exchange using the forms given in ref. [16] with $x_p=0.2$, but with $\alpha_\omega \neq \alpha_f$. The UPE amplitudes $P_0$, $P_-$ are described by pion exchange (with absorptive corrections) and similarly $S_0$, $D_0$, $D_-$ by B (and Z*) exchange forms. We allow a free normalization constant for each amplitude, $L_{\lambda\pm}$, except for $P_-$ which we relate to $P_0$ by an absorbed pion exchange form. We fix the $D_0$, $D_-$ phase difference to be $\pi$, and we take the B and Z trajectories as in ref. [17]. In addition to the $t$-dependent) Regge phase, we include, as extra parameters, constant decay phases between the amplitude pairs $D_0-P_0$, $D_0-S_0$ and $D_+-P_+$.

Considering that $K^-K^0$ production in the $A_2$ mass region is dominated by NPE, in particular by $D_+$, it is natural to ask how well the data determine the $S_0$ and $P_0$ amplitudes; especially since these amplitudes only contribute to $\langle Y_J^M\rangle$ with $J\leq 3$, $M\leq 1$, and that these moments have, in addition, contributions from the other amplitudes. We therefore proceed in stages. First we describe the higher moments, $J=4$, $M\leq 4$ and $J=2$, 3 with $M\geq 2$, in terms of $P_+$, $D_+$, $D_{2+}$, $D_0$ and $D_-$. Fig. 1b shows that a satisfactory fit** is obtained. Next we predict the contribution of these amplitudes to the lower moments; the result is shown by the continuous curves in fig. 1a. We see, for example, that $\langle Y_3^0\rangle$ is well-described by $P_+$, $D_+$ interference indicating that either $P_0$ is negligible or $P_0$, $D_0$ are incoherent. The evidence for non-zero $S_0$ and/or $P_0$ is seen by the discrepancy between the curves and the observed $\langle Y_0^0\rangle$, $\langle Y_2^0\rangle$ and $\langle Y_2^1\rangle$ moments. A non-zero $S_0$ contributes to these three moments *via* $|S_0|^2$, $S_0D_0$ and $S_0D_-$ interference, respectively, whereas

* We use Z to denote $2^{--}$ quantum number exchange [17]. B and Z exchange contribute respectively to the flip and non-flip components of $S_0$ and $D_0$.

** We do not include in the fit the first $t$ bin, centred on $-t=0.09$ (GeV/$c$)$^2$, due to the large acceptance corrections in this $t$ interval.

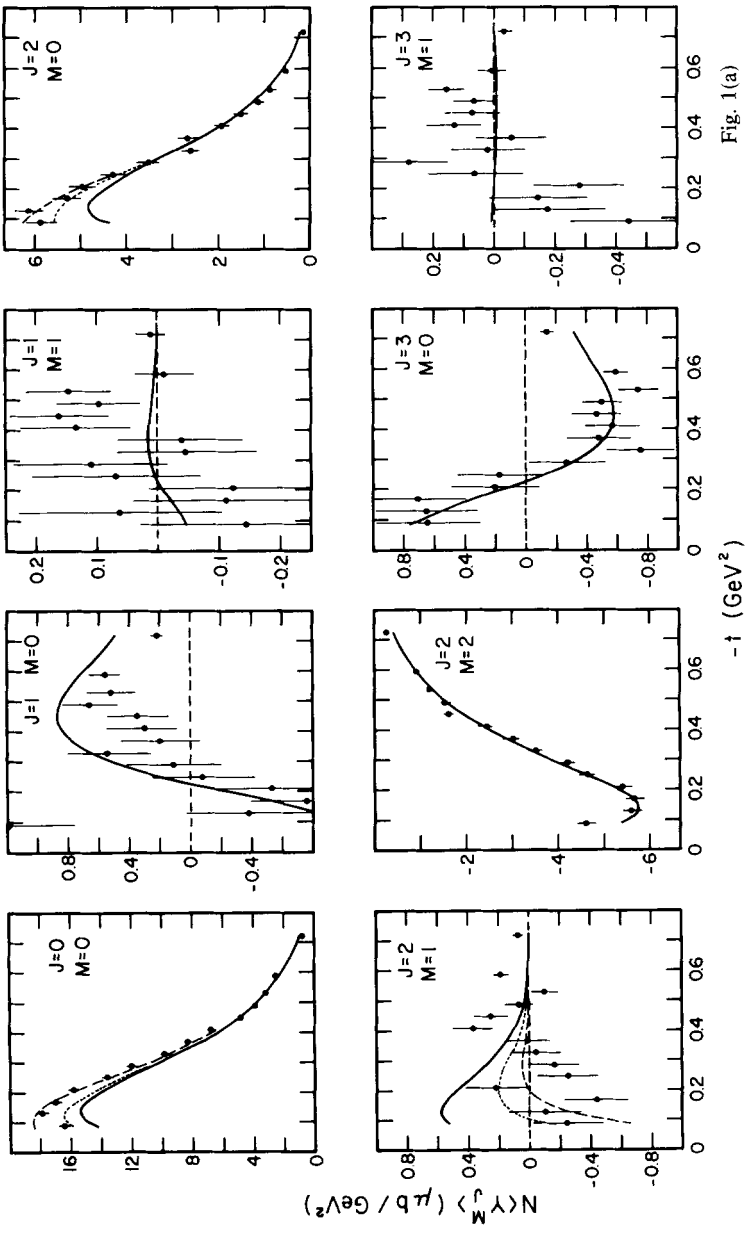


Fig. 1(a)

Fig. 1. The points represent the University of Geneva spectrometer data for $\pi^- p \to K^- K^0 p$ at 10 GeV/$c$ and are normalized so that $\sqrt{4\pi}\, N(Y_0^0) = d\sigma/dt$; they show the moments of the $K^-$ angular distribution in the $t$-channel helicity rest frame of the produced $K^- K^0$ system in the $A_2$ mass region, $1.2 < M < 1.4$ GeV. The continuous curves show a fit to the higher moments (b) and a prediction for the lower moments (a) in terms of just the D-wave and $P_+$ amplitudes. The dotted and dashed curves correspond respectively to the improvement obtained with the inclusion of $P_0$ and of $P_0$ together with $S_0$.

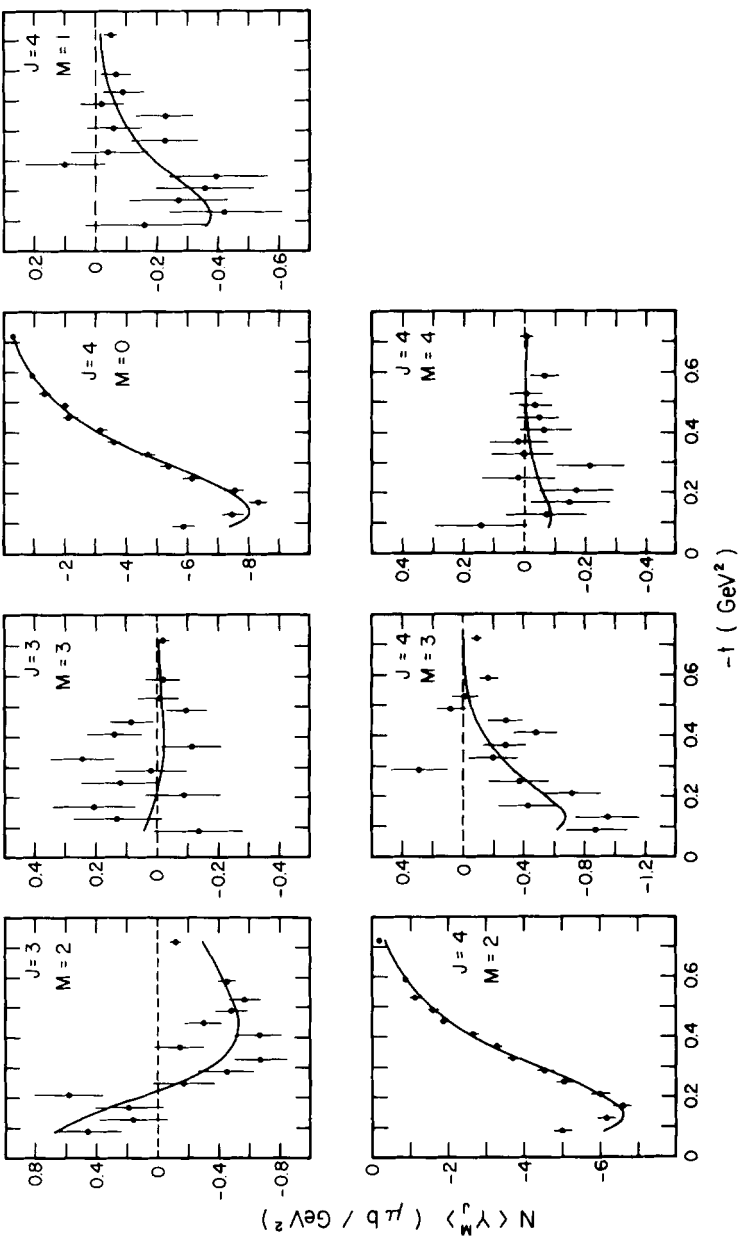


Fig. 1(b)

$P_0$ contributes *via* $|P_0|^2$, $|P_0|^2$ and $P_0P_-$, respectively. These alternative ways of removing the discrepancy are the origin of the $S_0/P_0$ wave ambiguity. Now we see that we need contributions which increase as $|t|$ decreases and this suggests a ($\pi$-exchange) $P_0$ contribution, rather than $S_0$. However, the inclusion of just $P_0$ would underfit $\langle Y_0^0 \rangle$ and overfit $\langle Y_2^0 \rangle$, and secondly it would have a magnitude in excess of that permitted by comparing $\pi^+ n \to K^- K^+ p$ and $\pi^- p \to K_S^0 K_S^0 n$ data. $P_0$ is forbidden in $K_S^0 K_S^0$ production and so $2N\langle Y_2^0 \rangle$ for this reaction should equal $N\langle Y_2^0 \rangle - 0.894|P_0|^2$ for $\pi^+ n \to K^- K^+ p$. The 6 GeV/$c$ data are compared in fig. 2. The line is obtained from the $K^- K^+$ data assuming the mass dependence of $P_0$ is given by the tail of the $\rho$ resonance decaying into the $K\bar{K}$ channel*. Increasing $P_0$

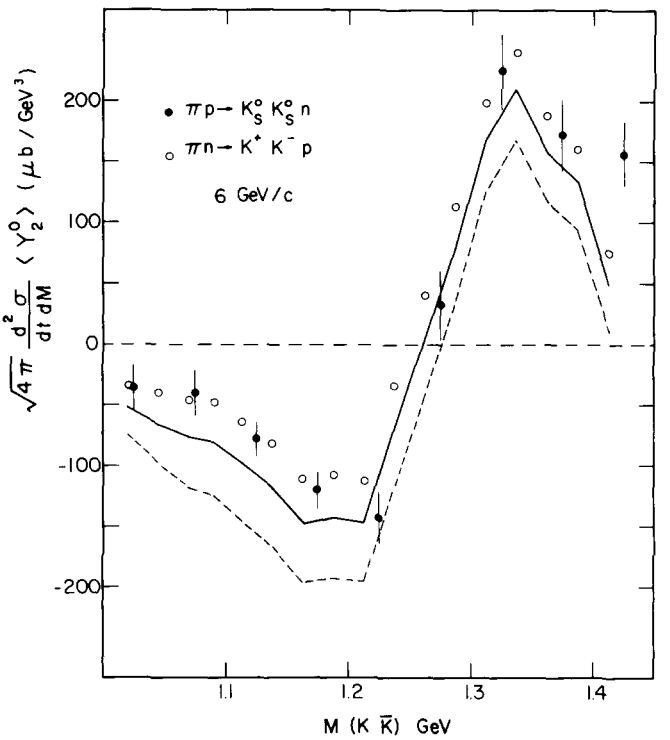


Fig. 2. The solid points, taken from ref. [14], are obtained from the $\langle Y_2^0 \rangle$ moment for $\pi^- p \to K_S^0 K_S^0 n$ for $-t < 0.2$ GeV$^2$ (ref. [3]) by normalizing to $\pi^+ n \to K^- K^+ p$ data for $-t < 0.08$ GeV$^2$. The continuous line is the prediction for the $K_S^0 K_S^0$ points obtained by subtracting the $P_0$ contribution from the $\pi^+ n \to K^- K^+ p \langle Y_2^0 \rangle$ moment (the open points). The dashed line corresponds to the $P_0$ which would be needed to describe the $K^- K^0$ data if the $S_0$ contribution was omitted.

* We take the form used in ref. [14] (see footnote 26), but do not use SU(3) for the normalisation. Rather we normalize the $\rho$ tail by requiring that $\rho$-f interference describes the $\langle Y_3^0 \rangle$ moments for the $K^- K^+$ production reactions[1].

destroys the agreement between the line and the $K_S^0K_S^0$ data. We take this to be the maximum $P_0$ allowed.

Including this $P_0$ contribution in $K^-K^0$ production leads, after allowing for the different beam energies and $t$ values, to the description given by the dotted lines on fig. 1a. The residual discrepancy is attributed to $S_0$. However it does not have the $t$ dependence expected of B exchange and it is necessary to include a Z-exchange contribution to $S_0$. The best fit to the moments is shown by the dashed curves in fig. 1a and the $t$ dependence of the $K^-K^0$ production amplitudes is shown in fig. 3. We note the dominance of $D_+$, the 'cross-over' zero in $P_+$; and that $D_0$ is compatible with the values obtained from charge-exchange $A_2^0$ production [18], see ref. [5].

Now we need to consider the $M_{KK}$ dependence of the $K^-K^0$ amplitudes. We repeat the analysis described in ref. [4], except that we fit all non-zero moments and include $P_-$, $D_-$, $D_{2+}$ effects. We fix $P_0$ (and $P_-$) to correspond to the $\rho$ resonance tail form described above, and we take $D_{2+} = 0.1D_+$ as found in the $A_2$ region. The results for $|S_0|$ are shown in fig. 4, together with the input value of $|P_0|$.

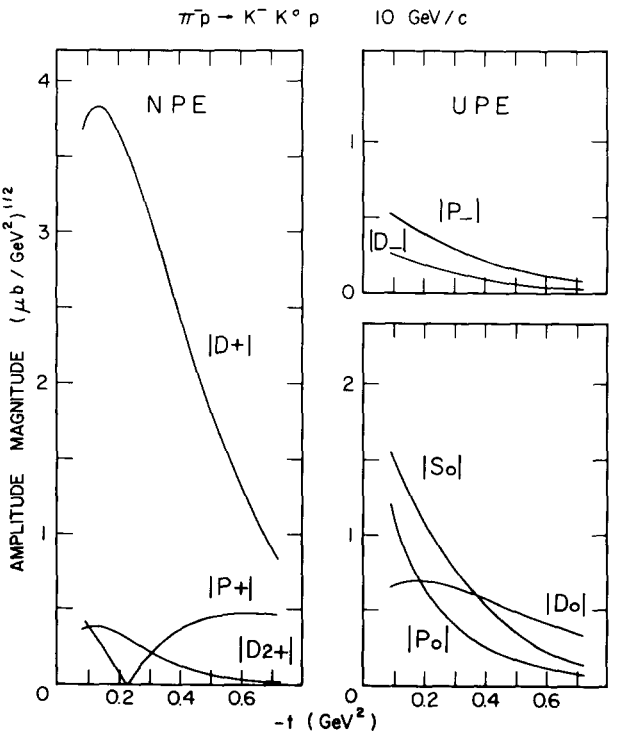


Fig. 3. The 10 GeV/$c$ $\pi^-p \to K^-K^0p$ amplitude magnitudes in the $A_2$ mass region, $1.2 < M < 1.4$ GeV, normalized so that their square gives the contribution to $d\sigma/dt$.

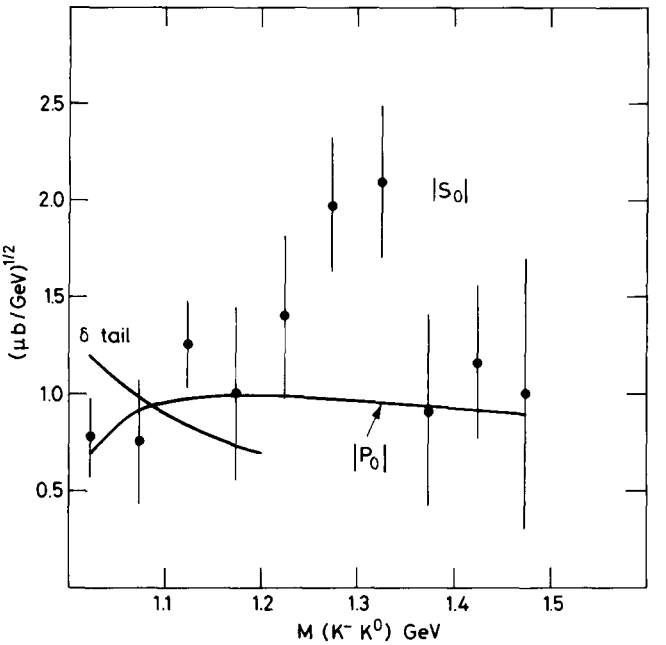


Fig. 4. The mass dependence of $|S_0|$ obtained from the 10 GeV/$c$ $\pi^- p \to K^- K^0 p$ data for the $t$ interval $0.07 < -t < 1$ GeV$^2$, shown together with the input $P_0$. The amplitudes are normalized so that their moduli squared give the contribution to $d\sigma/dM$. The $\delta$ tail prediction is that of subsect. 5.1.

## 4. D-wave $K^+K^-$ production

The data [1] for the reactions

$$\pi^- p \to K^- K^+ n, \tag{11}$$

$$\pi^+ n \to K^+ K^- p, \tag{12}$$

allow a study of $I = 0$, 1 $K\bar{K}$ states. In contrast to $K^- K^0$ production, only $I = 1$ exchange contributes to these reactions and UPE dominates in the forward direction. First we use the observed $J = 4$ moments of the $K\bar{K}$ distribution to determine D-wave production in the f and $A_2$ mass region.

### *4.1. $f \to K\bar{K}$ branching ratio*

We analyse the sum of the observed $\langle Y_4^M \rangle$ moments for the two reactions, as a function of $t$, in terms of the amplitudes $D_0$, $D_\pm$ describing $I = 0$, and $D_0$ describing $I = 1$, $K\bar{K}$ production. We use the data in the mass bin $1.25 < M < 1.3$ GeV to determine the $f \to K\bar{K}$ branching ratio. We take the pion-exchange form of eqs. (3)

and (4) for the dominant f-production amplitude $D_0^{I=0}$. We integrate $M^2|f_L^I|^2/q_\pi$ over the mass bin using

$$f_2^0 = \frac{m_f\sqrt{\Gamma_f^{\pi\pi}\Gamma_f^{K\bar{K}}}}{m_f^2 - M^2 - im_f\Gamma_f}, \tag{13}$$

where $\Gamma_f(M)$, $\Gamma_f^i(M)$ are given by eq. (10), $m_f = 1.275$ GeV and $\Gamma_f(m_f) = 0.180$ GeV. The parameter to be determined by the data is the product of the $f \to \pi\pi$ and $f \to K\bar{K}$ branching ratios,

$$x = \Gamma_f^{\pi\pi}\Gamma_f^{K\bar{K}}/\Gamma_f^2|_{M=m_f}.$$

The other $I = 0$ amplitudes are parametrized by conventional forms

$$D_- = -c_-\frac{\mu^2 - t}{\sqrt{-t}}D_0^{I=0},$$

$$D_+ = e^{-b_+ t}D_-.$$

We fix $|D_0^{I=1}|$ in terms of the known behaviour [18] of UPE $A_2$ production as found in the charge-exchange process $\pi^- p \to A_2^0 n$ and in the $K^-K^0$ analysis. To correct to the 1.25–1.3 GeV mass interval we integrate over an $A_2$ resonance form with $m_A = 1.31$ GeV, $\Gamma_A(m_A) = 102$ MeV and $A_2 \to K\bar{K}$ branching ratio of 4.7%. The best fit to the $J = 4$, $M \leq 2$ moments for $-t < 0.4$ GeV$^2$ is shown in fig. 5, and the amplitudes are shown in fig. 6. The corresponding parameter values are

$$x = 0.019 \pm 0.003, \qquad c_- = 0.6 \pm 0.1 \text{ GeV}^{-1},$$
$$b_\pi = 3.0 \pm 0.7 \text{ GeV}^{-2}, \qquad b_+ = 3.1 \pm 0.9 \text{ GeV}^{-2}. \tag{14}$$

The value of $b_\pi$ is typical of one-pion exchange, and taking the $f \to \pi\pi$ branching ratio to be 81%, the value found for $x$ implies

$$\text{B.R.}(f \to K\bar{K}) = (2.4 \pm 0.4)\%. \tag{15}$$

This result is in agreement with other independent determinations [2, 11, 19], but is smaller than the ANL value [1] of $(3.8 \pm 0.7)\%$ obtained from the same data. The ANL determination [1] compares $N\langle Y_4^0\rangle$ of $K^+K^-$ and $\pi^+\pi^-$ production data over the interval $0.08 < -t < 0.4$ GeV$^2$. There are two reasons for the discrepancy between these results. First, we find $D_0^{I=0}$, $D_\pm$ have a sizable effect, particularly at the larger $t$ values. Second, we renormalize the ANL $\pi^+\pi^-$ production data so that they extrapolate to the $\pi$ exchange pole prediction in the $\rho$ mass region*. If we were to omit this renormalization factor for the $\pi^+\pi^-$ data our result for the branching ratio would be increased by a factor of 1.25.

* The ANL group found [20] that the $\rho$ production amplitudes, extracted from their $\pi^+\pi^-$ data, fell below the $\pi$ exchange prediction by a factor 3.2/3.6.

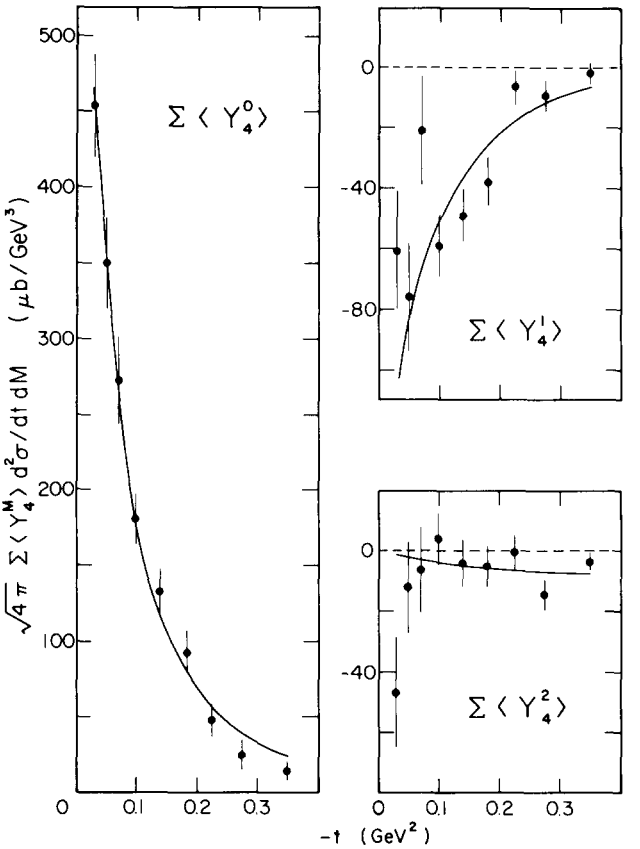


Fig. 5. The fit to the sum of the $J=4$ moments of the 6 GeV/$c$ data [1] for reactions (11) and (12), for $1.25 < M(K^-K^+) < 1.3$ GeV.

### 4.2. $f,f'$ and $A_2^0$ interference in $K^+K^-$ production

The $\langle Y_4^0 \rangle$ moments of the ANL data for reactions (11) and (12) show interesting structure, as a function of $M$, which has been interpreted [1, 21] in terms of interference between f, f' and $A_2$ resonance production. The sum and difference of these moments for processes (11) and (12) may be symbolically expressed in terms of these resonance production amplitudes:

$$\Sigma\langle Y_4^0 \rangle \sim |f|^2 + |f'|^2 + 2\,\mathrm{Re}(ff'^*) + |A_2|^2\,,$$

$$\Delta\langle Y_4^0 \rangle \sim \mathrm{Re}\,(fA_2^*) + \mathrm{Re}\,(f'A_2^*)\,.$$

The $\Sigma\langle Y_4^0 \rangle$ data shows clear evidence of the f-f' interference effect and allow a determination of the $f' \to \pi\pi$ branching ratio. On the other hand, the data for

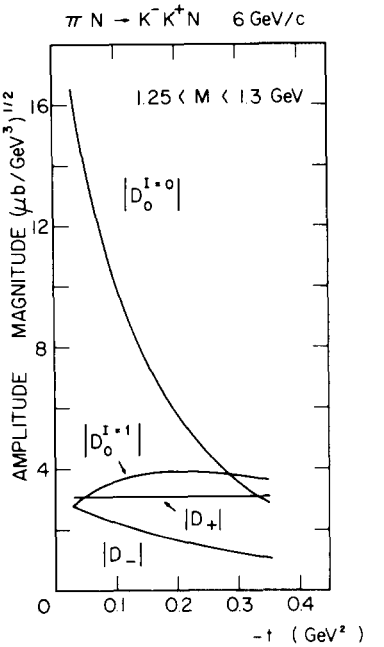


Fig. 6. The $K^-K^+$ production amplitudes resulting from the fit shown in fig. 5.

$\Delta\langle Y_4^0\rangle$ show little evidence for f-$A_2$ interference, but do show structure (at least for the $t$ band $0.08 < -t < 0.2$ GeV$^2$) which may be attributed to f'-$A_2$ interference. This is surprising, since we would have anticipated f-$A_2$ interference to dominate the f'-$A_2$ effect, and implies that f' and $A_2$ production should have important contributions from, respectively, the $I=0$ and 1 non-flip amplitudes* $D_{++;\lambda=0}$ (recall that f production proceeds dominantly *via* the pion-exchange amplitude, $D_{+-;\lambda=0}$). On the other hand, we have noted that the general properties of $A_2^0$ production, and in particular the $t$ dependence [18], are consistent with the dominance of the flip (B-exchange) amplitude, rather than the non-flip amplitude, for $-t < 0.15$ GeV$^2$. However, this is not a firm conclusion and so we allow the $\Delta\langle Y_4^0\rangle$ data to decide the flip, non-flip character $D_0^{I=1}$.

In our study of these interference effects we analyse the data for the sum and difference of the $\langle Y_4^M\rangle$ moments with $M \leq 2$ as a function of $M(K\bar{K})$. We parametrize the amplitudes as a function of $t$ and $M(K\bar{K})$ (see eqs. (8)–(10)), and fit to the data in the three available $t$ intervals (bounded by $t_{\min}$, $-0.08$, $-0.2$ and $-0.4$ GeV$^2$) simultaneously. In this amplitude analysis we include both $D_{+\pm;\lambda=0}$ for both $I=0$ and $I=1$ $K^+K^-$ production. The observed moments indicate that,

* We may assume $\lambda = 0$ since there is no evidence of f'-$A_2$ interference in $\Delta\langle Y_4^M\rangle$ with $M \neq 0$. The notation $D_{\lambda N\lambda N';\lambda}$ is that of eq. (2).

for $-t<0.4\ \mathrm{GeV}^2$, the $\lambda \neq 0$ amplitudes are small; and so we retain only contributions from $D_{+-;-}$ (absorbed $\pi$ exchange) and $D_+$ ($A_2$ exchange) for $I=0$ $K^+K^-$ production. We assume that $\lambda = 0$ f production is dominated by $\pi$ exchange, and we include a small contribution [5] from the tail of the $g$ resonance, $F_{+-;\lambda=0}$.

For $A_2$ production we can factor the amplitudes as in eq. (8)

$$D_\lambda^{I=1} = A_\lambda^{A_2}(t) B^{A_2}(M), \tag{16}$$

but for $I=0$ $K^+K^-$ production we must extend the formalism to include both the f and f′ resonances. We use the mass matrix approach to describe these overlapping resonances. For $\pi$ exchange the structure of the $I=0$ D-wave amplitude is given by eqs. (3) and (4) with

$$f(\pi\pi \to K\bar{K}) = \sum_{R,R'} g_R^{\pi\pi} [P(M)]_{R,R'} g_{R'}^{K\bar{K}}, \tag{17}$$

where the summations R and R′ are both over the f and f′ resonances, and where $(g_R^i)^2 \equiv m_R \Gamma_R^i$ are functions of $M$, the $K\bar{K}$ mass, as given by eq. (10)*. The mass propagator is given by

$$[P(M)]^{-1} = \begin{bmatrix} m_f^2 - M^2 - i m_f \Gamma_f & \delta \\ \delta & m_{f'}^2 - M^2 - i m_{f'} \Gamma_{f'} \end{bmatrix}, \tag{18}$$

with

$$\delta = \Delta - i g_f^{\pi\pi} g_f^{K\bar{K}} - i g_{f'}^{\pi\pi} g_{f'}^{K\bar{K}}, \tag{19}$$

where $\Delta$ is the mass mixing parameter.

We base the parametrization of the $t$ dependence of the production amplitudes on Regge exchange forms. Even with very flexible parametrizations** we are unable to produce a sizable f′-$A_2$ interference effect in $\Delta\langle Y_4^0\rangle$ and satisfactorily fit the data. The reason is clear: the f′-$A_2$ interference occurs *via*

$$\mathrm{Re}\,(D_{+-}^{I=0} D_{+-}^{I=1*} + D_{++}^{I=0} D_{++}^{I=1*})_{\lambda=0}. \tag{20}$$

The first term arises from $\pi$-B exchange and is limited in the f′ mass region by the absence of significant structure in the data in the f-$A_2$ mass region where this term would be much larger. Also from our knowledge of $A_2^0$ production [5, 18] an upper bound exists for $D_{++}^{I=1}$, and to produce appreciable f′-$A_2$ interference requires non-flip f′ production to be so large as to be in contradiction with the $\Sigma\langle Y_4^0\rangle$ data.

In the original ANL analysis [1, 21] of the $\langle Y_4^0\rangle$ moments alone, they did not consider the individual production amplitudes***; if, as the data implies, f′-$A_2$ interference occurs mainly *via* $\lambda = 0$ amplitudes, then it can be seen that their results violate the Schwartz-type inequalities $|f'| \cdot |A_2| \geq \mathrm{Re}\,(f' A_2^*)$.

* For the mass dependence of the total widths, $\Gamma_R$, the decay channels other than $\pi\pi$, $K\bar{K}$ are collectively associated with the momentum of the $\eta\eta$ channel.

** For example, allowing the amplitudes to have free ($t$-independent) phases, in addition to their Regge phase.

*** Also they did not attempt a simultaneous description of the data in the three available $t$ intervals.

Although the fit does not show significant interference structure in $\Delta\langle Y_4^0\rangle$, it does reproduce the observed structure in $\Sigma\langle Y_4^0\rangle$ through f-f' interference in the dominant $\pi$-exchange amplitude, $D_0$. The observed interference structure selects the negative sign of the coupling ratio $g_f^{\pi\pi}g_f^{K\bar{K}}/g_{f'}^{\pi\pi}g_{f'}^{K\bar{K}}$, corresponding to an f-f' mixing angle less than the magic angle [21]. The resulting description of the $\Sigma\langle Y_4^0\rangle$ data is shown in fig. 7 for the two extreme values of the $f' \to \pi\pi$ branching ratio, namely 0.5% and 1%. Here we have fixed the $f \to \pi\pi$, $f \to K\bar{K}$ and $f' \to K\bar{K}$ branching ratios to be 81%, 2.4% and 70% respectively, and set $m_{f'} = 1.515$ GeV, $\Gamma_{f'} = 60$ MeV and $\Delta = 0$. The fit is not sensitive to small variations of the latter three parameters.

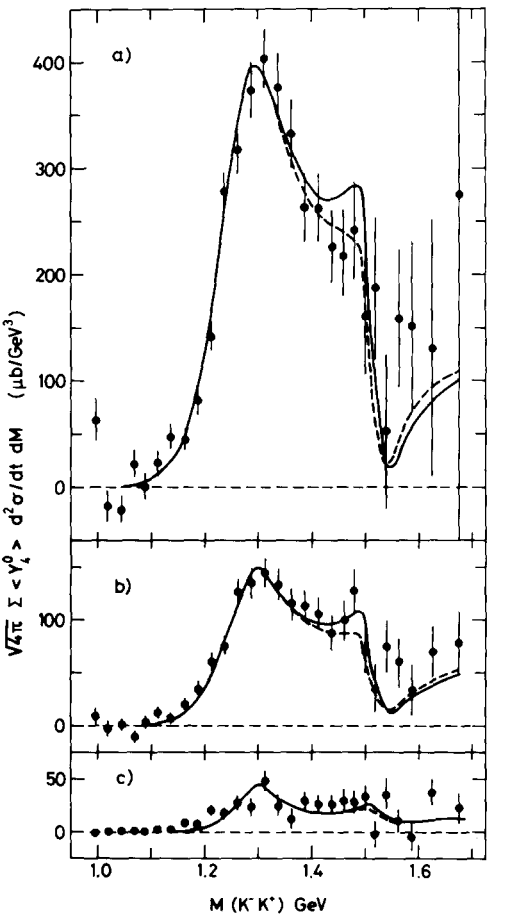


Fig. 7. The sum of the $J = 4$, $M = 0$ moments for the two $K^-K^+$ production reactions (eqs. (11) and (12)) at 6 GeV/$c$, for three $t$ intervals: (a) $-t < 0.08$, (b) $0.08 < -t < 0.2$, (c) $0.2 < -t < 0.4$ GeV$^2$. The data are from ref. [1]. The continuous and dashed curves correspond to an f, f', $A_2$ description of the data with an $f' \to \pi\pi$ branching ratio of 1% and 0.5% respectively.

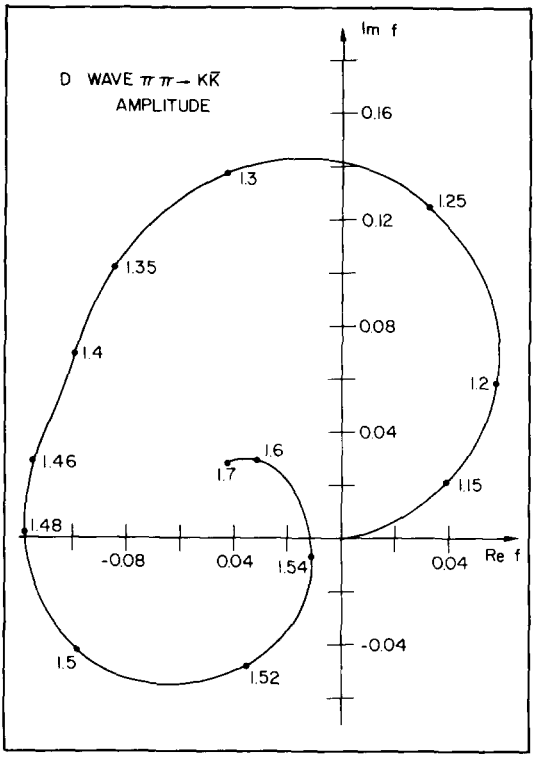


Fig. 8. The D-wave $\pi\pi \to K\bar{K}$ amplitude showing the f and f' resonant structure. The numbers on the curve are the c.m. energy in GeV.

The $f' \to \pi\pi$ branching ratio result of $0.75 \pm 0.25\%$ is consistent with the upper limit of 0.9% obtained from $K_S^0 K_S^0$ production by Beusch et al. [22]. The discrepancy with the ANL determination [1] of $(1.2 \pm 0.4)\%$ arises simply from our different input values of the $f \to K\bar{K}$ branching ratio (see subsect. 4.1). In fig. 8 we show the Argand plot for the $L = 2$, $I = 0$ $f(\pi\pi \to K\bar{K})$ amplitude, as given by eq. (17).

## 5. $\pi\pi \to K\bar{K}$ partial-wave analysis

The partial-wave analysis of $K\bar{K}$ production data is more complicated than that of $\pi\pi$ production. States of both even/odd $G$ parity can be produced *via* odd/even $G$-parity exchange (for example $\pi$/B exchange). Thus for each partial wave both $I = 0$ and $I = 1$ $K\bar{K}$ systems can be produced; states with $I + L$ even (for example S*, f, f') by $\pi$ exchange and states with $I + L$ odd (for example, $\delta$, $A_2$) by B exchange. The latter possibility is forbidden in $\pi N \to \pi\pi N$ processes.

As noted in sect. 4, in order to help unravel the $I=0$ and $I=1$ production amplitudes the ANL group [1] studied both

$$\pi^- p \to K^- K^+ n,$$

$$\pi^+ n \to K^- K^+ p,$$

for which the $K\bar{K}$ production amplitudes are of the form $(L^{I=0} \pm L^{I=1})$ respectively. However, even with perfect data on both processes further assumptions are necessary to carry out a $\pi\pi \to K\bar{K}$ partial-wave analysis.

At small $t$ only the $\langle Y_J^0 \rangle$ moments of the $K\bar{K}$ angular distribution are found to be appreciable, as anticipated from $\pi$-exchange dominance. It therefore appears reasonable to follow the procedure adopted for analysing $\pi\pi$ production [23], and to assume that only the nucleon flip amplitudes are non-zero. We will return to this point later, but for the moment we suppose it is true. The sum and the difference of the even-$J$ moments for the two reactions can then be expressed in terms of bilinear combinations of $(\lambda = 0)$ amplitudes containing only terms of the form

$$\begin{aligned} \Sigma\langle Y_J^0 \rangle: &\quad \mathrm{Re}(L^{\pi} L'^{\pi *}), \quad \mathrm{Re}\,(L^{\mathrm{B}} L'^{\mathrm{B}*}), \\ \Delta\langle Y_J^0 \rangle: &\quad \mathrm{Re}(L^{\pi} L'^{\mathrm{B}*}), \end{aligned} \tag{21}$$

and *vice versa* for the odd-$J$ moments. The amplitude superscript, which denotes the expected exchange mechanism, distinguishes between $I=0$ and $I=1$ $K\bar{K}$ production. The $\pi$-exchange amplitudes, $L^{\pi}$, produce $K\bar{K}$ systems with $I+L$ even, whereas the odd $I+L$ $K\bar{K}$ states may be associated with B exchange. In the actual analyses the $M \neq 0$ moments are included to take account of the small contributions from the $L_{\pm}$ amplitudes.

The ANL group [14] have used their data for the $t$ interval $-t < 0.08\ \mathrm{GeV}^2$ to determine the amplitudes $L^{\pi}$ and $L^{\mathrm{B}}$ in the mass region from the $K\bar{K}$ threshold to 1.6 GeV. To distinguish between the possible Barrelet-related solutions, they consider other information. In particular by comparing with $K_S^0 K_S^0$ production data [3] to limit the size of $P^{\pi}$, and by studying the $t$ dependence of the amplitudes, they clearly select the physical solution to be one which contains an $S^{\pi}$ enhancement around 1300 MeV. Moreover by requiring $P^{\pi}$ to be consistent with the behaviour expected for the high-mass tail of the $\rho$ meson they resolve the remaining phase ambiguity in favour of the solution in which the phase of $S^{\pi}$ advances slowly in the 1300 MeV mass region. The resonant D-wave is taken to be the reference amplitude and is assumed to be dominated by the $\pi$-exchange contribution to f and f' production.

We have repeated the above partial-wave analysis with the same assumptions, but using the sum and the difference of the moments for the two reactions rather than considering the reactions individually. From the Barrelet-related solutions we are led to select essentially the same solution.

To a very good approximation we also obtain the same results for the $L^{\pi}$ amplitudes by analysing only $\Sigma\langle Y_J^M \rangle$ for even $J$ and $\Delta\langle Y_J^M \rangle$ for odd $J$, in terms of just

the $\pi$-exchange amplitudes (together with small contributions from $L_{\pm}$). Again we use the data [1] for $-t<0.08\ \mathrm{GeV}^2$. We relate the amplitudes to $f_L(\pi\pi\to K\bar{K})$ using eqs. (3) and (4). The magnitudes of the partial-wave amplitudes, $f_L$, are shown in fig. 9. The neglect of B exchange is found not to distort the analysis. For example, although the $\Delta\langle Y_0^0\rangle$ moment shows that $S^{\mathrm{B}}$ is non-zero, we have $|S^{\mathrm{B}}|^2 \ll |S^{\pi}|^2$ for $-t<0.08\ \mathrm{GeV}^2$.

For the above analysis we required the value of the slope parameter, $b$, of eq. (4). Some idea of the value of $b$ is obtained by fitting the observed $J=0$, 4 moments [1, 24] to the form

$$\Sigma\langle Y_J^0\rangle = \frac{-At}{(t-\mu^2)^2}\,\mathrm{e}^{2b(t-\mu^2)}, \tag{22}$$

for $-t<0.4\ \mathrm{GeV}^2$. The results are shown in fig. 10. For $\Sigma\langle Y_4^0\rangle$ (dominated by $D^{\pi}$ at small $t$) and for $\Sigma\langle Y_0^0\rangle$ in the S* region (dominated by $S^{\pi}$ at small $t$) the values of $b$ are typical of pion exchange. However the results for $\Sigma\langle Y_0^0\rangle$ suggest a shallower slope for the S-wave in the 1300 MeV region. In the detailed amplitude analysis we found that the pion-exchange contribution has a slope $b_{\pi}\simeq 3\ \mathrm{GeV}^{-2}$ and so we used this value for $P^{\pi}$, $D^{\pi}$ and $F^{\pi}$. However we allowed the slope of

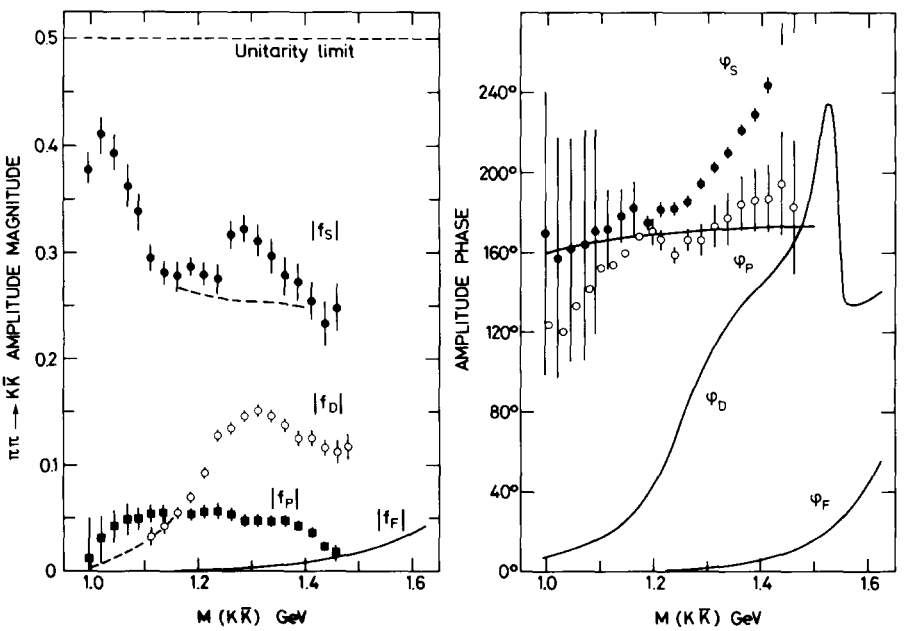


Fig. 9. The magnitude and phase of the $\pi\pi\to K\bar{K}$ amplitudes determined from the 6 GeV/$c$ ANL $K^-K^+$ production data [1]. The reference phase, $\phi_{\mathrm{D}}$, is taken from fig. 8. The $L=3$ amplitude corresponds to the tail of the g resonance [5]. For clarity the large errors for $\phi_{\mathrm{P}}$ near threshold are not shown. The results for $\phi_{\mathrm{P}}$ are compared with the $\rho$ tail phase.

the S-wave to have the mass dependence necessary to account for the behaviour shown in fig. 10, even though this only gives a small effect on the partial-wave amplitude (fig. 9) resulting from the $-t<0.08\ \mathrm{GeV}^2$ data. We return to this anomalous S-wave behaviour in the 1300 MeV mass region in a moment.

To summarize at this stage, we see that the S-wave is important throughout the mass region, with a threshold S* behaviour and structure at 1300 MeV. Provided we assume the dominance of nucleon-flip production amplitudes (for $-t<0.08\ \mathrm{GeV}^2$), this structure is to be attributed to the $I=0\ K\bar{K}$ S-wave, $S^{\pi}$. The amplitudes $P^{\pi}$ and $D^{\pi}$ are consistent with $\rho$ and f, f' resonant forms respectively. We now study the crucial $K\bar{K}$ S-wave in more detail, first in the mass region just above the $K\bar{K}$ threshold, the S* region, and then in the 1300 MeV region.

### 5.1. The $S^*$ region

To illuminate the S-wave production mechanism we analyse the sum and the difference of the moments, $\langle Y_J^0 \rangle$ with $J \leq 2$, of reactions (11) and (12) as functions of $t$ and $M$ in the threshold region, $M<1.1$ GeV. We input $P^{\pi}$, $P^{B}$, $D^{\pi}$, $D^{B}$ amplitudes in terms of $\rho$, $\phi$, f, $A_2$ Breit-Wigner forms. We parametrize the larger

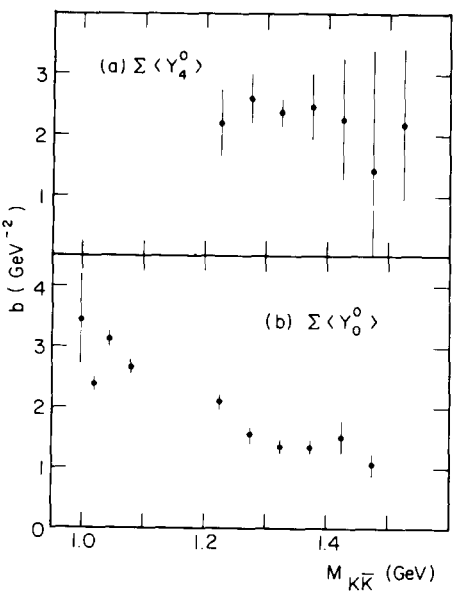


Fig. 10. The slopes, as defined by eq. (22), determined from the (a) $\langle Y_4^0 \rangle$ and (b) $\langle Y_0^0 \rangle$ moments for the sum of the two $K^-K^+$ production reactions at 6 GeV/$c$, for $-t<0.4\ \mathrm{GeV}^2$. The effect of $\phi$ production is seen in the slope found at 1.02 GeV.

amplitudes, $S^{\pi}$ and $S^{B}$, in terms of S* and $\delta$ resonant forms taking explicit account of the $K^+K^-$ and $K^0\bar{K}^0$ mass difference*. For example, the S-wave $\pi\pi \to K^-K^+$ partial-wave amplitude is of the form

$$f(\pi\pi \to K^-K^+) = \sqrt{\tfrac{1}{2}}(q_\pi q_c)^{1/2} g_{S^*}^{\pi\pi} g_{S^*}^{K\bar{K}} [m_\delta^2 - M^2 - iq_\eta (g_\delta^{\pi\eta})^2 - iq_0 (g_\delta^{K\bar{K}})^2]/\Delta ,$$

with

$$\Delta = [m_{S^*}^2 - M^2 - iq_\pi (g_{S^*}^{\pi\pi})^2 - i\bar{q}(g_{S^*}^{K\bar{K}})^2][m_\delta^2 - M^2 - iq_\eta (g_\delta^{\pi\eta})^2 - i\bar{q}(g_\delta^{K\bar{K}})^2]$$
$$+ [\tfrac{1}{2}(q_c - q_0) g_{S^*}^{K\bar{K}} g_\delta^{K\bar{K}}]^2 ,$$

where $q_c$, $q_0$, $q_\pi$, $q_\eta$ are the c.m. momenta in the $K^-K^+$, $K^0\bar{K}^0$, $\pi\pi$, $\pi\eta$ channels respectively, and $\bar{q} = \frac{1}{2}(q_0 + q_c)$. We take the $\delta$ parameters to be $m_\delta = 970$ MeV, $\Gamma_\delta^{\pi\eta} = 50$ MeV and $(g_\delta^{K\bar{K}})^2 = \frac{3}{2}(g_\delta^{\pi\eta})^2$. For the S* we input $m_{S^*} = 980$ MeV but let $g_{S^*}^{K\bar{K}}$ and $g_{S^*}^{\pi\pi}$ be free parameters.

We assume that $t$ dependence of the amplitudes is given by $\pi$ and B Regge exchange, with $\alpha_\pi = 0.83\ (t - \mu^2)$, $\alpha_B = -0.25 + 0.83t$, with $t$ in GeV$^2$, but we allow a free normalisation parameter for $S^B$ (and for $P^B$). The $S^{\pi}$–$S^{B}$ relative phase is fixed; the production phases by the $\pi$ and B exchange forms and the decay phases by the S* and $\delta$ resonant forms, with an additional background phase of about 85° for $S^{\pi}$, coming from the $\pi\pi \to \pi\pi$ channel [8].

This simple $\pi$-B exchange parametrization is able to describe all the features of the data** in the threshold mass region, $M < 1.1$ GeV, The $t$ dependence of the amplitudes at $M = 1.02$ GeV is shown in fig. 11. We do not quote the S* couplings since they are dependent on the choice of the S* mass; the $K^+K^-$ production data alone are insufficient to determine the mass and the partial widths of the S*. The mass dependence of the $I = 1$ amplitude, $S^B$, is compared with the prediction of the $K^-K^0$ data in fig. 4, after integrating $S^B$ over the $t$ interval $0.07 < -t < 1$ GeV$^2$ and allowing for the increase in $p_L$ to 10 GeV/$c$.

### 5.2. *The S-wave in the 1300 MeV region*

The S-wave $K\bar{K}$ mass spectrum obtained from $K^+K^-$ (and from $K_S^0K_S^0$) production data shows a significant bump at 1300 MeV. This structure was originally assigned [3] to the $I = 1$ $K\bar{K}$ channel, but the above analysis and that of ref. [14] attribute it to the $I = 0$ channel. In fact the mass dependence of $|f_S|$, fig. 9, is reminiscent of an $I = 0$ S-wave resonance on a smoothly falling S* background; however the phase of $f_S$ does not match this description. Also we remarked that

* The formalism is very similar to that used [25] to allow for the $K^-p$, $\bar{K}^0n$ mass difference in low-energy $K^-p$ scattering.

** The agreement of $|S^B|$ from the ANL data with the $\delta$ tail contribution has also been noted in ref. [26].

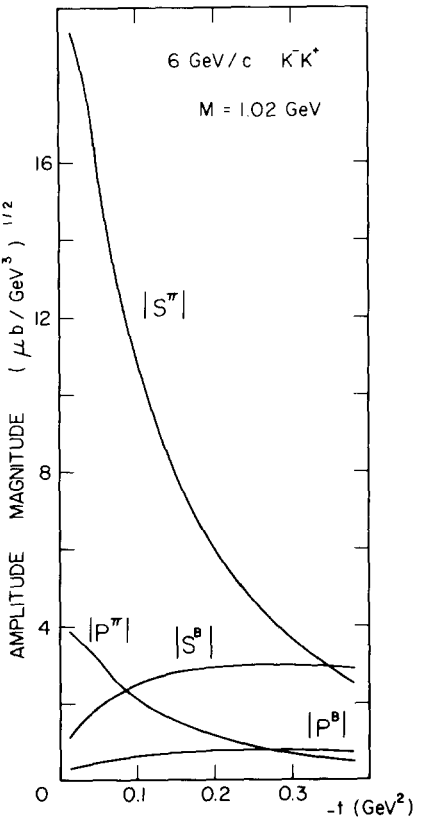


Fig. 11. The $t$ dependence of the 6 GeV/$c$ $K^-K^+$ production amplitudes at $M(K^-K^+) = 1.02$ GeV.

the $t$ dependence of the S-wave suggests sizable contributions other than $\pi$ exchange in this mass interval (see also the $K_S^0K_S^0$ data of ref. [3]). This effect can alternatively be seen in fig. 12 where we plot the S-wave contribution, $|S^{I=0}|^2 + |S^{I=1}|^2$, isolated from $K^+K^-$ data, using $\Sigma\langle Y_4^{0,2}\rangle$ and $\Sigma\langle Y_2^2\rangle$ to estimate the D-wave contribution to $\Sigma\langle Y_0^0\rangle$, and assuming the P-wave contribution is negligible. We also plot $-\Delta\langle Y_0^0\rangle$ since the higher moments indicate that this is dominantly due to $I = 0$, 1 S-wave interference. There is a striking difference between the S* region, where we found the $\pi$, B exchange description satisfactory, and the 1300 MeV region.

Also in sect. 3, we saw $K^-K^0$ production provided independent evidence of non-pion-exchange S-wave contributions in the 1300 MeV region. Moreover the $t$ dependence indicated that the non-flip amplitude, which we denote by $S^Z$, is more important than the flip amplitude, $S^B$, at small $t$.

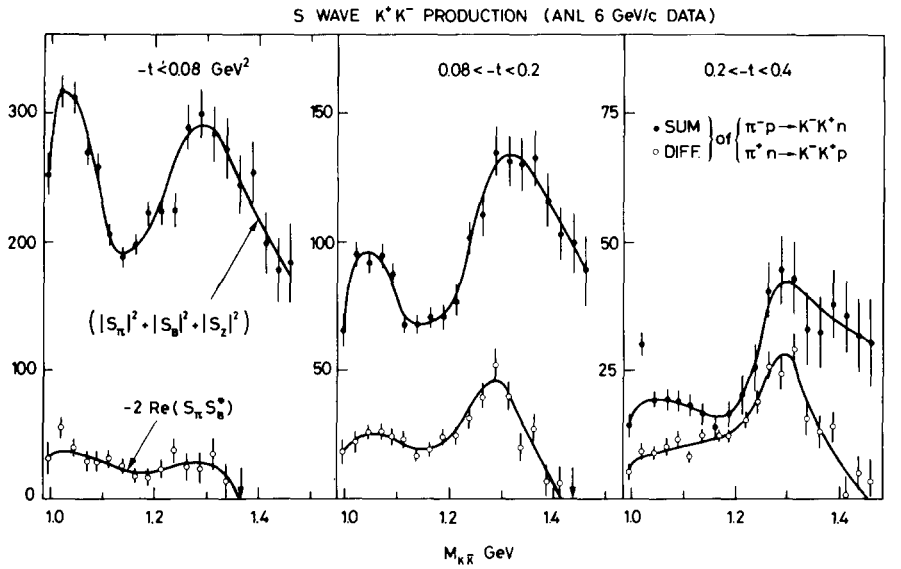


Fig. 12. The S-wave $K^-K^+$ contribution showing the different $t$ dependence in the threshold and 1300 MeV mass regions. The solid points are obtained from the 6 GeV/$c$ data [1] for $\Sigma\langle Y_4^{0,2}\rangle$, $\Sigma\langle Y_2^2\rangle$, $\Sigma\langle Y_0^0\rangle$. The open points are $-\Delta\langle Y_0^0\rangle$.

Recall that a crucial assumption in the $\pi^-p\to K^-K^+n$ and $\pi^+n\to K^-K^+p$ partial-wave analysis [14] was the dominance of the flip amplitudes $S^\pi$ and $S^B$. While this is a reasonable assumption for $I=0$ production, $S^\pi$, we see that it is dangerous for $I=1$ $K\bar{K}$ production for $-t<0.08$ GeV$^2$.

To demonstrate the inherent ambiguity that this can introduce in such analyses, we repeated the whole analysis but now including a fixed contribution $|S^Z|$ as determined by $|S_0|$ of the $K^-K^0$ data in the 1300 MeV region. We find that $|f_S|$ is reduced to a value indicated by the dashed curve in fig. 9, while the other amplitudes do not change appreciably. This is not surprising as, to a crude approximation, the data determine the sum $|S^\pi|^2+|S^Z|^2$.

In summary we see that the evidence for the structure in $S^{I=0}$ at 1300 MeV is not compelling and that their exist arguments to assign the bump to $S^{I=1}$ production.

## 6. The scalar mesons

The $K\bar{K}$ channel is a valuable source of information on the controversial $0^{++}$ meson states. These mesons are of unusual importance in particle spectroscopy because in addition to the conventional P-wave, $q\bar{q}$ nonet of the quark model, it has been proposed [12] that there is a low-lying nonet of S-wave $qq\bar{q}\bar{q}$ states. If

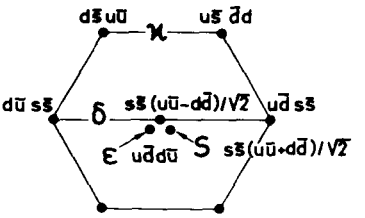


Fig. 13. The quark content of the $qq\bar{q}\bar{q}$ nonet.

multiquark states exist we can expect two nonets of $0^{++}$ mesons below about 1.5 GeV.

For a $0^{++}$ nonet let us denote the isotriplet members by $\delta$, the isodoublets by $\kappa$ and $\bar{\kappa}$, and the isosinglets by $\epsilon$ and S. Suppose that the S and $\epsilon$ mix magically in the conventional $q\bar{q}$ nonet, then $\epsilon$ and $\delta$ will be degenerate in mass, with the S state (which contains the $s\bar{s}$ pair) at a higher mass. On the other hand, if the S and $\epsilon$ states are magically mixed in the $qq\bar{q}\bar{q}$ nonet, then the quark content is as shown in fig. 13. That is, the S and $\delta$ and degenerate in mass and the $\epsilon$ lies at the lower mass. The resulting mass spectrum is sketched schematically in fig. 14. It was the approximate degeneracy of the observed S*(980) and $\delta(970)$ which prompted Jaffe [12] to assign these states to the $qq\bar{q}\bar{q}$ nonet, together with broad $\epsilon(\pi\pi)$ and $\kappa(K\pi)$ states. Indeed, the only obvious problem with this identification is the observed width of the $\delta \to \pi\eta$ decay; since $qq\bar{q}\bar{q} \to q\bar{q} + q\bar{q}$ are 'fall apart' decays, it should be much broader. Of course this approach raises the problem of observing another nearby $0^{++}$ nonet ($\epsilon'$, $\delta'$, $\kappa'$, S' of fig. 14).

The spectrum described above represents an idealized situation. We expect some violation of magic mixing. For example, in a $qq\bar{q}\bar{q}$ state one $q\bar{q}$ pair spends a fraction of the time in a colour octet state [12] or in a $0^-$ state. In either case this will lead to violations of magic mixing. Also the members of the two nonets can mix by gluon exchange.

All the non-strange $0^{++}$ mesons can couple to the $K\bar{K}$ channel. This highlights the importance of the isospin identification of the S-wave $K\bar{K}$ structure at 1.3 GeV. If an $I = 1$ state ($\delta'$) is confirmed in this mass region it will be clear evidence for the existence of two nonets.

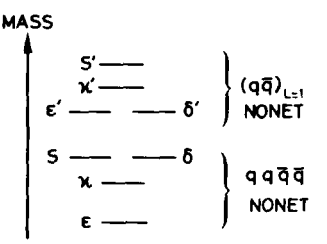


Fig. 14. Schematic mass spectrum for $0^{++}$ states.

Some time ago Morgan [6] reviewed the scalar mesons and attempted to accommodate them in a non-magically mixed $q\bar{q}$ nonet. In this description the $I = 0$ wave contained an S* resonance near the threshold of, and strongly coupled to, the $K\bar{K}$ channel, and a broad $\epsilon(1300)$ resonance coupled dominantly to the $\pi\pi$ channel. The recent data showing the narrow S-wave $K\bar{K}$ structure at 1300 MeV, with the possibility of an $I = 0$ component, opens the way to further (or different) $I = 0$ states.

The present knowledge of the magnitude and phase of the $I = 0$ S-wave in both the $\pi\pi \to \pi\pi$ [23, 27] and $\pi\pi \to K\bar{K}$ channels means a quantitative resonance analysis is possible [10]. We have attempted such a coupled channel multiresonance analysis in the 0.8–1.5 GeV mass region. Even allowing the ambiguity* in $|f_S|$ in the 1300 MeV mass regions, we are unable to obtain a satisfactory description of the data. We considered overlapping resonances using the mass matrix formalism, and also $M$-matrix parametrizations. Only the latter types of parametrization are able to reproduce the approximately constant behaviour of $\phi_S$ below 1.3 GeV. A typical (12 parameter) $M$-matrix fit is shown in fig. 15. In this example, the amplitudes have poles** on sheet II at $E = 0.986 - 0.007i$, $1.07 - 0.33i$ GeV, and on sheet III at $E = 1.37 - 0.17i$, $1.42 - 0.21i$ GeV; the S* is associated only with the first sheet-II

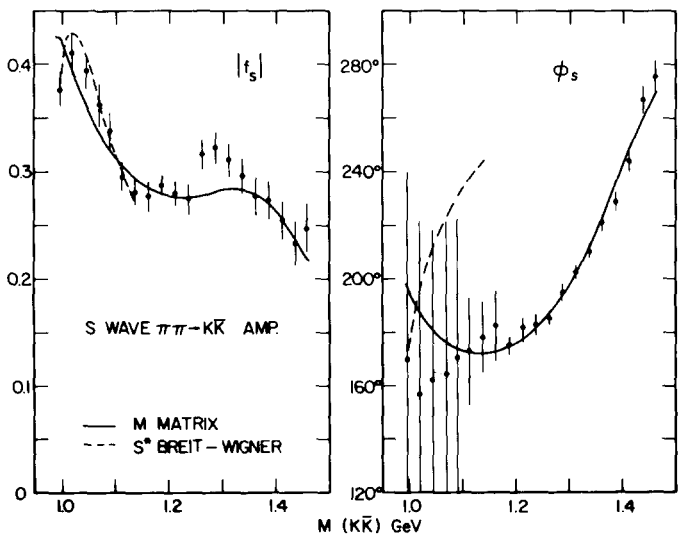


Fig. 15. The description of the S-wave $\pi\pi \to K\bar{K}$ amplitude in a coupled channel $M$-matrix analysis (continuous curves); and a S* Breit–Wigner plus background description (dashed curves).

* To do this we do not fit $|f_S|$ in the $1.25 < M < 1.35$ GeV mass region.

** The notation is as in ref. [8].

pole. Note that in a constant $M$-matrix (or constant scattering length) approach the S* is represented by a sheet-II pole alone. The behaviour of $\phi_S$ near threshold is not reproduced by a Breit–Wigner S* description which has nearby sheet-II and sheet-III poles [6, 8, 28].

A major problem in all fits* is the matching of the rapid decrease in $|f_S|$ just above the S* with the behaviour above 1.1 GeV. The slow variation of the phase, $\phi_S$, is found to rule out narrow structures ($\sim$200 MeV) in the 1.1–1.3 mass region. Recall that there is a solution for the $K^-K^+$ production amplitudes in which $\phi_S$ advances rapidly (ahead of the f resonance phase**) in the region, but this is surely unphysical since it requires the $S^B$, $P^\pi$ amplitudes to have the same rapid phase behaviour as $S^\pi$.

It is instructive to look at a simple S* Breit–Wigner resonance plus background fit to $|f_S|$ up to 1.15 GeV together with the $\pi\pi \to \pi\pi$ data. The form used is

$$f_{ij} = \frac{g^i_{S*} g^j_{S*} \sqrt{q_i q_j}}{m^2_{S*} - M^2 - i[(g^i_{S*})^2 q_i + (g^j_{S*})^2 q_j]},$$

where $i, j$ label the $\pi\pi$, $K\bar{K}$ channels. We include a linearly rising elastic background phase ($\delta_B$) in the $\pi\pi$ channel [8]. The result is given by the dashed curve on fig. 15, which also shows the prediction for $\phi_S$ assuming no background in the $K\bar{K}$ channel. Note the discrepancy in $\phi_S$; a satisfactory description of both $|f_S|$ and $\phi_S$ is difficult and requires a complicated amplitude structure. For completeness we give the parameter values corresponding to the fit:

$$m_{S*} = 1.005 \pm 0.003 \text{ GeV}, \qquad \delta_B \text{ (at 1 GeV)} = 89.0°,$$
$$(g^{\pi\pi}_{S*})^2 = 0.198 \pm 0.009 \text{ GeV}, \quad (g^{K\bar{K}}_{S*})^2 = 0.277 \pm 0.018 \text{ GeV},$$

which lead to a sheet-II pole at $E = 1.012 - i\ 0.030$ GeV, and a sheet-III pole at $E = 0.985 - i\ 0.065$ GeV.

## 7. Results and conclusions

We have performed partial-wave analyses of $K\bar{K}$ production data in the mass region from threshold to 1.5 GeV. The S-wave is important throughout the mass region showing, besides the S*, interesting structure at 1300 MeV. The higher partial waves are well described by $\rho$, f, f', $A_2$ resonance forms.

We attempted to resolve $I = 0$ and $I = 1$ S-wave contributions. We first analysed $K^-K^0$ production to estimate the $I = 1$ component. Although the amplitudes in the UPE sector are not well-determined, and have an S/P wave ambiguity, we found that the data imply a significant non-flip S-wave amplitude.

* The description of ref. [10] has the same difficulty.
** The observable is $|\phi_S - \phi_D|$.

Turning to $K^-K^+$ production, we first studied the D-wave contribution. We determined the $f \to K\bar{K}$ branching ratio to be $(2.4 \pm 0.4)\%$. Contrary to an earlier analysis [1, 21] we found that we could not describe the $\Delta\langle Y_4^0 \rangle$ data in terms of f'-$A_2$ (or f-$A_2$) interference. From the observed f-f' interference structure we determined the $f' \to \pi\pi$ branching ratio to be $(0.75 \pm 0.25)\%$.

We repeated the detailed ANL partial-wave analysis of $K^-K^+$ data, using their assumption of the dominance of flip amplitudes, and found essentially the same results. In particular the $I = 0$ S-wave, $f_S$, had, in addition to the S*, a significant bump at 1300 MeV, together with a slowly advancing phase $\phi_S$.

We stressed that the flip-dominance assumption is dangerous for the $I = 1$ S-wave contribution at small $t$. We showed this explicitly; we repeated the $K^-K^+$ analysis with an S-wave non-flip contribution as given by the $K^-K^0$ data. In this analysis $|f_S|$ was found to be smooth at 1300 MeV. We concluded that the isospin assignment of the S-wave structure at 1300 MeV is not resolved.

The implications of the $K\bar{K}$ analysis to the status of scalar mesons was discussed. The possibility of $I = 0$ and/or $I = 1$ states at 1300 MeV encourages the speculation of the existence of a second nonet of $0^{++}$ states; namely the $qq\bar{q}\bar{q}$ nonet proposed by Jaffe. However, even allowing the full ambiguity in $|f_S|$ at 1300 MeV we were unable to find any satisfactory multiresonance description of the $I = 0$ S-wave. The major problem, assuming the $\pi\pi \to \pi\pi$ amplitude is known, is to correlate the behaviour of $|f_S|$ and $\phi_S$ for the $\pi\pi \to K\bar{K}$ amplitude.

We thank N.M. Cason, D. Cohen, A.C. Irving, R. Jaffe, D. Morgan, C. Nef and A.B. Wicklund for valuable discussions and communications. We acknowledge the support of the British Science Research Council. One of us (E.N.O.) thanks the Turkish Government for support during a part of this work.

## References

[1] A.J. Pawlicki et al., Phys. Rev. D15 (1977) 3196.
[2] W. Wetzel et al., Nucl. Phys. B115 (1976) 208.
[3] N.M. Cason et al., Phys. Rev. Lett. 36 (1976) 1485;
V.A. Polychronakos et al., Phys. Rev. D19 (1979) 1317.
[4] A.D. Martin et al., Phys. Lett. 74B (1978) 417.
[5] A.D. Martin et al., Nucl. Phys. B140 (1978) 158.
[6] D. Morgan, Phys. Lett. 51B (1974) 71.
[7] D. Cohen, Proc. 5th EMS Conf., ed. E. Von Goeler and R. Weinstein, Boston (1977) p. 238;
A.J. Pawlicki et al., Phys. Rev. Lett. 37 (1976) 1666.
[8] A.D. Martin, E.N. Ozmutlu and E.J. Squires, Nucl. Phys. B121 (1977) 514.
[9] S.M. Flatté, Phys. Lett. 63B (1976) 324;
M. Cerrada et al., Phys. Lett. 62B (1976) 353;
M. Aguilar-Benitez et al., Nucl. Phys. B140 (1978) 73;
A.D. Martin, Proc. 13th Rencontre de Moriond, ed. J. Tran Thanh Van (1978) vol. 1, p. 363.

[10] P. Estabrooks, Phys. Rev. D19 (1979) 2678.
[11] N.M. Cason et al., Phys. Rev. Lett. 41 (1978) 271.
[12] R.L. Jaffe, Phys. Rev. D15 (1977) 267.
[13] R.L. Jaffe, and K. Johnson, Phys. Lett. 60B (1975) 201;
D. Robson, Nucl. Phys. B130 (1977) 328.
[14] D. Cohen et al., ANL preprint HEP-PR-78-22 (June, 1978).
[15] A.C. Irving and R.P. Worden, Phys. Reports 34 (1977) 117.
[16] A.C. Irving et al., Nucl. Phys. B149 (1979) 101.
[17] A.C. Irving, Nucl. Phys. B105 (1976) 491.
[18] M.J. Emms et al., Phys. Lett. 58B (1975) 117;
M.J. Corden et al., Nucl. Phys. B138 (1978) 235.
[19] M.J. Emms et al., Nucl. Phys. B96 (1975) 155.
[20] A.B. Wicklund et al., Phys. Rev. D17 (1978) 1197; private communication.
[21] A.J. Pawlicki et al., Phys. Rev. Lett. 37 (1976) 971.
[22] W. Beusch et al., Phys. Lett. 60B (1975) 101.
[23] P. Estabrooks and A.D. Martin, Nucl. Phys. B79 (1974) 301; B95 (1975) 322;
B. Hyams et al., Nucl. Phys. B64 (1973) 134.
[24] D. Cohen and A.B. Wicklund, private communication.
[25] R.H. Dalitz and S.F. Tuan, Ann. of Phys. 10 (1960) 307.
[26] A.C. Irving, Phys. Lett. 70B (1977) 217.
[27] W.D. Apel et al., Karlsruhe-Pisa collaboration, BNL-25056 (1978);
A.D. Martin and M.R. Pennington, Ann. of Phys. 114 (1978) 1.
[28] Y. Fujii and M. Fukugita, Nucl. Phys. B85 (1975) 179.

Nuclear Physics B145 (1978) 409–419


# HIGH-ENERGY BEHAVIOUR OF A DOUBLE DISCONTINUITY AND THE BARE POMERON

P. HOYER * and J. KWIECINSKI **
*Rutherford Laboratory, Chilton, Didcot, Oxon OX11 OQX, England*

Received 12 June 1978

The high-energy behaviour of a double discontinuity of the six-point amplitude is studied in the dual-resonance model and in a hybrid Feynman-diagram model. This discontinuity imposes, through unitarity, a bound on the intercept of the bare-pomeron singularity. It is shown that in both models the ordinary Regge trajectories which couple to two-body amplitudes decouple from the discontinuity. The origin of this decoupling is discussed. The asymptotic behaviour of the double discontinuity is controlled by sister trajectories in the dual-resonance model, and by the genuine three-particle Regge poles in a Feynman-diagram model. Insofar as the intercepts of these trajectories are lower than those of the usual Regge poles there is no strong constraint on the pomeron.

## 1. Introduction

The (bare) pomeron singularity in the topological expansion (or dual unitarisation) [1–3] *** is given by diagrams which have the topology of a cylinder. The dominant region of phase space which gives rise to the pomeron singularity corresponds to the production of two heavy clusters, both masses of which are of the order $s$. The same region of phase space is also responsible for the new, pomeron-like, singularity in a twisted dual-loop amplitude [4].

The asymptotic behaviour of the pomeron amplitude is closely connected with the scaling properties of the two-cluster production process. It is straightforward to show that if the amplitude for cluster production scales (i.e., if it depends only on scaling variables like $M_i^2/s$ where $M_i$ are the cluster masses), then the corresponding unitarity integral gives a pomeron singularity of intercept one.

These scaling properties appear to be very natural if the cylinder contribution is interpreted in a parton language. The pomeron in this picture corresponds to the (double) scattering of two *fast* valence quarks, unlike the reggeon amplitude which

* On leave from NORDITA, Copenhagen, Denmark.
** On leave from Institute of Nuclear Physics, Cracow, Poland.
*** The papers [3] are review papers.

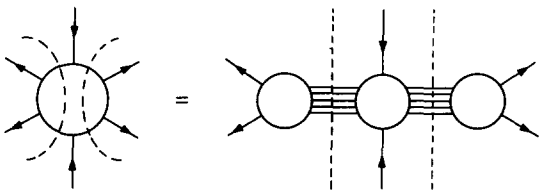

Fig. 1. The unitarity equation relating the double discontinuity of the six-point amplitude to the two-cluster production.

contains an additional damping factor due to a wee quark. It is this picture which underlines the QCD model for the pomeron singularity [5,6]. Explicit calculations done in two dimensions [6] showed, however, that the pomeron singularity was cancelled in the complete sum of diagrams. This cancellation may be a feature only of a two-dimensional model and might not appear in four dimensions [5].

The two-cluster production amplitude is related by unitarity to the double discontinuity of the six-point function, as shown in fig. 1. In the topological expansion scheme the six-point amplitude is the planar one and Regge-pole dominated (fig. 2) for high $s$, $M_1^2$ and $M_2^2$. It has been shown by Veneziano [7] using Schwartz inequalities that the amplitude corresponding to two heavy cluster production would scale (or, more precisely, would be bounded from *below* by some function which scales) provided that the ordinary (planar) Regge trajectories coupled to the double discontinuity of the six-point amplitude. There are no obvious reasons (like Steinmann relations [8] etc.) which would require the vanishing of the double dis-

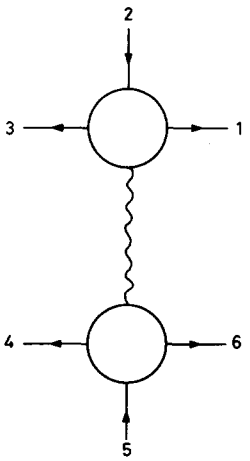


Fig. 2. The kinematics of the six-point amplitude; $s = (p_2 + p_5)^2$, $M_1^2 = (p_3 + p_4)^2$, $M_2^2 = (p_1 + p_6)^2$.

continuity of fig. 1 or the decoupling of Regge poles from it. Nevertheless, as observed by Veneziano [7] this decoupling does occur in the dual resonance model. A clarification of the reasons for this decoupling could lead to a better understanding of the bare-pomeron singularity in the dual unitarisation scheme.

In this paper we give an intuitive argument for why the ordinary reggeons decouple and show that there are contributions from other exchanges characteristic for multiparticle amplitudes. In sect. 2 we briefly discuss the relation between the 6-point amplitude and the two cluster production which follows from unitarity. In sect. 3 we discuss the double discontinuity of the six-point amplitude in the dual resonance model (DRM) and a hybrid Feynman diagram model. We exhibit the decoupling of the ordinary Regge poles within the DRM. A similar decoupling takes place also in the hybrid Feynman diagram model where the Regge poles are generated using two-particle amplitudes. We argue that the decoupling may be easily understood by inspecting the energy flow in the cut diagrams. We find that the high-energy behaviour of the double discontinuity in the DRM is governed by sister trajectories [9,10]. Within the hybrid Feynman diagram model the non-vanishing contribution is given by three-particle Regge poles [11]. Finally, in sect. 4 a brief discussion of the results is given.

## 2. Unitarity bound on two-cluster production

In order to demonstrate the relation between the double discontinuity of the six-point amplitude and the pomeron let us first consider a one-dimensional model with simple factorisation. The unitarity equation of fig. 1 takes the form

$$\frac{1}{2i}\,\mathrm{disc}_{M_1^2}\,\frac{1}{2i}\,\mathrm{disc}_{M_2^2}\,A_6 = g(M_1^2)\,g(M_2^2)\,A(s, M_1^2, M_2^2)\,, \tag{2.1}$$

where $A$ is a two-cluster production amplitude and $g(M_i^2)$ are coupling constants of a system of mass $M_i$ to the external particles. The couplings $g(M_i^2)$ can be obtained from the two-body amplitude. Regge-pole behaviour of this planar amplitude yields for large $M_i^2$:

$$g(M_i^2) = c(M_i^2)^{\alpha/2}\,, \tag{2.2}$$

where $\alpha$ is the Regge-trajectory intercept. The same Regge trajectory also contributes to the asymptotic behaviour of the 6-point amplitude for large $s$ and for $M_1^2 = x_1 s$, $M_2^2 = x_2 s$ (fig. 2). Assuming that this contribution has a non-vanishing double discontinuity one obtains:

$$\frac{1}{2i}\,\mathrm{disc}_{M_1^2}\,\frac{1}{2i}\,\mathrm{disc}_{M_2^2}\,A_6 = \beta(x_1, x_2)\,s^{\alpha}\,. \tag{2.3}$$

Combined with (2.1) and (2.2) this implies scaling of the two-cluster production

amplitude $A$:

$$A(s, M_1^2, M_2^2) = c^{-2}(x_1 x_2)^{-\alpha/2}\beta(x_1, x_2) \equiv A(x_1, x_2) . \tag{2.4}$$

Such a scaling behaviour gives a bare-pomeron singularity with intercept equal to one:

$$\operatorname{Im} A_P(s) = \frac{\text{const}}{s}\iint \mathrm{d}M_1^2 \mathrm{d}M_2^2 |A(s, M_1^2, M_2^2)|^2 = s \text{ const} \iint \mathrm{d}x_1 \mathrm{d}x_2 |A(x_1, x_2)|^2 . \tag{2.5}$$

This factorisable model illustrates in a simple way how the scaling properties may originate from unitarity and Regge behaviour. The simple factorisation is not, however, expected to hold, in general. The asymptotic (Regge) behaviour is built up from peripheral states rather than from states on parent trajectories. The peripheral states are expected to be highly degenerate and therefore arguments based on simple factorisation alone are not convincing. One can, however, apply Schwarz inequalities to the planar unitarity equation of fig. 1 [7]. It then follows that the two-cluster production amplitude is bounded from below by some function which scales, provided that ordinary Regge trajectories couple to the double discontinuity of the six-point amplitude. The Schwarz inequality is (fig. 3):

$$|A(M_1^2, M_2^2, s)|^2 \geqslant \frac{|(1/2i)\operatorname{disc}_{M_1^2}(1/2i)\operatorname{disc}_{M_2^2} A_6|^2}{[\operatorname{Im} A_4(M_1^2, t=0)\cdot \operatorname{Im} A_4(M_2^2, t=0)]} . \tag{2.6}$$

Assuming Regge behaviour for $\operatorname{Im} A_4$ and for the double discontinuity in the numerator with the same Regge trajectories in both i.e.,

$$\operatorname{Im} A_4(M_i^2, t=0) = c(M_i^2)^{\alpha(0)} , \tag{2.7}$$

$$\frac{1}{2i}\operatorname{disc}_{M_1^2}\frac{1}{2i}\operatorname{disc}_{M_2^2} A_6 = \beta(x_1, x_2)\, s^{\alpha(0)} , \tag{2.8}$$

one obtains

$$|A(M_1^2, M_2^2, s)|^2 \geqslant c^{-2}\beta^2(x_1, x_2)(x_1 \cdot x_2)^{-\alpha(0)} . \tag{2.9}$$

When combining with (2.5) (assuming some intrinsic cut-off in transverse momentum) this gives [7] a lower bound on the pomeron:

$$\operatorname{Im} A_P(s, t=0) \geqslant \text{const.}\, s . \tag{2.10}$$

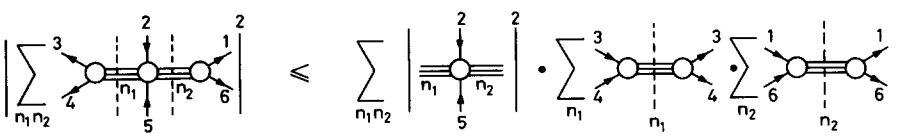


Fig. 3. Schwarz inequality which follows from the unitarity equation for the double discontinuity.

To conclude, the bound (2.9) requires two independent assumptions:

(1) planar unitarity, which leads to inequality (2.6) where all the amplitudes on the r.h.s. are the planar ones;

(2) the asymptotic behaviour for the double discontinuity and for the four-point amplitude is the same ($s^{\alpha}$).

## 3. High-energy behaviour of the double discontinuity

In sect. 2 we showed that the possible scaling behaviour of the two-cluster production amplitude depends upon whether the ordinary Regge trajectories couple in the double discontinuity of $A_6$. In this section we discuss this question within two models for $A_6$.

The kinematics of the 6-point function is defined by fig. 2. We are interested in the asymptotic limit where the following invariants are large:

$$s = s_{25} = (p_2 + p_5)^2 , \qquad s_{345} = (p_3 + p_4 - p_5)^2 ,$$

$$M_1^2 = s_{34} = (p_3 + p_4)^2 , \qquad s_{234} = (p_3 + p_4 - p_2)^2 ,$$

$$M_2^2 = s_{61} = (p_1 + p_6)^2 ,$$

The asymptotic behaviour of the 6-point amplitude is given by single Regge-pole exchange. We consider the configuration which is relevant to two-cluster production with ingoing and outgoing particles as in fig. 2. In this configuration $s$, $M_1^2$ and $M_2^2$ are positive while $s_{345}$ and $s_{234}$ are negative.

The double discontinuity of the six-point amplitude is defined by

$$\mathrm{disc}_{s_{34}}\mathrm{disc}_{s_{61}} A_6 = A_6(s_{34} + i\epsilon, s_{61} + i\epsilon) - A_6(s_{34} - i\epsilon, s_{61} - i\epsilon) \tag{3.1}$$

In the dual-resonance model, the Regge-pole limit of the $B_6$ function takes the following form when all large variables are negative [12]:

$$B_6 \sim \int_0^1 \mathrm{d}x_1 x_1^{-\alpha_{12}-1}(1-x_1)^{-\alpha_{23}-1} \int_0^1 \mathrm{d}x_2 x_2^{-\alpha_{56}-1}(1-x_2)^{-\alpha_{45}-1}$$

$$\times [-\alpha_{34}(1-x_1)(1-x_2) - \alpha_{61}x_1x_2 - \alpha_{234}x_1(1-x_2) - \alpha_{345}(1-x_1)x_2]^{\alpha_{123}} \tag{3.2}$$

where $\alpha_{ij}$, $\alpha_{ijk}$ are the linear Regge trajectories. The evaluation of the discontinuity (3.1) requires, however, knowledge of $B_6$ in limits where some of the variables ($\alpha_{34}$ and $\alpha_{61}$) are positive. Besides the contribution $B_6^{(\alpha)}$ obtained by analytic continuation of the expression (3.2) there is, in this region, a contribution $B_6^{(\beta)}$ from sister trajectories [9,10].

Let us first compute the double discontinuity of $B_6^{(\alpha)}$ in $\alpha_{34}$ and $\alpha_{61}$ for negative

$\alpha_{234}$ and $\alpha_{345}$. The singularities of $B_6^{(\alpha)}$ in $\alpha_{34}, \alpha_{61}$ are generated by the factor $(-z)^{\alpha_{123}}$ in the integral (3.2) where

$$z(\alpha_{34}, \alpha_{61}) = \alpha_{34}(1-x_1)(1-x_2) + \alpha_{61}x_1x_2 + \alpha_{234}x_1(1-x_2) + \alpha_{345}x_2(1-x_1) \tag{3.3}$$

The phases of the various terms in (3.1) are determined by:

$$\begin{aligned}
&(-z(\alpha_{34} + i\epsilon, \alpha_{61} + i\epsilon))^{\alpha_{123}} \\
&\quad = [e^{-i\pi\alpha_{123}}\theta(z) + \theta(-z)]\ |z|^{\alpha_{123}}, \\
&\quad (-z(\alpha_{34} - i\epsilon, \alpha_{61} + i\epsilon))^{\alpha_{123}} \\
&\quad = \{\theta(z)\ [e^{i\pi\alpha_{123}}\theta(x_1 + x_2 - 1) + e^{-i\pi\alpha_{123}}\theta(1 - x_1 - x_2)] + \theta(-z)\}|z|^{\alpha_{123}}, \\
&(-z(\alpha_{34} + i\epsilon, \alpha_{61} - i\epsilon))^{\alpha_{123}} \\
&\quad = \{\theta(z)[e^{-i\pi\alpha_{123}}\theta(x_1 + x_2 - 1) + e^{i\pi\alpha_{123}}\theta(1 - x_1 - x_2)] + \theta(-z)\}|z|^{\alpha_{123}}, \\
&(-z(\alpha_{34} - i\epsilon, \alpha_{61} - i\epsilon))^{\alpha_{123}} = [e^{i\pi\alpha_{123}}\theta(z) + \theta(-z)]|z|^{\alpha_{123}}\ .
\end{aligned} \tag{3.4}$$

Substituting this in (3.1) and (3.2) gives

$$\mathrm{disc}_{M_1^2}\ \mathrm{disc}_{M_2^2}\ B_6^{(\alpha)} = 0\ . \tag{3.5}$$

The decoupling (3.5) of ordinary Regge trajectories $\alpha$ holds only in the configuration relevant for *cluster production* i.e., for *negative* $s_{234}$ and $s_{345}$. In the configuration which corresponds to a cascade decay that is for positive $s_{234}$ and $s_{345}$ the double discontinuity of $B_6^{(\alpha)}$ is non-zero.

The contribution of the sister trajectory $\beta$ to the double discontinuity may be obtained using the results of refs. [9,10]. The amplitudes $B_6(s_{34} - i\epsilon, s_{61} + i\epsilon)$ and $B_6(s_{34} + i\epsilon, s_{61} - i\epsilon)$ are given by analytic continuation from the region where all large variables are negative, keeping

$$\eta \equiv \frac{s_{234}s_{345}}{s_{36}s_{61}} = 1$$

during the continuation. Hence the $\beta$ trajectory does not contribute to these amplitudes. The two other amplitudes in the discontinuity (3.1) have a non-vanishing $\beta$ contribution given by eq. (B.21) of ref. [10] and its complex conjugate. The expression for the double discontinuity in the DRM is thus

$$\begin{aligned}
&\mathrm{disc}_{s_{34}}\mathrm{disc}_{s_{61}}B_6 \\
&= \frac{-\pi^2}{2\beta_{123}\Gamma(\beta_{123})}\ \alpha_{34}^{\beta_{123}}\left[\left(-\frac{\alpha_{234}}{\alpha_{345}}\right)^{\beta_{123}-\alpha_{23}}\left(1 - \frac{\alpha_{234}}{\alpha_{34}}\right)^{-\beta_{123}+\alpha_{12}+\alpha_{23}}\right] \\
&\times \left[\left(-\frac{\alpha_{345}}{\alpha_{34}}\right)^{\beta_{123}-\alpha_{45}}\left(1 - \frac{\alpha_{345}}{\alpha_{34}}\right)^{-\beta_{123}+\alpha_{45}+\alpha_{56}}\right],
\end{aligned} \tag{3.6}$$

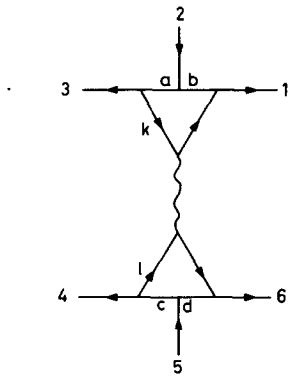


Fig. 4. The hybrid Feynman model for the six-point amplitude.

where $\beta_{123} = \frac{1}{2}(\alpha_{123} - 1)$. Because the $\alpha$ trajectory does not contribute (*cf.* eq. (3.5)), eq. (3.6) gives the leading contribution to the double discontinuity in the single-Regge limit.

Let us now consider the hybrid Feynman diagram for the 6-point amplitude as in fig. 4. We show in the appendix that the amplitude corresponding to this diagram may, in the single-Regge limit, be expressed in a form very similar to the dual-resonance amplitude (eq. (3.2)):

$$\Delta_\alpha = \int_0^1 \phi(\lambda_a \ldots \lambda_d)[-\lambda_a\lambda_c s_{34} - \lambda_b\lambda_d s_{16} - \lambda_a\lambda_d s_{345} - \lambda_b\lambda_c s_{234}]^{\alpha_{123}} \prod_i d\lambda_i \,. \tag{3.7}$$

The parameters $\lambda_i$ ($i$ = a, b, c, d) are Feynman parameters corresponding to the lines (a)–(d) in the diagram of fig. 4. The exact form of the function $\phi$ is irrelevant for our purposes. The vanishing of the double discontinuity of $A_6$ follows exactly as for the dual-resonance amplitude. It is again essential that the variables $s_{234}$ and $s_{345}$ are negative.

The physical origin of this decoupling which was difficult to see in the DRM is more transparent in the Feynman-diagram model. Taking the discontinuity in one of the variables (say $s_{34}$) implies that all the cut lines in the diagram are put on-shell *and* that their energy components have a common sign. This is illustrated for a simple ladder representation of the reggeon in fig. 5, where the arrows indicate positive energy flow. The (common) direction of the arrows is dictated by energy conservation in the part of the diagram to the left of the cutting.

It is now clear why the double discontinuity must vanish in the kinematic region under consideration. Taking a further discontinuity in $s_{61}$ would require the arrows on the lines (b) and (d) also to be directed to the left. This would violate energy conservation in the right-hand part of the diagram. In a "cascade" configuration on the

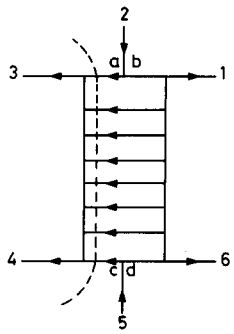


Fig. 5. Discontinuity of the single ladder amplitude in the variable $s_{34}$. The arrows indicate the energy flow.

other hand, where the directions of the lines 1 and 6 are reversed, there is no conflict with energy conservation and the double discontinuity is non-vanishing.

The above argument for the decoupling of ordinary Regge poles from the double discontinuity is evidently quite general. It applies to any diagram which has the structure of fig. 4, i.e., when the Regge pole is generated through insertions of four-point amplitudes.

A non-vanishing double discontinuity may be generated by two-particle irreducible insertions. This is realised in amplitudes with three-particle Regge poles [11]. As shown in fig. 6 the doubly cut three-particle ladder diagram is kinematically allowed.

## 4. Summary and discussion

Our study of the double discontinuity of the six-point function was motivated by its relation to the bare-pomeron singularity. We showed that if the asymptotic behaviour of the discontinuity in the single-Regge limit (fig. 2) is determined by the

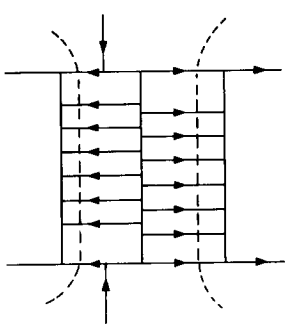

Fig. 6. Double discontinuity of the three-particle Regge pole.

ordinary Regge poles, then the intercept of the pomeron trajectory must be equal to, or above, one [7].

In both models that we considered, the dual-resonance model and a hybrid Feynman-diagram model, it turned out that the ordinary Regge poles did *not* contribute to the discontinuity. Moreover, we traced the reason for this decoupling to the pattern of energy flow in the two-particle insertion that generates the asymptotic behaviour. Taking the discontinuity in either $s_{34}$ or $s_{61}$ fixes the direction of energy flow in the cut lines (fig. 5), and the direction is opposite in the two cases. Consequently, the decoupling of the ordinary Regge poles is quite general, and there are no strong constraints on the pomeron intercept.

The fact that the discontinuity receives no contribution from ordinary Regge poles does not mean that it vanishes, however. In the DRM we found that the asymptotic behaviour is given by the first sister trajectory, $\beta = \frac{1}{2}\alpha - \frac{1}{2}$. This trajectory decouples from two-particle states and appears only in six-point, and higher, amplitudes [9,10]. While there were some indications previously * that the $\beta$ trajectory is linked to the pomeron, the present relation is much more direct. It implies, in particular, that if the $\beta$ trajectory has a higher intercept than the ordinary $\alpha$ trajectory, then the bare pomeron intercept is above one. This is not the case in the standard DRM, where $\beta$ is the leading trajectory only in the region $\alpha < -1$. (In the Neveu-Schwarz model, on the other hand, it has been shown [13] that $\beta_\pi > \alpha_\pi$ for $\alpha_\pi < +1$.)

In the hybrid Feynman diagram model we saw that Regge poles that are generated through two-particle irreducible insertions should have a non-vanishing double discontinuity. Such multiparticle Regge poles have been studied previously [11], and the present work suggests a relationship between them and the sister trajectories of the DRM. However, it is not clear that the Regge poles generated through multiparticle ladders have the rather unusual analytic properties exhibited by the $\beta$ trajectory. For example, the $\beta$ trajectory contributions to asymptotic limits in which the large variables have different signs are not in general related by analytic continuation (of the asymptotic form). Furthermore, the $\beta$ trajectory does not couple to two particles. The multi-ladder Regge poles of course do contribute to four-point amplitudes [11]. However, in these amplitudes the poles will be renormalised by two-particle insertions. Since such iterations do not contribute to the double discontinuity we studied in this paper, it could indeed turn out that the Regge pole governing the high-energy behaviour of the discontinuity is different from those seen in four-point amplitudes. In this case it should have a lower intercept than the ordinary Regge pole, as it lacks the two-particle insertions. This agrees with the bound given by the pomeron intercept.

Our results may also be compared with the calculations of the bare pomeron in two-dimensional QCD [6]. In that model, apparently due to the absence of transverse dimensions, the two-cluster production amplitude does not scale and there is no bare

* The papers [3] are review papers.

pomeron. Because of the simple factorization property of the states this implies that the "Regge pole" $\alpha$ decouples from the double discontinuity (2.1). This is consistent with the above results.

One of the authors (J.K) would like to thank Gabriele Veneziano for discussions and Joe Weis for discussions and useful correspondence. Both of us are grateful to Roger Phillips and Chan Hong-Mo for the hospitality of the Theory Division of the Rutherford Laboratory.

## Appendix

In this appendix we derive the representation (3.7) for the hybrid Feynman diagram. The amplitude corresponding to this diagram is given by the following expression

$$A_6 \sim \int d^4k\, d^4l \int_0^\infty \frac{x^{\alpha_{123}}}{(x-(k+l)^2)} \prod_{i=1}^{8} P_i\,, \tag{A.1}$$

where $P_i$ are the propagators corresponding to the various lines of the diagram. Introducing Feynman parametrization [14] and performing the loop interpretation we obtain:

$$A_6 \sim \int_0^\infty dx\, x^{\alpha_{123}} \int_0^\infty \frac{\Pi d\lambda_i \delta(\Sigma\lambda_i - 1)}{[D(\{\lambda_i\}, s_i)]^5}\,, \tag{A.2}$$

where

$$D = \lambda_g\left[x - \frac{\lambda_a\lambda_b s_{34} + \lambda_b\lambda_d s_{61} + \lambda_a\lambda_d s_{345} + \lambda_b\lambda_c s_{234}}{A\cdot B}\right] + \delta \equiv \lambda_g[x-\omega] + \delta. \tag{A.3}$$

$A$ and $B$ are equal to a sum over $\lambda$ parameters corresponding to the upper and lower vertices respectively, after neglecting terms $O(\lambda_g)$ which are negligible in the single-Regge limit. The function $D$ in (A.2) depends on the parameters $\lambda$ and upon invariants which are not large.

Rescaling the variable $\lambda_g$, for $\omega < 0$,

$$\lambda_g = \bar{\lambda}_g(x-\omega)^{-1}\,, \tag{A.4}$$

one arrives at the formula (3.7) after integrating over $x$ and $\bar{\lambda}_g$.

## References

[1] G. Veneziano, Phys. Lett. 52B (1974) 220; Nucl. Phys. B74 (1974) 365;
M. Ciafaloni, G. Marchesini and G. Veneziano, Nucl. Phys. B98 (1975) 472, 493.

[2] Chan Hong-Mo, J.E. Paton and Tsou Sheung Tsun, Nucl. Phys. B86 (1975) 479;
Chan Hong-Mo, J.E. Paton, Tsou Sheung Tsun and Ng Sing Wai, Nucl. Phys. B92 (1975) 13.
[3] Chan Hong-Mo and Tsou Sheung Tsun, Rutherford Laboratory preprint RL-76-080 (1976);
K. Konishi, Rutherford Laboratory preprint RL-76-095 (1976);
G.F. Chew and C. Rosenzweig, Lawrence Berkeley Laboratory preprint LBL-6783 (1977).
[4] Ch. B. Chiu and S. Matsuda, Nucl. Phys. B134 (1978) 463.
[5] F.E. Low, Phys. Rev. D12 (1975) 163;
S. Nussinov, Phys. Rev. Lett. 34 (1975) 1286; Phys. Rev. D14 (1976) 246;
J.F. Gunion and D.E. Soper, Phys. Rev. D15 (1977) 2617.
[6] R.C. Brower, J. Ellis, M.G. Schmidt and J.H. Weis, Nucl. Phys. B128 (1977) 131, 174;
M.B. Einhorn, E. Rabinovici, Nucl. Phys. B128 (1977) 421.
[7] G. Veneziano and J.H. Weis, private communications.
[8] R.C. Brower, C.E. de Tar and J.H. Weis, Phys. Reports 14 (1974) 259.
[9] P. Hoyer, N.A. Törnqvist and B.R. Webber, Phys. Lett. 61B (1976) 191;
P. Hoyer, Phys. Lett. 63B (1976) 50.
[10] P. Hoyer, N.A. Törnqvist and B.R. Webber, Nucl. Phys. B115 (1976) 429.
[11] B.M. McCoy and T.T. Wu, Phys. Rev. D12 (1975) 546, 578;
S.G. Matinyan and A.G. Sedrakyan, ZhETF Pisma 23 (1976) 588; 24 (1976) 240; [JETP Lett. 23 (1976) 538; 24 (1976) 214];
I.T. Drummond and I. Halliday, Nucl. Phys. B105 (1976) 293; B106 (1976) 493.
[12] Chan Hong-Mo, P. Hoyer and P.V. Ruuskanen, Nucl. Phys. B38 (1972) 125.
[13] C. Barratt, Nucl. Phys. B120 (1977) 147.
[14] R.J. Eden, P. Landshoff, D.I. Olive and J.C. Polkinghorne, The analytic $S$-matrix (Cambridge University Press, 1966).

Nuclear Physics B60 (1973) 26–44. North-Holland Publishing Company

# ANALYTICITY AND A FINITE-ENERGY SUM RULE FOR THE REGGEON-PARTICLE AMPLITUDE IN a + b → c + d + e

P. HOYER *
*Department of Theoretical Physics, Oxford University*

J. KWIECIŃSKI
*Rutherford High Energy Laboratory, Chilton, Didcot, Berkshire, and Institute of Nuclear Physics**, Cracow 23, Poland*

Received 23 February 1973

Abstract: We consider a single-Regge limit of the amplitude for the process a + b → c + d + e. In this limit the amplitude is proportional to the reggeon-particle amplitude for a + $i$ → c + d, where $i$ is a reggeon. We study the analytic structure of this amplitude using the dual resonance model and a perturbation theory model. We conclude that finite-energy sum rules can be derived, which relate the absorptive part of the amplitude at low $(p_c + p_d)^2$ to a part of the double-Regge vertex function of the original five-point amplitude. We discuss some phenomenological applications of the sum rules.

## 1. Introduction

In this paper we shall investigate the structure of the amplitude for the process a + b → c + d + e, where a, b, c, d and e are scalar particles, in the high-energy limit where $s_{ab} \to \infty$, $s_{de} \to \infty$ while $s_{cd}$ is kept fixed***, fig. 1. In such a limit the five-point amplitude is proportional to the reggeon-particle amplitude for a + $i$ → c + d, where $i$ is the exchanged reggeon. Although the singularity structure of the five-point function is rather complicated in general [1, 2] †, one may hope that its structure is simpler in a high-energy limit like that of fig. 1. This would then make possible the derivation of finite-energy sum rules [3; 4], which would be useful in the analysis of data for three-particle final states.

As was recently shown, there is an analogous situation in the case of inclusive reactions. The cross section for a + b → c + X is given by a discontinuity of the

* Supported partially by a grant from the University of Helsinki, Finland.
** Present address.
*** We use the notation $s_{ab} = (p_a + p_b)^2$, $s_{a\bar{c}} = (p_a - p_c)^2$, etc.
† In ref. [2] the problem of formulating finite-energy sum rules for five point amplitudes that relate the low-energy region in $s_{ab}$ to the single-Regge limit is considered. This paper also contains a discussion of the general analyticity structure of the amplitude.

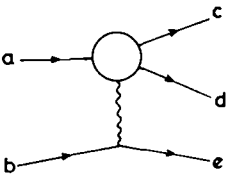


Fig. 1. The single-Regge limit of the process a + b → c + d + e.

amplitude for a + b + $\bar{c}$ → a + b + $\bar{c}$ in the forward direction [5], fig. 2a. In the limit when the missing mass is much smaller than the total energy, i.e. $s_{ab}/s_{ab\bar{c}} \gg 1$, the six-point amplitude is proportional to a reggeon-particle elastic amplitude (fig. 2b). In dual and ladder diagram models it turns out that the reggeon-particle amplitude has the singularity structure of a normal four-point function. Hence one may write down finite-mass sum rules [6], which connect the low missing-mass region with the triple-Regge limit. First applications of the FMSR to inclusive data are quite encouraging [7–9].

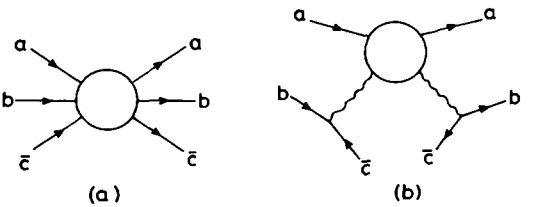


Fig. 2. (a) The six-point amplitude which is related to the inclusive reaction a + b → c + X. (b) A high-energy limit ($s_{ab}/s_{ab\bar{c}} \to \infty$ with $s_{b\bar{c}}$ fixed) of the amplitude in fig. 2a.

The reggeon-particle amplitude that we shall be concerned with here (fig. 1) is somewhat more general than the one encountered in inclusive distributions (fig. 2b). In the case of fig. 2b there is only one helicity amplitude contributing to the leading term, namely the one corresponding to a maximum helicity flip of the reggeons [10]. By contrast, there are many helicity states of the reggeon contributing [11] in fig. 1. The dependence on the helicity in this case can alternatively be seen as a dependence on the variable $\kappa = s_{cd}s_{de}/s_{ab}$. The reggeon-particle amplitude in fig. 1 also depends on the momentum transfer $s_{a\bar{c}}$. In the case of the inclusive reaction in fig. 2 the corresponding variables are equal to zero.

The structure of the amplitude for a + b → c + d + e in the double-Regge limit ($s_{cd} \to \infty$ in fig. 1) is already well-known [10, 11]. In this limit the amplitude decomposes into a sum of two terms, with cuts in $s_{cd}$ and in $s_{de}$, respectively. We shall in the following be concerned only with a part of the five-point amplitude which in the double-Regge limit gives the first term (with a cut in $s_{cd}$). This is also

the part which contains the poles in $s_{b\bar{c}}$ (when the reggeon is on-shell) and, according to the Steinmann relations [12], the normal threshold singularities and resonances in $s_{cd}$.

We investigate the singularity structure of this part of the amplitude in the single-Regge limit ($s_{cd}$ finite) using the dual resonance model (DRM) and a perturbation theory model. We find that when $\kappa = 0$ the reggeon-particle amplitude has the singularity structure of a normal four-point amplitude.

The FESR which follow from this analytic structure relate the absorptive part of the low $s_{cd}$ region to the first part of the double-Regge vertex. In the same way one can relate the other part of the double-Regge vertex to the low $s_{de}$ region.

When $\kappa \neq 0$ the reggeon-particle amplitude has singularities which are not present in normal four-point amplitudes. These singularities do not, however, contribute to the leading term in the discontinuity as $s_{cd} \to \infty$. The effect of the new singularities in the FESR is therefore that of an additional term which is independent of the cut-off.

In sect. 2 we discuss the structure of the amplitude in the double Regge limit. The single Regge limit is considered in sect. 3, where we investigate the analytic structure of two models, the dual resonance model and a perturbation theory model. The structure of the two models turns out to be very similar. In sect. 4 we discuss the modifications due to left-hand singularities and signature. All essential properties found in sect. 3 remain unaltered for the signatured amplitudes. The FESR are derived in sect. 5 and some applications are considered in sect. 6.

## 2. The double-Regge limit

We shall begin our investigation of the analytic structure of the five-point amplitude by considering the double-Regge limit (fig. 3). This is defined by letting $s_{ab}, s_{cd}, s_{de} \to \infty$ keeping $s_{a\bar{c}}, s_{b\bar{e}}$ and $\kappa = s_{cd}s_{de}/s_{ab}$ fixed. The structure of the amplitude in this limit has been investigated by several authors [10, 11, 13]. It has been shown that an amplitude with only right-hand cuts in the asymptotic variables takes the form*

$$T = (-s_{ab})^{\alpha_{b\bar{e}}}(-s_{cd})^{\alpha_{a\bar{c}}-\alpha_{b\bar{e}}} V_1(s_{b\bar{e}}, s_{a\bar{c}}; \kappa)$$

$$+ (-s_{ab})^{\alpha_{a\bar{c}}}(-s_{de})^{\alpha_{b\bar{e}}-\alpha_{a\bar{c}}} V_2(s_{a\bar{c}}, s_{b\bar{e}}; \kappa), \qquad (1)$$

where $\alpha_{b\bar{e}} \equiv \alpha(s_{b\bar{e}})$, etc. The vertex functions $V_1$ and $V_2$ are entire functions of $\kappa$.

The important feature of the decomposition of $T$ in eq. (1) is that only the first (second) term has a discontinuity in $s_{cd}(s_{de})$. If, according to duality, the Regge terms in eq. (1) are "built up" from resonances in $s_{cd}$ and $s_{de}$ we therefore

* This is true for amplitudes corresponding to planar Feynman diagrams and for planar dual models. For an example of the structure of a non-planar model see ref. [14].

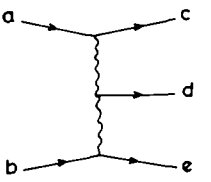


Fig. 3. The double Regge limit of the process a + b → c + d + e.

expect the first term in eq. (1) to be connected with the resonances in $s_{cd}$ and the second term with resonances in $s_{de}$. In fact, the residue of a resonance in $s_{cd}$ is a polynomial in $s_{de}$ and thus cannot contribute to the discontinuity in $s_{de}$ (i.e. to the second term in eq. (1)). The first term in eq. (1) also contains the poles in $\alpha_{b\bar{e}}$ when the reggeon $i$ goes on-shell. From the point of view of duality in the system $a + i \to c + d$ we therefore should consider only a part of the five-point amplitude $T$, which in the double-Regge limit gives the first term in eq. (1).

In deriving the FESR we shall start from a dispersion relation in $s_{cd}$ keeping $s_{ab}$, $s_{a\bar{c}}$, $s_{b\bar{e}}$ and $\kappa$ fixed (note that the limit $s_{ab} \to \infty$ has already been taken as in fig. 1). The reason for keeping $\kappa$ fixed is that we want the high-energy limit of the reggeon-particle amplitude ($s_{cd} \to \infty$) to be related to the double-Regge limit of the five-point function.

The variable $s_{de}$ can be expressed in terms of the independent variables as

$$s_{de} = \frac{\kappa s_{ab}}{s_{cd}} \; ; \tag{2}$$

substituting eq. (2) into the expression (1) for $T$ we get

$$T = (-s_{ab})^{\alpha_{b\bar{e}}} (-s_{cd})^{\alpha_{a\bar{c}} - \alpha_{b\bar{e}}} [V_1(s_{b\bar{e}}, s_{a\bar{c}}; \kappa) + (-\kappa)^{\alpha_{b\bar{e}} - \alpha_{a\bar{c}}} V_2(s_{a\bar{c}}, s_{b\bar{e}}; \kappa)]. \tag{3}$$

Both terms in eq. (3) now have a cut in $s_{cd}$, due to the relation (2). However, as discussed above only the first term can be dual to resonances in $s_{cd}$. The second term can be eliminated in either of two ways:

(i) By extrapolating to $\kappa = 0$. If $\alpha_{b\bar{e}} - \alpha_{a\bar{c}} > 0$ the second term in eq. (3) vanishes. As we shall see below the situation is analogous in the single-Regge limit. Thus at $\kappa = 0$ the reggeon-particle amplitude has only normal four-point singularities in $s_{cd}$ and a FESR can be derived. The FESR can be continued to $\alpha_{b\bar{e}} - \alpha_{a\bar{c}} < 0$ by subtracting out the term which is singular when $\kappa \to 0$.

(ii) By considering the amplitude $\widetilde{T}$:

$$\widetilde{T} = \frac{1}{2i \sin \pi(\alpha_{b\bar{e}} - \alpha_{a\bar{c}})} [e^{i\pi(\alpha_{b\bar{e}} - \alpha_{a\bar{c}})} T(s_{de} + i\epsilon)$$

$$- e^{-i\pi(\alpha_{b\bar{e}} - \alpha_{a\bar{c}})} T(s_{de} - i\epsilon)] \; . \tag{4}$$

In eq. (4), $T(s_{de} \pm i\epsilon)$ is the amplitude obtained in the single-Regge limit letting $s_{de} \to \infty$ above $(+i\epsilon)$ or below $(-i\epsilon)$ its cut. All other variables are to be evaluated in their physical limits. It follows from eq. (1) or eq. (3) that in the double-Regge limit

$$\tilde{T} = (-s_{ab})^{\alpha_{b\bar{e}}} (-s_{cd})^{\alpha_{a\bar{c}} - \alpha_{b\bar{e}}} V_1(s_{b\bar{e}}, s_{a\bar{c}}; \kappa) . \tag{5}$$

In the next section we consider the singularity structure of $\tilde{T}$ in the single Regge limit. It turns out that $\tilde{T}$ has certain singularities in $s_{cd}$ which are not present in normal four-point amplitudes. These come from the term $T(s_{de} - i\epsilon)$ in eq. (4), where the amplitude $T$ is evaluated in an unphysical limit. Such singularities cannot be determined from experimental data.

The additional singularities do not, however, contribute to the leading term (5) of $\tilde{T}$ in the double-Regge limit. This term is built up completely by the ordinary singularities in $s_{cd}$: The only effect of the extra singularities in the FESR is therefore to introduce a constant (i.e. cut-off independent) term on the l.h.s. of the sum rule.

This term vanishes in the limit $\kappa \to 0$, so that consistency with (i) is achieved.

## 3. The single-Regge limit

In this section we shall discuss the properties of the DRM and a perturbation theory model in the single-Regge limit shown in fig. 1. We consider amplitudes with only right-hand singularities, signature being introduced in the next section.

### *3.1. The dual resonance model*

In the single-Regge limit of fig. 1 the $B_5$ amplitude can be expressed in terms of the hypergeometric function* $F(a, b; c; z)$

$$B_5 = \Gamma(-\alpha_{b\bar{e}})(-\alpha_{ab})^{\alpha_{b\bar{e}}} [B_4(-\alpha_{cd}, -\alpha_{a\bar{c}} + \alpha_{b\bar{e}}) \times F\left(-\alpha_{b\bar{e}}, -\alpha_{cd}; 1 - \alpha_{b\bar{e}} + \alpha_{a\bar{c}}; \frac{\kappa}{s_{cd}}\right) + \left(\frac{\kappa}{s_{cd}}\right)^{\alpha_{b\bar{e}} - \alpha_{a\bar{c}}} \times B_4(-\alpha_{a\bar{c}}, -\alpha_{b\bar{e}} + \alpha_{a\bar{c}}) F(-\alpha_{a\bar{c}}, -\alpha_{cd} - \alpha_{a\bar{c}} + \alpha_{b\bar{e}}; 1 - \alpha_{a\bar{c}} + \alpha_{be}; \frac{\kappa}{s_{cd}})] . \tag{6}$$

From this expression we can see the following.

(i) If $\kappa = 0$ and $\alpha_{b\bar{e}} - \alpha_{a\bar{c}} > 0$,

$$B_5 = \Gamma(-\alpha_{b\bar{e}})(-\alpha_{ab})^{\alpha_{b\bar{e}}} B_4(-\alpha_{cd}, -\alpha_{a\bar{c}} + \alpha_{b\bar{e}}) . \tag{7}$$

* See ref. [15]. The definition of the hypergeometric function is given in ref. [16].

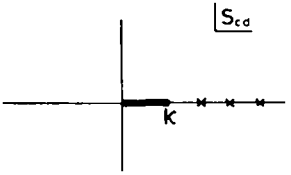


Fig. 4. The singularity structure in $s_{cd}$ of the amplitude $\tilde{T}$ in the dual resonance model. The crosses correspond to poles and the thick line to a cut.

In this case the reggeon-particle amplitude is given by a $B_4$ function. The derivation of the FESR can be done as for a four a four-point function. If $\alpha_{b\bar{e}} - \alpha_{a\bar{c}} < 0$ but, say, $\alpha_{b\bar{e}} - \alpha_{a\bar{c}} > -1$, we can consider the amplitude

$$B_5' = B_5 - \left(\frac{\kappa}{s_{cd}}\right)^{\alpha_{b\bar{e}} - \alpha_{a\bar{c}}} B_4(-\alpha_{ac}, -\alpha_{b\bar{e}} + \alpha_{ac})\,\Gamma(\alpha_{b\bar{e}})(-\alpha_{ab})^{\alpha_{b\bar{e}}} \qquad (8)$$

As $\kappa \to 0$ we find that $B_5'$ reduces to a $B_4$ function as in eq. (7). The FESR which were derived for $\alpha_{b\bar{e}} - \alpha_{a\bar{c}} > 0$ can thus be continued to $\alpha_{b\bar{e}} - \alpha_{a\bar{c}} < 0$ by substracting out the terms which are singular when $\kappa \to 0$. In the double-Regge limit (3) this means that only the first ($V_1$) of the two terms is present. The FESR are therefore going to relate an integral over the absorptive part in $s_{cd}$ to the first term in the double-Regge limit, as we already anticipated above.

(ii) When $\kappa \neq 0$ we can use the definition (4) to calculate $\tilde{T}$. The expression (6) for $T$ is real when the variables $\alpha_{ab}$ and $\alpha_{de}$ are negative. Continuing $\alpha_{de}$ to positive values, using eq. (2) and the $\pm i\epsilon$ prescription at the branch point $\alpha_{de} = 0$, we get

$$\tilde{T} = \Gamma(-\alpha_{b\bar{e}})(-\alpha_{ab})^{\alpha_{b\bar{e}}} B_4(-\alpha_{cd}, -\alpha_{a\bar{c}} + \alpha_{b\bar{e}})$$

$$\times F\left(-\alpha_{b\bar{e}}, -\alpha_{cd}; 1 - \alpha_{b\bar{e}} + \alpha_{a\bar{c}}; \frac{\kappa}{s_{cd}}\right). \qquad (9)$$

From eq. (9) one can directly see the singularity structure of $\tilde{T}$ in $s_{cd}$ (fig. 4). There is a series of poles corresponding to resonances at $\alpha_{cd} = n$, $n = 0, 1, 2, \ldots$. In addition the $F$-function gives rise to a cut $0 \leqslant s_{cd} \leqslant \kappa$. This cut corresponds to a singularity of $B_5$ on an unphysical sheet in $s_{de}$. Thus it cannot be determined directly from experimental data. However, we may still derive a useful FESR from the singularity structure of fig. 4. The cut $0 \leqslant s_{cd} \leqslant \kappa$ gives in the FESR rise to a term which is independent of the cut-off. It can therefore be eliminated by varying the cut-off.

### *3.2. The perturbation theory model*

Consider the five-point function $T$ generated by a sum of Feynman diagrams in

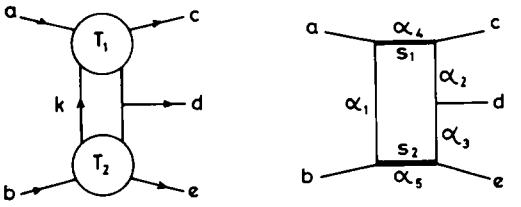


Fig. 5. (a) Diagrammatic representation of the perturbation theory model considered in the text. The internal lines correspond to scalar particles and the blobs $T_1$ and $T_2$ represent sums of planar Feynman diagrams. (b) The same amplitude as in fig. 5a; the thick lines indicate the energies which are dispersed in.

$\phi^3$ theory*. We may describe the amplitude by the diagram in fig. 5a, where the blobs $T_1$ and $T_2$ represent sums of planar Feyman diagrams. We assume that the amplitudes $T_1$ and $T_2$ satisfy unsubtracted dispersion relations:

$$T_1((p_a + k)^2, s_{a\bar{c}}) = \int_0^\infty \frac{\sigma_1(s_1, s_{a\bar{c}})\,ds_1}{(p_a + k)^2 - s_1}, \tag{10}$$

and similarly for the amplitude $T_2$. We shall also assume that $T_1$ and $T_2$ are Regge behaved at high energy. Thus as $s_1 \to \infty$,

$$\sigma_1(s_1, s_{a\bar{c}}) \simeq \beta_1(s_{a\bar{c}}) s_1^{\alpha_{a\bar{c}}}, \tag{11}$$

with a similar relation for $\sigma_2$ when $s_2 \to \infty$.

The five-point amplitude $T$ of fig. 5a can now be expressed as (we take the mass of the propagating particles to be $\mu$)

$$T = -ig \int \{\sigma_1(s_1, s_{a\bar{c}})\, \sigma_2(s_2, s_{b\bar{e}})\, ds_1\, ds_2 d^4k\} \{[k^2 - \mu^2]\, [(k + p_a - p_c)^2 - \mu^2]\, [(k + p_e - p_b)^2 - \mu^2]\, [(k + p_a)^2 - s_1]\, [(k - p_b)^2 - s_2]\}^{-1}. \tag{12}$$

Apart from the integrations over $s_1$ and $s_2$, $T$ has the structure of a simple box diagram (fig. 5b). Converting to the $\alpha$-representation [1], the integration over the loop momentum can be done. We get then

$$T = 2g\pi^2 \int \frac{\sigma_1(s_1, s_{a\bar{c}})\, \sigma_2(s_2, s_{b\bar{e}})\, ds_1\, ds_2 \prod_{i=1}^{5} d\alpha_i\, \delta\left(\sum_{i=1}^{5} \alpha_i - 1\right)}{[d + i\epsilon]^3}, \tag{13}$$

* For a review of the high-energy behaviour of Feynman diagrams, see ref. [1]. Models similar to that presented here have been studied by, for example, Drummond et al. [11] and Sanda [6].

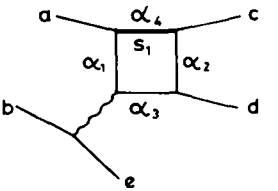


Fig. 6. The single-Regge limit of the amplitude shown in fig. 5.

where

$$d = \alpha_1\alpha_2 s_{a\bar{c}} + \alpha_1\alpha_3 s_{b\bar{e}} + \alpha_3\alpha_4 s_{cd} + \alpha_2\alpha_5 s_{de} + \alpha_4\alpha_5 s_{ab}$$
$$+ \alpha_1\alpha_4 m_a^2 + \alpha_2\alpha_4 m_c^2 + \alpha_2\alpha_3 m_d^2 + \alpha_3\alpha_5 m_e^2 + \alpha_1\alpha_5 m_b^2$$
$$- (\alpha_1 + \alpha_2 + \alpha_3)\mu^2 - \alpha_4 s_1 - \alpha_5 s_2 . \tag{14}$$

To find the structure of $T$ in the single Regge limit of fig. 1 we let $s_{ab} \to -\infty$ and $s_{de} \to -\infty$ keeping $s_{de}/s_{ab}$ fixed. When $-1 < \alpha_{b\bar{e}} < 0$ the leading contribution to the integral in eq. (13) comes from large $s_2$. Substituting the Regge expression (11) for $\sigma_2$ we find (the derivation is given in the appendix)

$$T = g\pi^3 \frac{\beta_2(s_{b\bar{e}})}{\sin \pi\alpha_{b\bar{e}}} \int_0^\infty ds_1\, \sigma_1(s_1, s_{a\bar{c}}) \int_0^1 \prod_{i=1}^4 d\alpha_i \frac{\delta\left(\sum_{i=1}^4 \alpha_i - 1\right)}{(d' + i\epsilon)^2}$$
$$\times (-\alpha_2 s_{de} - \alpha_4 s_{ab})^{\alpha_{b\bar{e}}} , \tag{15}$$

where $d'$ is obtained from $d$ by putting $\alpha_5 = 0$:

$$d' = \alpha_1\alpha_2 s_{a\bar{c}} + \alpha_1\alpha_3 s_{b\bar{e}} + \alpha_3\alpha_4 s_{cd} + \alpha_1\alpha_4 m_a^2 + \alpha_2\alpha_4 m_c^2$$
$$+ \alpha_2\alpha_3 m_d^2 - (\alpha_1 + \alpha_2 + \alpha_3)\mu^2 - \alpha_4 s_1 . \tag{16}$$

The structure of the amplitude $T$ in eq. (15) is essentially that of the box diagram in fig. 6, the reggeon being treated as a scalar particle. The only difference is that the integrand is multiplied by a factor $(-\alpha_2 s_{de} - \alpha_4 s_{ab})^{\alpha_{b\bar{e}}}$, which describes the correlations due to the Reggeon spin. It is interesting to note that the amplitude (15) looks very similar to the DRM in this respect [17].

Consider now the limit $\kappa \to 0$. This implies $s_{de} \to 0$ in eq. (15), so that the extra factor in the integrand reduces to $(-\alpha_4 s_{ab})^{\alpha_{b\bar{e}}}$. The singularity structure of $T$ is then determined by the zeroes of the denominator function $d'$ in eq. (15). Hence the reggeon-particle amplitude in fig. 6 has the singularity structure of a normal four-point function.

We must still verify that the integral over $s_1$ in eq. (15) converges. The behaviour of $\sigma_1(s_1, s_{a\bar{c}})$ at large $s_1$ is given by eq. (11) and ensures convergence of the representation (15) when $\alpha_{b\bar{e}} - \alpha_{a\bar{c}} > 0$. If $\alpha_{b\bar{e}} - \alpha_{a\bar{c}} < 0$ there is a singular term in $T$ when $\kappa \to 0$, proportional to $(-\kappa)^{\alpha_{b\bar{e}} - \alpha_{a\bar{c}}}$. The singularity does not depend on $s_{cd}$ and is therefore the same as the singularity in the double-Regge limit, eq. (3). As in the case of the DRM above we can subtract this singularity from the amplitude. The amplitude has then, for all values of $\alpha_{b\bar{e}} - \alpha_{a\bar{c}}$, only the singularities which come from the vanishing of the denominator function $d'$ in eq. (15).

If $\kappa \neq 0$ it can readily be seen that the amplitude $\tilde{T}$, defined by eqs. (4) and (15), has singularities in $s_{cd}$ which are not associated with zeroes of the denominator function $d'$. However, as in the case of the DRM these new singularities are not present in the leading term when $s_{cd} \to \infty$. In this limit the structure of $T$ is given by eq. (3). The only singularities of $\tilde{T}$ (eq. (5)) are those of the first term in eq. (3), and correspond to normal singularities in $s_{cd}$ (i.e. to zeroes of the denominator function).

If follows that also when $\kappa \neq 0$ the properties of the perturbation theory model (12) are similar to those of the DRM. An FESR can be derived, to which the new singularities contribute a term which does not depend on the cut-off. This term goes to zero in the limit $\kappa \to 0$.

## 4. Signature

Before we can write down the FESR we should construct amplitudes with definite signature in the $b\bar{e}$ and $a\bar{c}$ channels. Such amplitudes are most conveniently described using variables which are symmetric (or antisymmetric) under crossing. We shall begin be defining as set of such variables. We then discuss the effects of signature in the double Regge limit. Finally we use the DRM to study the properties of the signatured amplitude in the single-Regge limit.

### *4.1. Crossing-symmetric variables*

In the double-Regge limit (fig. 3) all the large variables have simple properties under crossing. For example under line reversal in the $a\bar{c}$ channel (i.e. $a \leftrightarrow \bar{c}$) $s_{ab} = -s_{\bar{c}b}$. This is no longer true in the single Regge limit (fig. 1). The three large variables $s_{ab}$, $s_{\bar{c}b}$ and $s_{de}$ are related through

$$s_{de} = s_{ab} + s_{\bar{c}b} \tag{17}$$

(we ignore terms like $s_{cd}/s_{ab}$ which vanish in the single-Regge limit). From eq. (17) we can see that $s_{de}$ is symmetric when $a \leftrightarrow \bar{c}$. Instead of $s_{ab}$ we shall choose as our independent variable the combination $\sigma$, which is antisymmetric when $a \leftrightarrow \bar{c}$:

$$\sigma = \tfrac{1}{2}(s_{ab} - s_{\bar{c}b}) . \tag{18}$$

Both $s_{de}$ and $\sigma$ are antisymmetric under $b \leftrightarrow \bar{e}$.

In analogy with four-point amplitudes we shall use the crossingodd variable $\nu$,

$$\nu = (p_a + p_c) \cdot p_d = s_{cd} + \tfrac{1}{2}(s_{a\bar{c}} - s_{b\bar{e}} - 2m_c^2 - m_d^2), \tag{19}$$

to describe the reggeon-particle amplitude (instead of $s_{cd}$). Finally we define the variable

$$\kappa_s = -\frac{\upsilon s_{de}}{\sigma} \tag{20}$$

which is symmetric both under $a \leftrightarrow \bar{c}$ and $b \leftrightarrow \bar{e}$, and replaces $\kappa = s_{cd}s_{de}/s_{ab}$ used above.

### *4.2. The double-Regge limit*

Let $T_{\tau_1\tau_2}$ be an amplitude with signature $\tau_1$ in the $b\bar{e}$ channel and $\tau_2$ in the $a\bar{c}$ channel. This amplitude can be constructed by adding four terms as in fig. 7, where a cross indicates that the reggeon line is to be twisted. The double-Regge limit of the amplitude in fig. 7a is given in eq. (1). The other amplitudes in fig. 7 are similar, except that they have left-hand cuts in some of the large variables. The full amplitude is then [13, 18, 19]

$$\begin{aligned} T_{\tau_1\tau_2} = {} & [(-\sigma)^{\alpha_{b\bar{e}}} + \tau_1(\sigma)^{\alpha_{b\bar{e}}}]\,[(-\upsilon)^{\alpha_{a\bar{c}} - \alpha_{b\bar{e}}} + \tau_1\tau_2(\upsilon)^{\alpha_{a\bar{c}} - \alpha_{b\bar{e}}}]\, V_1(s_{b\bar{e}}, s_{a\bar{c}}; \kappa) \\ & + [(-\sigma)^{\alpha_{a\bar{c}}} + \tau_2(\sigma)^{\alpha_{a\bar{c}}}]\,[(-s_{de})^{\alpha_{b\bar{e}} - \alpha_{a\bar{c}}} \\ & + \tau_1\tau_2(s_{de})^{\alpha_{b\bar{e}} - \alpha_{a\bar{c}}}]\, V_2(s_{a\bar{c}}, s_{b\bar{e}}; \kappa). \end{aligned} \tag{21}$$

The structure of $T_{\tau_1\tau_2}$ in the double-Regge limit is similar to that of the amplitude $T$ (eq. (1)). There are two terms in eq. (21), the first of which has cuts in $\sigma$ and $\upsilon$, and the second in $\sigma$ and $s_{de}$. As before, only the first term in eq. (21) can be dual to resonances in $\upsilon$. The second term may be eliminated either by taking the limit $\kappa_s \to 0$ (which implies $s_{de} \to 0$ in eq. (17)) or, if $\kappa_s \neq 0$, by defining a new amplitude $\tilde{T}_{\tau_1\tau_2}$.

Analogously to what was done in sect. 2, we define $\tilde{T}_{\tau_1\tau_2}$ by an analytic continuation in $s_{de}$. In the physical limit of the amplitude $T_{\tau_1\tau_2}$ all variables approach their cuts from above ($+i\epsilon$). We denote this limit of $T_{\tau_1\tau_2}$ by $T_{\tau_1\tau_2}(s_{de} + i\epsilon)$. We now define the limit $T_{\tau_1\tau_2}(s_{de} - i\epsilon)$, where all variables approach their cuts from above except $s_{de}$, which approaches from below ($-i\epsilon$). $T_{\tau_1\tau_2}(s_{de} - i\epsilon)$ can be obtained from the physical limit by continuig $s_{de}$ along a circle, keeping $\sigma$ and $\upsilon$ fixed. This is illustrated in fig. 8 for the case of a term with a righthand cut in $s_{de}$.

When continuing $s_{de}$ we have to take care not to encircle the branch points at $s_{ab} = 0$ and $s_{\bar{c}b} = 0$, as these variables would then be evaluated in an unphysical

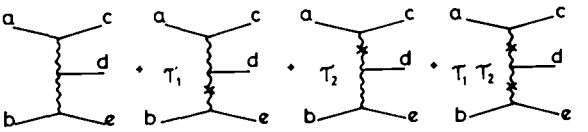


Fig. 7. The four terms which have to be added to obtain a definite signature $\tau_1$ in the $b\bar{e}$ channel and $\tau_2$ in the $a\bar{c}$ channel. A cross indicates that the reggeon line is to be twisted.

limit. It follows from eqs. (17) and (18) that this is ensured if $|s_{de}/\sigma| < 2$ during the continuation. This restriction is of course, only relevant in the single-Regge limit.

The definition of $\tilde{T}_{\tau_1\tau_2}$ is the same as that of $\tilde{T}$, given by eq. (4):

$$\tilde{T}_{\tau_1\tau_2} = \frac{1}{2i\sin\pi(\alpha_{b\bar{e}} - \alpha_{a\bar{c}})}\left[e^{i\pi(\alpha_{b\bar{e}} - \alpha_{a\bar{c}})}T_{\tau_1\tau_2}(s_{de} + i\epsilon)\right.$$

$$\left. - e^{-i\pi(\alpha_{b\bar{e}} - \alpha_{a\bar{c}})}T_{\tau_1\tau_2}(s_{de} - i\epsilon)\right] . \tag{22}$$

In the double-Regge limit only the first term of $T_{\tau_1\tau_2}$ (eq. (21)) contributes to $\tilde{T}_{\tau_1\tau_2}$:

$$\tilde{T}_{\tau_1\tau_2} = [(-\sigma)^{\alpha_{b\bar{e}}} + \tau_1(\sigma)^{\alpha_{b\bar{e}}}]\,[(-\upsilon)^{\alpha_{a\bar{c}} - \alpha_{b\bar{e}}}$$

$$+ \tau_1\tau_2(\upsilon)^{\alpha_{a\bar{c}} - \alpha_{b\bar{e}}}]\, V_1(s_{b\bar{e}}, s_{a\bar{c}}; \kappa) . \tag{23}$$

We therefore expect that the $\upsilon$-discontinuity of $\tilde{T}_{\tau_1\tau_2}$ in eq. (23) is dual to normal singularities (resonances) in $\upsilon$.

### *4.3. The single-Regge limit*

We shall now investigate the structure of $\tilde{T}_{\tau_1\tau_2}$ in the single-Regge limit (fig. 1) using the DRM. In this model $T_{\tau_1\tau_2}$ is a sum of four $B_5$ functions as in fig. 7. A twist on a reggeon line indicates that the ordering of two particles is to be reversed.

The amplitude for the diagram in fig. 7a is given in eq. (6), and the other three amplitudes can be obtained by replacing $a \leftrightarrow \bar{c}$, $b \leftrightarrow \bar{e}$. All amplitudes consist of two terms, of which only the first contributes to $\tilde{T}_{\tau_1\tau_2}$. The expression for $\tilde{T}_{\tau_1\tau_2}$ in the single-Regge limit is thus

$$\tilde{T}_{\tau_1\tau_1} = \Gamma(-\alpha_{b\bar{e}})[(-\sigma)^{\alpha_{b\bar{e}}} + \tau_1(\sigma)^{\alpha_{b\bar{e}}}]$$

$$\times\left[\left(1 + \frac{1}{2}\frac{\kappa_s}{\upsilon}\right)^{\alpha_{b\bar{e}}} B_4(-\alpha_{cd}, -\alpha_{a\bar{c}} + \alpha_{b\bar{e}})F\left(-\alpha_{b\bar{e}}, -\alpha_{cd}; 1 - \alpha_{b\bar{e}} + \alpha_{a\bar{c}}; \frac{\kappa_s/\upsilon}{1 + \frac{1}{2}\kappa/\upsilon}\right)\right.$$

$$\left. + \tau_1\tau_2\left(1 - \frac{1}{2}\frac{\kappa_s}{\upsilon}\right)^{\alpha_{b\bar{e}}} B_4(-\alpha_{a\bar{d}}, -\alpha_{a\bar{c}} + \alpha_{b\bar{e}})F\left(-\alpha_{b\bar{e}}, -\alpha_{a\bar{d}}; 1 - \alpha_{b\bar{e}} + \alpha_{a\bar{c}}; -\frac{\kappa_s/\upsilon}{1 - \frac{1}{2}\kappa_s/\upsilon}\right)\right]$$

(24)

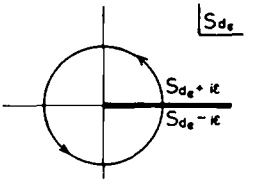


Fig. 8. The path of continuation in $s_{de}$ used in the definition of $T_{\tau_1\tau_2}(s_{de}-i\epsilon)$. The singularity structure is that of an amplitude with a right-hand cut in $s_{de}$. Note that the branch point of an amplitude with a left-hand cut in $s_{de}$ is similarly encircled.

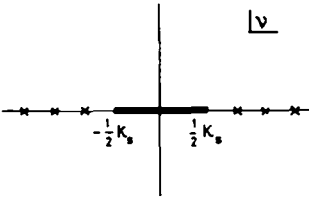


Fig. 9. The singularity structure in $s_{cd}$ of the signatured amplitude $\tilde{T}_{\tau_1\tau_2}$ in the dual resonance model. Crosses correspond to poles and the thick line to a cut.

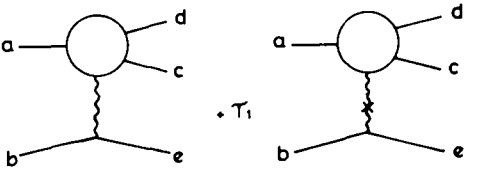


Fig. 10. The two $B_5$ functions given by eq. (25) in the text.

If in eq. (24) we let $\kappa_s \to 0$ we find that $\tilde{T}_{\tau_1\tau_2}$ reduces to a sum of $B_4$ functions. The only singularities of $\tilde{T}_{\tau_1\tau_2}$ in $\upsilon$ are then the resonance poles. When $\kappa_s \neq 0$ $\tilde{T}_{\tau_1\tau_2}$ has, in addition, a cut in $\upsilon$ for $-\frac{1}{2}\kappa_s \leqslant \upsilon \leqslant \frac{1}{2}\kappa_s$ (see fig. 9). Hence the properties of the signatured amplitude are very similar to those of the non-signatured amplitude that we discussed in the previous section.

There are two more $B_5$ functions which contribute to the single-Regge limit, in addition to the four shown in fig. 7. They are shown in fig. 10. Denoting their combined contribution by $B_5(s,u)$ we have

$$B_5(s,u) = \Gamma(-\alpha_{b\bar{e}})[(-\sigma)^{\alpha_{b\bar{e}}} + \tau_1(\sigma)^{\alpha_{b\bar{e}}}]\left(1+\frac{1}{2}\frac{\kappa_s}{\upsilon}\right)^{\alpha_{b\bar{e}}}$$

$$\times B_4(-\alpha_{cd}, -\alpha_{a\bar{d}})F\left(-\alpha_{b\bar{e}}, -\alpha_{cd}; -\alpha_{cd}-\alpha_{a\bar{d}}; \frac{\kappa_s/\upsilon}{1+\frac{1}{2}\kappa_s/\upsilon}\right). \tag{25}$$

The singularity structure of $B_5(s,u)$ is the same as that of $\tilde{T}_{\tau_1\tau_2}$ in eq. (24) and shown in fig. 9. $B_5(s,u)$ is symmetric under $a \leftrightarrow \bar{c}$ and vanishes exponentially [19] in the double-Regge limit. It must therefore be superconvergent.

We have now investigated all amplitudes that contribute to the single-Regge limit in the DRM. The properties of the amplitudes with definite signature in the $b\bar{e}$ and $a\bar{c}$ channels are completely analogous to the properties of the amplitude with only right-hand singularities, discussed in sect. 3. The conclusions about the singularity structure which we reached in that section are therefore valid for the full amplitude with right- and left-hand singularities.

A similar analysis can be done using the perturbation theory model described in sect. 3. The conclusions reached are the same as for the DRM.

## 5. The finite-energy sum rules

We define the reggeon-particle amplitude $f_i(\upsilon, s_{a\bar{c}}, s_{b\bar{e}}, \kappa_s)$ for the process $a + i \to c + d$ (fig. 1) by the relation

$$\tilde{T}_i = \beta^i_{b\bar{e}}(s_{b\bar{e}})\frac{\tau_i + e^{-i\pi\alpha_i(s_{b\bar{e}})}}{\sin\pi\alpha_i(s_{b\bar{e}})}\,\sigma^{\alpha_i(s_{b\bar{e}})}f_i\,. \tag{26}$$

In eq. (26), $\tilde{T}_i$ is the amplitude related as in eq. (22) to the amplitude $T_i$ for the process $a + b \to c + d + e$, the reggeon $i$ being exchanged in the $b\bar{e}$ channel (fig. 1). $\beta^i_{b\bar{e}}$ is the reggeon-particle-particle vertex function, and the definition of the variables $\sigma$, $\upsilon$ and $\kappa_s$ is given in eqs. (18), (19) and (20).

From our discussion above we expect that $f_i$, as a function of $\upsilon$, has the normal singularities of a four-point function when $\kappa_s = 0$. If $\kappa_s \neq 0$ there are additional singularities which do not, however, contribute to the limit $|\upsilon| \to \infty$ of $f_i$. In the DRM these additional singularities take the form of a cut $-\frac{1}{2}\kappa_s \leqslant \upsilon \leqslant \frac{1}{2}\kappa_s$ (see fig. 9).

According to (23) and 26) the behaviour of $f_i$ as $\upsilon \to \infty$ is

$$f_i = \sum_j \beta^j_{a\bar{c}}(s_{a\bar{c}})\frac{\tau_i\tau_j + \exp\left[-i\pi(\alpha_j(s_{a\bar{c}}) - \alpha_i(s_{b\bar{e}}))\right]}{\sin\pi\left[\alpha_i(s_{b\bar{e}}) - \alpha_j(s_{a\bar{c}})\right]}$$

$$\times \upsilon^{\alpha_j(s_{a\bar{c}}) - \alpha_i(s_{b\bar{e}})}V^d_{ij}(s_{b\bar{e}}, s_{a\bar{c}}; \kappa)\,, \tag{27}$$

where $V_{ij}^{\mathrm{d}}$ is the part of the reggeon ($i$) -- reggeon ($j$) – particle (d) vertex which is multiplied by $\upsilon$ (i.e. $V_1$ in eq. (21)).

The FESR for the amplitude $f_i$ can now be derived in the standard way [3, 4]. They are

$$c_i^{(n)}(s_{\mathrm{b}\bar{\mathrm{e}}}, s_{\mathrm{a}\bar{\mathrm{c}}}; \kappa_s) + \int_{\upsilon_0}^{N} \mathrm{d}\nu\, \nu^n \,\mathrm{Im}\,[f_i(\nu + i\epsilon) + (-1)^{n+1} f_i(-\nu - i\epsilon)]$$

$$= \sum_j [1 + (-1)^{n+1} \tau_i \tau_j]\, \beta_{\mathrm{a}\bar{\mathrm{c}}}^j(s_{\mathrm{a}\bar{\mathrm{c}}})\, V_{ij}^{\mathrm{d}}(s_{\mathrm{b}\bar{\mathrm{e}}}, s_{\mathrm{a}\bar{\mathrm{c}}}; \kappa_s)$$

$$\times \frac{N^{\alpha_j(s_{\mathrm{a}\bar{\mathrm{c}}}) - \alpha_i(s_{\mathrm{b}\bar{\mathrm{e}}}) + n + 1}}{\alpha_j(s_{\mathrm{ac}}) \quad \alpha_i(s_{\mathrm{b}\bar{\mathrm{e}}}) + n + 1}, \tag{28}$$

where

$$\mathrm{Im}\, f_i(\nu \pm i\epsilon) = \frac{1}{2i}[f_i(\nu \pm i\epsilon, s_{\mathrm{a}\bar{\mathrm{c}}}, s_{\mathrm{be}}, \kappa_s) - f_i(\nu \mp i\epsilon, s_{\mathrm{a}\bar{\mathrm{c}}}, s_{\mathrm{b}\bar{\mathrm{e}}}, \kappa_s)]\ .$$

The integral in eq. (28) is over the normal four-point singularities of $f_i$ (i.e. pole terms, resonances, etc.). The additional singularities of $f_i$ contribute the term $c_i^{(n)}$.

As discussed in the previous sections, $c_i^{(n)}(s_{\mathrm{b}\bar{\mathrm{e}}}, s_{\mathrm{a}\bar{\mathrm{c}}}; \kappa_s)$ vanishes as $\kappa_s \to 0$. In the DRM it is readily seen that

$$c_i^{(n)}(s_{\mathrm{b}\bar{\mathrm{e}}}, s_{\mathrm{a}\bar{\mathrm{c}}}; \kappa_s) \propto (\kappa_s)^{n+1} \qquad \text{as} \qquad \kappa_s \to 0\,. \tag{29}$$

For small $\kappa_s$ the higher moment sum rules are thus less sensitive to the unknown term $c_i^{(n)}$.

## 6. Applications

At present the only way of obtaining $\mathrm{Im}\, f_i(\nu)$ in eq. (28) from experimental data is to assume that the absorptive part is dominated by the resonance contributions. The consistency of eq. (28) with the data can then be tested by varying the cut-off $N$. This should be done at several values of $\kappa_s$ and $n$, so that the restriction (29) can be applied.

Such an application of the FESR is analogous to a recent analysis [8] of quasi-two-body reactions using the inclusive FMSR. However, it should give considerably more information, as not only the total production cross section of the resonances but also their decay distributions can be correlated. In addition, one can avoid certain resonances whose production mechanisms are not clearly understood (e.g., Q may contribute to K + f → anything but not to K + f → K + $\pi$).

In general the two parts of the double-Regge vertex have to be generated separately by summing over resonances in $s_{cd}$ and in $s_{de}$ (and their crossed channels). In some applications, however, the two parts can be related to each other by exchange-degeneracy arguments. This happens in particular when particle d is a $\pi$-meson and the reggeons exchanged are any of the four meson trajectors f-$\rho$-$\omega$-$A_2$. As we think this case may be of practical interest we shall discuss it in some detail here.

Consider the system $ab\bar{c}\bar{d}e = K^-K^+K^+\pi^-\bar{K}^0$ in the double-Regge limit as in fig. 11a (all particles are treated as incoming). As in sect. 4 we shall assume that the contribution of a given exchange $(\alpha_i(s_{b\bar{e}}), \alpha_j(s_{a\bar{c}}))$ to the amplitude $T$ is of the form

$$T(i,j) = [(-\sigma)^{\alpha_{b\bar{e}}} + \tau_i \sigma^{\alpha_{b\bar{e}}}]\,[(-\nu)^{\alpha_{a\bar{c}} - \alpha_{b\bar{e}}} + \tau_i\tau_j{}^{\alpha_{a\bar{c}} - \alpha_{b\bar{e}}}]\, V_1(i,j)$$

$$+ [(-\sigma)^{\alpha_{a\bar{c}}} + \tau_j \sigma^{\alpha_{a\bar{c}}}]\,[(-s_{de})^{\alpha_{b\bar{e}} - \alpha_{a\bar{c}}} + \tau_i\tau_j s_{de}^{\alpha_{b\bar{e}} - \alpha_{a\bar{c}}}]\, V_2(j,i)\,. \qquad (30)$$

The full amplitude is

$$T = T(A_2^+, f) + T(A_2^+, \rho^0) + T(\rho^+, \omega) + T(\rho^+, A_2^0)\,. \qquad (31)$$

By drawing the duality diagrams it is easy to see that the only planar diagram is the one where the particles a, b, c, d, e are ordered as in fig. 11a. This means that the full amplitude $T$ should have only a right-hand cut in each of the variables $\sigma$, $\nu$ and $s_{de}$. Hence six of the eight terms in eq. (30) have to cancel in the sum (31). This gives six relations between the vertex functions $V_k(i,j)$, $k = 1,2$.

Six further relations can be obtained by considering the system $ab\bar{c}\bar{d}e = K^+K^-\bar{K}^0\pi^-K^+$ (fig. 11b). Combined with isospin invariance these relations imply that all non-zero vertex functions $V_k(i,j)$ are degenerate ($k = 1, 2$):

$$V_k(A_2^+, f) = V_k(\rho^+, \omega) = V_k(A_2^+, \rho^0)$$

$$= -V_k(f, A_2^+) = -V_k(\omega, \rho^+) = -V_k(\rho^0, A_2^+)\,, \qquad k = 1, 2$$

Finally, observing that the process in fig. 11a is identical to the one in fig. 11b,

$$V_1(A_2^+, f) = V_2(A_2^+, f)\,.$$

It follows that all the vertex functions are related.

The degeneracy of the vertex functions means that the full double-Regge vertex can be obtained by summing the resonances in only one system, e.g. in $s_{cd}$. Consistency with the sum of resonance in the other system ($s_{de}$) then requires that the two sets of resonances must be related. These predictions make the application of the FESR particularly interesting to reactions where f, $\rho$, $\omega$ or $A_2$ are the dominating exchanges.

We are grateful to all our colleagues for helpful discussions. One of us (J.K.) is indebted to Dr. R.J.N. Phillips for his kind hospitality at the Theory Division of the Rutherford Laboratory, where this work has been done.

## Appendix

In this appendix we shall derive the explicit expressions for the perturbation theory amplitude $T$ in the single- and double-Regge limits. The definition of $T$ in the non-asymptotic region is given by eqs. (13) and (14). We shall assume that $-1 < \alpha_{b\bar{e}}, \alpha_{a\bar{c}} < 0$. It is straightforward to continue the expressions to arbitrary values of the momentum transfers.

In the single Regge limit $s_{ab} \to -\infty$, $s_{de} \to -\infty$ while $s_{de}/s_{ab}$, $s_{cd}$, $s_{b\bar{e}}$ and $s_{a\bar{c}}$ remain fixed. The leading contribution to the integral in eq. (13) comes from large $s_2$. Substituting the leading behaviour of $\sigma_2$,

$$\sigma_2(s_2, s_{b\bar{e}}) \simeq \beta_2(s_{b\bar{e}}) s_2^{\alpha_{b\bar{e}}}, \qquad s_2 \to \infty, \tag{A.1}$$

in eq. (13), the integral over $s_2$ can be explicitly done. We get

$$T = g\pi^3 \beta_2(s_{b\bar{e}})\, \alpha_{b\bar{e}}\, (\alpha_{b\bar{e}} - 1)\, \frac{e^{-i\pi\alpha_{b\bar{e}}}}{\sin \pi\alpha_{b\bar{e}}}$$

$$\times \int_0^\infty \sigma_1(s_1, s_{a\bar{c}})\, ds_1 \int_0^1 \prod_{i=1}^{5} d\alpha_i \frac{\delta\left(\sum_{i=1}^{5} \alpha_i - 1\right) \alpha_5^{-\alpha_{b\bar{e}} - 1}}{[d'' + i\epsilon]^{2-\alpha_{b\bar{e}}}}, \tag{A.2}$$

where

$$d'' = \alpha_5(\alpha_2 s_{de} + \alpha_4 s_{ab}) + \alpha_1\alpha_2 s_{a\bar{c}} + \alpha_1\alpha_2 s_{b\bar{e}}$$

$$+ \alpha_3\alpha_4 s_{cd} + \alpha_1\alpha_4 m_a^2 + \alpha_2\alpha_4 m_c^2 + \alpha_2\alpha_3 m_d^2 + \alpha_3\alpha_5 m_e^2$$

$$+ \alpha_1\alpha_5 m_b^2 - (\alpha_1 + \alpha_2 + \alpha_3)\mu^2 - \alpha_4 s_1 . \tag{A.3}$$

Because the large variables $s_{de}$ and $s_{ab}$ both are multiplied by $\alpha_5$ in eq. (A.3), the leading contribution to $T$ comes from small $\alpha_5$. If we scale $\alpha_5$,

$$\alpha_5 = \frac{x}{\alpha_2 s_{de} + \alpha_4 s_{ab}}, \tag{A.4}$$

the integral over $x$ can be extended from zero to infinity. The expression for $T$ is then

$$T = g\pi^3\beta_2(s_{b\bar{e}})\alpha_{b\bar{e}}(\alpha_{b\bar{e}} - 1)\frac{e^{-i\pi\alpha_{b\bar{e}}}}{\sin\pi\alpha_{b\bar{e}}}\int_0^\infty ds_1\,\sigma_1(s_1, s_{a\bar{c}})$$

$$\times\int_0^1\prod_{i=1}^4 d\alpha_i\,\delta\left(\sum_{i=1}^4\alpha_i - 1\right)(-\alpha_2 s_{de} - \alpha_4 s_{ab})^{\alpha_{b\bar{e}}}\int_0^\infty dx\,\frac{x^{-\alpha_{b\bar{e}}} - 1}{[d' - x + i\epsilon]^{2-\alpha_{b\bar{e}}}}\,, \tag{A.5}$$

where the expression for $d'$ is given in eq. (16). The integral over $x$ in (A.5) can be done explicitly and we then obtain the expression (15) for $T$ in the single-Regge limit.

Next consider the double-Regge limit. We have to let $s_{cd} \to \infty$ keeping $s_{a\bar{c}}$, $s_{b\bar{e}}$ and $\kappa = s_{cd}s_{de}/s_{ab}$ fixed in the expression (15) for $T$. Again, the dominant contribution comes from large $s_1$. Substituting the Regge behaviour (11) of $\sigma_1$ we get

$$T = -g\pi^4\frac{\beta_1(s_{a\bar{c}})\beta_2(s_{b\bar{e}})}{\sin\pi\alpha_{a\bar{c}}\sin\pi\alpha_{b\bar{e}}}e^{-i\pi\alpha_{a\bar{c}}}\alpha_{a\bar{c}}\int_0^1\prod_{i=1}^4 d\alpha_i\,\delta\left(\sum_1^4\alpha_i - 1\right)$$

$$\times\frac{\alpha_4^{-\alpha_{a\bar{c}}} - 1}{(d''' + i\epsilon)^{1-\alpha_{a\bar{c}}}}(-\alpha_2 s_{de} - \alpha_4 s_{ab})^{\alpha_{b\bar{e}}}\,, \tag{A.6}$$

where

$$d''' = \alpha_3\alpha_4 s_{cd} + \alpha_1\alpha_2 s_{a\bar{c}} + \alpha_1\alpha_3 s_{b\bar{e}} + \alpha_1\alpha_4 m_a^2$$

$$+ \alpha_2\alpha_4 m_c^2 + \alpha_2\alpha_3 m_d^2 - (\alpha_1 + \alpha_2 + \alpha_3)\mu^2\,. \tag{A.7}$$

If we define the new integration variable $z$ by

$$\alpha_4 = \frac{\alpha_2\kappa}{s_{cd}}z\,, \tag{A.8}$$

we get for the leading term in $T$,

$$T = -g\pi^4\frac{\beta_1(s_{a\bar{c}})\beta_2(s_{b\bar{e}})}{\sin\pi\alpha_{a\bar{c}}\sin\pi\alpha_{b\bar{e}}}(-s_{ab})^{\alpha_{a\bar{c}}}(-s_{de})^{\alpha_{b\bar{e}} - \alpha_{a\bar{c}}}e^{-i\pi\alpha_{a\bar{c}}}\alpha_{a\bar{c}}$$

$$\times\int_0^1\prod_{i=1}^3 d\alpha_i\,\delta\left(\sum_{i=1}^3\alpha_i - 1\right)\alpha_2^{\alpha_{b\bar{e}} - \alpha_{a\bar{c}}}\int_0^\infty dz\,z^{-\alpha_{a\bar{c}}-1}\frac{(1+z)^{\alpha_{be}}}{(\bar{d} + \alpha_2\alpha_3\kappa z + i\epsilon)^{1-\alpha_{a\bar{c}}}}\,, \tag{A.9}$$

where

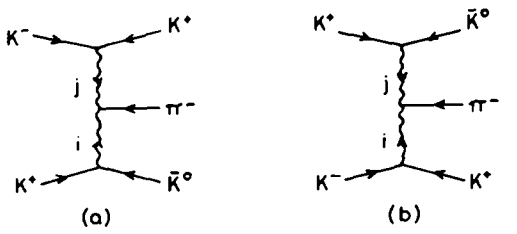


Fig. 11. (a) The double-Regge limit of the process $K^- + K^* \to K^- + \pi^+ + K^0$. All particles are treated as incoming. (b) The same reaction as in fig. 11a, but with a change in the particle ordering: a ⟷ b, c ⟷ e.

$$\bar{d} = \alpha_1\alpha_2 s_{a\bar{c}} + \alpha_1\alpha_3 s_{b\bar{e}} + \alpha_2\alpha_3 m_d^2 - (\alpha_1 + \alpha_2 + \alpha_3)\mu^2 \tag{A.10}$$

The denominator $(\bar{d} + \alpha_2\alpha_3\kappa z + i\epsilon)^{1-\alpha_{a\bar{c}}}$ in (A9) can be changed into an exponential using the formula

$$\frac{1}{(z+i\epsilon)^\mu} = \frac{e^{-i\pi\mu}}{\Gamma(\mu)} \int_0^\infty e^{\lambda(z+i\epsilon)} \lambda^{\mu-1}\, d\lambda\,. \tag{A.11}$$

The resulting expression for $T$ can then be expressed in terms of the confluent hypergeometric function* $\psi(a, b; x)$. This function can be written [20] as a sum of two entire functions $\phi(a, b; x)$, which establishes the structure (1) of $T$ in the double-Regge limit. The explicit expression for the vertex function $V_1$ in eq. (1) is

$$V_1(s_{b\bar{e}}, s_{a\bar{c}}; \kappa) = -g\pi^4 \frac{\beta_1(s_{a\bar{c}})\beta_2(s_{b\bar{e}})}{\sin\pi\alpha_{a\bar{c}} \sin\pi\alpha_{b\bar{e}}} \frac{\Gamma(\alpha_{b\bar{e}} - \alpha_{a\bar{c}})}{\Gamma(-\alpha_{a\bar{c}})}$$

$$\times \int_0^1 \prod_{i=1}^3 d\alpha_i \delta\left(\sum_{i=1}^3 \alpha_i - 1\right) \alpha_3^{\alpha_{a\bar{c}} - \alpha_{b\bar{e}}} \int_0^\infty d\lambda\, \lambda^{-\alpha_{b\bar{e}}} e^{\lambda(\bar{d} + i\epsilon)}$$

$$\times \phi(-\alpha_{b\bar{e}}, \alpha_{a\bar{c}} - \alpha_{b\bar{e}} + 1; -\alpha_2\alpha_3\lambda\kappa). \tag{A.12}$$

The amplitude $T$ being symmetric, $V_1$ and $V_2$ are the same functions in this model.

## References

[1] R.J. Eden, P.V. Landshoff, D.I. Olive and J.C. Polkinghorne, The analytic $S$-matrix (Cambridge University Press, Cambridge 1966), and references therein.

* Ref. [20].

[2] S. Humble, Daresbury preprint DNPL/P 102 (1972).
[3] R. Dolen, D. Horn and C. Schmid, Phys. Rev. 166 (1968) 1768.
[4] R.J.N. Phillips and G. Ringland, High energy physics, vol. V, ed. E.H.S. Burhop (Academic Press, New York 1972), and references therein.
[5] A.H. Mueller, Phys. Rev. D2 (1970) 2963.
[6] J. Kwieciński, Nuovo Cimento Letters 3 (1972) 619;
A.I. Sanda, Phys. Rev. D6 (1972) 280;
M.B. Einhorn, J.E. Ellis and J. Finkelstein, Phys. Rev. D5 (1972) 2063.
[7] S.D. Ellis and A.I. Sanda, Phys. Letters 41B (1972) 87;
D.P. Roy and R.G. Roberts, Phys. Letters 40B (1972) 555;
J. Finkelstein, Phys. Rev. D6 (1972) 931.
[8] P. Hoyer, R.G. Roberts and D.P. Roy, Nucl. Phys. B56 (1973) 173; Phys. Letters 44B (1973) 258.
[9] Chan Hong-Mo, H.I. Miettinen and R.G. Roberts, Nucl. Phys. B54 (1973) 411.
[10] C.E. DeTar and J.H. Weis, Phys. Rev. D4 (1971) 3141.
[11] I.T. Drummond, P.V. Landshoff and W.J. Zakrzewski, Nucl. Phys. B11 (1969) 383.
[12] O. Steinmann, Helv. Phys. Acta 33 (1960) 257, 347;
H. Araki, J. Math. Phys. 2 (1960) 163.
[13] J.H. Weis, Phys. Rev. D5 (1972) 1043.
[14] R. Roth, Phys. Rev. D6 (1972) 2274.
[15] A. Białas and S. Pokorski, Nucl. Phys. B10 (1969) 399.
[16] A. Erdélyi (ed.), Higher transcendental functions, vol. 1 (McGraw-Hill, New York, 1953) p. 56.
[17] Chan Hong-Mo, P. Hoyer and P.V. Ruuskanen, Nucl. Phys. B38 (1972) 125.
[18] I.T. Drummond, P.V. Landshoff and W.J. Zakrzewski, Phys. Letters 28B (1969) 676.
[19] W.J. Zakrzewski, Nucl. Phys. B14 (1969) 458.
[20] A. Erdélyi, ref. [16], p. 255.

# Regge Poles and Finite-Energy Sum Rules for Kaon-Nucleon Scattering

GURU VACHAN DASS
*Theoretical Physics Division, A.E.R.E., Harwell, Berks., England*
*and*
*Theoretical Studies Group, Rutherford Laboratory, Chilton, Didcot, Berks., England*

AND

C. MICHAEL
*Rutherford Laboratory, Chilton, Didcot, Berks., England*

(Received 17 June 1968)

Generalized finite-energy sum rules (FESR) for kaon-nucleon scattering are evaluated to determine the $t$ dependence and other properties of the relevant Regge-exchange amplitudes: $P$, $P'$, $A_2$, $\rho$, and $\omega$. The FESR's have been evaluated (a) with the available phase-shift analyses for the low-energy $KN$ system as input and (b) in the resonance-saturation approximation with all the appropriate resonances of which $J^P$ is known. For the $K^+p$ system, the phase-shift analysis of Lea *et al.* has been used; for the $\bar{K}N$ system, the multichannel effective-range analysis of Kim, and the resonance-plus-background analysis of Armenteros *et al.* Matching energies of $\sqrt{s}=2$ GeV and $\sqrt{s}=2.15$ GeV have been used for the cases (a) and (b), respectively. In terms of the definite helicity flip amplitudes, $A$ (which is the full forward amplitude at $t=0$) and $B$, we find that assuming the $\rho$ contribution to be known, the non-spin-flip contributions for the various Regge poles are similar to those deduced from high-energy fits; however, the spin-flip contributions of the high-energy fits are inconsistent with our FESR results. For example, the factorization ratio $(\nu B/A)$ for the $A_2$, $P$, $P'$, and $\omega$ contributions, where $\nu$ is $(s-u)/4M$, is found to have the opposite sign to that used in previous high-energy fits. As far as our results go, the FESR's are consistent with the usual explanation of the crossover phenomenon in terms of a single genuine $\omega$ Regge pole, though we cannot regard this conclusion as very strong, because of the poor available input data. We find no evidence of a wrong-signature nonsense zero in $\alpha_\omega$ for $-t\lesssim 0.8$ (GeV/$c$)$^2$; we find $(\nu B/A)_\omega=+(1$–$3)$ for $-t\lesssim 0.6$ (GeV/$c$)$^2$. There is some evidence for an exchange degeneracy between the $\omega$ and the $P'$ for this ratio, because we also find evidence for $(\nu B/A)_{P,P'}\approx+1$. There is some evidence for the no-compensation mechanism for the $P'$, with $\alpha_{P'}=0$ at $-t\sim 0.5$ (GeV/$c$)$^2$, which, however, would make the $\omega$ and $P'$ trajectories quite nondegenerate. For the $A_2$, we find $\nu B/A\sim+10$, which would be expected if the $A_2$ were degenerate with the $\rho$. Our determination of the signs of the spin-flip amplitudes $B$ allows us to predict the $K^\pm p$ polarizations semiquantitatively; our results agree with the available $K^-p$ polarization data, while the previous Regge models gave the wrong sign of this polarization. Our new signs for the $B$ amplitudes also improve the agreement of the conventional Regge model with the available $K^+n$ charge-exchange cross section without invoking a $\rho'$ contribution. On the basis of getting good agreement between the FESR results and the Regge expectations, we are able to choose a particular set of low-energy input data as our favored one: We prefer Kim's coupling constants $g_A^2$ and $g_Z^2$ for the Born terms, a negligible $Y_1^*$ (1385) coupling (as also found by Kim), and the nonresonant-type solution IV for the $K^+p$ phase-shift analysis. We have also considered FESR's for amplitudes with the wrong crossing properties, generalizing the Schwarz superconvergence relations. A simple model to remove the infinities expected in the case of Schwarz FESR's is seen to be in good agreement with the low-energy data, at least at $t=0$.

## 1. INTRODUCTION

IF an amplitude decreases sufficiently fast with increasing energy, one can use dispersion relations to derive superconvergence relations (SCR) for this amplitude.[1,2] One may use a Regge-pole parametrization for the asymptotic behavior of the scattering amplitude in question. It has been shown recently, however, that one can generalize SCR's to cases in which the amplitude does not superconverge [i.e. behave as (energy)$^{-1-\epsilon}$ where $\epsilon>0$ as energy $\to\infty$]; one essentially subtracts the supposedly known asymptotic part (given, for example, by Regge poles) to write an SCR for the remainder (full amplitude minus Regge part). These Reggeized superconvergence relations or finite-energy sum rules (FESR's) which relate integrals of the full amplitude only over a finite low-energy region to Regge-pole parameters are very important tools in detecting inadequacies of either the low-energy data or the Regge-pole parameters (as determined by fits to high-energy data alone) depending upon which of the two is known better. The FESR's can predict[3] some features of the low- (high-) energy data, given only the high- (low-) energy data. It is this aspect of the FESR's that interests us in this paper.

It is instructive to trace the essential history of the origin of the FESR's. De Alfaro *et al.*[1] pointed out that if an analytic function (for example, a scattering amplitude at a fixed momentum transfer) $f(\nu)$ satisfying a dispersion relation

$$f(\nu)=\frac{1}{\pi}\int_{-\infty}^{\infty}\frac{\mathrm{Im}f(\nu')d\nu'}{\nu'-\nu} \tag{1}$$

[1] See, e.g., V. de Alfaro, S. Fubini, G. Furlan, and G. Rossetti, Phys. Letters **21**, 576 (1966).

[2] G. V. Dass and C. Michael, Phys. Rev. **162**, 1403 (1967), and references therein.

[3] R. Dolen, D. Horn, and C. Schmid, Phys. Rev. **166**, 1768 (1968).

is subject to the asymptotic bound, for energy $\nu \to \infty$,

$$|f(\nu)| < \nu^{\gamma}, \quad \gamma < -1, \tag{2}$$

it must satisfy the SCR

$$\int_{-\infty}^{\infty} \mathrm{Im} f(\nu)\, d\nu = 0. \tag{3}$$

For amplitudes that are odd under crossing symmetry, this SCR takes the form of an integral over only positive energies:

$$\int_{0}^{\infty} \mathrm{Im} f(\nu) d\nu = 0. \tag{4}$$

One can, of course, also derive similar SCR's for the amplitudes $\nu^{2n} f(\nu)$, where $n$ is any positive integer, provided the asymptotic behavior permits that derivation. Appealing to Regge-pole theory for the asymptotic behavior, if one chooses the appropriate crossing odd amplitude which corresponds to the exchange of a trajectory that lies sufficiently low to satisfy the condition $\gamma < -1$ [Eq. (2)], the SCR gives a sum rule for the imaginary part of the amplitude. Hopefully, the high-energy part gives a negligible contribution to Eq. (4) which, therefore, gives a condition on the low-energy imaginary parts only. Such sum rules have been studied quite extensively.[2] If the leading Regge term allows only $\gamma > -1$, but is known from high-energy fits, one may study the difference [$f(\nu)$ − the leading Regge term]. For instance, the $P'$ Regge pole was predicted by Igi[4] by a study of the difference of the $\pi N(+)$ amplitude in the forward direction and the $P$ Regge pole contribution to this amplitude. More recently, Igi and Matsuda,[5] Logunov, Soloviev, and Tavkhelidze,[6] and Dolen, Horn, and Schmid[3] have employed this technique further for $\pi N$ scattering. The FESR's can be derived,[3] for example, by starting with the SCR for the amplitude from which the sum of all the Regge contributions with $\gamma > -1$ has been subtracted. These FESR's hold quite generally for any analytic function that can be expanded at high energies $\nu$ ($\geq$ a certain number $\nu_1$ at which one believes this asymptotic behavior to have been established) in terms of a Regge-pole parametrization. These FESR's take the form[3]

$$\frac{1}{\nu_1^{n+1}} \int_{0}^{\nu_1} \nu^n \,\mathrm{Im} f(\nu,t)\, d\nu = \sum_i \frac{\beta_i \nu_1^{\alpha_i}}{(\alpha_i + n + 1)}, \tag{5}$$

where the contribution of a single Regge pole $i$ is given by

$$f_{\mathrm{Regge}}(\nu,t) = \frac{\beta_i(t) \nu^{\alpha_i(t)}}{\sin \pi \alpha_i(t)} (\pm 1 - e^{-i\pi\alpha_i(t)}), \tag{6}$$

the various symbols having their usual meaning. For meson-baryon scattering, we have chosen $\nu$ to be $\nu = (s-u)/4M$, where $s$, $t$, and $u$ are the usual Mandelstam variables and $M$ is the nucleon mass. It is important[3] to realize that the point $\gamma = -1$ does not have any special role for the FESR's; every Regge-pole contribution, irrespective of whether the trajectory lies high or low, occurs in the same form in the FESR. Also,[3] the various Regge poles contribute to the FESR with the same weight as in the amplitude $f(\nu)$. This makes the FESR's particularly suited to investigate the properties of the Regge poles as they occur at high energies by evaluating only low-energy integrals. One should remember, however, that the derivation of the FESR's assumes that for $\nu > \nu_1$, $f = f_{\mathrm{Regge\ poles}}$ only; if the function $f$ cannot be expanded in terms of a Regge-pole parametrization, one has to reexamine the whole issue all over again. For example, Regge cuts would have to be represented approximately as a superposition of poles, etc.

There is another side of development of the history of the FESR's. So far, we have mentioned finite-energy integrals over only Im$f$. It is possible to consider FESR's for Re$f$ or for combinations of Re$f$ and Im$f$ also. Gilbert[7] wrote down a similar dispersion relation some years ago. More recently, Liu and Okubo[8] and Olsson[9] and Barger and Phillips[10] have investigated such FESR's for $\pi N$ scattering. The idea is to consider a function $G(\nu,t)$ which has analyticity properties very similar to those of $f(\nu,t)$ and which also depends on another parameter $m$. For special values of $m$, Im$G$ reduces to Im$f$; otherwise, Im$G$ involves both Re$f$ and Im$f$ in general. For example, for $t=0$, one can use $G = (\mu^2 - \nu^2)^{m/2} f$, where $\mu$ is the meson mass and $G$ has the same singularity structure as $f$. The FESR's for $G$ have exactly the same form as for $f$ above. We evaluate these generalized FESR's involving both the real and imaginary parts of the scattering amplitude for various moments $m$; the added advantage of these FESR's for $m \neq$ even integral is that they provide information on the phase of the high-energy amplitude also.

Kaon-nucleon scattering, in its various charge and hypercharge modes, is more complicated than pion-nucleon scattering from the theoretical point of view; it has the added disadvantage of poorer experimental information. Regge-pole theory for $KN$ scattering is less well determined than for $\pi N$ scattering; more types of Regge poles are possible and less information at high energies is available. FESR's are, therefore, of special importance in determining those characteristics of $KN$ Regge poles which cannot be determined otherwise, from high-energy Regge fits alone. The absence of high-

[4] K. Igi, Phys. Rev. Letters **9**, 76 (1962); Phys. Rev. **130**, 820 (1962).
[5] K. Igi and S. Matsuda, Phys. Rev. **163**, 1622 (1967); Phys. Rev. Letters **18**, 625 (1967).
[6] A. A. Logunov, L. D. Soloviev, and A. N. Tavkhelidze, Phys. Letters **24B**, 181 (1967).
[7] W. Gilbert, Phys. Rev. **108**, 1078 (1957).
[8] Y. Liu and S. Okubo, Phys. Rev. Letters **19**, 190 (1967).
[9] M. G. Olsson, Phys. Letters **26B**, 310 (1968).
[10] V. Barger and R. J. N. Phillips, Phys. Letters **26B**, 730 (1968); C. Michael, Phys. Letters **26B**, 392 (1968) gives further evidence on $B^{(+)}$.

energy data on polarization in any channel in elastic $KN$ scattering has led to ambiguities in the phases of the Regge-pole amplitudes (especially the spin-flip amplitude $B$) because data on high-energy $d\sigma/dt$ alone cannot determine these phases; this has led to predictions of $K^-p \to K^-p$ polarization of the wrong sign as compared to the recent polarization data[11] (though the energy of this experiment is rather low for comparison with a Regge-pole model). Our FESR analysis brings out this inadequacy of the previous Regge fits, predicts the phases of the amplitudes at high energies, and this then leads to the correct sign and magnitude of the expected polarization. The present analysis also confirms some of the notions in current Regge phenomenology and predicts some new ones.

In Sec. 2, we summarize some information on the Regge poles relevant to the $KN$ system. In Sec. 3, we discuss the FESR's that we want to evaluate and also our low-energy data input. In Sec. 4, the results of evaluating the FESR's are discussed along with some relevant information from meson-meson scattering FESR's. Section 5 is devoted to the discussion of some other sum rules related to the Schwarz[12] superconvergence relations. Section 6 gives our predictions for polarization in $K^{\pm}p$ elastic scattering and for the $K^+n$ charge-exchange cross section, both of which have been regarded as weak points of Regge-pole phenomenology. The conclusions are given in Sec. 7. Some preliminary results have been published elsewhere.[13]

## 2. REGGE POLES FOR $KN$ SCATTERING

The usual invariant amplitudes[14] $A'$ (which we call $A$) and $B$ receive contributions from different Regge poles[15] in the $t$ channel ($K\bar{K} \to N\bar{N}$):

$$f(K^-p \to K^-p) = f_P + f_{P'} + f_\omega + f_\rho + f_{A_2}, \quad (7a)$$

$$f(K^+p \to K^+p) = f_P + f_{P'} - f_\omega - f_\rho + f_{A_2}, \quad (7b)$$

$$f(K^-n \to K^-n) = f_P + f_{P'} + f_\omega - f_\rho - f_{A_2}, \quad (7c)$$

$$f(K^+n \to K^+n) = f_P + f_{P'} - f_\omega + f_\rho - f_{A_2}, \quad (7d)$$

$$f(K^-p \to \bar{K}^0n) = 2f_\rho + 2f_{A_2}, \quad (7e)$$

$$f(K^+n \to K^0p) = -2f_\rho + 2f_{A_2}, \quad (7f)$$

where $f$ stands for either $A$ or $B$; the subscripts refer to the contributing Regge pole.[15] We shall use the amplitudes

$$f^{(+)} = \tfrac{1}{2}[f(K^-p \to K^-p) + f(K^+p \to K^+p)] = f_P + f_{P'} + f_{A_2} \quad (8a)$$

and

$$f^{(-)} = \tfrac{1}{2}[f(K^-p \to K^-p) - f(K^+p \to K^+p)] = f_\rho + f_\omega, \quad (8b)$$

which receive contributions from Regge poles of positive and negative signature, respectively. If one had good experimental data on all the amplitudes on the left-hand sign of Eq. (7), one could invert Eq. (7) to extract information on all the four Regge contributions ($P+P'$), $\omega$, $\rho$, and $A_2$. One gets

$$4(f_P + f_{P'}) = f_{K^-p} + f_{K^+p} + f_{K^-n} + f_{K^+n}, \quad (9a)$$

$$4f_{A_2} = f_{K^-p} + f_{K^+p} - f_{K^-n} - f_{K^+n}, \quad (9b)$$

$$4f_\rho = f_{K^-p} - f_{K^+p} - f_{K^-n} + f_{K^+n}, \quad (9c)$$

$$4f_\omega = f_{K^-p} - f_{K^+p} + f_{K^-n} - f_{K^+n}, \quad (9d)$$

$$4f_\rho = f_{K^-p \to \bar{K}^0n} - f_{K^+n \to K^0p}, \quad (9e)$$

$$4f_{A_2} = f_{K^-p \to \bar{K}^0n} + f_{K^+n \to K^0p}. \quad (9f)$$

Since the amplitudes for $K^{\pm}n$ scattering are not sufficiently well determined, we cannot very reliably separate the Regge contributions beyond that in Eq. (8).

The zeros of the amplitudes $A$ and $B$ as a function of $t$ for a definite Regge pole are very conveniently studied by the FESR approach. These zeros may arise from the trajectory passing through some special $\alpha$ values for which the amplitude develops special properties (for example, the $\alpha$ value may be physically impossible or the amplitude may develop a ghost and so on). The FESR determination of the $t$ dependence of the amplitudes, therefore, could help one to determine the behavior of the trajectory near these zeros: whether it chooses sense or chooses nonsense, what is the ghost-eliminating mechanism, etc. Depending on which amplitude one is considering, one may also determine whether or not the relevant Regge trajectory goes through zero in the $t$ region studied by finding whether or not the appropriate integral over the relevant amplitude passes through zero as a function of $t$; this is useful only if (a) the zero of $\beta_i(t)$ on the right-hand side of Eq. (5) [if $\beta_i(t)$ be proportional to some positive power of $\alpha_i(t)$] is not cancelled by the factor $(\alpha_i+n+1)$ in the denominator at the $t$ value for which $\alpha_i(t)=0$, and if (b) the contribution of the particular pole for which $\alpha_i(t)$ passes through zero is not masked by that of the other poles in the Regge summation. The various possible modes of behavior of the trajectory couplings have been given by Chiu, Chu, and Wang[16]; we use their notation for the different mechanisms of coupling.

Let us summarize some relevant information on the different Regge poles:

(*a*) $\omega$. At a given lab energy, the experimental $d\sigma/dt$ for ($\bar{p}p \to \bar{p}p$) and ($K^-p \to K^-p$) near the forward direction is bigger and steeper as a function of $t$ than the

[11] C. Daum *et al.*, Nucl. Phys. **B6**, 273 (1968).
[12] J. H. Schwarz, Phys. Rev. **159**, 1269 (1967); **162**, 1671 (1967); Nuovo Cimento **54A**, 529 (1968).
[13] G. V. Dass and C. Michael, Phys. Rev. Letters **20**, 1066 (1968).
[14] W. Rarita, R. J. Riddell, Jr., C. B. Chiu, and R. J. N. Phillips, Phys. Rev. **165**, 1615 (1968).
[15] R. J. N. Phillips and W. Rarita, Phys. Rev. **139**, B1336 (1965); Phys. Rev. Letters **15**, 807 (1965).
[16] C. B. Chiu, S.-Y. Chu, and L.-L. Wang, Phys. Rev. **161**, 1563 (1967).

$d\sigma/dt$ for $(pp \to pp)$ and $(K^+p \to K^+p)$, respectively, and therefore the $\bar{p}p$ and $pp$ (and similarly, $K^-p$ and $K^+p$) $d\sigma/dt$'s cross over near the forward direction at $t=t_c\sim-0.13$ (we use units GeV$=1$, $\hbar=c=1$). The usual explanation[14,15,17] of this crossover phenomenon in terms of the $\omega$ Regge pole can be shown, when combined with the factorization theorem for the Regge-pole residues and the real analyticity for the unfactored residues, to lead to the conclusion that the $\omega$ would essentially "decouple from all physics" at $t=t_c$; i.e., the $\omega$-exchange residue functions vanish at $t=t_c$ for every helicity amplitude in every reaction. This explanation has been shown[17] to lead to difficulties in $\pi^0$ photoproduction, $\gamma p \to \pi^0 p$, because the data do not show any sign of a dip in the measured $d\sigma/dt$ at $t\simeq t_c$. A recent FESR calculation[18] for $\gamma p \to \pi^0 p$ confirms this difficulty. It would be of interest to see what evidence the FESR's give for $KN$ scattering. The crossover phenomenon only requires that the imaginary part of the helicity-nonflip amplitude $A$ for the $\omega$ should vanish at $t=t_c$; the usual explanation, however, puts a much stronger constraint on the $\omega$ contribution; it requires the real and imaginary parts of both $A_\omega$ and $B_\omega$ to vanish at $t=t_c$. It is of interest to study the behavior of the real part of $A$ and both the real and imaginary parts of $B$ for the trajectory corresponding to the $\omega$ quantum numbers in the $t$ channel ($I=0$, $G$ negative, and $J^P=1^-$). The FESR calculation, if the input low-energy data were complete and reliable, is capable of giving all this information and also may determine the trajectory function $\alpha_\omega(t)$. If, for example, one finds that at $t=t_c$, only $\mathrm{Im}A_\omega=0$, but $\mathrm{Im}B_\omega\neq0$, $\mathrm{Re}B_\omega\neq0$, and $\mathrm{Re}A_\omega\neq0$, one would tend to believe the conjecture that the usual[14,15] $\omega$ Regge pole is an effective mixture of a genuine $\omega$ Regge pole and some other contribution $\bar{\omega}$ such that $\mathrm{Im}(A_\omega+A_{\bar{\omega}})=0$ at $t=t_c$; no such restriction being placed on $\mathrm{Re}(A_\omega+A_{\bar{\omega}})$ or $\mathrm{Im}(B_\omega+B_{\bar{\omega}})$ or $\mathrm{Re}(B_\omega+B_{\bar{\omega}})$, all of which may be nonzero at $t=t_c$. If the effective $\omega$ contribution in the process $\gamma p \to \pi^0 p$ and in $NN$ and $KN$ scattering were indeed from a genuine single Regge pole, the absence of the zero at $t=t_c$ in the first process and the presence of this zero in the later two processes could be understood if one were to give up the factorization theorem. A recent FESR study[19] of the $\omega$ Regge contribution in $KN$ scattering within the resonance saturation approximation shows, as partly expected, that the sum-rule integrals for the amplitudes $\mathrm{Im}A_\omega$ and $\mathrm{Im}\nu B_\omega$ do have this zero at $t\sim t_c$. A possible suggestion of Ref. 19 was to cast doubts on the factorization theorem. It seems unjustified to conclude from this evidence of a zero in only the lowest-moment sum rules for $\mathrm{Im}A_\omega$ and $\mathrm{Im}B_\omega$ at $t=t_c$ that the factorization theorem could be overthrown. The point is that one should study the behavior of $\mathrm{Re}A_\omega$ and $\mathrm{Re}B_\omega$ also (and preferably, the higher moment sum rules also for all the amplitudes $\mathrm{Re}A_\omega$, $\mathrm{Im}A_\omega$, $\mathrm{Re}B_\omega$, and $\mathrm{Im}B_\omega$) near $t=t_c$ in all the relevant processes to arrive at such a conclusion. If one finds that at $t=t_c$, $\mathrm{Re}A_\omega\neq0$ and/or $\mathrm{Re}B_\omega\neq0$ for $KN$ scattering, one already knows that the effective $\omega$ is more than a single pole and that one should not expect factorization to hold for such a mixture. Unfortunately, the resonance saturation approximation does not give any reliable information about the real parts of the amplitudes. We return to our evaluation of the FESR's in Sec. 3; we hope to do better than the resonance approximation.

To our knowledge, the only high-energy Regge fit[15] (to $KN$ scattering) that takes the $\omega$ contribution into account is unable to determine it very well; actually, $B_\omega=0$ was used.[15] An FESR calculation for $KN$ scattering, therefore, becomes very important for a study of the $\omega$ contribution: in particular to find whether $B_\omega$ is really very small; also, one might learn something about $A_\omega$.

Contogouris *et al.*[20] have determined the $\omega$ trajectory ($\alpha_\omega=0.45+0.9t$) by studying, as a function of $t$ and $s$, the quantity

$$X(s,t)=\frac{d\sigma}{dt}(\pi^+p\to\rho^+p)+\frac{d\sigma}{dt}(\pi^-p\to\rho^-p)-\frac{d\sigma}{dt}(\pi^-p\to\rho^0n),$$

which receives contributions from $\omega$-like Regge poles. The $\omega$ contribution to $X(s,t)$ has a dip at $t=-0.5$ and this mainly determines the position of $\alpha_\omega=0$. While this is the only direct determination of $\alpha_\omega(t)$ (using high-energy data) known to us, the position of $\alpha_\omega=0$ ($t=-0.5$) needs confirmation. A careful analysis of the $\pi N \to \rho N$ data shows that the dip in $X(s,t)$ which could arise due to a peak in $d\sigma/dt(\pi^-p\to\rho^0n)$ or a dip in $d\sigma/dt(\pi^\pm p\to\rho^\pm p)$ arises mainly from the 4-GeV/$c$ data for $d\sigma/dt(\pi^+p\to\rho^+p)$; one would normally expect it to show up also in the $(\pi^-p\to\rho^-p)$ data which, however, do not go to large enough $|t|$ to allow the conclusion of such a dip; the $(\pi^-p\to\rho^0n)$ data also do not have a peak at about $t=-0.5$. Their analysis[20] also shows this dip at only 4 GeV/$c$. A detailed Regge-pole analysis of $\pi N \to \rho N$ and $KN \to K^*_{890}N$ by Dass and Froggatt[21] shows that the evidence for this dip is not strong, though the $\chi^2$ does get reduced slightly by using $\alpha_\omega=0.45+0.9t$. One would like to get some confirmation about this type of $\omega$ trajectory. Actually, our FESR analysis does not show this zero in $\alpha_\omega$.

Since one cannot very reliably separate the $\rho$ and $\omega$ contributions in our FESR calculation because of the

[17] V. Barger and L. Durand, III, Phys. Rev. Letters **19**, 1295 (1967).
[18] P. Di Vecchia, F. Drago, and M. L. Paciello, Nuovo Cimento **55A**, 809 (1968).
[19] P. Di Vecchia, F. Drago, and M. L. Paciello, Phys. Letters **26B**, 530 (1968).
[20] A. P. Contogouris, J. T. T. Van, and H. J. Lubatti, Phys. Rev. Letters **19**, 1352 (1967).
[21] G. V. Dass and C. D. Froggatt (to be published in Nucl. Phys.).

unsatisfactory state of the $Kn$ data, we shall deduce the properties of the $\omega$ contribution from the difference $f^{(-)}-f_\rho$, taking the $\rho$ to be well-known from the high-energy $KN$ fits[22] which make use of the $(\pi^-p\to\pi^0n)$ and $(\pi^-p\to\eta^0n)$ data and factorization constraints. We believe that the $\rho$ Regge pole is well-determined by high-energy fits, assuming that factorization is good for the $\rho$ contribution and the effects of $\rho'$ contribution are not very large.

(*b*) $A_2$. This is the well-known Regge trajectory which contributes to the process $\pi^-p\to\eta n$.

Most of the $\pi N\to\eta N$ and $KN\to KN$ Regge fits use a curved or a rather flat (slope $\approx 0.4$) $A_2$ trajectory with no zero of $\alpha_{A_2}$ in the region $-t=0\to 0.8$, while a recent $KN\to K\Delta$ Regge analysis[23] used a much steeper trajectory (slope $\approx 1$). The occurrence of zeros in $\alpha_{A_2}$ causes a ghost in the amplitude $A_{A_2}$ and raises the question of how this ghost is eliminated. Also, one can have many choices for the behavior of the amplitude $B_{A_2}$ near $\alpha_{A_2}=0$. Matsuda and Igi[24] evaluated FESR's for the $KN$ system for the $A_2$ contribution in the resonance saturation approximation. In the resonance approximation, however, $f_{A_2}=f_\rho$ [see Eqs. (9b) and (9c)] because one does not include any $K^+p$ and $K^+n$ resonances. This approximation $\mathrm{Im}f_\rho=\mathrm{Im}f_{A_2}$ (no $S=+1$ resonances) directly leads to results based on the argument of exchange degeneracy between the $\rho$ and the $A_2$. However, experimentally, $\mathrm{Im}(f_{K^+p}-f_{K^+n})$ is not identically zero; this makes $\mathrm{Im}f_\rho-\mathrm{Im}f_{A_2}$ nonzero. The differences between the $\rho$ and the $A_2$ arising because of this will therefore not be reproduced by the resonance approximation. For the $\omega$ contribution, on the other hand, the resonance approximation seems more reliable because it only assumes that the background contribution to $\mathrm{Im}f_{K^-n}+\mathrm{Im}f_{K^-p}$ equals $\mathrm{Im}f_{K^+p}+\mathrm{Im}f_{K^+n}$.

The high-energy fits to $d\sigma/dt(\pi N\to\eta N)$ and $d\sigma/dt(KN\to KN)$ do not determine the phase of the amplitude $B_{A_2}$. Because of a lack of polarization data in these reactions, as pointed out in Sec. 1, the FESR's are very useful in predicting the phases of $A_{A_2}$ and $B_{A_2}$. Indeed, the sign of $(B/A)_{A_2}$ turns out to be opposite to the one used in some high-energy fits. This, combined with the further ill-determined signs of $(B/A)_{P,P'}$ from the high-energy fits led to a negative polarization for $K^-p\to K^-p$ scattering. With the signs we suggest for $B/A$ for the different contributions, one gets a positive polarization which agrees with the available experimental data.[11]

(*c*) *P and P'*. For the vacuum exchanges again, the high-energy data do not determine the sign of $B/A$ and our FESR analysis is able to pin down the sign of $(B_P+B_{P'})/(A_P+A_{P'})$, though we cannot separate the $P$ and $P'$ contributions unambiguously.

While the $P$ trajectory is always assumed to be rather flat, some recent analyses[10,16] indicate that $\alpha_{P'}$ should go through zero at $t\simeq -0.55$ and the no-compensation mechanism should be followed to parametrize the amplitudes $A_{P'}$ and $B_{P'}$; this gives double dips (zeros) in $\mathrm{Im}A_{P'}$ and $\mathrm{Im}B_{P'}$ at $\alpha=0$. Though our analysis allows one to study only $f^{(+)}$ and not $f_{P'}$ directly (except in the resonance approximation), a dip in $f^{(+)}$ will result (and indeed, it does) if $P'$ did choose the no-compensation mechanism.

(*d*) $\rho$. We assume that the $\rho$ contribution is correctly given by most of the high-energy fits and we do not take into account any possible $\rho'$ Regge pole.

## 3. THE FESR's

### A. Generalities

For the FESR's, one needs amplitudes having definite crossing symmetry and the $f^{(\pm)}$ are suitable for this purpose. The amplitudes $\nu A^{(+)}$, $B^{(+)}$, $A^{(-)}$, and $\nu B^{(-)}$ are all odd under crossing; we consider the generalized FESR's for the amplitude

$$a(\nu,t,m)=(M/4\pi^2)(\nu_0^2-\nu^2)^{m/2}F(\nu,t)\,, \qquad (10)$$

where $m$ is a variable which could be nonintegral and $\nu_0=\mu+t/4M$. The energy dependence of $F(\nu,t)$ at high energies is parametrized in the form

$$F(\nu,t)=\textstyle\sum_i \nu(\nu_0^2-\nu^2)^{[\alpha_i(t)-\delta]/2}\chi_i(t)\,, \qquad (11)$$

where $F(\nu,t)$ may be one of the four amplitudes $\nu A^{(+)}$, $B^{(+)}$, $A^{(-)}$, and $\nu B^{(-)}$ for which $\delta=0,2,1,1$, respectively, $\chi_i(t)$ is a real function of $t$, and $\alpha_i(t)$ is the Regge trajectory function; the sum runs over the relevant Regge terms [see Eq. (8)]. At high energies, the parametrization in Eq. (11) resembles the usual Regge expansion,[14,15] so that one can directly use the high-energy Regge parameters in Eq. (11). If one writes a superconvergence relation for the difference of the full amplitude and the Regge contribution and uses analyticity to match the amplitudes evaluated below $\nu_1$ with the Regge parametrization evaluated above $\nu_1$, the set of generalized FESR's takes the form

$$\int_0^{\nu_1} d\nu\,\mathrm{Im}a(\nu,t,m)=\sum_i \frac{\mathrm{Im}a_i(\nu_1,t,m)}{\alpha_i(t)+m+2-\delta}\frac{(\nu_1^2-\nu_0^2)}{\nu_1}\,, \qquad (12)$$

where we have chosen the matching energy to be $\nu_1=1.53$ (which corresponds to $\sqrt{s}=2$, $p_{\mathrm{lab}}=1.46$). The derivation of these FESR's in Eq. (12) runs closely parallel to the derivation of the sum rule Eq. (5) in Sec. 1. For computational convenience, we have considered only integral $m=-2$ to 3 at $t=0$ and $m=0$ to 3 for $t\neq 0$. In principle, one could consider nonintegral values of $m$ also. Indeed, we have evaluated some special sum rules for nonintegral moments; we come to these in Sec. 5. For even $m$, the left-hand side of the FESR (12) requires $(-)^{m/2}$ Im$F$ from the $\Lambda\pi$ threshold to $\nu_1$ together with the $\Lambda$ and $\Sigma$ pole terms. For odd $m$, $(-)^{(m+1)/2}$ Re$F$ is required in the region above the $KN$ threshold and the $\Lambda$ and $\Sigma$ pole terms and Im$F$ below

[22] A. Derem and G. Smadja, Nucl. Phys. **B3**, 628 (1967).
[23] M. Krammer and U. Maor, Nuovo Cimento **52A**, 308 (1967).
[24] S. Matsuda and K. Igi, Phys. Rev. Letters **19**, 928 (1967); **20**, (E) 781 (1968); CERN Topical Conference, 1968 (unpublished).

this threshold. For $K^+p$ scattering, there are no contributions below the physical $KN$ threshold. Indeed, no real parts are needed below the physical threshold; this motivates our particular choice of $\nu_0$ and of the weighting factor in Eq. (10). The above FESR's have the advantage that by varying $m$ one can study the phase of the Regge amplitude; this is not possible in the usual narrow-resonance approximation.

For $m=-2$, $t=0$, our sum rule for the amplitude $A^{(-)}$ is the usual forward dispersion relation[25]; the sum rule for $B^{(+)}$ is the spin-flip dispersion relation considered, in some way, by Igi[4] (for $\pi N$ scattering) along with his dispersion relation for the $A^{(+)}$ amplitude to predict the $P'$. Note that these dispersion relations require the amplitude evaluated at threshold and involve the evaluation of a principal-value integral. Some of our $m=0$, $t=0$ sum rules have already been considered.[26] For example, Lusignoli *et al.* have considered the separate amplitudes $\nu(A_P+A_{P'})$, $\nu A_{A_2}$, $A_\rho$, and $A_\omega$ at $t=0$; Razmi and Ueda have evaluated the sum rules for $m=0$, $t=0$ for the $\nu A^{(+)}$ and $A^{(-)}$ amplitudes and also for the amplitudes $A_{K^+n}\pm A_{K^-n}$ and related them to the Regge parameters of Phillips and Rarita[15]; Chan and Yen considered the $t=0$ sum rule for $A_\rho$, used $SU(3)$ symmetry to relate the $\rho K\bar{K}$ vertex to the $\rho\pi\pi$ vertex, and made use of the $\pi N$ charge-exchange data in addition to the $KN$ data to predict finally the coupling constants $g_{\Lambda KN}^2$ and $g_{\Sigma KN}^2$; Yoshimura also considered the forward amplitude to investigate the symmetry of the factorized residue functions for the $\rho$ and the $(\omega,\varphi)$ trajectories. To our knowledge, FESR's for the other $m$ values have not been investigated for $KN$ scattering so far.

For $m=0$ and $t\neq 0$, however, the FESR analyses for $KN$ scattering have been used only in the resonance saturation approximation wherein one can explicitly separate the $\omega$,[19] $\rho$,[24] and $A_2$ [24] contributions. In addition to the other difficulties mentioned in Sec. 2 about the resonance approximation, one would always prefer to use a more exact form of the low-energy amplitudes $A$ and $B$ on the left-hand side of Eq. (12).

### B. Input Data

We use phase-shift analyses for $(K^-p\to K^-p)$ and $(K^+p\to K^+p)$ scattering up to the matching energy $\sqrt{s}=2$. For $K^+p$ scattering, Lea *et al.*[27] have found several solutions in this energy region; we used a solution of type I which suggests an inelastic $P_{11}$ resonance and also a nonresonant solution of type IV. Solutions of type II gave amplitudes $A$ and $B$ very similar to those for type I, while solutions of type III are not favored by the authors.[27] The forward-dispersion relation for the amplitude $A$ for $K^+p$ scattering is already built into their analysis because they used $\mathrm{Re}A(t=0)$ calculated from this dispersion relation as part of the data in their $\chi^2$ minimization. For $K^-p$ scattering, the situation is complicated by the presence of the Born terms ($\Lambda$ and $\Sigma$) and inelastic channels ($\pi\Lambda$ and $\pi\Sigma$) below the $\bar{K}N$ threshold. Fortunately, Kim[28] has done a multichannel analysis of $\bar{K}N$, $\pi\Lambda$, and $\pi\Sigma$ data using a $K$-matrix–effective-range parametrization for the partial-wave amplitudes; he used data from threshold up to $P_{\mathrm{lab}}=550$ MeV/$c$. In the unphysical region, we use the direct extrapolation of his parametrization though we allow the $Y_1^*(1385)$ coupling to have its broken $SU(3)$ value[29] as well as the almost negligible value found by Kim. This gives us an idea of what sort of errors to expect from uncertainties in the parametrization of the unphysical region.[30] For the $\Lambda$ and $\Sigma$ pole terms, we use Kim's values[25]

$$g_\Lambda^2/4\pi=13.5\,,\quad g_\Sigma^2/4\pi=0.2\,, \tag{13}$$

or alternatively, Zovko's values[25] of 5.7 and 1.7, respectively, for these couplings. We take Zovko's values to be typical of some[31] of the $KN$ forward dispersion relation results.[32–34] For the region 780–1220 MeV/$c$, Armenteros *et al.*[35] have a preliminary phase-shift analysis using simple backgrounds plus (finite-width) resonances. This still leaves the gaps (550–780 MeV/$c$) and (1220–1460 MeV/$c$). Lacking any better procedure, we extrapolated the energy-dependent fits of Armenteros *et al.*[35] to the region 550–1460 MeV/$c$ and confirmed that they still reproduced the experimental $K^-p$ total cross sections.[36] This extrapolation is wrong for each partial wave separately because some of the background amplitudes exceed the unitarity limit; for the full amplitudes $A$ and $B$ which are resonance dominated, however, we

[25] J. K. Kim, Phys. Rev. Letters **19**, 1079 (1967); N. Zovko, Phys. Letters **23**, 143 (1966).

[26] M. S. K. Razmi and Y. Ueda, Phys. Rev. **162**, 1738 (1967); Nuovo Cimento **52A**, 948 (1967); C. H. Chan and Y. L. Yen, Phys. Rev. **165**, 1565 (1968); M. Lusignoli, M. Restignoli, G. Violini, A. Borgese, and M. Colocci, Nuovo Cimento **51A**, 1136 (1967); M. Yoshimura, Tokyo Report, 1967 (unpublished).

[27] A. T. Lea, B. R. Martin, and G. C. Oades, Phys. Rev. **165**, 1770 (1968), and private communication.

[28] J. K. Kim, Phys. Rev. Letters **19**, 1074 (1967).

[29] R. L. Warnock and G. Frye, Phys. Rev. **138**, B947 (1965).

[30] Also, we do not include any $D$ waves below the $\bar{K}N$ threshold. Otherwise, we construct the partial-wave amplitudes and the full amplitudes $A$ and $B$ directly using his tabulated parameters (Ref. 28).

[31] See, e.g., M. Lusignoli, M. Restignoli, G. A. Snow, and G. Violini, Nuovo Cimento **45A**, 792 (1966).

[32] In principle, one could extrapolate the older constant-scattering-length parametrization of Kim (Ref. 33) into the unphysical region instead of using the more recent effective-range parametrization (Ref. 28). It has been shown, however, (Ref. 34) that by using the stability of the couplings $g_\Lambda^2$ and $g_\Sigma^2$ as a criterion for the compatibility of the extrapolated amplitude in the unphysical region with the known total cross sections in the physical region, one can reject the older parametrization (Ref. 33) in favor of the new one (Ref. 28) which we use.

[33] J. K. Kim, Phys. Rev. Letters **14**, 29 (1965).

[34] C. H. Chan and F. T. Meiere, Phys. Rev. Letters **20**, 568 (1968).

[35] R. Armenteros, M. Ferro-Luzzi, D. W. G. Leith, R. Levi-Setti, A. Minten, R. D. Tripp, H. Filthuth, V. Hepp, E. Kluge, H. Schneider, R. Barloutaud, P. Granout, J. Meyer, and J. P. Porte, Nucl. Phys. **B3**, 592 (1967).

[36] In order to study how crucially our results depend on this extrapolation, we changed the matching energy to $\sqrt{s}=1.9$ which coincides with the higher-energy end of the experiment of Armenteros *et al.* (Ref. 35) and also we changed the point where the Armenteros *et al.* parametrization takes over the Kim parametrization to 670 MeV/$c$. Making both the changes does not introduce any significant changes in our results.

believe this extrapolation to be a fair approximation. This is better than the narrow-resonance saturation approximation which does not even reproduce the experimental total cross sections. The parametrization of Armenteros *et al.* agrees approximately with the experimental $K^-p$ polarization of Cox *et al.*[37] from 1100 to 1350 MeV/$c$, which already involves an extrapolation. This shows that our extrapolation may not be very bad for the total amplitudes $A$ and $B$.

The $K^-n$ analysis of Armenteros *et al.*[33] is less reliable since it does not reproduce the total cross sections as well. Also, the only $K^+n$ analysis is 0–813 MeV/$c$ so that, as pointed out above, we cannot appeal to the neutron data to separate the isospin contributions beyond those in Eq. (8). We do evaluate FESR's for moments $m=0, 2$ for all the four contributions $(P+P')$, $A_2$, $\rho$, and $\omega$ in the narrow-width resonance saturation approximation taking all the known resonances (of which $J^P$ is known) from Rosenfeld *et al.*[38] This takes one up to an effective cutoff energy $\sqrt{s}=2.15$.[39] If one believes in the conjecture[40] that the Pomeranchuk trajectory is mostly built from the nonresonating background at low energies, one can regard the $P+P'$ results in the resonance approximation to be a representation of the $P'$.

Let us remind ourselves of the various possibilities in the input data: (a) coupling strength of $Y_1^*(1385)$ [the Kim value or the broken $SU(3)$ value]; (b) solution I or solution IV for $K^+p$ scattering; and (c) Zovko's or Kim's values [the latter are very similar to $SU(3)$ values] for the pole-term couplings. Actually, we use the $SU(3)$ values for $f=0.36$ for the resonance-approximation results instead of the Kim values.

These variations in the input data set mean eight different evaluations of each FESR at each $t$ value. We use the difference, if any, of the results for different data sets to estimate the errors shown in the figures, the central value shown being the one for our favored data set, to be discussed later.

### C. Choice of $\nu_1$

One would, in principle, like a high value of $\nu_1$, corresponding to say $P_{\text{lab}}\sim 5$ GeV/$c$, for the assumption of the Regge behavior having become established at $\nu_1$ to be valid. We have no alternative to choosing $\nu_1$ corresponding to $\sqrt{s}\sim 2$ GeV because the low-energy data do not allow one to do so either with the phase-shift analysis or in the resonance approximation. Though it is certainly desirable to choose a comparatively high $\nu_1$, one need not wait until phase-shift analysis for kaon nucleon scattering extends to momenta as high as 5 GeV/$c$. Our value of $\nu_1=1.53$ is not too unreasonable if one were to keep in mind the fact that the extrapolation of the Regge amplitude down to $\nu_1$ should represent only a local average of the amplitude and the wiggles (resonances) start appearing only below $\sqrt{s}\sim 2$. Some other calculations[19,24,41] have also used low matching energies like $\sqrt{s}\sim 2$. A high $\nu_1$ would ensure that the right-hand side of the FESR [Eq. (12)] did represent *the* amplitude at that $\nu_1$. The choice of a low $\nu_1$ would give one only the extrapolation (to $\nu_1$) of the high-energy Regge amplitude; this may or may not be *the* amplitude at $\nu_1$ because the low-energy wiggles might be important at a low $\nu_1$. Furthermore, lower-lying Regge trajectories could be important for a low $\nu_1$. In our case, it seems that both these effects are rather small because the agreement of the sum-rule results with the extrapolations of the high-energy Regge amplitudes is quite good in general [see Sec. 4 (A)], at least so far as the question of the over-all normalization is concerned.

### D. Sum Rules with Different Moments

The FESR's of Eq. (12) are not equally useful in the form given above for all values of $m$. In principle, the ones with large $m$ are also equally valid, but their usefulness decreases with increasing $m$ because the higher the $m$ value, the greater is the weight given to the input data immediately below $\nu_1$ in the evaluation of the FESR integral. One cannot make $m$ too small either. With $m$ very small (negative and large), the low-energy data around $\nu=\nu_0$ would be weighted heavily and the sum-rule integrals would be far more sensitive to the low-energy data than to Regge poles; such ones, for example, might call for an accurate knowledge of high partial waves near threshold and in the nearby unphysical region. Since one has to resort to an extrapolation procedure to know the amplitudes in the unphysical region, it is better not to try to learn something about Regge poles from the high-inverse-moment sum rules. From this point of view, the choice $\nu_0=\mu+t/4M$ is better than $\nu_0=0$ because with the latter accurate information of the amplitude in the unphysical region (e.g., analog of scattering length) would be required down to $\nu_0=0$ as an input datum for the low-$m$ sum rules; with the former, this information at only the physical threshold is needed. One needs to know the amplitude at threshold for the $m=-2$ sum rules. Since one does not have this information except for $t=0$ ($t\neq 0$ is unphysical at threshold), we considered $m=-2$ only for $t=0$. Summarizing, therefore, one should consider sum rules with $m\geqslant 0$ as appropriate for giving information on Regge poles. Also, in general, the $m=$ even integral sum rules should be more reliable than the

[37] C. R. Cox *et al.*, in *Proceedings of the Heidelberg International Conference on Elementary Particles 1967*, edited by H. Filthuth (Interscience Publishers, Inc., New York, 1968) Contribution No. 253.

[38] A. H. Rosenfeld, N. Barash-Schmidt, A. Barbaro-Galtieri, L. R. Price, P. Soding, C. G. Wohl, M. Roos, and W. J. Willis, Rev. Mod. Phys. **40**, 77 (1968).

[39] This is different from $\sqrt{s}=2$ which is our matching energy in the case of the complete data input. The reason is that we have included some resonances higher in mass than $\sqrt{s}=2$. At the point $\sqrt{s}=2.15$, the higher known resonance next to the highest (in mass) one that we have included should take over.

[40] H. Harari, Phys. Rev. Letters **20**, 1395 (1968).

[41] S.-Y. Chu and D. P. Roy, Phys. Rev. Letters **20**, 958 (1968).

$m$=odd integral ones because the latter (former) require real (imaginary) parts of the amplitudes in the physical region.

### E. Different $t$ Values

In principle, fixed-$t$ dispersion relations are valid for all physical $t$ and because the FESR's are derived from these, one should expect the FESR's to be valid for all the physical $t$ values for which the high-energy Regge expansion holds. Since the Regge poles in question are the mesonic ones in the $t$ channel, one expects the range of validity to be approximately $t=0$ to $-1$. This immediately requires one to know the input amplitudes out to $-t\sim 1$. While for comparatively high $s$, $-t\sim 1$ is in the physical scattering region where experiments can give information on the scattering amplitude, one has to resort to extrapolations in the case of the low-$s$ amplitudes that are input data for the FESR integrals. At the physical threshold, for example, $-t=1$ is well away from the only physical point $t=0$. Similarly, in the unphysical region (below the $KN$ threshold), one has to resort to extrapolation in order to get the $-t=1$ amplitudes. While the $t=0$ extrapolation into the unphysical region can be put to some test[34] by forward dispersion relations, no such reliable test exists for the $t\neq 0$ extrapolations. As $-t$ increases, the range of $s$ values for which this extrapolation to unphysical $t$ values becomes necessary increases. This range is small for $t\sim 0$. Lacking any subtler method of analytic continuation in $\cos\theta_s$, we have used the common Legendre expansion of the scattering amplitudes to extrapolate to unphysical $t$ values the low-$s$ amplitudes which are input data for the sum-rule integrals.

There is a further complication, however. Suppose one were to use $\nu_0=0$. It so happens that with the physical masses, the effective $\nu$ value for some terms can vanish for quite low $-t$ values. The $\Lambda$ pole term has $\nu_\Lambda\gtrless 0$ for $-t\lesssim 0.23$ approximately; the $\Sigma$ pole term has $\nu_\Sigma\gtrless 0$ for $-t\lesssim 0.59$ approximately; at $-t=2$, $\nu_\Lambda$, $\nu_\Sigma$, $\nu_{Y_1^*(1385)}$, and $\nu_{Y_0^*(1405)}$ are all negative. This leads to apparent difficulties for the nonintegral and the inverse-moment sum rules. Actually they can be circumvented in the case of genuine FESR's by a proper treatment of the relevant contributions, but they do weight the input data in a rather sensitive manner. For the sum rules to be described in the Sec. 5, however, one cannot avoid this problem and one has to have some prescription to stay away from the $t$ region where such things happen. The choice $\nu_0=\mu+t/4M$ (and not $\nu_0=0$) is very welcome in this respect because now the difficulty due, for example, to $\nu_\Lambda=0$ does not arise; $\nu_\Lambda$ cannot become equal to $\nu_0$ for any real $t$. The $\nu_0=0$ troubles creep in again at $t=-4M\mu$, but this is at $-t\approx 1.9$ and quite far away from the region of interest to us. This point needs special treatment in $\pi N$ scattering because of the small pion mass. There is another possibility, however. $\nu_\Lambda^2-\nu_0^2$ can vanish when $\nu_\Lambda=-\nu_0$; this happens at $-t\sim 1.05$ and calls for a special treatment of the pole term for this $t$ value; we have not gone beyond $-t\lesssim 1$ in practice. Not all sum rules (for any $m$), therefore, are equally simple and valid in their innocent form of Eq. (12) for all $t$. For the genuine FESR's which we have dealt with so far, the trouble due to $\nu_\Lambda=-\nu_0$ can be circumvented by a proper analytic treatment of the pole; this can be seen by looking at the contour along which the original FESR is evaluated, and deforming it in a harmless manner. For some other sum rules (see Sec. 5), one has to stay away from this point and also use proper definitions of the sum rules; luckily, this does not happen for $-t<1$. One should note that the $\Lambda$ pole term is the lowest-$s$ contribution and creates difficulties at the lowest $-t$ value. If one can take care of these difficulties or if one does not go as far as the point at which the $\Lambda$ pole term starts calling for a sensitive treatment, one has automatically guarded oneself against the similar troubles from the other (higher $s$) contributions.

## 4. RESULTS AND DISCUSSION

Before coming to results of our evaluation of the FESR's of Eq. (12), we record some formulas which we have used. The spin-flip amplitude $B$ and the usual non-spin-flip amplitude $A$ are given in terms of the partial-wave amplitudes $f_{l\pm}$ referring to $J=l\pm\frac{1}{2}$ for a given $s$-channel isospin state as[42]

$$\begin{bmatrix} B(s,t) \\ A(s,t) \end{bmatrix} = \frac{4\pi}{k^2}\sum_{l=1}^{\infty} P_l'(\cos\theta)\Big\{(E+M)(f_{l-}(s)-f_{l+}(s)) \times \begin{bmatrix} 1 \\ M-W \end{bmatrix} + (E-M)(f_{(l-1)+}(s) - f_{(l+1)-}(s))\begin{bmatrix} 1 \\ M+W \end{bmatrix}\Big\}, \quad (14)$$

where $k$ is the c.m. momentum, $\theta$ is the c.m. scattering angle, $s=W^2$, and $E=(k^2+M^2)^{1/2}$. The amplitude $A'$ (which we have called $A$ throughout) is related to the amplitudes $A$ and $B$ by the equation[14]

$$A\equiv A'=A+\nu B/(1-x), \quad x=t/4M^2. \quad (15)$$

In terms of $A$ and $B$, experimental quantities are given by[14]

$$\sigma_{\text{tot}}(s)=(1/p)\,\text{Im}A(s,t=0), \quad (16a)$$

$$\frac{d\sigma}{dt}(s,t)=\frac{1}{\pi s}\left(\frac{M}{4k}\right)^2\left[(1-x)|A|^2-x\left(\frac{p^2+sx}{1-x}\right)|B|^2\right], \quad (16b)$$

$$P(s,t)=-\frac{\sin\theta}{16\pi\sqrt{s}}\frac{\text{Im}(AB^*)}{d\sigma/dt}, \quad (16c)$$

[42] See, e.g., Ref. 2.

where $p$ is the pion lab momentum and $P(s,t)$ is the polarization defined relative to the normal $(\mathbf{q}_i \times \mathbf{q}_f)$ to the scattering plane, $\mathbf{q}_i$ and $\mathbf{q}_f$ being the initial and final pion momenta.

Coming to the contributions of the various Born diagrams [$\Lambda$, $\Sigma$, $Y_0^*(1405)$, and $Y_1^*(1385)$] to the amplitudes $A$ and $B$, one gets[43]

$$A_\Lambda{}^0=\frac{g_{\Lambda KN}{}^2(M-m_\Lambda)}{m_\Lambda{}^2-s}, \quad B_\Lambda{}^0=\frac{g_{\Lambda KN}{}^2}{m_\Lambda{}^2-s}, \tag{17a}$$

$$A_\Sigma{}^1=\frac{g_{\Sigma KN}{}^2(M-m_\Sigma)}{m_\Sigma{}^2-s}, \quad B_\Sigma{}^1=\frac{g_{\Sigma KN}{}^2}{m_\Sigma{}^2-s}, \tag{17b}$$

$$A_{Y_0^*(1405)}{}^0=\frac{g_{Y_0^*KN}{}^2(M+m_{Y_0^*})}{m_{Y_0^*}{}^2-s}, \quad B_{Y_0^*(1405)}{}^0=\frac{g_{Y_0^*KN}{}^2}{m_{Y_0^*}{}^2-s}, \tag{17c}$$

where the normalization of the coupling constants is $g_{N\pi N}{}^2/4\pi=14.6$ and the superscripts refer to the total isospin in the $s$ channel. The coupling constants $g_{\Sigma KN}{}^2$ and $g_{\Lambda KN}{}^2$ are for a pseudoscalar-type meson-baryon vertex and their $SU(3)$ symmetry values are given in terms of $g_{\pi N}{}^2$ and the $F$-$D$ mixing parameter $f$ by

$$g_\Lambda{}^2\equiv g_{\Lambda KN}{}^2=\tfrac{1}{3}(1+2f)^2 g_{\pi N}{}^2, \tag{18a}$$

$$g_\Sigma{}^2\equiv g_{\Sigma KN}{}^2=(1-2f)^2 g_{\pi N}{}^2, \tag{18b}$$

where the currently quoted value of $f$ is $\sim 0.36$. The effective Lagrangian for the $Y_0^*KN$ vertex is

$$\mathfrak{L}=g_{Y_0^*KN}\bar{Y}_0^* N\bar{K}+\text{H.c.},$$

where the constant $g_{Y_0^*KN}{}^2/4\pi$ can be determined by relating the Lagrangian calculation with the dispersion-theoretic calculation. In the latter, one introduces a $\delta$ function in the appropriate absorptive parts appearing in the dispersion relation and can compare the pole residue obtained in this way with the coupling constant. In the case of $Y_0^*$, however, one has to extrapolate below the physical $\bar{K}N$ threshold. Warnock and Frye[29] did this with the Dalitz-Tuan model and we use their value $g_{Y_0^*}{}^2/4\pi=0.32$. For the $Y_1^*(1385)$, we use their broken $SU(3)$ value, $g_{Y_1^*KN}{}^2/4\pi=1.9/M^2$, where the relevant Lagrangian is

$$g_{Y_1^*KN}(\bar{Y}_1^*)_\mu N\partial_\mu\bar{K}+\text{H.c.}.$$

Again, the structure of the $Y_1^*$ Born term could be determined by means of the dispersion-theoretic calculation. One gets[44]

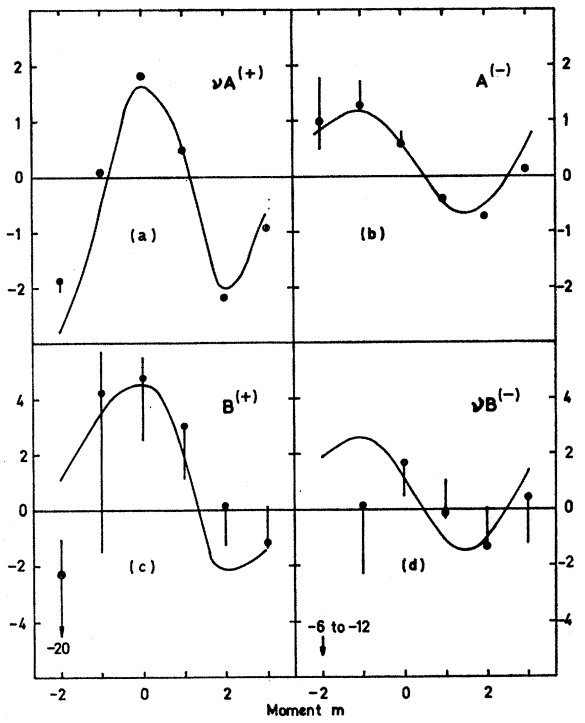


FIG. 1. Evaluation of Eq. (12) (units, GeV=1) at $t=0$ for different moments $m$ and amplitudes $F$. This is the same as Fig. 1 of Ref. 13. The points are the sum-rule results for our favored data set [Kim's corrected (Ref. 43) coupling constants and unphysical region and a nonresonant $K^+p$ solution], with the error bars showing the extent of the values obtained using the other choices discussed in the text. The continuous curves represent the extrapolations (to our matching energy $\sqrt{s}=2$) of high-energy Regge fits of solution 2 of Phillips and Rarita (Ref. 15) for $A^{(+)}$, $A^{(-)}$, and $B^{(-)}$ ($B\omega\equiv 0$). For $B^{(+)}$, we use the FESR result of Barger and Phillips (Ref. 10) and the Regge fit of Derem and Smadja (Ref. 22).

$$B_{Y_1^*}{}^1=\frac{g_{Y_1^*KN}{}^2}{(m_{Y_1^*}{}^2-s)}\left(\frac{1}{2}-t+\frac{[(m_{Y_1^*}+M)^2-\mu^2][(m_{Y_1^*}-M)^2-\mu^2-2Mm_{Y_1^*}]}{6m_{Y_1^*}{}^2}\right), \tag{19a}$$

$$A_{Y_1^*}{}^1=\frac{g_{Y_1^*KN}{}^2}{(m_{Y_1^*}{}^2-s)}\left(\frac{1}{2}-t(M+m_{Y_1^*})+\frac{[(M+m_{Y_1^*})^2-\mu^2]}{6m_{Y_1^*}{}^2}\right.$$
$$\left.\times\{(M+m_{Y_1^*})[(m_{Y_1^*}-M)^2-\mu^2]-m_{Y_1^*}(M^2+\mu^2-m_{Y_1^*}{}^2)\}\right). \tag{19b}$$

[43] The conventional Born terms used in many calculations on $KN$ forward dispersion relations have a factor $M_p/M_Y$ for the $\Lambda$ and $\Sigma$ pole terms, relative to the usual definition of the coupling constants. This has been noted, among others, by Chan and Meiere (Ref. 34).

[44] The $Y_1^*(1385)$ contribution to $A_{A_2}$ and $A_\rho$ in Ref. 24 has the wrong $t$ dependence. See S. Matsuda and K. Igi, Phys. Rev. Letters **20**, 781 (E) (1968). On reevaluation, their $A_{A_2}$ sum rule results change.

The values of the $Y_0^*(1405)$ and $Y_1^*(1385)$ coupling constants that we use may not be extremely accurate, but they are sufficiently good for our purpose: (a) We have used both of them in the resonance approximation calculation (of which the results are only qualitative anyway), and (b) we have used the $Y_1^*(1385)$ contribution also to provide estimates of errors due to parametrization of the unphysical region in the calculation with the phase-shift analyses input.

In order to evaluate the contributions of the resonances decaying physically into the $\bar{K}N$ channel, one has only to use Eq. (14) above along with the following:

$$f_{l\pm}=\frac{e^{i\delta_{l\pm}}\sin\delta_{l\pm}}{k}, \tag{20}$$

$$\mathrm{Im}f_{l\pm}(s)=\mathrm{Im}\frac{\Gamma_{el}/2k}{M-W-\frac{1}{2}i\Gamma_{\mathrm{tot}}}\simeq\frac{\pi\Gamma_{el}}{2k}\delta(M-\sqrt{s}), \tag{21}$$

$\delta_{l\pm}$ being the elastic-scattering phase shift for the appropriate partial wave.

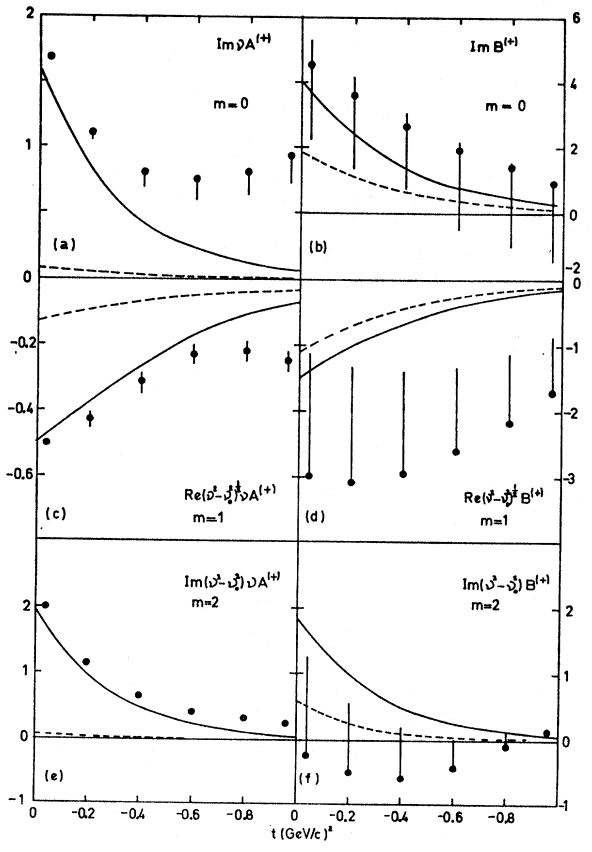


FIG. 2. Evaluation of Eq. (12) (units, GeV=1) for $m=0$, 1, and 2 for the amplitudes $A^{(+)}$ and $B^{(+)}$ for $0<-t<1$. The points and error bars have the same meaning as for Fig. 1. The dashed curve is the $A_2$ contribution as deduced by an extrapolation (to $\sqrt{s}=2$) of solution 1 of Ref. 22. The full-line curves represent the expected Regge contributions to the (+) amplitudes at $\sqrt{s}=2$, our matching energy. For $A_P$, $A_{P'}$ we used solution 1 of Phillips and Rarita as such; for $B_P$, $B_{P'}$, we used $(\nu B/A)_{P,P'}=1$.

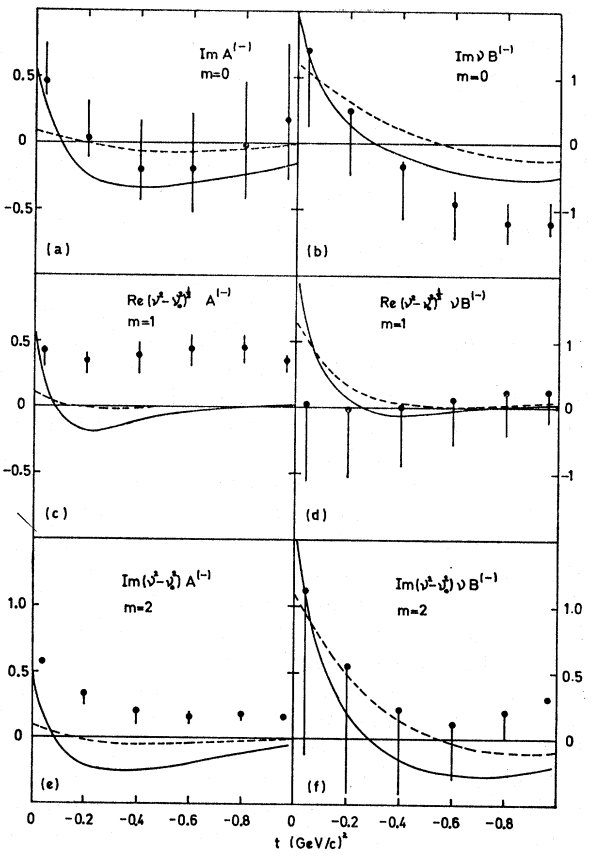


FIG. 3. Evaluation of Eq. (12) (units, GeV=1) for $m=0$, 1, and 2 for the amplitudes $A^{(-)}$ and $B^{(-)}$ for $0<-t<1$. The points and error bars have the same meaning as for Fig. 1. The dashed curve is the $\rho$ contribution as deduced by an extrapolation (to $\sqrt{s}=2$) of solution 1 of Ref. 22. The full-line curves represent the expected Regge contributions to the (−) amplitudes at $\sqrt{s}=2$, our matching energy. For $A_\omega$, we used solution 1 of Phillips and Rarita as such; for $B_\omega$, we used $(\nu B/A)_\omega=1.5$.

Now we turn to our results. We first discuss the case of the data input involving the phase shift and then, the resonance saturation results.

### A. $t=0$

For $t=0$, we plot the results of evaluating the left-hand side of Eq. (12) versus $m$; this gives one a feeling for the relative importance of the different moments $m$ and the phase of the amplitude in question. We recall that FESR's with $m$ odd involve the real part and those with $m$ even involve the imaginary part of the amplitude. For even $m$, the sum rules for the amplitude $A$ could be evaluated directly by using total cross sections when a higher matching energy might be employed. Some earlier work for the $m=0$ sum rules has been mentioned already in Sec. 3. The vertical error bars in Fig. 1 give an estimate of the difference arising from using different input low-energy data, the central dots are for our favored set which has the Kim couplings for the $\Lambda$ and $\Sigma$ pole terms, a negligible $Y_1^*$ coupling (as in

Kim's solution[28]) and a nonresonant $K^+p$ solution. This notation has been followed in Figs. 2 and 3, also. The smooth curves in Fig. 1 represent extrapolations to 1.53 GeV of high-energy Regge fits to the 6–20 GeV data. We used solution 2 of Phillips and Rarita.[15] (Using solution 1 would make very slight differences in the comparison of the Regge curve with our points.) For $\nu A^{(+)}$ and $A^{(-)}$, the Phillips-Rarita parameters show a good agreement with our points remembering that a confrontation of data below 1.53 GeV and above 6 GeV is what is being presented. For $\nu B^{(-)}$, the Phillips-Rarita solution had $\nu B/A=+11$ for the $\rho$ and $B_\omega=0$; these fit with our results approximately, the real part ($m$ odd) results not being in good agreement. As pointed out earlier, the reason for their[15] choice $B_\omega=0$ is that the high-energy data were not good enough to determine it well. Hopefully, the agreement could be improved by taking $B_\omega\neq 0$. Indeed, we do use $(\nu B/A)_\omega=1.5$ as a typical expected sample value in all the subsequent comparisons of the sum-rule results with the extrapolations to $\nu_1$ of the high-energy Regge fits; we were led to this choice of $(\nu B/A)_\omega$ by a comparison of the sum-rule results for $B^{(-)}$ and the known $\rho$ contribution. For $B^{(+)}$, reasonable agreement can be obtained only by using the more recent[22] result of an analysis of the process $K^-p\to\bar{K}^0n$ that $\nu B/A=+8.3$ for the $A_2$ (rather than $\sim -8$ as in the Phillips and Rarita[15] analyses) and also the recent FESR result[10] in $\pi N$ scattering that $\nu B/A=+1$ (rather than negative as in the Phillips-Rarita analyses[15]) for the $P$ and $P'$. The fact that our results require $\nu B/A$ = positive for all the contributions to the (+) amplitudes is very important (especially for the $A_2$) and we return to it in Sec. 6. That high-energy data alone cannot determine the sign of $\nu B/A$ is clearly brought out by the four solutions that Reeder and Sarma[45] obtain for the $A_2$ trajectory couplings. This ambiguity in the determination of the sign of $\nu B/A$ is removed by our analysis and we are able to pick out their solution 3 (which resembles the Derem-Smadja solution,[22] but differs from the Phillips-Rarita solutions[15]) as our favored one. As noted by Reeder and Sarma, this has definite experimental consequences for the polarization in $K^-p\to\bar{K}^0n$ (and actually, also for the $K^\pm p\to K^\pm p$ processes which are more easily accessible for polarization measurements; see Sec. 6); their[45] neutron polarization near the forward direction is about $-50\%$ for solution 3 as compared to about $-100\%$ for the solutions having the opposite sign of $\nu B/A$.

One sees that the agreement of our results with the extrapolation of the high-energy Regge fits is not very good (especially for the $B$ amplitudes) for $m=-2$ and $-1$. For $m=-2$, the FESR for $A^{(-)}$ (which is the forward-dispersion relation evaluated, for example, by Kim[25]) is much more sensitive to low-energy data and to coupling constants ($g_\Lambda^2$ and $g_\Sigma^2$) than it is to the Regge contribution. Indeed, we regard our FESR's for $m=-2$ and $m=-1$ (which we evaluate only for $t=0$) as providing a consistency check on the input data set rather than teaching us something about the relevant Regge poles. Actually, Fig. 1 shows that there is some inconsistency in our data set since one can see that our $m=-2$ results for the $B$ amplitudes cannot be attributed to lower-lying Regge contributions, but imply some error in the $P$ waves near threshold, or in Kim's treatment of the unphysical region which we adopt, etc. It is precisely these $B$ amplitudes which are much more sensitive to the Born-term coupling constants than are the $A$ amplitudes.

### B. Favored Data Set

One should consider several independent sum rules in choosing one's "favored data set" and, in particular, in determining the coupling constants $g_\Lambda^2$ and $g_\Sigma^2$ because of the sensitivity of different sum rules to different aspects of the input data. For example, the forward dispersion relation (the $A^{(-)}$ sum rule for $m=-2$, $t=0$) is nearly as well satisfied by Zovko's coupling constants plus a "broken $SU(3)$" value for $Y_1^*(1385)$ coupling as with our favored set. Our choice of the favored set was based on a study of the whole family of our sum rules.

It is obvious that since total cross-section data are ingredients of the $K^+p$ phase-shift analysis that we use as our data input, one does not expect our results using the $K^+p$ solutions I and IV to be significantly different for the $A$ amplitudes. For $\mathrm{Im}A^{(\pm)}$, especially at $t=0$, this is strictly true because of the optical theorem; for $\mathrm{Re}A^{(+)}$ also, it is true because of the fact that the forward-dispersion relation was built into the $K^+p$ analysis of Lea *et al.*[27] Indeed, we find that the FESR results for the two $K^+p$ solutions are essentially the same for the $A$ amplitude. From our point of view, the main difference between the two $K^+p$ solutions is in the $B^{(\pm)}$ amplitudes and we use this difference to select our favored data set. Also, the difference between the Kim and Zovko-Born couplings is more important for the $B^{(\pm)}$ amplitudes than for the $A^{(\pm)}$ amplitudes. The reason for this becomes clear if we consider, as an example, the $\Lambda$ contribution in Eq. (17a) which shows that while the coupling constants have their full strength in the $B$ amplitudes, their contribution to the $A$ amplitude is weakened by the factors $M-m_\Lambda$ and $\nu_\Lambda$ (the value of $\nu$ for $\sqrt{s}=m_\Lambda$), both $\nu_\Lambda$ (in the region of interest to us) and $M-M_\Lambda$ being much less than 1 in our units. One has

$$A_\Lambda^0=(M-m_\Lambda+\nu_\Lambda/(1-x))B_\Lambda^0. \tag{22}$$

The $B$ amplitudes, therefore, are more important than the $A$ amplitudes as a guide to the choice of the favored set. The third type of variation that we have considered [$Y_1^*(1385)$ contribution] can contribute to both the $A^{(\pm)}$ and $B^{(\pm)}$ amplitudes almost equally

[45] D. D. Reeder and K. V. L. Sarma, Phys. Rev. **172**, 1566 (1968).

strongly, and the variation it causes depends in detail upon which sum rule one is considering.

For choosing between the different input data sets, we compared our predictions for these different data sets with the expected (extrapolated down to $\nu_1=1.53$) Regge contribution. Let us restrict our attention to $t=0$ because this comparison is more reliable for $t=0$. In fact, the $t$ dependence of the results with different data sets is quite similar and, if anything, the data set which we favor on the basis of our considerations at $t=0$ is also the favored one for our $t\neq 0$ results. For the $B^{(-)}$ amplitude, for example, our FESR results for $m=-1$, 1, 2, and 3 have the same and the opposite signs to that expected from the Regge extrapolation for the $K^+p$ solutions IV and I, respectively; for $m=-2$, our results are quite different from the expected one possibly because of the extreme sensitivity of this sum rule to the very-low-energy data; for $m=0$, the magnitude is in much better agreement with the Regge expectation for solution IV. The $B^{(+)}$ results are not completely in favor of solution IV; solutions I and IV are better for $m=2$ and 3, respectively; $m=0$ and $\pm 1$ results are about equally good for both the solutions; $m=-2$ results are not good for either. On the whole, therefore, the nonresonant solution IV is preferable to the resonant solution I. As for the difference between the Kim and Zovko couplings and the presence or almost absence of the $Y_1^*$ contribution, one has to consider the $A$ sum rules also. For the $A^{(-)}$ results, the results are surely better for the Kim couplings than for the Zovko ones for $m=0$, 1, $-2$, $-1$, the results for $m=2$ and 3 being about the same for both the cases. In some cases, the combination (Zovko's couplings + full $Y_1^*$ contribution) is only slightly worse than the choice (Kim couplings + almost no $Y_1^*$ contribution), though the latter is, in some other cases, much better (for example, the $m=0$ result for the $A^{(-)}$ amplitude). When the combination (Kim couplings + full $Y_1^*$ contribution) is significantly different from the combination (Kim couplings + almost no $Y_1^*$ contribution), it is generally worse than the latter (for example, the $m=-2$ case for $A^{(-)}$). On the whole, therefore, the preferred choice is (a) Kim's Born couplings for the $\Lambda$ and the $\Sigma$ contributions, (b) almost zero $Y_1^*(1385)$ contribution, as found by Kim,[28] and (c) the nonresonant $K^+p$ solution IV. We hope that when future analyses of low-energy kaon-nucleon scattering become sufficiently well determined, one would not have to rely on a comparison with the extrapolation of the Regge result; under the present circumstances, we found this to be a useful possibility. It may very well happen that only two or one or none of the three choices that we have preferred is the true one and that the combination of the three is only a close approximation to the true representation of the data; this must await better and more complete phase-shift analyses than those available at present. It is unfortunate that, as found by Queen *et al.*,[46] all recent parametrizations of the low-energy $\bar{K}N$ scattering amplitude are inconsistent with the remainder of our knowledge of the $KN$ interactions because they do not satisfy the important constraint that the Born coupling constants $g_\Lambda^2$ and $g_\Sigma^2$ defined by the dispersion relations be energy-independent. Queen *et al.*[46] have suggested that future parametrizations of the experimental data should incorporate more theoretical constraints (for example, their important consistency requirement of the constancy of $g_\Lambda^2$ and $g_\Sigma^2$). As mentioned in Sec. 3, Chan and Meiere[34] have shown, in a somewhat related context, that the constant-scattering-length extrapolation (with Kim's[33] parameters) into the unphysical region leads to inconsistencies because the coupling constants $g_\Lambda^2$ and $g_\Sigma^2$ tend to vary wildly and even become negative for different allowed values of a certain parameter $\beta$. Hopefully, things will improve in future and a future FESR analysis of $KN$ scattering will be more informative than it is now.

### C. $t\neq 0$

The results carry information in the form of dips and zeros in the various Regge contributions as a function of $t$. For $t\neq 0$, one should rely upon the results of only those FESR's which agree reasonably well at $t=0$ with the Regge expectation. We have shown the results for the (+) and (−) amplitudes for $m=0$, 1, and 2 in Figs. 2 and 3, respectively. The smooth full-line curves in these figures are the sum of all the relevant Regge contributions (extrapolated down to our matching energy) and the dashed curves are for the $\rho$ (for Fig. 3) contribution in the case of the (−) amplitudes and the $A_2$ (for Fig. 2) contribution in the case of the (+) amplitudes. The $\rho$ and $A_2$ contributions are extrapolations from the results of Derem and Smadja.[22] For the $A_2$, we have used their solution 1. Their other solution is very similar. The $A_P$, $A_{P'}$ and $A_\omega$ contributions are taken from solution I (which is very similar to their solution II which we have used only for our Fig. 1) of Phillips and Rarita.[15] $B_P$, $B_{P'}$, and $B_\omega$ are determined by using our qualitative (for all $t$) conclusions (confirmed for the $P$ and $P'$ by the $\pi N$ FESR results of Barger and Phillips[10]) that $\nu B/A=+1$ for $P$ and $P'$ and $\nu B/A=+1.5$ for the $\omega$. The curves do not represent, therefore, true high-energy Regge fits; they are partly motivated by the FESR results. With the high-energy Regge fit[14,15] extrapolations taken as such, even the signs of the spin-flip amplitudes $B$ would not agree with ours. The curves are meant to represent what we believe the extrapolation of high-energy Regge fits should look like. Detailed Regge fits to high-energy data incorporating our FESR "prejudices" about the phases and

[46] N. M. Queen, S. Leeman, and F. E. Yeomans, Birmingham University Report (unpublished).

magnitudes of the various contributions are in progress.[47]

For $A^{(+)}$ and $m=0$, we find [Fig. 2(a)] slight evidence of a dip (presumably due to the $P'$ contribution) at $-t=0.5$; this agrees with the conclusions of Barger and Phillips,[10] who studied the $\pi N$ sum rules. From high-energy fits, it appears that the $P'$ trajectory is less strongly coupled to the $KN$ system than to the $\pi N$ system; Phillips and Rarita[15] found that at $t=0$, for example,

$$(A_{KN}/A_{\pi N})_{P'}=(B_{KN}/B_{\pi N})_{P'}=0.29.$$

Indeed, we find a less pronounced dip than in the $\pi N$ case. This dip is consistent with its interpretation as a double zero in $A_{P'}$ according to the no-compensation mechanism if $\alpha_{P'}=0$ at this $t$ value. Such a dip could not be attributed to the $P$ contribution because the $P$ trajectory is rather flat and is not expected to go through zero at such a low value of $-t$. Also, it could not be due to the $A_2$ contribution because the latter is much smaller than the $P$ and $P'$ contributions to $A^{(+)}$. The $m=1$ [Fig. 2(c)] results for the $A^{(+)}$ (involving $\mathrm{Re}A^{(+)}$) are also consistent with the presence of this dip in the $P'$ contribution; here, however, the $A_2$ contribution is not negligible and the conclusion cannot be definite because the same dip could be attributed to the $A_2$ contribution. The extrapolations of the Regge fits down to our matching energy seems to be systematically below the FESR results for the $A^{(+)}$ amplitude. This can be due to a number of reasons. (a) The extrapolation of the Regge fits to as low an energy as $\sqrt{s}=2$ may not be completely justified; (b) the high-energy fits may be inconsistent with the FESR results, in which case either the low-energy data or the high-energy fits need to be reexamined. [It is worth remarking that our results for the $A^{(+)}$ sum rules are fairly reliable especially for $m=0$ in the sense that the vertical error bars are small and the different input data sets do not lead to very different results. The small error bars for $m=2$ in Fig. 2(e) are *a priori* expected because of the relatively small weight given to the very-low-energy data in the high-$m$ sum rules.] The disagreement at large $-t\sim 1$ is not as bad as it looks because the plotted Regge extrapolation did not take into account the no-compensation mechanism for the $P$ and $P'$.

Coming to the results for the $B^{(+)}$ amplitude shown in Figs. 2(b), 2(d), and 2(f), we see that, as pointed out in Sec. 4 B, the vertical bars are quite big and a difference in the input data sets causes an appreciable difference in the results. The two $K^+p$ solutions give fairly different results. (For $B^{(-)}$, the variation caused by varying the $K^+p$ solution is much larger than the one caused by varying the $Y_1^*$ or the $\Lambda$ and $\Sigma$ couplings for the same $K^+p$ solution.) It is difficult to draw any strong conclusion from the $B^{(+)}$ results partly because of the very big errors. The agreement is not good for our favored data set, though it is reasonable for $m=0$ [Fig. 2(b)] within the rather large error bars. In $A^{(+)}$, the $A_2$ trajectory contribution is masked by $P$ and $P'$; not so in $B^{(+)}$ for $m=1$ [Fig. 2(d)] where real parts are involved. In this case, our results, *as they stand*, show no evidence of a zero for $-t<0.8$ approximately so that the Chew mechanism (or the no-compensation mechanism) type nonsense-choosing zero is excluded. Either a Gell-Mann type nonsense-choosing zero or else no zero of $\alpha_{A_2}$ in this range is possible.[48] Unfortunately, this conclusion is in direct contradiction to the results of Chu and Roy,[41] who considered the sum rule corresponding to $\int \mathrm{Im}B d\nu$ and $\int \nu^2 d\nu\ \mathrm{Im}B$ for the $A_2$ contribution to photoproduction; they conclude that their results strongly favor the Chew or the no-compensation mechanism over that of Gell-Mann; they did find a zero in the zero-moment sum rule and they thought that the behavior of their second-moment sum rule suggests strongly a double-zero behavior. It is true that our data input is not extremely reliable for the real parts (Sec. 4 D) and that our conclusion cannot be regarded as absolutely final, but it appears that their conclusion is not final either. Their second-moment sum rule does have a definite single zero, even though one could perhaps regard it as only a slight displacement of a double-zero–type behavior. We believe that more conclusive evidence is needed to decide the issue one way or the other. In fact, considerations of exchange degeneracy between the $\rho$ and the $A_2$ would tend to support our conclusion. Also, the $\pi\eta\to\pi\rho$ FESR's support our conclusion.

The results for the $(-)$ amplitudes are shown in Fig. 3 for $m=0$, 1, and 2. We assume the $\rho$ to be given and investigate the $\omega$ contribution which is our main interest in the $(-)$ amplitudes. Turning to $m=0$ [Fig. 3(a)] for $A^{(-)}$ which should be dominated by the $\omega$, we do find solutions (using Kim's coupling constants) in which the imaginary part changes sign for $-t\sim 0.2$ as is needed to explain the crossover phenomenon. There appears to be some dilution, however, by lower-lying Regge poles or else the data are not sufficiently reliable since we find no corresponding zero either in $\mathrm{Re}A^{(-)}(m=1)$ [Fig. 3(c)] which is well nigh constant as a function of $t$, or in the $m=2$ moment for $A^{(-)}$. Actually, the FESR results for the $m=2$ moment of $A^{(-)}$ [Fig. 3(e)] are quite insensitive to the considered variations in the input data and could be reliable except for the fact that all the variations we have allowed (for the $A$ amplitudes) are in the very-low-energy data to which the $m=2$ are insensitive by construction.[49] The present

[47] G. V. Dass, C. Michael, and R. J. N. Phillips (unpublished).

[48] Exchange degeneracy of the $A_2$ with the $\rho$ would suggest that the $A_2$ trajectory passed through zero at $-t\sim 0.5$, while high-energy Regge fits to $\pi N\to\eta N$ and to the $\bar{K}N$ charge-exchange data tend to favor a flatter (or curved) trajectory with no such zero.

[49] For the $B$ amplitudes, however, we have allowed big variations at all energies because the two $K^+p$ solutions give quite different spin-flip amplitudes at even high energies. At low energies, the different choices for the couplings $g_A^2$, $g_Z^2$, and $g_{Y_1^*(1385)^2}$ provide this variation.

experimental situation does not allow one to consider any variations (for the $A$ amplitudes) in the higher-energy end of our input data—the region which is weighted heavily for high positive $m$ values; it is possible that allowing for such variations would reproduce results consistent with the usual zero[17] in the effective $\omega$ contribution to the $(-)$ amplitudes. We do not regard the absence of a crossover in the $m=1$ results as a serious difficulty because of the extent to which the real parts of the input data are reliable. We return to the question of the reliability of our sum rules involving the real parts in Sec. 4 D.

The case of the $B^{(-)}$ amplitudes is shown in Fig. 3(b), 3(d), and 3(f). The error bars here are bigger, in general, than for $A^{(-)}$. Overlooking again the $m=1$ [Fig. 3(d)] results which involve real parts and which are very sensitive to the input data variations (particularly, the $K^+p$ solution), we find that after subtracting the known $\rho$ contribution, the $m=0$ results [Fig. 3(b)] for the effective $\omega$ contribution to $B^{(-)}$ show a behavior similar to the one for $A^{(-)}$ for $m=0$. Within the error bars shown, the $m=2$ results [Fig. 3(f)] are also consistent with the occurrence of the usual crossover at $-t\sim 0.2$.

We find no evidence in the $B^{(-)}$ sum rules of any additional zero in $B_\omega$ (a sense-nonsense zero at the wrong-signature unphysical point $\alpha_\omega=0$) for $-t<1$ which is inconsistent with $\alpha_\omega=0.45+0.9t$ found by Contogouris *et al.*[20] (see also Sec. 2), from a $\pi N\to\rho N$ analysis; our results tend to favor a flatter trajectory (if the zero at $t=t_c$ is not to be associated with $\alpha_\omega=0$). Also, we find $(\nu B/A)_\omega=+1$ to $+3$ for $0<-t<0.7$. This shows that the amplitude $B_\omega$ could be appreciably more important than $A_\omega$ in this $t$ region and it is not a good approximation to set $B_\omega=0$[15] in a Regge fit. One can get a qualitative estimate of $(\nu B/A)_\omega$ at $t=m_\omega^2$ by assuming the $\omega$ and $\rho$ dominance of the isoscalar and isovector nucleon form factors, respectively. It has been shown by Rarita *et al.*[14] that

$$\left(\frac{\omega_{\rm lab}B}{A}\right)_\rho\equiv\frac{R_-}{R_+}=\frac{34.8}{13.7}\simeq 2.54 \tag{23}$$

at $t=m_\rho^2$, assuming factorization for the $\rho$ residues and using the results in their Sec. V (xii). Using the known proton and neutron magnetic moments and charges and the fact that the isovector part is the $\rho$ contribution and the isoscalar part is the $\omega$ contribution, one can deduce from the ratio of the isoscalar and isovector total magnetic moments that

$$\frac{B_\omega}{B_\rho}=\frac{(\gamma_1+2M\gamma_2)_\omega}{(\gamma_1+2M\gamma_2)_\rho}\approx 0.2\,, \tag{24}$$

where the residues $\gamma_1$ and $\gamma_2$ are defined by Ball and Wong.[50] Similarly, since the isovector and isoscalar charges are equal, $A_\omega/A_\rho\simeq(\gamma_1)_\omega/(\gamma_1)_\rho=1$. Hence $\omega_{\rm lab}B_\omega/A_\omega\simeq 0.5$ at $t=m_\omega^2$, assuming $m_\omega^2\simeq m_\rho^2$. Keeping in mind the various approximations that we have made on the way, the comparison of this number $(\nu B/A)_\omega$ of $\sim+0.5$ with our value ($+1$ to $+3$), though it involves an extrapolation in $t$, is qualitatively satisfactory. On the other hand, in their fit to $NN$ data, Rarita *et al.*[14] used $\nu B/A\approx -6$ for the $\omega$, which they took as the predominant spin-flip contribution to fit the $pp$ polarization data. Their model is in conflict with the recent $\bar{p}p$ polarization data of Daum *et al.*[11] at 2–3 GeV/$c$. This lends support to the conclusion that additional important spin-flip contributions (for example, $\rho$, $A_2$, and $\omega$ correctly) should be included in a Regge fit to $NN$ scattering to achieve agreement with experiment. We have seen that the sign of $\nu B/A$ used by Rarita *et al.*[14] is negative for $P$, $P'$, and $\omega$; our results want this sign to be positive for all these three contributions. It may very well be that if the Regge parameters are constrained to be consistent with the FESR results, one would get agreement with experimental data on $NN$ and $N\bar{N}$ scattering.

### D. How Good Are Our Input Data? Implications for Different Moments

A word about the extent to which our results for the FESR's with different moments are reliable is now in order. Here we want to consider this question in the light of our input data. These remarks are supplementary to those of Sec. 3D. To get some idea of how well our input data determined the low-energy amplitudes $A$ and $B$ which went into our FESR integrals, we compared our amplitudes $A$ with some forward-dispersion-relation calculations. Unfortunately, there is not very much else to compare with, especially at $t\neq 0$. Im$A$ at $t=0$ is, of course, all right because all our input data reproduce the observed total cross sections. However, one still has not confirmed that the $t\neq 0$ amplitudes $A^{(\pm)}$ are correct. Our extrapolation of the parametrization of Armenteros *et al.*[35] below their region introduces very small discontinuities in Im$A$ (and similarly, in Im$B$) at the point ($p_{\rm lab}=550$ MeV/$c$) where the parametrization of Armenteros *et al.* takes over the Kim[28] parametrization. For Re$A(K^+p\to K^+p)$, the agreement is very good. The situation about Re$A(K^-p\to K^-p)$ is not very good. We (a) overestimate it in the region 550–780 MeV/$c$ (the region between the analyses of Kim and Armenteros *et al.*), (b) more or less agree with the results of a very recent forward-dispersion-relation calculation by Carter[51] in the region of the analysis of Armenteros *et al.*, and (c) underestimate it in the region (1220–1460 MeV/$c$); all this, in such a manner that the area under the plot of Re$A(K^-p\to K^-p)$ versus $\nu$ is about the same as for Carter's numbers. Our $m=$ odd (real parts of $A^{(\pm)}$ involved) sum rules always have factors of $(\nu^2-\nu_0^2)^{m/2}$ multiplying the amplitude; this

[50] J. S. Ball and D. Y. Wong, Phys. Rev. **133**, B179 (1964).

[51] A. A. Carter, Cavendish Laboratory Report No. HEP 68-10 (unpublished).

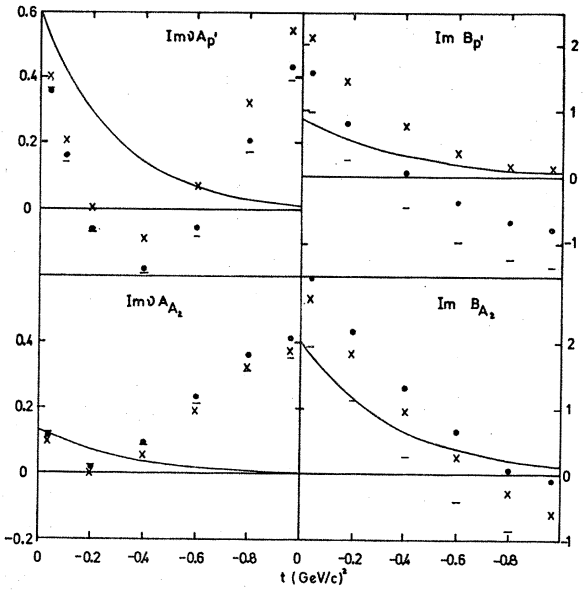


FIG. 4. Evaluation of Eq. (12) (units, GeV=1) for $m=0$, $\nu_0=0$ in the resonance saturation approximation for the contributions $f_{P+P'}$ (identified as $f_{P'}$), $f_{A_2}$ of Eq. (9) with all the bound states and resonances (Ref. 38) (of which $J^P$ is known) included. The full-line curves are the Regge expectation as for Figs. 2 and 3 evaluated at $\sqrt{s}=2.15$( Ref. 39). The crosses (×) are for corrected Kim coupling constants (Ref. 43) $g_\Lambda^2$ and $g_\Sigma^2$ and a negligible $Y_1^*(1385)$ contribution, the resonance analog of our favored data set; the points are for $SU(3)$ couplings $g_\Lambda^2$ and $g_\Sigma^2$ ($g_{\pi N}^2\sim 14.5$ and $f=0.36$) and $g_{Y_1^*(1385)}^2=1.9/M^2$; the lines are for uncorrected Zovko's couplings (Ref. 43) $g_\Lambda^2$ and $g_\Sigma^2$, and $g_{Y_1^*}^2=1.9/M^2$.

places a greater or smaller weighting on the high-energy region of our input data than on the low-energy region, depending upon whether $m$ is positive or negative. If this weighting is not too strong, our results for $m$ odd may be reliable. Otherwise, this makes our results for $m$ odd sum rules less reliable than those for the $m$ even (imaginary parts involved) sum rules because of this different weighting of the two regions in which our real parts of the $A^{(\pm)}$ amplitudes do not reproduce very well the results of Carter. It is obvious that one would be very lucky if the $t$ dependence of the $m$ odd sum rules came out correctly, given the fact that the input data set might be bad enough to make them wrong at even $t=0$. Our $m=3$ results have not been shown because these would grossly over estimate the higher-energy end of the input data. The $m=\pm 1$ results are not bad at $t=0$ (see Fig. 1); the $t$ dependence may not be correct (see Figs. 2 and 3).

We have no way to check our $B$ amplitudes and these are particularly sensitive to variations in the input data; one can believe only those conclusions (we have mentioned only such ones) which stand inspite of these variations. Again, we rely on our sum-rule results for Im$B$ more than on Re$B$. Summarizing, therefore, we regard our $m$ even sum rules as more reliable than the $m$ odd ones.

We wish to emphasize that our data input is a good representation of all the known experimental data, though it may not be the only possible unique representation. For example, it reproduces the known total cross section (both elastic and reaction ones) and the known differential cross sections from threshold up to our matching energy; these indeed are the ingredients of the data on which the phase-shift analyses which we have used were based. Also correctly reproduced are the available data on polarization in $K^-p$ scattering even in the region 1100–1350 MeV/$c$,[37] in which some extrapolation beyond the region of Armenteros *et al.* is already involved. The forward-dispersion relation for $K^+p$ scattering, being built into the analysis of Lea *et al.*,[27] guarantees our Re$A(K^+p\to K^+p)$ at $t=0$ being correct. The only obvious imperfections in our input are (a) Re$A(K^-p\to K^-p)$ is not well reproduced. This weakens our $m$ odd results somewhat. (b) There is a slight discontinuity in Im$B$ and Re$A(K^-p\to K^-p)$ at the point of changeover from the Kim parametrization to the parametrization of Armenteros *et al.*; the discontinuities in Im$B$ are not very crucial because these are very small compared to the other more important ambiguities like $g_\Lambda^2$, $g_\Sigma^2$, and $g_{Y_1^*}^2(1385)$ for the $B$ amplitude; the discontinuities in Im$A$ are negligibly small anyway; the one in Re$A(K^-p\to K^-p)$ is not negligible. Nonetheless, an over-all average of Re$A(K^-p)$ as a function of energy is nearly correctly given, when compared with Carter's numbers.

### E. Resonance Saturation Approximation

We have evaluated (with $\nu_0=0$) the $m=0$ and $m=2$ results for the separate contributions $(P+P')$, $A_2$, $\omega$, and $\rho$ in the resonance approximation. For $m=0$, the results are shown in Fig. 4 for the $P+P'$ and $A_2$ and in Fig. 5 for the $\rho$ and the $\omega$. As mentioned in Sec. 2, we expect the resonance-saturation-approximation results to be quite reliable for the $\omega$. Keeping in mind the rather large uncertainties in the known resonance parameters, we thought it good enough to work within the approximation of narrow-width resonances and therefore not to worry about the energy dependence of the relevant width, etc. The full-line curves in Figs. 4 and 5 are the expected Regge contributions extrapolated down to $\sqrt{s}=2.15$,[39] evaluated as for Figs. 2 and 3. The crosses are for Kim coupling constants for the $\Lambda$ and $\Sigma$ terms (corrected[43] for the factors $M_p/M_Y$) and a negligible $Y_1^*(1385)$ contribution; the points are for $SU(3)$ couplings for the $\Lambda$ and $\Sigma$ terms ($g_{\pi N}^2=14.5$ and $f=0.36$) and a broken $SU(3)$ value[29] for the $Y_1^*$ coupling; the broken lines are for Zovko couplings (not corrected[43] for the factors $M_p/M_Y$) for the $\Lambda$ and $\Sigma$ terms and a broken $SU(3)$ value[29] for the $Y_1^*$ coupling; these cases were chosen as indicative of the errors and uncertainties involved, within the resonance approximation. Assuming[40] that the $P+P'$ contribution of Eq. (9a) is only $P'$ contribution in the resonance approximation, the results for all the four contributions are summarized below. One must remember[41] that the resonance ap-

proximation can give only crude results and that slight shifts in the positions of the expected zeros (as a function of $t$) or double zeros becoming broken into two nearby zeros (and vice versa) or other similar things are likely to happen in the resonance-saturation results. We have taken the resonance parameters from Rosenfeld *et al.*[38] and have included all the relevant resonances of which $J^P$ is known.

$P'$. A single zero in the $B$ sum rule and an almost double zero in the $A$ sum rule (a similar behavior for the $m=2$ results) confirm our more exact FESR result that the $P'$ trajectory seems to choose the no-compensation mechanism type coupling ($\alpha_{P'}=0$ at $-t\sim 0.5$). The agreement with the Regge curves is not good, possibly because the relevant Regge fits did not incorporate this feature of the $P'$ coupling.

$\omega$. The results for both $m=0$ and $m=2$ indicate zeros in the $A_\omega$ and $B_\omega$ at $-t\sim 0.1$ which is expected on the basis of the usual explanation[17] of the crossover phenomenon. The agreement with the Regge curves is fairly good. We recall that one can believe the resonance-approximation results for the $\omega$ to be reasonably correct. Again, we do not see evidence of a second zero (at $-t\sim 0.5$) in $B_\omega$ as expected due to a wrong-signature sense-nonsense zero if one accepts $\alpha_\omega=0.45+0.9t$.[20] The results for the $\omega$ also, therefore, confirm our more exact FESR results given already. While this paper was being written up, we saw a paper by Di Vecchia *et al.*[19] who evaluated the $m=0$ case with the older (1967) resonance parameters of Rosenfeld *et al.*,[52] neglecting the $Y_1^*(1385)$ contribution, as suggested by Kim.[28]

$\rho$. We do not rely very much on our resonance results for the $\rho$ and $A_2$, both of which have been evaluated for $m=0$ by Matsuda and Igi.[24,44] For the $\rho$, the sense-nonsense zero in $B_\rho$ is at about the right place, the $m=2$ result behaving similarly. The Regge $A_\rho$ is very small and is not very well given by the resonance approximation, though the Kim case with no $Y_1^*(1385)$ is not far out from the Regge curve.

$A_2$. The $m=0$ results have been evaluated by Mitsuda and Igi[24,44] with the older 1967 resonance parameters of Rosenfeld *et al.*[52] The results are consistent with a double zero in $A_{A_2}$ at $-t\sim 0.2$ and a single zero in $B_{A_2}$ at $t\approx -0.6$, both of which, if at the same $t$ value, could result from a no-compensation mechanism for the $A_2$ (as for $P'$), though $A_{A_2}$ is numerically somewhat small in magnitude and also sensitive to the inclusion or omission of certain resonances. Also, the $m=2$ result for $A_{A_2}$ shows two zeros (at $-t\approx 0.13$ and 0.5; similarly for $A_\rho$) and not a double zero as for $m=0$. The $m=2$ result for $B_{A_2}$ is similar to that for $m=0$; it has a single zero at $-t\approx 0.4$.

On the whole, therefore, our resonance approximation results give support to our more exact results obtained with phase-shift analyses as input data.

[52] A. H. Rosenfeld, A. Barbaro-Galtieri, W. T. Podolsky, L. R. Price, Matts Roos, P. Soding, W. J. Willis, and C. G. Wohl, Rev. Mod. Phys. **39**, 1 (1967).

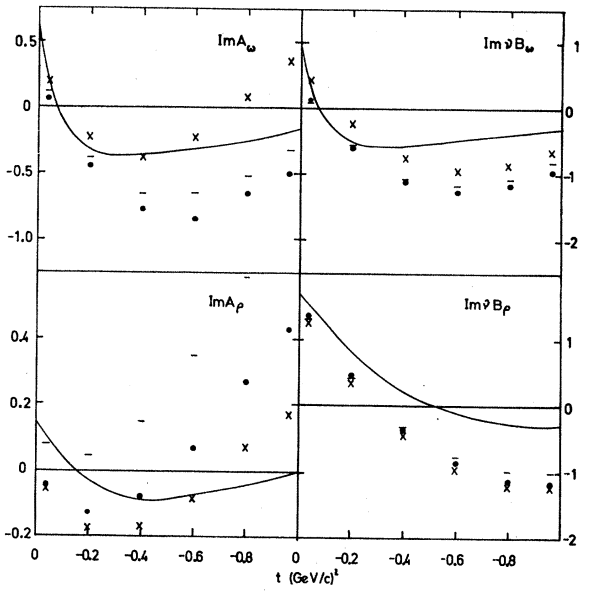


FIG. 5. Evaluation of Eq. (12) (units, GeV=1) for $m=0$, $\nu_0=0$ in the resonance saturation approximation for the contributions $f_\rho$, and $f_\omega$ of Eq. (9) with all the bound states and resonances (Ref. 38) (of which $J^P$ is known) included. The full-line curves are the Regge expectation as for Figs. 2 and 3 evaluated at $\sqrt{s}=2.15$ (Ref. 39). The crosses (×) are for corrected Kim coupling constants (Ref. 43) $g_\Lambda^2$ and $g_\Sigma^2$ and a negligible $Y_1^*(1385)$ contribution, the resonance analog of our favored data set; the points are for $SU(3)$ couplings $g_\Lambda^2$ and $g_\Sigma^2$ ($g_{\pi N}^2\sim 14.5$ and $f=0.36$) and $g_{Y_1^*(1385)}^2=1.9/M^2$; the lines are for uncorrected Zovko's couplings (Ref. 41) $g_\Lambda^2$ and $g_\Sigma^2$, and $g_{Y_1^{*2}}=1.9/M^2$.

### F. Relevant Meson-Meson Scattering FESR Analyses in Resonance Approximation

By considering the process $KK\to KK$, one can show that the zero in the residue of the helicity-nonflip amplitude for the $\omega$ contribution has a zero nearer to $t=0$ than the zero in the $\rho$ residue which in, for example, the $\pi\pi\to\pi\pi$ calculation of Schmid[53] is at $-t\simeq 0.3$. This is encouraging for the usual[17] $\omega$-crossover explanation which would indeed want it at $-t\simeq 0.15$. For the other trajectories, the $KK\to KK$ calculation does not give very unambiguous results.

One could consider the process $\pi\rho\to\pi\eta$ to get information on $B_{A_2}$. If one uses Eq. (12c) of Ademollo *et al.*[54] in their Eq. (12b), one can deduce that $B_{A_2}/\alpha_{A_2}$ has no zero for $-t<1.4$ approximately. This could mean the Gell-Mann nonsense-choosing mechanism $\beta\sim\alpha$ near $\alpha=0$ if $\alpha_{A_2}$ goes through zero for $-t<1.4$; otherwise,[55] it could mean the Chew mechanism or the no-compensation type coupling ($\beta\sim\alpha^2$ near $\alpha=0$). Also, the $SU(3)$ symmetry limit results of Ademollo *et al.*[54] include exchange degeneracy between the $\rho$ and $A_2$; this implies $\beta_{A_2}\sim\alpha_{A_2}$ near $\alpha_{A_2}=0$.

[53] C. Schmid, Phys. Rev. Letters **20**, 628 (1968).
[54] M. Ademollo, H. R. Rubinstein, G. Veneziano, and M. A. Virasoro, Phys. Rev. Letters **19**, 1502 (1967).
[55] The results of Ademollo *et al.* (Ref. 54) favor the possibility that $\alpha_{A_2}$ does go through zero for $-t<1.4$.

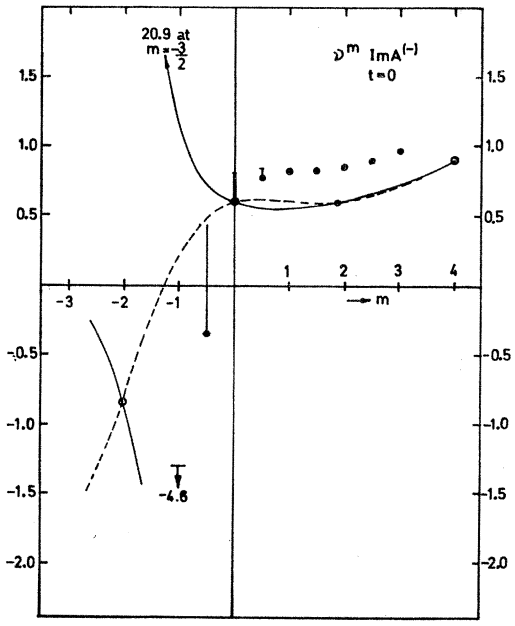


FIG. 6. Evaluation of Eq. (33) at $t=0, \lambda=m_K$ in the normalization of Eq. (12) (units, GeV=1) for various $m$ values. For $m$ even, the whole thing is a genuine FESR, shown by circles where the naive Regge expectation (evaluated as a sum of genuine $\omega$ and $\rho$ Regge poles as for Figs. 2 and 3) and the modified Regge expectation coincide. The full line is the naive Regge expectation having two infinite discontinuities at $m=-1.52(=-1-\alpha_\omega)$ and $m=-1.57(=-1-\alpha_\rho)$; the dashed curve is the modified version incorporating the $m$ plane pole plus background model and has no infinities at the points $m=-1.52, -1.57$. The integral in Eq. (33) is shown by points and error bars in the same notation as for the other figures. For $m=-1.5$, the integral varies from $-8.6$ to $-21.7$ for the various input data sets; this agrees better with the dashed curve. An ideal agreement with the dashed curve would mean $\tilde{f}(m)=0$.

## 5. OTHER SUM RULES

The finite-energy sum rules that we have considered so far depend on analyticity and a Regge-like parameterization of the high-energy data. However, one may evaluate relations which depend in a more sensitive fashion on the Regge-pole approximation. Effectively what one does is to evaluate the Froissart-Gribov representation of the $l$-plane amplitude $a(l)$ using the finite-energy trick to continue the representation to smaller $l$ values. We shall discuss this procedure in terms of the Khuri plane[56] which is much simpler for practical evaluation, while the correspondence between leading Regge poles and leading Khuri poles is maintained. Let us take $\nu_0$ to be zero to simplify the discussion further and consider a typical amplitude $A^{(-)}(\nu,t)$ which is an odd function of $\nu$. Then at fixed $t$, say, $t=0$, we consider the following relations:

$$0=\int_0^\infty \mathrm{Im}\left[\left(-\frac{\nu^2}{\lambda^2}\right)^{m/2} A^{(-)}(\nu)\right]d\nu, \qquad (25)$$

$$b(m)=\int_0^\infty \mathrm{Re}\left[\left(-\frac{\nu^2}{\lambda^2}\right)^{m/2} A^{(-)}(\nu)\right]d\nu, \qquad (26)$$

$$f(m)=\int_0^\infty \left(\frac{\nu}{\lambda}\right)^m \mathrm{Im}A^{(-)}(\nu)d\nu. \qquad (27)$$

The expression on the right-hand side of Eq. (25), which is the usual generalized SCR we have discussed previously, is zero from crossing and analyticity. Equation (26) is not zero, and defines an analytic function of $m$, $b(m)$. There is a relation between Eqs. (26) and (27): $f(m)=b(m)\sin\frac{1}{2}m\pi$. Equation (27) similarly defines an analytic function of $m$, $f(m)$, which is the same function as was discussed by Khuri[56] (noting that $\nu$ is proportional to $\cos\theta_t$ for our kinematics). Thus one expects $f(m)$ to have poles at $m=-\alpha-1, -\alpha+1, -\alpha+3, \cdots$ if there is a pole in $a(l)$ at $l=\alpha$. Assuming that the highest $l$-plane singularity is at $l=\alpha$, one must seek a method of analytic continuation to discuss Eqs. (25)–(27) for $m>-\alpha-1$ and this is provided by the finite-energy trick. We evaluate the integrals from $\nu_1$ to $\infty$ using a Regge parametrization of the high-energy data and obtain, if $A^{(-)}(\nu)\sim\sum\beta e^{-i(\pi/2)(\alpha-1)}(\nu/\lambda)^\alpha$,

$$0=\int_0^{\nu_1} \mathrm{Im}\left[\left(-\frac{\nu^2}{\lambda^2}\right)^{m/2} A^{(-)}(\nu)\right]d\nu - \sum \lambda\beta \frac{\sin[\frac{1}{2}\pi(\alpha+m+1)](\nu_1/\lambda)^{\alpha+m+1}}{\alpha+m+1}, \qquad (28)$$

$$b(m)=\int_0^{\nu_1} \mathrm{Re}\left[\left(-\frac{\nu^2}{\lambda^2}\right)^{m/2} A^{(-)}(\nu)\right]d\nu + \sum \lambda\beta \frac{\cos[\frac{1}{2}\pi(\alpha+m+1)](\nu_1/\lambda)^{\alpha+m+1}}{\alpha+m+1}, \qquad (29)$$

$$f(m)=\int_0^{\nu_1} \left(\frac{\nu}{\lambda}\right)^m \mathrm{Im}A^{(-)}d\nu - \sum \lambda\beta \frac{\sin[\frac{1}{2}\pi(\alpha+1)](\nu_1/\lambda)^{\alpha+m+1}}{\alpha+m+1}. \qquad (30)$$

In these equations, the summation is over the relevant Regge poles ($\rho$ and $\omega$ for the $A^{(-)}$ amplitude). Equation (28) can clearly be continued in $m$ beyond $-\alpha-1$ and this is the technique we have been employing in the previous sections. Equations (29) and (30), however, have poles in $b(m)$ and $f(m)$, as we have noted, and to continue these one must make a model for the $m$-plane amplitude as a pole plus background:

$$b(m)=\sum \frac{\lambda\beta}{(\alpha+m+1)}+\tilde{b}(m). \qquad (31)$$

[56] N. N. Khuri, Phys. Rev. Letters **10**, 420 (1963); Phys. Rev. **132**, 914 (1963); D. Z. Freedman and J.-M. Wang, *ibid.* **153**, 1596 (1967).

Then, Eqs. (29) and (30) may be written as

$$\tilde{b}(m)=\int_0^{\nu_1}\mathrm{Re}\left[\left(-\frac{\nu^2}{\lambda^2}\right)^{m/2}A^{(-)}(\nu)\right]d\nu+\sum\frac{\lambda\beta}{\alpha+m+1}$$
$$\times\left[\cos[\tfrac{1}{2}\pi(\alpha+m+1)]\left(\frac{\nu_1}{\lambda}\right)^{\alpha+m+1}-1\right], \quad (32)$$

$$\tilde{f}(m)\equiv\sin(\tfrac{1}{2}\pi m)\,\tilde{b}(m)=\int_0^{\nu_1}\left(\frac{\nu}{\lambda}\right)^m\mathrm{Im}A^{(-)}(\nu)d\nu$$
$$-\sum\frac{\lambda\beta}{\alpha+m+1}\{\sin[\tfrac{1}{2}\pi(\alpha+1)]$$
$$\times(\nu_1/\lambda)^{\alpha+m+1}+\sin(\tfrac{1}{2}\pi m)\} \quad (33)$$

and the latter equations (32) and (33) are in a form suitable to continue to values of $m$ larger than $-\alpha-1$. We note that Schwarz[12] has considered expressions in Eqs. (27) and (30) for $m$ odd (for $m$ even this is the form of the FESR's used by Dolen *et al.*[3]) and has argued that $f(m)$ is zero at these nonsense, wrong-signature values if third double-spectral-function effects are negligible. However, $f(m)$ may even be infinite, as is exhibited in Eq. (30).

Before evaluating relations such as Eq. (32), one should discuss the choice of $\nu_0$ and $\lambda$ and possible $t$-dependent singularities. As they stand, $b(m)$ and $f(m)$ are singular for $t\simeq-0.23$ when $\nu_\Lambda=0$; such left-hand cuts in $t$ are well known in the physical partial-wave amplitudes $a(l)$, of course. Thus we see that $\tilde{b}(m)$ must contain these cuts and we may learn rather little from evaluating the relations numerically—what we seek, of course, is some representation which will minimize the background term in the region of interest.

Equation (33) with $\nu_0=0$ has the advantage that only imaginary parts of the data are required; thus at $t=0$ for $A^{(\pm)}$ the data are essentially the total cross sections and are reliable. Choosing $A^{(-)}$ since this is expected to have effectively only one contribution with $\alpha\simeq0.5$ at $t=0$, we plot in Fig. 6, with error bars as usual, the integral in Eq. (33) and compare with the Regge terms. The normalization used is similar to that for the usual FESR's [Eq. (12)] considered previously, rather than as in Eq. (33). The $m$-plane pole model using $\lambda=0.494$ (since $\cos\theta_t=\nu/\mu$ at $t=0$) is the more plausible and is shown dashed, together with the naive result of setting $f(m)=0$. Though the normalization of the high-energy parameters is not very reliable (because the agreement for $m>0$ is not good even for $m$ values corresponding to genuine FESR's) in this context, we see that the Schwarz condition $f(m)=0$ for $m=-1$ is not satisfied, while $\tilde{f}(m)=0$ (shown dashed) is a more plausible assumption. For even $m$, $f(m)=0$ and one has the FESR's evaluated by Dolen, Horn, and Schmid.[3]

In Fig. 7, we show the results of evaluating the analogs of Eq. (32) at $t=0$, for the four amplitudes

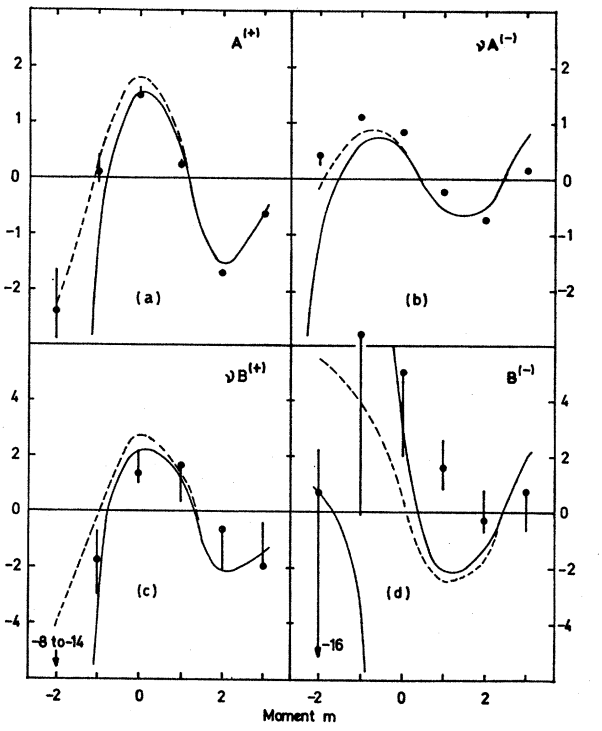


FIG. 7. Evaluation of the analogs of Eq. (32) at $t=0$ for $-2\leqslant m$ (integral only) $\leqslant 3$ for the four amplitudes $A^{(+)}$, $\nu A^{(-)}$, $\nu B^{(+)}$, and $B^{(-)}$. The normalization is the same as for Eq. (12) (units, GeV=1). Also, $\nu_0=\mu+t/4M$ was used. The points and error bars have the same meaning as for the other figures; they are for the left-hand side of Eq. (12) evaluated for the wrong crossing-symmetry amplitudes $A^{(+)}$, $\nu A^{(-)}$, $B^{(-)}$, and $\nu B^{(+)}$ and correspond to the integral in Eq. (32). The naive (full line) and the modified (dashed line) Regge expectations are calculated with the same high-energy parameters as for Figs. 2 and 3 and for $\lambda=m_K$. The infinities at $m=-1-\alpha_i$, $-2-\alpha_i$, $-1-\alpha_i$, and $\alpha_i$ for the amplitudes $A^{(+)}$, $\nu A^{(-)}$, $\nu B^{(+)}$, and $B^{(-)}$, respectively, (where $\alpha_i$ refers to any contributing Regge pole) occur for the unmodified (full line) case $[b(m)=0]$, but not in the modified model $[\tilde{b}(m)=0]$ which agrees better with the low-energy integrals.

$A^{(+)}$, $\nu A^{(-)}$, $\nu B^{(+)}$, and $B^{(-)}$. In this case, to avoid the necessity for real-part data below the physical $KN$ threshold, we used $\nu_0=\mu+t/4M$ as for the FESR's. Indeed the integrals evaluated are formally the same as for the FESR's of Eq. (12) except for an interchange of the (+) and (−) labels. Again the high-energy contribution (within a 10% error due to neglecting $\nu_0^2$ relative to $\nu_1^2$) is in good agreement if $\tilde{b}(m)=0$ (dashed line) and not if $b(m)=0$ (continuous line).

Using this value of $\nu_0$, there is no $t$ singularity until $\nu_0=-\nu_\Lambda$ at $t\simeq-1.05$, so that the $t$ dependence of the expression should be of value if the background is really negligible. We find the $P'$ dip again in $A^{(+)}$ but no $\omega$ crossover at all for $A^{(-)}$. In view of the extra assumptions involved in carrying the model in Eq. (31) to $t\neq0$ for these sum rules, we are not able to make a definite conclusion about this apparent lack of $\omega$ crossover. Introduction of adjustable parameters (to fix up, for example, the $\omega$ crossover for $A^{(-)}$) would reduce the chances of learning more from these sum rules.

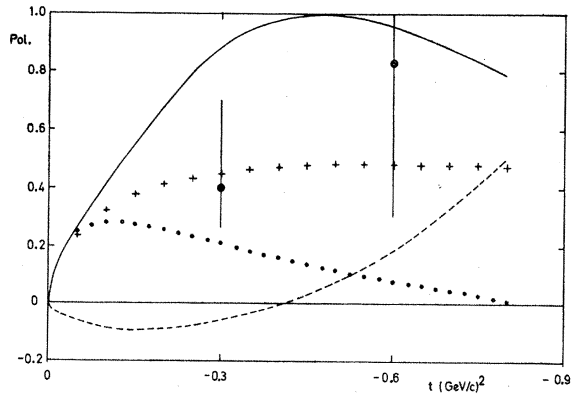


FIG. 8. $K^{\pm}p$ polarizations at $P_{\text{lab}}=1.46$ GeV/$c$ versus $t$. Continuous and dashed curves are for $K^{-}p$ scattering and are the predictions for choices (I) and (II), respectively, as described in the text. The points with error bars are from Ref. 11; the error bars represent the range of values in this energy region. The $K^{+}p$ predictions are shown with crosses and dots for choices (I) and (II), respectively.

In conclusion, we have shown that the "off $l$-shell" Regge-pole contributions can be calculated by using the wrong-crossing generalized moment sum rules. These depend on the $m$-plane background amplitude which seems to be negligible for our value of $\nu_1$ and $m$ sufficiently large.

## 6. PREDICTIONS

In order to predict any specific feature of $KN$ scattering, it is necessary to extract the invariant amplitudes and their energy dependence from our FESR results. Having obtained the invariant amplitudes, one can calculate any observable like $d\sigma/dt$ and polarization for $KN$ scattering at high energies or a local energy-averaged value at lower energies. For instance, the modulus and phase of the $K_2^0p \to K_1^0p$ regeneration amplitude can be evaluated; it is dominated by the $\omega$-exchange contribution.

If the FESR evaluations had negligibly small errors, the extraction of the invariant amplitudes could be accomplished by fitting the left-hand side of Eq. (12) to a sum of effective poles and determining the $\alpha_i(t)$ and $\beta_i(t)$ for each amplitude at each $t$ value from the results for the different $m$ values. In practice, however, these errors are not small, and we choose a less ambitious procedure (which we call I): We employ effective trajectories[57] $\alpha(t)$ deduced qualitatively from previous high-energy fits, in order to extract the effective residues $\beta(t)$ from our $m=0$ and $m=1$, FESR results with our favored data set. This is somewhat inconsistent since the phase of the amplitude may not correspond with the trajectory $\alpha(t)$. An alternative (which we call II) is to use (as mentioned previously in Sec. 4C and employed for Figs. 2–7) the high-energy fits of Phillips and Rarita[15] and of Derem and Smadja[22] with the modifications that $\nu B/A=+1$, $+1$, $+1.5$ for $P$, $P'$, and $\omega$ respectively—although this representation of our FESR results is quantitatively rather poor, especially for $\mathrm{Re}A^{(-)}$ and $\mathrm{Re}B^{(+)}$ [Figs. 3(c) and 2(d), respectively]. We believe that these choices (I) and (II) represent qualitatively the correct amplitudes; the quantitatively exact answer may perhaps lie in between the two if and when the predictions with (I) and (II) differ appreciably.[58]

In Fig. 8, we show the $K^{\pm}p$ polarizations resulting from the above two choices for $p_{\text{lab}}=1.46$ GeV/$c$, our matching energy. Also shown is an energy-averaged representation of the $K^{-}p$ polarization data of Daum *et al.*[11] from 1.4 to 2.3 GeV/$c$, the error bars showing the range of values encountered in their energy region. The experimental values lie between our predictions for the two choices, (I, the FESR results) and (II, the expected extrapolation of the modified high-energy Regge fit), at least up to $-t\sim 0.6$ beyond which the reliability of these predictions decreases. In our preliminary report[13] on the sum-rule evaluations, we had used a modification of choice (I): we did not use directly the FESR results for $\mathrm{Re}A^{(-)}$ and $\mathrm{Re}B^{(-)}$, but determined them from the FESR results for the corresponding imaginary parts ($\mathrm{Im}A^{(-)}$ and $\mathrm{Im}B^{(-)}$, respectively), assuming some effective $\alpha$ values; this leads to predictions, for $K^{-}p$ polarization, of about 40% at $-t\sim 0.3$ and about 100% at $-t\sim 0.6$ (as is indeed observed[11] experimentally), with the $K^{+}p$ ($K^{-}p$) polarization being larger than the $K^{-}p$ ($K^{+}p$) polarization for $-t$ less (greater) than approximately 0.3.

We hope that our results will be qualitatively valid also at higher energies[58] with, of course, a reduction in normalization. Previous high-energy fits with $B_\omega=0$ and the opposite sign of $B_{A_2}$ had predicted a large negative $K^{-}p$ polarization and a small $K^{+}p$ polarization. One should note that in an exchange-degeneracy limit for the residues (at all $t$ values) where $\nu B/A$ is the same for $\rho$ and $A_2$, the polarization will be zero for $K^{+}n$ and $K^{-}p$ charge-exchange scattering. Further, if $P'$ and $\omega$ (as well as the $\rho$ and $A_2$) were also each degenerate in their trajectories and residue functions, the polarization and the real part of the forward-scattering amplitude would both be zero in the $K^{-}p$ case and both positive in the $K^{+}p$ case. Also, the two charge-exchange cross sections would be identical, $K^{-}p \to \bar{K}^0n$ having a purely imaginary amplitude and $K^{+}n \to K^0p$, a purely real one.

Another source of difficulty for the Regge-pole model in the intermediate-energy region has been the $K^{+}n$ charge-exchange data at 2.3 GeV/$c$, as discussed by

[57] The effective $\alpha$ values we used for our $m=0$ and $m=1$ results are $(0.9+0.3t)$ for $\mathrm{Im}A^{(+)}$; $(0.6+0.4t)$ for $\mathrm{Im}B^{(+)}$; $(0.5+0t)$ for $\mathrm{Re}A^{(+)}$ and $\mathrm{Re}B^{(+)}$; $(0.5+0.6t)$ for $\mathrm{Im}A^{(-)}$ and $\mathrm{Re}A^{(-)}$, and $(0.5+0.8t)$ for $\mathrm{Im}B^{(-)}$ and $\mathrm{Re}B^{(-)}$. Only the $\mathrm{Im}B^{(+)}$ sum rule for $m=0$ is sensitive to the chosen $\alpha$ values because the corresponding denominator is just $\alpha$.

[58] Future high-energy fits (Ref. 47) incorporating the information that the FESR's give can help to make these predictions quantitative.

Rarita and Schwarzchild,[59] who found that the conventional Regge fits gave only half the differential cross section needed in the peak region ($-t\sim0.2$). This process is spin-flip-dominated with the $\rho$ and $A_2$ trajectory exchanges contributing; the sign change of the spin-flip amplitude $B_{A_2}$ (retaining everything else unchanged as in Ref. 59) is enough to increase the predictions by up to 50% for $-t\sim0.2$ without the need to introduce a $\rho'$ contribution. Hopefully, a researching[47] of the parameters after one takes into account this sign change will make theory agree with the experimental cross section even better.

## 7. CONCLUSIONS

We have seen that FESR's can provide a very useful tool to determine several features of Regge-pole parameters. If one had a complete and well-determined phase-shift analysis, one could hopefully learn something also about the lower-lying Regge poles which would not be very important to the high-energy fits, but could be important at the low matching energy that we have to use. Even with the present state of the low-energy $KN$ phase-shift analysis, we have learnt some useful things. We now summarize these.

$\omega$. Our sum-rule results, as far as they go, are consistent with the usual explanation of the crossover phenomenon. These results are based mainly on the sum rules involving the imaginary parts of the amplitudes $A$ and $B$. Our sum-rule results involving the real parts are not as reliable as the ones for imaginary parts. If it were not for the lack of a zero in $\mathrm{Re}A_\omega$ as determined by our sum rules for $\mathrm{Re}A^{(-)}$, we should be unreserved about our confirmation of the usual $\omega$-crossover mechanism of only a single pole with all residues passing through zero at $t=t_0$ because of factorization.

We find no evidence of a wrong-signature nonsense zero in $B_\omega$ for $-t\lesssim0.8$. This is in contradiction with what is expected for a trajectory function $\alpha_\omega=0.45+0.9t$ found by Contogouris *et al.*[20] from an analysis of the $\omega$ contribution in the reaction $\pi N\to\rho N$. Our FESR results would prefer a flatter trajectory for the effective $\omega$ contribution.

We find $(\nu B/A)_\omega=+1$ to $+3$ for $-t\lesssim0.6$ which, again, is in contradiction to what has been assumed in high-energy fits which have taken this ratio to be either zero[15] or negative.[14]

*P and P'*. We find $(\nu B/A)_{P,P'}\sim+1$ which is, again, of opposite sign to that in high-energy fits. This agrees with the $\pi N$ FESR results of Barger and Phillips.[10] Also, we find some evidence of the no-compensation mechanism type coupling for the $P'$, $\alpha_{P'}$ passing through zero at $-t\sim0.5$. Our results support exchange degeneracy of $P'$ and $\omega$ for the ratio of the residues $\nu B/A$, though $\alpha_{P'}$ and $\alpha_\omega$ are not found to be degenerate. For example, we suggest that $\alpha_{P'}$ has a zero at $-t\sim0.5$, while $\alpha_\omega$ has no zero for $-t\lesssim0.8$.

$\rho$. We have not really learnt anything about the $\rho$-trajectory contribution from the present analysis. We have taken the $\rho$ Regge pole to be well known and used it to teach us something about the $\omega$ pole.

$A_2$. Our results would want $(\nu B/A)_{A_2}=+10$ (nearly the same as for $\rho$) which, again, is of opposite sign to that previously used in some high-energy fits.[15]

The situation is somewhat confused about the type of mechanism of coupling that the $A_2$ chooses. Our sum-rule results (and also the $\pi\eta\to\pi\rho$ FESR's in the resonance approximation) would prefer either the Gell-Mann mechanism, or else no zero in $\alpha_{A_2}$ for $-t<1$ approximately, while the resonance-approximation FESR's for the $KN$ system could be consistent with the no-compensation mechanism and the photoproduction sum rules of Chu and Roy[41] would perhaps like either the Chew mechanism or the no-compensation mechanism. A really convincing FESR analysis in this context would be very welcome.[60] Again, our results support exchange degeneracy of $\rho$ with $A_2$ for the ratio of the residues $\nu B/A$ for $t\sim0$. We cannot really say very much about the $A_2$ trajectory; our input data are not accurate enough to allow one to calculate $\alpha_{A_2}$ explicitly.

We have not considered the possibility of more than one $t$-channel pole having the quantum numbers of the $\rho$ and $A_2$. Our $A_2$ and $\omega$ contributions, therefore, are only effective ones.

*Favored data set.* Though the input data are not very well determined, a choice of the favored data set which leads to the best agreement with extrapolations down to our matching energy of the high-energy Regge fits is possible. This may not be *the* correct and final representation of the data at low energies (up to $\sqrt{s}=2$ for our purpose). We would prefer Kim's couplings $g_\Lambda^2$ and $g_\Sigma^2$ for the Born diagrams, a negligible $Y_1^*(1385)$ coupling (as found by Kim) and the nonresonant (type IV) $K^+p$ phase-shift solution of Lea *et al.*[27]

*Predictions.* Having been able to determine the signs and the $t$ dependence of the Regge-pole spin-flip contributions in $KN$ scattering, we see that the older signs of $\nu B/A$ for $P$, $P'$, $\omega$, and $A_2$ are not consistent with our results. If we take them as our sum rules prefer, we are able to predict quite confidently the expected polarization in $K^+p$ and $K^-p$ elastic scattering and our prediction agrees with the available[11] experimental data on $K^-p$ polarization while the previous fits gave the wrong sign of the polarization. Also, we are able to remove, at least partially, the other difficulty that the Regge-pole theory meets in the $KN$ system: The $K^+n\to K^0p$ $d\sigma/dt$ comes out in better agreement with the experimental

[59] W. Rarita and B. M. Schwarzschild, Phys. Rev. **162**, 1378 (1967).

[60] Note that our result (either the Gell-Mann mechanism or $\alpha_{A_2}\neq0$ for $-t\lesssim0.8$) is based mainly on our $\mathrm{Re}B^{(+)}$ sum rule which, apart from involving real parts, gets non-negligible contributions from the $P'$. If one had $|\mathrm{Re}B_{P'}|$ for $-t\sim1$ much larger than $|\mathrm{Re}B_{P'}|$ for $-t\sim0$ one could perhaps allow a zero in the $\mathrm{Re}B_{A_2}$ sum rule and, therefore, a Chew or a no-compensation type mechanism which corresponds to $B\sim\alpha^2$ near $\alpha=0$.

data than the previous older prediction because of the change of sign of the ratio $(\nu B/A)_{A_2}$.

*Other sum rules.* We have considered generalized Schwarz sum rules which evaluate the "off $l$-shell" amplitudes in the Khuri plane. We find the background to be small in general, so that these relations are satisfied with Regge-pole parameters alone. The $t$ dependence of these relations implies that the background amplitude has cuts, however, and this limits the applications, since further parameters to describe the background will then be needed.

## ACKNOWLEDGMENTS

We are grateful to Dr. R. J. N. Phillips for his interest and discussions.

PHYSICAL REVIEW VOLUME 175, NUMBER 5 25 NOVEMBER 1968

# Analyticity and Broken $SL(2,C)$ Symmetry for Regge Families*

P. K. Kuo† AND James F. Walker‡

*Laboratory for Nuclear Science and Physics Department, Massachusetts Institute of Technology, Cambridge, Massachusetts 02139*

(Received 17 July 1968)

Explicit constraints on the mass dependence of daughter Regge trajectories, near zero mass, are obtained for fermion trajectories contributing to $\pi N$ scattering. Both the analyticity and the group-theoretic approaches are investigated. We find agreement between these two methods, but disagreement between our constraints and those previously published. For the dependence on the mass $W$ of the $k$th daughter trajectory with parity designation $\pm$, we find that $\alpha_k^{(\pm)}(W)=\sigma-k\pm A(\sigma-k+\frac{1}{2})W+[B_1+B_2(\sigma-k)(\sigma-k+1)+A^2(\sigma-k+\frac{1}{2})]W^2\pm\cdots$, where $\sigma$, $A$, $B_1$, and $B_2$ are constants over the family. For each of the two methods, we stress the assumptions leading to the MacDowell symmetry evident above.

## I. INTRODUCTION

In a recent paper[1] it has been pointed out that two different approaches to daughter Regge trajectories, analyticity and group-theoretic, lead to the same results for the scattering of spinless particles. Mathematically the equivalence of these two approaches has been established.[2] Namely, in order to make the analycity requirement for scattering amplitudes compatible with Lorentz invariance and Regge behavior, it is necessary and sufficient to classify singularities according to the irreducible representations of the homogeneous Lorentz group $SL(2,C)$. However, at the practical level, the ways by which these approaches lead to a given result differ considerably. At present their relationship is by no means trivial.[3] In this paper we compare these approaches for fermion trajectories, with particular emphasis on the mass formula that they yield. Even though the two methods agree, we find that each of the methods seems to have some advantages over the other. We reserve a more detailed discussion of this point for later. The mass formula that we obtain does not agree completely with that obtained previously by Domokos and Surányi,[4] hereafter referred to as DS, using their group-theoretic method. In order to facilitate comparison, our group-theoretic approach closely parallels that of DS. In our approach this disagreement is resolved by recognizing some subtleties associated with the use of wave functions having nonphysical angular momentum values.

In Sec. II we examine the implication of analyticity on the $\pi N$ scattering amplitude near $u=0$ ($u$ is the square of the momentum transfer for exchange scattering) in some detail, using the method of Ref. 1. In Sec. III we use our apparently modified version of the perturbation theory developed in DS to reproduce the results of Sec. II. Section IV contains some discussion concerning the relative merit of the two approaches and the degree to which the daughters are determined by experiment.

## II. ANALYTICITY APPROACH TO $\pi N$ SCATTERING AMPLITUDE

The $\pi N$ scattering is dominated in the backward region by the exchange of fermion trajectories. For this reason we go to the $u$ channel and define the invariant

* Work supported in part by the U. S. Atomic Energy Commission under Contract No. AT(30-1)2098.

† Present address: Department of Physics, Johns Hopkins University, Baltimore, Maryland.

‡ Present address: Department of Physics and Astronomy, University of Massachusetts, Amherst, Massachusetts.

[1] J. B. Bronzan, C. E. Jones, and P. K. Kuo, Phys. Rev. **175**, 2200 (1968).

[2] G. Domokos and G. L. Tindle, Phys. Rev. **165**, 1906 (1968).

[3] L. Jones and H. K. Shepard, Phys. Rev. **175**, 2117 (1968).

[4] G. Domokos and P. Surányi, in *Proceedings of the Topical Conference on High-Energy Collision of Hadrons* (CERN, Geneva, 1968), Vol. 1, p. 494.

7.B.1 Nuclear Physics B13 (1969) 644-650. North-Holland Publ. Comp., Amsterdam

# EXCHANGE DEGENERACY, DUALITY AND REGGE CUTS*

C. MICHAEL**
*High Energy Physics Division*
*Argonne National Laboratory, Argonne, Illinois* 60439

Received 20 August 1969

Abstract: Duality leads to exchange degeneracy for Regge trajectories, and empirical evidence is presented that such a degenerate scheme is not satisfied. A substantial improvement results from the inclusion of Regge cut corrections. These corrections are discussed, separating for clarity the P and non-P contributions to the cut. Application is made to pairs of line reversed reactions such as $\bar{K}N$ and KN charge exchange, and $\pi^+p \to K^+\Sigma^+$ and $K^-p \to \pi^-\Sigma^+$.

## 1. INTRODUCTION

The concept of the duality of resonance poles with Regge poles [1] leads to many consequences, although the concept can at best be approximate for the physical amplitude because of the limitations of pole dominance and because the energy average necessary for the application of duality is imprecise. In such a dual scheme, the absence of resonance poles in channels with exotic quantum numbers leads [2] to exchange degenerate Regge trajectories which have residue functions related in magnitude and have the mechanism of nonsense-choosing at the intercept of the trajectory with zero and negative integers. However, the empirical $\rho$, $\omega$, $P'$ and $A_2$ trajectories determined from analyzing $\pi N$, KN and $\pi N \to \eta N$ data [3] are not degenerate, and have the mechanism of sense-choosing with a special cross over zero for $\rho$ and $\omega$, and the mechanism of no-compensation for the $P'$. As previous calculations have shown, [4] the inclusion of Regge cuts in an exchange degenerate scheme tends to restore agreement with experiment. We discuss the effect of such cuts in a qualitative manner which avoids the differences of detail between formulations of their contribution. In particular we discuss separately the dominant effects from the asymptotic imaginary elastic scattering amplitude (P) and those from the non-asymptotic pole contributions such as $P'$, $\omega$, $\rho$ and $A_2$. We illustrate the consequences of such cuts both for single pole exchange and for exchange degenerate trajectories, and we discuss the experimental consequenses for cross sec-

* Work supported by the U. S. Atomic Energy Commission.
** On leave of absence from Rutherford High Energy Laboratory, Chilton, Didcot. Address from Sept. 1969: TH Division, CERN, Geneva.

tions and polarizations with particular emphasis on line reversed pairs of reactions such as ($K^-p \to \bar{K}^0 n$ and $K^+n \to K^0 p$) and ($\pi^+p \to K^+\Sigma^+$ and $K^-p \to \pi^-\Sigma^+$).

## 2. REGGE CUTS

The eikonal, Glauber or absorption approaches to Regge cuts in inelastic reactions all give substantially similar results. Details may vary, for instance the triple and higher multiplicity exchanges are not treated equivalently. However, near the forward direction (say for $-t < 0.6$ (GeV/$c$)$^2$) single and double scattering dominate and the cuts come from P and non-P elastic scattering modifications to the pole. Coherent inelastic processes [5] may modify the expressions somewhat but these effects should not be dominant.

A convenient approximate expression for the double scattering term is

$$A_{\text{cut}}(\nu,t) = \frac{i}{16\pi^2 \nu}\int\int dt_1 dt_2\, \tau A_{\text{pole}}(\nu,t_1)[A^{\text{in}}_{\text{el.}}(\nu,t_2) + A^{\text{out}}_{\text{el.}}(\nu,t_2)]\,, \qquad (1)$$

where $\tau = T^{-\frac{1}{2}}\theta(T)$ and $T = -t_1^2 - t_2^2 - t^2 + 2tt_1 + 2tt_2 + 2t_1t_2$ and our amplitude is normalized as the $\pi$N non flip amplitude so that $\sigma_{\text{tot}} = \text{Im}\,A/p$ where $\nu$ and $p$ are the pion lab. energy and momentum. For a spin flip amplitude the double scattering term is relatively smaller since the single scattering vanishes for $t_1 = 0$ and thus the convolution is reduced. One may alternatively consider the multiple scattering projected in $l$ or $b$ and the results are equivalent. For instance, the flatter $t$ dependence of the cut term is equivalent to the absorption correction in low partial waves; and the spin flip amplitude lies in higher partial waves and is thus less affected by such absorption.

### 2.1. P-*Contribution*

The P-contribution to $A_{\text{cut}}$ wil have a phase almost 180° from $A_{\text{pole}}$ since $iA_{\text{el.}}$ is negative and real. This destructively interfering cut contribution is inevitable in the type of model we are considering and agrees well with data, in contrast to the opposite sign resulting from the $iA^*_{\text{el.}}$ in a unitarity-based approach. Since the P-cut has less rapid $t$ dependence than the pole term the two contributions may cancel completely for larger ($-t$) and such zeroes explain the $\rho$ and $\omega$ crossover and the effective no-compensation mechanism [6] for the P'.

The exact phase of the P-cut will depend on the phase variations of the pole with $t$ since the convolution integral samples all negative $t$ values. If the phase of the pole term rotates anticlockwise with decreasing $t$, then the P-cut phase relative to the pole term will be greater than 180° at $t = 0$ since the convolution has contributions from $-t_1 > 0$; and less than 180° for moderate $t$ values where the main contributions in the integral come from $t_1 \approx \approx t_2 \approx \frac{1}{4}t$. Since the spin-flip amplitude will be affected less by the cuts, such a deviation in phase of the non-flip amplitude from 180° will give a

small polarization. If the spin-flip ($B$) and non-spin-flip ($A$) amplitudes have the same phase in the pole term, then the polarization which has the sign of $\mathrm{Im}A^*B$ will be positive near $t = 0$ and will change sign by moderate $t$ values. A calculation by Blackmon for $\pi p \to \eta n$ illustrates this quantitatively [4].

2.2. *Non-P contributions*

Pole-pole cuts are expected to contribute although absorption by asymptotic elastic scattering only [7] does not include them. Such cuts lie about 0.5 lower than the poles in the $\alpha$ plane and will be important up to moderate energies. In particular they have a phase which may be estimated from eq. (1) and is of the order of the sum of the phases of the amplitudes evaluated at $\frac{1}{4}t$ plus $90^\circ$. Thus the phase is not near $180^\circ$ and they contribute substantially to polarization unlike the P-cuts which are suppressed. The $P'\rho$ cut in $\pi$N charge exchange is an example and it builds a polarization more positive than the $P\rho$ cut alone and gives a more rapid energy dependence. Such pole-pole cuts are also invoked to explain the exchange in those processes where no single pole has the required quantum numbers, but evidence from such experiments in inconclusive [8].

## 3. EXCHANGE DEGENERACY AND LINE REVERSAL

3.1. *Kaon charge exchange*

Line reversed reactions such as $K^-p \to \bar{K}^0n$ and $K^+n \to K^0p$ provide a sensitive testing ground for exchange degeneracy. The absence of direct channel resonances in the latter reaction leads to strong constants on the exchanged $t$-channel Regge poles from duality. The $\rho$ and $A_2$ exchanges must cancel in the imaginary part of the $K^+n \to K^0p$ amplitude and they are thus degenerate in trajectory and their contributions will be $90^\circ$ out of phase. The relative sign of their contribution is opposite for $K^-p \to \bar{K}^0n$ and they build a rotating phase ($-e^{-i\pi\alpha(t)}$) amplitude of the same modulus as the real $K^+n \to K^0p$ amplitude. Thus the cross sections for the two processes should be equal, and furthermore there should be no polarization since the $\rho$ and $A_2$ contribute in the same relative strength to both spin amplitudes. The fig. 1 shows that the $K^+n \to K^0p$ cross section is larger at low energies by about a factor of 2 and may become comparable at 5 GeV/$c$.

The effect of the P-cut will be to reduce the amplitude for $\bar{K}$ charge exchange slightly less than that for K charge exchange since in the latter case the phase of the "pole" term does not vary with $t$. Thus the P-cut has the opposite effect from that needed. The non-P cuts, however, are asymmetric between the two processes and provide an explanation of the effect. In $\bar{K}$N and KN elastic scattering the dominant non-P exchanges are the exchange degenerate trajectories $P'$ and $\omega$ which contribute as $P' + \omega$ and $P' - \omega$ respectively. The latter combination is purely real while the former has the same modulus but a rotating phase ($-e^{-i\pi\alpha(t)}$) and so is mostly imaginary at $t \approx 0$. The non-P pole cuts are then exactly negative imaginary for $K^+n \to K^0p$ and approximately negative imaginary at small $t$ for $K^-p \to$

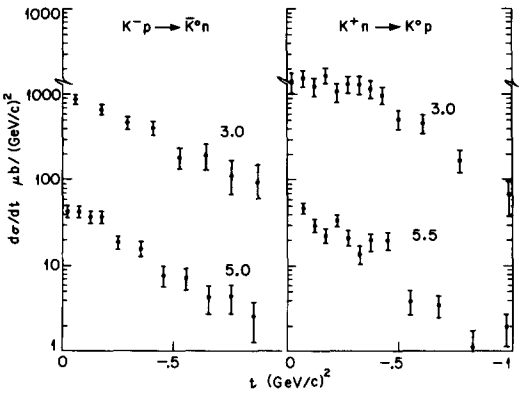


Fig. 1. Differential cross-section data from ref. [9] is compared for $K^-p \to \bar{K}^0n$ and $K^+n \to K^0p$.

$\to \bar{K}^0n$. Thus these cuts will only destructively interfere in the case of $K^-p \to \bar{K}^0n$, and the larger $K^+n \to K^0p$ cross section is predicted correctly. We take this as evidence of the importance of pole-pole cuts when effects from the predominant P-cut are suppressed.

The polarization may then be predicted for $K^-p \to \bar{K}^0n$ to be small and positive at small $t$ and turning negative at moderate $t$ from the P-cut, and positive and increasing from zero at $-t>0$ from the P' and $\omega$ cut; and for $K^+n \to K^0p$ the polarizations will be large and positive coming from the P' and $\omega$ cut alone. A measurement of the polarization for both processes at comparable energies would allow confirmation of this cut-modified degeneracy scheme.

3.2. *Hypercharge exchange*

Similar reasoning applies to the pair of line reversed reactions $\pi^+p \to$ $\to K^+\Sigma^+$ and $K^-p \to \pi^-\Sigma^+$. The degenerate $K^*(1^-)$ and $K^*(2^+)$ exchanges analogous to $\rho$ and $A_2$ will be $90^0$ out of phase. The resulting equality of cross sections is compared with data in fig. 2. The continuous curves are a one pole Regge interpolation of the data which does not distinguish the two reactions. Thus the fact that the $\pi^+p \to K^+\Sigma^+$ data fits reasonably well while the $K^-p \to \pi^-\Sigma^+$ data lies consistently high implies that *experimentally*

$$\frac{d\sigma}{dt}(K^-p \to \pi^-\Sigma^+) > \frac{d\sigma}{dt}(\pi^+p \to K^+\Sigma^+) .$$

In order to estimate the cut effects one must have recourse to SU(3) which, combined with duality, leads to the duality diagram approach [11] which predicts that the $K^*$ poles will contribute with such strength that the $K^-p \to \pi^-\Sigma^+$ amplitude will be real while $\pi^+p \to K^+\Sigma^+$ will have rotating phase. The P contribution should factorize so that $P_{\pi^+p}P_{K^+\Sigma^+} = P_{K^-p}P_{\pi^-\Sigma^+}$ and thus the sum of terms $(P_{\pi^+p} + P_{K^+\Sigma^+})$ and $(P_{K^-p} + P_{\pi^-\Sigma^+})$ as needed in eq. (1) will be the same to first order. The non-P poles in elastic scatter-

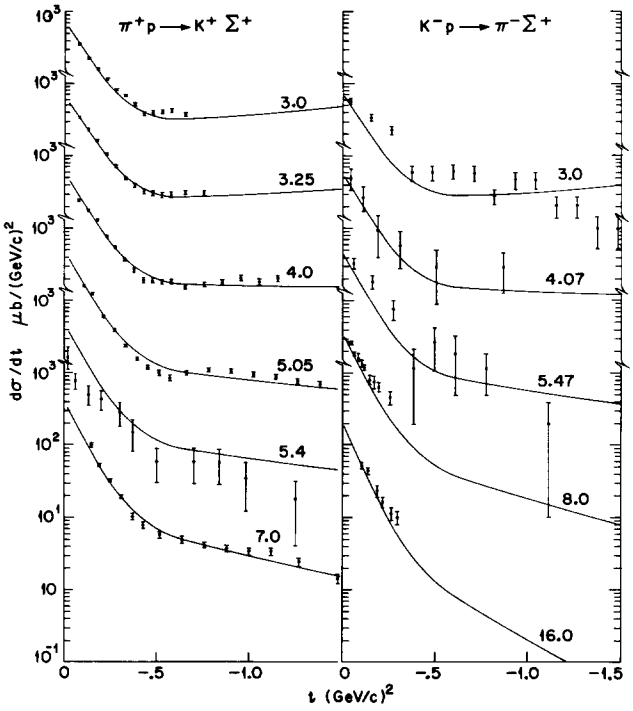


Fig. 2. Differential cross-section data from ref. [10] is compared for $\pi^+p \rightarrow K^+\Sigma^+$ and $K^-p \rightarrow \pi^-\Sigma^+$. The curves are single-pole Regge interpolations of the data and are equal at a given energy for both reactions.

ing are such that for $t \approx 0$ the imaginary part is larger in $(K^-p + \pi^-\Sigma^+)$ than in $(\pi^+p + K^+\Sigma^+)$ and the latter combination has a substantial negative real part [12]. Then both P and non-P cuts suppress the $K^-p \rightarrow \pi^-\Sigma^+$ reaction more and lead to a modified result *opposite* to the experimental evidence. The polarization is predicted to be positive for $\pi^+p \rightarrow K^+\Sigma^+$ from both P and non-P cuts while only the non-P cuts contribute for $K^-p \rightarrow \pi^-\Sigma^+$ and they lead to a polarization suppressed for small $t$ and positive for larger $|t|$. The measured polarization [10] for $\pi^+p \rightarrow K^+\Sigma^+$ is indeed positive for $0.2 < -t < 0.6(GeV/c)^2$ although it is apparently suppressed near $t = 0$.

## 4. SUMMARY

(i) The Regge cut modifications of dual exchange degenerate Regge-trajectories provide an attractive picture which explains high energy data satisfactorily.

(ii) Evidence from the non-equality of $\bar{K}N$ and $KN$ charge exchange con-

firms the need for absorptive effects from non-asymptotic elastic scattering; the larger absorption from $\bar{K}N$ relative to KN being responsible.

(iii) The line reversed pair of reactions $\pi^+p \to K^+\Sigma^+$ and $K^-p \to \pi^-\Sigma^+$ are not consistent with the scheme in relative magnitude. The experimental evidence is not conclusive but the simplest explanation is that the total cross sections satisfy

$$\sigma(\pi^+p)+\sigma(K^+\Sigma^+)>\sigma(K^-p)+\sigma(\pi^-\Sigma^+)$$

in the 3 - 8 GeV/$c$ energy range despite the SU(3)-duality diagram-factorization arguments we presented.

(iv) Polarization predictions are presented.

The author thanks Professor V. Barger, Professor D. Cline, Professor D. Reeder and Professor M. Blackmon for useful discussions. Hospitality at the University of Wisconsin, Madison, where this work was started is gratefully acknowledged, and Dr. K. C. Wali and Dr. R. C. Arnold are thanked for their hospitality at the Argonne National Laboratory.

## REFERENCES

[1] R. Dolen, D. Horn and C. Schmid, Phys. Rev. 166 (1968) 1768;
C. Schmid, Phys. Rev. Letters 20 (1968) 689;
G. Veneziano Nuovo Cimento 57A (1968) 190.
[2] V. Barger, Phys. Rev. 179 (1969) 1371;
C. Schmid, Nuovo Cimento Letters 1 (1969) 165;
R. H. Capps, Phys. Rev. Letters 22 (1969) 215;
J. Madula et al., Phys. Rev. Letters 22 (1969) 1147;
V. Barger and C. Michael, Experimental aspects of dual theories for baryons, Phys. Rev. (to be published).
[3] G. V. Dass, C. Michael and R. J. N. Phillips, Nucl. Phys. B9 (1969) 549;
V. Barger and R. J. N. Phillips, Meson exchanges from simultaneous analysis of $\pi$N scattering data and dispersion sum rules, Wisconsin preprint COO-223 (April 1969).
[4] R. C. Arnold and M. L. Blackmon, Phys. Rev. 176 (1968) 2082;
C. Michael, Nucl. Phys. B8 (1968) 431;
M. L. Blackmon and G. R. Goldstein, Phys. Rev. 179 (1969) 1480;
M. L. Blackmon, Phys. Rev. 178 (1969) 2385;
C. Lovelace, CERN TH 1047 (1969).
[5] F. Henyey, G. L. Kane, J. Pumplin and M. H. Ross, Phys. Rev. Letters 21 (1968) 946 and Phys. Rev., to be published.
[6] V. Barger and R. J. N. Phillips, Phys. Letters 29B (1969) 676.
[7] G. Cohen-Tannoudji, et al., Nuovo Cimento 48A (1967) 1075.
[8] C. Michael, Phys. Letters 29B (1969) 230.
[9] J. Badier et al., Saclay CEA Report R-3037 (1966);
P. Astbury et al., Phys. Letters 16 (1965) 328; 23 (1966) 396;
Y. Goldschmidt-Clermont et al., Phys. Letters 27B (1968) 602;
D. Cline, J. Penn and D. Reeder, Wisconsin Preprint (1968).
[10] S. M. Pruss et al., Phys. Rev. Letters 23 (1969) 189,
W. A. Cooper, et al., Phys. Rev. Letters 20 (1968) 472;
J. Badier et al., Saclay CEA Report R-3037 (1966);
J. S. Loos et al., Phys. Rev. 173 (1968) 1330;

D. Birnbaum et al., presented by G. Belletini in Proceedings of 14th international conference on high energy phisics, Vienna 1968, edited by J. Prentki and J. Steinberger, CERN, p. 358.
[11] H. Harari, Phys. Rev. Letters 22 (1969) 562;
J. Rosner, Phys. Rev. Letters 22 (1969) 689;
[12] J. Rosner, Phys. Rev. Letters 21 (1968) 950.

# AMBIGUITIES IN REGGE ANALYSES AND COMPARISON WITH PHASE SHIFTS

C. DAUM, C. MICHAEL and C. SCHMID
*CERN, Geneva, Switzerland*

Received 15 January 1970

We discuss a simple rotation in the flip non-flip plane, which is undetermined in conventional Regge fits (i.e., those without FESR), and which thus affects the conclusions about mechanism choosing at $\alpha = 0$. Our $t$ independent effective pole analysis of $K^{\pm}p$ elastic scattering naturally continues down to $p_{\mathrm{Lab}} = 1.45$ GeV/$c$, where a rotation invariant comparison with the $K^{+}p$ phase shifts is made.

Regge pole phenomenology provides a framework for obtaining the amplitudes of high energy processes. However in conventional analyses [i.e., those without FESR *], there are several features which should be discussed in detail:

i) the uniqueness of the fits;

ii) the zeros of the amplitudes and more specifically the mechanisms at $\alpha = 0$, etc.. The knowledge of these zeros is crucial for duality comparisons;

iii) the predictive power of such fits.

Most fits have been done in a $t$-dependent manner which necessitated a priori assumptions about zeros and mechanisms for each pole residue. We want to determine such zeros in an unbiased way and therefore we perform our analysis at each fixed $t$ value independently. We consider meson-baryon scattering ($0^{-}\frac{1}{2}^{+} \to 0^{-}\frac{1}{2}^{+}$). Within a model employing a fixed number of Regge poles, one can discuss the uniqueness of the fits. We shall show that:

a) there is a simple rotation operation in the spin flip-spin non-flip plane which leaves unchanged the cross-section and polarization at each $t$ separately, while intermixing the Regge residue function. This operation affects all conventional Regge analyses (i.e., those without FESR). However, if one works modulo the rotation, one can investigate simply any remaining ambiguities in the analysis;

b) the intermixing of Regge residues can modify the zeros in residue functions and change the interpretation of mechanisms;

c) the effective Regge pole model has predictive power coming from the connection between the phase of the amplitude and its energy dependence. However, the Regge predictions must be tested in a manner invariant under the rotation.

When $d\sigma/dt$ and $P$ data are available, one has only two real numbers to determine the four components of the two complex amplitudes $A'$ and $B$. An analysis employing several Regge poles gives one further constraint since the phase is obtained from the energy dependence †. To remove the above rotation degeneracy, one must either measure $R$ or $A$ parameters or compare to amplitudes obtained through phase shift analysis.

We define amplitudes $a$ and $b$ [2] such that

$$d\sigma/dt = C(|a|^2 + |b|^2)$$

$$P\, d\sigma/dt = -2C\, \mathrm{Im}\, ab^*$$

$a$ is the conventional $A'$ amplitude. For elastic scattering $C = (1 - t/4M^2)/(16\pi p_{\mathrm{L}}^2)$, where $p_{\mathrm{L}}$ is the meson lab. momentum, $M$ the target mass. With $q$ the centre-of-mass momentum, we have

$$b = \frac{\sqrt{-t}\, p_{\mathrm{L}}\, B\, (1 + t/4q^2)^{\frac{1}{2}}}{2M(1 - t/4M^2)}$$

We now consider the $(a, b)$ plane ( and *not* the complex plane)

* We perform a Regge analysis without FESR for the following reasons: a) possibility to confront high energy results with FESR; b) for our application to $K^{\pm}p$ scattering, though they were useful when no polarization data existed [1], the FESR have poorly known contributions from the Born poles, unphysical region and $K^{-}p$ phase shift region.

† When there is only one Regge pole (as in $\pi$N charge exchange), one may determine from only $d\sigma/dt$ data two extra quantities, the phases of $A'$ and $B$. These phases are equal.

$$\overrightarrow{\mathrm{Re}} = (\mathrm{Re}\, a,\ \mathrm{Re}\, b)$$

$$\overrightarrow{\mathrm{Im}} = (\mathrm{Im}\, a,\ \mathrm{Im}\, b)$$

In vector notation the measured quantities are given by

$$\mathrm{d}\sigma/\mathrm{d}t = C(\overrightarrow{\mathrm{Re}} \cdot \overrightarrow{\mathrm{Re}} + \overrightarrow{\mathrm{Im}} \cdot \overrightarrow{\mathrm{Im}})$$

$$P\mathrm{d}\sigma/\mathrm{d}t = 2C\overrightarrow{\mathrm{Re}} \cdot \overrightarrow{\mathrm{Im}}$$

$\mathrm{d}\sigma/\mathrm{d}t$ is a scalar product, $P\mathrm{d}\sigma/\mathrm{d}t$ a vector product and both are invariant under a rotation in the spin flip-non-flip plane about the normal.

Reggeology gives restrictions on the phase (angle in the comples plane) from energy dependence, but this Regge phase is *invariant* under rotations in the $(a,b)$ plane. Since for each Regge pole $\mathrm{R}_j$ we have

$$\overrightarrow{\mathrm{Re}_j} = \frac{\mp 1 - \cos \pi\alpha_j}{\sin \pi\alpha_j} \overrightarrow{\mathrm{Im}_j}$$

Then any sum of pole amplitudes may be rotated in the $(a, b)$ plane without changing the complex phases. A Regge cut can in general be considered as a sum of effective poles and will also be invariant ‡.

The parameters $A$ and $R$ are related to $|a|^2 + |b|^2$ and $\mathrm{Re}(ab^*)$ which are clearly not invariant under such rotations and will allow, within a Regge pole model, a complete determination of the amplitudes. However, they have only been measured in $\pi$N scattering [3]. Also near $t = 0$ one may use limited $t$ continuity arguments as in $\pi$N charge exchange [4] to limit the rotation angle since the forward cross-section dip implies substantial spin flip.

Particular mechanisms such as "nonsense" and "Chew" for + signatured trajectories at $\alpha = 0$ are not invariant concepts and can be rotated into one another. Therefore they cannot be determined in an unbiased way in a traditional Regge fit. Dynamical zeros may also be moved in a similar way.

In order to discuss any remaining ambiguities in a Regge fit, we must first arbitrarily fix the over-all orientation in the $(a\text{-}b)$ plane. We choose this over-all orientation such that $b(P) = 0$ at all $t$, which is not a physical constraint on the Pomeron, but is merely a *convention*; equally well we could have chosen $b = 0$ for any other of the poles in the model. In the past, it was known that $b_{\mathrm{P}}$ was poorly determined [5]; we emphasize that our result has nothing to do with the Pomeron per se, but rotates all poles in the problem equally.

As an illustration we shall now discuss the Regge analysis of $\mathrm{K}^{\pm}\mathrm{p}$ elastic scattering. We use $\mathrm{d}\sigma/\mathrm{d}t$ and $P$ data [6,7] between $P_{\mathrm{L}} = 1.45$ and 15 GeV/$c$. The $\mathrm{d}\sigma/\mathrm{d}t$ data were smoothed in $t$ and normalized at $t = 0$ to the forward amplitude obtained from $\sigma_{\mathrm{TOT}}$ [8] and dispersion relation real parts [9]. All data are interpolated to obtain points at $t$ values in steps of 0.1 from $t = 0$ to $t = -1.0$ (GeV)$^2$. We use a conventional effective pole model, where effective poles represent the combined effects of poles and cuts. This implies that we cannot use factorization.

Since there are no good data on $\mathrm{K}^+\mathrm{n}$ elastic scattering (in particular no polarizations) nor on $\mathrm{K}^0$ regeneration on protons, charge exchange will not give any constraints on the $\mathrm{K}^{\pm}\mathrm{p}$ elastic amplitudes which we set out to determine. Therefore we do not include charge exchange data, and we only determine the definite linear combination of $t$ channel isospins, which corresponds to $\mathrm{K}^{\pm}\mathrm{p}$ elastic scattering, namely, $\rho + \omega \equiv \mathrm{V}$ and $\mathrm{A}_2 + \mathrm{f}_0 \equiv \mathrm{T}$. We assume that the coupling of $\phi$ and $f'$ to $\mathrm{N}\bar{\mathrm{N}}$ is weak and can be neglected. We are left with three poles: P, T, V. For simplicity, we assume that the trajectories of V and T are degenerate $\alpha_{\mathrm{V}} = \alpha_{\mathrm{T}} = \alpha_{\mathrm{M}}$ (M = meson), but the residues must not be taken degenerate since such strong exchange degeneracy would not represent the data quantitatively [7]. For numerical stability, we fix the two trajectory functions, $\alpha_{\mathrm{P}}$ and $\alpha_{\mathrm{M}}$ at various values. Here we shall show two cases; a non-zero P slope [S]: $\alpha_{\mathrm{P}} = 1 + 0.3\ t$, $\alpha_{\mathrm{M}} = 0.5 + 0.9\ t$; and a flat P [F]: $\alpha_{\mathrm{P}} = 1$, $\alpha_{\mathrm{M}} = 0.5 + t$. In a subsequent publication we shall discuss the evidence that the data prefer the former choice. As described above, we work at each $t$ separately in order to remove prejudices about zeros of residues; we concentrate on $t \neq 0$. In order to fix the over-all orientation in the $(a,b)$ plane we chose the convention $B_{\mathrm{P}} \equiv 0$ at all $t$; thus we are left with five unknown residues at each $t$ value: $\gamma_{\mathrm{P}}$, $\gamma_{\mathrm{T}}$, $\gamma_{\mathrm{V}}$, $\beta_{\mathrm{T}}$, $\beta_{\mathrm{V}}$ (where $\mathrm{Im}\, A' = \gamma\nu^{\alpha}$, $\mathrm{Im}\, B = \beta\nu^{\alpha-1}$ and $\nu = \omega_{\mathrm{L}} + t/4M$).

For $0 \leqslant -t \leqslant 0.5$ and each $\alpha$ choice, we obtained fits at each $t$ value which led to a unique solution in which each residue function was remarkably continuous in $t$. Using first a lowest momentum of 2.75 GeV/$c$ for the fits, we extended this to 1.45 GeV/$c$ and found substantially the same solution. Consequently we retained 1.45 GeV/$c$ as a lowest momentum and were encouraged by the reasonable fits, particularly for $\mathrm{K}^+\mathrm{p}$, at this momentum. We analyzed the fitting procedure in order to understand the uniqueness; we

‡ However, a specific model, such as the absorption prescription for the cut discontinuity, is not invariant under these rotations.

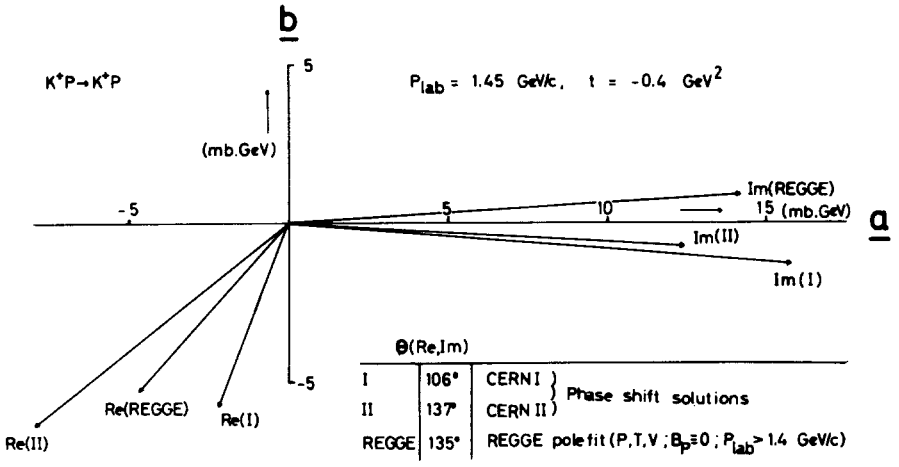


Fig. 1. Amplitudes for $K^+p$ elastic scattering at 1.45 GeV/$c$ and $t = -0.4$ GeV$^2$, in the spin flip-non-flip plane from the Regge pole model S described in the text, and from the phase shift solutions of ref. 10. The Regge amplitudes $\vec{\mathrm{Re}}$ and $\vec{\mathrm{Im}}$ may be rotated simultaneously as described in the text; $\theta$(Re,Im) is the angle between these two vectors.

found that $\gamma_P$ was determined by the higher energy data in $\sigma(K^-) + \sigma(K^+)$, and then $\gamma_V$ and $\beta_T$ were determined in a unique way from the data on $\sigma(K^-) - \sigma(K^+)$ and $P\sigma(K^-) + P\sigma(K^+)$, respectively. $\gamma_T$ and $\beta_V$ are then identified from the lower energy data on $\sigma(K^-) + \sigma(K^+)$ and from $P\sigma(K^-) + P\sigma(K^+)$. $\gamma_T$ and $\beta_V$ are in general less well determined, but out to $|t| = 0.5$ one obtains a unique solution. For $|t| > 0.5$, the ambiguities (in particular a four-fold ambiguity affecting $\beta_V$ and $\gamma_T$) will be discussed in another publication.

We summarize our results for $-t \leq 0.5$ (with $\beta_P \equiv 0$ of course); $\gamma_V$ has the usual cross over zero at $t \approx -0.15$, $\beta_V$ has a zero at $-0.45$; both $\gamma_T$ and $\beta_T$ have ghost killing zeros at $\alpha_M = 0$; $\beta_V$ and $\beta_T$ are almost equal in agreement with exchange degeneracy.

We pass now to the comparison of our Regge predictions for the phase and spin dependence of the $K^+p$ amplitudes at 1.45 GeV/$c$ with those from phase shift analysis [10]. We show in fig. 1 a typical comparison for the amplitudes in the ($a$, $b$) plane. Since we may rotate the Regge amplitudes about the normal to the plane, we must compare invariant quantities. Possible candidates are $|\vec{\mathrm{Re}}|$, $|\vec{\mathrm{Im}}|$ and $\theta$(Re,Im). However, it is more convenient to compare first the two fitted quantities $\mathrm{d}\sigma/\mathrm{d}t \sim |\vec{\mathrm{Re}}|^2 + |\vec{\mathrm{Im}}|^2$ and $P\mathrm{d}\sigma/\mathrm{d}t \sim |\vec{\mathrm{Re}}||\vec{\mathrm{Im}}| \sin\theta(\mathrm{Re},\mathrm{Im})$. The real test is then the comparison of a third invariant which can be $\theta$(Re,Im) or else $\phi = |\vec{\mathrm{Re}}|/|\vec{\mathrm{Im}}|$, the latter being the tangent of the "average Regge phase". Such a third invariant is the prediction of Regge in this context. In fig. 2 these four quantities (of which

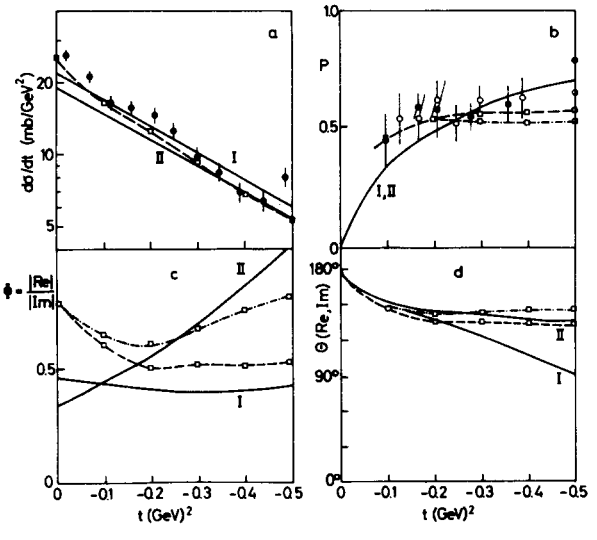


Fig. 2. Comparison for $K^+p$ elastic scattering at 1.45 GeV/$c$ against $t$. Solid lines are phase shift solutions I and II of ref. 10. The squares are our fixed $t$ Regge predictions which are connected to guide the eye by a dashed line for trajectories S ($\alpha_P = 1 + 0.3\,t$, $\alpha_M = 0.5 + 0.9\,t$) and a dot-dash line for trajectories F($\alpha_P = 1$, $\alpha_M = 0.5 + 1.0\,t$). a) Differential cross-section, data from Bettini et al. [6]. b) Polarization, data [6] from Anderson et al. (black circles) and Asbury et al. (open circles). c) The ratio $\phi$ of lengths of the vectors $\vec{\mathrm{Re}}$ and $\vec{\mathrm{Im}}$. d) The angle $\theta$ between the vectors $\vec{\mathrm{Re}}$ and $\vec{\mathrm{Im}}$, see fig. 1.

only three are independent) are compared for both our sets of Regge trajectories S, F and for

both phase shift solutions I, II [10]. The polarization data clearly show the need of higher partial waves in the phase shift analysis to give a sharper rise at small $t$. In the $\theta$ plot, fig. 2d, the Regge prediction is seen to be rather independent of the choice of trajectories, and the Regge prediction shows a preference for the phase shift solution II, which is the solution most in accord with exchange degeneracy expectations [7]. In fig. 2c, $\phi$ which is related to the phase and thus to the $\alpha$ values, shows a larger difference between the predictions from our two choices. These predictions are in qualitative agreement with the phase shift amplitudes except at $t \approx 0$. Here, our $\phi$ values are obtained from fits to the energy dependence of $\sigma_{TOT}$ for $K^{\pm}p$ and, at $t = 0$, lie 0.1 higher than Carter's value [9]. The phase shift estimates [10] of $\phi$ at $t = 0$ do not vary smoothly with energy, and may change appreciably in more refined analyses.

Having seen that the invariant comparison to phase shift amplitudes is fairly good, one may now fix the orientation of the Regge solutions at each $t$ value separately from the phase shifts. If solution II is essentially correct, the Regge solution should be rotated clockwise (see fig. 1) and the angle corresponds to $\beta_p/\gamma_p \sim -0.5$. However, solution I would be compatible with $\beta_p/\gamma_p$ as large as +2.0. This same angle intermixes the $\beta$ and $\gamma$ residues for both V and T poles as well.

The methods of amplitude extraction employed in phase shift analysis and in Regge analysis are at fixed $s$ and $t$, respectively, and are quite independent of each other. It is most encouraging that when one is able to confront the two methods, they agree qualitatively. Moreover, the Regge approach even allows us to discriminate among phase shift solutions giving equally good fits to the data. Provided relevant quantities are asked of it, the predictive power of Regge pole analysis is evident.

*References*


1. G. V. Dass and C. Michael, Phys. Rev. 175 (1968) 1774;
   G. V. Dass, C. Michael and R. J. N. Phillips, Nucl. Phys. B9 (1969) 549.
2. W. Rarita, R. J. Riddell Jr., C. B. Chiu and R. J. N. Phillips, Phys. Rev. 165 (1968) 1615.
3. B. Amblard, G. Cozzila, Y. Ducros, M. Hansroul, A. de Lesquen, J. P. Merlo, J. Morchet and L. Van Rossum, Lund Intern. Conf. on Elementary particles, 1969.
4. R. J. N. Phillips and W. Rarita, Phys. Rev. 139 (1965) B1336;
   G. Höhler, J. Baacke and G. Eisenbeiss, Phys. Letters 22 (1966) 203.
5. C. Michael, Phys. Letters 26B (1968) 392;
   V. Barger and R. J. N. Phillips, Phys. Letters 26B (1968) 730.
6. S. Andersson et al., Phys. Letters 30B (1969) 56;
   A. Bettini et al., Phys. Letters 16 (1965) 83;
   C. Daum et al., Nucl. Phys. B6 (1968) 273;
   J. G. Asbury et al., Phys. Rev. Letters 23 (1969) 194;
   J. A. Danysz et al., Nucl. Phys. B14 (1969) 161;
   J. Debaisieux et al., Nuovo Cimento 44A (1966) 142;
   M. N. Foccaci et al., Phys. Letters 19 (1965) 441;
   W. de Baere et al., Nuovo Cimento 45A (1966) 885;
   J. Banaigs et al., Nucl. Phys. B9 (1969) 640;
   J. Gordon et al., Phys. Letters 21 (1966) 117;
   N. Booth et al., Phys. Rev. Letters 23 (1969) 193;
   J. Mott et al., Phys. Letters 23 (1966) 171;
   L. S. Schroeder et al., Phys. Rev. 176 (1968) 1648;
   K. J. Foley et al., Phys. Rev. Letters 11 (1963) 503;
   Chih-Yung Chien et al., Phys. Letters 28B (1969) 615;
   M. Aderholz et al., Phys. Letters 24B (1967) 434;
   K. J. Foley et al., Phys. Rev. Letters 15 (1965) 45;
   G. A. Rebka, J. Rothberg, A. Etkin, P. Glodis, J. Greenberg, V. W. Hughes, K. Kondo, D. C. Lu, S. Mori and P. A. Thompson, Yale preprint (1969).
7. S. Andersson, C. Daum, F. C. Erné, J. P. Lagnaux, J. C. Sens, C. Schmid and F. Udo, Polarization measurements in medium energy elastic scattering and high energy models, IIIrd Intern. Conf. on High energy collisions, Stony Brook (1969), to be published.
8. W. Baker et al., Phys. Rev. 129 (1963) 2288;
   W. Galbraith et al., Phys. Rev. 138 (1965) B913;
   A. N. Diddens et al., Phys. Rev. 132 (1963) 2721;
   R. J. Abrams et al., Phys. Letters 30B (1969) 564.
9. A. A. Carter, The Argand diagrams of the KN and $\bar{K}N$ forward scattering amplitudes, Cambridge preprint 68/10 (1968).
10. S. Andersson et al., Phys. Letters 30B (1969) 56.


* * * * *

Nuclear Physics B63 (1973) 431–444. North-Holland Publishing Company

# THE PRODUCTION OF REGGE RECURRENCES

C. MICHAEL
*CERN, Geneva*

Received 19 June 1973

Abstract: For resonance states lying on a given Regge trajectory, the two-body production mechanism as a function of the excitation of the recurrence state is discussed. A dual resonance model suggests general features for the Regge-Regge-particle coupling involved in such production. An application is made to the high energy production in $\pi N \to \pi\pi N$ of $\rho$, $f_0$ and g mesons with emphasis on the relative production cross sections, the relative $t$-dependences, the ratio of natural to unnatural parity exchange and the helicity dependence.

## 1. Introduction

There is no complete theory of two-body reactions at high energies. The salient features of the data, however, can be described in a $t$-channel complex angular momentum approach. The exchange of a Regge pole is found [1] to explain the energy dependence and phase of certain amplitudes (net helicity flip $n = 1$ in particular). The $t$-dependence of the Regge residue function can be evaluated from duality considerations. In particular the dual resonance model, $B_4$, gives a natural scale of $1/\alpha'$ to the energy $s$ and so defines a residue $\beta(t)$ that should be essentially constant in $t$. The resulting $t$-dependence is indeed observed [1] experimentally for those amplitudes that have been found to be Regge-behaved. Other helicity amplitudes have a more complicated behaviour and in a complex angular momentum approach this implies the presence of Regge cuts.

Resonance states have been found to lie on exchange-degenerate Regge trajectories which are essentially linear in $m^2$. The highest lying such trajectory for a given set of quantum numbers (the parent or leading trajectory) is well established (for example $\rho - f_0 - g$; $\omega - A_2$; $K^* - K^{**}$ etc). The relative couplings (partial widths) of such Regge recurrence states to a given channel ($\pi\pi$ etc.) have been studied. For instance, a dual resonance $B_4$ model gives an $(\frac{1}{4}e)^J$ decrease of the partial widths for large $J$. The daughter states implied by such dual models are much more model dependent. They will be affected by any unitarization or any absorption of low partial waves needed to make the dual resonance model more physical.

At high energies, it becomes possible to produce Regge recurrence states in quasi

two-body reactions, for example $\pi N \to \rho N$, $\pi N \to f_0 N$, $\pi N \to gN$ etc. At a given energy, from a combined study of the different states on the leading Regge trajectory†, one can discuss the $J$-dependence of (i) the resonance production cross section, (ii) the slope of the differential cross section in $t$ and any eventual shrinking or anti-shrinking with $J$, (iii) the ratio of different exchanges (for example $\pi$ to $A_2$ exchange in $\pi N \to \pi\pi N$) and the ratio of different helicity amplitudes, (iv) the relative absorption corrections to the Regge pole exchange.

The next section reviews models that allow a discussion of the relative production of Regge recurrences. The on-shell exchange coupling (or equivalently the decay matrix element) is first discussed. The off-shell or Regge exchange coupling relevant to the production process is then discussed in different models. The dual resonance model is found to give the most complete treatment and this is related to analyses [2] using the inclusive triple Regge limit and finite mass sum rules (duality for Regge-particle amplitudes). Appendix A contains relevant definitions and clarifications.

The third section, together with appendix B, represents the specific results for the particle-Regge exchange-Regge production vertex from dual resonance models. Compared to the finite mass sum rule approach, a similar decrease of the ratio of natural parity exchange to unnatural parity exchange with increasing excitation $J$ is found, while, unlike that approach, no systematic anti-shrinking of the $t$-dependence with increasing mass is present in the dual model vertex. An analysis of the helicity structure of the Regge exchange coupling is made, and the problem of the unwanted crossing matrix zeroes in the $s$-channel helicity $\pi$-exchange amplitudes is resolved.

## 2. Regge recurrence production

As a prelude, the relative production cross section for a spin-$J$ resonance of mass $m$ in the process $a + b \to m + e$ by r-exchange is discussed. On the r-particle exchange pole, this can be related to the decay matrix element for $m \to a + r$. Thus, for $\pi$ exchange from a $\pi$ beam, the recurrence production cross section is related to the $\pi\pi$ partial width of the spin-$J$ resonance, see also appendix A.

Historically, the partial widths of spin-$J$ resonances were first estimated [3] from the centrifugal barrier suppression factors for a decay in a box of radius $R$

$$m_J \Gamma_J(m) \sim g_J q \left[qR\, h_J^{(1)}(qR)\right]^{-2},$$

where $h_J^{(1)}$ is a spherical Hankel function of the first kind. For a linear Regge trajec-

† As well as the dependence of two-body reactions on $J = \alpha(m^2)$ of the produced parent state, the dependence on $m^2$ for fixed-$J$ is also of interest. Thus, using vector dominance, one can relate the data on electroproduction ($m^2 < 0$) and photoproduction ($m^2 = 0$) of $\pi$ mesons on nucleons to the data on $\pi N \to \pi\pi N$ with the dimeson system in a P-wave for a range of values of $m^2$ across the $\rho$ meson width.

tory, $qR \sim \sqrt{J}$, and thus for large $J$, $\Gamma(J)$ decreases as $g_J J^{-J}$. With the dynamical assumption [4] of a constant $g_J$, this is a very rapid decrease of the partial width with $J$. The usefulness of the centrifugal barrier factor lies rather in describing the large $q$ behaviour of the width for fixed-$J$ which is independent of assumptions about $g_J$.

A more reliable estimate of the $J$-dependence of the coupling $\Gamma_{cd}(J)$ arises from considering the elastic scattering amplitude for c + d → c + d. For the imaginary part of the amplitude, duality relates the average direct channel resonance contribution to the Regge exchange amplitude. The $t$-dependence of the exchange amplitude then gives an estimate of the relative strength of different partial waves. For an amplitude with $t$-dependence $e^{\frac{1}{4}R^2 t}$, the contribution of the spin-$J$ partial wave contains a factor

$$a(J) \sim e^{-J(J+1)/q^2R^2} .$$

Thus partial waves with $J \sim qR$ will be dominant while those with $J \gg qR$ will be suppressed. For a Regge pole exchange amplitude, $\frac{1}{4}R^2$ has the form $\alpha' \log(\alpha' s)$ and then $q^2R^2 \sim \alpha' s \log \alpha' s$. A direct channel resonance of partial width $\Gamma_{cd}$ and total width $\Gamma_T$ will contribute a bump to the imaginary part of the amplitude $a(J)$ of height $\Gamma_{cd}/\Gamma_T$ and of extent in $s$ (or $m^2$) of $m_J \Gamma_T$. Thus $a_J$ will receive an average imaginary part of magitude $m_J \Gamma_{cd}$. Then such duality considerations allow an estimate of the coupling of a spin $J \sim \alpha' s = \alpha' m^2$ parent resonance to the channel cd:

$$m_J \Gamma_{cd}(J) \sim e^{-J/\log J} .$$

This is a much slower decrease with $J$ than that found for the centrifugal barrier with constant $g_J$.

A more explicit example of such a dual estimation of the strength of the $J^{th}$ partial wave from the $t$-dependence of the high energy amplitude is the $B_4$ dual resonance model itself. Using the $\pi\pi \to \pi\pi$ dual amplitude [5, 6] gives for the leading trajectory:

$$m_J \Gamma_{\pi\pi}(J) = \frac{q^2}{2J+1} \frac{q}{m} \frac{(2\alpha' q^2)^J}{\alpha'(J-1)!} \frac{1}{c_J} ,$$

where $c_J \sim 2^J$ for large $J$, and is defined in appendix B. When the relevant isospin factors are included, this expression gives a reasonable account [6] of the $\pi\pi$ partial widths: 0.85 $\Gamma_\rho$ and 0.34 $\Gamma_\rho$ are predicted for the $f_0$ and g respectively as against experimental values [7] of $\sim$ 0.9 $\Gamma_\rho$ and $\sim$ 0.5 $\Gamma_\rho$. Comparison of the g and $\rho$ partial widths provides the most interesting test, since this is insensitive to any exchange degeneracy breaking. For large $J$, and with linear trajectory $J = \alpha' m^2$, the above expression has a $J$-dependence

$$m_J \Gamma(J) \sim (\tfrac{1}{4}e)^J$$

Such a slow $(\frac{1}{4}e)^J$ exponential decrease is common to all dual model approaches.

In the production of Regge recurrence states at high energy, the coupling or Regge residue that enters is (see appendix A) $R_\lambda^J(t, m^2)$. When extrapolated to the particle exchange pole ($\alpha(t) = 0$ or 1 as appropriate). $R$ is related to the decay matrix element as function of $J = \alpha(m^2)$ discussed above. Thus, the essentially new feature of interest in production is the interplay of the $t$, $J = \alpha(m^2)$, and $\lambda$ dependence of the coupling.

The $n$-point dual resonance model allows [8] an explicit calculation of the coupling $R_\lambda^J(t, m^2)$ and the results are presented in appendix B and discussed in detail in the next section. Here, such a $B_n$ calculation is compared with other approaches that have been suggested. The inclusive process a + b → anything + e, is related to the forward a + b + $\bar{e}$ → a + b + $\bar{e}$ amplitude. The exchange of a Regge trajectory $\alpha_r(t)$ coupled to $b\bar{e}$, then leads to the consideration of the forward Regge particle scattering amplitude r + a → r + a. Duality techniques applied to r + a → r + a relate the triple Regge amplitude at large $m^2$ to resonance contributions at small $m^2$. The triple Regge amplitude has a term $(s/m^2)^{2\alpha(t)}$ which correlates the $t$- and $m^2$-dependence, and this is conjectured [2] to be valid on average for $m^2$ in the resonance region. This gives rise to a production cross section for anything of mass $m^2$ which has a $t$-dependence antishrinking as $e^{-t2\alpha' \log m^2}$ with increasing $m^2$. The same factor $(s/m^2)^{2\alpha(t)}$ also comes† from taking the double Regge limit in the exclusive process a + b → c + d + e. Here duality techniques need to be applied [9] to the r + a → c + d amplitude for varying $m^2$.

The $(s/m^2)^{2\alpha(t)}$ factor also yields a faster fall off with $m^2$ when the exchanged trajectory $\alpha(t)$ is higher lying. Thus natural parity exchange ($\alpha(t) \sim 0.5 + t$) will become less important relative to unnatural parity exchange ($\alpha(t) \sim 0 + t$) as $m^2$ increases at fixed-$s$.

In practice for $\alpha(m^2)$ in the range 1 to 2, the leading trajectories should dominate the r + a → r + a and r + a → c + d processes, and such dual predictions will be relevant to parent resonance production. For higher $m^2$, however, just as for particle-particle scattering, the leading trajectory resonances will no longer dominate the amplitudes. Thus, there is no conflict with the result (sect. 3) from the dual resonance model that there is, in general, no antishrinking of the $t$-dependence with $m^2$ for the production of parent trajectory states.

Complementary to the complex angular momentum plane approach to the energy dependence, the dual absorptive model [10] or geometric model seeks to describe the momentum transfer dependence of two-body reactions. Thus the $t$-dependence of the production cross section is predicted in such a model, and its dependence on

† Reggeizing the two-body a + b → m + e production amplitude gives an expression $\beta(t)\, P_{\alpha(t)}(\cos\theta_t)$. For large $s$, at $t \neq 0$, $\cos\theta_t \to s(2q_{am}q_{be})^{-1}$; and for large mass $m^2$, $q_{am} \sim m^2(4t)^{-\frac{1}{2}}$. Thus, $P_{\alpha(t)}(\cos\theta_t)$ behaves as $(s/m^2)^{\alpha(t)}$. To have reasonable analytic behaviour, however, $\beta(t)$ must contain a factor $(q_{am}q_{be})^{\alpha(t)}$ and then the resultant two-body Regge exchange amplitude has no explicit kinematic dependence on $m^2$.

the external mass $m$ of a produced resonance can be found. Indeed, if a universal radius of peripherality $R_0$ is supposed for all exchange reactions, then the $t$-dependence $J_\lambda(R_0\sqrt{-t'})$ is independent of $m^2$. Remembering the motivation *via* duality with peripheral resonances at low energy, one might rather expect the average angular momentum $L_0 \sim qR$ to be independent of $m^2$. Then taking account of the dependence on $m^2$ of the final state momentum $q_f$, leads to a $J_\lambda(R_0\sqrt{-t'}\,\sqrt{q}/\sqrt{q_f})$ behaviour. This shows a shrinking of the $t$-dependence with increasing $m^2$ since $q_f$ decreases. For large $s/m^2$, however, this effect gives a $t$-dependence independent of $m^2$.

## 3. Regge recurrence excitation in the dual resonance model

Explicit calculations with a naturality conserving meson vertex and a naturality changing meson vertex are reproduced in appendix B. These vertices can be applied to natural parity meson production ($J^P = 0^+, 1^-, 2^+, 3^-$, etc.) from pseudo-scalar mesons by the exchange of natural or unnatural parity Regge trajectories. The applications will be most fruitful, if the amplitudes under consideration are Regge behaved in $s$-dependence and phase and have the $t$-dependence characteristic of dual resonance couplings.

For vector meson production on nucleons (PN → VN) the $n = 1$ natural parity isoscalar exchange amplitude ($\omega - f_0$) is indeed found [13] to have the Regge $s$-dependence: $(-t')^{\frac{1}{2}}(\alpha' s)^{\alpha(t)}\,\Gamma(1-\alpha(t))\,\xi_+(t)$ where $\xi_+$ is the signature factor $(\mp 1 - e^{-i\pi\alpha(t)})$. The $\rho - A_2$ charge exchange $n = 1$ amplitude is relatively small and hard to isolate without polarization data. The $n = 1$ unnatural parity charge exchange ($\pi$) producing $\rho$ with $\lambda = 0$ in the $s$-channel frame is also found [14, 15] to have the shrinking $s$-dependence of a Regge trajectory exchange. The $t$-dependence of this amplitude is found [16] to be $(\mu^2 - t)^{-1}\sqrt{-t'}\,e^{bt}$ with $b = 4.4\,\mathrm{GeV}^{-2}$ at 17.2 GeV/$c$. This can be compared [1] with the Regge limit of a dual model expression $\beta(t)\,\Gamma(-\alpha(t))\,\xi_+(t)\,(\alpha' s)^{\alpha(t)}$ where $\beta(t)$ is the product of the $\pi\rho$ and $N\bar{N}$ residues. In the range $0 < -t < 0.2\ \mathrm{GeV}^2$, this latter expression behaves approximately as $(\mu^2 - t)^{-1}\,\beta(t)\,e^{ct}$ where, at 17.2 GeV/$c$, $c = 3.8$ for $\alpha' = 0.9$ and $c = 4.3$ for $\alpha' = 1.0$. Comparing with the empirical values, the $t$-dependence of $\beta(t)$, thus defined with the duality scale of $s$ of $1/\alpha'$, is almost constant apart from $\sqrt{-t}$ factors. This reggeized $\pi$-exchange gives a natural prediction for the exponential form factor that would have been needed for elementary $\pi$-exchange.

Bearing in mind these expectations of which amplitudes should be Regge behaved, some applications are presented of the dual resonance model couplings of Regge recurrences. Details are given in appendix B.

### *3.1. The ratio of natural parity exchange to unnatural parity exchange*

The $\pi$ exchange Regge couplings to recurrence states of spin $J$ and helicity $\lambda$, $U_\lambda^J(t, m^2)$, has the structure of the decay matrix element of the state to $\pi\pi$, and

an off-shell correction factor $X^J_\lambda$ which, for the $s$-channel helicity frame, is the product of a low order polynomial in $t$ and a $(-t)^{\frac{1}{2}|\lambda|}$ factor. For natural parity exchange, the Regge coupling $N^J_\lambda(t, m^2)$ has the structure of a decay matrix element, times a factor $\sqrt{-t}/p_a$ coming from the naturality change, and an off-shell correction factor. Because of this $\sqrt{-t}/p_a$ factor, $N^J_1(m^2)/U^J_0(m^2) \sim m^{-1}$ for increasing $J$, or $\alpha(m^2)$, at fixed-$t$. Explicitly evaluating the factors in appendix B, gives $N^J_1/U^J_0 \sim \sqrt{-t}$, $0.70\sqrt{-t}$ and $0.56\sqrt{-t}$ for $J = 1$, 2 and 3 production ($\rho$, $f_0$, g) respectively at $t \sim 0$.

This dependence is similar to the $(m^2)^{\alpha U(0) - \alpha N(0)}$ or $m^{-1}$ dependence arising on average in the finite mass sum rule approach. Experimental evidence supporting this dependence has been given [2], in particular a comparison of $I_t = 0$ natural parity exchange and $I_t = 1$ unnatural parity exchange in $\pi N \to \rho N$ and $\pi N \to gN$. $\pi^- p \to \pi^- \pi^+ n$ data also show [15] a relative decrease of natural parity exchange with increasing $\pi\pi$ mass. The contribution of the $\pi$ cut makes this more difficult to analyze quantitatively, however.

### *3.2. Slope dependence on $m^2$*

The $t$ dependences of the Regge vertices are given by the factors $X^J_\lambda(t, m^2)$ which are presented in appendix B. The $t$-dependence is different for different helicity amplitudes and also different for $s$- or $t$-channel frames. The $t$-dependence is not of exponential form, and is characterized by the linear term in $t$ at small-$t$; $R^J_\lambda \sim (-t)^{\frac{1}{2}|\lambda|}(1 + b^J_\lambda t + \ldots)$. The slope of the $t$-dependence of the production amplitude as a function of excitation $J = \alpha(m^2)$ is characterized by $b(J)$. An antishrinking of the spin-$J$ production cross section with $t$ means a decrease of $b$ with increasing $m^2$ at fixed energy $s$. For large-$J$ and $\lambda_t = 0$, the $\pi$-exchange coupling does have an antishrinking behaviour of the slope $b$ as approximately $b^J_{\lambda_t = 0}(m^2) \sim -\frac{1}{2}\alpha' \log(m^2)$, similar to that found in the finite mass sum rule approaches from the $(s/m^2)^{\alpha(t)}$ factor. The same coupling in the $s$-channel frame ($\lambda_s = 0$), however, has a strongly shrinking behaviour $b^J_{\lambda_s = 0}(m^2) \sim m^2$ coming from the crossing matrix. For the lowest spin states, one finds explicitly:

$b_\rho = 0$, $b_{f_0} = 0.8$ and $b_g = 1.2$ for $\lambda_s = 0$ $\pi$ exchange;

$b_\rho = 0$, $b_{f_0} = 0$ and $b_g = 0.14$ for $\lambda_s = \pm 1$ natural parity exchange;

$b_\rho = 0$, $b_{f_0} = -0.9$ and $b_g = -1.4$ for comparison from a $-\alpha' \log \alpha' m^2$ antishrinkage. These slope factors $b^J$ represent the change in slope for different Regge recurrences at the meson vertex. An overall $t$-dependence coming from the Regge pole exchange factors and the baryon vertex have also to be added of course.

The $\lambda_s = 0$ $\pi$-exchange amplitude in $\pi N \to \rho N$ seems to be Regge behaved as discussed above. The comparison of this amplitude with those for $f_0$ and g production should be a particularly appropriate test of the predictions. Data indicate [15] that the $s$-channel helicity slope parameter is constant within errors from the $\rho$ to $f_0$

region in $\pi N \to \pi\pi N$ at 17.2 GeV/$c$. The analysis assumes a common slope for all amplitudes at a given mass, however, although the $\rho$ and $f_0$ $\lambda_s = 0$ amplitudes should dominate. A separation of these contributions and an extension to the g-meson region are needed to clarify experimentally the shrinkage or antishrinkage of the slope with $J$.

### 3.3. Crossing matrix zeroes

Consider $\pi$-exchange producing natural parity mesons. On the $\pi$-exchange pole, the only coupling in the $t$-channel helicity frame is $R^J_{\lambda_t=0}(m^2)$. Assuming that this is the only helicity coupling for all $t$, would then give an $s$-channel helicity structure $R^J_{\lambda_s}(t, m^2) = d^J_{\lambda_s 0}(\cos\chi(t))\, R^J_{\lambda_t=0}(t, m^2)$. Thus the zeroes of the $d^J$ function in $t$ would be present in the $s$-channel helicity couplings. For $J = 1$ production this yields $R^{J=1}_{\lambda_s=0}(t, m^2) \sim \cos\chi(t) \sim (t + m^2 - \mu^2)$ which has a zero in the physical region at $t = -m^2 + \mu^2 \sim -0.6$. At high energies, the data show [16] no sign of such a zero. Such zeroes can only be removed by introducing non-zero $t$-channel couplings to $\lambda_t \neq 0$. The full dual resonance model vertex, indeed, contains such reggeized $\pi$-couplings to $\lambda_t \neq 0$ amplitudes (vanishing at $\alpha(t) = 0$ of course). Then crossing to the $s$-channel helicity frame, the combination of contributions from different $t$-channel helicities no longer has the crossing matrix zeroes. Appendix B establishes this explicitly. For $J = 1$ production, for example, $R^{J=1}_{\lambda_s=0}(t, m^2)$ is a constant and the unwanted zero is removed naturally.

It is these additional helicity couplings of the Regge exchange that are important. They emerge naturally from the dual model structure and indicate that the $s$-channel helicity amplitudes have a simpler structure in $t$ compared to the $t$-channel helicity amplitudes. Thus the dual model Regge vertex structure justifies the assumption of simple $s$-channel helicity couplings that have been made empirically. For instance, the surprising constancy [16] in $t$ of the ratio $\gamma_s$ of S- to P-wave $\pi\pi$ production in $\lambda_s = 0$ is naturally explained; this is related to the above discussion of the filling in of the crossing matrix zeroes. A model approach to $\pi$-exchange [17] takes the $s$-channel helicity amplitudes obtained by crossing the $t$-channel Born term and then arbitrarily replaces $t$ by $\mu^2$ in all factors except for the essential $(-t)^{\frac{1}{2}n}/(\mu^2 - t)$ dependence. This has the feature found naturally in the dual vertices of removing the $t$-structure coming from the crossing matrix, but also goes further since it introduces an absorption correction or cut in the $n = 0$ amplitude which has flip at both Regge vertices.

The additional Regge couplings also play a role in making the $\lambda_t = 2$ production amplitudes significant for $t$-values of the order of 1 GeV$^2$. Thus, taking as an example $A_2$ or $K^{**}$ production by natural parity exchange, the helicity $\lambda_t = 2$ or $\lambda_s = 2$ contribution can be estimated from the formulae of appendix B and will be significant.

## 4. Conclusion

The most reliable component of the dual resonance model should be the vertex couplings for mesons on leading trajectories. Problems of daughter states, fermions, and unitarity corrections are thereby avoided. The Regge exchange coupling to produce leading Regge trajectory recurrence states has been evaluated to give the following results.

(a) The production amplitudes for Regge recurrence states can be predicted from a knowledge of the $J = 1$ amplitude. The resonance production amplitude decreases as $(\frac{1}{4}e)^{\frac{1}{2}J}$ for large $J$.

with increasing $J$.

(c) The variation of $t$-dependence with helicity and $J$ has been discussed. Certain $s$-channel helicity amplitudes show a shrinkage of $t$-dependence with increasing $J$.

(d) Additional Regge couplings have been found that fill in the crossing matrix zeroes and so yield $s$-channel helicity amplitudes with simple $t$-dependence.

These results are simplest to apply in practice to amplitudes that are Regge behaved. Experimental evidence supporting (b) and (d) has been presented. Many specific predictions are contained in the couplings evaluated in appendix B. A successful analysis of the particle-Regge-Regge coupling may then give information that can be used to tackle the intriguing problem of understanding why the absorption corrections (or Regge cut effects) in the $n = 0$ $\pi N \to \pi\pi N$ amplitude appear [18, 15] to decrease with increasing $m^2$ (or $J$) relative to the $\pi$-pole contribution.

I gratefully acknowledge discussions with P. Hoyer, A.D. Martin and B. Petersson.

## Appendix A. Definitions of production amplitudes

Consider the process a + b → m + e where m is a spin-$J$ resonance of helicity $\lambda$ which decays with invariant mass $m$ into two spinless particles c and d. In the rest frame of m, the direction of $p_c$ is described by spherical polar angles $\theta$ and $\phi$ in a frame with $O_y$ normal to the a + b → m + e scattering plane and $O_z$ either along $p_a$ in the $t$-channel frame or along $-p_e$ in the $s$-channel frame. The helicity amplitude for the a + b → c + d + e process can thus be factorized

$$A^{\mu_b\mu_a}_{\mu_e}(s, t, m^2, \cos\theta, \phi) = \sum_{\lambda} A^{\mu_b\mu_a J}_{\mu_e}(s, t, m^2)$$

$$\times [m_J^2 - m^2 - im_J\Gamma_T(m^2)]^{-1} M_J d^J_{\lambda 0}(\cos\theta)\, e^{i\lambda\phi} \qquad (A.1)$$

where $M_J$ is the decay matrix element of m into c + d and is related to the partial width by

$$m_J \Gamma_{cd}(m^2) = \frac{1}{2J+1} \frac{q}{8\pi m} |M_J|^2 \tag{A.2}$$

The exchange of a Regge pole r of trajectory $\alpha(t)$, signature $\tau$, and lowest particle state of spin $j_0$, then gives an a + b → m + e amplitude:

$$A^{\mu_b \mu_a J}_{\mu_e \lambda}(s, t, m^2) = R^J_{\mu_a \lambda}(t, m^2) [-\tau - e^{-i\pi\alpha(t)}] (\alpha' s)^{\alpha(t)} \alpha' \Gamma(j_0 - \alpha(t)) R_{\mu_b \mu_e}(t) \tag{A.3}$$

$R^J_{\mu_a \lambda}(t, m^2)$ is the required coupling of the exchanged reggeon r of momentum transfer $t$ to the incoming particle a and the produced state of mass $m$, spin $J$ and helicity $\lambda$.

Some relations between these amplitudes and the observable differential cross sections are

*A.1. Inclusive cross section a + b → anything + e.*

From the generalized optical theorem, this can be related to the discontinuity of the forward three-particle a + b + $\bar{e}$ scattering amplitude $A(s, t, m^2)$

$$\frac{d\sigma}{dt\, dm^2} = \frac{1}{128\pi^2 s q_i^2} \operatorname{disc} A(s, t, m^2) . \tag{A.4}$$

An average over helicity labels is implied. For $s/m^2$ large and $m^2$ also large, a triple Regge behaviour has the form

$$A(s, t, m^2) \sim \left(\frac{s}{m^2}\right)^{2\alpha_r(t)} (m^2)^{\alpha_0(0)} , \tag{A.5}$$

where $\alpha_0$ is the exchange trajectory (pomeron or other) intercept in the reggeon (r) - particle (a) total cross section.

*A.2. Exclusive cross section a + b → c + d + e.*

$$\frac{d\sigma}{dt\, dm^2\, d\Omega} = \frac{1}{64\pi s q_i^2} \frac{1}{(2\pi)^3} \frac{q_{cd}}{4m} |A^{\mu_b \mu_a}_{\mu_e}(s, t, m^2, \cos\theta, \phi)|^2 , \tag{A.6}$$

where an average over initial and sum over final helicities is implied. For $s/m^2$ large and $m^2$ also large, there exists a double Regge limit with the form

$$A \sim \left(\frac{s}{m^2}\right)^{\alpha_r(t_{be})} (m^2)^{\alpha(t_{ac})} . \tag{A.7}$$

*A.3. Spin J production in a + b → c + d + e and resonance production.*

The $Y_L^M(\theta, \phi)$ moments of the observable of eq. (A.6) can be used to try and extract the spin-$J$, helicity-$\lambda$ component in the cd final state channel. Resonance states in this channel should have Breit-Wigner shapes in their $m^2$-dependence. Integrating over the resonance line shape in $m^2$, and multiplying by $\Gamma^J_{tot}(m^2)/\Gamma^J_{cd}(m^2)$ to correct for the branching ratio, then gives the resonance production cross section. Because of unitarity, this is also related to the factorized production amplitude defined in eq. (A.1), by

$$\rho^J_{\lambda\lambda} \frac{d\sigma}{dt} = \frac{1}{64\pi s q_i^2} \left| A^{\mu_b \mu_a J}_{\mu_e \lambda}(s, t, m_J^2) \right|^2 , \tag{A.8}$$

where a helicity average over $\mu_a$ and $\mu_b$ and sum over $\mu_e$ is implied.

As a further clarification, the information contained in the $m^2$- or $J$-dependent observables A.1 to A.3 is illustrated at the $\pi$-exchange pole, $t = \mu^2$, in $\pi N \to \pi\pi N$: A.1 is related to $\sigma^{tot}_{\pi\pi}(m^2)$; A.2 is related to $(d\sigma/dt)_{\pi\pi}(m^2, \cos\theta)$; A.3 is related to $m_J \Gamma^J_{\pi\pi}(m_J)$.

## Appendix B. Explicit dual resonance model couplings

Particle – Regge pole exchange – Regge recurrence production coupling residues $R^J_\lambda(t, m^2)$ are evaluated from dual resonance models. Isospin and signature factors are neglected, since the dynamical dependence on the variables is under study. Triple meson vertices are considered which are naturality conserving (for example $\pi + \pi \to \rho$, $f_0$, g etc.) or naturality changing (for example $\pi + A_2 \to \rho$, $f_0$, g etc., or $\pi + \rho \to \omega$, $A_2$ etc.).

*B.1. Naturality conserving vertex*

From factorizing the dual $n$-point function $B_n$ into two pieces on a leading pole $m$ at $\alpha(m^2) = J$ in an internal subenergy, the following expression for the process a + b → m + e arises [11]

$$V^J_{\mu_1 \ldots \mu_J} = g^2 \frac{(\sqrt{2\alpha'})^J}{\sqrt{J!}} \int du\, u^{-1-\alpha(s)} (1-u)^{-1-\alpha(t)} \prod_{i=1}^{J} (p^\mu_a u - p^\mu_e (1-u)). \tag{B.1}$$

This must be contracted with the polarization tensor $\epsilon^J_{\mu_1 \ldots \mu_J}(\lambda)$ to obtain the helicity amplitudes. In the rest frame of $m$, where $p$ has spherical polar co-ordinates $\theta$ and $\phi$,

$$\epsilon^J_{\mu_1 \ldots \mu_J} p^{\mu_1} p^{\mu_2} \ldots p^{\mu_J} = \frac{(p)^J}{\sqrt{C_J}} d^J_{\lambda 0}(\cos\theta)\, e^{i\lambda\phi} \tag{B.2}$$

where $C_J = (2J)!\, 2^{-J}/(J!)^2$. A further property of the polarization tensor is

$$\epsilon^J_{\mu_1 \ldots \mu_J} = \sum_{\lambda_1 \lambda_2} (J - r, r, \lambda_2, \lambda_1 \mid J, \lambda)\, \epsilon^r_{\mu_1 \ldots \mu_r}(\lambda_1)\, \epsilon^{J-r}_{\mu_{r+1} \ldots \mu_J}(\lambda_2)\,. \tag{B.3}$$

Then expanding the product in eq. (B.1) gives terms in $(p_a^\mu)^r(-p_e^\mu)^{J-r}$ and eqs. (B.2) and (B.3) can be used to simplify the expression. In the $s$-channel helicity frame, $-p_e$ is along $O_z$ and has magnitude $s/2m$ for large-$s$, while $p_a$ has $z$-component $p_a \cos\chi$ and $x$-component $p_a \sin\chi$ where

$$\begin{aligned} p_a^2(t) &= \lambda(m^2, t, a^2)/4m^2\,, \\ p_a(t)\cos\chi(t) &= (m^2 + t - a^2)/2m\,, \\ p_a(t)\sin\chi(t) &= (-t)^{\frac{1}{2}}\,. \end{aligned} \tag{B.4}$$

For large-$s$, the Regge limit of eq. (B.1), gives the Regge residue, defined as in appendix A,

$$U^J_\lambda(t, m^2) = g \frac{(2\alpha')^{\frac{1}{2}J}}{\sqrt{\alpha' J!\, c_J}} p_a^J(v^2)\, X^J_\lambda(t, m^2)\,, \tag{B.5}$$

where $\alpha(t) = \alpha'(t - v^2)$ and in the $s$-channel helicity frame

$$X^J_\lambda(t, m^2) = p_a^{-J}(v^2) \sum_{r=0}^{J} \frac{(p_a(t))^r (2\alpha' m)^{r-J}}{(J-r)!} \frac{\Gamma(-\alpha(t) + J - r)}{\Gamma(-\alpha(t))}$$

$$\times \left(\frac{(J+\lambda)!(J-\lambda)!}{(r+\lambda)!\,(r-\lambda)!}\right)^{\frac{1}{2}} d^r_{\lambda 0}(\cos\chi(t))\,. \tag{B.6}$$

This latter expression reduces to the product of a factor $(-t)^{\frac{1}{2}|\lambda|}$ and a polynomial in $t$ of order $J - |\lambda|$ or less.

For the $t$-channel frame, the result is the same as eq. (B.5) and (B.6) except for the interchange of $r$ and $J - r$ in the first three factors in the numerator of eq. (B.

On shell at $\alpha(t) = 0$ the expressions simplify to

$$X^J_{\lambda_s} = d^J_{\lambda_s 0}(\cos\chi(v^2)), \qquad X^J_{\lambda_t} = \delta_{\lambda_t 0}. \tag{B.7}$$

The first term in (B.5) is the decay matrix element for m → a + on shell exchange particle. The above $B_n$ results are for a theory of scalar particles with lowest states at $\alpha(m^2) = 0$. In practice, for the naturality conserving vertex $\pi$ + ($\pi$ exchange) → $\rho$, $f_0$, g etc., the produced resonances have trajectories with $\alpha(m^2) = 1$ as lowest state. This can be incorporated into a $B_5$ model for $\pi + \pi \to \pi + \pi + \epsilon$ (where $\epsilon$ is a $J^P = 0^+$ state) in the same way as into the $B_4$ model [5, 6] for $\pi\pi \to \pi\pi$. The resulting $B_5$ expression agrees with the $B_4$ matrix element on shell, and gives the same result for the Regge vertex as eq. (B.5) except for the replacement of the $\sqrt{J!}$ factor in the denominator by $\sqrt{(J-1)!}$.

The $t$-dependence of the correction factor $X(t)$ can be expressed, for small-$t$, as

$$X^J_\lambda(t, m^2) = (1 + t\, b^J_\lambda(m^2) + O(t^2))(-t)^{\frac{1}{2}|\lambda|}. \tag{B.8}$$

Neglecting $a^2$ and $v^2$, gives a general result

$$b^J_{\lambda_s=0} = b^J_{\lambda_t=0} + \frac{J(J+1)}{m^2},$$

$$b^J_{\lambda_t=0} = \frac{-2J}{m^2} - \alpha' \sum_{r=2}^{J} \frac{J!}{(J-r)!}\,\frac{1}{r}(\alpha' m^2)^{-r}. \tag{B.9}$$

Similarly, the $t$-dependence of $\Sigma_\lambda |X^J_\lambda|^2$ is characterized at small-$t$ by $2\, b^J_{\lambda_t=0}$.

Explicit off-shell correction factors for $a^2 = v^2 = \mu^2$ and $p_a = \frac{1}{2}m(1 - 4\mu^2/m^2)^{\frac{1}{2}}$ in the $s$-channel helicity frame are

$$p_a X^1_0 = \tfrac{1}{2}m, \qquad p_a X^1_1 = -(-\tfrac{1}{2}t)^{\frac{1}{2}},$$

$$p_a^2 X^2_0 = \tfrac{1}{4}\{(m^2 + 2\mu^2) + (t - \mu^2)(2 - 1/\alpha' m^2)\},$$

$$p_a^2 X^2_1 = (-\tfrac{3}{8}t)^{\frac{1}{2}} t\, m, \qquad p_a^2 X^2_2 = -\tfrac{1}{4}\sqrt{6}\, t,$$

$$p_a^3 X^3_0 = \frac{1}{8m}\{(m^4 + 6m^2\mu^2) + (t - \mu^2)(6m^2 - \frac{3}{\alpha'} - \frac{2}{\alpha' m^2 \alpha'})\},$$

$$p_a^3 X^3_1 = -\tfrac{1}{4}\sqrt{-3t}\,\{(m^2 + \mu^2) + (t - \mu^2)(1 - 1/\alpha' m^2)\},$$

$$p_a^3 X^3_2 = -\tfrac{1}{8}t\, m\sqrt{30}, \qquad p_a^3 X^3_3 = -\tfrac{1}{4}\sqrt{5}\,(-t)^{\frac{3}{2}}. \tag{B.10}$$

For the $t$-channel frame, similarly

$$p_a(t) X_0^1 = p_a(\mu^2) \left(1 + \frac{3(\mu^2 - t)}{m^2 - 4\mu^2}\right), \qquad p_a(t) X_1^1 = \frac{\sqrt{-t}(t - \mu^2)}{\sqrt{2}\sqrt{m^2 - 4\mu^2}\, m} . \quad \text{(B.11)}$$

*B.2. Naturality changing vertex*

From the $B_5$ dual resonance model for five pseudo-scalar mesons [12], one can extract the vertex for producing natural parity meson Regge recurrences by the exchange of a natural parity Regge trajectory $\alpha(t) - 1 = \alpha'(t - \upsilon^2)$. Extracting the leading trajectory spin $J$-pole in the cd channel and taking the Regge limit $s \to \infty$, gives a resonance production coupling together with the decay amplitude. Factorizing off the decay matrix element and picking out in the $s$-channel helicity frame the coefficient of $d^J_{\lambda 0}(\cos\theta) e^{i\lambda\phi}$ (see eq. (A.1)) gives the production Regge residue

$$N^J_\lambda(t, m^2) = \bar{g} \frac{(2\alpha')^{\frac{1}{2}J}}{\sqrt{(J-1)!}} \left(\frac{J+1}{\alpha' c_J J}\right)^{\frac{1}{2}} p_a^J(\upsilon^2) \frac{\sqrt{-t}}{p_a(\upsilon^2)} X^J_\lambda(t, m^2) ,$$

$$X^J_\lambda(t, m^2) = p_a^{1-J}(\upsilon^2) \sum_{r=1}^{J} \frac{(p_a(t))^{r-1} (2\alpha' m)^{r-J}}{(J-r)!}$$

$$\times \frac{\Gamma(-\alpha(t) + J - r + 1)}{\Gamma(-\alpha(t) + 1)} \left(\frac{r(r+1)(J+\lambda)!\,(J-\lambda)!}{J(J+1)(r+\lambda)!\,(r-\lambda)!}\right)^{\frac{1}{2}}$$

$$\times \{d^r_{1\lambda}(\cos\chi(t)) + d^r_{-1\lambda}(\cos\chi(t))\} , \quad \text{(B.12)}$$

which is again a polynomial in $t$ of order $J - |\lambda|$ or less together with a factor $(-t)^{\frac{1}{2}|\lambda|}$.

For on-shell exchange at $t = \upsilon^2$

$$X^J_\lambda(\upsilon^2, m^2) = d^J_{1\lambda}(\cos\alpha(\upsilon^2)) + d^J_{-1\lambda}(\cos\alpha(\upsilon^2)) , \quad \text{(B.13)}$$

and in the $t$-channel frame

$$X^J_{\lambda_t}(\upsilon^2, m^2) = \delta_{\lambda_t, \pm 1} . \quad \text{(B.14)}$$

Specific forms of the off-shell correction factor in the $s$-channel helicity frame, where $p_a = p_a(\upsilon^2)$ and $a = \mu$, are

$$X_0^J = 0\,,$$

$$X_1^1 = 1\,, \qquad p_a X_1^2 = \frac{m^2 + v^2 - \mu^2}{2m}\,, \qquad p_a X_2^2 = \sqrt{-t}\,,$$

$$p_a^2 X_1^3 = \frac{1}{4m^2}\left[(m^2 + v^2 - \mu^2)^2 + m^2 v^2 + (t - v^2)\,(m^2 - 1/\alpha')\right]\,,$$

$$p_a^2 X_2^3 = \sqrt{\tfrac{5}{2}}\,\frac{\sqrt{-t}}{2m}(m^2 + v^2 - \mu^2)\,, \qquad p_a^2 X_3^3 = -\tfrac{1}{4}\sqrt{15}\,t\,. \tag{B.16}$$

In the $t$-channel helicity frame

$$p_a X_1^2 = p_a(t) + \frac{(1 - \alpha(t))\cos\chi(t)}{2\alpha' m}\,, \qquad p_a X_2^2 = \frac{1 - \alpha(t)}{2\alpha' m}\sin\chi(t)\,. \tag{B.17}$$

## References


[1] C. Michael, Proc. of the 4th Int. Conf. on high energy collisions, Oxford, (RHEL, 1972); Proc. of the 16th Int. Conf. on high energy physics, Batavia, (NAL, 1973).
[2] P. Hoyer, R.G. Roberts and D.P. Roy, Nuclear Phys. B56 (1973) 173.
[3] J. Blatt and V. Weisskopf, Theoretical nuclear physics, (John Wiley and Sons, New York, 1952).
[4] F. von Hippel and C. Quigg, Phys. Rev. D5 (1972) 624.
[5] C. Lovelace, Phys. Letters 28B (1968) 624.
[6] J. Shapiro, Phys. Rev. 179 (1969) 1345.
[7] Particle Data Group, Rev. Mod. Phys. 45 (1973) (to be published).
[8] D. Alessandrini, D. Amati, M. Le Bellac and D. Olive, Phys. Reports 1 (1971) 269; H.M. Chan and T.S. Tsun, Phys. Rev. D4 (1971) 156.
[9] P. Hoyer and J. Kwiecinski, Rutherford preprint RPP/T46 (1973).
[10] H. Harari, Ann. of Phys. 63 (1971) 432.
[11] D.K. Campbell, D.I. Olive and W. Zakrewski, Nuclear Phys. B14 (1969) 319.
[12] K. Bardakci and H. Ruegg, Phys. Letters 28B (1969) 671.
[13] C. Michael, CERN TH. 1627 (1973).
[14] P. Estabrooks and A.D. Martin, Phys. Letters 42B (1972) 229.
[15] P. Estabrooks and A.D. Martin, CERN TH. 1647 (1973).
[16] P. Estabrooks and A.D. Martin, Phys. Letters 41B (1972) 350; CERN TH. 1668 (1973).
[17] P. Williams, Phys. Rev. D1 (1970) 1312.
[18] W. Ochs and F. Wagner, MPI Munich preprint (1973).

Nuclear Physics B82 (1974) 282–312. North-Holland Publishing Company

# HIGH-ENERGY PRODUCTION AND DECAY OF VECTOR AND TENSOR MESONS

A.C. IRVING and C. MICHAEL
*CERN, Geneva*

Received 18 March 1974

Abstract: The available charge-exchange data for $\pi N \to \rho N$, $\pi N \to \omega N$ and $\rho - \omega$ interference effects in the momentum range 6–17 GeV/$c$ are analyzed. Duality considerations are used to constrain as much as possible the exchanged Regge poles and also to relate their contributions to those made by the same Regge exchanges in $\pi N \to f^0 N$ and $\pi N \to A_2 N$. Combined with an empirical investigation of the Regge cut contributions, this allows a simultaneous description of vector and tensor meson production. The resulting amplitudes are used to predict interference effects in the common $K\bar{K}$ decay channel of $f^0$ and $A_2$. Other predictions include $K^*(1420)$ and $\overline{K}^*(1420)$ production, and many polarization effects.

## 1. Introduction

With the increasing abundance of data on resonance production processes, it has become possible to investigate closely the structure of the exchange amplitudes. The usefulness of a description in terms of $t$-channel Regge-pole exchange with $s$-channel modifications (cuts or absorption) has been confirmed [1]. The simplest approach would be to restrict the Regge-pole exchanges by dual constraints (exchange degeneracy, etc.), factorization and SU(3), and to restrict the cuts to amplitudes of zero over-all helicity flip $n$. We shall pursue such a simple approach with its considerable predictive power and shall try to identify any possible indications for relaxing the constraints.

The advent of spectrometer data on the production of higher mass resonances will introduce a further exciting line of investigation. Higher mass (and spin) resonances are produced in reactions that have the same exchange quantum numbers as their basic counterparts (e.g. $\pi N \to f^0 N$ or $\pi N \to gN$ relative to $\pi N \to \rho N$). It is thus a challenge to existing theories to account for the production mechanisms of such states. Dual theories, both more generally through local duality applied to finite mass sum rules [2, 3], and more specifically from the explicit dual model vertex structure [4], have characteristic predictions to make. We use these ideas to make a preliminary study of tensor meson production based on the knowledge of vector meson production.

In sect. 2, we discuss the available data (6–17 GeV/$c$) on $\pi N \to \rho N$ and $\pi N \to \omega N$

and establish models for the exchange contributions. Interference effects between $\rho$ and $\omega$ production amplitudes are observable as a result of $\rho$–$\omega$ electromagnetic mixing in the $\pi\pi$ decay, and also from comparison with the SU(3) related processes $KN \to K^*N$ and $\bar{K}N \to \bar{K}^*N$. Our decomposition of the $\rho$ and $\omega$ production amplitudes into exchange contributions is consistent with data on such interference effects and, in sect. 3, we discuss predictions for nucleon polarization observables which will provide further insight into the amplitude structure.

Armed with a model for vector meson production, in sect. 4, we use the dual model expectations as a guide in discussing the charge-exchange tensor meson production reactions $\pi N \to f^0 N$ and $\pi N \to A_2 N$. The available data are well described. As an additional sensitive test, we present, in sect. 5, predictions for the interference effects to be seen in the $K\bar{K}$ decay channel which is common to $A_2$ and $f^0$. Likewise $K^*(1420)$ and $\bar{K}^*(1420)$ production are discussed.

Conclusions are presented in sect. 6.

## 2. Vector-meson production

Spin-1 meson production on nucleons involves six helicity amplitudes which are connected to the observable density matrix elements as follows (see also appendix A)

$$\sigma_0^{\mathrm{u}} = \rho_{00}\mathrm{d}\sigma/\mathrm{d}t = |P^0_{++}|^2 + |P^0_{+-}|^2 = |P_0|^2 ,$$

$$\sigma_-^{\mathrm{u}} = (\rho_{11} - \rho_{1-1})\mathrm{d}\sigma/\mathrm{d}t = |P^-_{++}|^2 + |P^-_{+-}|^2 = |P_-|^2 ,$$

$$\sigma^{\mathrm{n}} = (\rho_{11} + \rho_{1-1})\mathrm{d}\sigma/\mathrm{d}t = |P^+_{++}|^2 + |P^+_{+-}|^2 = |P_+|^2 ,$$

$$\sqrt{2}\ \mathrm{Re}\,\rho_{10}\mathrm{d}\sigma/\mathrm{d}t = \mathrm{Re}\,(P^-_{++}P^{0*}_{++} + P^-_{+-}P^{0*}_{+-}) , \tag{2.1}$$

where

$$P^{\pm}_{\lambda\nu} = \sqrt{\tfrac{1}{2}}(H^{+1}_{\lambda\nu} \pm H^{-1}_{\lambda\nu}) .$$

Allowance [5, 6] can be made for the presence of S-wave background under the P-wave vector meson signal. Thus the modulus of $\lambda = 0$ and 1 unnatural parity exchange contributions ($\sigma_0^{\mathrm{u}}$ and $\sigma_-^{\mathrm{u}}$), their interference $\mathrm{Re}\,\rho_{10}$, and the natural parity exchange contribution $\sigma^{\mathrm{n}}$ can be separated. Further separation of the amplitudes requires, at present, assumptions about the nature of the exchange contributions. In principle, however, polarization observables will allow [7] a determination of the moduli and relative phases of each amplitude. In practice, an incomplete set of polarization measurements (e.g. polarized target without recoil polarization analysis) will allow stringent tests of the assumptions to be made about exchange amplitudes.

*2.1.* $\pi^- p \to \rho^0 n$

The quantum numbers allowed in the $t$-channel are such that only a restricted set of Regge-pole exchanges should contribute. These are discussed in turn.

*2.1.1. $\pi$ exchange.* We treat the pion as a Regge pole with a slope just like any other particle exchange. The proximity of the $J = 0$ $\pi$-pole to the physical region implies that the Regge description is essentially the same for small $t$ as a one-particle exchange expression. From consideration of the Chew-Frautschi plot for unnatural parity mesons we expect

$$\alpha_\pi(t) = \alpha'(t - \mu^2) = 0.82(t - \mu^2) ,$$

where $\mu$ is the pion mass and the value of $\alpha'$ comes from assuming linear exchange degenerate trajectories $\pi - \mathrm{H}$ or $\eta - \mathrm{B}$. The $J = 0$ $\pi$-pole couples only to $\lambda_t = 0$ $\rho$ mesons ($\lambda_s$ and $\lambda_t$ refer respectively to $s$- and $t$-channel helicity frames). Away from the nonsense zero at $\alpha_\pi(t) = 0$, however, a Regge $\pi$ trajectory should couple to $\lambda_t \neq 0$ and this contribution could become significant for $-t \sim 0.5$ GeV$^2$. A simple estimate of a reasonable strength for such a $\lambda_t = 1$ contribution comes [4] from the structure of the dual resonance model vertex. This yields, for the $t$-channel helicity frame,

$$\frac{\pi_-^t}{\pi_0^t} = \frac{2\sqrt{-t}(\mu^2 - t)}{m(m^2 - \mu^2 - 3t)} . \tag{2.2}$$

where $m = m_\rho$ and $\pi_-^t$ vanishes at $t = \mu^2$ as discussed previously. In terms of $s$-channel helicity amplitudes, this takes on the simple form [4]

$$\frac{\pi_-^s}{\pi_0^s} = \frac{2\sqrt{-t}}{m} . \tag{2.3}$$

The more popular assumption of taking $\pi_-^t = 0$ leads to $\pi_-^s/\pi_0^s = 2\sqrt{-t}\, m/(m^2 + t - \mu^2)$, which is significantly different in the neighbourhood of the zero of $\pi_0^s$ at $-t = m^2 - \mu^2$.

At the nucleon vertex, the $\pi$ Regge trajectory couples to the helicity flip only. Thus its contribution to $P_{+-}^0$ and $P_{+-}^-$ will be in the above ratio. A simple parametrization for the $\lambda_s = 0$ amplitude valid up to moderate $t$-values is

$$\pi_{+-}^0 = \frac{\sqrt{-t}\, g_\pi}{\mu^2 - t} \frac{m}{\sqrt{m^2 - 4\mu^2}} \mathrm{e}^{b_\pi t} \mathrm{e}^{-\frac{1}{2} i\pi\alpha_\pi(t)} \left(\frac{p_\mathrm{L}}{p_0}\right)^{\alpha_\pi(t)-1} , \tag{2.4}$$

where $p_\mathrm{L}$ is lab momentum and $p_0$ is chosen for convenience as 17.2 GeV/$c$. A constant factor has been included to assist the identification of $g_\pi$ with the residue of the $t$-channel $\pi$ exchange pole (appendix A).

*2.1.2. $A_2$ exchange.* The $A_2$ Regge pole may couple to the amplitudes $P^+_{+-}$ and $P^+_{++}$. We expect a trajectory

$$\alpha_A(t) = 0.5 + \alpha' t.$$

The ratio of flip to non-flip coupling at the nucleon vertex may be related by factorization to that found in $\pi N \to \eta N$ and KN charge exchange. In terms of the invariant coupling A' and A for such processes we have $A_2$ exchange ratios

$$\frac{A^+_{+-}}{A^+_{++}} = \frac{-\sqrt{-t}}{2m_N}\frac{A}{A'} = \frac{\sqrt{-t}}{r}, \tag{2.5}$$

and thus $r \sim 0.5$ for the vector dominance expectation [8] $A/A' \sim -3.7$, while $r \sim 0.25$ for the empirical values of $A/A' \sim -8$ found in effective pole fits to $0^-\tfrac{1}{2}^+ \to 0^-\tfrac{1}{2}^+$ processes [9]. A parametrization for the $s$ and $t$ dependence of the $A_2$ exchange pole contribution is

$$A^+_{+-} = -t' g_A e^{b_A t} e^{-\frac{1}{2}i\pi\alpha_A(t)} \left(\frac{p_L}{p_0}\right)^{\alpha_A(t)-1}. \tag{2.6}$$

*2.1.3. Cut contribution.* The contributions from the $\pi$ and $A_2$ Regge poles have long been known [10] to be insufficient to describe the data on $\pi N \to \rho N$. In particular, the data are non-zero in the forward direction, while the Regge contributions all vanish as $t' \to 0$. It is traditional [10] to incorporate a background, Regge cut, or absorptive correction $C$ which does not vanish as $t' \to 0$. This can be motivated from $s$-channel Born term or dual arguments, via absorption of low partial waves, or from a $\pi$-pomeron Regge cut. Our interest lies in an empirical description of the data, however, so that we shall be content with a parametrization of the cut $C$. The simplest assumption is that $C$ only contributes to the $s$-channel helicity non-flip amplitude $H^1_{+-}$. This leads to equal amounts of cut in $P^-_{+-}$ and $P^+_{+-}$. The phase and energy dependence of $C$ may be obtained from the experimental data and some theoretical assumptions. Since Re $\rho_{10}$ experimentally [6] has its extremum value relative to $P_0$ and $P_-$, this implies that $P_0$ and $P_-$ have the same phase (phase coherence). Thus the phase of $C$ and of the $\pi$ exchange contributions must be similar. Consideration of their interference in $P_+$ also leads to constraints [5] on their relative phase as a function of $t$. A compromise, which also has the virtue of being the naive absorption model result, is to take the phase from an effective trajectory

$$\alpha_C(t) = 0 + \tfrac{1}{2}\alpha' t\,.$$

The energy dependence of the cut contribution is model-dependent – as a simple approximation we take the energy dependence to be given by the same effective trajectory as the phase. Thus the cut is approximated for convenience by an effective (non-factorizing) pole with the above trajectory. Thus our parametrization is

$$C^{+}_{+-} = C^{-}_{+-} = g_C e^{b_C t} e^{-\frac{1}{2} i\pi\alpha_C(t)} \left(\frac{p_L}{p_0}\right)^{\alpha_C(t)-1} . \tag{2.7}$$

*2.1.4. Our model.* Our combination of $\pi$ and $A_2$ pole exchange and effective cut $C$ differs from that of Estabrooks et al. [11] only in details: the $\lambda_t = 1$ $\pi$-exchange coupling and the $A_2$ nucleon non-flip couplings are retained. A further possible contribution – with $A_1$ quantum number exchange – will be reconsidered subsequently. Thus we have, in the $s$-channel helicity frame

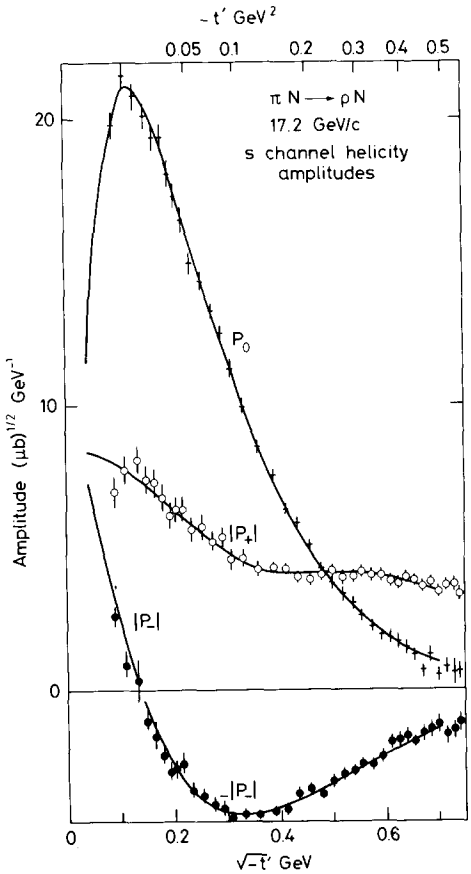


Fig. 1. The moduli of the production amplitudes for $\pi^- p \to \rho^0 n$ at 17.2 GeV/$c$. The points are the $s$-channel helicity amplitudes of ref. [12] extracted from the data of ref. [13] and the curves are the fit of the model described in the text. For clarity, $\pm|P_{-}|$ is plotted to exhibit the 180° phase change of $P^{-}_{+-}$ near $\sqrt{-t'} = 0.15$ GeV.

Table 1
Parameters for the models defined in the text in subsect. 2.1 ($\pi^- p \to \rho^0 n$), subsect. 2.2 ($\pi^- p \to \omega^0 n$) and subsect. 4.1 ($\pi^- p \to f^0 n$) [Quantities in square brackets were not varied in the fits; the normalization of $g_\pi$ is calculated in appendix A.]

$\pi N \to \rho N$

| $g_\pi$ ($\sqrt{\mu b}$) | $g_A/g_\pi$ (GeV$^{-3}$) | $g_C/g_\pi$ (GeV$^{-1}$) | $b_\pi$ (GeV$^{-2}$) | $b_A$ (GeV$^{-2}$) | $b_C$ (GeV$^{-2}$) | $r$ (GeV) |
|---|---|---|---|---|---|---|
| [6.0] | 5.17 | −1.42 | 4.51 | 3.24 | 6.45 | [0.5] |

$\pi N \to \omega N$

| $g_B$ ($\sqrt{\mu b}$) | $g_\rho/g_A$ | $g_Z/g_B$ (GeV) | $C_B/g_B$ (GeV$^{-1}$) | $C_\rho/g_B$ (GeV$^{-1}$) | $b_{C_B}$ (GeV$^{-2}$) | $b_{C_\rho}$ (GeV$^{-2}$) |
|---|---|---|---|---|---|---|
| 6.0 | 2.0 | 0.54 | −0.20 | −0.048 | 0.97 | [$= b_{C_B}$] |

$\pi N \to f^0 N$

| $g_\pi$ ($\sqrt{\mu b}$) | $g_A/g_\pi$ (GeV$^{-3}$) | $g_C/g_\pi$ (GeV$^{-1}$) | $g_{C_2}/g_\pi$ (GeV$^{-2}$) | $b_\pi$ (GeV$^{-2}$) | $b_A$ (GeV$^{-2}$) | $b_C$ (GeV$^{-2}$) |
|---|---|---|---|---|---|---|
| [8.4] | 1.35 | −0.84 | −0.575 | [4.51] | [3.24] | 3.89 |

$$P^0_{+-} = \pi^0_{+-} \quad , \quad P^0_{++} = 0,$$

$$P^-_{+-} = \left(\frac{\pi^s_-}{\pi^s_0}\right)\pi^0_{+-} + C_{+-} \quad , \quad P^-_{++} = 0,$$

$$P^+_{+-} = A^+_{+-} + C_{+-} \quad , \quad P^+_{++} = A^+_{++} \, . \tag{2.8}$$

The moduli of $P_0, P_-$ and $P_+$ obtained [11,12] from an analysis of the 17.2 GeV/$c$ $\pi^- p \to \pi^+\pi^- n$ data [13] determine the parameters introduced above. The normalization (see appendix A) fixes $g_\pi$; $b_\pi$ is given by the $t$ dependence of $P_0$; the small $t$-value of $P_+$ or $P_-$ yields $g_C$; the $t$ dependence of $P_-$ constrains $b_C$ and then the shape of $P_+$ as a function of $t$ is sufficient to determine $g_A$ and $b_A$. The fit is shown in fig. 1. Parameters are given in table 1.

The energy dependence [11, 14] from 6–17.2 GeV/$c$ is then a stringent cross check on the above determination. The break seen [14] at 4–6 GeV/$c$ in the $t$ dependence of $P^s_0$ is not accounted for, but the energy dependence out to $t \sim -0.3$ is

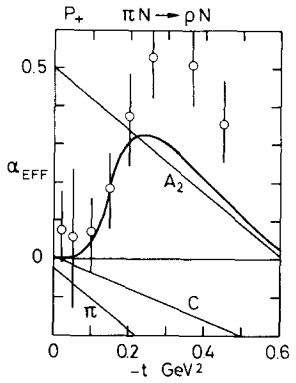


Fig. 2. $\alpha_{\text{eff}}$ for $|P_+|^2$ as extracted from the 6 GeV/$c$ [14] and 17.2 GeV/$c$ [13] $\pi^- p \to \rho^0 n$ data in ref. [11] and the prediction of the model (curve). The trajectories assumed for the $\pi$, $A_2$ and cut C contributions are also shown.

satisfactory. Among other possibilities, either a $\pi$ trajectory of slope $\frac{1}{2}\alpha'$ exactly phase coherent with the cut $C$, or a small low-lying correction to $P_0^S$ could be tolerated by the data. The energy dependence of $P_-^S$ is in agreement with our model, while the crucial test comes from $\alpha_{\text{eff}}$ for $P_+$ as shown in fig. 2. Here the striking relative increase of natural parity exchange from 6 to 17.2 GeV/$c$ is accounted for by the $A_{++}^+$ contribution at small $t$, the $A_{++}^+ - C_{+-}$ destructive interference at moderate $t$, and the $A_2$ dominance at larger $t$. Previous interpretations [15] of $\pi N \to \rho N$ data have had much larger $C$ contributions relative to $A_2$ at $t \sim -0.3$ to $-0.5$, so that a much lower value of $\alpha_{\text{eff}}$ [close to $\alpha_C(t)$] had been expected.

Our fit with the dual model estimate of $\pi_-^t/\pi_0^t$ (eq. (2.2)) is a considerable improvement over taking $\pi_-^t$ zero when $P_0^S$ would have had a zero at $t \sim -0.5$ and the cut would have [11] a much flatter $t$ dependence ($b_C \sim 1.0$). As a compromise, one can take $\pi_-^t/\pi_0^t$ at about 0.5 of the dual vertex value eq. (2.2) when the cut $t$ dependence is very reasonable ($b_C \sim 3.0$). An equally acceptable fit can then be obtained by allowing $r$ to be reduced to 0.25. This compromise description gives a similar value of $\alpha_{\text{eff}}$ for $P_+$, and allows an improved description of the $\rho$–$\omega$ interference phases. Since our present aim is to retain as simple a description as possible in order to extend our analysis to the $f^0$ production amplitudes, we shall retain the dual model expression for $\pi_-^t/\pi_0^t$ of eq. (2.2).

### 2.2. $\pi N \to \omega N$

We again discuss in turn the various expected exchange contributions. We consider data for the average of $\pi^- p \to \omega n$ and $\pi^+ n \to \omega p$ so that any possible [15] $\pi$ exchange via $\rho$–$\omega$ electromagnetic mixing will not contribute.

*2.2.1. B exchange.* The unnatural parity meson spectrum is consistent with $\pi$ – H and $\eta$ – B exchange degenerate trajectories split apart by about 0.23. Thus we take the B trajectory as

$$\alpha_B = -0.25 + \alpha' t \ .$$

To allow for the splitting of the trajectories, and relate B to $\pi$ by exchange degeneracy, we use

$$\frac{B}{\pi} = -\frac{g_B}{g_\pi} \frac{\Gamma(-\alpha_B)}{\Gamma(-\alpha_\pi)} \frac{\sin\frac{1}{2}\pi\alpha_B}{\cos\frac{1}{2}\pi\alpha_\pi} i e^{-\frac{1}{2}i\pi(\alpha_B - \alpha_\pi)} \left(\frac{p_L}{p_0}\right)^{\alpha_B - \alpha_\pi} . \tag{2.9}$$

For strong exchange degeneracy we would have $g_B = g_\pi$; however since $\alpha_\pi \neq \alpha_B$ this comparison depends on $p_L$. A dual theory would lead to comparison at $\alpha$'s = 1 or $p_L = 1/(2m_N\alpha')$ which yields $g_B = 0.5\, g_\pi$ as an expectation. The helicity couplings of the B exchange are taken from the same model as for the $\pi$ (eq. (2.3)). The dual vertex factor ensures a pure $\lambda_t = 0$ coupling at $\alpha(t) = 0$ but can also be evaluated at $\alpha(t) = 1$. This yields, at $t = m_B^2$, a ratio of $\omega$ production with $\lambda_t = 0$ to all of 0.2. This can be compared directly with the branching fraction of $\omega$ with $\lambda_t = 0$ in B decay to $\omega\pi$ which experimentally is quoted [16] as 0.10–0.16. Thus the dual vertex factor successfully reproduces the predominant $\lambda_t = 1$ coupling at $\alpha(t) = 1$, the B mass value.

*2.2.2. $\rho$ exchange.* This is expected to be exchange degenerate with the $A_2$ exchange in $\rho$ production and we write $\alpha_\rho(t) = \alpha_A(t)$ and

$$\frac{\rho}{A_2} = \frac{g_\rho}{g_A} i \tan\tfrac{1}{2}\pi\alpha_A \ , \tag{2.10}$$

where $g_\rho = g_A$ for strong exchange degeneracy of the couplings.

*2.2.3. Cut C.* The B-pole contribution discussed above gives rise to phase coherence for $P_-$ and $P_0$ and a specific ratio from eq. (2.3). The $\rho$ contribution has a dip at $\alpha_\rho(t) = 0$ in $P_+$. To take account of possible deviations from these expectations in the data, we introduce a cut in the $n = 0$ amplitude. Guided by the absorption model expectation of cuts mainly 180° out of phase with their respective poles, we parametrize the phase and $t$ dependence of the cut as

$$C^{\pm}_{+-} = (i e^{-\frac{1}{2}i\pi\alpha_B(t)} c_B e^{b_B t} + i e^{-\frac{1}{2}i\pi\alpha_\rho(t)} c_\rho e^{b_\rho t}) \left(\frac{p_L}{p_0}\right)^{\alpha_C(t)-1} . \tag{2.11}$$

As discussed subsequently, data imply $C_B > C_\rho$, so we take $\alpha_C(t) = \alpha_B(t)$ for the energy dependence of the cut.

*2.2.4. $J^{PC}I = 2^{-+}1$ exchange.* Unnatural parity exchange amplitudes in vector

meson production with nucleon non-flip coupling can only receive contributions from the exchange of axial mesons ($A_1$ – D nonet) and their $J^{PC} = 2^{-+}$ exchange degenerate partners (no resonance state known). Thus in $\pi N \to \rho N$, $A_1$ exchange could contribute, but aside from other problems the $A_1$ contribution has a zero at $\alpha(t) = 0$ (from signature and absense of known $J^{PC} = 0^{-+}$ state), while the $\pi$ contribution has a pole at $\alpha(t) = 0$. Thus the $\pi$ is doubly favoured over the $A_1$ at $\alpha(t) \sim 0$. Conversely, in $\omega$ production, the B exchange contribution has a signature zero at $\alpha(t) = 0$, while the $Z$ ($J^P I^G = 2^- 1^+$) exchange contribution would not vanish at $\alpha(t) \sim 0$ and could be relatively important. The only clue for the helicity coupling of $Z$ exchange at the meson vertex comes from the ratio of $A_1 \to \rho(\lambda) + \pi$ with $\lambda = 0$ and 1 in models [17]. This leads to a dominant $\lambda_t = 0$ coupling and for simplicity we use eq. (2.3) to give the $s$-channel $Z^-_{++}$ to $Z^0_{++}$ coupling ratio. For the $t$ dependence of Z exchange, we make the economical assumption that all the unnatural parity exchanges have similar slopes which leads to

$$\frac{Z_{++}}{B_{+-}} = \frac{g_Z/g_B}{\sqrt{-t'}} \frac{\cos\frac{1}{2}i\pi\alpha_Z}{\sin\frac{1}{2}i\pi\alpha_B} \frac{\Gamma(1-\alpha_Z)}{\Gamma(-\alpha_B)} \left(\frac{p_L}{p_0}\right)^{\alpha_Z - \alpha_B}, \tag{2.12}$$

where $g_Z$ controls the strength (sign unknown) and $\alpha_Z$ is taken as $0 + \alpha' t$.

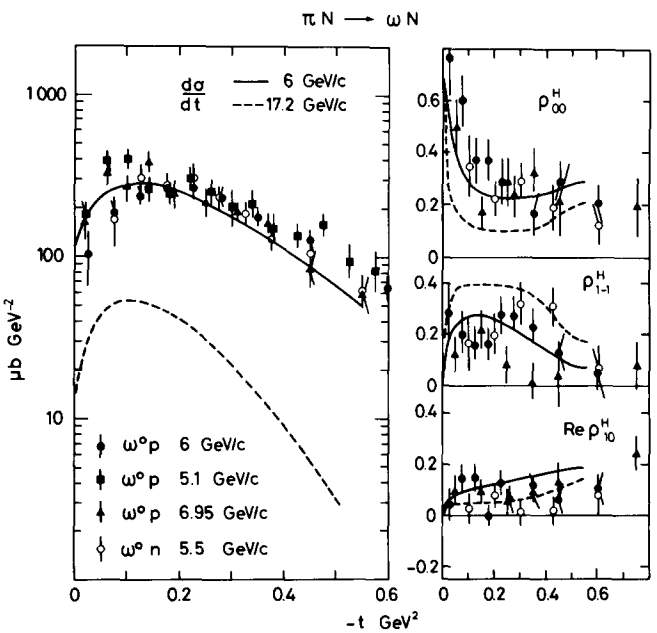


Fig. 3. The data [18, 19] and model fit to $\pi N \to \omega N$ cross section and $s$-channel density matrix elements at 6 GeV/$c$. The cross-section data at 5.5, 6.95 and 5.1 GeV/$c$ have been scaled by 0.82, 1.38 and 0.70, respectively [i.e. by $(p_L/6)^{-2.25}$] to an effective momentum of 6 GeV/$c$. The model prediction for $\pi N \to \omega N$ at 17.2 GeV/$c$ is shown by dotted curves.

*2.2.5. Our model.* In summary the contributions considered are

$$P^0_{+-} = B^0_{+-}\,, \qquad P^0_{++} = Z^0_{++}\,,$$

$$P^-_{+-} = B^-_{+-} + C^-_{+-}\,, \qquad P^-_{++} = Z^-_{++}\,,$$

$$P^+_{+-} = \rho^+_{+-} + C^+_{+-}\,, \qquad P^+_{++} = \rho^+_{++}\,. \tag{2.13}$$

Insufficient data on $\pi N \to \omega N$ exist to extract a reliable energy dependence of the different components. Thus we consider data [18, 19] in the region of 6 GeV/$c$, where it is best measured, and attempt to describe it with the above contributions linked to the previous model for $\rho$ production. Some information from $\rho$–$\omega$ interference phases is also anticipated.

Setting $g_Z = 0$, a considerable breaking of exchange degenerary for B is necessary (three times expectation) and the large experimental value of $\rho_{00}$ at small $t$ is not reproduced. The latter can be achieved readily by including a Z exchange contribution. The parameters of a satisfactory description of the data (see fig. 3) are shown in

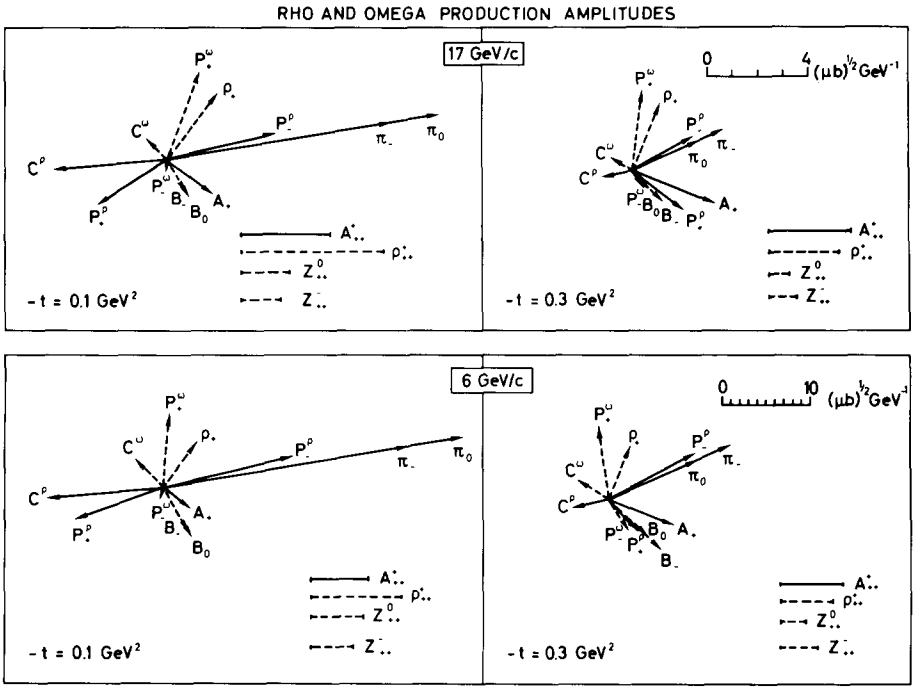


Fig. 4. Argand diagrams of our $\rho$ and $\omega$ production amplitudes with nucleon helicity flip, at 6 and 17.2 GeV/$c$, for $-t$ = 0.1 and 0.3 GeV$^2$. For ease of comparison the 6 GeV/$c$ amplitudes are scaled by the constant factor 6/17.2 ($\rho(\omega)$ production amplitudes are shown by solid (dotted) lines). Also shown are the magnitudes of the (incoherent) contributions $\rho^+_{++}$, $A^+_{++}$, $Z^0_{++}$ and $Z^-_{++}$.

table 1. As shown in the Argand diagram of fig. 4, the cut C has its phase mainly antiparallel to $B_-$ to achieve the required $P_+/P_-$ ratio ($\rho_{1-1}$ large and positive). A small contribution ($C_\rho$) antiparallel to $\rho$ serves to swing the resultant of $P_-^\omega$ anticlockwise into better agreement with the $\rho-\omega$ interference phase data (sect. 3). One unpleasant feature is that $g_\rho/g_A \sim 2$, unlike the dual expectation of unity. This might be caused by normalization uncertainties in comparing the cross section for producing a wide resonance ($\rho$) with a narrow one ($\omega$). However, in appendix A we discuss such normalization questions and no major uncertainty seems present.

A direct test of this exchange decomposition of $\omega$ production is in the energy dependence to higher energies and fig. 3 shows the 17 GeV/$c$ prediction.

## 3. Polarization and interference effects in vector-meson production

The decomposition of the $\rho$ and $\omega$ amplitudes discussed in sect. 2 is shown in the Argand diagrams of fig. 4. Characteristic features are the $t$ and $s$ depenence of the phase of $P_{+-}^+$ for $\rho$ production, due to the interference between the cut C and $A_2$ contributions. The phase of $C^\omega$ is rather constant with energy and momentum transfer and influences the phases of $P_\pm$ for $\omega$ production as previously discussed. The non-flip nucleon couplings to Z, $\rho$ and $A_2$ are also all significant and will give substantial polarization effects.

### *3.1. Interference effects*

The relative phases of $\rho$ and $\omega$ production amplitudes are observable from the electromagnetic $\rho-\omega$ mixing in the $\pi\pi$ decay channel and via SU(3) from a comparison of K* and $\overline{K^{*0}}$ production. The $\rho-\omega$ mixing in observable $P_i$ (i.e. $P_+$, $P_-$ or $P_0$) is controlled [20] by the bilinear combination of production amplitudes

$$P^i_{++}(\rho)P^i_{++}(\omega)^* + P^i_{+-}(\rho)P^i_{+-}(\omega)^*$$

$$= \xi_i[|P^i_{++}(\rho)|^2 + |P^i_{+-}(\rho)|^2]^{\frac{1}{2}}[|P^i_{++}(\omega)|^2 + |P^i_{+-}(\omega)|^2]^{\frac{1}{2}} e^{i\phi_i} . \qquad (3.1)$$

Thus the relative phase $\phi_i$ can be measured directly (with no ambiguities), while the coherence $\xi_i$ can only be determined if the $\omega \to \pi\pi$ branching ratio is well known. The relation to K* production from SU(3) is

$$\sqrt{2}\,P^i(K^*) = P^i(\omega) + P^i(\rho) , \qquad \sqrt{2}\,P^i(\overline{K^*}) = P^i(\omega) - P^i(\rho) , \qquad (3.2)$$

where the phases are such that K* production would be real for exchange degenerate Regge poles in $\rho$ and $\omega$ production. Thus for observables:

$$|P^i(K^*)|^2 - |P^i(\overline{K^*})|^2 = 2\mathrm{Re}[P^i_{++}(\rho)P^i_{++}(\omega)^* + P^i_{+-}(\rho)P^i_{+-}(\omega)^*]$$

$$= 2\xi_i[|P^i_{++}(\rho)|^2 + |P^i_{+-}(\rho)|^2]^{\frac{1}{2}}[|P^i_{++}(\omega)|^2 + |P^i_{+-}(\omega)|^2]^{\frac{1}{2}} \cos\phi_i . \qquad (3.3)$$

Table 2
$\rho-\omega$ interference phases

| Amplitude | $-t$ | 6 GeV/$c$ | | | 17.2 GeV/$c$ | | |
|---|---|---|---|---|---|---|---|
| | (GeV$^2$) | $\phi$ (degree) | $\xi$ | $\phi$ data (degree) | $\phi$ (degree) | $\xi$ | $\phi$ data (degree) |
| | 0–0.08 | 69 | 0.54 | 70 ± 30 | 69 | 0.43 | |
| $P_0$ | 0.08–0.2 | 69 | 0.77 | | 69 | 0.68 | |
| | 0.2 –0.45 | 69 | 0.81 | 45 ± 30 | 69 | 0.84 | |
| | 0–0.08 | 218 | 0.47 | | 218 | 0.36 | |
| $P_-$ | 0.08–0.2 | 106 | 0.38 | 70 ± 25 | 106 | 0.32 | |
| | 0.2 –0.45 | 87 | 0.71 | 120 ± 15 | 87 | 0.64 | |
| | 0–0.08 | 93 | 0.36 | 75 ± 30 | 180 | 0.19 | |
| $P_+$ | 0.08–0.2 | 188 | 0.38 | 140 ± 20 | 241 | 0.64 | 205 ± 15 |
| | 0.2 –0.45 | 241 | 0.84 | 170 ± 20 | 255 | 0.95 | 230 ± 7 |

The phase ($\phi$) and coherence ($\xi$) are defined in the text (eq. (3.1)). The preliminary data for $\phi$ is taken from refs. [14] (6 GeV/$c$) and [11] (17.2 GeV/$c$). The observed strength of $\rho-\omega$ interference effects in $\pi N \to \pi\pi N$ data is controlled by $\xi\Gamma(\omega \to \pi\pi)$. Compared to the usual assumption of complete coherence ($\xi = 1$), our predictions for $\xi$ will result in values of $\Gamma(\omega \to \pi\pi)$ enhanced by $1/\xi$.

Thus the difference of K* and $\overline{\text{K}^*}$ observables yields similar information to $\rho-\omega$ interference, but uses the assumption of SU(3) and gives only $\xi_i \cos\phi_i$. The relative normalization of K* and $\overline{\text{K}^*}$ is also difficult to obtain with good precision experimentally. A comparison with preliminary $\rho-\omega$ interference and K* $-$ $\overline{\text{K}^*}$ data at 6 GeV/$c$ [14] is presented in table 2 and fig. 5. The two types of data agree generally with each other and with the expectations of our models for $\rho$ and $\omega$ production.

Since the $\omega \to \pi\pi$ branching ratio is not well determined, the coherence $\xi$ has not been determined experimentally. The relative coherence, however, is found [14] to be smaller for $P_+$ than for $P_-$ or $P_0$ and this is in general accord with our expectations. The change in phase with increasing $|t|$ of $P^+_{++}$ for $\rho$ production as the $A_2$ takes over from the cut combined with the relatively important $P^+_{++}$ contributions yields a too-pronounced swing in $\rho-\omega$ interference phase for $P_+$. This feature can be improved by resorting to the solution (sect. 2) for $\rho$ production with $\pi^t_-/\pi^t_0$ reduced and a consequent less steep $t$ dependence of the cut and less dominant $P^+_{++}$ contributions. The phase of $\lesssim 90°$ between the B and $\pi$ exchange in $P_0$, and the phase of $\gtrsim 90°$ between $\rho$ and $\omega$ production in $P_-$ are well reproduced by our model amplitudes. A strong energy dependence of the $\rho-\omega$ phase for $P_+$ is also indicated in table 2.

The K* and $\overline{\text{K}^*}$ charge-exchange observables are in acceptable agreement except for $P_-$. Here, aside from a small effect due to $\frac{1}{3}\rho_{SS}$ present in the data, the effects of SU(3) breaking must be considered. This could be due to cuts which are not SU(3)

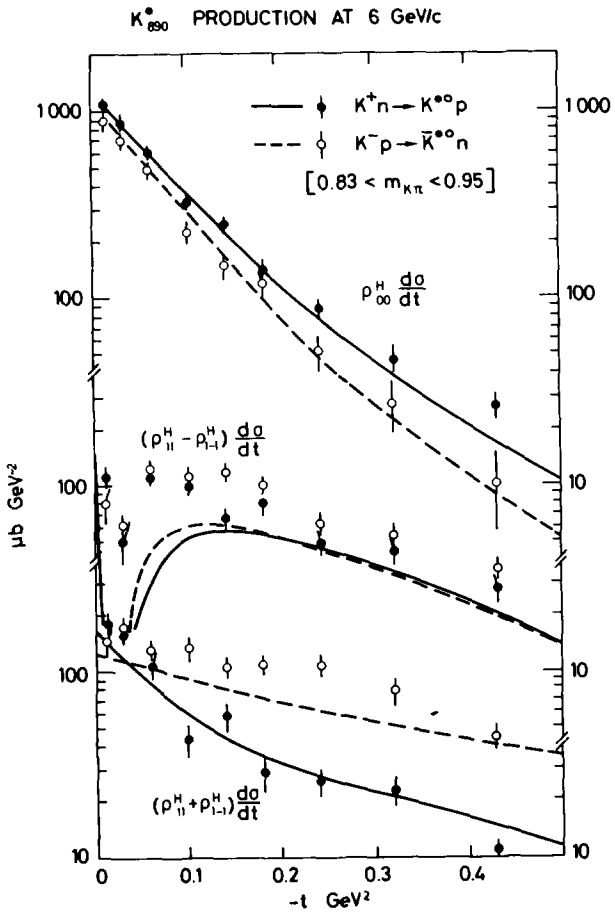


Fig. 5. Our SU(3) prediction and K* production data at 6 GeV/c ($\rho^{H}_{00}(d\sigma/dt)$, $(\rho^{H}_{11} \pm \rho^{H}_{1-1})$ $(d\sigma/dt)$). For the comparison with the preliminary data of ref. [14], which contains $\frac{1}{3}\rho_{SS}$ in each component and uses the mass cut ($0.83 < m_{K\pi} < 0.95$ GeV), the prediction has been multiplied by a factor 0.443.

octets in the $t$-channel – a serious possibility since the pomeron exchange is not empirically an SU(3) singlet and also Regge-Regge cuts can contribute. An alternative explanantion lies in SU(3) broken mass values which enter into the expression for the crossing matrix used to obtain the $s$-channel $\pi$ exchange contributions to $P_-$ from the $t$-channel expressions in which $\lambda_t = 0$ is dominant (eq. (2.2)). Thus for the vertex $a \to m$ by $\pi$ exchange

$$\frac{\pi^s_-}{\pi^s_0} = \frac{2m\sqrt{-t'}}{m^2 + \mu^2 - a^2} . \tag{3.4}$$

This ratio is larger for $K \to K^*$ than for $\pi \to \rho$ processes. Thus in agreement with the data, a larger value of $P_-/P_0$ for $\overline{K^*}$ (or $K^*$) compared to $\rho$ would be expected since the destructive interference of the cut enhances the effect beyond $t = -\mu^2$.

### 3.2. Polarization effects

Fig. 6 shows predictions for $\rho$ and $\omega$ production polarization, as well as for $\gamma N \to \pi^+ N$ where vector dominance ($\gamma \sim \rho - \omega/2.8$) has been used. The polarization plotted, $P_n$, is that arising from natural parity exchange alone

$$P_n \sigma_n = -2\,\mathrm{Im}(P^+_{++} P^{+*}_{+-}), \qquad P\sigma = P_n \sigma_n + P_u \sigma_u . \tag{3.5}$$

In our model $P_u$ is zero for $\rho$ production and thus for $\rho$ production and to a good approximation for photoproduction $P_n$ can be equated with $P\sigma/\sigma_n$, which is the quantity plotted as data [21] in fig. 6. The structure in the polarization arises from the phase of $P^+_{+-}$, which swings from the phase of $C^\rho$ to that of $A_2$ as $|t|$ increases and which thus passes through 90° relative to $P^+_{++} = A_{++}$ at an intermediate $t$-value. The energy dependence of $P_N$ for $\pi N \to \rho N$ and $\gamma N \to \pi^+ N$ is also characteristic of our model with its significant $A_2 - C^\rho$ interference which shifts with energy.

$P_u$ for $\omega$ production depends on the sign of the $Z$ contribution which has not been determined. The effect of introducing an exchange degenerate $A_1$ contribution in $\pi N \to \rho n$ will be very small as argued previously and this is shown quantitatively for our choice of $A_1$–Z trajectory in table 3. Such small $A_1/\pi$ ratios will not affect differential cross section and density matrix observables in which they enter quadratically, while polarization effects are linear in $A_1/\pi$ and so could become significant at $|t| \sim 0.3$ or larger.

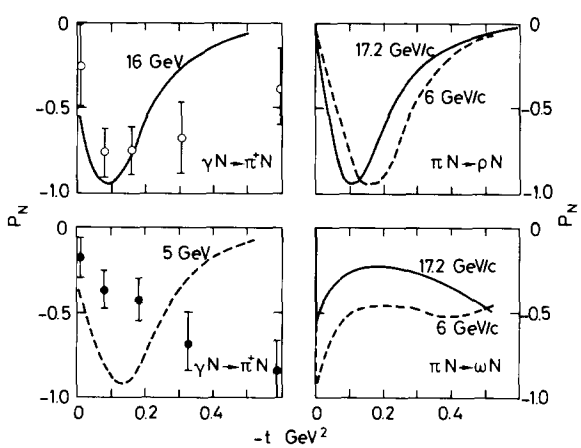


Fig. 6. Predicted nucleon polarization in vector meson production. The more reliably estimated natural parity exchange component (see eq. (3.5)) is shown. The prediction for $\gamma p \to \pi^+ n$ obtained from vector dominance is compared with data [21] at 5 and 16 GeV/$c$.

Table 3
The ratio of $Z(J^PI^G = 2^-1^+)$ to B exchange in helicity zero amplitudes at 17.2 GeV/$c$ (as deduced from our model) and the exchange degeneracy prediction for the equivalent quantity $A_1/\pi$ in $\rho$ production

| $-t$ (GeV$^2$) | $\lvert Z_0/B_0\rvert$ | $\lvert A_{10}/\pi_0\rvert$ |
|---|---|---|
| 0.05 | 1.76 | 0.0094 |
| 0.1 | 1.24 | 0.023 |
| 0.3 | 0.67 | 0.112 |

Further polarized target observables can be measured [7] with the target polarization in the scattering plane. Quantities which are interference effects between natural and unnatural parity exchange can then be analysed. Thus the relative phase of $P^0_{+-}$ and $P^+_{++}$, for instance, can be tested in $\pi N \to \rho N$. Such observables can be constructed from our parametrizations for the amplitudes and checked from the Argand diagrams of fig. 4.

## 4. Tensor meson production

### *4.1. Introduction*

Spin-2 meson production on nucleons involves 10 helicity amplitudes which are related to density matrix elements and decay angular distribution moments as described in appendix A. The combinations which correspond to specific exchange naturality are

$$D^0_{\lambda\nu} = H^0_{\lambda\nu}, \qquad D^{1\pm}_{\lambda\nu} = \sqrt{\tfrac{1}{2}}(H^1_{\lambda\nu} \pm H^{-1}_{\lambda\nu}), \qquad D^{2\pm}_{\lambda\nu} = \sqrt{\tfrac{1}{2}}(H^2_{\lambda\nu} \mp H^{-2}_{\lambda\nu}). \quad (4.1)$$

$D^{1+}$ and $D^{2+}$ are the natural parity exchange amplitudes.

For spin-2 production, removing the spin 0 and 1 background in the decay channel is much more difficult than the analogous problem for spin-1 production. The presently available data on tensor meson production are also considerably less complete than for the vector production we have discussed. This leads us to try to combine our models for the exchange amplitudes in vector meson production with some additional theoretical input to describe the tensor meson amplitudes. This proves very useful as a preliminary study of tensor meson production.

Application of local duality to Regge + particle total cross sections [2] or to Regge + particle → particle + particle amplitudes [3] allows a general discussion of the relative production mechanisms for states of different mass but similar exchange quantum numbers. A much more specific analysis can be made by employing [4] the Regge recurrence production vertices in the dual resonance model. The latter

(dual boost model) yields specific expressions for the $t$ dependence and helicity dependence of the Regge-pole exchange vertices for producing states on the same Regge trajectory (e.g. $\rho$–f–g or $\omega$–$A_2$). We shall employ and investigate such dual model relations. The other necessary contribution, the cuts, will be deduced from the experimental data as far as possible.

*4.2. $\pi N \to f^0 N$*

The exchange contributions will be the same as those for $\pi N \to \rho N$ discussed in sect. 2 and we present here the "dual boost" predictions for $f^0$ production relative to $\rho$.

*4.2.1. $\pi$ exchange.* At $t = \mu^2$ the coupling reduces to the relevant partial decay width to $\pi\pi$. The dual boost prediction of $\Gamma_f \sim 0.85\,\Gamma_\rho$ is smaller than the experimental [6] ratio $\Gamma_f \sim 1.03\,\Gamma_\rho$. However, the discrepancy is not serious – a factor of 1.1 in the production amplitude only. Our $f^0$ model is normalized to the experimental width as described in appendix A.

The $\lambda_t = 0, 1, 2$ or $\lambda_s = 0, 1, 2$ contributions from Reggeized $\pi$ exchange have been calculated [4]. In the $s$-channel the helicity coupling ratios, normalized to 1 at $t = \mu^2$ for $\lambda_t = 0$, are given by

$$p_a^2 X_0^s = \tfrac{1}{4}[m^2 + 2\mu^2 + (t - \mu^2)(2 - 1/\alpha' m^2)] ,$$

$$p_a^2 X_{1-}^s = \tfrac{1}{2}\sqrt{-3t'}\,m ,$$

$$p_a^2 X_{2-}^s = -\tfrac{1}{2}\sqrt{3}\,t' , \qquad (4.2)$$

where $4p_a^2 = m^2 - 4\mu^2$ and $m$ is the tensor meson mass. The $t$-dependence of $f^0$ production relative to $\rho$ production is given by the dual vertex factor

$$\pi^i_{+-} = g^f_\pi X^s_i \frac{\sqrt{-t'}}{\mu^2 - t} e^{b_\pi t} e^{-\frac{1}{2} i\pi\alpha_\pi(t)} \left(\frac{p_L}{p_0}\right)^{\alpha_\pi(t)-1} . \qquad (4.3)$$

Compared to eq. (2.4), the only difference in $t$-dependence comes from the factor $X_i^s$. Thus for $\lambda_s = 0$, $\pi^0_{+-}$ is a steeper function of $t$ for $f^0$ production than for $\rho$ production, since $X_0^s$ is at small $t$ equivalent to an exponential with slope 0.9 $\mathrm{GeV}^{-2}$. This is a very clean prediction, characteristic of the dual vertex factor, since the more general dual approaches [2, 3] predict, on the contrary, an $f^0$ $t$-dependence less steep than for the $\rho$. These latter approaches are, however, less specific since they apply to the sum of all helicity contributions.

*4.2.2. $A_2$ exchange.* The ratio of natural parity exchange to unnatural parity exchange is expected to decrease with higher masses produced in all dual-based approaches [2, 4]. The specific "dual boost" model gives $g_A/g_\pi \sim 0.7$ of the $\rho$-produc-

tion ratio. The ratio of $\lambda_s = 2$ to $\lambda_s = 1$ is also specified:

$$\frac{A^{2+}_{+-}}{A^{1+}_{+-}} = \frac{2m\sqrt{-t'}}{m^2 + v^2 - \mu^2}, \tag{4.4}$$

where $\alpha_{A_2}(v^2) = 1$.

The $t$-dependence of $A^{1+}$ is expected to be the same for $f^0$ as $\rho$ production and the ratio $r$ of ++ to +− nucleon couplings is also retained.

$$A^{1+}_{+-} = -g_A\, t' e^{b_A t}\, e^{-\frac{1}{2}i\pi\alpha_A(t)} \left(\frac{p_L}{p_0}\right)^{\alpha_A(t)-1}. \tag{4.5}$$

*4.2.3. C exchange.* In specific absorption models, the cut strength is tied to the $\pi$-pole strength and $t$ dependence. Thus no substantial change from $\rho$ to $f^0$ would have been expected. In practice, data show [6, 22] a reduction in $g_c/g_\pi$ (at small $t$) of $\sim 0.7$ in going from the $\rho$ to $f^0$. No explanation exists except for the possibility that some of the cut could come from $A_2$ absorption which would then decrease by such a factor as discussed above. Data analysis also indicates [12] the necessity of an $n = 1$ cut in the amplitude $H^2_{+-}$ which vanishes like $\sqrt{-t'}$ instead of $(-t')^{\frac{3}{2}}$ as the pole contributions. Thus we choose a parametrization

$$C^{1+}_{+-} = C^{1-}_{+-} = g_C\, e^{b_C t}\, e^{-\frac{1}{2}i\pi\alpha_C(t)} \left(\frac{p_L}{p_0}\right)^{\alpha_C(t)-1},$$

$$C^{2+}_{+-} = C^{2-}_{+-} = \sqrt{-t'}\, g_{C_2}\, e^{b_C t}\, e^{-\frac{1}{2}i\pi\alpha_C(t)} \left(\frac{p_L}{p_0}\right)^{\alpha_C(t)-1}, \tag{4.6}$$

where $\alpha_C(t)$ is chosen the same as for $\rho$ production.

*4.2.4. Our model.* In summary our exchange contribution are

$$D^0_{+-} = \pi^0_{+-},$$

$$D^{1-}_{+-} = \pi^{1-}_{+-} + C^{1-}_{+-}, \quad D^{1+}_{+-} = A^{1+}_{+-} + C^{1+}_{+-}, \quad D^{1+}_{++} = A^{1+}_{++},$$

$$D^{2-}_{+-} = \pi^{2-}_{+-} + C^{2-}_{+-}, \quad D^{2+}_{+-} = A^{2+}_{+-} + C^{2+}_{+-}, \quad D^{2+}_{++} = A^{2+}_{++}. \tag{4.7}$$

A complete separation of $J = 2$ effects from $J = 0$ and 1 in the $f^0$ region exists [12] at 17.2 GeV/$c$. This was achieved by parameterizing the $f^0$ production amplitudes and we show the result in fig. 7. Our dual boost plus $\rho$-production model approach is easily able to reproduce the amplitudes as shown in the figure. The parameters are given in table 1. In this description of $f^0$ amplitudes the $\pi$ contributions were completely fixed as described above; the $A_2$ contributions were fixed except for $g_A/g_\pi$ which is forced to be substantially smaller than the dual value; $g_C$, $b_C$ and

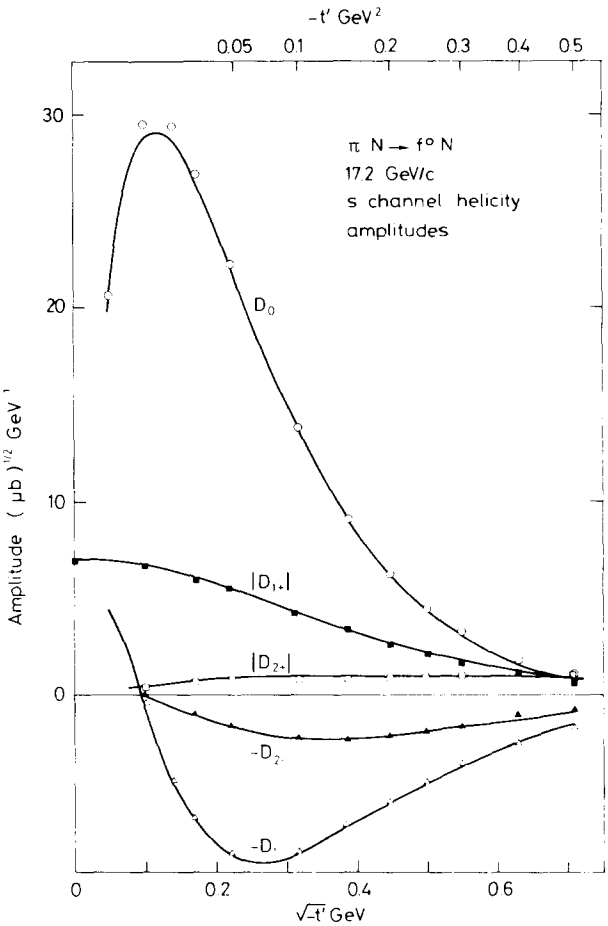


Fig. 7. The $f^0$ production amplitudes at 17.2 GeV/$c$. The points are the amplitudes as extracted in ref. [12] and the curves are our model reconstruction of them.

$g_{C_2}$ were free and obtain reasonable values. Thus the dual vertex factors with little freedom reproduce the whole complex structure of the $f^0$ production amplitudes. In particular, $D_0$ is given entirely by the $\pi$ contribution and the shrinkage of slope compared to $\rho$ production is exactly predicted. The fraction of natural parity exchange in $f^0$ production is relatively small as predicted by the dual approaches and is consequently not well determined. We are thus unable to confirm the expected decrease in $g_A/g_\pi$ from $\rho$ to f of 0.7. Our $f^0$ production amplitudes are consistent with lower energy data. Such data exist either as bounds on $J = 2$ contributions [23] or with specific background assumptions [19] to separate out the $f^0$ component (see fig. 8).

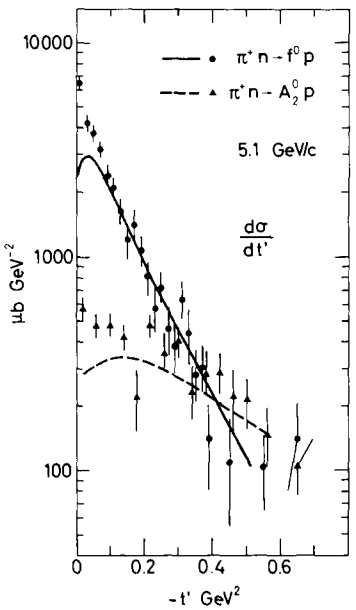


Fig. 8. $f^0$ and $A_2$ production differential cross sections at 5.1 GeV/*c*. The points are those of ref. [19] and the curve is the model prediction.

### *4.3. $\pi N \to A_2 N$ charge exchange*

Available data on $\pi^- p \to A_2^0 n$ or $\pi^+ n \to A_2^0 p$ afford little help in constructing a model. A combination of exchange degeneracy relations applied to $\pi N \to f^0 N$, and dual boost relations applied to $\pi N \to \omega N$ give strong predictive power. The more so, since exchange degeneracy breaking has been investigated while comparing $\pi N \to \rho N$ with $\pi N \to \omega N$ and the dual boost relations have been tested in going from $\pi N \to \rho N$ to $\pi N \to f^0 N$. For the individual exchanges we assume the following.

*4.3.1. B exchange.* This is taken as exchange degenerate with the $f^0$ production $\pi$ exchange contributions employing the same $B/\pi$ ratio as eq. (2.9) with $g_B/g_\pi$ fixed at the $\rho-\omega$ value.

*4.3.2. $\rho$ exchange.* This is taken as exchange degenerate to the $A_2$ exchange amplitudes in $f^0$ production together with the factor $g_\rho/g_A = 2$ used in relating $\rho$ to $\omega$ production (eq. (2.10)). Note that this factor of 2 largely compensates for the fact that the $g_A/g_\pi$ ratio in $f^0$ production was much less than the dual boost value from $\rho$ production. That the dual prediction persists is not unreasonable, since $\rho$ exchange in $\pi \to A_2$ shares the same coupling as $A_2$ exchange in $\pi \to \rho$ when evaluated at the common $A_2$ pole and $\rho$ pole.

*4.3.3. Z exchange.* The ratio of Z to B is as in eq. (2.12) with $g_Z/g_B$ fixed at the $\omega$ production value (table 1) and B exchange as above.

*4.3.4. Cut contributions.* The effective cut in $\omega$ production $(C/g_B)_\omega$ is scaled by the same factor as the $f^0$ cut is in relation to the $\rho$ cut:

$$(C/g_B)_{A_2} = (C/g_B)_\omega \, (g_C/g_\pi)_{f^0} \, (g_C/g_\pi)_\rho^{-1} \, . \tag{4.8}$$

The $t$ dependence of the $\omega$ cut is already very flat, so that it is maintained unchanged for the $A_2$ production cut. In the same spirit, we also introduce an helicity 2 cut with the ratio of $C_2/C$ the same as in $f^0$ production $(g_{C_2}/g_C)$.

*4.3.5. Our model.* In summary, the exchange contributions are

$$D^0_{+-} = B^0_{+-} \, , \quad D^i_{+-} = B^i_{+-} + C^i_{+-} \, , \quad D^j_{+-} = \rho^j_{+-} + C^j_{+-} \, ,$$

$$D^0_{++} = Z^0_{++} \, , \quad D^i_{++} = Z^i_{++} \, , \qquad D^j_{++} = \rho^j_{++} \, , \tag{4.9}$$

where $i = 1-, 2-$ and $j = 1+, 2+$.

The model is completely specified in advance by a mixture of theoretical and phenomenological constraints. The predicted differential cross section for $A_2$ production is compared with some data at 5.1 GeV/$c$ [19] in fig. 8 and the agreement is seen to be reasonable. Better data in the $3\pi$ or $\eta\pi$ decay mode, including density matrix elements or decay moments, would be of great interest in testing our ideas for the charge-exchange production of $A_2$.

Mearge evidence [24] on the energy dependence of $\pi^+ n \to A_2^0 p$ suggests a decrease of cross section with $\alpha_{\text{eff}} \sim 0$ consistent with the dominant unnatural exchange in our model.

Finally, in this section, we review the status of the dual boost factors which proved so useful in constructing tensor meson production amplitudes. In relating $f^0$ production to $\rho$ production, the $\pi$ exchange contribution is completely specified. The agreement is reasonable for the normalization $(\Gamma_f/\Gamma_\rho)$, and excellent for the $t$-dependence of the $\lambda_s = 0$ amplitude $(b_\pi^f - b_\pi^\rho \sim 0.9 \text{ GeV}^{-2})$. The helicity structure proposed also avoids the problem of crossing matrix zeros in $P_0$ and $D_0$ and at the same time gives a satisfactory account of the measured helicity couplings on the exchange degenerate B-meson pole ($B \to \omega\pi$ dominantly $\lambda_\omega = 1$). The expected suppression of natural parity exchange relative to unnatural parity exchange in going from $\rho$ to $f_0$ production is found in our analysis, but is stronger than anticipated. The same comparison between $\omega$ and $A_2$ production is closer to the expectation of the dual vertex model. A similar comparison of natural parity exchanges in data for $\pi N \to \rho N$ and $\pi N \to A_2 N$ with $I_t = 0$ also suggests [1] that they decrease somewhat more rapidly for the production of higher spin resonances than in the model.

## 5. Interference effects in $f^0$ and $A_2$ production

An Argand diagram of the $f^0$ and $A_2$ production amplitudes of our model at 17.2 GeV/$c$ is shown in fig. 9. Compared to the $\rho-\omega$ situation (fig. 4) the most noticeable difference lies in $D^f_{1+}$ which is dominated by the cut and so remains near 180° compared to $D^\rho_{1+}$. Thus (unlike $\rho$, $\omega$ production) the phase difference between $f^0$ and $A_2$ natural parity production amplitudes varies little with $-t$ ($\sim 120°$). The dominant unnatural parity-exchange amplitudes have a phase approximately 90° ahead for f production compared to $A_2$ production.

Just as for $\rho$ and $\omega$ production, the relative phase between $f^0$ and $A_2$ production amplitudes is observable – and in two independent ways. The K*(1420) and $\overline{K^*}$(1420) charge-exchange production reactions are related by SU(3) to $f^0$ and $A_2$ analogously to eqs. (3.2) and (3.3). Fig. 10 shows the prediction of our model for the production cross-sections of these mesons compared with data [25, 26] near 4 GeV/$c$. Normalization uncertainties, particularly with a deuterium target, make this a rather imprecise test. Relatively well normalized data with density matrix element information would be needed to investigate the interference effects properly.

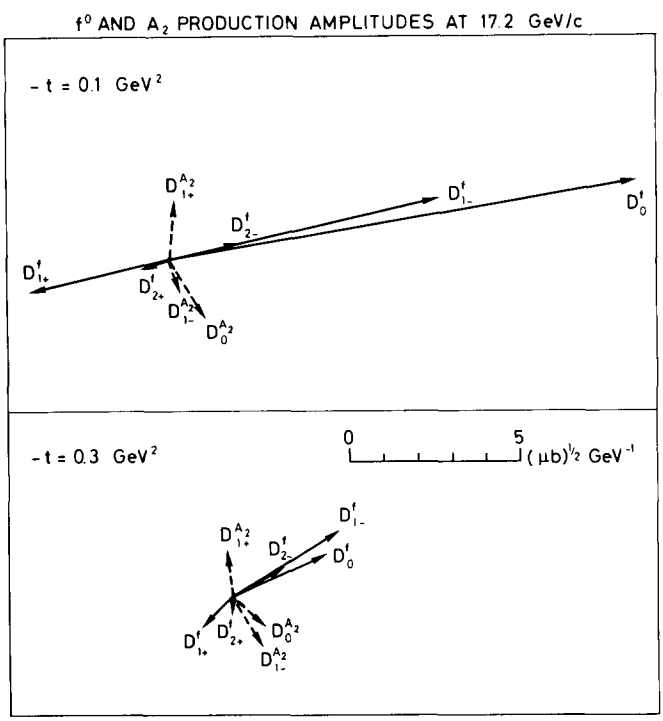


Fig. 9. Argand diagram of the model nucleon flip amplitudes for $f^0$ (solid lines) and $A_2$ (dotted) production at 17.2 GeV/$c$ at $-t$ = 0.1 and 0.3 GeV$^2$. For clarity the (exceedingly small) amplitudes $D^{A_2}_{2\pm}$ are not shown.

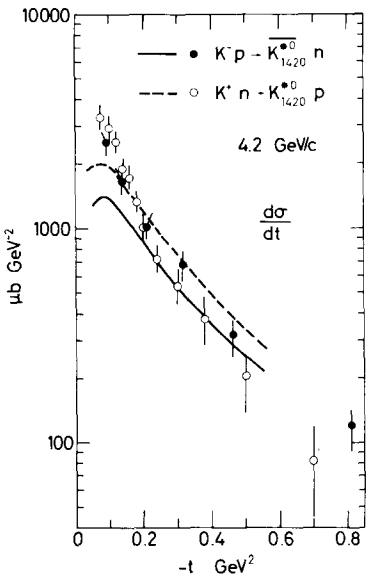


Fig. 10. Comparison of our SU(3) predictions for $K^-p \to \overline{K}^{*0}(1420)n$ (solid line) and $K^+n \to K^{*0}(1420)p$ (dotted line) with the 4.2 GeV/$c$ data [25, 26] (solid and open points, respectively). The 4.6 GeV/$c$ deuterium data of ref. [26] has been scaled by $(4.2/4.6)^{-2}$ to an effective momentum of 4.2 GeV/$c$.

A more complete test in principle, analogous to $\rho$–$\omega$ interference, is provided [27] by the common decay channel of $f^0$ and $A_2$ into $K\bar{K}$. Both mesons can decay by strong interactions with comparable strength into $K^0\bar{K}^0$ and $K^+K^-$ and interferences between their combined production and decay amplitudes will result. Generalizing eqs. (A.3)–(A.7) of appendix A this gives observable combinations of the form

$$\sum_{\mu} |F^i_\mu(s,t)\, B^f(m) + A^i_\mu(s,t)\, B^{A_2}(m)|^2 , \tag{5.1}$$

where $F^i_\mu$ and $A^i_\mu$ ($i = 0, 1\pm, 2\pm$) represent production amplitudes (assumed approximately constant in $K\bar{K}$ invariant mass $m$) and $B^f$ and $B^{A_2}$ are the decay factors of eq. (A.5). The phase and modulus of these decay factors are illustrated in fig. 11. The mass, width and branching ratio parameters used are collected in appendix B. The relative phase $\delta_f - \delta_{A_2}$ of the $f^0$ and $A_2$ resonance decay factors is also shown as a function of $K\bar{K}$ mass in fig. 11. This is of interest since it is the variation of this phase with $m$ that allows the ambiguity in the sign of the relative f and $A_2$ production phase to be resolved. Thus, like $\rho$–$\omega$ interference, a more complete measurement is possible in principle and with no SU(3) assumptions. The relevance of the relative phase depending on $m$ is understood on considering the interference term in eq. (5.1):

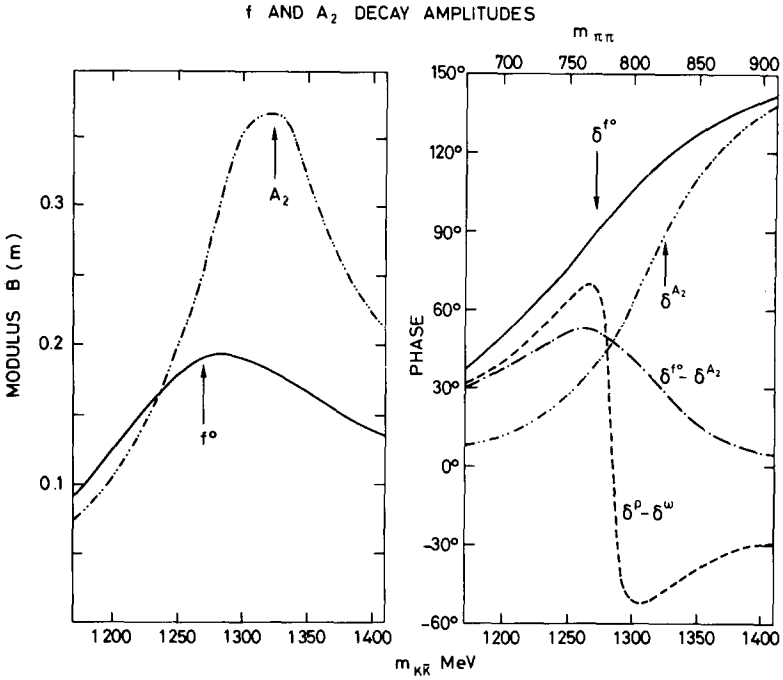


Fig. 11. The modulus and phase of the $f^0 \to K^+K^-$ (full curve) and $A_2 \to K^+K^-$ (double-dotted curve) Breit-Wigner decay amplitudes $B(m_{K\bar{K}})$ [eq. (A.5)]. The mass, width and branching ratios used are discussed in appendix B. We also compare the resonance phase differences $\delta^{f}-\delta^{A_2}$ (single-dotted curve) and $\delta^{\rho}-\delta^{\omega}$ (dashed) where the mass scales are chosen to coincide at $m_{K\bar{K}} = 1270$, $m_{\pi\pi} = 770$ MeV ($(m, \Gamma)_{\rho} = (772, 143)$; $(m, \Gamma)_{\omega} = (784, 10)$ MeV).

$$\sum_{\mu} \mathrm{Re}(F^i_{\mu} A^{i*}_{\mu} B^{f}(m) B^{A_2}(m)^*)$$
$$= \xi_i \{\sum_{\mu} |F^i_{\mu}|^2\}^{\frac{1}{2}} \{\sum_{\mu} |A^i_{\mu}|^2\}^{\frac{1}{2}} |B^{f}(m)|\, |B^{A_2}(m)| \cos(\phi_i + \delta_f(m) - \delta_{A_2}(m)). \quad (5.2)$$

The known $m$ variation of $B$ and thus $\delta$ then allows the $f-A_2$ relative production phase $\phi_i$ to be uniquely determined.

In practice this effect can be well controlled since, because of isospin, the $f^0-A_2$ interference changes sign both with the change from proton to neutron target (as for $\rho-\omega$ interference) and with the change from $K^+K^-$ to $K^0\bar{K}^0$ decay channel. An easy way to visualize the respective signs for the four relevant processes is via duality diagrams as shown in fig. 12. Thus processes (b) and (c) $\pi^-p \to K^-K^+n$ and $\pi^+n \to K^0\bar{K}^0p$ have real production phase duality diagrams (like $KN \to K^*(1420)N$) while (a) and (d), $\pi^-p \to K^0\bar{K}^0n$ and $\pi^+n \to K^+K^-p$, have rotating phase (like $\bar{K}N \to \bar{K}^*(1420)N$). Thus for processes (b) or (c) the production phases will be as drawn for the Argand diagram of fig. 9, while for (a) or (d) an extra 180° is needed.

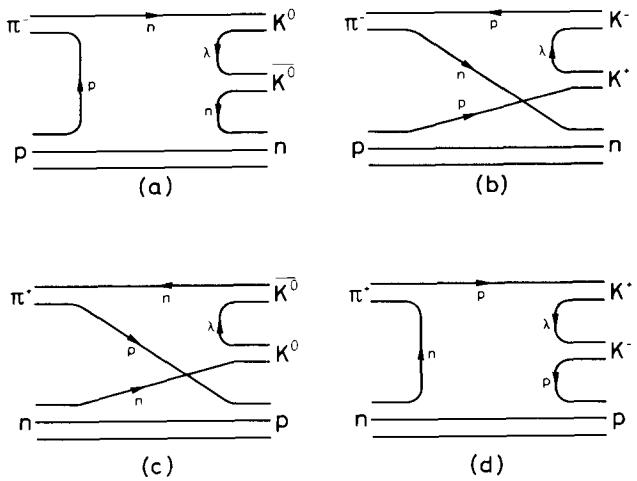


Fig. 12. Duality diagrams for the four processes: (a) $\pi^- p \to K^0 \bar{K}^0 n$, (b) $\pi^- p \to K^- K^+ n$, (c) $\pi^+ n \to K^0 \bar{K}^0 p$ and (d) $\pi^+ n \to K^+ K^- p$.

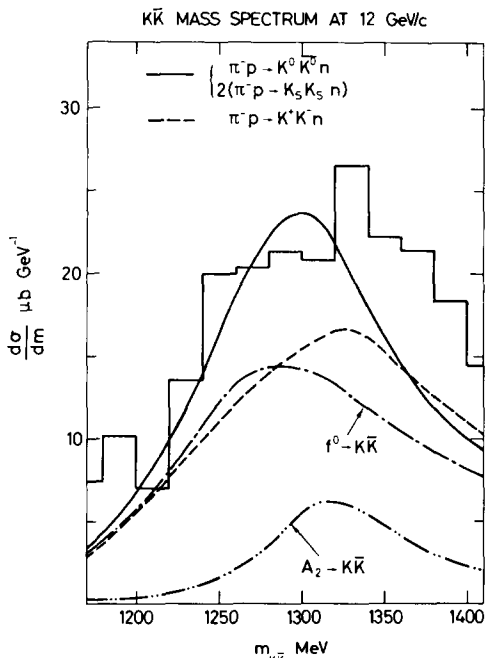


Fig. 13. The predicted $K\bar{K}$ mass spectrum ($|t| < 0.5$ GeV$^2$) for $\pi^- p \to K^+ K^- n$ and $\pi^- p \to K^0 \bar{K}^0 n$ at 12 GeV/$c$ is compared with the $\pi^- p \to K^0_S K^0_S n$ data of ref. [29].

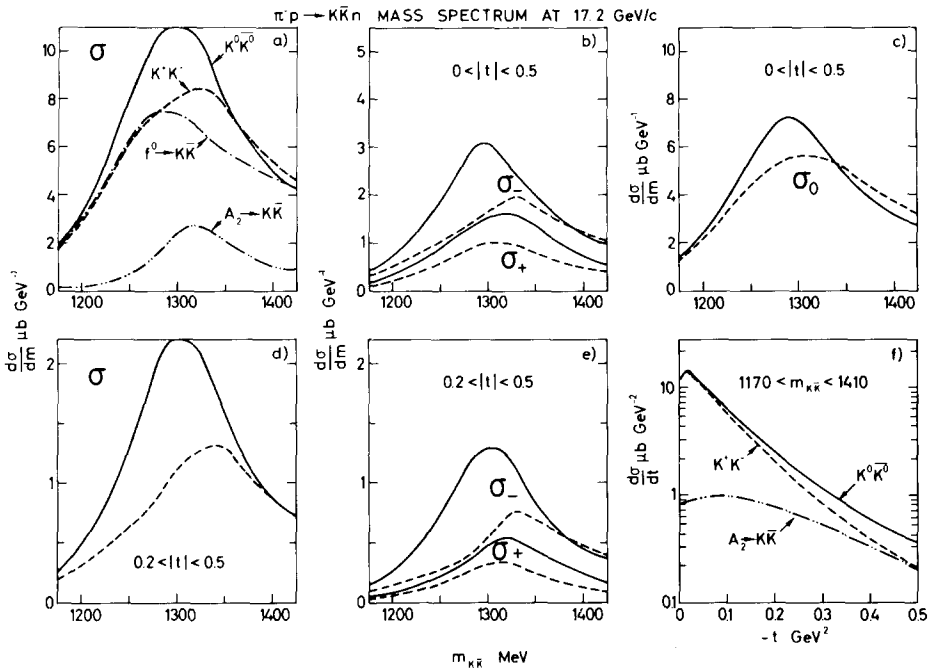


Fig. 14. The predicted mass spectrum $d\sigma/dm$ of $\pi^- p \to K\bar{K}n$ at 17.2 GeV/$c$ integrated over $|t| < 0.5$ GeV$^2$ ((a) (b) and (c)) and over $0.2 < |t| < 0.5$ GeV$^2$ ((d) and (e)). (a) and (d) show $\sigma$, the full mass spectrum; (c) shows the helicity zero contribution $\sigma_0$; and the helicity one and two contributions are given by their natural ($\sigma_+$) and unnatural ($\sigma_-$) parity contributions in (b) and (e). (f) shows $d\sigma/dt$ integrated over the region $1170 < m_{K\bar{K}} < 1410$ MeV as a function of $t$. The $\pi^- p \to K^0\bar{K}^0 n$ ($K^+K^-n$) predictions are shown by full (dashed) curves. Contributions proceeding via $f^0$ ($A_2$) production are shown by single- (double-) dotted curves.

As an example, consider the contribution to $|D_0|^2$. At $m \sim m_{f^0}$ the $f^0$ Breit-Wigner phase is $\sim 50°$ ahead of the $A_2$ resonance decay phase (see fig. 11) and the $f^0$ production amplitude is $\sim 70°$ ahead of the $A_2$ production (see fig. 9) so that the overall relative phase will be $\sim 120°$ (destructive) for (b) or (c) and $\sim 120° + 180°$ (constructive) for reactions (a) or (d).

More comprehensive predictions are shown in figs. 13, 14 and table 4 for different combinations of observables in $\pi N \to K\bar{K}N$. Fig. 14 shows the various components of $d\sigma/dm$ for $|t|$ cuts of $0 < |t| < 0.5$ and for $0.2 < |t| < 0.5$ GeV$^2$. The latter cut samples the region of largest production phase difference in $D_{1-}$ so exhibiting larger interference effects in $d\sigma_-/dm$ and hence in $d\sigma/dm$ ($d\sigma_+/dm$ is small and the helicity zero production phase difference is independent of $t$ in our model). A general feature of the predicted mass spectra of figs. 13 and 14 is that the maxima of both $\pi^- p \to K^- K^+ n$ and $\pi^- p \to K^0\bar{K}^0 n$ are shifted from the position of the dominant $f^0$ (1270 MeV) towards higher masses (to 1325 and 1300 MeV, respectively).

Table 4
The predicted normalized moments of the $K\bar{K}$ angular distribution in $\pi^- p \to K\bar{K}n$ at 17.2 GeV/$c$ and $m_{K\bar{K}} = 1310$ MeV ($\langle Y_0^0 \rangle = 1/\sqrt{4\pi}$)

| Moment | $K^0\bar{K}^0$ | $K^+K^-$ |
|---|---|---|
| $\langle Y_0^2 \rangle$ | 0.132 | 0.140 |
| $\langle Y_2^2 \rangle$ | −0.010 | −0.009 |
| $\langle Y_0^4 \rangle$ | 0.089 | 0.118 |
| $\langle Y_1^4 \rangle$ | 0.081 | 0.082 |
| $\langle Y_1^2 \rangle$ | 0.062 | 0.051 |
| $\langle Y_2^4 \rangle$ | 0.032 | 0.030 |
| $\langle Y_3^4 \rangle$ | 0.011 | 0.013 |
| $\langle Y_4^4 \rangle$ | 0.002 | 0.001 |

For $\pi^- p \to K^- K^+ n$ (or equivalently $\pi^+ n \to K^0 \bar{K}^0 p$) the shift is more marked and a definite asymmetry around 1325 MeV is anticipated.

Also shown in fig. 14 is $d\sigma/dt$ (in the mass region $1.17 < m < 1.41$ GeV) for $\pi^- p \to K^+ K^- n$ and $\pi^- p \to K^0 \bar{K}^0 n$. The interference effects are seen to be small. Another way to exhibit the data is to show the normalized moments $\langle Y_M^L \rangle$ (eq. (A.6)) for $K\bar{K}$ production. However, these are predicted to have very weak $m$ dependence and small interference effects. This is understandable since in general each $\langle Y_M^L \rangle$ is a sum over many exchange components whose contributions tend to be diluted. In table 4 we give the predicted values of the $\langle Y_M^L \rangle$ at $m = 1310$ MeV, where the $K\bar{K}$ spectra are approximately maximal. Only the $\langle Y_M^4 \rangle$ moments will be independent of S- and P-wave background uncertainties.

To make maximum use of interference effects, care of these $J < 2$ contributions and of accurate relative normalization will be needed experimentally. Another source of uncertainty is the precise $f^0 \to K\bar{K}$ (and to a lesser extent $A_2 \to K\bar{K}$) branching ratio. The quoted [28] value of $f^0 \to K\bar{K}/f^0 \to \text{all} = 0.05 \pm 0.03$ is based on data samples in which the effects of $f^0 - A_2$ interference have had to be taken into account in principle. Thus, since we have a reasonable model for the relative strength and phase of $f^0$ and $A_2$ production in $\pi N \to K\bar{K}N$, we are in a position to re-evaluate the $f^0 \to K\bar{K}$ branching ratio. As an example, fig. 13 shows data [29] on $\pi^- p \to K^0 \bar{K}^0 n$ at 12 GeV/$c$, together with our (absolute) prediction* including $f^0 - A_2$ interference and using $f^0 \to K\bar{K}/f^0 \to \text{all} = 0.025$. Taking account of the normalization error on the data, and the possible contribution of S- and P-wave $K\bar{K}$; this yields a $K\bar{K}$/all branching ratio $0.025 \pm 0.01$. Our curves in fig. 14 are evaluated with this branching ratio which has the virtue of being closer to the theoretical

* This contrasts with the experimental analysis [29] of the same data which added incoherently $f^0$ and $A_2$ and, estimating equal contributions of the two resonances, compared with the then existing $f^0$ production data in the $\pi\pi$ mode and claimed $f^0 \to K\bar{K}/f^0 \to \pi\pi \sim 0.05$.

value from SU(3). Thus, ideal mixing in the tensor meson nonet gives equal $f^0K\bar{K}$ and $A_2K\bar{K}$ couplings and allowing for D-wave phase space $\Gamma_{f^0K\bar{K}} = 0.7$ $\Gamma_{A_2K\bar{K}} \sim 3.4$ MeV, i.e. $\Gamma(f^0 \to K\bar{K})/\Gamma(f^0 \to \text{all}) \sim 0.02$.

## 6. Conclusions

(i) The simple exchange-model ideas of exchange-degenerate, factorizing, SU(3) symmetric $t$-channel Regge poles, together with empirical cuts in over-all non-flip amplitudes, have proved a very useful guide to the data. Exchange-degeneracy breakings of up to factors of 2 have been found necessary, in particular between $\rho$ and $A_2$ exchanges in vector meson production. It is important to consider *a priori* all allowed pole exchanges (i.e. B, $A_1$, Z ...) and then argue why their contributions might be negligible (as for $A_1$ exchange in $\pi N \to \rho N$).

(ii) The dual boost factors provide an economical description of higher spin meson production. The predicted mass/spin dependence of the natural/unnatural pole couplings, meson vertex helicity couplings and production $t$ dependences proved very satisfactory in the case of $\rho$ and $f^0$ production. The dual vertex helicity couplings were also shown to describe well the dominantly $\lambda_\omega = 1$ decay $B \to \omega\pi$.

(iii) The empirically determined cut in $\rho$ production has a remarkably steep $t$ dependence, although this can be alleviated by modifying the $\pi^t_-/\pi^t_0$ ratio. For $f^0$ production the cut is relatively smaller at $t = 0$ and is less steep. No convincing theoretical explanation exists, although one possible contributory factor was discussed.

(iv) Improved data on the charge-exchange production of $\omega$, $A_2$ and $f^0$ over a range of energies will allow many of the above feature to be clarified. Together with polarization data, or data on the $K\bar{K}$ decay of $f^0 - A_2$ (predictions for which were presented), many more model-independent lines of analysis become accessible. Our preliminary study of tensor meson production can easily be extended to higher spin mesons – for instance the spin-3 states $g$ and $\omega^*(3^-)$. Thus the systematics of the dependence of the production amplitudes on the external mass and spin can be established as soon as the relevant data becomes available.

(v) Our preliminary analysis of $f^0 - A_2$ interference in $\pi N \to K\bar{K}N$ (in which the important role of the production amplitudes is emphasized) allows an estimate to be made of the $f^0 \to K\bar{K}/f^0 \to$ all branching ratio which we find to be $0.025 \pm 0.010$.

We are grateful to Alan Martin and Penny Estabrooks for helpful discussions and communications.

## Appendix A. Normalization and spin

Consider the process $a + b \to m + e$, where m is a spin-$J$ resonance of helicity $\lambda$ which decays with invariant mass $m$ into two spinless particles c and d. In the rest

frame of m, the direction of $\boldsymbol{p}_c$ is described by spherical polar angles $\theta$ and $\phi$ in a frame with Oy normal to the scattering plane and Oz either along $\boldsymbol{p}_a$ in the $t$-channel frame or along $-\boldsymbol{p}_e$ in the $s$-channel frame. The helicity amplitude for a + b → c + d + e can be factorized into a production amplitude $A^J$ and a decay matrix element $M^J$

$$A^{\mu_a}_{\mu_e\mu_b}(s,t,m^2,\theta,\phi) = \sum_\lambda A^{J\lambda\mu_a}_{\mu_e\mu_b}(s,t,m^2)\frac{M^J\, \mathrm{d}^J_{\lambda 0}(\cos\theta)\mathrm{e}^{i\lambda\phi}}{m_J^2 - m^2 - im\Gamma_T(m)}, \tag{A.1}$$

where

$$|M^J|^2 = \frac{8\pi m}{q}(2J+1)\, m_J \Gamma_{cd}(m)\,. \tag{A.2}$$

We normalize A such that the differential cross section

$$\frac{\mathrm{d}\sigma}{\mathrm{d}t\,\mathrm{d}m^2\mathrm{d}\Omega} = \frac{1}{(2\pi)^3}\overline{\sum_\mu}\frac{q_{cd}}{4m}|A^{\mu_a}_{\mu_c\mu_b}(s,t,m^2,\theta,\phi)|^2\,, \tag{A.3}$$

where an average over initial spin states and sum over final spin states is implied.

Integrating over the decay angular distribution exhibited in eq. (A.1)

$$\frac{\mathrm{d}\sigma}{\mathrm{d}t\,\mathrm{d}m^2} = \overline{\sum_{\mu,\lambda}}|A^{J\lambda\mu_a}_{\mu_c\mu_b}(s,t,m^2)B^J(m)|^2\,, \tag{A.4}$$

where

$$B^J(m) = \frac{[m_J\Gamma_{cd}(m)/\pi]^{\frac{1}{2}}}{m_J^2 - m^2 - im\Gamma_T(m)} \tag{A.5}$$

are the decay factors relevant.

The generalization to the expectation value of the angular decay moments $Y^L_M(\theta,\phi)$ gives

$$\langle Y^L_M\rangle = \frac{1}{\sqrt{4\pi}}\sum_{\lambda,\lambda'}\frac{2J+1}{\sqrt{2L+1}}\langle JJ00|L0\rangle(-1)^{\lambda'}\langle J\lambda{-}\lambda'|LM\rangle\rho^J_{\lambda\lambda'}\,, \tag{A.6}$$

with

$$\rho^J_{\lambda\lambda'}(m^2)\frac{\mathrm{d}\sigma}{\mathrm{d}t\,\mathrm{d}m^2} = \overline{\sum_\mu}\,\mathrm{Re}[A^{J\lambda\mu_a}_{\mu_e\mu_b}(s,t,m^2)B^J(m)A^{J\lambda'\mu_a}_{\mu_e\mu_b}(s,t,m^2)^*\,B^J(m)^*]\,. \tag{A.7}$$

For resonance production it is convenient to introduce production amplitudes averaged over the resonance mass spectrum and corrected for all decay modes. Thus

the natural definition of a production cross section is to integrate over the resonance peak:

$$\frac{\mathrm{d}\sigma}{\mathrm{d}t} = \frac{\Gamma_T}{\Gamma_{cd}} \int_{m_L^2}^{m_H^2} \mathrm{d}m^2 \frac{\mathrm{d}\sigma}{\mathrm{d}t\,\mathrm{d}m^2}$$

$$= \frac{I(m_L^2, m_H^2)}{(2s_a+1)(2s_b+1)} \sum_{\mu,\lambda} |A^{J\lambda\mu_a}_{\mu_e\mu_b}(s,t,m_J^2)|^2 , \qquad \text{(A.8)}$$

which introduces the average production amplitudes. The average $I$ is defined so that it is unity for a narrow resonance. In general, it depends on the mass dependence of the production amplitudes $A^J$ and the decay factors $B^J$:

$$I(m_L^2, m_H^2) = \frac{\Gamma_T}{\Gamma_{cd}} \int_{m_L^2}^{m_H^2} \mathrm{d}m^2 |B^J(m)|^2 \sum_{\mu,\lambda} |A^J(m^2)|^2 / \sum_{\mu,\lambda} |A^J(m_J^2)|^2 . \qquad \text{(A.9)}$$

Analogous averaged results hold for the moments and density matrix elements of resonance production. For explicit expressions and an extension to a mixture of spin states see ref. [23].

In the special case of $\pi$ exchange at $t = \mu^2$, however, the dependence of the production amplitude on $m^2$ is known and can be used to obtain the normalization of $\rho$ and $f^0$ production. Thus $A^J$ contains [6] an additional factor of $M^J$ controlling the production of resonance $J$ by $\pi$ exchange. Thus

$$I_\pi = \frac{1}{\pi} \frac{\Gamma_T(m_J)}{\Gamma_{cd}(m_J)} \int_{m_L^2}^{m_H^2} \mathrm{d}m^2 \frac{m_J \Gamma_{cd}(m^2)}{|m_J^2 - m^2 - im\Gamma_T(m^2)|^2} \frac{q_J m}{m_J q} \frac{\Gamma_{cd}(m^2)}{\Gamma_{cd}(m_J^2)} . \qquad \text{(A.10)}$$

This, combined with the Chew-Low formula [6], enables the production cross section at $t \to \mu^2$ to be normalized

$$\frac{(t-\mu^2)^2}{-t'} \frac{\mathrm{d}\sigma}{\mathrm{d}t}\bigg|_{t=\mu^2} = \frac{2\pi}{m_N^2 p_L^2} \frac{g^2}{4\pi} C_I (2J+1) m_J \Gamma_{cd}(m_J) I_\pi . \qquad \text{(A.11)}$$

The right-hand side at $p_L = 17.2$ GeV/$c$, with $g^2/4\pi = 14.4$, taking $I_\pi = 1$, has a value $(6.55)^2$ $\mu$b for $\rho$ production ($I = 1$; $c_I = 1$; $\Gamma(m_J) = 0.143$) and a value of $(9.2)^2$ for $f^0$ production ($I = 0$; $c_I = \frac{2}{3}$; $\Gamma_{\pi\pi}(m_J) = 0.81 \times 0.182$). These values are used for normalizing our production amplitudes by equating them to $g_\pi^2 e^{2b_\pi \mu^2}$ (see table 1). Representative values of $I_\pi(m_L^2, m_H^2)$ calculated from the $\pi\pi$ phase shifts [6] are

$$I_\pi^\rho(0.490, 0.689) = 0.495 , \qquad I_\pi^\rho(0.078, 1.562) = 1.028 .$$

Thus about $\pm 3\Gamma$ in $m$ is needed to have $I_\pi^\rho \sim 1$. For the $f^0$, with $\pm 3\Gamma$ mass range

$I_\pi^f = 0.96$. Thus our normalization of the $\rho$ and f production amplitudes corresponds in practice to taking a mass range of $\pm 3\Gamma$. For the $\omega$, which is very narrow, our prescription depends less on the production amplitude and is equivalent to taking the whole signal – to which $\pm 3\Gamma$ is a good approximation.

## Appendix B. Decay amplitudes for $f^0$ and $A_2$

To evaluate the resonance decay factors $B(m)$ (eq. (A.5) of Appendix A) we need the dependence of the total width $\Gamma_T$ and partial width $\Gamma_{cd}$ on subenergy $m$. For a D-wave resonance it is customary to use a centrifugal barrier factor

$$\Gamma(m) = \left(\frac{q}{q_R}\right)^5 \Gamma(m_R) \frac{D_2(q_R R)}{D_2(qR)},$$

where $D_2(x) = 9 + 3x^2 + x^4$, $q$ is the decay momentum into the relevant channel, and $R$ is a constant representing the radius of interaction.

For the $f^0$ we take [6] (in GeV units): $m_f = 1.27$, mass dependence of $\Gamma_T$ from $\Gamma_T(m_f) = 0.182$, $R = 3.5$ with $q$ as $\pi\pi$ decay momentum; mass dependence of $\Gamma_{K\bar{K}}$ from $\Gamma_{K\bar{K}}(m_f)/\Gamma_T = 0.025$ (see text), $R = 3.5$ with $q$ as $K\bar{K}$ decay momentum.

For the $A_2$ we take [30] $m_{A_2} = 1.324$; mass dependence of $\Gamma_T$ from $\Gamma_T(m_{A_2}) = 0.104$, $R = 3.5$ with $q$ as a $\pi\rho$ decay momentum; mass dependence of $\Gamma_{K\bar{K}}$ from $\Gamma_{K\bar{K}}(m_{A_2})/\Gamma_T = 0.06$ [31], $R = 3.5$ with $q$ as $K\bar{K}$ decay momentum.

## References


[1] C. Michael, Proc. 16th Int. Conf. on high-energy physics, Chicago-Batavia, 1972 (NAL, Batavia, Ill., 1973) vol. 3, p. 165;
R. Diebold, Proc. 2nd Int. Conf. on elementary particles, Aix-en-Provence, 1973, J. de Phys. Suppl. 34 Cl-1973, p. 284.
[2] P. Hoyer, R.G. Roberts and D.P. Roy, Nucl. Phys. B56 (1973) 173.
[3] P. Hoyer and J. Kwiecinski, Nucl. Phys. B60 (1973) 26.
[4] C. Michael, Nucl. Phys. B63 (1973) 431.
[5] P. Estabrooks and A.D. Martin, Phys. Letters 41B (1972) 350.
[6] P. Estabrooks et al., Proc. AIP Conf. on particles and fields, Tallahassee, 1973 (AIP, New York, 1973) p. 37.
[7] G.C. Fox, Proc. 2nd Int. Conf. on polarization and polarized targets, Berkely, 1971, Caltech. preprint CALT-63-334 (1971);
J.D. Kimel and E. Reya, Nucl. Phys. B58 (1973) 513.
[8] C. Michael, Springer Tracts in modern physics, ed. G. Höhler, (Springer Verlag, Berlin, 1970) vol. 55, p. 174.
[9] H. Pilkuhn et al., Nucl. Phys. B65 (1973) 460.
[10] G.L. Kane and M. Ross, Phys. Rev. 177, (1969) 2353;
C.D. Froggatt and D. Morgan, Phys. Rev. 187 (1969) 2044;
G.C. Fox, Proc. Conf. on phenomenology in particles physics, Pasadena, 1971 (Cal. Inst. Tech., Pasadena, Calif., 1971), p. 703.

[11] P. Estabrooks, A.D. Martin and C. Michael, Nucl. Phys. B72 (1974) 454.
[12] A.D. Martin, Proc. 4th Int. Symp. on multiparticle hadrodynamics, Pavia, 1973; CERN TH. 1741.
[13] G. Grayer et al., Proc. 4th Int. Conf. on high-energy collisions, Oxford, 1972 (Rutherford High Energy Laboratory, Chilton, Didcot, Berks., 1972), RHEL-72-001, vol. 2, p. 26.
[14] D.S. Ayres, Proc. AIP Conf. on particles and fields, Tallahassee, 1973 (AIP, New York, 1973) p. 302;
R. Diebold, quoted in ref. [1] and private communication.
[15] R.D. Field and D.P. Sidhu, Phys. Rev. D10 (1974) 89;
M. Ross, F.S. Henyey and G.L. Kane, Nucl. Phys. B23 (1970) 269.
[16] S.U. Chung et al., Phys. Letters 47 B (1973) 526;
V. Chaloupka, Proc. 2nd Int. Conf. on elementary particles, Aix-en-Provence, 1973, J. de Phys. Suppl., 34 11-12 Cl-1973, p. 213; CERN preprint D.Ph. II/Phys. 73–33 (1973).
[17] F. Gilman, M. Kugler and S. Meshkov, SLAC Pub. 1235 (1973).
[18] J.C. Anderson et al., Phys. Letters B45 (1973) 165;
L.E. Holloway et al., Phys. Rev. D8 (1973) 2814;
J.A. Mathews et al., Phys. Rev. Letters 26 (1971) 400.
[19] N. Armenise et al., Nuovo Cimento 65A (1970) 637.
[20] A.S. Goldhaber, G.C. Fox and C. Quigg, Phys. Letters 30B (1969) 249.
[21] G.C. Morehouse et al., Phys. Rev. Letters 25 (1970) 835;
D.J. Sherden et al., Phys. Rev. Letters 30 (1973) 1230;
C. Geweniger et al., Phys. Letters 29B (1969) 41;
H. Burfeindt et al., Phys. Letters 33B (1970) 509.
[22] W. Ochs and F. Wagner, Phys. Letters 44B (1973) 2[illegible].
[23] J.A. Charlesworth et al., Nucl. Phys. B65 (1973) 253.
[24] J.T. Carroll et al., Phys. Rev. Letters 25 (1970) 1393.
[25] M. Aguilar-Benitez et al., Phys. Rev. D4 (1971) 2858.
[26] K. Buchner et al., Nucl. Phys. B45 (1972) 333.
[27] C. Michael and V. Ruuskanen, Phys. Letters 35B (1971) 47;
J. Rosner, Proc. Conf. on phenomenology in particle physics, Pasadena, 1971 (Cal. Inst. Tech., Pasadena, Calif., 1971) p. 387.
[28] Particle Data Group, Rev. Mod. Phys. 45 No. 2, Part II (1973).
[29] W. Beusch et al., Phys. Letters 25B (1967) 357.
[30] G. Conforto et al., Phys. Letters 45B (1973) 154.
[31] V. Chaloupka et al., Phys. Letters 44B (1973) 211.

Nuclear Physics B72 (1974) 474–480. North-Holland Publishing Company

# A STUDY OF DUALITY OF THE $\pi\pi$ SCATTERING AMPLITUDE

A. UKAWA and M. FUKUGITA
*Department of Physics, University of Tokyo, Tokyo 113, Japan*

Y. OYANAGI
*National Laboratory for High Energy Physics, Oho-machi, Tsukuba-gun, Ibaraki 300-32, Japan*

Received 27 September 1973
(Revised 31 December 1973)

Abstract: Dual structure of the $\pi\pi$ scattering amplitude has been investigated in terms of the finite energy sum rule using recent phase-shift data. The amplitude shows properties quite consistent with the simple dual model in the framework of the two component theory of duality.

Extensive study of dipion peripheral production has given information on $\pi\pi$ scattering in the low-energy region and has enabled us to investigate a relation between direct-channel resonances and crossed-channel Regge exchange, called duality. In this paper we present an analysis of $\pi\pi$ scattering by constructing the amplitude in the Regge region in terms of finite energy sum rules using recent phase-shift data [1–3].

We must include two resonance towers with different signatures in the direct channel to study the relation between trajectories with different signatures in the crossed channel. For the input of our analysis, we choose the partial-wave solution of the Wisconsin-Toronto group [2] (from $\sqrt{s} = 0.60$ to 1.48 GeV), which covers the $\rho$- and f-meson regions†.

A set of sum rules with a continuous moment is written in terms of the integral of a crossing-odd amplitude:

$$S(t, \epsilon) = \int_{\nu_0}^{\nu_N} \mathrm{d}\nu \, \mathrm{Im} \, [(\nu^2 - \nu_0^2)^{-(\epsilon+2)/2} \, \mathrm{e}^{i\pi(\epsilon+2)/2} \, T(\nu, t)] \, , \tag{1}$$

† The solution of ref. [2] seems to have two flaws at a glance [3, 4], i.e., one is the absence of the S*(980) and the other is the early onset of inelasticity. The contribution of S*(980) to the integral of the FESR, however, is negligible because of its small elastic width, and the early onset of inelasticity may not have a serious effect after integration. On the other hand we do not take the LBL solution [3], because of its large f-wave contribution which is inconsistent with recent experiment [4].

where $\nu = \frac{1}{2}(s-u)$. For $I_t = 0$ and 2, we make $T$ crossing odd, multiplying the original amplitudes by $\nu$. We evaluate the integral up to $\sqrt{s} = 1.48$ GeV over the region $0 \leqslant -t \leqslant 2.4$ (GeV/$c$)$^2$ with moments $-4 \leqslant \epsilon \leqslant -1$†. Since the finite energy sum rules are known to be well saturated by low-lying resonances provided the cut-off is chosen midway between two adjacent resonances, [5, 6] our cut-off at $\sqrt{s} = 1.48$ GeV, which lies midway between f and g mesons, is appropriate to test the duality.

$I_t = 1$. The integral (1), for each moment $\epsilon$, exhibits the phase of the amplitude given by the effective trajectory $\alpha_\rho(t) = 0.5 + 1.1t$. In fig. 1 we present the $t$-dependences of both the imaginary and real parts of the scattering amplitude in a Regge region, which are given by $(\alpha_\rho + 1)S(t, -2)$ and $(\alpha_\rho + 2)S(t, -3)/\sqrt{\nu_N^2 - \nu_0^2}$, respectively, assuming $T \sim \nu^{\alpha_\rho}$. Both imaginary and real parts exhibit the behaviour characteristic of $\rho$ Regge pole exchange with the Gell-Mann mechanism [7]: the imaginary part has single zeros at $t \simeq -0.4$, $-1.4$ and $-2.3$ (GeV/$c$)$^2$, while the real part has double zeros at $t \simeq -0.4$ and $-2.3$ (GeV/$c$)$^2$ and has a maximum at $t \simeq -1.5$ (GeV/$c$)$^2$.

In order to test the resonance dominance of the imaginary part of the non-diffractive amplitude, which is one of the requisites for the duality, we also show in fig. 1 the imaginary part of the amplitude calculated from the integral saturated by $\rho$, f and $\epsilon'(1260)$ (second daughter of f) resonances††. The figure shows that the $\rho$ Regge pole exchange amplitude is built of the sum of $\rho$, f and $\epsilon'$ in the direct channel. We have made the same analysis including two more resonances $\rho'(1590)$ and g [8] in addition to $\rho$, f and $\epsilon'$ and choosing the cut-off at 1.81 GeV and found single zeros at $t \simeq -0.4$, $-1.4$ and $-2.1$ (GeV/$c$)$^2$ in agreement with the results above. This indicates that the structure of the imaginary part of the amplitude remains unchanged as the cut-off is taken higher.

It should be noted in particular that the amplitude near the first zero is described by the Regge *pole* exchange in contrast to the helicity non-flip amplitude in meson-baryon scattering, where the imaginary part has a zero at $t \simeq -0.2$ (GeV/$c$)$^2$. The prediction based on a low-energy $\pi\pi$ model [9], which gives a zero near $t = -0.2$, does not agree with the FESR analysis, unless the partial waves higher than the leading resonances contribute unexpectedly. If this feature of the $\pi\pi$ scattering amplitude persists at high energy, a considerable contribution from lower partial waves is required and the smaller radius of the peripheral $\pi\pi$ interaction ($R \approx 0.8$ fm) which is consistent with the position of the first zero at $-t \simeq 0.4$ (GeV/$c$)$^2$ would not be sufficient to assure the observed behaviour, particularly beyond the first zero.

† For the low-energy region ($\sqrt{s} < 0.6$ GeV) where phase-shift data are lacking, we extrapolated the partial-wave amplitudes consistently with the current algebra requirements. Our results do not depend on the details of the extrapolation.

†† The resonance parameters are determined by a fitting procedure to the partial-wave amplitudes of ref. [2], each amplitude being assumed as a sum of a Breit-Wigner form and a constant background term. The parameters are: $m_\rho = 0.782$, $\Gamma_\rho = 0.137$, $x_\rho = 0.93$; $m_f = 1.261$, $\Gamma_f = 0.183$, $x_f = 0.78$; $m_{\epsilon'} = 1.316$, $\Gamma_{\epsilon'} = 0.267$, $x_{\epsilon'} = 0.73$ (in GeV units). A change of the parametrization, especially of $\epsilon'$, has little influence on the results.

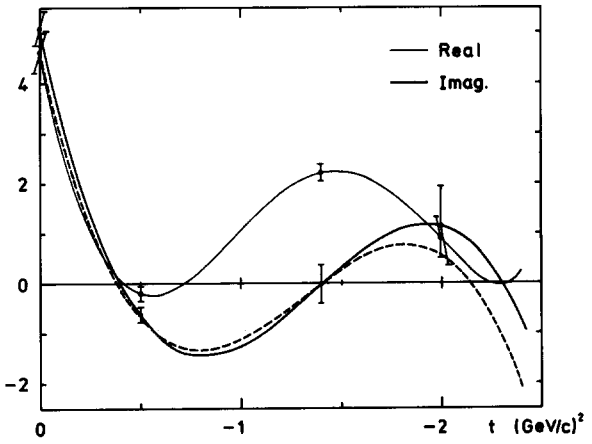


Fig. 1. $t$-dependences of the imaginary and real parts of the $I_t = 1$ scattering amplitude in the Regge region (solid curve), given by

$$\sqrt{\nu_N^2 - \nu_0^2}\, T(\nu_N, t) = i(\alpha_\rho + 1)S(t, -2) + (\alpha_\rho + 2)S(t, -3)/\sqrt{\nu_N^2 - \nu_0^2},$$

where $\nu_N$ stands for the cut-off of the integral. The errors shown are those calculated from the data of ref. [2]. The dashed curve represents the imaginary part of the amplitude calculated by resonance saturation. (The amplitudes are in units of GeV.)

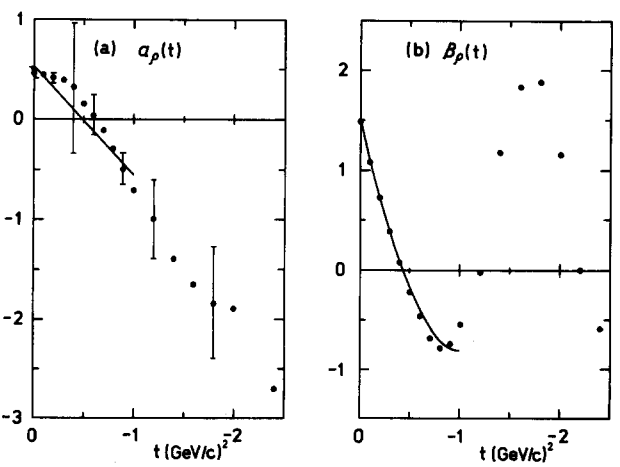


Fig. 2. $\rho$ Regge-pole parameters, $\alpha_\rho(t)$ (a) and $\beta_\rho(t)$ (b), determined in a $t$-independent manner (circles) as well as a $t$-dependent manner for $0 < -t < 1$ (GeV/$c$)$^2$ (solid curve). The errors for $\alpha_\rho(t)$ are only typical. ($\beta_\rho(t)$ is in units of GeV.)

The remarkable feature also seen in fig. 1 is the $t$-channel Regge pole behaviour which persists in the large $|t|$ region as far as $t \simeq -2.4$ (GeV/$c$)$^2$. Although we are in the region of the third double spectral function in the integration for large $|t|$, the sum rule is expected to be written safely because of the absence of a dual $(s, u)$ term in the $I_t = 1$ combination, $(s, t) - (u, t)$. In addition to this, the absence of an $(s, u)$ term implies that the amplitude is described in terms of Regge-pole exchange in the $t$-channel even in the backward direction, so that, as we observe in fig. 1, the imaginary part of the amplitude at fixed $u$ cancels when averaged over an energy interval $\Delta s \approx 2$ (GeV)$^2$, while the real part gives a positive value in agreement with the $\rho$-f exchange degeneracy in the $u$- as well as $s$-channels.

The Regge-pole parameters, $\alpha_\rho(t)$ and $\beta_\rho(t)$, determined in a $t$-independent manner are shown in fig. 2 †. They are consistent with roughly straight trajectory with $\alpha_\rho(0) \simeq 0.5$ and $\alpha'_\rho \simeq 1$ (GeV/$c$)$^{-2}$ and the residue function $\beta_\rho(t) \sim 1/\Gamma[\alpha_\rho(t)]$. We have estimated $\beta_\rho(m_\rho^2)$, which is related to the $\rho$-width in the $t$-channel, in terms of a $t$-dependent analysis assuming a linear trajectory and a quadratic parametrization in $t$ for $\beta_\rho(t)$ in the forward region $0 \leqslant |t| \leqslant 1$ (GeV/$c$)$^2$. This analysis gives $\alpha_\rho(t) = 0.52 + 1.08\,t$ and $\Gamma_\rho \simeq 0.15$ GeV, consistent with the $\rho$ meson width in the $s$-channel $\Gamma_\rho \simeq 0.13$ GeV*.

$I_t = 0$. The two component theory of duality [10] assumes that the imaginary part of the amplitude in the forward region is given by the sum of f Regge and pomeron exchanges which are dual to $s$-channel resonances and the non-resonating background part, respectively. This assumption has been ascertained in the case of meson-baryon scattering by separating the ordinary Regge amplitude in terms of the resonance approximation in the $s$-channel [11–13]. The saturation of the $\rho$-exchange amplitude by the $s$-channel resonances allows us to expect they also saturate f-exchange in the $I_t = 0$ amplitude.

The integral corresponding to the imaginary part of the $I_t = 0$ combination of the resonant amplitude is presented in fig. 3(a) in the forward region up to $t = -1.0$ (GeV/$c$)$^2$, together with that of the full amplitude. The resonant part has the qualitative features of single Regge-pole exchange with the Gell-Mann mechanism like the $\rho$-exchange, and is quite consistent with the $\rho$-f exchange degeneracy. To make it clear the imaginary part of the $\rho$ exchange contribution to the $I_t = 1$ amplitude multiplied by $\frac{3}{2}$ is added in the same figure. The slight difference between the two amplitudes is due to our cut-off of the integral and will become smaller with alternating signs as the cut-off is taken higher.

On the other hand the non-resonating background part shows a diffraction-like $t$-dependence as is seen in fig. 3(b). The magnitude of the forward peak corresponds to the asymptotic total cross section $\sigma_{\pi\pi} \simeq 28$ mb. Although this value seems a bit larger ($\sigma_{\pi\pi}^{\mathrm{exp}} \simeq 18$ mb [14]) it should not be taken too seriously, since it depends on the choice of a partial-wave solution and the separation of the background part.

† The residue $\beta_\rho(t)$ is normalized as $\sigma_{\pi^+\pi^-}^{\mathrm{tot}} - \sigma_{\pi^+\pi^+}^{\mathrm{tot}} = 16\pi\,\beta_\rho(0)\,s^{\alpha_\rho(0)-1}$.

* See third footnote of this paper.

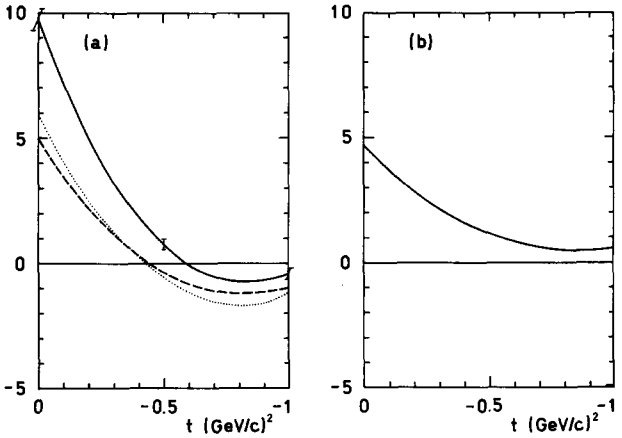


Fig. 3. (a) the integral $S(t, -2)$ corresponding to the imaginary part of the $I_t = 0$ amplitude (solid curve) and the resonance saturation for the integral (dashed curve) as a function of $t$. The $\rho$ exchange contribution to the $I_t = 1$ amplitude multiplied by $\frac{3}{2}$ is also shown (dotted curve). (b) the non-resonating background part which is obtained by subtracting the resonance contribution from the integral corresponding to the full amplitude.

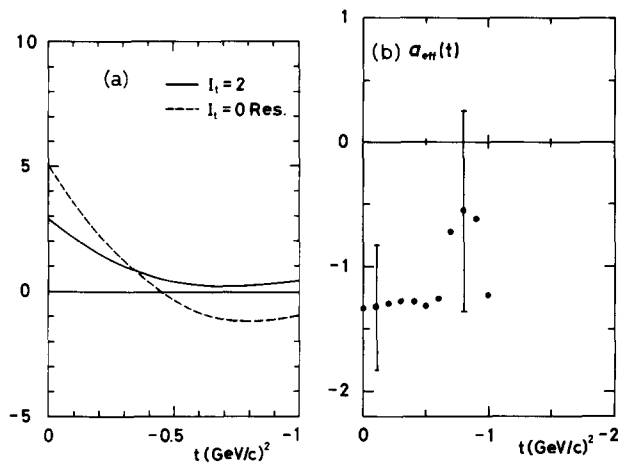


Fig. 4. (a) the integral $S(t, -2)$ corresponding to the imaginary part of the $I_t = 2$ amplitude (solid curve) as compared with the imaginary part of the $I_t = 0$ resonant amplitude (dashed curve). (b) the effective Regge-pole trajectory for the $I_t = 2$ amplitude determined in a $t$-independent manner for $0 < -t < 1$ (GeV/$c$)$^2$.

These results are in good agreement with the conjecture of the two component theory of duality in that the resonant and background parts are dual to ordinary Regge and pomeron exchanges, respectively.

We now refer to the real part, which is sensitive to the ill-determined phase shift of the $I_s = 2$ d-wave $\delta_2^2$ (due to the crossing matrix and the factor $q\nu \sim \nu^2$ in the integrand). We have found that the integral corresponding to the real part of the $I_t = 0$ amplitude has a zero at $t \simeq -0.6\ (\mathrm{GeV}/c)^2$ contrary to the expected behaviour of the sum of the pomeron and f exchanges. This discrepancy originates from the large exotic phase $\delta_2^2$ of our input [2]†.

$I_t = 2$. The integral corresponding to the imaginary part of the $I_t = 2$ amplitude is about half of that of the $I_t = 0$ resonant amplitude at $t = 0$ (fig. 4a), although no Regge pole is exchanged in the $I_t = 2$ channel. As for this superconvergence-type integral, we are confronted with a disastrous cut-off problem [15], i.e., the magnitude of the $s$-channel resonances grows as $\nu^{\alpha_\rho(t)}$, so that cancellation between the contributions from resonances with different signatures is not expected even if the exchange degeneracy holds exactly (a simple estimation of the integral with exact exchange degeneracy gives ~54% of the integral for the $I_t = 0$ resonant part). The exoticity of the $t$-channel, however, is supported by two observations: (i) the integral has a structureless $t$-dependence, (ii) effective one-pole analysis gives $\alpha_{\mathrm{eff}}(t) < 0$ for all $t$ (fig. 4b).

We have investigated the properties of the amplitude for $\pi\pi$ scattering as model-independently as possible using recent partial-wave analyses. The results presented above are strongly suggestive of the dual structure which is abstracted from the simple $B_4$ model in the framework of the two-component theory.

One of the authors (Y.O.) is thankful to the Sakkokai Foundation for financial support.

## References

[1] J.P. Baton, G. Laurens and J. Reignier, Phys. Letters 33B (1970) 528.
[2] J.T. Carroll, R.N. Diamond, M.W. Firebaugh, W.D. Walker, J.A.J. Matthews, J.D. Prentice and T.S. Yoon, Phys. Rev. Letters 28 (1972) 318.
[3] S.D. Protopopescu, M. Alston-Garnjost, A. Barbaro-Galtieri, S.M. Flatté, J.H. Friedman, T.A. Lasinski, G.R. Lynch, M.S. Rabin and F.T. Solmitz, Phys. Rev. D7 (1973) 1279.
[4] G. Grayer, B. Hyams, C. Jones, P. Schlein, W. Blum, H. Dietl, W. Koch, E. Lorenz, G. Lütjens, W. Männer, J. Meissburger, W. Ochs, U. Stierlin and P. Weilhammer, Proc. of the 3rd Int. Conf. on experimental meson spectroscopy, Philadelphia, 1972.

† If we artificially decrease this phase, say, by a factor 2, which is consistent with the scattering length approximation based on dispersion relations, the zero at $t \simeq -0.6\ (\mathrm{GeV}/c)^2$ mentioned above disappears, while the qualitative features of the other amplitudes remain unchanged (this makes $\sigma_{\pi\pi} \simeq 20$ mb).

[5] M. Ademollo, H.R. Rubinstein, G. Veneziano and M.A. Virasoro, Phys. Rev. 176 (1968) 1904.
[6] G. Veneziano, Nuovo Cimento 57A (1968) 190.
[7] G. Kaiser, Nucl. Phys. B43 (1972) 345.
[8] B. Hyams, C. Jones, P. Weilhammer, W. Blum, H. Dietl, G. Grayer, W. Koch, E. Lorenz, G. Lütjens, W. Männer, J. Meissburger, W. Ochs, U. Stierlin and F. Wagner, Max Planck Institute preprint MPI-PAE/Exp. El. 28 (1973).
[9] J.L. Basdevant, C.D. Frogatt and J.L. Petersen, Phys. Letters 41B (1972) 173, 178; J.L. Basdevant and C. Shomblond, Phys. Letters 45B (1973) 48.
[10] H. Harari, Phys. Rev. Letters 20 (1968) 1395; P.G.O. Freund, Phys. Rev. Letters 20 (1968) 235.
[11] H. Harari and Y. Zarmi, Phys. Rev. 187 (1969) 2230.
[12] M. Fukugita and T. Inami, Nucl. Phys. B44 (1972) 490.
[13] T.A. Lasinski, Nucl. Phys. B29 (1971) 125.
[14] W.J. Robertson, W.D. Walker and L. Davis, Durham preprint (1972); C. Caso, F. Conte, G. Tomasini, P. Benz, P. Schilling, S. Ratti, D. Teodoro, G. Vegni, L. Mosca and C. Lewin, Nuovo Cimento 3A (1972) 287.
[15] C. Schmid, Phys. Rev. Letters 20 (1968) 628; R. Dolen, D. Horn and C. Schmid, Phys. Rev. 166 (1968) 1768.

Nuclear Physics B72 (1974) 454–460. North-Holland Publishing Company

# EXCHANGE MECHANISMS FOR $\pi^- p \to \rho^0 n$ AND $\rho - \omega$ INTERFERENCE

P. ESTABROOKS ‡*, A.D. MARTIN ‡‡* and C. MICHAEL
*CERN, Geneva*

Received 15 November 1973

Abstract: The 17 GeV/$c$ $\pi^- p \to \rho^0 n$ production amplitudes are decomposed into $\pi$, $A_2$ and non-evasive exchange contributions. Independent support for this description comes from the observed $\rho$-$\omega$ interference effects and from the energy dependence of $\rho^0$ production data.

The reaction $\pi^- p \to \rho^0 n$ is well-known historically as a process in which $\pi$ exchange can be studied. However, it has also been noted that simple one-pion exchange does not provide a complete description of the production mechanisms [1, 2]. Here we investigate the non $\pi$ exchange contributions and present a simple phenomenological model which describes the helicity structure and $t$ dependence of the 17.2 GeV/$c$ $\rho^0$ production data [3]. Examination of the energy dependence and of $\rho$-$\omega$ interference effects provides support for our description.

The $\rho$ production ** amplitude combinations $P_0$, $P_+$ and $P_-$ can be extracted [4, 5] from $\pi^- p \to \pi^- \pi^+ n$ cross-section and density matrix data. $P_0$ describes helicity zero dipion production and $P_+$ ($P_-$) describe helicity 1 production by natural (unnatural) parity exchange to leading order in energy. Neglect of $A_1$ quantum number exchange ensures [5] that $P_0$ and $P_-$ are single amplitudes and their relative phase, $\varphi$, can also be determined. $P_+$ is an incoherent sum of amplitudes with and without helicity flip at the nucleon vertex (of which the former is expected to dominate).

The $P$-wave amplitudes † obtained from the high statistics 17.2 GeV/$c$ data [3] are shown in fig. 1 for the $t$ channel (Gottfried-Jackson) frame. For our present purposes, the $s$-channel decomposition could equally well be used, but the $t$ channel allows a somewhat clearer separation of the modifications to $\pi$ exchange.

‡ Supported by the National Research Council of Canada.
‡‡ On leave of absence from the University of Durham, Durham.
* Present address: University of Durham, Durham.
** That is the $P$-wave $\pi^- \pi^+$ production amplitudes in the $\rho$ mass region.
† We consider only the solution with $P_0$ and $P_-$ essentially phase coherent which was shown [6] to be the physical solution for $-t < 0.2$ GeV$^2$.

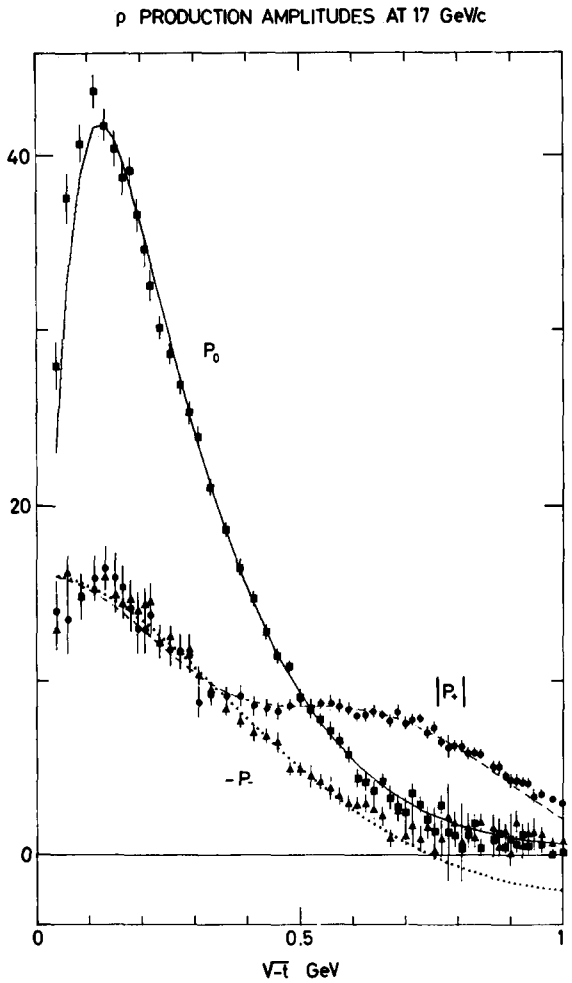


Fig. 1. The $\rho$ production amplitudes in the $t$-channel frame at 17.2 GeV/$c$. The points are the results of an amplitude analysis of the CERN-Munich $\pi^- p \to \pi^- \pi^+ n$ data for $700 < M_{\pi\pi} < 850$ MeV. The curves are the results of the fit to the amplitudes in the interval $0.005 < -t < 0.5$ GeV$^2$ that is described in the text. The values of the parameters are $g_C/g_\pi = -1.21$, corresponding to a cut strength of 0.93 of that in the Williams model [7], $g_A/g_\pi = 8.2$, $b_\pi = 0.6$ GeV$^{-2}$, $b_C = 0.8$ GeV$^{-2}$, $b_A = 2.5$ GeV$^{-2}$ and $\alpha'_A - \alpha'_C = 0.43$ GeV$^{-2}$ ($\chi^2 = 0.7$ per degree of freedom).

Elementary one-pion exchange only couples to $P_0$ in the $t$-channel frame. The non-zero values of $P_\pm$, which moreover do not vanish in the forward direction, thus imply an additional contribution which is not (evasive) pole exchange. Such a cut effect is expected [7, 2] to be most important in the $s$-channel net helicity non-flip amplitude $H^1_{+-}$. The cut, $C$, then contributes equally to $P_+$ and $P_-$ in the $s$-channel,

and on crossing to the $t$-channel contributes to $P_+$, $P_-$, $P_0$ in the ratio $1 : \cos\chi : \sin\chi$, where $\chi$ is the $s$-$t$ crossing angle ($\sin\chi > 0$). The inclusion of $C$ allows an adequate description of $P_-$, but the observed ratio of $|P_+|$ to $|P_-|$ as a function of $t$ necessitates the introduction of a natural parity exchange contribution ($A_2$ exchange) which interferes destructively with $C$ in $P_+$. This leads us to the parametrization

$$P_0 = \pi + C\sin\chi\,, \qquad P_- = C\cos\chi\,, \qquad P_+ = A_2 + C\,, \tag{1}$$

where the $t$ dependence is parametrized as

$$\begin{aligned} \pi &= g_\pi \frac{\sqrt{-t}}{\mu^2 - t}\, e^{b_\pi t}\, e^{-\frac{1}{2} i\pi\alpha_\pi}\,, \\ C &= g_C\, e^{b_C t}\, e^{-\frac{1}{2} i\pi\alpha_C}\,, \\ A_2 &= -t\, g_A\, e^{b_A t}\, e^{-\frac{1}{2} i\pi\alpha_A}\,, \end{aligned} \tag{2}$$

with $\alpha_i = \alpha_0^i + \alpha_i' t$ determining the phase of the $i$th contribution.

The phase difference between $\pi$ and $C$ is controlled by the relative phase, $\varphi$, of $P_0$ and $P_-$, which is consistent with $\varphi = 180°$ for all $-t$ less than 0.5 GeV$^2$. $P_0$ and $P_-$ determine the $\pi$ and $C$ contributions, and then, given the phase difference * $\alpha_A - \alpha_C$, $|P_+|$ determines the $A_2$ exchange contribution. We take $\alpha_C = \alpha_\pi$ and, at $t = 0$, $\alpha_A - \alpha_C = 0.5$. Allowing a linear dependence on $t$ of the $A_2$-$C$ phase difference, we obtain the overall fit ** in the $t$ region $-0.005$ to $-0.5$ GeV$^2$ shown in fig. 1.

The simple parametrization of eqs. (1) and (2) is an excellent description of the 17.2 GeV/$c$ data out to $-t = 0.5$ GeV$^2$. The description of $P_+$ is also reasonable in the region beyond $-0.5$ GeV$^2$, where this amplitude dominates. Two possible contributions which have been neglected could easily be incorporated without changing the essential features. First, from processes such as $KN \to KN$, $\pi N \to \eta N$, and from the non-zero polarization in $\gamma p \to \pi^+ n$, there is some evidence for a small $A_2$ helicity non-flip coupling at the nucleon vertex. Such a coupling will be important for polarization predictions in $\pi N \to \rho N$, but enters the unpolarized observables only as a small correction to the $t$ dependence of $A_2$ and a small reduction of coherence between $C$ and $A_2$ in $P_+$. Secondly, a reggeized $\pi$ exchange can have a $\lambda_t = \pm 1$ coupling (vanishing at $t = \mu^2$ of course) to $P_-$. This coupling is present in dual Born models [8] and is such as to fill in the crossing matrix zero ($\cos\chi = 0$ at $-t \sim 0.6$ GeV$^2$) in $P_-$ in the $t$-channel frame (or equivalently in $P_0$ in the $s$-channel frame). Fig. 1 indeed indicates the need for such a contribution to $P_-$ at large $t$.

* The data impose bounds to this phase difference. At $-t \sim 0.05$, $|\alpha_A - \alpha_C| \lesssim 0.6$ decreasing to $|\alpha_A - \alpha_C| \lesssim 0.2$ at $-t \sim 0.5$ GeV$^2$.

** As $|P_+|^2$ has a quadratic dependence on $A_2$, a second solution exists. This is found to be unphysical, having an $A_2$ contribution whose phase, relative to $C$, varies extremely rapidly with $t$, and whose magnitude shows an anomalously rapid $t$ dependence.

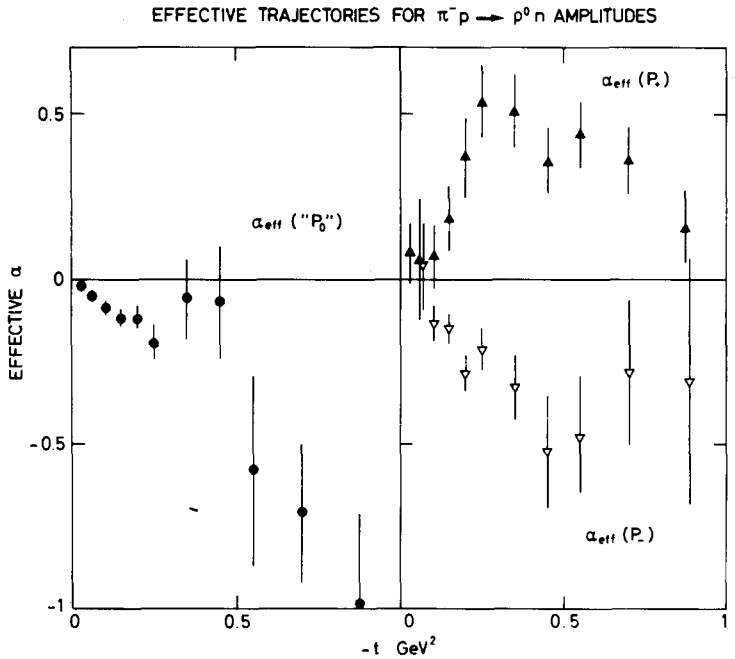


Fig. 2. The effective trajectories, calculated using $s$-channel amplitude components obtained by analysing $\pi^- p \to \pi^- \pi^+ n$ data in the energy range 4–17 GeV/$c$.

Having established a parametrization for the phase and $t$ dependence of the $\pi$, $C$ and $A_2$ contributions for $-t < 0.5$ GeV$^2$, we look at the energy dependence that would arise from the phase-energy relationship. Fig. 2 shows the effective trajectories, $\alpha_{\text{eff}}(t)$, for $P_0$, $P_+$ and $P_-$ (in the $s$-channel) obtained * by analyzing $\pi^- p \to \pi^- \pi^+ n$ data, refs. [3, 10–13], in the energy range 4 to 17 GeV/$c$. In the model of eq. (1), the $s$-channel $P_0$ is pure $\pi$ exchange and $\alpha_\pi = 0.5\ (t - \mu^2)$ is a reasonable compromise trajectory. Qualitatively, the structure of $\alpha_{\text{eff}}$ for $P_+$ can be easily understood with our description. $C$ is the dominant contribution at small $t$ ($\alpha_C \approx \alpha_\pi$) and $A_2$ domintates at $t \sim -0.5$, while there is a cancellation at intermediate $t$ values ($t \sim -0.25$) which leads to an $\alpha_{\text{eff}}$ above the $A_2$ trajectory. However, although the $t$ behaviour is correct, the phase-energy prediction is approximately 0.2 lower than $\alpha_{\text{eff}}$ obtained from the data.

At 17.2 GeV/$c$, $\rho$-$\omega$ interference effects have been shown [14] to be largest in $P_+$ in the interval $0.1 < -t < 0.4$ GeV$^2$ and we shall concentrate on this amplitude. Fig. 3 shows a breakdown of $P_+$ into its $C$ and $A_2$ components, as determined above,

* The method used is described in ref. [9], except that here we use the $s$-channel observable $(\rho_{00} + \frac{1}{3}\rho_{SS})\, d\sigma/dt$ in the place of $|P_0|^2$. This is an update of that calculation and includes high statistics $\pi^- p \to \pi^- \pi^+ n$ data at 6 GeV/$c$ [13] as well as the high statistics 17 GeV/$c$ data.

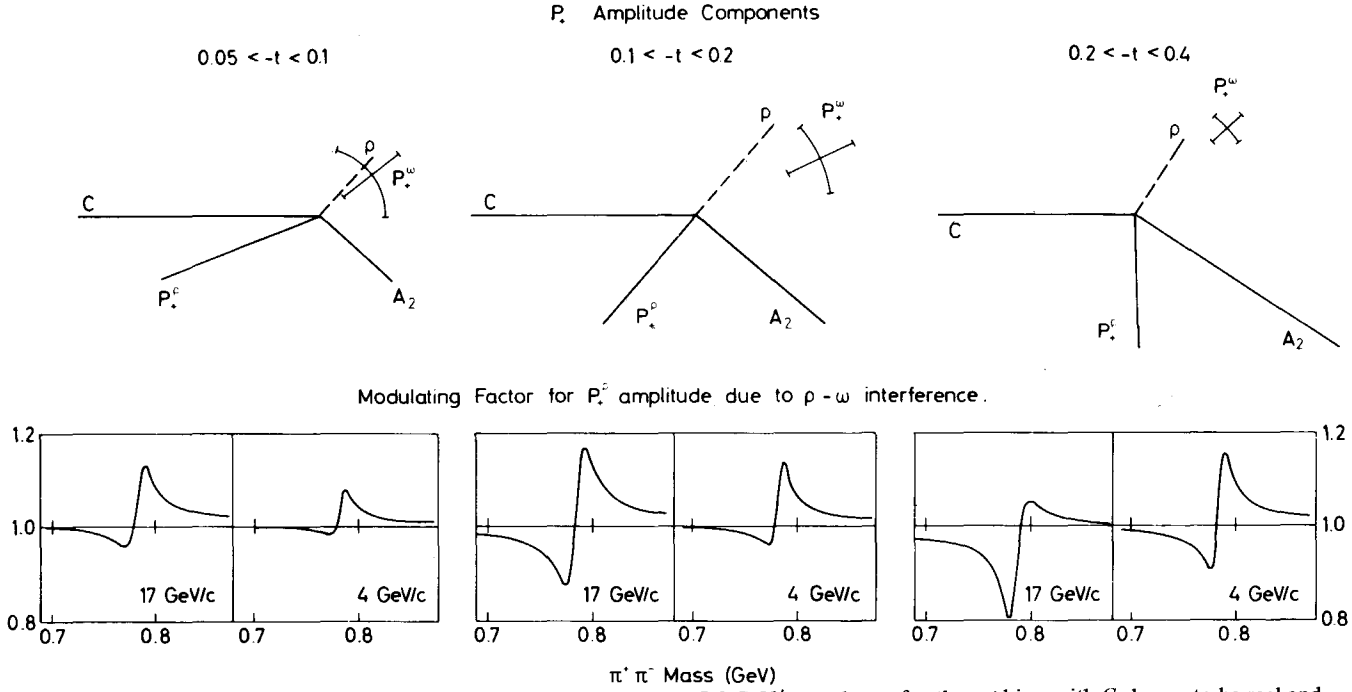


Fig. 3. The (complex) $C$ and $A_2$ contributions to $P_+$ for $\rho$ production at 17.2 GeV/$c$ are shown for three $t$ bins, with $C$ chosen to be real and negative. The dashed line indicates the $\rho$ exchange contribution to $\pi^- p \to \omega n$ obtained assuming $\rho$-$A_2$ exchange degeneracy. The $P_+$ amplitudes for $\pi^- p \to \rho^0 n$ $(C + A_2)$ and $\pi^- p \to \omega n$ $(\rho)$ then yield the $\rho$-$\omega$ modulating factors shown at 17 GeV/$c$ which can then be compared with the observed effects in ref. [14] (a 7 MeV resolution is folded in as described in ref. [14]). Conversely the crosses are the predictions for $P_+^\omega$ obtained from the values of $|P_+^\omega/P_+^\rho|$ and $\phi$ tabulated in ref. [14]. The 4 GeV/$c$ predictions for the modulating factor (with a 3 MeV mass resolution folded in) come from scaling $C$ relative to $A_2$ and $\rho$ by an energy dependence $\alpha_A - \alpha_C = 0.5 \pm 0.4\, t$.

The $\rho$-$\omega$ modulating factor as a function of $\pi\pi$ mass $m$ is given by

$$+ P_+^\omega(m_\rho^2 - m^2 - im_\rho\Gamma_\rho)\eta/P_+^\rho(m_\omega^2 - m^2 - im_\omega\Gamma_\omega)|^2 ,$$

where the $\rho$-$\omega$ mixing enters through $\eta$ which is approximately [18]

$$i[\Gamma(\omega \to \pi^+\pi^-)/\Gamma(\rho \to \pi^+\pi^-)]^{\frac{1}{2}}.$$

The $\rho$ parameters are taken from ref. [6] while we use $\Gamma(\omega \to \pi^+\pi^-)/\Gamma(\omega \to \text{all}) = 0.0175$ and $\Gamma_\omega = 10$ MeV.

for three relevant $t$ intervals. The phase of $P_+$ relative to $P_-$ can thus be obtained. For $\pi^- p \to \omega n$, $\rho$ quantum number exchange contributes to $P_+$. Since B quantum number exchange in $\pi N \to \omega N$ is smaller than $\pi$ exchange in $\pi N \to \rho N$, the B cut should be small compared to $\rho$ exchange *. Unfortunately, there are no data on $|P_+|$ for $\pi N \to \omega N$ at or near 17 GeV/$c$. Thus, the modulus, as well as the phase, must be estimated before a $\rho$-$\omega$ interference pattern can be predicted. The simplest model is to take exchange degenerate $\rho$ and $A_2$ contributions: $\rho = iA_2 \tan \frac{1}{2}\pi\alpha_A(t)$. This then ensures, *via* SU(3), a real $KN \to K^*N$ amplitude in agreement with duality for an exotic direct channel process. Constructing $P_+$ for $\omega$ production in this way then yields the $\rho$-$\omega$ modulating factors shown in fig. 3. Conversely, the relative moduli and phases of the $\rho$ and $\omega$ production amplitudes $P_+$ derived from fitting the experimental data at 17.2 GeV/$c$ [14], yield the $P_+$ amplitudes for $\omega$ production that are shown by crosses in fig. 3. These estimates are in reasonable accord with the $\rho$-$A_2$ exchange degeneracy prescription. In particular the change of phase of $P_+$ with $t$, required by the observed $\rho$-$\omega$ effects, is well reproduced by the admixture of $C$ and $A_2$ contributions to $P_+$ for $\pi^- p \to \rho^0 n$.

Further confirmation comes from the observed ratio [15] of $|P_+|$ in $K^- p \to \bar{K}^{*0} n$ and $K^+ n \to K^{*0} p$. $P_+$ for $K^+ n \to K^{*0} p$ ($C+A_2+\rho$ exchange) is suppressed since the resultant of $A_2+\rho$, which is predominantly real, cancels with the real $C$ contribution. On the other hand, for $K^- p \to \bar{K}^{*0} n$ ($C+A_2-\rho$ exchange), the resultant of $A_2-\rho$ is approximately imaginary and adds incoherently to $C$.

The exchange degeneracy of $\rho$ and $A_2$ leads to a zero of the $\rho$ contribution at $\alpha_\rho = 0$ which is not observed in $P_+$ obtained from the available $\pi^+ n \to \omega p$ data at 6–7 GeV/$c$ [16, 17]. Thus, some modification at larger $t$ or at lower energy to $P_+$ in $\omega$ production will be necessary. Insight into this effect should come from a study of the $\rho$-$\omega$ effects in the 4–6 GeV/$c$ Argonne [13] $\pi^- p \to \pi^- \pi^+ n$ (and $\pi^+ n \to \pi^- \pi^+ p$) data. In fig. 3, we predict the $\rho$-$\omega$ modulating factor for $P_+$ at 4 GeV/$c$, using the 17 GeV/$c$ amplitude components, $\rho$-$A_2$ exchange degeneracy and the phase-energy relation. The observed effect in $P_+$, for $0.08 < -t < 0.2$, in the preliminary data [13] at 4 GeV/$c$ indicates a somewhat larger relative $\rho$-$\omega$ production phase ($240 \pm 20°$) than that predicted by the model ($\approx 210°$).

In summary, we have presented a simple picture for the main features of the $t$ and $s$ dependence of $\pi^- p \to \rho^0 n$ data and $\rho$-$\omega$ interference patterns. For $\pi^- p \to \rho^0 n$, the dominant contributions are $\pi$ exchange (unnatural parity exchange coupling to $t$-channel helicity zero $\rho$ mesons); a cut $C$ (over-all $s$-channel helicity non-flip which thus contributes to unnatural and natural parity exchange), and an $A_2$ contribution in natural parity exchange which interferes destructively with the cut contribution. The natural parity exchange amplitude for $\pi N \to \omega N$, as seen through $\rho$-$\omega$ interference, is consistent with a $\rho$ contribution exchange degenerate to the $A_2$ contribution in $\pi N \to \rho N$.

* This is consistent with the small $\rho$-$\omega$ interference effects observed in $P_-$ (cf., ref. [14]).

It is a pleasure to thank the members of the CERN-Munich collaboration and the Argonne spectrometer group for providing us with data. In particular we thank G. Grayer, W. Männer, R. Diebold, S. Kramer and A. Wicklund for their interest in this work.

## References

[1] G.L. Kane and M. Ross, Phys. Rev. 177 (1969) 2353;
C.D. Froggatt and D. Morgan, Phys. Rev. 187 (1969) 2044.
[2] G.C. Fox, Proc. of Cal. Tech. Conf., Phenomenology in particle physics, p. 703 (1971).
[3] G. Grayer et al., Proc. of 4th Conf. on high energy collisions, Oxford (1972) vol. 2, p. 26.
[4] C.D. Froggatt and D. Morgan, Phys. Letters 40B (1972) 655.
[5] P. Estabrooks and A.D. Martin, Phys. Letters 41B (1972) 350.
[6] P. Estabrooks et al., CERN preprint TH. 1661; Proc. of the Tallahasse Conf. on $\pi\pi$ scattering, 1973 (AIP, New York).
[7] M. Ross, F.S. Henyey and G.L. Kane, Nucl. Phys. B23 (1970) 269;
P.K. Williams, Phys. Rev. D1 (1970) 1312.
[8] C. Michael, Nucl. Phys. B63 (1973) 431.
[9] P. Estabrooks and A.D. Martin, Phys. Letters 42B (1972) 229.
[10] F. Bulos et al., Phys. Rev. Letters 26 (1971) 1453.
[11] J.A.J. Matthews et al., Nucl. Phys. B32 (1971) 366.
[12] S. Barish and W. Selove, to be published (1973).
[13] D.S. Ayres et al., ANL/HEP 7318 and 7320; Proc. of the Tallahasse Conf. on $\pi\pi$ scattering, 1973 (AIP, New York).
[14] P. Estabrooks, A.D. Martin, G. Grayer, B. Hyams, C. Jones, P. Weilhammer, W. Blum, H. Dietl, W. Koch, E. Lorenz, G. Lütjens, W. Männer, J. Meissburger and U. Stierlin, to be published.
[15] C. Michael, Nucl. Phys. B57 (1973) 292.
[16] J.A.J. Matthews et al., Phys. Rev. Letters 26 (1971) 400.
[17] J.C. Anderson et al., Phys. Letters 45B (1973) 165.
[18] A.S. Goldhaber, G.C. Fox and C. Quigg, Phys. Letters 30B (1969) 249.

Nuclear Physics B72 (1974) 413–453. North-Holland Publishing Company

# CONSTRUCTION OF PHENOMENOLOGICAL $\pi\pi$ AMPLITUDES

J.L. BASDEVANT
*Laboratoire de Physique Théorique et Hautes Energies, Paris* *

C.D. FROGGATT ** and J.L. PETERSEN
*NORDITA, Copenhagen*

Received 18 December 1973

Abstract: We give a comprehensive description of our scheme for applying the Roy equations to $\pi\pi$ phenomenology. The method is applied to recent high statistics $\pi\pi$ experiments. The complete set of amplitudes consistent with these experiments and with the theoretical constraints of analyticity, crossing and unitarity are presented. We consider the implications of these results and discuss future experiments which could remove the final ambiguities in the low-energy $\pi\pi$ amplitude.

## 1. Introduction

Our ambition, in performing this phenomenological analysis of $\pi\pi$ scattering, is to describe the low-energy $\pi\pi$ experimental situation in a language as simple and as model-independent as possible, sticking to properties derived from fundamental principles. Within the context of present experimental information, the outcome of our work is to point out what is known about $\pi\pi$ scattering and what remains to be measured in order to have complete information, i.e. what are the "useful" measurements. Our most important results have already been given in refs. [1–4], and, in this paper, we give a complete account of the method and techniques. Of course, our program is such that we can readily incorporate new measurements as soon as they are available. We must emphasize that, at this stage, we do not have any other theoretical ambition than analyzing the data. We believe that it is only once this phenomenological description is done thoroughly that one can attempt to understand theoretically the dynamics of the low-energy $\pi\pi$ system, or to test various dynamical assumptions, since there is a considerable dispersion in the experimental results at present.

We proceed in two steps. First, we elicit the classes of $\pi\pi$ amplitudes consistent

* Postal address: Laboratoire de Physique Théorique et Hautes Energies, Université Paris VI - Tour 16 - 1er étage - 2, Place Jussieu, 75221 Paris CEDEX 05.
** On leave from Dept. of Natural Philosophy, Glasgow University, Glasgow G12 8QQ.

with crossing, analyticity and unitarity requirements. Then we find the subclass which agrees with experimental results. Our basic starting point consists in the rigorous equations derived by Roy [5] on the basis of fixed momentum transfer dispersion relations and crossing symmetry. In sect. 2 we recall these equations and explain how we use them. In spirit, our work may be compared to what has been done in the past decade on $\pi$N scattering [6], the difference being that the experimental $\pi$N information is much more accurate and abundant, while theoretical constraints on $\pi\pi \to \pi\pi$, which is a closed system under crossing, are more stringent. Roy's equations express the crossing property directly on physical partial-wave amplitudes and it was advocated by Basdevant, le Guillou and Navelet [7] that they should be used for such an analysis. Besides us, several groups [8–10] have attempted this and the results may be considered qualitatively similar although a particular parametrization in the case of Bonnier and Gauron [8] and a specific interpretation of the data in the case of Pennington and Protopopescu [10] have led these authors to conclusions which are too restrictive in our opinion, although correct within their particular assumptions.

An important byproduct of our work is of a theoretical nature. In fact, we have gained considerable insight into various previous theoretical approaches to $\pi\pi$ scattering and their results [11]. The Chew-Mandelstam equations, which are well-defined approximations to Roy's equations [7], must be reinterpreted as relations approximately satisfied by the amplitude. In some recent model calculations [12] which used the unphysical region constraints it was claimed that the presence of the $\rho$-meson in the $I = l = 1$ amplitude leads to more or less unique s-waves; by being able to produce explicit counterexamples, we have shown these conclusions to be much too restrictive. Recently Piguet and Wanders [13] have also shown this using the unphysical region constraints, therefore it is not necessary to further analyze this point: the unphysical region constraints may be just as useful as the physical ones but it is more difficult to use them safely when continuing to the physical region (e.g. the $\rho$-mass). Our most important observation concerns the number of parameters which are necessary in order to specify the low-energy $\pi\pi$ amplitude. In fact, we have found essentially the same number of degrees of freedom as in the Born term of a Lagrangian model. For instance, the interplay of crossing and unitarity is not strong enough to determine the $\pi\pi$ amplitude uniquely once the existence of the $\rho$ meson is fixed: one can impose the presence of an arbitrary $I = 0$ s-wave resonance etc. . . . . One of the ambiguities is reminiscent of the Castillejo-Dalitz-Dyson ambiguity. Mathematically, the Roy equations bear much resemblance with the approach initiated by Atkinson [14] in recent years within the Mandelstam representation, and it may be possible that they contain the CDD ambiguity noticed by Atkinson and Warnock [15]. This observation is in particular relevant to the question of constructing $\pi\pi$ amplitudes constrained by the low-energy current algebra conditions [16, 17]: in fact, the existence of the $\rho$ meson and of an isoscalar s-wave resonance cannot be established without specifying further the dynamics, for instance by requiring the absence of CDD poles [17] (if this is possible)

or by referring to a specific Lagrangian [18] (this has been noticed in a different context by Lehman [19]). These theoretical results are mentioned in sect. 3. The conclusion that can be drawn is that it is absolutely necessary to supplement crossing and unitarity with very precise dynamical properties – and not just a few low energy parameters – in order to specify the $\pi\pi$ amplitude. We have not been able to use criteria such as asymptotic properties, duality or current algebra conditions in a secure way to discriminate among our solutions; we feel that new theoretical tools or definitions are necessary in order to do so.

Sect. 4 contains the results of our phenomenological analysis, concentrating on the energy region from threshold to 1.1 GeV. This analysis uses, besides the $\rho$ parameters, various sets of data concerning the $I = l = 0$ phase shift $\delta_0^0$ in the region $500\ \text{MeV} \leqslant M_{\pi\pi} \leqslant 1100\ \text{MeV}$ coming from pion production experiments. We then examine *a posteriori* the implications of other measurements such as $\delta_0^0$ in the low-energy region – e.g. from $K_{e4}$ experiments – and the $I = 2$ s-wave phase $\delta_0^2$. The first important observation is that there is at present no compelling argument to fix the s-wave $I = 0$ scattering length $a_0^0$ better than within the limits $-0.05 \leqslant a_0^0 \leqslant 0.7\ m_\pi^{-1}$. In particular we cannot confirm that Weinberg's predictions ($a_0^0 \sim 0.15$–$0.19$) are established. Secondly, as an effect of the ambiguities, one cannot discriminate between the phases $\delta_0^0$ of three different groups [20–22] which, in the region $500\ \text{MeV} \leqslant M_{\pi\pi} \leqslant 900\ \text{MeV}$ are similar in behaviour, but are roughly equally spaced from one another by 5° to 10°. However, once $a_0^0$ and a particular experimental set of $\delta_0^0$ and inelasticities $\eta_0^0$ up to 100 MeV have been selected, then relatively crude information about the high energy behaviour is sufficient to determine the $\pi\pi$-amplitudes below 1 GeV, within small uncertainties. Hence we are able (a) to discuss the implcations of a given set of experimental results and to compare it with other sets, and (b) to indicate how further experiments (and what experiments) can resolve these final ambiguities.

## 2. Theoretical framework

### *2.1. Roy's equations*

The technique for obtaining physical partial wave equations is quite old [23]. The $\pi\pi$ equations have been written by Roy [5], and further analyzed by Basdevant, Le Guillou and Navelet [7] (BGN). We shall only mention the basic features of interest for the present work. For simplicity we consider the $\pi^0\pi^0$ amplitude $F^{00}(s,t,u)$ and denote by $A^{00}(s,t)$ its $s$-channel absorptive part (our notations and conventions are given in appendix A). The $t$-dependent subtraction function of fixed-$t$ dispersion relations can be expressed in terms of the forward amplitude [5, 7], and we write the dispersion relation as (we use pion mass units $m_\pi = 1$)

$$F^{00}(s,t,u) = a_0^{00} + \frac{t(t-4)}{\pi} \int_4^\infty \frac{ds'}{s'(s'-4)} A^{00}(s',0) \left[\frac{1}{s'-t} + \frac{1}{s'+t-4}\right]$$

$$+ \frac{1}{\pi} \int_4^\infty ds' A^{00}(s',t) \left[\frac{1}{s'-s} + \frac{1}{s'-u} - \frac{1}{s'} - \frac{1}{s'+t-4}\right] , \tag{2.1}$$

where $a_0^{00}$ is the s-wave scattering length, and where the absorptive part can be expanded in partial waves

$$A^{00}(s',t) = \sum_{l=0}^{\infty} (2l+1) \operatorname{Im} f_l^{00}(s') P_l \left(1 + \frac{2t}{s'-4}\right) \tag{2.2}$$

in the intersection of the large Lehmann-Martin ellipses *, i.e.

$$4 \geqslant t \geqslant -28 . \tag{2.3}$$

After projecting $F^{00}(s,t,u)$ onto partial waves, using the $t-u$ symmetry in the direct channel (Bose statistics),

$$f_l^{00}(s) = \frac{1}{2} \int_{-1}^{1} F^{00}(s,t,u) P_l(z) \, dz$$

$$= \int_0^1 F^{00}(s,t,u) P_l(z) \, dz = \frac{2}{s-4} \int_{\frac{1}{2}(4-s)}^{0} F^{00}(s,t,u) P_l \left(1 + \frac{2t}{s-4}\right) dt , \tag{2.4}$$

and using eqs. (2.1) and (2.2), one obtains a set of relations for partial-wave amplitudes

$$f_l^{00}(s) = a_0^{00} \delta_{l0} + \sum_{l'} (2l'+1) \int_4^\infty ds' K_l^{l'}(s,s') \operatorname{Im} f_{l'}^{00}(s') , \tag{2.5}$$

where the kernels can easily be deduced from the above equations. The relations (2.5) are well defined, i.e. the summation over $l'$ converges, provided $s$ is in the range

$$-4 \leqslant s \leqslant 60 , \tag{2.6}$$

(this range may be extended considerably, both rigorously [25] and by phenomenological arguments [7]). Taking isospin into account is only an algebraic complication, we refer the reader e.g. to BGN [7].

These equations are rigorously derived from axiomatic field theory, they are necessary conditions for crossing to hold since they originate from the $s-u$ symmetric eq. (2.1), but they are not sufficient and must be supplemented [5, 7] by another set of relations expressing the $t-u$ symmetry of the amplitude defined by eq. (2.1)

$$\int_{-1}^{1} F^{00}(s,t,u) P_{2l+1}(z) \, dz \equiv 0 . \tag{2.7}$$

* See for instance ref. [24].

However, it can be seen [5, 7] that these supplementary conditions involve only higher partial waves $l' \geqslant 2$, and do not constrain the s-wave (more generally, the s- and p-waves in the full isospin treatment). Therefore, for $l' = 0$ (and $l' = 1$), eq. (2.5) is a complete expression of the crossing symmetry that the total amplitude enjoys; in particular, Martin's [26] and Roskies' [27] relations for s- and p-waves may be deduced from it.

Roy has furthermore argued that if the absorptive parts $\mathrm{Im}\, f_l(s)$ are known in the inelastic region $s \geqslant 16$, the elastic unitarity relation

$$\mathrm{Im}\, f_l(s) = \rho(s)[(\mathrm{Re}\, f_l(s))^2 + (\mathrm{Im}\, f_l(s))^2] \tag{2.8}$$

with $\mathrm{Re}\, f_l(s)$ as defined by eq. (2.5) (which is an identity for $\mathrm{Im}\, f_l$) provides a system of non-linear singular integral equations defining $\mathrm{Im}\, f_l$, and hence the amplitude, in the elastic region.

*2.2. Basic properties of the equations*

In the realistic case with charged pions, the equations have the form

$$f_l^I(s) = \begin{pmatrix} a_0^0 \\ 0 \\ a_0^2 \end{pmatrix} \delta_{l0} + \tfrac{1}{3}(2a_0^0 - 5a_0^2)\frac{s-4}{4} \begin{pmatrix} \delta_{l0} \\ \tfrac{1}{6}\delta_{l1} \\ -\tfrac{1}{2}\delta_{l0} \end{pmatrix}$$

$$+ \sum_{I'=0}^{2} \sum_{l'=0}^{1} \int_4^\infty K_{ll}^{I'I'}(s,s')\, \mathrm{Im}\, f_{l'}^{I'}(s')\, \mathrm{d}s' + \phi_l^I(s)\,, \tag{2.9}$$

where $a_0^0$ and $a_0^2$ are the s-wave scattering lengths, and where $\phi_l^I(s)$ is a well defined sum of higher partial-wave contributions ($l' \geqslant 2$)

$$\phi_l^I(s) = \sum_{I'=0}^{2} \sum_{l'=2}^{\infty} \int_4^\infty K_{ll}^{I'I'}(s,s')\, \mathrm{Im}\, f_{l'}^{I'}(s')\, \mathrm{d}s' \tag{2.10}$$

(see BGN for further details concerning the kernels $K_{ll}^{I'I'}$).

The fundamental advantage of the relations (2.9) over the unphysical region crossing constraints [26–27] is that they relate physically accessible quantities. The price to pay is of course that they involve an infinite number of partial waves.

It has been shown by BGN that in the so-called "s–p approximation" i.e. setting $\mathrm{Im}\, f_{l'}(s) \equiv 0$ for $l' \geqslant 2$ in (2.9) one obtains the Chew-Mandelstam equations [28], which appear as well defined approximations to exact equations. However, Lovelace pointed out [29] that the Chew-Mandelstam equations could not have physically reasonable solutions owing to their behaviour at $s = \infty$. Therefore the presence of the higher wave contribution $\phi_l^I(s)$ (or its analytic continuation above $s = 60$) is crucial mathematically. However, if $\phi_l^I(s)$ is small in the low energy region, as turns out to be the case in practice (see further on), we see that the Chew-Mandelstam

equations must be reinterpreted as relations which must be approximately saturated by the amplitude, and not as equations whose exact solutions should be close to physical amplitudes.

We now come to a very important property of eq. (2.9) which we shall use in the following. In the right-hand side of (2.9) there are three terms: a polynomial subtraction term, an integral over s- and p-waves, and $\phi_l^I(s)$. The polynomial satisfies all crossing constraints trivially. It has been shown by BGN that the integral over s- and p-waves satisfies all Martin inequalities and Roskies relations automatically whatever the values of the $\mathrm{Im} f_{l'}^{I'}(s)$ $l' = 0,1$ provided they are positive. The "true" $\phi_l^I(s)$, i.e. as calculated if we knew $\mathrm{Im} f_{l'}^{I'}(s)$ $l' \geqslant 2$ exactly, satisfies the constraints by itself also. But, if we construct a function $\phi_l^I(s)$ which satisfies the constraints, and choose some functions $\mathrm{Im} f_{l'}^{I'}(s) \geqslant 0$ $(l' = 0,1)$, then $f_l^I(s)$ as defined by the right-hand side of (2.9) will automatically comply with all requirements of crossing whatever $\mathrm{Im} f_{l'}^{I'}$ are chosen.

### 2.3. Driving terms

In order to use eq. (2.9) in practice, we split the $s'$ integration into two parts, introducing some cutoff parameter $N$

$$f_l^I(s) = \text{S.T.} + \sum_{I'=0}^{2} \sum_{l'=0}^{1} \int_4^N K_{lI}^{l'I'}(s,s') \,\mathrm{Im} f_{l'}^{I'}(s')\, \mathrm{d}s' + d_l^I(s)\,, \tag{2.11}$$

where S.T. is the first-order polynomial subtraction term written in eq. (2.9), and $d_l^I(s)$ is called a driving term. The driving term consists of two pieces

$$d_l^I(s) = d_1^{lI}(s) + d_2^{lI}(s)\,. \tag{2.12}$$

The first piece $d_1^{lI}(s)$ is the contribution of all waves for $s' > N$, and the second $d_2^{lI}(s)$ of higher waves $l' \geqslant 2$ for $s' < N$, i.e.

$$d_1^{lI}(s) = \sum_{I'=0}^{2} \sum_{l'=0}^{\infty} \int_N^{\infty} K_{lI}^{l'I'}(s,s') \,\mathrm{Im} f_{l'}^{I'}(s')\, \mathrm{d}s'\,, \tag{2.13a}$$

$$d_2^{lI}(s) = \sum_{I'=0}^{2} \sum_{l'=2}^{\infty} \int_4^N K_{lI}^{l'I'}(s,s') \,\mathrm{Im} f_{l'}^{I'}(s')\, \mathrm{d}s'\,. \tag{2.13b}$$

We choose for $N$ an energy squared above which a Regge representation of the amplitude is convenient. Therefore the evaluation of $d_1^{lI}$ is quite simple if we compute the Regge contribution in the original dispersion relation (2.1) and project the result on partial waves, e.g. for the $\pi^0\pi^0$ amplitude we would have

$$d_1^{l\pi^0\pi^0}(s) = \frac{1}{2} \int_{-1}^{1} \mathrm{d}z\, P_l(z) \frac{1}{\pi} \int_N^{\infty} \mathrm{d}s' \,[a(s',t)\, A^{00}(s',0) + b(s',t,s) A^{00}(s',t)]\,, \tag{2.14}$$

where $a(s',t)$ and $b(s',t,s)$ can be read off from eq. (2.1).

For $d_2^{II}(s)$ we make the rather drastic approximation of retaining only the resonance contributions and neglecting completely the low-energy part. The main justification is phenomenological: higher partial wave $\pi\pi$ amplitudes are very small at low energies, and the neglected contributions fall well within the errors we shall allow on the estimation of the driving terms, if we restrict ourselves to studying the equations in a limited energy region above threshold, e.g. $4 \leqslant s \leqslant 60\ m_\pi^2$.

In practice, we have chosen $N = 110\ m_\pi^2$ i.e. half way between the $f_0$ and g resonances. The $f_0$ resonance contributes to $d_2^{II}$; we have taken a mass $M_{f_0} = 1269$ MeV and an elastic partial width $\Gamma_{f_0}^{el} = 125$ MeV. To estimate $d_1^{II}$ we assume a Regge pole plus pomeron exchange behaviour; for the Regge exchange component we take exchange degenerate $\rho + f_0$ poles with the Lovelace-Veneziano residue function [30] evaluated for a universal $\rho$ coupling constant of $f^2/4\pi = 2.4$. The diffractive component is represented as a simple pomeron exchange pole with a slope $\alpha'_P = 0.4\ \text{GeV}^{-2}$ and parameters chosen to give an asymptotic cross section $\sigma_\infty = 1/m_\pi^2 \sim 20$ mb and a logarithmic slope for the differential cross section of $b = 10\ (\text{GeV}/c)^{-2}$ at $s = 10\ \text{GeV}^2$. In s- and p-waves, the resulting driving terms can be approximately parametrized between threshold and $N$ by

$$d_l^I(s) = (s-4) \sum_{k=1}^{3} d_{l,k}^I (s-4)^{k-1} \ . \tag{2.15}$$

The coefficients, $d_{l,k}^I$, are given in table 2. The major contribution to $d_0^0(s)$ comes from the $f_0$ resonance, while pomeron exchange provides the dominant part of $d_0^2(s)$ and $d_1^1(s)$ is quite small. The errors that must be attached to the estimation of the driving terms come from phenomenological (or experimental) uncertainties, e.g. errors on $\Gamma_{f_0}^{el}$, $\sigma_\infty$, the $\rho$ residue function $\gamma_\rho(t)$, and theoretical uncertainties – neglecting low-energy contributions in (2.13b), and not imposing in this work the supplementary conditions (2.7). (In an exact theory it should not matter whether one computes the driving terms in eq. (2.14), and the similar one for $d_2^{II}$, using the full integration range $-1 \leqslant \cos\theta \leqslant 1$ or only half of it $0 \leqslant \cos\theta \leqslant 1$, owing to Bose statistics. In an actual parametrization the two results are generally different, but one can easily check that in practice the discrepancy is very small at low energies – less that 1% for $s < 5$ – and in particular for $0 \leqslant s \leqslant 4$; it increases with energy to become quite large above $1(\text{GeV})^2$.

We must emphasize that eq. (2.15) is only a representation of the computed driving terms, valid to first approximation in the region $10 < s < N$ where they are not negligible numerically. However, in the region $0 \leqslant s \leqslant 4$ this approximation is very poor, and eq. (2.15) violate the unphysical region crossing constraints, whereas the computed driving terms do not. One can even construct driving terms which satisfy all crossing constraints exactly [8], and which agree with eq. (2.15) for $10 < s < N$ well within the errors that we allow.

Our qualitative results are somewhat independent of the exact values of the driving terms, provided the order of magnitude is correct, and therefore our experimental ignorance of $\pi\pi$ Regge parameters is not a practical drawback here.

*2.4. Definition and construction of the solutions*

Once the driving terms $d_l^I(s)$ are known, eq. (2.11) becomes a system of non linear singular integral equations for the amplitude in the region $4 \leqslant s \leqslant N$ when put together with the unitarity condition

$$\operatorname{Im} f_l^I(s) = \rho(s)|f_l^I(s)|^2 + \frac{1-(\eta_l^I(s))^2}{4\rho(s)} \tag{2.16}$$

if the elasticity parameters $\eta_l^I(s)$ are given (for the notations, and definition of $\rho(s)$ and $\eta_l^I(s)$ see appendix A), and we want to investigate the classes of amplitudes satisfying these equations.

However, in the present work, we are primarily interested in studying the $\pi\pi$ amplitudes below 1.1 GeV, i.e. for $4 \leqslant s \lesssim 60$. In that region, one knows phenomenologically that higher partial wave amplitudes $l \geqslant 2$ are small and essentially real, therefore unitarity (2.16) is not a strong constraint on these waves and we shall concentrate on the s- and p-wave equations $l = 0, 1$. Once these equations are solved, in a sense we will now describe, higher partial-wave amplitudes are known without any further iteration of the equations [7] for $4 \leqslant s \lesssim 60$, and the resulting total amplitude satisfies fixed $t$ dispersion relations, crossing and unitarity for $s \lesssim 60$ to a very good accuracy [7]. We do not attempt to use eqs. (2.11) and (2.16) as integral equations – for instance through an iteration scheme – for technical and mathematical reasons (e.g. we do not know *a priori* the multiplicity of solutions corresponding to given values of the scattering lengths and driving terms). Instead we define a solution, i.e. a unitary and crossing symmetric amplitude at low energies, by the following criterion.

"$\epsilon$-criterion": Since $f_l^I(s)$ as defined by eq. (2.11) for $l = 0, 1$, in terms of $\operatorname{Im} f_{l'}^{I'}(s')$, (a) satisfies all crossing and positivity constraints whatever the value of $\operatorname{Im} f_{l'}^{I'}(s') > 0$ [7], and (b) has by construction [7] the imaginary part $\operatorname{Im} f_l^I(s)$, we define a solution to eq. (2.11) by requiring that all three amplitudes $f_0^0(s), f_1^1(s)$, $f_0^2(s)$ also satisfy unitarity $\operatorname{Im} f_l^I(s) = \sqrt{(s-4)/s}\,|f_l^I(s)|^2$ to a given accuracy $\epsilon$ (e.g. 1%) in the eleastic region.

We confine ourselves to the elastic region and do not extend the range of our criterion to $s = N$, which is possible in principle (see eqs. (2.11) and (2.16)), because the elasticity parameters $\eta_l^I(s)$ are not sufficiently well measured up to $s = N$ at present. However, we shall make full use of the important experimental observation [21, 22, 31–35] that $\pi\pi$ amplitudes are nearly elastic up to the $K\bar{K}$ threshold ($\eta_l^I(s) \sim 1$ $s < 4m_K^2$) and we choose the elastic region to be $s < 4m_K^2$ (indeed $4\pi$ inelasticity seems weaker than 1% below the $K\bar{K}$ threshold, this sets the order of magnitude of $\epsilon$). Above $s = 4m_K^2$, we check *a posteriori* that the deviation of $f_l^I(s)$ from the unitarity relation (2.16) is compatible with the errors we can accept on the values of $\eta_l^I(s)$ and the driving terms.

In order to realize this, we first choose $\operatorname{Im} f_l^I(s)$ to be the imaginary part of an amplitude $g_l^I(s)$ parametrized so that it satisfies elastic unitarity exactly below $s = 4m_K^2$,

and inelastic unitarity (2.16) with a given $\eta_l^I(s)$ above that energy

$$\mathrm{Im}\, f_l^I(s) = \mathrm{Im}\, g_l^I(s)\ . \tag{2.17}$$

We then compute $f_l^I(s)$ by eq. (2.11) and we fix the parameters in $g_l^I(s)$ by minimizing the quantity

$$\|f - g\| = \int_4^{60} \omega(s)|f_l^I(s) - g_l^I(s)|^2\, \mathrm{d}s\ , \tag{2.18}$$

where $\omega(s)$ is a positive weight function (the CERN program MINUIT was used). In practice we have chosen

$$\|f - g\| = \sum_{i=1}^{P} \omega_i |f_l^I(s_i) - g_l^I(s_i)|^2\ , \tag{2.19}$$

the $s_i$ being a set of points (typically 5 to 10 points) in the region $4 \leqslant s_i \leqslant 60$. One of the points chosen is threshold, so that we minimize in particular on the s-wave slopes $b_0^0$, $b_0^2$ and the p-wave scattering length $a_1^1$ defined in appendix A (the s-wave scattering lengths are subtraction constants in eq. (2.11)).

To prevent the parametrization from playing a crucial role, we have used two very different analytic forms, which both lead to the same results in practice. The first is a simple $K$-matrix approach

$$g_l^I(s) = [K_l^I(s)^{-1} + C_\pi(s)]^{-1}\ , \tag{2.20}$$

where $C_\pi(s)$ is the Chew-Mandelstam function

$$C_\pi(s) = \frac{2}{\pi}\sqrt{\frac{s-4}{s}}\log\frac{\sqrt{4-s}+\sqrt{-s}}{2}\ ,$$

and the $K$-matrix can be taken as a rational function in $s$

$$K_l^I(s) = \frac{a_0^I\delta_{l0} + a_1^I(s-4) + a_2^I(s-4)^2 + \ldots}{1 + C_1^I(s-4) + C_2^I(s-4)^2 + \ldots}\ , \tag{2.21}$$

which is elastic up to infinity. Inelasticity may be introduced by adding to eq. (2.21) a term of the form $H_l^I(s)\, C_K(s)$ where $H_l^I(s)$ is another rational function and

$$C_K(s) = \frac{2}{\pi}\left\{\sqrt{\frac{s-4m_K^2}{s}}\log\frac{\sqrt{4m_K^2-s}+\sqrt{-s}}{2m_K} - \sqrt{m_K^2-1}\ A\tan\frac{1}{\sqrt{m_K^2-1}}\right\}\ . \tag{2.22}$$

This method is simple and practical, however, it is not well suited for incorporating a given inelasticity, and another method, fully described in appendix B, consists in expressing the partial wave $S$-matrix elements as products of rational functions:

$$S_l^I(s) = [1 + 2i\sqrt{\frac{s-4}{s}}\, g_l^I(s)]$$

$$= \frac{z-z_R^*}{z-z_R}\,\frac{z+z_R}{z+z_R^*}\,\frac{i-az^n}{i+az^n}\cdot\ldots \qquad (2.23)$$

[where $z_R$ is complex (resonance pole), $a$ is real and $n$ is an odd integer, see appendix B], $z$ being a conformal variable which unfolds the appropriate Riemann sheets and is defined in appendix B. Within this parametrization it is easy to insert a given inelasticity for $s \geqslant 4m_K^2$, in particular the S* effect [21, 22, 31–35]. The two s-wave scattering lengths $a_0^0$ and $a_0^2$, which determine the subtraction terms in eq.(2.11), are of course among the parameters in eqs. (2.21) and (2.23).

Once the minimization is achieved, we may adopt the following philosophy. The functions $f_l^I(s)$ are analytic in $s$ and are by construction the projections of a crossing symmetric total amplitude which satisfies fixed $t$ dispersion relations, while the $g_l^I(s)$ are analytic in $s$ and satisfy unitarity (2.16) with given inelasticities. Furthermore in the region of interest we have

$$|f_l^I(s) - g_l^I(s)| \leqslant \epsilon\,, \qquad 4 \leqslant s \leqslant 60\,. \qquad (2.24)$$

Therefore we consider both $f_l^I$ and $g_l^I$ as approximations to the same amplitude which is analytic, unitary and crossing symmetric, and we call either of them a solution. Once we are in the vicinity of a solution (if it exists) it is sufficient to iterate the equations in order to obtain the numerical solution (provided we have fixed a sufficient number of conditions for it to be unique). However it is worth emphasizing that we are also buidling explicit analytic models of $\pi\pi$ amplitudes, i.e. the functions $g_l^I(s)$, which are unitary and satisfy crossing in the sense of our $\epsilon$-criterion, and which can be used in other applications.

It may happen eventually that by undertaking a more complete treatment of the equations – e.g. using the supplementary conditions [5, 7] – one may be able to exclude some of our solutions. However, we think that in trying to do this at present we may eliminate physically acceptable solutions since our theoretical and phenomenological knowledge is not sufficiently accurate and complete (e.g. if we choose the inelastic threshold to be $s = 4m_K^2$, we cannot take strictly $\epsilon = 0$ in our $\epsilon$-criterion, since a theorem by Martin [24] says that the $\pi\pi$ amplitude must vanish identically if the $4\pi$ inelasticity vanishes anywhere between $s = 16$ and $s = 20$). In other words, given an arbitrary set of s- and p-waves, one can always construct driving terms so that eq. (2.11) is satisfied; however, these driving terms will in general be in contradiction with phenomenological estimates (e.g. averaged asymptotic cross sections orders of magnitude too large, or even negative) and we can exclude them, but it is only experimental and phenomenological arguments which can discriminate between our solutions at present.

### 2.5. Higher partial waves

Once we have determined s- and p-wave amplitudes, higher partial waves are computed directly by eq. (2.11) which we may write as

$$f_l^I(s) = \sum_{I'=0}^{2} \sum_{l'=0}^{1} \int_4^N K_{ll}^{l'I'}(s,s') \operatorname{Im} f_{l'}^{I'}(s')\, ds'$$

$$+ \frac{(s-4)^l}{\pi} \int_4^N ds' \frac{\operatorname{Im} f_l^I(s')}{(s'-4)^l(s'-s)} + \tilde{d}_l^I(s), \qquad l \geqslant 2 \tag{2.25}$$

where we have redefined the driving term in order to extract the explicit direct channel right-hand cut contribution which has the good threshold behaviour [7], and which contains the direct channel resonances (e.g. the $f_0$ for $l = 2, I = 0$) that we put in by hand. In the region $4 \leqslant s \leqslant 60$ unitarity is a very weak contraint on these waves, therefore we shall define the phase shift by the approximate relation

$$\tan \delta_l^I(s) \simeq \sqrt{\frac{s-4}{s}} \operatorname{Re} f_l^I(s), \tag{2.26}$$

(we may check *a posteriori* that neglecting the low-energy contribution in the second term of the r.h.s. of (2.25) is a good approximation).

In eq. (2.25), the first term i.e. the s- and p-wave contribution, is the dominant one at low energies, until the effects of direct channel resonances are felt. We remark that for $l \geqslant 2$ it is important to compute the driving terms by projecting on the whole range $-1 \leqslant \cos\theta \leqslant 1$ [see eq. (2.14)] if we want to preserve the threshold behaviour without invoking the supplementary conditions (2.7) which we have not studied or used here.

### 2.6. Basic phenomenological assumptions

In all this work we have restricted ourselves to a particular set of $\pi\pi$ amplitudes defined by physical criteria which we now enumerate.

(a) We assume the existence of the $I = l = 1$ $\rho$-resonance, and we impose its mass $m_\rho$ and width $\Gamma_\rho$ (varying these parameters within experimental errors). The p-wave scattering length itself $a_1^1$ is computed from the equations, it is not imposed.

(b) We assume that to a good approximation (1%) inelasticity starts at $s = 4m_K^2$ and not at $s = 16m_\pi^2$. Our treatment of the inelasticity will be described in sect. 4.

(c) The Regge parameters and higher partial-wave resonances enable us to estimate the driving terms, as described above, within definite error bands which we do not transgress.

(d) We also assume that the exotic $I = 2$ s-wave is non-resonant below 1 GeV, and we forbid resonance poles in our parametrization of this amplitude.

*2.7. Unsubtracted dispersion relation*

Under plausible assumptions – Pomeranchuk theorem and non-dominance of the real part over the imaginary part asymptotically – the $I_t = 1$ amplitude satisfies an unsubtracted dispersion relation

$$2F^0(s,t) + 3F^1(s,t) - 5F^2(s,t) = \frac{1}{\pi}\int_4^\infty \Delta(s',t)\left[\frac{1}{s'-s} - \frac{1}{s'-u}\right] ds' , \qquad (2.27)$$

where

$$\Delta(s,t) \equiv 2A^0(s,t) + 3A^1(s,t) - 5A^2(s,t) ,$$

a consequence of which is the Olsson sum rule [36]:

$$L \equiv 2a_0^0 - 5a_0^2 = \frac{3}{4\pi^2}\int_4^\infty \frac{ds}{\sqrt{s(s-4)}} [\sigma_{tot}^{\pi^+\pi^-}(s) - \sigma_{tot}^{\pi^+\pi^+}(s)] , \qquad (2.28)$$

[cf. also eq. (A.7)].

Assuming $\Delta(s,t)$ is dominated by $\rho$-exchange at high energies

$$\Delta(s,t) \simeq \gamma_\rho(t)\, s^{\alpha_\rho(t)} , \qquad s > N, \qquad (2.29)$$

it is natural to split eq. (2.28) into two parts

$$L = L_{sp} + L_\infty , \qquad (2.30)$$

where $L_{sp}$ is the s- and p-wave contribution to the right-hand side of (2.28) for $s \leqslant N$, and $L_\infty$ includes the higher wave $l \geqslant 2$ and asymptotic $s > N$ contributions. Choosing $N \approx 110 m_\pi^2$, the only $l \geqslant 2$ resonance to be taken into account is the $f_0$ and we obtain

$$L_\infty \approx \frac{40\,\Gamma_{f_0}^{el}}{m_{f_0}(m_{f_0}^2 - 4)} + \frac{8}{\pi}\frac{\gamma_\rho(0)}{N^{\frac{1}{2}}} . \qquad (2.31)$$

We may incorporate eqs. (2.27) and (2.28) in our analysis. However, in eq. (2.30) $L_\infty$ is quite important (20 to 30% of the total) and this requires a good knowledge of the $\rho$ residue function. Therefore, in order not to bias our results, we prefer to operate backwards and, for each of our solutions, to use eqs. (2.27) and (2.28) to extract the implications concerning $\gamma_\rho(t)$ [1, 2, 37]. For instance we can define $L_\infty$ as the value which saturates eq. (2.30) once s- and p-waves are known, and then compare it with the available (rather ill-defined) experimental information.

## 3. Theoretical results

We did not encounter any basic technical obstacle in carrying out our programme. The most important problem was to discover the actual multiplicity of solutions,

and to know how many constraints were necessary for a solution to be unique. The usefulness of the Roy equations, both theoretical and phenomenological, as argued in ref. [7] is established by observing that (a) we have found no published model which satisfies our criterion, and (b) simple analytic forms which fit the data will in general violate the equations grossly. However, for several models which incorporate the $\rho$ meson by construction [12, 38], we can produce amplitudes which are close to the model predictions near threshold ($s \lesssim m_\rho^2$) and do satisfy the criterion.

Our most interesting result concerns the multiplicity of the solutions. We have already explained this in ref. [1]. Our assumptions of subsect. 2.6 do not put stronger constraints on the s-wave scattering lengths $a_0^0$ and $a_0^2$ than to lie in a domain outlined in fig. 1 of ref. [1]. By no means does one obtain quasi-uniqueness as hinted by some model calculations [12] based on the unphysical region crossing contraints. Since our amplitudes satisfy these contraints they are explicit counter-examples to the uniqueness claim. There are however some restrictions: for instance the values $a_0^0 = a_0^2 = 0$ can be reached only by introducing an exotic $I = 2$ resonance in contradiction with our assumption (2.6d).

Once $a_0^0$, $a_0^2$, $m_\rho$ and $\Gamma_\rho$ are fixed, the very low-energy parameters (i.e. the p-wave scattering length and the s-wave effective ranges) are essentially determined. Furthermore all amplitudes in our domain are such that $\delta_0^0(m_\rho) > 0$ and $\delta_0^2(m_\rho) < 0$ so that, as a nearly trivial consequence of crossing, each s-wave amplitude possesses a zero in the region $0 \leqslant s \leqslant 4$ or near it (e.g. if $a_0^2 > 0$ (or $a_0^0 < 0$) the zero of $f_0^2$ (or $f_0^0$) lies in the physical region $s > 4$). However there remains an arbitrariness in the $l = I = 0$ phase; one can choose the energy at which $\delta_0^0$ passes through e.g. 90°.

To summarize, in order to obtain a more or less unique set of amplitudes under our previous assumptions we need to specify five parameters which can be taken as $a_0^0$, $a_0^2$, $m_\rho$, $\Gamma_\rho$ and the energy where $\delta_0^0 = 90°$.

Our findings are qualitatively similar to those of Morgan and Shaw [39]. These authors found that in addition to imposing $m_\rho$, $\Gamma_\rho$ they could fix at least 4 more parameters which they took to be $a_0^0/a_0^2$, $\delta_0^0$ (600 MeV), $\delta_0^0$ (900 MeV) and $\delta_0^2(m_\rho)$. Our more complete treatment of crossing allows us to reduce this number to 3 and for arbitrary values within a domain of these 3 parameters we do find consistent solutions *. It is quite easy to understand these results by referring to the Born term of a Lagrangian containing a contact $-\frac{1}{4!}\lambda(\boldsymbol{\pi}\cdot\boldsymbol{\pi})^2$ term, a scalar interaction $\frac{1}{2} m_\epsilon g_\epsilon (\boldsymbol{\pi}\cdot\boldsymbol{\pi})\epsilon$ and a vector interaction $g_\rho \epsilon_{ijk}\pi_i \partial_\mu \pi_j \rho_k^\mu$ as represented in fig. 1. In Born approximation the amplitude depends on five parameters, i.e. $\lambda$, $m_\rho$, $m_\epsilon$, $g_\rho^2$, $g_\epsilon^2$ which can be eliminated in favour of $a_0^0$, $a_0^2$, $m_\rho$, $\Gamma_\rho$, and a combination of $m_\epsilon$ and $\Gamma_\epsilon$ and which are all uncorrelated by crossing. Using the notation of Chew and Mandelstam

$$A^{\pi\pi}_{\alpha\beta\gamma\delta}(s,t,u) = A(s,t,u)\,\delta_{\alpha\beta}\delta_{\gamma\delta} + A(t,s,u)\,\delta_{\alpha\gamma}\delta_{\beta\delta} + A(u,t,s)\,\delta_{\alpha\delta}\delta_{\beta\gamma}\,, \tag{3.1}$$

* We are indebted to Dr. G. Shaw for a clarifying correspondence on this point.

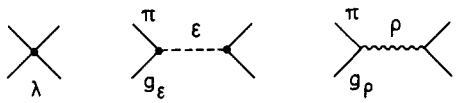


Fig. 1. Born terms of a Lagrangian model in $\pi\pi$ scattering. All crossed diagrams are understood to be present.

we would have

$$A^{\text{Born}}(s,t,u) = \lambda + g_\epsilon^2 \frac{m_\epsilon^2}{m_\epsilon^2 - s} + g_\rho^2 \left[\frac{s-u}{m_\rho^2 - t} + \frac{s-t}{m_\rho^2 - u}\right], \tag{3.2}$$

and, in Born approximation

$$32\pi\, m_\pi a_0^0 = 5\lambda + g_\epsilon^2 \left[\frac{3m_\epsilon^2}{m_\epsilon^2 - 4m_\pi^2} + 2\right] + 16 g_\rho^2 \frac{m_\pi^2}{m_\rho^2}, \tag{3.3a}$$

$$32\pi\, m_\pi a_0^2 = 2\lambda + 2g_\epsilon^2 - 8 g_\rho^2 \frac{m_\pi^2}{m_\rho^2}, \tag{3.3b}$$

so that

$$2a_0^0 - 5a_0^2 = \frac{3}{4\pi}\left[\frac{g_\epsilon^2 m_\pi}{m_\epsilon^2 - 4m_\pi^2} + \frac{3g_\rho^2 m_\pi}{m_\rho^2}\right] \geqslant \frac{9m_\pi}{m_\rho^2}\frac{g_\rho^2}{4\pi}, \tag{3.4}$$

which shows that the value $a_0^0 = a_0^2 = 0$ cannot be reached in the absence of an exotic pole. It is known that one can unitarize such a Lagrangian by using e.g. the Padé method [40] and preserve approximately its crossing properties provided the coupling constants are not too large (notice that our domain lies inside $-0.1 \leqslant a_0^0 \leqslant 0.8$, $-0.2 \leqslant a_0^2 < 0.15$ so that on an absolute scale, e.g. axiomatic bounds [41] $a_0^0 \geqslant -7.5$, $a_0^2 \geqslant -7.1$, we are dealing with very small scattering lengths) and unitarity effects will not change the basic character of the Born term. We remark that allowing for an exotic resonance would add two more parameters, as would the introduction of another $I = 0$ resonance.

The fact that one can choose, at given $a_0^0$ and $a_0^2$, the energy where $\delta_0^0 = 90°$ is highly reminiscent of the CDD ambiguity. Since Roy's equations have some similarities with the equations considered by Atkinson [14] within the Mandelstam representation, we may be in the presence of the same CDD ambituity as noticed by Atkinson and Warnock [15]. However, our ambiguities may also come from the fact that we have not really taken care of the asymptotic properties of the equations – we lump any deviation at high energies in the errors attributed to the driving terms. In any case, this is a very interesting problem to which we hope to come back.

To conclude, we are comforted to understand our results in the simple language of Lagrangian field theory and, perhaps, within $S$-matrix theory as developed by Atkinson [14], although it may be disappointing that the uniqueness hopes of the

low-energy bootstrap [11] and of some models are disproved. In a phenomenological language, crossing constrains the low energy parameters but not the striking features of the low-energy $\pi\pi$ amplitudes i.e. the resonances. In order to determine the physical amplitude, we must incorporate in our analysis some experimental information about the s-waves, which we shall now do.

## 4. Phenomenological results

In this section we supplement the phenomenological assumptions of subsect. 2.6 by requiring agreement with all available experimental information on the $\pi\pi$ system below 1.1 GeV. Most of the information comes from recent high statistics $\pi^+\pi^-$ production experiments [20–22, 31–35]. Apart from the rho meson parameters, these experiments mainly constrain the isoscalar s-wave phase shift $\delta_0^0$ in the region 500 MeV $\leqslant M_{\pi\pi} \leqslant$ 1100 MeV. Measurements of other quantities are examined *a posteriori* and are found to be insufficiently accurate at present to select further between our solutions.

### *4.1. Further phenomenological assumptions*

Therefore we now further restrict our set of $\pi\pi$ amplitudes and require agreement with the following additional physical information.

(e) There is a strong cusp or S* effect causing $\delta_0^0$ to accelerate through 180° and a sharp onset of inelasticity at the $K\bar{K}$ threshold [21, 22, 31–35].

(f) The isoscalar s-wave phase shift $\delta_0^0$ in the mass range 500 MeV $\leqslant M_{\pi\pi} <$ 900 MeV must lie in the between-down [42] or up-down [22] bands.

When we undertook this analysis the isoscalar phase shift $\delta_0^0$ was assumed to be of the between-down type [42] and our most detailed results were obtained using the Saclay [20] and Berkeley [21] phases. Chew-Low extrapolation results from the high statistics CERN-Munich experiment [33–35] were in good agreement with the Berkeley phases. However a recent amplitude analysis [22] yields phases noticeably higher than previous results. We therefore also present our preliminary analysis of these new solution 1 (CM-EM1) phases [22]. It should be remarked here that another analysis [35] of the same data, based on slightly different assumptions regarding the structure of the dipion production amplitudes, leads to phases closer to those from Chew-Low extrapolation than to CM-EM1 (see fig. 5 below). Very grossly, there is a 5° to 10° difference between the Saclay (SAC) and the Berkeley (BKLY) phases and a similar difference between the latter and the CM-EM1 phases. It is convenient to analyze the results obtained by fitting on a given data set and then to see how the results are altered when another set is chosen. We adopt the criterion that the $\chi^2$ per experimental point must be less than 2 to define a "fit" to the data.

The conformal variable $z$, described in appendix B, is well suited to describe a given behaviour in the region of the $K\bar{K}$ threshold and the results presented in this

Table 1
Fixed parameters in the Saclay and Berkeley solutions [cf. eqs. (B.6), (B.15), (B.17)]

| | |
|---|---|
| $z_{S^*} = 0.928 - i\,0.0740$ | $E_{S^*} = 998 - i\ 66$ MeV |
| $z_\rho = 0.468 - i\,0.0126$ | $E_\rho = 767 - i\ 67$ MeV |
| $z_{\rho'} = 0.539 + i\,0.0088$ | $E_{\rho'} = 1630 - i\,120$ MeV |
| $z_{\rho'} = 0.537 - i\,0.0107$ | $X_{\rho'} = 0.36$ |
| $\alpha_1^1 = 0.872$ | |

section were all derived in terms of this variable. In particular the S* effect is described by a pole in the $z$ variable, the parameters of which were found by fitting to the inelasticity $\eta_0^0(s)$ of ref. [21] and to a given set of phases $\delta_0^0$ below the $K\bar{K}$ threshold. In addition, the phase at the $K\bar{K}$ threshold was constrained to be 180° to conform with the experimental vanishing of the $Y_1^0$ moment [21]. These S* parameters were found to be essentially independent of the behaviour below 800 MeV and are given in table 1. We remark here that a much narrower S* pole is used to fit the CERN phases. We also investigated the sensitivity of our results to the existence of an $\epsilon'$ resonance in $f_0^0(s)$ above 1100 MeV.

In order to obtain good input output agreement for the p-wave above 800 MeV within this parametrization, we found it necessary to include a background singularity. For convenience we choose to represent this background by an inelastic $\rho'$ resonance either under the f or the g meson. The parameters taken for this $\rho'$ resonance and for the $\rho$ resonance itself are also given in table 1. The $I = 2$ s-wave amplitude is taken to be purely elastic. For a full discussion of our parametrization, we refer the interested reader to appendix B.

The driving term parameters to be substituted in eq. (2.15) were calculated as described in subsect. 2.3 and are listed in table 2. We estimate the errors due to uncertainties in experimental quantities and neglected contributions to be less than 30% for $d_0^0(s)$ and 50% for $d_1^1(s)$ and $d_0^2(s)$.

### *4.2. General description of solutions s- and p-waves*

The multiplicity of solutions described in sect. 3 is reduced, firstly, by fixing the isoscalar s-wave amplitude near the $K\bar{K}$ threshold and above to satisfy the

Table 2
Driving term parameters

| $k$ / $(l,I)$ | 1 | 2 | 3 |
|---|---|---|---|
| (0,0) | $9.12 \times 10^{-4}$ | $9.78 \times 10^{-5}$ | 0 |
| (1,1) | $1.36 \times 10^{-4}$ | $8.36 \times 10^{-6}$ | $1.75 \times 10^{-7}$ |
| (0,2) | $5.09 \times 10^{-4}$ | $6.32 \times 10^{-5}$ | $-3.78 \times 10^{-7}$ |

phenomelogocial requirement e). In this way, we are reduced to just one solution for each point in the explored region of the $(a_0^0, a_0^2)$ plane as outlined in fig. 1 of ref. [1]. Secondly, we require the isoscalar s-wave phase shift $\delta_0^0$ to satisfy condition f). This reduces the number of possible $\pi\pi$ amplitudes further leaving, for any given set of experimental phase shifts, only a very narrow band of finite extent in the $(a_0^0, a_0^2)$ plane. This allowed region, hereafter called a universal curve, following Morgan and Shaw [39], is shown in fig. 2 for each of the three sets of experimental phase shifts $\delta_0^0$. We note there is a systematic downward displacement of the universal curve associated with the upward displacement of the experimental phase shifts $\delta_0^0$ in passing from the Saclay to the CM-EM1 results. If we allow for all of the uncertainties in the physical input, we find an error band associated with each of these curves – viz., for fixed $a_0^0$, the uncertainty in $a_0^2$ is $\Delta a_0^2 = \pm 0.007$. The major contribution to this estimated error comes from allowing for the possible existence of an $\epsilon'$ resonance. The effect of including an $\epsilon'$ resonance is to displace the universal curve upwards.

It is interesting to compare the universal curves of fig. 2 with the results from the soft meson theory of low-energy $\pi\pi$ interactions due to Weinberg [43]. The assumptions of linearity and current algebra give

$$L \equiv 2a_0^0 - 5a_0^2 = 18a_1^1 = \frac{3}{4\pi F_\pi^2} = 0.60 \pm 0.06 \tag{4.1}$$

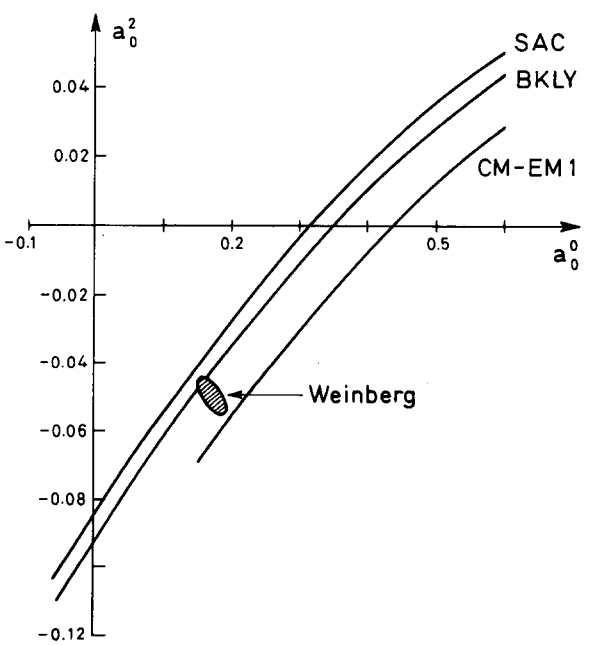


Fig. 2. Universal curves correlating the two s-wave scattering lengths for the Saclay (SAC), Berkeley (BKLY) and CM-EM1 phase shifts respectively. The estimated error band associated with each of these curves is discussed in the text.

for the universal curve, where $F_\pi$ is the PCAC constant. The further assumption of non exoticity for the $\sigma$ term implies

$$a_0^0/a_0^2 = -\tfrac{7}{2} \ , \tag{4.2}$$

and combined with eq. (4.1) gives the Weinberg predictions for the scattering lengths, shown in fig. 2. The universal curves of fig. 2 are reproduced by the following approximate parametrizations,

$$\text{SAC:} \quad 2a_0^0 - 8a_0^2 = 0.62 + (a_0^0 - 0.2)^2 \pm 0.06 \ , \tag{4.3}$$

$$\text{BKLY:} \quad 2a_0^0 - 8a_0^2 = 0.69 + (a_0^0 - 0.2)^2 \pm 0.06 \ , \tag{4.3}$$

$$\text{CM-EM1:} \quad 2a_0^0 - 8a_0^2 = 0.84 + (a_0^0 - 0.25)^2 \pm 0.06 \ , \tag{4.5}$$

where the quoted error is estimated in the same way as $\Delta a_0^2$ above. Furthermore both the Saclay and Berkeley data restrict the isoscalar s-wave scattering length to the range

$$-0.05 < a_0^0 < 0.6 \ , \tag{4.6}$$

while the CM-EM1 phases require $a_0^0 > 0.15$.

The p-wave scattering length $a_1^1$ is rather stable and close to the Weinberg value $0.33 \pm 0.03$, whereas the linear approximation prediction $a_1^1 = \frac{1}{18}L$ is not well satisfied except for s-wave scattering lengths close to the Weinberg values.

The variation of the s- and p-wave scattering lengths and s-wave slopes [defined in eq. (A.4)] along the universal curve is given in tables 3 and 4 for the Saclay and CM-EM1 phase shifts. Fixing $a_0^0$ essentially determines all these low energy parameters. The isoscalar s-wave slope, in particular, has a qualitatively different behaviour to that of the linear approximation, which gives $b_0^0 = \frac{1}{3}L$ and $b_0^2 = -\frac{1}{6}L$. Future analyses of low energy $\pi\pi$ experiments, such as $K_{e4}$ decay, should be constrained in their choice of $a_0^0$ and $b_0^0$ so as to be compatible with the results spanned by tables 3 and 4.

In figs. 3–5 we show three typical solutions for each of the three different sets of experimental phase shifts. The three curves in each figure illustrate the spread of allowed behaviour below 500 MeV for a given set of experimentally determined s-wave phase shifts above 500 MeV, with the present statistical accuracy of the experiments. In each case we give the two extreme solutions and an intermediate solution which, for the Saclay and Berkeley phase shifts, corresponds to the Weinberg scattering lengths. For the CM-EM1 phase shifts, the Weinberg predictions correspond to the lowest allowed values for the scattering lengths. In fig. 5 we also include the phase shifts $\delta_0^0$ obtained from a simple Chew-Low extrapolation [33] of the CERN-Munich data and from an amplitude analysis based on spin and phase coherence [35], in order to illustrate the ambiguities involved in $\pi\pi$ phase-shift analyses. The resolution of these ambiguities in $\pi\pi$ phase-shift analysis is an important problem for future $\pi\pi$ phenomenology; a possible approach is suggested in subsect. 4.5.

Table 3.
Low energy s- and p-wave parameters calculated for the Saclay phase shifts

| $a_0^0$ | $b_0^0$ | $a_0^2$ | $b_0^2$ | $a_1^1$ |
|---|---|---|---|---|
| −0.056 | 0.15 ± 0.03 | −0.103 ± 0.007 | −0.061 ± 0.007 | 0.030 ± 0.002 |
| 0.16 | 0.21 ± 0.03 | −0.037 ± 0.007 | −0.065 ± 0.007 | 0.032 ± 0.002 |
| 0.30 | 0.19 ± 0.03 | −0.006 ± 0.007 | −0.074 ± 0.007 | 0.035 ± 0.002 |
| 0.58 | 0.03 ± 0.03 | +0.047 ± 0.007 | −0.096 ± 0.007 | 0.040 ± 0.002 |

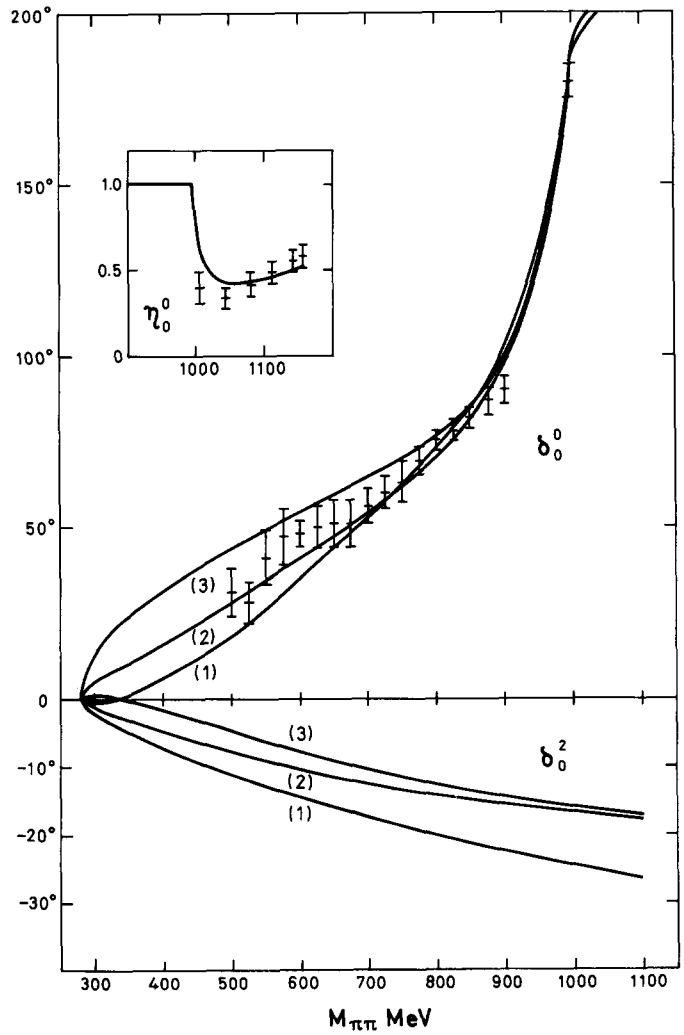


Fig. 3. Typical solutions for the s-wave amplitudes fitted to Saclay phase shifts. The curves correspond to (1) $a_0^0 = -0.06$, (2) $a_0^0 = 0.16$ and (3) $a_0^0 = 0.58$.

Table 4
Low energy s- and p-wave parameters calculated for the CM-EM1 phase shifts

| $a_0^0$ | $b_0^0$ | $a_0^2$ | $b_0^2$ | $a_1^1$ |
|---|---|---|---|---|
| 0.17 | 0.32 ± 0.03 | −0.066 ± 0.007 | −0.083 ± 0.007 | 0.040 ± 0.002 |
| 0.31 | 0.30 ± 0.03 | −0.030 ± 0.007 | −0.090 ± 0.007 | 0.042 ± 0.002 |
| 0.40 | 0.27 ± 0.03 | −0.010 ± 0.007 | −0.093 ± 0.007 | 0.042 ± 0.002 |
| 0.59 | 0.14 ± 0.03 | +0.028 ± 0.007 | −0.106 ± 0.007 | 0.045 ± 0.002 |

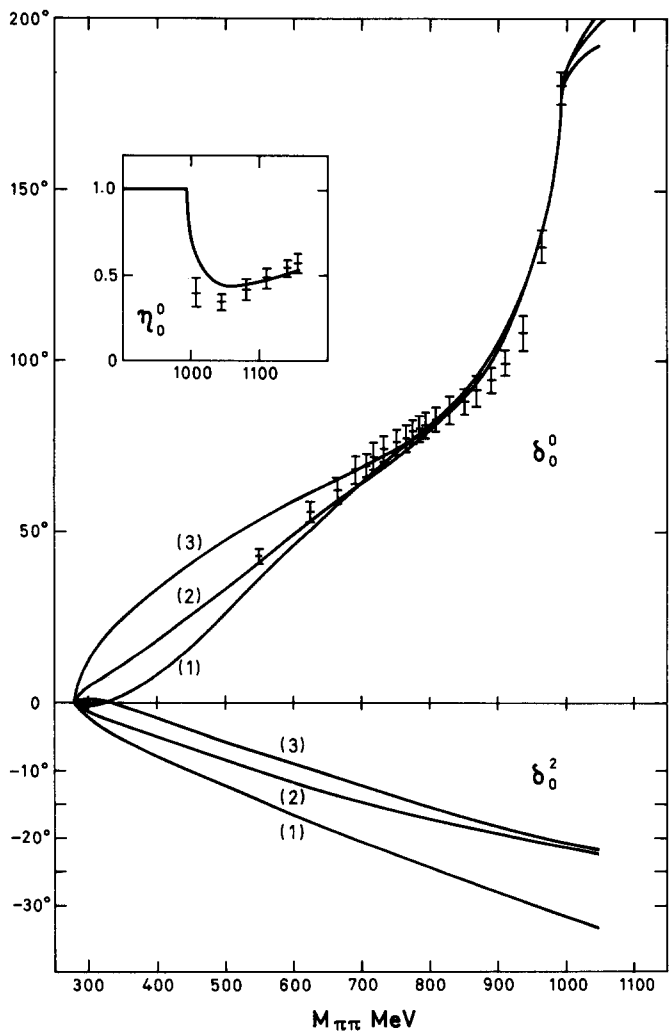


Fig. 4. Typical solutions for the s-wave amplitudes fitted to the Berkeley data. The curves correspond to (1) $a_0^0 = -0.05$, (2) $a_0^0 = 0.17$ and (3) $a_0^0 = 0.59$.

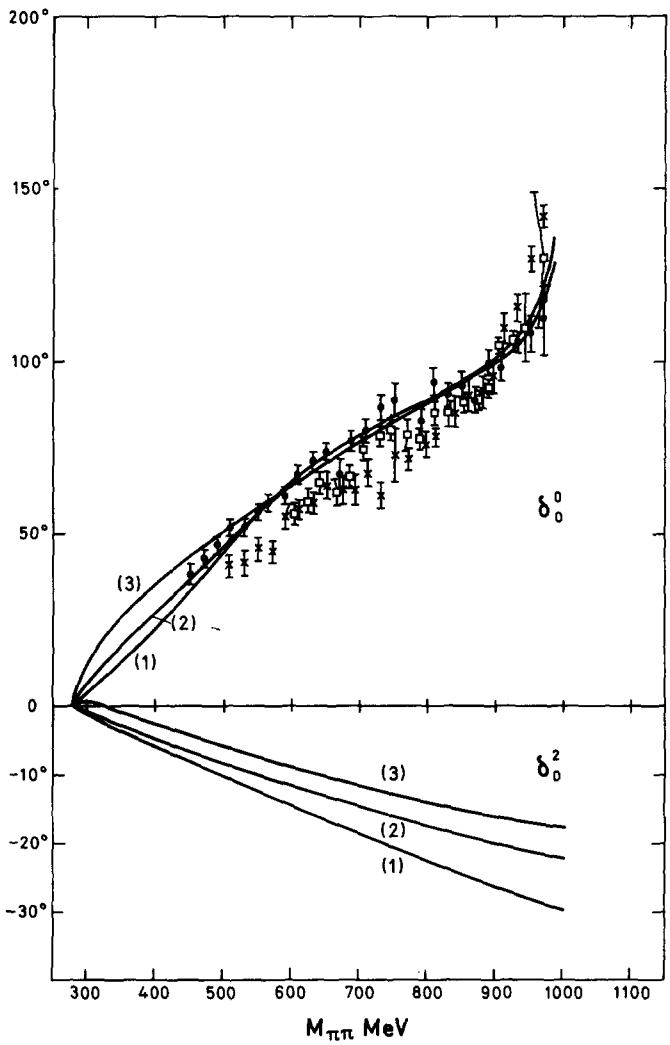


Fig. 5. Typical solutions for the s-wave amplitudes fitted to the CM-EM1 phase shifts [22] ⧺. Also shown are the phases of Grayer et al. [33] ⧖ and Hyams et al. [35] ⧗ from the same experiment. The curves correspond to (1) $a_0^0 = 0.17$, (2) $a_0^0 = 0.31$ and (3) $a_0^0 = 0.59$.

In table 5, we give the mathematical and associated physical parameters for the Saclay and Berkeley solutions shown in figs. 3 and 4. As well as the s- and p-wave scattering lengths and s-wave slopes, we tabulate the mass and width $m_\epsilon$, $\Gamma_\epsilon$ associated with the $\epsilon$ resonance pole and the d- and f-wave scattering lengths.

In contrast to our set of $\pi\pi$ amplitudes covering the whole range (4.6), Pennington and Protopopescu [10] have claimed that imposing the Berkeley data in the Roy

Table 5
Variable parameters in the Saclay (SAC) and Berkeley (BKLY) solutions [cf. eqs. (B.6), (B.15), (B.17)]. These solutions do not contain an $\epsilon'$ resonance above 1100 MeV and therefore lie in the lower parts of the error bands associated with the universal curves in fig. 2

| Param. | SAC 1 | SAC 2 | SAC 3 | BLKY 1 | BKLY 2 | BKLY 3 |
|---|---|---|---|---|---|---|
| $a_0^0$ | −0.058 | 0.165 | 0.583 | −0.054 | 0.169 | 0.587 |
| $a_0^2$ | −0.105 | −0.038 | 0.042 | −0.115 | −0.048 | 0.032 |
| $a_1^1$ | 0.0303 | 0.0324 | 0.0408 | 0.0336 | 0.0351 | 0.0431 |
| $b_0^0$ | 0.154 | 0.210 | 0.057 | 0.178 | 0.248 | 0.097 |
| $b_0^2$ | −0.064 | −0.068 | −0.101 | −0.071 | −0.075 | −0.102 |
| $m_\epsilon$ | 569 MeV | 407 MeV | 267 MeV | 517 MeV | 439 MeV | 309 MeV |
| $\Gamma_\epsilon$ | 672 MeV | 875 MeV | 732 MeV | 477 MeV | 671 MeV | 624 MeV |
| $a_2^0 \times 10^4$ | 15.9 | 15.7 | 21.8 | 17.9 | 17.2 | 23.1 |
| $a_2^2 \times 10^4$ | −1.96 | −0.49 | 5.77 | −1.11 | 0.38 | 6.63 |
| $a_3^1 \times 10^4$ | 0.14 | 0.41 | 1.26 | 0.15 | 0.46 | 1.35 |
| Re $z_\epsilon$ | 0.721 | 0.718 | 0.655 | 0.656 | 0.670 | 0.614 |
| Im $z_\epsilon$ | −0.224 | −0.326 | −0.411 | −0.196 | −0.282 | −0.368 |
| $\alpha_0^0$ | 0.683 | 0.970 | 1.55 | 0.673 | 0.933 | 1.56 |
| $\beta_0^0$ | −0.332 | −0.296 | −0.411 | −0.456 | −0.339 | −0.458 |
| Re $\bar{z}_0^0$ | 1.31 | 1.10 | 1.01 | 1.21 | 1.18 | 0.939 |
| Im $\bar{z}_0^0$ | 1.13 | 1.47 | 1.19 | 0.860 | 1.25 | 1.14 |
| $\theta_1$ | −41° | −63° | −55° | −53° | −62° | −83° |
| $\theta_2$ | 25° | −2° | −1° | 11° | 1° | 5° |
| $\alpha_0^2$ | 0.914 | 1.07 | 1.28 | 0.909 | 1.06 | 1.27 |
| $\beta_0^2$ | −0.239 | −1.00 | −1.00 | −0.476 | −0.884 | −0.406 |
| Re $\bar{z}_0^2$ | 1.62 | 0.075 | 0.371 | 0.347 | 0.069 | 0.000 |
| Im $\bar{z}_0^2$ | 1.26 | 1.00 | 0.929 | 1.41 | 1.06 | 1.00 |
| $\beta_1^1$ | −0.174 | −0.140 | 0.015 | −0.120 | −0.095 | 0.040 |

equations leads to a well defined scattering length $a_0^0 = 0.15 \pm 0.07$. It appears that this result follows from their strict use of the Berkeley band of phase shifts down to 500 MeV [10, 44]. This is partly illustrated in fig. 4, where the first data point favours our solution 2. However our three solutions have a reasonable $\chi^2$ when compared to the full data set and we feel it would be unwise to rely heavily on the phase near 500 MeV to select a solution of the Weinberg type.

In our solutions, the $I = 2$ s-wave phase shift $\delta_0^2$ is strongly correlated to the behaviour of $\delta_0^0$. It is clear that measuring $\delta_0^2$ with good accuracy, i.e. a true error of $\pm 3°$, in the region from 450 MeV to 900 MeV, could constrain the $\pi\pi$ amplitude appreciably. However it should be remarked that the $\delta_0^2$ phase depends on both $a_0^0$ and on the $\delta_0^0$ used in the fit (see figs. 3–5). The downward displacement of the

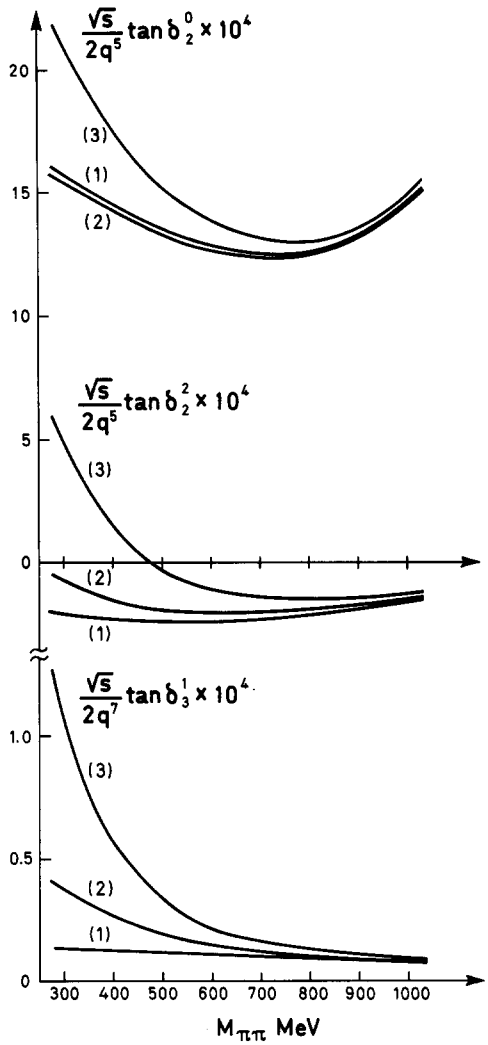


Fig. 6. Behaviour of the d- and f-wave amplitudes below 1 GeV for the three Saclay solutions of fig. 3.

universal curve in passing from the Saclay to the CM-EM1 phase results in a larger (numerically) $\delta_0^2$ phase. In any case the present experimental information on $\delta_0^2$ is not yet precise enough to discriminate between our band of solutions.

### *4.3. Higher partial waves*

The d- and f- partial-wave amplitudes are calculated as described in subsect. 2.5.

Table 6
Behaviour of the d- and f-wave phase shifts below 1 GeV. Errors include the effect of all experimental and theoretical uncertainties

| $M_{\pi\pi}$ (MeV) | $\delta_2^0$ | $\delta_2^2$ | $\delta_3^1$ |
|---|---|---|---|
| 400 | 0° .07 ± 0° .01 | 0° .00 ± 0° .01 | 0° .002 ± 0° .001 |
| 600 | 0° .9 ± 0° .1 | −0° .1 ± 0° .1 | 0° .04 ± 0° .02 |
| 800 | 3° .5 ± 0° .5 | −0° .5 ± 0° .2 | 0° .2 ± 0° .1 |
| 1000 | 11° ± 2° | −1° .0 ± 0° .6 | 0° .8 ± 0° .2 |

and we plot the quantities

$$K_l^I(s) = \frac{\sqrt{s}}{2q^{2l+1}} \tan \delta_l^I \tag{4.7}$$

in fig. 6 for our Saclay solutions. The $K_l^I(s)$ tend to the scattering lengths $a_l^I$ at threshold and we see that the scattering length approximation, $K_l^I(s) = a_l^I$, can be grossly violated for energies below 1 GeV. We note that the isoscalar d-wave scattering length $a_2^0$ has a rather stable value within our set of solutions – it is dominated by the $\rho$ and the "$\epsilon$". The $I = 2$ d-wave scattering length is comparatively small ($\rho$–"$\epsilon$" cancellation) while the f-wave scattering length $a_3^1$ is dominated by the threshold singularities. The behaviour of the d- and f-waves are similar to fig. 6 for our solutions fitted to the Berkeley or CM-EM1 phases. Since the values are quite stable we tabulate the d- and f-wave phase shifts for the mass region below 1 GeV in table 6. The errors allow for the spread between the three solutions and uncertainties in the experimental phases $\delta_0^0$, the driving terms and other input parameters such as the elastic partial decay width of the $f_0$ resonance. The values of these higher wave phases at 1 GeV are in good agreement with experimental values [20, 21, 22, 35]. Below 1 GeV the d- and f-waves are more accurately defined by our phenomenelogical determination than by experiment at the present level of statistics. We therefore suggest that in future ππ phase-shift analyses below 1 GeV, the phenomenological d- and f-wave phases of table 6 should be used as input (checking *a posteriori* that they agree with the data). In particular we remark that the CM-EM1 d-wave phase shifts [22] appear to be too large below 800 MeV.

### *4.4. The Regge ρ residue function*

We have evaluated the asymptotic contribution $L_\infty$ (defined in subsect. 2.7) to the Olsson sum rule for our three sets of solutions and the values obtained are shown in fig. 7. The error band associated with each of these curves, due to all the uncertainties in the input, corresponds to $\Delta L_\infty = \pm 0.05$. The contributions of the $f_0$ resonance and Regge $\rho$ exchange with the Lovelace-Vaneziano [30] residue function were evaluated using eq. (2.31) and are indicated by dashed lines in fig. 7. We see that our solutions tend to favour an effective Regge $\rho$ exchange residue function

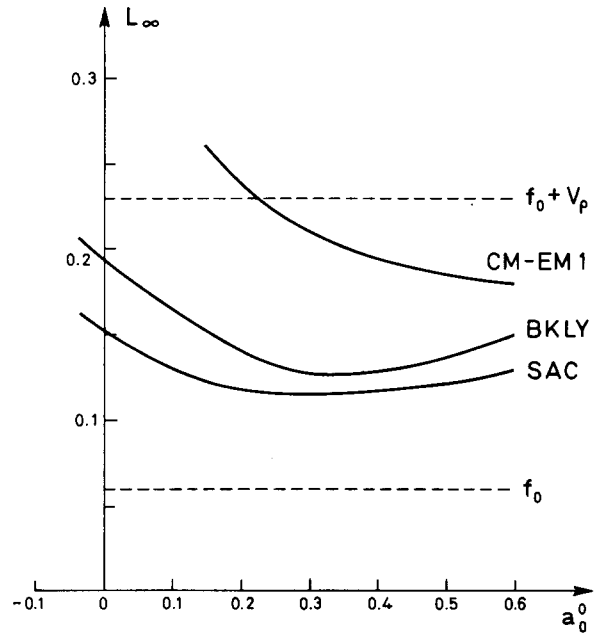


Fig. 7. Asymptotic contributions $L_\infty$ to the Olsson sum rule. The dashed lines indicate the contributions from the $f_0$ resonance and Regge $\rho$ exchange with the Lovelace-Veneziano residue function, $V_\rho$.

at $t = 0$ somewhat smaller than the Lovelace-Veneziano value. In particular our Saclay and Berkeley solutions suggest that the Veneziano $B_4$ model predicts high energy amplitudes too large by about a factor of two[+], and that the zero of the effective residue function is nearer the geometrical absorption value, $t = -0.2$ GeV$^2$, than the nonsense value, $t = -0.6$ GeV$^2$ [37].

### 4.5. *Future selection between solutions using the $\pi^+\pi^-$ $Y_1^0$ moment*

Our isoscalar s-wave amplitudes for a particular set of experimental phase shifts above 500 MeV differ mostly below the rho (see figs. 3–5) and have an uncertainty of between $\pm 5°$ and $\pm 10°$ at 500 MeV. More accurate information on $\delta_0^0$ near 500 MeV and below would be a great help in further restricting our set of $\pi\pi$ amplitudes, as exemplified in the work of Pennington and Protopopescu [10, 44] discussed above. The rho meson no longer dominates the amplitude in this mass region and it is more dificult to extract reliable s- and p-wave phase shifts from $\pi^+\pi^-$ production experiments. Partial information may still be accessible however, in the

[+] A similar phenomenon has been found in other circumstances [45].

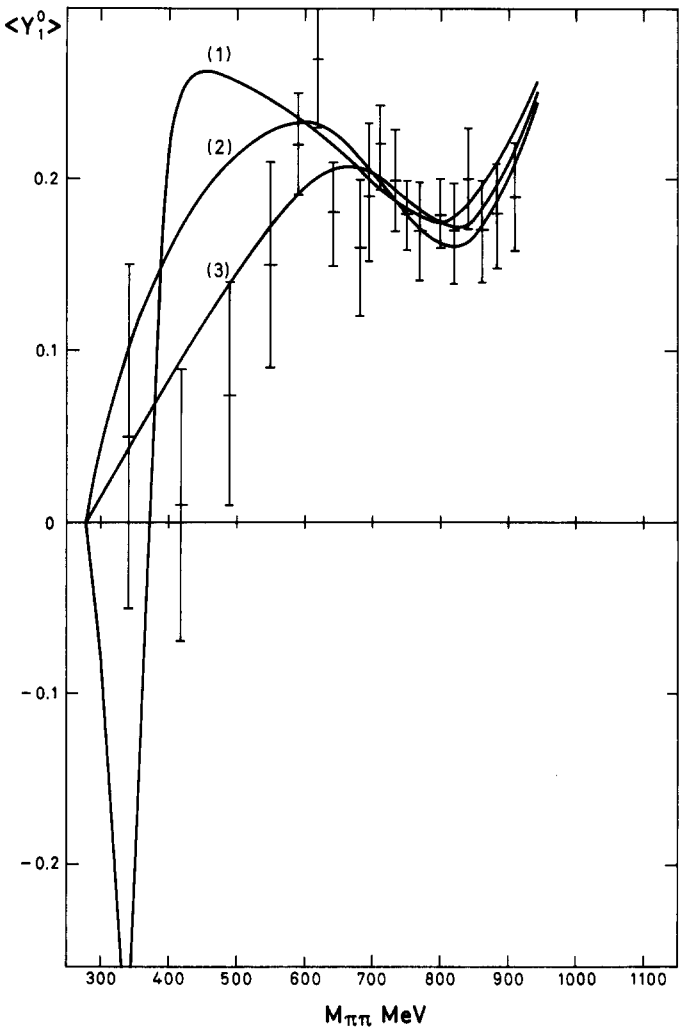


Fig. 8. Normalized extrapolated $\langle Y_1^0 \rangle$ moment for the Saclay data compared to the solutions of fig. 3.

form of the $Y_1^0$ moment of the $\pi\pi$ angular distribution. In fact the normalized $\langle Y_1^0 \rangle$ moments, which are proportional to the backward forward asymmetry, have been published for the Saclay and Berkeley experiments [20, 21]. This quantity has been calculated for all our solutions and is shown in figs. 8–9 together with the experimental values. There is a tendency for the large values of $a_0^0$ compared to Weinberg (i.e. $a_0^0 \geqslant 0.3$) to be favoured. However we would not rule out any of our solutions on this basis at present, but only point out that reliable experimental information on this quantity could do so.

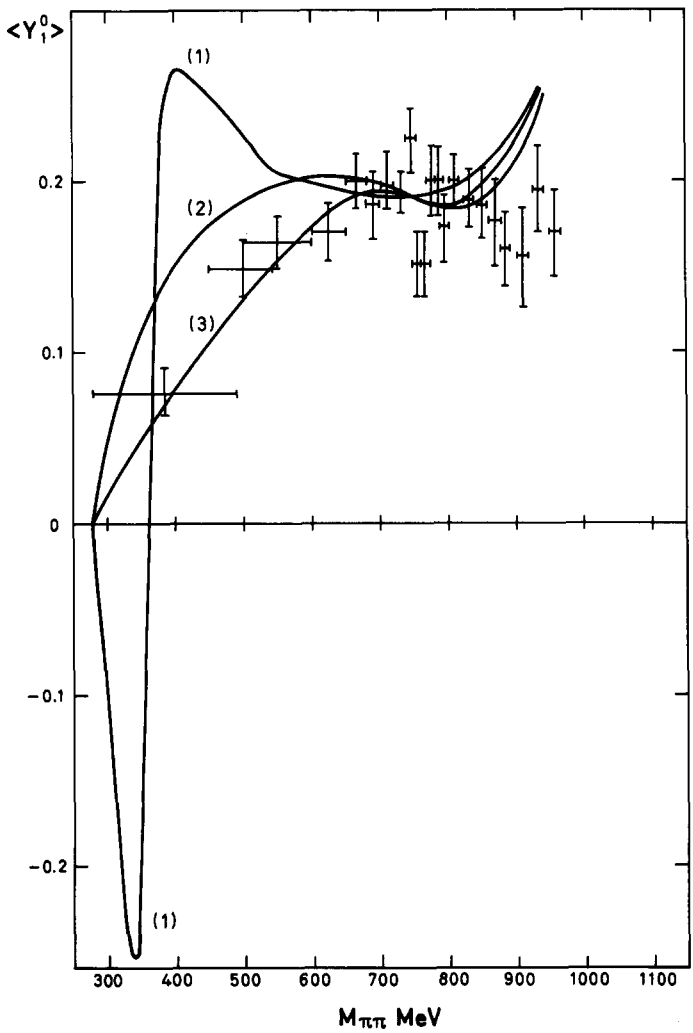


Fig. 9. Normalized extrapolated $\langle Y_1^0 \rangle$ moment for the Berkeley data compared to the solutions of fig. 4.

There are theoretical grounds [11, 22] for believing that the unnormalized moment, $N\langle Y_1^0\rangle$, is a cleaner quantity to extrapolate for the reaction $\pi N \to \pi\pi N$. In the CM-EM1 phase-shift analysis it was found convenient to use the combination $N\langle Y_1^0\rangle - \sqrt{\frac{28}{27}}\, N\langle Y_3^0\rangle$, which removes the main d-wave effects and essentially extrapolates to the quantity

$$\langle \tilde{Y}_1^0\rangle\ \sigma_{\mathrm{el}}^{+-} \equiv 4\sqrt{\frac{\pi}{3}}\frac{1}{q^2}\ \sin\delta_1^1\,(2\sin\delta_0^0\cos(\delta_0^0-\delta_1^1)+\sin\delta_0^2\cos(\delta_0^2-\delta_1^1)). \qquad (4.8)$$

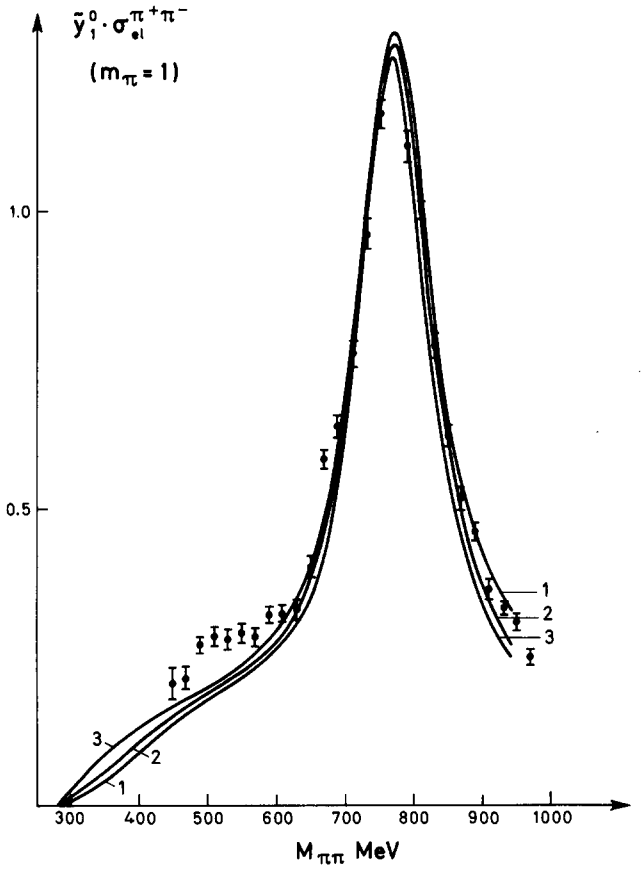


Fig. 10. Unnormalized $\langle \tilde{Y}_1^0 \rangle \sigma_{el}^{+-}$ moment, defined in eq. (4.8), computed from the CM-EM1 (and 2) phases and compared to the solutions of fig. 5.

We have evaluated this quantity for the CM-EM phase shifts and indeed it is found to be invariant in going from their (favoured) solution 1 to their solution 2 phase shifts. In the absence of the original data on the moments we have treated these values as data points in fig. 10, where we compare them to the predictions from our three solutions of fig. 5. None of our solutions is able to reproduce the behaviour of this quantity in the region below 600 MeV and we feel this is a serious anomaly which should be investigated further. This is reflected in the low-energy structure of the p-wave amplitude from the CERN analysis shown in fig. 11 which, similarly, we are unable to reconcile with the Roy equations. The CM-EM solution 2 p-wave phase shifts [22] are also shown in fig. 11 and are even more difficult to reproduce.

We should like to emphasize again that the Roy equations are able to predict d and higher waves accurately below 1 GeV. From our point of view there is, thefore,

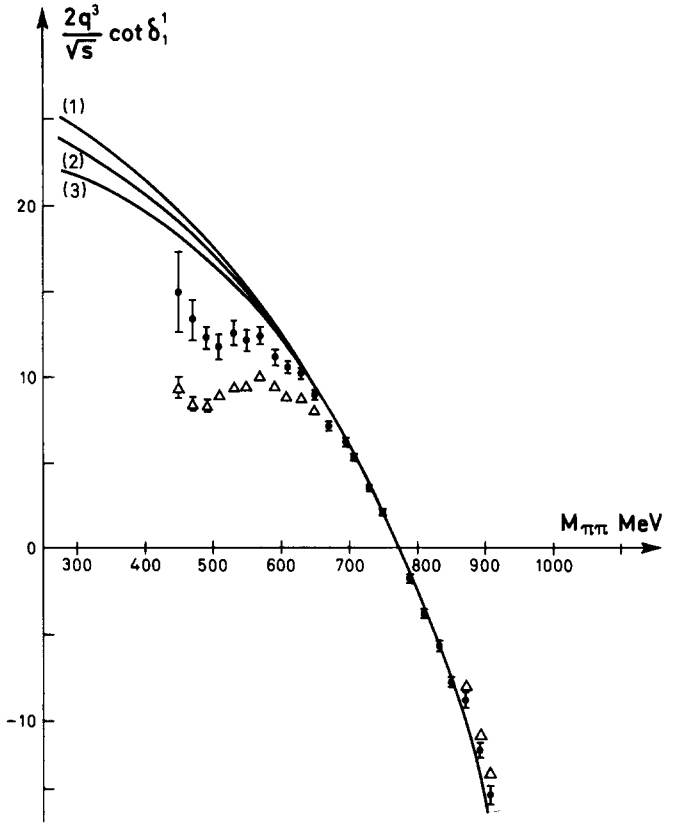


Fig. 11. The quantity $(2q^3/\sqrt{s})\cot\delta_1^1$ evaluated for the CM-EM1 • and CM-EM solution 2 $\dot{\Delta}$ p-wave phase shifts [22]. The curves correspond to the three solutions of fig. 5.

no advantage in working with $\langle Y_1^0\rangle - \sqrt{\frac{28}{27}}\langle Y_3^0\rangle$ rather than with $\langle Y_1^0\rangle$ itself. In fact values of the unnormalized $Y_1^0$ moment could be just as useful input into our analysis as the isoscalar s-wave phase shifts. Since $\langle Y_1^0\rangle\,\sigma_{el}^{+-}$ is more directly accessible experimentally, it could replace $\delta_0^0$ as item (f) in our list of assumed phenomenoligical information. We therefore urge experimentalists to publish values of this quantity, obtained by extrapolation or amplitude analysis. A direct $\pi\pi$ phase-shift analysis of these data could then be made within our approach, in which other moments could be predicted and checked *a posteriori* or used as additional phenomenological input.

### *4.7. Information on $\pi\pi$ scattering from other sources*

We conclude with some remarks about other sources of information on low energy $\pi\pi$ scattering. The $I = 2$ s-wave phase shift $\delta_0^2$ is correlated to the behaviour

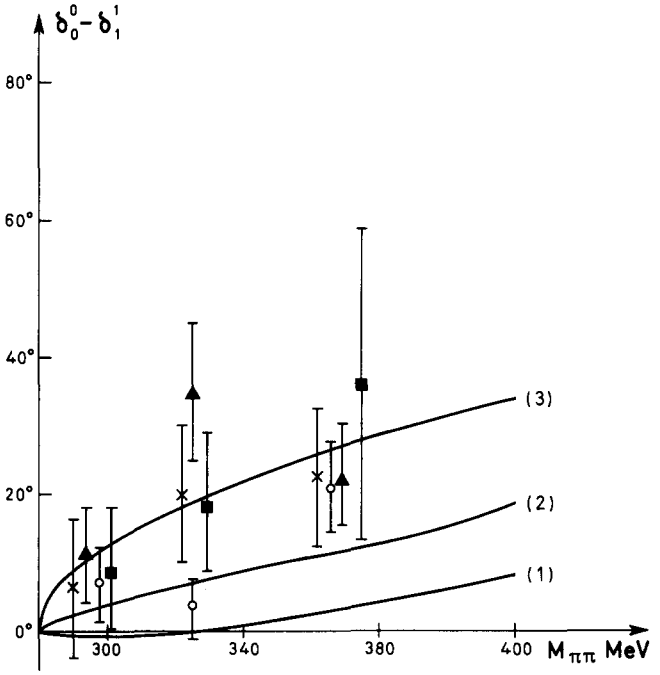


Fig. 12. Recent $K_{e4}$ results compared to the three Berkeley solutions of fig. 4. Data points from Beier et al. [46] ⊖ and from Zylbersztein et al. [46]: ⊻ ⊥ $\chi^2$ points, ⊥ maximum likelihood, ▮ Pais Treiman method.

of $\delta_0^0$ as shown in figs. 3–5. As mentioned above, the measurement of $\delta_0^2$ with good accuracy in $\pi^+\pi^+$ or $\pi^-\pi^-$ production experiments would help to constrain the $\pi\pi$ amplitude and, in each case, would select between the solutions with the small and large values of $a_0^0$. However the dispersion in the present $I = 2$ data [1, 42] encompasses all of our solutions.

The most direct experimental method of selecting between our solutions in favour of a definite s-wave scattering length is, of course, from $K_{e4}$ measurements. In fig.12 we compare our three Berkeley solutions from fig. 5 with the most recent $K_{e4}$ results [46]. The curves for a given value of $a_0^0$ are very similar for our Saclay and CM-EM1 solutions, due to the correlation we find between $a_0^0$ and the slope $b_0^0$. It appears that a negative value for $a_0^0$ can be ruled out but, otherwise any value within the range (4.6) is allowed by present measurements. Clearly a more accurate $K_{e4}$ experiment could provide a sensitive determination of $a_0^0$. As mentioned earlier, future analyses of $K_{e4}$ decay should make use of the phenomenological correlation between $a_0^0$ and $b_0^0$ given in tables 3 and 4.

Via analytic continuation, the amplitudes for other processes can be related to the $\pi\pi$ phase shifts. In particular the behaviour of the elastic $\pi$N d-wave amplitude

close to the physical threshold is very sensitive to the value of $a_0^0$. The most detailed analysis [47] favours $a_0^0 \sim 0.1$ and claims that the errors are small enough to rule out a scattering length as large as 0.6.

We should like to thank Professors J. Hamilton and A. Martin for their constant interest and suggestions. Much useful advice arose from conversations and correspondence with Drs. D. Atkinson, B. Bonnier, P. Gauron, R.C. Johnson, G. Laurens, D. Morgan, M.R. Pennington, C. Schmid and G. Shaw. We also thank Dr. C. Schomblond for her help and Professors M. Gourdin and G. Snow for useful remarks. Finally one of us (CDF) gratefully acknowledges the hospitality of NORDITA.

## Appendix A. Notation

We use partial-wave amplitudes $f_l^I(s)$ for orbital angular momentum $l$ and isospin $I$. These are related to the real phase shift $\delta_l^I(s)$ and elasticity coefficient $\eta_l^I(s)$ by

$$f_l^I(s) = (\eta_l^I(s)\, e^{2i\delta_l^I(s)} - 1)/2i\rho(s)\,, \tag{A.1}$$

where $\rho(s) \equiv \sqrt{(s-4)/s}$ (we use units $\hbar = c = m_\pi = 1$).

Scattering lengths $a_l^I$ are defined as

$$a_l^I = \lim_{s\to 4^+} f_l^I(s)/q^{2l}\,, \tag{A.2}$$

where $q$ is the c.m. three-momentum,

$$q^2 = \tfrac{1}{4}(s-4)\,. \tag{A.3}$$

For s-waves we define the slopes $b_0^0$ and $b_0^2$ as

$$b_0^I = \lim_{s\to 4^+} (\mathrm{Re}\, f_0^I(s) - a_0^I)/q^2\,. \tag{A.4}$$

For the detailed form of the Roy equations we refer to BGN [7].

Taking the limit as $s \to 4^+$ of these equations one gets identically

$$b_0^0 = \tfrac{1}{3}(2a_0^0 - 5a_0^2) - 4\frac{(a_0^0)^2}{\pi} + \frac{16}{\pi}\int_4^\infty \frac{ds'}{s'(s'-4)^2}\left[A^0(s',0) - (a_0^0)^2\sqrt{\frac{s'-4}{s'}}\right]$$

$$+\frac{16}{\pi}\int_4^\infty \frac{ds'}{s'^2(s'-4)}\left[\tfrac{1}{3}A^0(s',0) - A^1(s',0) + \tfrac{5}{3}A^2(s',0)\right]\,, \tag{A.5}$$

$$b_0^2 = -\tfrac{1}{6}(2a_0^0 - 5a_0^2) - 4\frac{(a_0^2)^2}{\pi} + \frac{16}{\pi}\int_4^\infty \frac{ds'}{s'(s'-4)^2}\left[A^2(s',0) - (a_0^2)^2\sqrt{\frac{s'-4}{s'}}\right]$$

$$+\frac{16}{\pi}\int_4^\infty \frac{ds'}{s'^2(s'-4)}\left[\tfrac{1}{3}A^0(s',0) + \tfrac{1}{2}A^1(s',0) + \tfrac{1}{6}A^2(s',0)\right]. \qquad \text{(A.6)}$$

Here $A^I(s,t)$ is the absorptive part of the invariant amplitude $F^I(s,t)$ (cf. sect. 2).

We also make use of the following sum rules based on unsubtracted forward dispersion relations:

$$L \equiv 2a_0^0 - 5a_0^2 = \frac{4}{\pi}\int_4^\infty \frac{ds'}{s'(s'-4)}\left[2A^0(s',0) + 3A^1(s',0) - 5A^2(s',0)\right], \qquad \text{(A.7)}$$

(Olsson's sum rule),

$$a_1^1 = \frac{16}{3\pi}\int_4^\infty ds' \frac{2s'-4}{s'^2(s'-4)^2} A^1(s',0)$$

$$+\frac{2}{9\pi}\int_4^\infty \frac{ds'}{s'^2}\left[2A^0(s',0) + 3A^1(s',0) - 5A^2(s',0)\right]. \qquad \text{(A.8)}$$

Taking the limit $s \to 4^+$ in the Roy equation for $f_1^1(s)$ one obtains Wander's sum rule

$$2a_0^0 - 5a_0^2 - 18a_1^1 = -\frac{96}{\pi}\int_4^\infty ds' \frac{2s'-4}{s'^2(s'-4)^2} A^1(s',0)$$

$$+\frac{16}{\pi}\int_4^\infty \frac{ds'}{s'^2(s'-4)}\left[2A^0(s',0) + 3A^1(s',0) - 5A^2(s',0)\right], \qquad \text{(A.9)}$$

which of course is also a consequence of eqs. (A.7) and (A.8).

## Appendix B. Parametrization of s- and p-wave $\pi\pi$ amplitudes

In this appendix we describe in some detail the parametrizations adopted for s- and p-waves ($f_0^0(s), f_1^1(s), f_0^2(s)$).

We shall primarily be working with the $S$-matrix element

$$S_l^I(s) = \eta_l^I(s)\, e^{2i\delta_l^I(s)}$$

$$= 1 + 2i\sqrt{\frac{s-4}{s}}\, f_l^I(s)$$

$$= 1 - 2\sqrt{\frac{4-s}{s}}\, f_l^I(s). \qquad \text{(B.1)}$$

We want to write $S_l^I$ as a rational function of a suitably chosen variable $z$ which will automatically introduce the physically relevant thresholds. The advantages of this scheme over the more familiar $K$-matrix formalism are (i) we can explicitly ensure that no physical sheet singularities occur; (ii) the parameters are directly related to the location of singularities and thus for the most part have a simple physical significance of their own and (iii) we are able to treat the important $l = I = 0$ $\pi\pi \to K\bar{K}$ inelasticity without having to parametrize ($K$-) matrix elements having to do with the reactions $\pi\pi \to K\bar{K}$ and $K\bar{K} \to K\bar{K}$, in which we have no direct interest here.

The variable $z$ will differ for the three amplitudes above for reasons which will become clear below. We therefore treat the parametrization of each amplitude individually.

*B.1. Parametrization of $f_0^0(s)$*

Here the physically relevant thresholds are $s = 0$, $s = 4$ and $s = 4m_K^2$. The variable $z$ which we chose will map the $q$-plane cut along $(-\infty, -q_I)$ $(q_I, \infty)$, $(i, i\infty)$ and $(-i\infty, -i)$ onto the unit circle $|z| < 1$ such that

$$q_I = \sqrt{m_K^2 - 1}\,,$$

$$q \in (-q_I, q_I) \to z \in (-1, 1)\,,$$

$$1^{st} \text{ sheet } (\mathrm{Im}\, q > 0) \to |z| < 1\,, \qquad \mathrm{Im}\, z > 0\,,$$

$$2^{nd} \text{ sheet } (\mathrm{Im}\, q < 0) \to |z| < 1\,, \qquad \mathrm{Im}\, z < 0\,. \tag{B.2}$$

The transformation $q \to z$ is given by

$$q^2 = \frac{R^2 z^2}{(z^2 - z_0^2)(z^2 - z_0^{*2})}\,,$$

$$z_0 = e^{i\theta}\,, \quad \tan\theta = 1/q_I\,, \qquad \theta \approx 16^\circ.3\,,$$

$$R = \frac{2q_I}{m_K} \approx 1.92\,. \tag{B.3}$$

Fig. 13 is the $z$-plane image of the four-sheeted $s$-plane Riemann surface. The circle and the real axis divide the $z$-plane into four domains which are the images respectively of the four sheets of $s$.

From eq. (B.3) it follows that the four complex numbers $z_i$, $i = 1,2,3,4$ with

$$z_2 = -z_1\,, \qquad z_3 = -z_1^{-1}\,, \qquad z_4 = z_1^{-1} = -z_3\,, \qquad |z_1| < 1, \quad \mathrm{Im}\, z_1 > 0\,, \tag{B.4}$$

will be the images of the same complex number in the $s$-plane, however, pertaining to sheet number $i$.

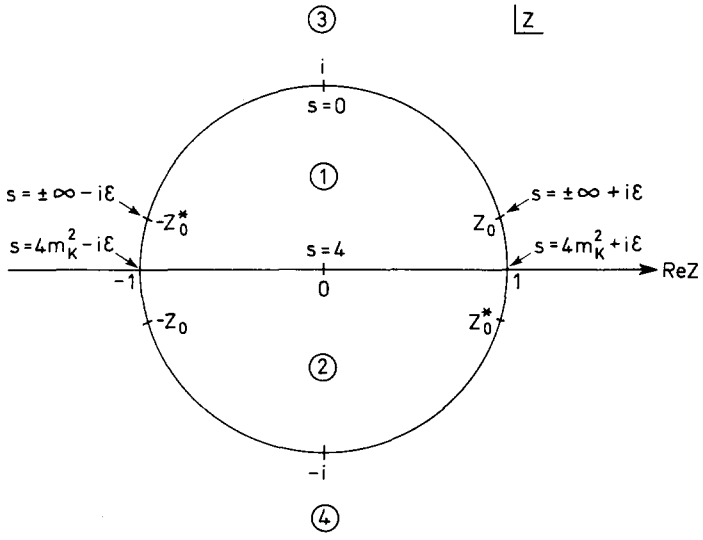


Fig. 13. $z$-plane image pertaining to eq. (B.3) of the four-sheeted Riemann surface for $s$.

Time-reversal invariance, elastic unitarity (we assume $\eta_0^0(s) \equiv 1$ on $4 \leqslant s \leqslant m_K^2$ in the parametrization) and analyticity requires the $S$-matrix element (B.1) to satisfy

$$S_0^0(-z^*) = [S_0^0(z)]^* ,$$

$$S_0^0(-z) = [S_0^0(z)]^{-1} ,$$

$$S_0^0 \text{ holomorphic in } |z| < 1 , \qquad \operatorname{Im} z > 0 ,$$

$$S_0^0 \text{ meromorphic in } |z| < 1 . \tag{B.5}$$

These will be satisfied by the following rational parametrization

$$S_0^0(z) = \mathcal{R}(z; z_\epsilon)\ \mathcal{R}(z; z_{S^*}) \times \frac{i+z}{i-z}\ \frac{i-\alpha_0^0 z}{i+\alpha_0^0 z}\ \frac{i-\beta_0^0 z^3}{i+\beta_0^0 z^3}\ \mathcal{R}(z; \bar{z}^0_0) , \tag{B.6}$$

where

$$\mathcal{R}(x;y) \equiv \frac{(x-y^*)(x+y)}{(x-y)(x+y^*)} . \tag{B.7}$$

We first outline the mathematical significance of the various factors in eq. (B.6).

The first factor, $\mathcal{R}(z;z_\epsilon)$ in eq. (B.6) introduces a pole at $z = z_\epsilon$ corresponding to an $\epsilon$-meson of mass $m_\epsilon$ and width $\Gamma_\epsilon$ such that $z_\epsilon$ is the image of the point $s_\epsilon$

on the second sheet, where

$$s_\epsilon = (m_\epsilon - \tfrac{1}{2} i \Gamma_\epsilon)^2 .$$

The factor $\mathcal{R}(z; z_{S^*})$ likewise describes an S* resonance.

The third factor in eq. (B.6) introduces a pole at $z = i$ corresponding to the $1/\sqrt{s}$ singularity at $s = 0$ (cf. eq. (B.1)).

The fourth factor in eq. (B.6) introduces a zero in $S_0^0(s)$ in the range $0 \leqslant s \leqslant 4$ on either the 1st or 3rd sheet (according to whether $\alpha_0^0 > 1$ or $\alpha_0^0 < 1$) and a corresponding pole on the 2nd (virtual bound state) or the 4th sheet. The presence of this factor is required for any reasonable low-energy behaviour of $f_0^0(s)$. From eq. (B.1) we see that the position of this zero will be given by the equation

$$f_0^0(s) = \frac{1}{2} \sqrt{\frac{s}{4-s}} , \tag{B.8}$$

which will always have a solution on $-2 < \sqrt{s} < 2$ ($\sqrt{s} < 0$ on the 3rd sheet, $\sqrt{s} > 0$ on the 1st sheet). The position of the zero we calculate approximately in terms of the low-energy parameters $a_0^0$ and $b_0^0$. From the definition eq. (A.4) and unitarity we get to order $(q^2)$ on $0 \leqslant s \leqslant 4$

$$f_0^0(s) = a_0^0 + b_0^0 q^2 - \sqrt{4-s}\,(\tfrac{1}{2}(a_0^0)^2 + q^2[a_0^0 b_0^0 + \tfrac{1}{2}(a_0^0)^4 - \tfrac{1}{4}(a_0^0)^2]) . \tag{B.9}$$

For all our solutions the corresponding solution to eq. (B.8) has $|\sqrt{s}| \lesssim 1$. We therefore expect the approximation (B.9) to be adequate in view of the crossing constraint

$$\operatorname{Im} f_0^0(s) = O(s^{\frac{3}{2}}) \qquad \text{for } s \to 0^- .$$

The remaining parameters $\beta_0^0$ and $\operatorname{Re} \bar{z}_0^0$, $\operatorname{Im} \bar{z}_0^0$ in the last two factors in eq. (B.6) are chosen so as to reproduce the behaviour

$$\operatorname{Re} f_0^0(s) = a_0^0 + b_0^0 q^2 + O(q^4) ,$$

as $s \to 4^+$, for the given values of $z_\epsilon$, $z_{S^*}$ and $\alpha_0^0$. Whenever this is possible in more than one way, that solution (in terms of $\beta_0^0$, $\operatorname{Re} \bar{z}_0^0$ and $\operatorname{Im} \bar{z}_0^0$) is chosen which corresponds to the most distant singularities in the $z$-plane (cf. the discussion below).

We next comment on the physical significance of the parameters as given in tables 1 and 5.

*B.1.1. The S* resonance.* The experimental structure which identifies the dynamical properties of the S* is the peculiar behaviour of $\delta_0^0$ and $\eta_0^0$: below the $K\bar{K}$ threshold ($z = 1$) $\delta_0^0$ increases slowly to $\delta_0^0 \simeq 90°$ in the 900 MeV region; then on a short interval just before the $K\bar{K}$ threshold $\delta_0^0$ increases rapidly to 180°; above $s = 4 m_K^2$ $\eta_0^0$ exhibits a corresponding rapid drop from 1 to a minimum value of 0.3–0.5. The choice of parametrization (i.e. the choice of $z$) is heavily biased in favour of functions with important square-root branch points at $s = 4 m_K^2$ : $S_0^0(z)$ will be regular

at $z = 1$ and $(\mathrm{d}/\mathrm{d}z)\, S_0^0(z)|_{z=1}$ will be proportional to the strength of the cusp-effect. One can still, within the present parametrization, describe a fully elastic $f_0^0$. By eqs. (B.4) this requires the singularity structure to be invariant under $z \to z^{-1}$, however. For an approximately elastic $f_0^0(s)$ we would thus be forced to have, besides the factors $\mathcal{R}(z;z_\epsilon)$ and $\mathcal{R}(z;z_{S*})$ in eq. (B.6), additional factors $\mathcal{R}(z;z'_\epsilon)$ and $\mathcal{R}(z;z'_{S*})$ with

$$z'_\epsilon \approx z_\epsilon^{-1}\,, \qquad z'_{S*} \approx z_{S*}^{-1}\,.$$

However, the contribution of a term $\mathcal{R}(z;z_r)$ to the phase shift is

$$\delta(z;z_r) = A \tan \frac{-2z\ \mathrm{Im}\, z_r}{|z_r|^2 - z^2}\,. \tag{B.10}$$

Thus we see that the two factors $\mathcal{R}(z;z_\epsilon)\,\mathcal{R}(z;z_{S*})$ (with values of $z_\epsilon$ and $z_{S*}$ as given in tables 1 and 5) will already reproduce the qualitative behaviour of $\delta_0^0$ as summarized above. In particular the agreement would be completely spoiled if we had a factor $\mathcal{R}(z;z'_{S*})$ with $z'_{S*} \simeq z_{S*}^{-1}$: the rapid rise in $\delta_0^0$ would then disappear. We thus conclude that the presence of this rapid rise and the fact that it takes place over the interval from 90° to 180° is strong evidence for an interpretation of the S* as a 2nd sheet pole not accompanied by a 3rd sheet pole, as would be the case for a less inelastic object [+]. We have argued that near $z = 1$ we must have $\mathcal{R}(z;z'_{S*}) \simeq 1$ This requires

$$|\mathrm{Im}\, z'_{S*}| \ll |\mathrm{Re}\, z'_{S*} - 1|\,.$$

In practice we encounter no difficulty in fitting the data without an $\mathcal{R}(z;z'_{S*})$ term at all, corresponding to $\mathrm{Im}\, z'_{S*} = 0$.

We conclude that there is strong experimental evidence for the S* as a 2nd sheet pole with a mass very close to $4\, m_K^2$. The width is given essentially by the length of the energy interval over which $\delta_0^0$ increases from 135° to 180° (say) and/or the length of the energy interval over which $\eta_0^0$ drops to its minimum. This parameter is much harder to get from present experiments than the mass. The data of ref. [22] thus require a value of $\Gamma_{S*}$ an order of magnitude smaller than that given in table 1. In principle, however, $\Gamma_{S*}$ must be considered an experimentally well defined parameter.

*B.1.2. The $\epsilon$-resonance.* The $\epsilon$ is a much more elusive object than the S* and thus our published values for $m_\epsilon$ and $\Gamma_\epsilon$ in table 5 need some comments.

We first point out that the set of functions

$$\left\{ \frac{i - az^n}{i + az^n}\,, \quad |a| < 1\,, \quad n > 0 \text{ odd integer} \right\}$$

[+] If one wants to describe the observed drop in $\eta_0^0$ in connection with a behaviour of $\delta_0^0$ like in the so called up-solution above 800 MeV, one must in fact use a factor $R(z;z'_{S*})$. That was done in ref. [3]. In this work, however, we only consider the implications of the "down-solution" above $m_\rho$ (cf. ref. [21]).

is a complete set of functions on the space of elastic $S$-matrices defined on $-1 \leqslant z \leqslant 1$ (i.e. on $4 \leqslant s \leqslant 4\, m_K^2$). This means that we can fit any conceivable experimental phase shift with arbitrary accuracy using functions $S_0^0(z)$ having singularities only for $|z| > 1$. That again implies that even a seemingly clearly resonating phase shift (like $\delta_1^1$, see below) can be fitted with arbitrary accuracy without using a second sheet resonance pole [48]. This observation implies that it is not only very difficult to determine the $\epsilon$-pole position but the problem of finding the singularities corresponding to a set of experimental phase shifts with finite accuracy (however good) does not even in principle have a unique solution. This statement is true for any parametrization: it is a feature known as instability in theories of analytic extrapolation [49]. One therefore needs to reformulate the problem (which was "improperly posed"). We do this by assuming first that on the second sheet at most 3 poles need be considered. These 3 poles are the ones pertaining to $z_\epsilon$, $z_{S^*}$ and (for sufficiently large values of $a_0^0$ – cf. table 5) a virtual bound state coming from the fourth factor in eq. (B.6). Second, we require that the contribution to $\delta_0^0$ coming from singularities outside the circle $|z| = 1$ is "as smooth as possible" inside $|z| = 1$. In the present work we shall make no attempt to formalize this last principle, but from results on extrapolation theory pertaining to analogous situations [49] we expect that, once such a principle has been sharply defined, one can prove that as experimental errors on $\delta_0^0$ go to zero (i) the 3 poles on the 2nd sheet will converge to unique and well defined positions provided the assumption that at most 3 poles exist on the 2nd sheet is correct and (ii) the contribution to $S_0^0$ coming from singularities outside $|z| = 1$ will converge to a well defined function inside $|z| = 1$, whereas the actual singularity positions outside $|z| = 1$ are not expected to have any significance and no convergence of these can be expected since the approximation scheme neglects the presence of branch-point singularities on $|z| = 1$.

In the present work we have imposed smoothness of the contribution of background singularities (those with $|z| \geqslant 1$) (a) by limiting their number and (b) by requiring them to be as far away as possible (cf. the discussion of the parameters $\beta_0^0$, Re $\bar{z}_0^0$ and Im $\bar{z}_0^0$). However crude this treatment of the background singularities may be, it represents a refinement over our methods used for ref. [2]. Accordingly we feel that our values for $\Gamma_\epsilon$ in that paper may have been overestimated (cf. table 5 for our new values).

The disentangeling of the contribution from the three 2nd sheet poles is still a serious one. For the S* we feel the situation is rather well defined as explained above, however, and for the remaining two we are effectively helped by the Roy-eqs. in that, once we chose a particular value of $a_0^0$, these eqs. predict the corresponding value of $b_0^0$ and therefore the position of the pole in the 4th factor in eq. (B.6) as explained above. Thereby the ambiguity in the $\epsilon$-pole position is reduced.

We thus feel that our published $\epsilon$-pole positions represent a little more than the results of an arbitrary fit, but we strongly emphasize that, due to the inherent difficulties in its definition, the actual numbers should be treated with great care. The test of our scheme will be to see whether $z_\epsilon$ as we have defined it will converge to a unique position as experimental errors decrease with time.

*B.2. Parametrization of $f_1^1(s)$*

There are two essential differences compared to the parametrization of $f_0^0(s)$:
(i) near $s = 4\,m_K^2$

$$f_1^1(s) = \tilde{f}_1^1(s) + O((s - 4\,m_K^2)^{\frac{3}{2}}) , \tag{B.13}$$

where $\tilde{f}_1^1(s)$ is regular at $s = 4\,m_K^2$;
(ii) near $s = 4$

$$\delta_1^1 \propto a_1^1 q^3 .$$

Condition (i) is satisfied automatically by writing $S_1^1$ as a (rational) function of the new variable

$$z_1 \equiv \tfrac{1}{4} z(3 - z^2) , \tag{B.14}$$

where $z$ is given by eq. (B.3). Then the condition (B.13) just means that $S_1^1(z_1)$ is regular at $z_1 = \frac{1}{2}$ (the image of $s = 4\,m_K^2$).

Condition (ii) is satisfied by formally treating $f_1^1$ as an s-wave with zero scattering length and slope $= a_1^1$.

Simplifying a little the low energy treatment as compared to the case of $f_0^0$ we then write

$$S_1^1(z_1) = \mathcal{R}(z_1; z_\rho) \frac{(i+z_1)(i-\alpha_1^1 z_1)(i-\beta_1^1 z_1^3)}{(i-z_1)(i+\alpha_1^1 z_1)(i+\beta_1^1 z_1^3)}$$

$$\times\ \mathcal{R}(z_1; z_{\rho'})\ \mathcal{R}(z_1; z'_{\rho'}) . \tag{B.15}$$

Here $z_\rho$ is the image in the $z_1$ plane of the point

$$s = (m_\rho - \tfrac{1}{2} i\,\Gamma_\rho)^2$$

on the second sheet.

The two last factors have been included in order to be able to vary the detailed behaviour of $\delta_1^1$ in the 900–1000 MeV region as required by the Roy equations. We found it natural to represent these background-terms by an inelastic $\rho'$ (cf. table 1), but by no means do we claim to have predicted a $\rho'$ by the Roy equations.

*B.3. Parametrization of $f_0^2(s)$*

In this amplitude no $K\bar{K}$ threshold is present and, for simplicity, we take $f_0^2(s)$ to be elastic from threshold to $s = \infty$. That is, we take $S_0^2$ to be a rational function of the new variable $z_2$ given by

$$q^2 = \frac{4z_2^2}{(z_2^2 - 1)^2} \quad . \tag{B.16}$$

We thuse write

$$S_0^2(z_2) = \mathcal{R}(z_2; e^{i\theta_1})\, \mathcal{R}(z_2; e^{i\theta_2})$$

$$\times \frac{i+z_2}{i-z_2}\, \frac{i-\alpha_0^2 z_2}{i+\alpha_0^2 z_2}\, \frac{i-\beta_0^2 z_2^3}{i+\beta_0^2 z_2^3}\, \mathcal{R}(z_2; \bar{z}_0^2)\,. \tag{B.17}$$

Here $\theta_1$ and $\theta_2$ are free real parameters in the interval $(-\frac{1}{2}\pi, \frac{1}{2}\pi)$ (i.e. for simplicity we allow real axis poles on the left-hand cut). The parameters $\alpha_0^2$, $\beta_0^2$, $\bar{z}_0^2$ are then fixed in terms of the scattering length $a_0^2$ and the slope $b_0^2$ in complete analogy to what was done for $f_0^0(s)$ above.

## References


[1] J.L. Basdevant, C.D. Froggatt and J.L. Petersen, Phys. Letters 41B (1972) 173.
[2] J.L. Basdevant, C.D. Froggatt and J.L. Petersen, Phys. Letters 41B (1972) 178.
[3] J.L. Basdevant, C.D. Froggatt and J.L. Petersen, Proc. Int. Conf. on $\pi\pi$ scattering and associated topics, Tallahassee, 1973.
[4] J.L. Basdevant, B. Bonnier, C. Schomblond, C.D. Froggatt and J.L. Petersen, Comm. to Aix en Provence Int. Conf. on elementary particles, September 1973.
[5] S.M. Roy, Phys. Letters 36B (1971) 353.
[6] J. Hamilton and W.S. Woolcock, Rev. Mod. Phys. 35 (1963) 737;
G. Höhler and R. Strauss, Z. Phys. 232 (1970) 205;
E. Pietarinen, Nuovo Cimento 12A (1972) 522;
E. Pietarinen, Nucl. Phys. B49 (1972) 315;
G. Höhler et al., Nucl. Phys. B39 (1972) 237;
H. Nielsen, Nucl. Phys. B33 (1971) 152.
[7] J.L. Basdevant, J.C. Le Guillou and H. Navelet, Nuovo Cimento 7A (1972) 363.
[8] B. Bonnier and P. Gauron, Nucl. Phys. B52 (1973) 506.
[9] J.C. Le Guillou and J.L. Basdevant, Ann. Inst. Henri Poincaré 17 (1972) 221.
[10] M.R. Pennington and S.D. Protopopescu, Phys. Rev. D7 (1973) 1429, 2591.
[11] J.L. Petersen, Phys. Reports 2 (1971) 155;
J.L. Basdevant, Springer tracts in Mod. Phys. 61 (1972) 1.
[12] J.C. Guillou, A. Morel and H. Navelet, Nuovo Cimento 5A (1971) 659;
B. Bonnier and P. Gauron, Nucl. Phys. B21 (1970) 465.
[13] O. Piguet and G. Wanders, Nucl. Phys. B46 (1972) 295.
[14] D. Atkinson, Nucl. Phys. B7 (1968) 375; B8 (1968) 377; B13 (1969) 415; B23 (1970) 397;
J. Kupsch, Nucl. Phys. B11 (1969) 573; B12 (1969) 155; Nuovo Cimento 66A (1970) 202; Comm. Math. Phys. 19 (1970) 65.
[15] L. Castillejo, R.H. Dalitz and F.J. Dyson, Phys. Rev. 101 (1956) 453;
D. Atkinson and R.L. Warnock, Phys. Rev. 188 (1969) 2098.
[16] L.S. Brown and R.S. Goble, Phys. Rev. Letters 20 (1968) 346;
R. Arnowitt, H.H. Friedman, P. Nath and R. Suitor, Phys. Rev. Letters 20 (1968) 475;
A.M.S. Amatya, A. Pagnamenta and B. Renner, Phys. Rev. 172 (1968) 1755;
H.J. Schnitzer, Phys. Rev. D2 (1970) 1621.
[17] J.S. Kang and B.W. Lee, Phys. Rev. D3 (1971) 2814.

[18] J.L. Basdevant and B.W. Lee, Phys. Rev. D2 (1970) 1680.
[19] H. Lehmann, Phys. Letters 41B (1972) 529;
G. Ecker and J. Honerkamp, Nucl. Phys. B52 (1973) 211.
[20] J.P. Baton, G. Laurens and J. Reignier, Phys. Letters 25B (1967) 419; Nucl. Phys. B3 (1967) 349; Phys. Letters 33B (1970) 525, 528;
G. Laurens, Thesis, Saclay report CEA-N-1497 (1971).
[21] S.D. Protopopescu et al., Phys. Rev. D7 (1973) 1279.
[22] P. Estabrooks et al., Proc. Int. Conf. on $\pi\pi$ scattering and associated topics, Tallahassee, 1973.
[23] R. Oehme, Phys. Rev. 100 (1955) 1503; 102 (1956) 1174;
R.H. Capps and G. Takeda, Phys. Rev. 103 (1956) 1877;
G.F. Chew, M.L. Goldberger, F.E. Low and Y. Nambu, Phys. Rev. 106 (1957) 1337;
F. Steiner, Fortschr. Phys. 19 (1971) 115;
J. Baacke and F. Steiner, Fortschr. Phys. 18 (1970) 67.
[24] A. Martin, Scattering theory: unitarity, analyticity and crossing (Springer, 1969).
[25] G. Mahoux, S.M. Roy and G. Wanders, Nucl. Phys. B70 (1974) 297.
[26] A. Martin, Nuovo Cimento 47A (1967) 265;
G. Auberson, O. Brander, G. Mahoux and A. Martin, Nuovo Cimento 65A (1970) 743.
[27] A.P. Balachandran and J. Nuyts, Phys. Rev. 172 (1968) 1821;
R. Roskies, Nuovo Cimento 65A (1970) 467;
J.L. Basdevant, G. Cohen-Tannoudji and A. Morel, Nuovo Cimento 64A (1969) 585.
[28] G.F. Chew and S. Mandelstam, Phys. Rev. 119 (1960) 467.
[29] C. Lovelace, Nuovo Cimento 21 (1961) 305.
[30] C. Lovelace, Phys. Letters 28B (1968) 264; Proc. of Conf. on $\pi\pi$ and $K\pi$ interactions, Argonne National Laboratory (1969);
J.A. Shapiro, Phys. Rev. 179 (1969) 1345.
[31] M. Alston-Garnjost et al., Phys. Letters 36B (1971) 152.
[32] S.M. Flatté et al., Phys. Letters 38B (1972) 232.
[33] G. Grayer et al., Experimental meson spectroscopy 1972, Proc. of the Third Int. Conf. Philadelphia, 1972; ed. K.W. Lai and A.H. Rosenfeld.
[34] G. Grayer et al., Contribution to the 16th Int. Conf. on high energy physics, Batavia, Sept. 1972.
[35] B. Hyams et al., Proc. Int. Conf. on $\pi\pi$ scattering and associated topics, Tallahassee, 1973.
[36] M.G. Olsson, Phys. Rev. 162 (1967) 1338.
[37] J.L. Basdevant and C. Schomblond, Phys. Letters 45B (1973) 48.
[38] J.L. Basdevant and J. Zinn-Justin, Phys. Rev. D3 (1971) 1865.
[39] D. Morgan and G. Shaw, Phys. Rev. D2 (1970) 520; Nucl. Phys. B10 (1969) 261.
[40] J.L. Basdevant, Fortschr. Phys. 20 (1972) 283.
[41] B. Bonnier and R. Vinh Mau, Phys. Letters 24B (1967) 477;
A.K. Common, Nuovo Cimento 63 (1969) 451.
[42] R. Diebold, Proc. of the 16th Int. Conf. on high energy physics, Batavia, 1972.
[43] S. Weinberg, Phys. Rev. Letters 17 (1966) 616.
[44] M.R. Pennington and S.D. Protopopescu, Proc. Int. Conf. on $\pi\pi$ scattering and associated topics, Tallahassee, 1973.
[45] C. Schmid, Proc. of the Amsterdam Int. Conf. on elementary particles 1971 (North-Holland, Amsterdam, 1972).
[46] A. Zylbersztejn et al., Phys. Letters 38B (1972) 457;
E.W. Beier et al., Phys. Rev. Letters 29 (1972) 511; 30 (1973) 399.
[47] H. Nielsen and G.C. Oades, Comm. to Aix-en-Provence Int. Conf. on elementary particles, September 1973.

[48] J. Hamilton and B. Tromborg, Partial-wave amplitudes and resonance poles (Oxford University Press, 1972).
[49] R.E. Cutkosky, Ann. of Phys. 54 (1969) 350;
J. Pišút, Springer tracts in Mod. Phys. 55 (1970) 43;
E. Pietarinen, Nuovo Cimento 12A (1972) 522.

IISc-CTS-12/99
ZU-TH 10/00
BUTP-99/33

# Roy equation analysis of $\pi\pi$ scattering

May 30, 2000

B. Ananthanarayan[a], G. Colangelo[b], J. Gasser[c] and H. Leutwyler[c]

[a] Centre for Theoretical Studies, Indian Institute of Science
Bangalore, 560 012 India
[b] Institute for Theoretical Physics, University of Zürich
Winterthurerstr. 190, CH-8057 Zürich, Switzerland
[c] Institute for Theoretical Physics, University of Bern
Sidlerstr. 5, CH-3012 Bern, Switzerland

**Abstract**

We analyze the Roy equations for the lowest partial waves of elastic $\pi\pi$ scattering. In the first part of the paper, we review the mathematical properties of these equations as well as their phenomenological applications. In particular, the experimental situation concerning the contributions from intermediate energies and the evaluation of the driving terms are discussed in detail. We then demonstrate that the two $S$-wave scattering lengths $a_0^0$ and $a_0^2$ are the essential parameters in the low energy region: Once these are known, the available experimental information determines the behaviour near threshold to within remarkably small uncertainties. An explicit numerical representation for the energy dependence of the $S$- and $P$-waves is given and it is shown that the threshold parameters of the $D$- and $F$-waves are also fixed very sharply in terms of $a_0^0$ and $a_0^2$. In agreement with earlier work, which is reviewed in some detail, we find that the Roy equations admit physically acceptable solutions only within a band of the ($a_0^0$,$a_0^2$) plane. We show that the data on the reactions $e^+e^- \to \pi\,\pi$ and $\tau \to \pi\,\pi\,\nu$ reduce the width of this band quite significantly. Furthermore, we discuss the relevance of the decay $K \to \pi\,\pi\,e\,\nu$ in restricting the allowed range of $a_0^0$, preparing the grounds for an analysis of the forthcoming precision data on this decay and on pionic atoms. We expect these to reduce the uncertainties in the two basic low energy parameters very substantially, so that a meaningful test of the chiral perturbation theory predictions will become possible.

**Pacs:** 11.30.Rd, 11.55.Fv, 11.80.Et, 13.75.Lb
**Keywords:** Roy equations, Dispersion relations, Partial wave analysis, Meson-meson interactions, Pion-pion scattering, Chiral symmetries

# Contents

# 1 Introduction

The present paper deals with the properties of the $\pi\pi$ scattering amplitude in the low energy region. Our analysis relies on a set of dispersion relations for the partial wave amplitudes due to Roy [1]. These equations involve two subtraction constants, which may be identified with the $S$-wave scattering lengths, $a_0^0$ and $a_0^2$. We demonstrate that the subtraction constants represent the essential parameters in the low energy region – once these are known, the Roy equations allow us to calculate the partial waves in terms of the available data, to within small uncertainties. Given the strong dominance of the two $S$-waves and of the $P$-wave, it makes sense to solve the equations only for these, using experimental as well as theoretical information to determine the contributions from higher energies and from the higher partial waves. More specifically, we solve the relevant integral equations on the interval $2M_\pi < \sqrt{s} < 0.8\,\mathrm{GeV}$. One of the main results of this work is an accurate numerical representation of the $S$- and $P$-waves for a given pair of scattering lengths $a_0^0$ and $a_0^2$.

Before describing the outline of the present paper, we review previous work concerning the Roy equations. Roy's representation [1] for the partial wave am-

plitudes $t_l^I$ of elastic $\pi\pi$ scattering reads

$$t_\ell^I(s) = k_\ell^I(s) + \sum_{I'=0}^{2} \sum_{\ell'=0}^{\infty} \int_{4M_\pi^2}^{\infty} ds'\, K_{\ell\ell'}^{II'}(s,s')\, \mathrm{Im}\, t_{\ell'}^{I'}(s')\,, \tag{1.1}$$

where $I$ and $\ell$ denote isospin and angular momentum, respectively and $k_\ell^I(s)$ is the partial wave projection of the subtraction term. It shows up only in the $S$- and $P$-waves,

$$k_\ell^I(s) = a_0^I\, \delta_\ell^0 + \frac{s-4M_\pi^2}{4M_\pi^2}\,(2a_0^0 - 5a_0^2)\,\left(\frac{1}{3}\,\delta_0^I\,\delta_\ell^0 + \frac{1}{18}\,\delta_1^I\,\delta_\ell^1 - \frac{1}{6}\,\delta_2^I\,\delta_\ell^0\right). \tag{1.2}$$

The kernels $K_{\ell\ell'}^{II'}(s,s')$ are explicitly known functions (see appendix A). They contain a diagonal, singular Cauchy kernel that generates the right hand cut in the partial wave amplitudes, as well as a logarithmically singular piece that accounts for the left hand cut. The validity of these equations has rigorously been established on the interval $-4M_\pi^2 < s < 60M_\pi^2$.

The relations (1.1) are consequences of the analyticity properties of the $\pi\pi$ scattering amplitude, of the Froissart bound and of crossing symmetry. Combined with unitarity, the Roy equations amount to an infinite system of coupled, singular integral equations for the phase shifts. The integration is split into a low energy interval $4M_\pi^2 < s' < s_0$ and a remainder, $s_0 < s' < \infty$. We refer to $s_0$ as the *matching point*, which is chosen somewhere in the range where the Roy equations are valid. The two $S$-wave scattering lengths, the elasticity parameters below the matching point and the imaginary parts above that point are treated as an externally assigned input. The mathematical problem consists in solving Roy's integral equations with this input.

Soon after the original article of Roy [1] had appeared, extensive phenomenological applications were performed [2]–[8], resulting in a detailed analysis and exploitation of the then available experimental data on $\pi\pi$ scattering. For a recent review of those results, we refer the reader to the article by Morgan and Pennington [9]. Parallel to these phenomenological applications, the very structure of the Roy equations was investigated. In [11], a family of partial wave equations was derived, on the basis of manifestly crossing symmetric dispersion relations in the variables $s\,t + t\,u + u\,s$ and $s\,t\,u$. Each set in this family is valid in an interval $s_0 < s < s_1$, and the union of these intervals covers the domain $-28M_\pi^2 \leq \mathrm{Re}\; s \leq 125.3M_\pi^2$ (for a recent application of these dispersion relations, see [12]). Using hyperbolae in the plane of the above variables, Auberson and Epele [13] proved the existence of partial wave equations up to $\mathrm{Re}\; s = 165M_\pi^2$. Furthermore, the manifold of solutions of Roy's equations was investigated, in the single channel [14]–[16] as well as in the coupled channel case [17]. In the late seventies, Pool [18] provided a proof that the original, infinite set of integral equations does have at least one solution for $\sqrt{s_0} < 4.8\,M_\pi$, provided that the driving terms are not too large, see also [19]. Heemskerk and Pool also examined

numerically the solutions of the Roy equations, both by solving the $N$ equation [19] and by using an iterative method [20].

It emerged from these investigations that – for a given input of $S$-wave scattering lengths, elasticity parameters and imaginary parts – there are in general many possible solutions to the Roy equations. This non-uniqueness is due to the singular Cauchy kernel on the right hand side of (1.1). In order to investigate the uniqueness properties of the Roy system, one may – in a first step – keep only this part of the kernels, so that the integral equations decouple: one is left with a single channel problem, that is a single partial wave, which, moreover, does not have a left hand cut. This mathematical problem was examined by Pomponiu and Wanders, who also studied the effects due to the presence of a left hand cut [14]. Investigating the infinitesimal neighbourhood of a given solution, they found that the multiplicity of the solution increases by one whenever the value of the phase shift at the matching point goes through a multiple of $\pi/2$. Note that the situation for the usual partial wave equation is different: There, the number of parameters in general increases by two whenever the phase shift at infinity passes through a positive integer multiple of $\pi$, see for instance [21, 22] and references cited therein.

After 1980, interest in the Roy equations waned, until recently. For instance, in refs. [23] these equations are used to analyze the threshold parameters for the higher partial waves, relying on the approach of Basdevant, Froggatt and Petersen [5, 6]. The uncertainties in the values of $a_0^0$ and $a_0^2$ are reexamined in refs. [24]. In recent years, it has become increasingly clear, however, that a new analysis of the $\pi\pi$ scattering amplitude at low energies is urgently needed. New $K_{e4}$ experiments and a measurement of the combination $a_0^0 - a_0^2$ based on the decay of pionic atoms are under way [25]–[29]. It is expected that these will significantly reduce the uncertainties inherent in the data underlying previous Roy equation studies, provided the structure of these equations can be brought under firm control. For this reason, the one-channel problem has been revisited in great detail in a recent publication [30], while the role of the input in Roy's equations is discussed in ref. [31].

The main reason for performing an improved determination of the $\pi\pi$ scattering amplitude is that this will allow us to test one of the basic properties of QCD, namely the occurrence of an approximate, spontaneously broken symmetry: The symmetry leads to a sharp prediction for the two $S$-wave scattering lengths [32]–[40]. The prediction relies on the standard hypothesis, according to which the quark condensate is the leading order parameter of the spontaneously broken symmetry. Hence an accurate test of the prediction would allow us to verify or falsify that hypothesis [34]. First steps in this program have already been performed [35]–[39]. However, in the present paper, we do not discuss this issue. We follow the phenomenological path and ignore the constraints imposed by chiral symmetry altogether, in order not to bias the data analysis with theoretical prejudice. In a future publication, we intend to match the chiral perturbation

theory representation of the scattering amplitude to two loops [40] with the phenomenological one obtained in the present work.

Finally, we describe the content of the present paper. Our notation is specified in section 2. Sections 3 and 4 contain a discussion of the background amplitude and of the driving terms, which account for the contributions from the higher partial waves and from the high-energy region. As is recalled in section 5, unitarity leads to a set of three singular integral equations for the two $S$-waves and for the $P$-wave. The uniqueness properties of the solutions to these equations are discussed in section 6, while section 7 contains a description of the experimental input used for energies between 0.8 and 2 GeV. In particular we also discuss the information concerning the $P$-wave phase shift, obtained on the basis of the $e^+e^- \to \pi\pi$ and $\tau \to \pi\pi\nu$ data. In section 8, we describe the method used to solve the integral equations for a given input. The resulting universal band in the $(a_0^0,a_0^2)$ plane is discussed in section 9, where we show that, in the region below 0.8 GeV, any point in this band leads to a decent numerical solution for the three lowest partial waves. As discussed in section 10, however, the behaviour of the solutions above that energy is consistent with the input used for the imaginary parts only in part of the universal band – approximately the same region of the $(a_0^0,a_0^2)$ plane, where the Olsson sum rule is obeyed (section 11). The solutions are compared with available experimental data in section 12, and in section 13, we draw our conclusions concerning the allowed range of $a_0^0$ and $a_0^2$. The other threshold parameters can be determined quite accurately in terms of these two. The outcome of our numerical evaluation of the scattering lengths and effective ranges of the lowest six partial waves as functions of $a_0^0$ and $a_0^2$ is given in section 14, while in section 15, we describe our results for the values of the phase shifts relevant for $K \to \pi\pi$. Section 16 contains a comparison with earlier work. A summary and concluding remarks are given in section 17.

In appendix A we describe some properties of the Roy kernels, which are extensively used in our work. The background from the higher partial waves and from the high energy tail of the dispersion integrals is discussed in detail in appendix B. In particular, we show that the constraints imposed by crossing symmetry reduce the uncertainties in the background, so that the driving terms can be evaluated in a reliable manner. In appendix C we discuss sum rules connected with the asymptotic behaviour of the amplitude and show that these relate the imaginary part of the $P$-wave to the one of the higher partial waves, thereby offering a sensitive test of our framework. Explicit numerical solutions of the Roy equations are given in appendix D and, in appendix E, we recall the main features of the well-known Lovelace-Shapiro-Veneziano model, which provides a useful guide for the analysis of the asymptotic contributions.

## 2 Scattering amplitude

We consider elastic $\pi\pi$ scattering in the framework of QCD and restrict our analysis to the isospin symmetry limit, where the masses of the up and down quarks are taken equal and the e.m. interaction is ignored[1]. In this case, the scattering process is described by a single Lorentz invariant amplitude $A(s,t,u)$,

$$\begin{aligned}\langle \pi^d(p_4)\pi^c(p_3)\,\mathrm{out}|\pi^a(p_1)\pi^b(p_2)\,\mathrm{in}\rangle &= \delta_{fi} + \\ (2\pi)^4 i\,\delta^4(P_f-P_i)\{\delta^{ab}\delta^{cd}A(s,t,u) &+ \delta^{ac}\delta^{bd}A(t,u,s) + \delta^{ad}\delta^{bc}A(u,s,t)\}\,.\end{aligned}$$

The amplitude only depends on the Mandelstam variables $s$, $t$, $u$, which are constrained by $s+t+u=4M_\pi^2$. Moreover, crossing symmetry implies

$$A(s,t,u) = A(s,u,t)\,.$$

The $s$-channel isospin components of the amplitude are given by

$$\begin{aligned}T^0(s,t) &= 3A(s,t,u) + A(t,u,s) + A(u,s,t)\ \ , \\ T^1(s,t) &= A(t,u,s) - A(u,s,t)\ \ , \\ T^2(s,t) &= A(t,u,s) + A(u,s,t)\ \ .\end{aligned} \tag{2.1}$$

In our normalization, the partial wave decomposition reads

$$\begin{aligned}T^I(s,t) &= 32\,\pi\sum_\ell (2\ell+1)\,P_\ell\left(1+\frac{2t}{s-4M_\pi^2}\right)t_\ell^I(s)\ \ , \\ t_\ell^I(s) &= \frac{1}{2i\sigma(s)}\left\{\eta_\ell^I(s)\,e^{2i\delta_\ell^I(s)}-1\right\}\ \ , \\ \sigma(s) &= \sqrt{1-\frac{4M_\pi^2}{s}}\,.\end{aligned} \tag{2.2}$$

The threshold parameters are the coefficients of the expansion

$$\mathrm{Re}\,t_\ell^I(s) = q^{2\ell}\left\{a_\ell^I + q^2\,b_\ell^I + q^4\,c_\ell^I + \ldots\right\}\ \ , \tag{2.3}$$

with $s=4(M_\pi^2+q^2)$.

The isospin amplitudes $\vec{T}=(T^0,T^1,T^2)$ obey fixed-$t$ dispersion relations, valid in the interval $-28M_\pi^2 < t < 4M_\pi^2$ [41]. As shown by Roy [1], these can be written in the form[2]

$$\begin{aligned}\vec{T}(s,t) &= (4M_\pi^2)^{-1}\,(s\,\mathbf{1}+t\,C_{st}+u\,C_{su})\,\vec{T}(4M_\pi^2,0) \\ &+ \int_{4M_\pi^2}^\infty ds'\,g_2(s,t,s')\,\mathrm{Im}\,\vec{T}(s',0) + \int_{4M_\pi^2}^\infty ds'\,g_3(s,t,s')\,\mathrm{Im}\,\vec{T}(s',t)\,.\end{aligned} \tag{2.4}$$

[1] In our numerical work, we identify the value of $M_\pi$ with the mass of the charged pion.

[2] For an explicit representation of the kernels $g_2(s,t,s')$, $g_3(s,t,s')$ and of the crossing matrices $C_{st}$, $C_{su}$, we refer to appendix A.

The subtraction term is fixed by the $S$-wave scattering lengths:

$$\vec{T}(4M_\pi^2, 0) = 32\,\pi\,(a_0^0, 0, a_0^2)\,.$$

The Roy equations (1.1) represent the partial wave projections of eq. (2.4). Since the partial wave expansion of the absorptive parts converges in the large Lehmann–Martin ellipse, these equations are rigorously valid in the interval $-4M_\pi^2 < s < 60M_\pi^2$. If the scattering amplitude obeys Mandelstam analyticity, the fixed-$t$ dispersion relations can be shown to hold for $-32M_\pi^2 < t < 4M_\pi^2$ and the Roy equations are then also valid in a larger domain: $-4M_\pi^2 < s < 68M_\pi^2$ (for a review, see [42]). In fact, as we mentioned in the introduction, the range of validity can be extended even further [11, 13], so that Roy equations could be used to study the behaviour of the partial waves above $\sqrt{68}\,M_\pi = 1.15\,\mathrm{GeV}$, where the uncertainties in the data are still considerable. In the following, however, we focus on the low energy region. We assume Mandelstam analyticity and analyze the Roy equations in the interval from threshold to

$$s_1 = 68M_\pi^2 \;\;, \qquad \sqrt{s_1} = 1.15\,\mathrm{GeV} \;\;.$$

# 3 Background amplitude

The dispersion relation (2.4) shows that, at low energies, the scattering amplitude is fully determined by the imaginary parts of the partial waves in the physical region, except for the two subtraction constants $a_0^0, a_0^2$. In view of the two subtractions, the dispersion integrals converge rapidly. In the region between 0.8 and 2 GeV, the available phase shift analyses provide a rather detailed description of the imaginary parts of the various partial waves. Our analysis of the Roy equations allows us to extend this description down to threshold. For small values of $s$ and $t$, the contributions to the dispersion integrals from the region above 2 GeV are very small. We will rely on Regge asymptotics to estimate these. In the following, we split the interval of integration into a low energy part ($4M_\pi^2 \le s' \le s_2$) and a high energy tail ($s_2 \le s' < \infty$), with

$$\sqrt{s_2} = 2\,\mathrm{GeV} \;\;, \qquad s_2 = 205.3\,M_\pi^2 \;\;.$$

For small values of $s$ and $t$, the scattering amplitude $\vec{T}(s,t)$ is dominated by the contributions from the subtraction constants and from the low energy part of the dispersion integral over the imaginary parts of the $S$- and $P$-waves. We denote this part of the amplitude by $\vec{T}(s,t)_{\scriptscriptstyle SP}$. The corresponding contribution to the partial waves is given by

$$t_\ell^I(s)_{\scriptscriptstyle SP} = k_\ell^I(s) + \sum_{I'=0}^{2}\sum_{\ell'=0}^{1}\int_{4M_\pi^2}^{s_2} ds'\,K_{\ell\ell'}^{II'}(s,s')\,\mathrm{Im}\,t_{\ell'}^{I'}(s') \;\;. \tag{3.1}$$

The remainder of the partial wave amplitude,

$$d_\ell^I(s) = \sum_{I'=0}^{2}\sum_{\ell'=2}^{\infty}\int_{4M_\pi^2}^{s_2} ds'\, K_{\ell\ell'}^{II'}(s,s')\,\mathrm{Im}\, t_{\ell'}^{I'}(s') + \sum_{I'=0}^{2}\sum_{\ell'=0}^{\infty}\int_{s_2}^{\infty} ds'\, K_{\ell\ell'}^{II'}(s,s')\,\mathrm{Im}\, t_{\ell'}^{I'}(s') \quad , \tag{3.2}$$

is called the *driving term*. It accounts for those contributions to the r.h.s. of the Roy equations that arise from the imaginary parts of the waves with $\ell = 2, 3, \ldots$ and in addition also contains those generated by the imaginary parts of the $S$- and $P$-waves above 2 GeV. By construction, we have

$$t_\ell^I(s) = t_\ell^I(s)_{\scriptscriptstyle SP} + d_\ell^I(s) \quad . \tag{3.3}$$

For the scattering amplitude, the corresponding decomposition reads

$$\vec{T}(s,t) = \vec{T}(s,t)_{\scriptscriptstyle SP} + \vec{T}(s,t)_d \quad . \tag{3.4}$$

We refer to $\vec{T}(s,t)_d$ as the *background amplitude*.

The contribution from the imaginary parts of the $S$- and $P$-waves turns out to be crossing symmetric by itself. In this sense, crossing symmetry does not constrain the imaginary parts of the $S$- and $P$-waves[3]. The symmetry can be exhibited explicitly by representing the three components of the vector $\vec{T}(s,t)_{\scriptscriptstyle SP}$ as the isospin projections of a single amplitude $A(s,t,u)_{\scriptscriptstyle SP}$ that is even with respect to the exchange of $t$ and $u$. The explicit expression involves three functions of a single variable [11, 36]:

$$A(s,t,u)_{\scriptscriptstyle SP} = 32\pi\left\{\tfrac{1}{3}W^0(s) + \tfrac{3}{2}(s-u)W^1(t) + \tfrac{3}{2}(s-t)W^1(u) + \tfrac{1}{2}W^2(t) + \tfrac{1}{2}W^2(u) - \tfrac{1}{3}W^2(s)\right\} \quad . \tag{3.5}$$

These are determined by the imaginary parts of the $S$- and $P$-waves and by the two subtraction constants $a_0^0, a_0^2$:

$$\begin{aligned} W^0(s) &= \frac{a_0^0\, s}{4M_\pi^2} + \frac{s(s-4M_\pi^2)}{\pi}\int_{4M_\pi^2}^{s_2}\frac{ds'\,\mathrm{Im}\, t_0^0(s')}{s'(s'-4M_\pi^2)(s'-s)} \quad , \\ W^1(s) &= \frac{s}{\pi}\int_{4M_\pi^2}^{s_2}\frac{ds'\,\mathrm{Im}\, t_1^1(s')}{s'(s'-4M_\pi^2)(s'-s)} \quad , \\ W^2(s) &= \frac{a_0^2\, s}{4M_\pi^2} + \frac{s(s-4M_\pi^2)}{\pi}\int_{4M_\pi^2}^{s_2}\frac{ds'\,\mathrm{Im}\, t_0^2(s')}{s'(s'-4M_\pi^2)(s'-s)} \quad . \end{aligned} \tag{3.6}$$

The representation

$$A(s,t,u) = A(s,t,u)_{\scriptscriptstyle SP} + A(s,t,u)_d \tag{3.7}$$

[3]The asymptotic behaviour of the scattering amplitude does tie the imaginary part of the $P$-wave to the contributions from the higher partial waves, see appendix C.1.

yields a manifestly crossing symmetric decomposition of the scattering amplitude into a leading term generated by the imaginary parts of the $S$- and $P$-waves at energies below $s_2$ and a background, arising from the imaginary parts of the higher partial waves and from the high energy tail of the dispersion integrals.

# 4 Driving terms

In the present paper, we restrict ourselves to an analysis of the Roy equations for the $S$- and $P$- waves, which dominate the behaviour at low energies. The background amplitude only generates small corrections, which can be worked out on the basis of the available experimental information. The calculation is described in detail in appendix B. In particular, we show that crossing symmetry implies a strong constraint on the asymptotic contributions.

The resulting numerical values for the driving terms are well described by polynomials in $s$, or, equivalently, in the square of the center of mass momentum $q^2 = \frac{1}{4}(s - 4M_\pi^2)$. By definition, the driving terms vanish at threshold, so that the polynomials do not contain $q$-independent terms. In view of their relevance in the evaluation of the threshold parameters, we fix the coefficients of the terms proportional to $q^2$ with the derivatives at threshold and also pin down the term of order $q^4$ in the $P$-wave, such that it correctly accounts for the background contribution to the effective range of this partial wave. The remaining coefficients of the polynomial are obtained from a fit on the interval from threshold to $s_1$. The explicit result reads

$$\begin{aligned} d_0^0(s) &= 0.116\,q^2 + 4.79\,q^4 - 4.09\,q^6 + 2.69\,q^8 \quad , \\ d_1^1(s) &= 0.00021\,q^2 + 0.038\,q^4 + 0.94\,q^6 - 1.21\,q^8 \quad , \\ d_0^2(s) &= 0.0447\,q^2 + 1.59\,q^4 - 6.26\,q^6 + 5.94\,q^8 \quad , \end{aligned} \tag{4.1}$$

where $q$ is taken in GeV units (the range $4M_\pi^2 < s < 68M_\pi^2$ corresponds to $0 < q < 0.56\,\mathrm{GeV}$). The driving term of the $I = 0$ $S$-wave is larger than the other two by an order of magnitude. It is dominated almost entirely by the contribution from the $D$-wave with $I = 0$. In $d_1^1(s)$, the $D$- and $F$-waves nearly cancel, so that the main contributions arise from the region above 2 GeV. The term $d_0^2(s)$ picks up small contributions both from low energies and from the asymptotic domain. The above polynomials are shown as full lines in fig. 1. The shaded regions represent the uncertainties of the result, which may be represented as $d_\ell^I(s) \pm e_\ell^I(s)$, with

$$\begin{aligned} e_0^0(s) &= 0.008\,q^2 + 0.31\,q^4 - 0.33\,q^6 + 0.41\,q^8 \quad , \\ e_1^1(s) &= 0.002\,q^2 + 0.06\,q^4 - 0.17\,q^6 + 0.21\,q^8 \quad , \\ e_0^2(s) &= 0.005\,q^2 + 0.20\,q^4 - 0.32\,q^6 + 0.39\,q^8 \quad . \end{aligned} \tag{4.2}$$

Above threshold, the error bars in $d_0^0(s)$, $d_1^1(s)$ and $d_0^2(s)$ roughly correspond to 6%, 1% and 4% of $d_0^0(s)$, respectively.

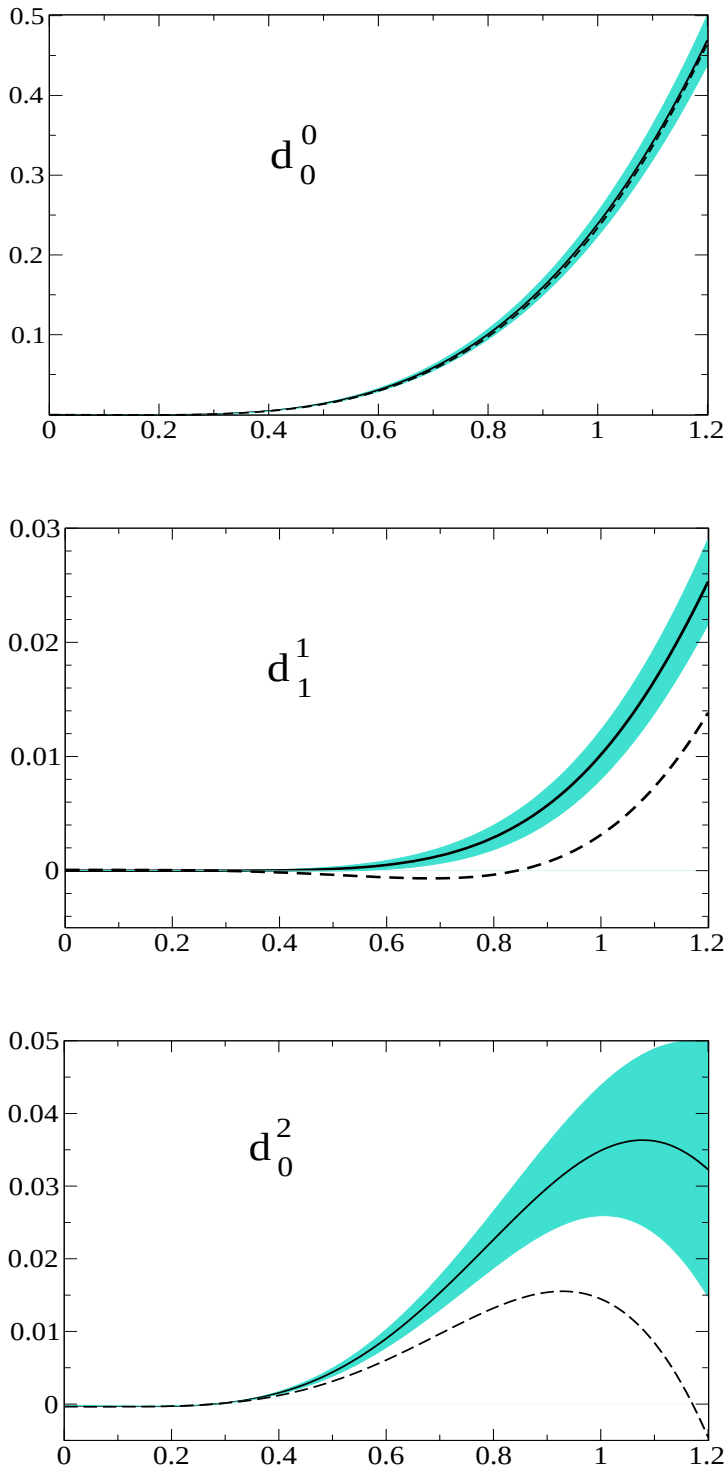


Figure 1: Driving terms versus energy in GeV. The full lines show the result of the calculation described in appendix B. The shaded regions indicate the uncertainties associated with the input of that calculation. The dashed curves represent the contributions from the $D$- and $F$-waves below 2 GeV.

As far as $d_0^0(s)$ is concerned, our result roughly agrees with earlier calculations [3, 6]. Our values for $d_1^1(s)$ and $d_0^2(s)$, however, are much smaller. The bulk of the difference is of purely kinematic origin: The values taken for $s_2$ are different. While we are working with $\sqrt{s_2} = 2\,\mathrm{GeV}$, the values used in refs. [3] and [6] are $\sqrt{53}\,M_\pi \simeq 1\,\mathrm{GeV}$ and $\sqrt{110}\,M_\pi \simeq 1.5\,\mathrm{GeV}$, respectively. The value of $s_2$ enters the definition of the driving terms in eq. (3.2) as the lower limit of the integration over the imaginary parts of the $S$- and $P$-waves. We have checked that, once this difference in the range of integration is accounted for, the driving terms given in these references are consistent with the above representation. Note however, that our uncertainties are considerably smaller, and we do rely on this accuracy in the following. It then matters that not only the range of integration, but also the integrands used in [3, 6] differ from ours: In these references, it is assumed that, above the value taken for $s_2$, the behaviour of the $S$- and $P$-wave imaginary parts is adequately described by a Regge representation.

The difference between such a picture and our representation for the background amplitude is best illustrated with the simple model used in the early literature, where the asymptotic region is described by a Pomeron term with $\sigma_{tot} = 20\,\mathrm{mb}$ and a contribution from the $\rho$-$f$-trajectory, taken from the Lovelace-Shapiro-Veneziano model (appendix E). As discussed in detail in appendix B.4, the assumption that an asymptotic behaviour of this type sets in early is in conflict with crossing symmetry [43]. In particular, the model overestimates the contribution to the driving terms from the region above 1.5 GeV, roughly by a factor of two. Either the value of $\sigma_{tot}$ or the residue of the leading Regge trajectory or both must be reduced in order for the model not to violate the sum rule (B.6). The manner in which the asymptotic contribution is split into one from the Pomeron and one from the leading Regge trajectory is not crucial. For any reasonable partition that obeys the sum rule (B.6), the outcome for the driving terms is approximately the same. The result for $d_1^1(s)$ and $d_0^2(s)$ is considerably smaller than what is expected from the above model. The leading term $d_0^0(s)$, on the other hand, is dominated by the resonance $f_2(1275)$ and is therefore not sensitive to the behaviour of the imaginary parts in the region above 1.5 GeV.

# 5 Roy equations as integral equations

Once the driving terms are pinned down, the Roy equations for the $S$- and $P$-waves express the real parts of the partial waves in terms of the $S$-wave scattering lengths and of a principal value integral over their imaginary parts from $4M_\pi^2$ to $s_2$. Unitarity implies that, in the elastic domain $4M_\pi^2 < s < 16M_\pi^2$, the real and imaginary parts of the partial wave amplitudes are determined by a single real parameter, the phase shift. If we were to restrict ourselves to the elastic region, setting $s_2 = 16M_\pi^2$, the Roy equations would amount to a set of coupled, nonlinear singular integral equations for the phase shifts. We may extend this

range, provided the elasticity parameters $\eta_\ell^I(s)$ are known. On the other hand, since the Roy equations do not constrain the behaviour of the partial waves for $s > 68M_\pi^2$, the integrals occurring on the r.h.s. of these equations can be evaluated only if the imaginary parts in that region are known, together with the subtraction constants $a_0^0$, $a_0^2$, which also represent parameters to be assigned externally.

In the present paper, we do not solve the Roy equations in their full domain of validity, but use a smaller interval, $4M_\pi^2 < s < s_0$. The reason why it is advantageous to use a value of $s_0$ below the mathematical upper limit, $s_0 < s_1$, is that the Roy equations in general admit more than one solution. As will be discussed in detail in section 6, the solution does become unique if the value of $s_0$ is chosen between the $\rho$ mass and the energy where the $I = 0$ $S$-wave phase passes through $\pi/2$ – this happens around 0.86 GeV. In the following, we use

$$\sqrt{s_0} = 0.8\,\mathrm{GeV} \quad , \qquad s_0 = 32.9\,M_\pi^2 \quad .$$

In the variable $s$, our matching point is nearly at the center of the interval between threshold and $s_1 = 68\,M_\pi^2$. We are thus solving the Roy equations on the lower half of their range of validity, using the upper half to check the consistency of the solutions so obtained (section 10). Our results are not sensitive to the precise value taken for $s_0$ (section 9).

The Roy equations for the $S$- and $P$-waves may be rewritten in the form

$$\begin{aligned}\mathrm{Re}\,t_\ell^I(s) = k_\ell^I(s) &+ \int\!\!\!\!\!\!-_{4M_\pi^2}^{s_0} ds' K_{\ell\,0}^{I\,0}(s,s')\,\mathrm{Im}\,t_0^0(s') + \int\!\!\!\!\!\!-_{4M_\pi^2}^{s_0} ds' K_{\ell\,1}^{I\,1}(s,s')\,\mathrm{Im}\,t_1^1(s') \\ &+ \int\!\!\!\!\!\!-_{4M_\pi^2}^{s_0} ds' K_{\ell\,0}^{I\,2}(s,s')\,\mathrm{Im}\,t_0^2(s') + f_\ell^I(s) + d_\ell^I(s) \quad , \end{aligned} \tag{5.1}$$

where $I$ and $\ell$ take only the values $(I,\ell)$ =(0,0), (1,1) and (2,0). The bar across the integral sign denotes the principal value integral. The functions $f_\ell^I(s)$ contain the part of the dispersive integrals over the three lowest partial waves that comes from the region between $s_0$ and $s_2$, where we are using experimental data as input. They are defined as

$$f_\ell^I(s) = \sum_{I'=0}^{2} \sum_{\ell'=0}^{1} \int\!\!\!\!\!\!-_{s_0}^{s_2} ds' K_{\ell\ell'}^{II'}(s,s')\,\mathrm{Im}\,t_{\ell'}^{I'}(s') \quad . \tag{5.2}$$

The experimental input used to evaluate these integrals will be discussed in section 7, together with the one for the elasticity parameters of the $S$- and $P$-waves.

One of the main tasks we are faced with is the construction of the numerical solution of the integral equations (5.1) in the interval $4M_\pi^2 \le s \le s_0$, for a given input $\{a_0^0, a_0^2, f_\ell^I, \eta_\ell^I, d_\ell^I\}$. Once a solution is known, the real part of the amplitude can be calculated with these equations, also in the region $s_0 \le s \le s_1$.

# 6 On the uniqueness of the solution

The literature concerning the mathematical structure of the Roy equations was reviewed in the introduction. In the following, we first discuss the situation for the single channel case – which is simpler, but clearly shows the salient features – and then describe the generalization to the three channel problem we are actually faced with. For a detailed analysis, we refer the reader to two recent papers on the subject [30, 31] and the references quoted therein.

## 6.1 Roy's integral equation in the one-channel case

If we keep only the diagonal, singular Cauchy kernel in (1.1), the partial wave relations decouple, and the left hand cut in the amplitudes disappears. Each one of the three partial wave amplitudes then obeys the following conditions:
i) In the interval between the threshold $s = 4M_\pi^2$ and the matching point $s = s_0$, the real part is given by a dispersion relation

$$\mathrm{Re}\, t(s) = a + (s - 4M_\pi^2)\, \frac{1}{\pi} \int\!\!\!\!\!\!-_{4M_\pi^2}^{\infty} ds'\, \frac{\mathrm{Im}\, t(s')}{(s' - 4M_\pi^2)\,(s' - s)}\ . \tag{6.1}$$

ii) Above $s_0$, the imaginary part $\mathrm{Im}\, t(s)$ is a given input function

$$\mathrm{Im}\, t(s) = A(s), \qquad s \geq s_0\ . \tag{6.2}$$

iii) For simplicity, we take the matching point in the elastic region, so that

$$t(s) = \frac{1}{\sigma(s)} e^{i\delta(s)} \sin\delta(s)\ \ , \qquad 4M_\pi^2 \leq s \leq s_0\ \ , \tag{6.3}$$

where $\delta(s)$ is real and vanishes at threshold. We refer the reader to [30] for a precise formulation of the regularity properties required from the amplitude and from the input absorptive part. As a minimal condition, we must require

$$\lim_{s \nearrow s_0} \mathrm{Im}\ t(s) = A(s_0)\ \ . \tag{6.4}$$

Otherwise, the principal value integral does not exist at the matching point.

Equations (6.1)–(6.4) constitute the mathematical problem we are faced with in this case: Determine the amplitudes $t(s)$ that verify these equations for a given input of scattering length $a$ and absorptive part $A(s)$. Once a solution is known, the real part of the amplitude above $s_0$ is obtained from the dispersion relation (6.1), and $t(s)$ is then defined on $4M_\pi^2 \leq s < \infty$. The following points summarize the results relevant in our context:

1. Elastic unitarity reduces the problem to the determination of the real function $\delta(s)$, defined in the interval $4M_\pi^2 \leq s \leq s_0$. The amplitude $t(s)$ is then obtained from (6.3).

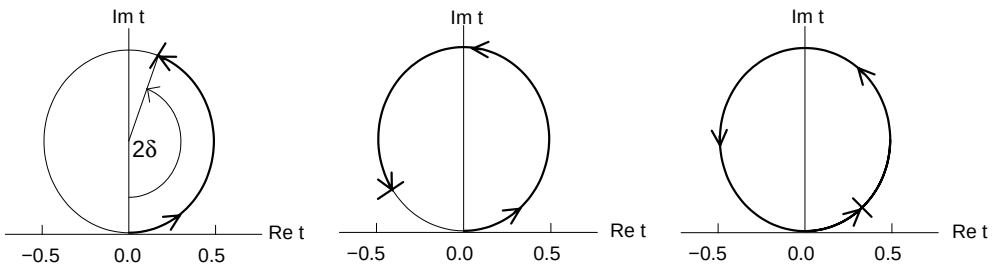


a) $m = 0$ b) $m = 1$ c) $m = 2$

Figure 2: Boundary conditions on the phase $\delta(s_0)$ for solving Roy's integral equation. Figs. a,b,c represent the cases $0 < \delta(s_0) < \pi/2$, $\pi/2 < \delta(s_0) < \pi$ and $\pi < \delta(s_0) < 3\pi/2$, respectively. In fig. c, the phase winds around the Argand circle slightly more than once.

2. A given input $\{a, A(s)\}$ does not, in general, fix the solution uniquely – in addition, the value of the phase at the matching point plays an important role. Indeed, let $t(s)$ be a solution and suppose first that the phase at the matching point is positive. For $0 < \delta(s_0) < \pi/2$, the infinitesimal neighbourhood of $t(s)$ does not contain further solutions. For $\delta(s_0) > \pi/2$, however, the neighbourhood contains an $m$-parameter family of solutions. The integer $m$ is determined by the value of the phase at the matching point ($[x]$ is the largest integer not exceeding $x$):

$$m = \left[\frac{2\delta(s_0)}{\pi}\right] \quad . \tag{6.5}$$

For a monotonically increasing phase, the index $m$ counts the number of times $\delta(s)$ goes through multiples of $\pi/2$ as $s$ varies from threshold to the matching point. We illustrate the situation for $m = 0, 1, 2$ in figure 2.

3. If the value of the phase at the matching point is negative, the problem does not in general have a solution. In order for the problem to be soluble at all, the input must be tuned. For $-\pi/2 < \delta(s_0) < 0$, for instance, we may keep the absorptive part $A(s)$ as it is, but tune the scattering length $a$. This situation may be characterized by $m = -1$: Instead of having a family of solutions containing free parameters, the input is subject to a constraint. Once a solution does exist, it is unique in the sense that the infinitesimal neighbourhood does not contain further solutions.

4. Consider now the case displayed in fig. 2a, where the phase at the matching point is below $\pi/2$. This corresponds to the situation encountered in the coupled channel case, for our choice of the matching point. According to the

above statements, a given input $\{a, A(s)\}$ then generates a locally unique solution – if a solution exists at all. We take it that uniqueness also holds globally, see [15].

The solution may be constructed in the following manner: Consider a family of unitary amplitudes, parametrized through $c_1, \ldots, c_n$. For any given amplitude, evaluate the right and left hand sides of eq. (6.1) and calculate the square of the difference at $N$ points in the interval $4M_\pi^2 \leq s \leq s_0$. Finally, minimize the sum of these squares by choosing $c_1, \ldots, c_n$ accordingly. Since the solution is unique, it suffices to find one with this method – it is then the only one.

## 6.2 Cusps

In general, the solutions are not regular at the matching point, but have a cusp (branch point) there: $\delta(s) = \delta(s_0) + C(s_0 - s)^\gamma + \ldots$, with $\gamma > 0$. The phenomenon arises from our formulation of the problem – the physical amplitude is regular there. We conclude that, even if a mathematical solution can be constructed for a given input $\{a, A(s)\}$, it will in general not be acceptable physically, because it contains a fictitious singularity at the matching point. The behaviour of the phase is sensitive to the value of the exponent: If $\gamma$ is close to 1, the discontinuity in the derivative is barely visible, while for small values of $\gamma$, it manifests itself very clearly.

The strength of the singularity is determined by the constant $C$, whose value depends on the input used. In particular, if the scattering length $a$ is varied, while the absorptive part $A(s)$ is kept fixed, the size of $C$ changes. We may search for the value of $a$ at which $C$ vanishes. Although the singularity does not disappear entirely even then, it now only manifests itself in the derivatives of the function (for the solution to become analytic at $s_0$, we would need to also adapt the input for $A(s)$). In view of the fact that our solutions are inherently fuzzy, because the values of the input are subject to experimental uncertainties, we consider solutions with $C \simeq 0$ or $\gamma \simeq 1$ as physically acceptable and refer to these as solutions without cusp.

The search for solutions without cusp can be implemented as follows. Instead of fixing $a$, constructing solutions in the class of functions with a cusp and then determining the value of $a$ at which the cusp disappears, we may simply consider parametrizations that do not contain a cusp, treating the scattering length $a$ as a free parameter, on the same footing as the set $c_1, \ldots, c_n$ used to parametrize the phase shift and minimizing the difference between the left and right hand sides of eq. (6.1). We have verified that if a solution without cusp does exist, this procedure indeed finds it: Allowing for the presence of cusps does not lead to a better minimum.

The net result of this discussion is that the scattering length $a$ must match the input for $A(s)$ – it does not represent an independent parameter. When

| | range of $s_0$ | range of $\delta_0^0$ | range of $\delta_1^1$ | $m$ |
|---|---|---|---|---|
| I | $1 < \sqrt{s_0} < 1.15$ | $\pi < \delta_0^0 < \frac{3}{2}\pi$ | $\frac{1}{2}\pi < \delta_1^1 < \pi$ | 2 |
| II | $0.86 < \sqrt{s_0} < 1$ | $\frac{1}{2}\pi < \delta_0^0 < \pi$ | $\frac{1}{2}\pi < \delta_1^1 < \pi$ | 1 |
| III | $0.78 < \sqrt{s_0} < 0.86$ | $0 < \delta_0^0 < \frac{1}{2}\pi$ | $\frac{1}{2}\pi < \delta_1^1 < \pi$ | 0 |
| IV | $0.28 < \sqrt{s_0} < 0.78$ | $0 < \delta_0^0 < \frac{1}{2}\pi$ | $0 < \delta_1^1 < \frac{1}{2}\pi$ | $-1$ |

Table 1: Multiplicity of solutions in the coupled channel case. The multiplicity index $m$ is the number of free parameters occurring in the solutions of the Roy equations, if the matching point $s_0$ is in the interval indicated (in GeV units). Also displayed is the variation of the physical phases $\delta_0^0$ and $\delta_1^1$ on that interval.

solving the Roy equations, we can at the same time also determine the value of $a$ that belongs to a given input for the high energy absorptive part. The conclusion remains valid even if the matching point is above the first inelastic threshold, provided the elasticity parameter $\eta$ is known and sufficiently smooth at the matching point. For a thorough analysis of the issue, we refer to [31].

## 6.3 Uniqueness in the multi-channel case

In the multichannel case, we need to determine three functions $\delta_0^0, \delta_1^1$ and $\delta_0^2$ for a given input $\{a_0^0, a_0^2, f_\ell^I, \eta_\ell^I, d_\ell^I\}$. The multiplicity index $m$ of the infinitesimal neighbourhood of a given solution is displayed in table 1 [31], for various values of the matching point $s_0$. The table contains the following information. In the situations indicated with the labels I and II, the infinitesimal neighbourhood of a given solution contains a family of solutions, characterized by 2 and 1 free parameters, respectively. In case III, the solution is unique in the sense that the neighbourhood does not contain further solutions, while in case IV a solution only exists if the input is subject to a constraint ($m = -1$, compare paragraph 3 in section 6.1). In order to uniquely characterize the solution in case I, for instance, we thus need to fix two more parameters – in addition to the input – say the position of the $\rho$ resonance and its width, or the position of the $\rho$ resonance and the value of $s$ where the $I = 0$ phase passes through $\pi/2$, and similarly for II. In the following, we stick to case III, where the solution is unique for a given input. As discussed above, each of the three partial waves will in general develop a cusp at the matching point $s_0$, unless some of the input parameters take special values.

The situation encountered in practice is the following. Let $0.1 < a_0^0 < 0.6$, and let $f_\ell^I$, $\eta_\ell^I$ and $d_\ell^I$ be fixed as well. For an arbitrary value of the scattering length $a_0^2$, the solution in general develops a strong cusp in the $P$-wave. This cusp can be removed by tuning $a_0^2 \to \bar{a}_0^2$, using for instance the method described in the single channel case above. Remarkably, it turns out that the solutions so obtained are nearly free of cusps in the two $S$-waves as well. The problem manifests itself almost exclusively in the $P$-wave, because our matching point is

rather close to the mass of the $\rho$, where the imaginary part shows a pronounced peak. If $a_0^2$ is chosen to slightly differ from the optimal value $\bar{a}_0^2$, a cusp in the $P$-wave is clearly seen. We thus obtain a relation between the scattering lengths $a_0^0$ and $a_0^2$. This is how the so-called *universal curve*, discovered a long time ago [44], shows up in our framework. We will discuss the properties of this curve in detail below.

In principle, we might try to also fix $a_0^0$ with this method, requiring that there be no cusp in one of the two $S$-waves. The cusps in these are very weak, however – the procedure does not allow us to accurately pin down the second scattering length. The choice $a_0^0 = -0.2$, for instance, still leads to a fully acceptable solution. On the other hand, we did not find a solution in the class of smooth functions for $a_0^0 = -0.5$. This shows that the analyticity properties that are not encoded in the Roy integral equations (5.1) do constrain the range of admissible values for $a_0^0$, but since that range is very large, the constraint is not of immediate interest, and we do not consider the matter further. In our numerical work, we consider values in the range $0.15 < a_0^0 < 0.30$ and use the center of this interval, $a_0^0 = 0.225$, as our reference point.

# 7 Experimental input

In this section, we describe the experimental input used for the elasticity below the matching point at $\sqrt{s_0} = 0.8\,\mathrm{GeV}$ and for the imaginary parts of the $S$- and $P$-waves in the energy interval between $\sqrt{s_0}$ and $\sqrt{s_2} = 2\,\mathrm{GeV}$. The references are listed in [45]–[59] and for an overview, we refer to [9, 60]. The evaluation of the contributions from the higher partial waves and from the asymptotic region ($s > s_2$) is discussed in detail in appendix B.

## 7.1 Elasticity below the matching point

The Roy equations allow us to determine the phase shifts of the $S$- and $P$-waves only if – on the interval between threshold and the matching point – the corresponding elasticity parameters $\eta_0^0(s)$, $\eta_1^1(s)$ and $\eta_0^2(s)$ are known. On kinematic grounds, the transition $2\pi \to 4\pi$ is the only inelastic channel open below our matching point, $\sqrt{s_0} = 0.8\,\mathrm{GeV}$. The threshold for this reaction is at $E = 4\,M_\pi \simeq 0.56\,\mathrm{GeV}$, but phase space strongly suppresses the transition at low energies – a significant inelasticity only sets in above the matching point. In particular, the transition $\pi\pi \to K\bar{K}$, which occurs for $E > 2\,M_K \simeq 0.99\,\mathrm{GeV}$, does generate a well-known, pronounced structure in the elasticity parameters of the waves with $I = 0, 1$. Below the matching point, however, we may neglect the inelastic reactions altogether and set

$$\eta_0^0(s) = \eta_1^1(s) = \eta_0^2(s) = 1 \quad , \qquad \sqrt{s} < 0.8\,\mathrm{GeV} \quad .$$

We add a remark concerning the effects generated by the inelastic reaction $2\pi \to 4\pi$, which are analyzed in ref. [57]. In one of the phase shift analyses given there (solution A), the inelasticity $1 - \eta_1^1(s)$ reaches values of order 4%, already in the region of the $\rho$-resonance. The effect is unphysical – it arises because the parametrization used does not account for the strong phase space suppression at the $4\pi$ threshold[4]. For the purpose of the analysis performed in ref. [57], which focuses on the region above 1 GeV, this is immaterial, but in our context, it matters: We have solved the Roy equations also with that representation for the elasticities. The result shows significant distortions, in particular in the $P$-wave.

## 7.2 Input for the $I = 0, 1$ channels

The experimental information on the $\pi\pi$ phase shifts in the intermediate energy region comes mainly from the reaction $\pi N \to \pi\pi N$. A rather involved analysis is necessary to extract the $\pi\pi$ phase shifts from the raw data, and several different representations for the phases and elasticities are available in the literature. The main source of experimental information is still the old measurement of the reaction $\pi^- p \to \pi^-\pi^+ n$ by the CERN–Munich (CM) collaboration [49], but there are also older, statistically less precise data, for instance from Saclay [45] and Berkeley [48], as well as newer ones, such as the data of the CERN-Cracow-Munich collaboration concerning pion production on polarized protons [54] and those on the reaction $\pi^- p \to \pi^0\pi^0 n$, obtained recently by the E852 collaboration at Brookhaven [59]. For a detailed discussion of the available experimental information, we refer to [9, 57, 60].

For our purposes, energy-dependent analyses are most convenient, because these yield analytic expressions for the imaginary parts, so that the relevant integrals can readily be worked out. To illustrate the differences between these analyses, we plot the corresponding imaginary parts in fig. 3, both for the $I = 0$ $S$-wave and for the $P$-wave. The representations of refs. [47, 55, 57] do not extend to 2 GeV, but they do cover the range between 0.8 and 1.7 GeV. Unitarity ensures that the contributions generated by the imaginary parts of the $S$- and $P$-waves in the region between 1.7 and 2 GeV are very small, so that we may use these representations also there without introducing a significant error. For the $P$-wave, the differences between the various parametrizations are not dramatic, but for the $I = 0$ $S$-wave, they are quite substantial. Despite these differences, the result obtained for the dispersive integrals are similar, at least in the range where we are solving the Roy equations. This can be seen in fig. 4, where we plot the value of the dispersion integral $f_0^0$, defined in eq. (5.2). The only visible difference is between parametrization B of ref. [57] and the others. In order of magnitude, the effect is comparable to the one occurring if the scattering length $a_0^0$ is shifted by 0.01. It arises from the difference in the behaviour of the $S$-wave imaginary part

[4] We thank Wolfgang Ochs for this remark.

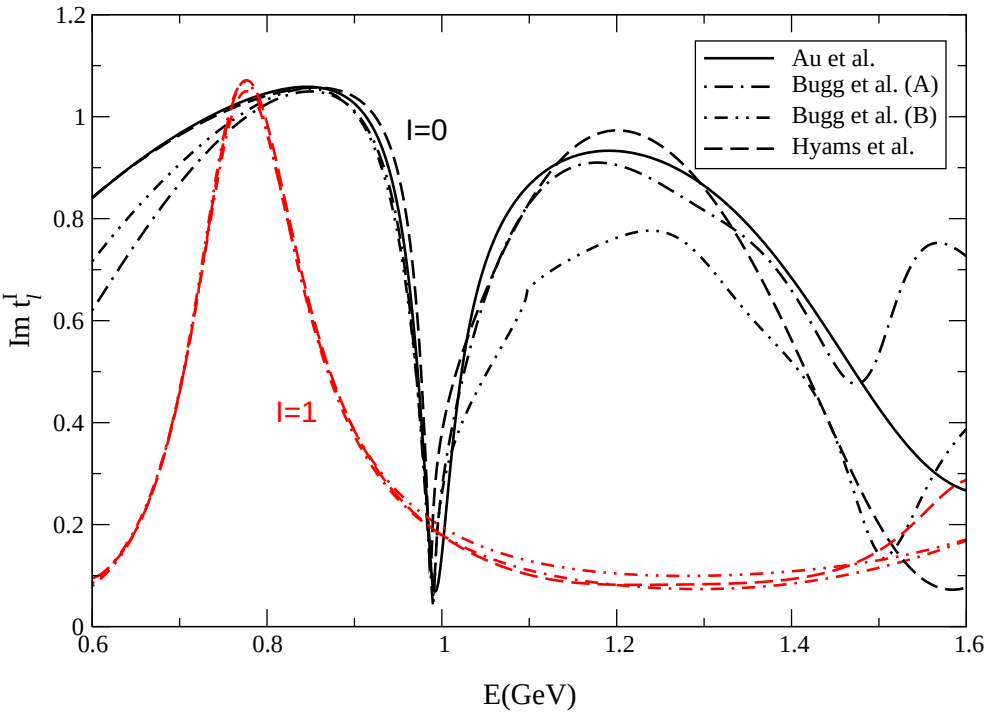


Figure 3: Comparison of the different input we used for the imaginary parts of the $I = 0$ and $I = 1$ lowest partial waves above the matching point at 0.8 GeV.

in the region between 1 and 1.5 GeV. The phase shift analysis of Protopopescu et al. [48] does not cover that region, as it only extends to 1.15 GeV, but those of Au, Morgan and Pennington [55] as well as Bugg, Sarantsev and Zou [57] do. Both of these include, aside from the CM data, additional experimental information, not included in the analysis of Hyams et al. [47].

In the following, we rely on the representation of Au et al. [55] for the $S$-wave and the one of Hyams et al. [47] for the $P$-wave (the analysis of Au et al. does not include the $P$-wave). We have verified that, using [47] also for the $S$-wave would not change our results below the matching point, beyond the uncertainties to be attached to the solutions, anyway. On the other hand, Au et al. [55] yield a more consistent picture above the matching point – for this reason we stick to that analysis. More precisely, we use the solution denoted by $K_1$(Etkin) in ref. [55], table I. That solution contains a narrow resonance in the 1 GeV region, which does not occur in the other phase shift analyses. In our opinion, the extra state is an artefact of the representation used: A close look reveals that the occurrence of this state hinges on small details of the $K$-matrix representation. In fact, the resonance disappears if two of the $K$-matrix coefficients are slightly modified, for instance with $(-c_{12}^0, -c_{22}^0) = (3.1401, 2.8447) \to (3.2019, 2.6023)$.

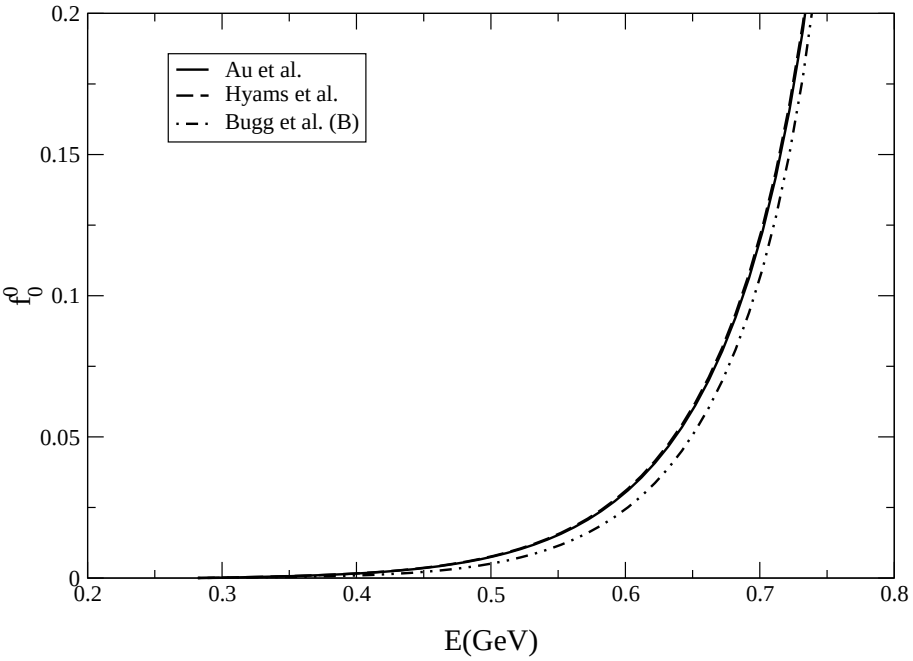


Figure 4: Comparison of the results obtained for the dispersion integral $f_0^0$ with the various imaginary parts shown in fig. 3.

## 7.3 Phase of the $P$-wave from $e^+e^- \to \pi^+\pi^-$ and $\tau \to \pi^-\pi^0\,\nu_\tau$

For the $P$-wave, the data on the processes $e^+e^- \to \pi^+\pi^-$ and $\tau \to \pi^-\pi^0\,\nu_\tau$ yield very useful, independent information. The corresponding transition amplitude is proportional to the pion form factor $F_{e.m.}(s)$ of the electromagnetic current and to the form factor $F_V(s)$ of the charged vector current, respectively. The data provide a measurement of the quantities $|F_{e.m.}(s)|$ and $|F_V(s)|$ in the time-like region, $s > 4M_\pi^2$.

In the isospin limit, the two form factors coincide: The currents only differ by an isoscalar operator that carries odd $G$-parity, so that the pion matrix elements thereof vanish. While the isospin breaking effects in $|F_V(s)|$ are very small, $\rho-\omega$ interference does produce a pronounced structure in the electromagnetic form factor. The $\omega$-resonance generates a second sheet pole in the isoscalar matrix elements, at $s = (M_\omega - i\,\frac{1}{2}\,\Gamma_\omega)^2$. The residue of the pole is small, of order $O(m_d - m_u, e^2)$, but in view of the small width of the $\omega$, the denominator also nearly vanishes for $s = M_\omega^2$. Moreover, the pole associated with the exchange of a $\rho$ occurs in the immediate vicinity of this point, so that the transition amplitude involves a sum of two contributions that rapidly change with $s$, both in magnitude and phase. Since the interference phenomenon is well understood, it can be corrected for. When this is done, the data on the two processes $e^+e^- \to \pi^+\pi^-$ and $\tau \to \pi^-\pi^0\nu$ are in remarkably good agreement (for a review, see [61, 62]).

We denote the phase of the vector form factor by $\phi(s)$,

$$F_V(s) = |F_V(s)|\, e^{\,i\,\phi(s)} \quad .$$

In the elastic region $4M_\pi^2 < s < 16M_\pi^2$, the final state interaction exclusively involves $\pi\pi$ scattering, so that the Watson theorem implies that the phase $\phi(s)$ coincides with the $P$-wave phase shift,

$$\phi(s) = \delta_1^1(s) \quad , \qquad 4M_\pi^2 < s < 16M_\pi^2 \quad .$$

In fact, phase space suppresses the inelastic channels also in this case – the available data on the decay channel $\tau \to 4\,\pi\,\nu_\tau$ show that, for $E < 0.9\,\mathrm{GeV}$, the inelasticity is below 1%, so that the phase of the form factor must agree with the $P$-wave phase shift, to high accuracy [63].

In the region where the singularity generated by $\rho$-exchange dominates, in particular also in the vicinity of our matching point, the form factor is well represented by a resonance term and a slowly varying background. Quite a few such representations may be found in the recent literature. Since the uncertainties in the data (statistical as well as systematic) are small, these parametrizations agree quite well. In the following, we use the Gounaris-Sakurai representation of ref. [64] as a reference point. That representation involves a linear superposition of three resonance terms, associated with $\rho(770)$, $\rho(1450)$ and $\rho(1700)$. We have investigated the uncertainties to be attached to this representation by (a) comparing the magnitude of the form factor with the available data[5], (b) comparing it with other parametrizations, (c) varying the resonance parameters in the range quoted in ref. [64] and (d) using the fact that analyticity imposes a strong correlation between the phase of the form factor and its magnitude. On the basis of this analysis, we conclude that the $e^+e^-$ and $\tau$ data determine the phase of the $P$-wave at $0.8\,\mathrm{GeV}$ to within an uncertainty of $\pm 2^\circ$. A detailed comparison between the phase of the form factor and the solution of the Roy equations for the $P$-wave will be given in section 12.2.

## 7.4 Phases at the matching point

In the framework of our analysis, the input used for $s \geq s_0$ enters in two ways: (i) it specifies the value of the three phases at the matching point and (ii) it determines the contributions to the Roy equation integrals from the region above that point. Qualitatively, we are dealing with a boundary value problem: At threshold, the phases vanish, while at the matching point, they are specified by the input. The solution of the Roy equations then yields the proper interpolation between these boundary values. The behaviour of the imaginary parts above the matching point is less important than the boundary values, because it only affects the slope and the curvature of the solution.

[5] We are indebted to Simon Eidelman and Fred Jegerlehner for providing us with these.

| $\delta_0^0$ | $\delta_1^1$ | $\delta_1^1 - \delta_0^0$ | reference |
|---|---|---|---|
| 81.7 ± 3.9 | 105.2 ± 1.0 | 23.4 ± 4.0 | [46, 47] |
| 90.4 ± 3.6 | 115.2 ± 1.2 | 24.8 ± 3.8 | [50] s-channel moments |
| 85.7 ± 2.9 | 116.0 ± 1.8 | 30.3 ± 3.4 | [50] t-channel moments |
| 81.6 ± 4.0 | 108.1 ± 1.4 | 26.5 ± 4.2 | [48] table VI |
| 80.9 | 105.9 | 25.0 | [46, 47] |
| 79.5 | 106.1 | 26.5 | [57] solution A |
| 79.9 | 106.8 | 26.9 | [57] solution B |
| 80.7 | – | – | [55] solution $K_1$ |
| 82.0 | – | – | [55] solution $K_1$(Etkin) |

Table 2: Value of the phases $\delta_0^0$ and $\delta_1^1$ at 0.8 GeV. The first three rows stem from analyses of the data at a fixed value of the energy ("energy independent"), while the remaining entries are obtained from a fit to the data that relies on an explicit parametrization of the energy dependence ("energy dependent analysis").

We now discuss the available information for the phases $\delta_0^0$ and $\delta_1^1$ at the matching point. The values obtained from the high energy, high statistics $\pi N \to \pi\pi N$ experiments are collected in table 2. In those cases where the published numbers do not directly apply at 0.8 GeV, we have used a quadratic interpolation between the three values of the energy closest to this one. The errors given in the third column are obtained by adding those from the first two columns in quadrature. For the energy dependent entries, the error analysis is more involved – only ref. [48] explicitly quotes an error. The scatter seen in the table partly arises from the fact that different methods of analysis are used. The corresponding systematic uncertainties are not covered by the error bars quoted in the individual phase shift analyses: Taken at face value, the numbers listed in the table are contradictory, particularly in the case of the $P$-wave. For a thorough discussion of the experimental discrepancies, we refer to [60].

As discussed above, both the statistical and the systematic uncertainties of the $e^+e^-$ and $\tau$ data are considerably smaller. They constrain the phase of the $P$-wave at 0.8 GeV to a narrow range, centered around the value $\delta_1^1(s_0) = 108.9^\circ$ obtained with the Gounaris-Sakurai representation of the form factor in ref. [64]:

$$\delta_1^1(s_0) = 108.9^\circ \pm 2^\circ \quad . \tag{7.1}$$

The comparison with the numbers listed in the second column of the table shows that this value is within the range of the results obtained from $\pi N \to \pi\pi N$.

Unfortunately, the $e^+e^-$ and $\tau$ data only concern the $P$-wave. To pin down the $I = 0$ $S$-wave, we observe that the overall phase of the scattering amplitude drops out when considering the difference $\delta_1^1 - \delta_0^0$, so that one of the sources of systematic error is absent. Indeed, the third column in the table shows that the outcome of the various analyses is consistent with the assumption that the

fluctuations seen are of statistical origin. The statistical average of the energy independent analyses yields $\delta_1^1(s_0) - \delta_0^0(s_0) = 26.6^\circ \pm 3.7^\circ$, with $\chi^2 = 2$ for 2 degrees of freedom (as the numbers are based on the same data, we have inflated the error bar – the number given is the mean error of the three data points). The remaining entries in the table neatly confirm this result. Combining it with the one in the fourth row, which is based on independent data, we finally arrive at

$$\delta_1^1(s_0) - \delta_0^0(s_0) = 26.6^\circ \pm 2.8^\circ \quad . \tag{7.2}$$

Since the value for $\delta_1^1$ comes from the data on the form factor, while the one for the difference $\delta_1^1 - \delta_0^0$ is based on the reaction $\pi N \to \pi\pi N$, these numbers are independent, so that it is legitimate to combine them. Adding errors quadratically, we obtain

$$\delta_0^0(s_0) = 82.3^\circ \pm 3.4^\circ \quad . \tag{7.3}$$

In the following, we rely on the two values for the phases at the matching point given in eqs. (7.1) and (7.3). We emphasize that the $\pi N \to \pi\pi N$ data are consistent with these – in fact, the result of the energy-dependent analysis quoted in the fourth row of the table is in nearly perfect agreement with the above numbers. We are exploiting the fact that the $e^+e^-$ and $\tau$ data strongly constrain the behaviour of the $P$-wave in the region of the $\rho$, thus reducing the uncertainties in the value of $\delta_1^1$ at the matching point.

For the principal value integrals to exist, we need to continuously connect the values of the imaginary parts calculated from the phases at the matching point with those of the phase shift representation we wish to use. This can be done, either by slightly modifying the parameters occurring in the representation in question or with a suitable interpolation of the phases between the matching point and $K\bar{K}$ threshold. We have checked that our results do not depend on how that is done, as long as the interpolation is smooth. Note that, for the representation $K_1$(Etkin) [55] – our reference input for the imaginary part of the $I = 0$ $S$-wave – an interpolation is not needed: The last row of table 2 shows that, at the matching point, this representation nearly coincides with the central value in eq. (7.3).

## 7.5 Input for the $I = 2$ channel

The uncertainties in this channel are rather large. The current experimental situation is summarized in fig. 5, where we show the data points from the two main experiments [51, 53], and five different parametrizations that we will use as input. The central one is our best fit to the data of the Amsterdam–CERN–Munich collaboration (ACM) [53] solution B (which we call from now on ACM(B)) with a parametrization *à la* Schenk [65]. To cover the rather wide scatter of the data, we have varied the input in this channel, using the five curves shown in the figure,

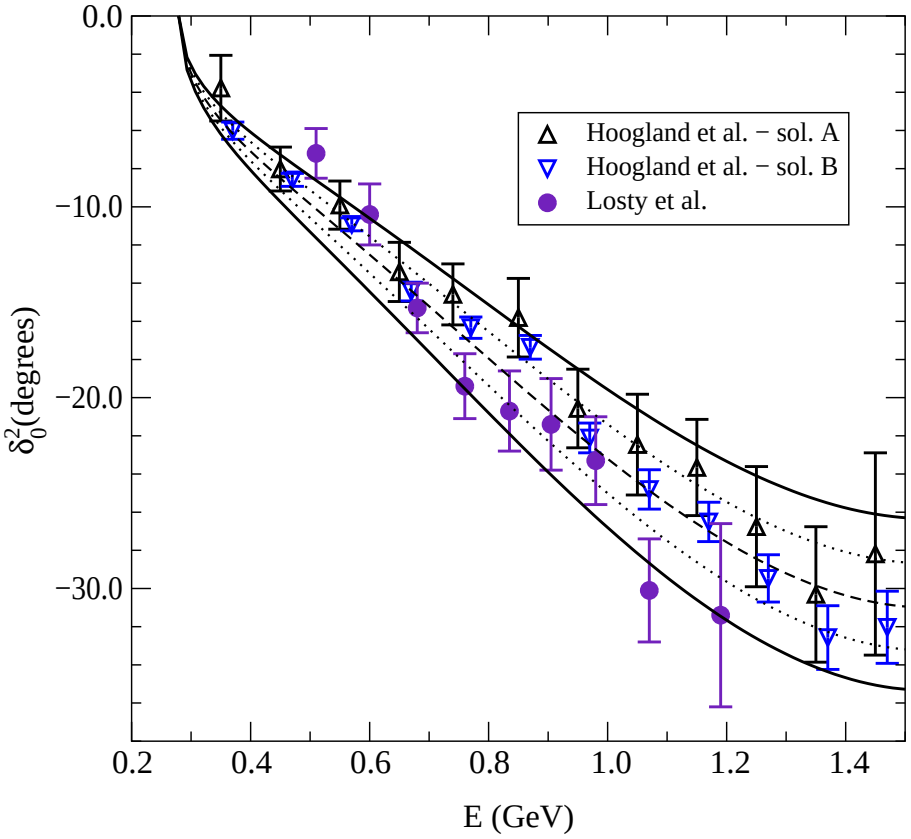


Figure 5: Different data sets for the $S$-wave in the $I = 2$ channel and curves that we have used as input in the Roy equation analysis.

together with $\eta_0^2 = 1$ (note that for the Roy equation analysis, only the value of the scattering length $a_0^2$ and the behaviour of the imaginary part above 0.8 GeV matter).

# 8 Numerical solutions

In the preceding section, the input required to evaluate the r.h.s. of our system of equations was discussed in detail. In the present section, we describe the numerical method used to solve this system and illustrate the outcome with an example.

## 8.1 Method used to find solutions

We search for solutions of the Roy equations by numerically minimizing the square of the difference between the left and right hand sides of eq. (5.1) in the region between threshold and 0.8 GeV. As we are neglecting the inelasticity in this

region, the real and imaginary parts of $t_\ell^I(s)$ are determined by a single real function, the phase $\delta_\ell^I(s)$. In principle, the minimization should be performed over the whole space of physically acceptable functions $\{\delta_0^0(s),\ \delta_1^1(s),\ \delta_0^2(s)\}$, but for obvious practical reasons we restrict ourselves to functions described by a simple parametrization. We will use the one proposed by Schenk some time ago [65], allowing for an additional parameter in the polynomial part:

$$\tan\delta_\ell^I = \sqrt{1-\frac{4M_\pi^2}{s}}\, q^{2\ell}\left\{A_\ell^I + B_\ell^I q^2 + C_\ell^I q^4 + D_\ell^I q^6\right\}\left(\frac{4M_\pi^2 - s_\ell^I}{s-s_\ell^I}\right)\ , \qquad (8.1)$$

The first term represents the scattering length, while the second is related to the effective range:

$$a_\ell^I = A_\ell^I\ , \qquad b_\ell^I = B_\ell^I + \frac{4}{s_\ell^I - 4M_\pi^2}\,A_\ell^I - \frac{1}{M_\pi^2}\left(A_\ell^I\right)^3\delta_{\ell 0}\ . \qquad (8.2)$$

In each channel, one of the five parameters is fixed in order to ensure the proper value of the phase at $s_0$. Moreover the $S$-wave scattering lengths $a_0^0$ and $a_0^2$ are identified with the two constants that specify the subtraction polynomials in the Roy equations. As discussed in sect. 6, we need to tune the value of $a_0^2$ in order to avoid cusps. Treating this parameter on the same footing as the others, we are dealing altogether with $15-3-1=11$ free variables, to be determined by a minimization procedure. Our choice of $s_0$ ensures that the solution is unique, and therefore the method is safe: The choice of a bad parametrization would manifest itself in a failure of the minimization method – the minimum would not yield a decent solution.

The square of the difference between the left and right hand sides of the Roy equations is calculated at 22 points between threshold and $s_0$ for each of the three waves, so that the sum of squares ($\Delta^2_{\rm Roy}$) contains 66 terms. The minimization of the function ($\Delta^2_{\rm Roy}$) over 11 parameters can be handled by standard numerical routines [66]. Our procedure does generate decent solutions: The differences between the left and right hand sides of the Roy equations are not visible on our plots – they are typically of order $10^{-3}$. The equations could be solved even more accurately by allowing for more degrees of freedom in the parametrization of the phases, but, in view of the uncertainties in the input, the accuracy reached is perfectly sufficient. Note also that the exact solution corresponding to a given input contains cusps. We have checked that these are too small to matter: Enlarging the space of functions on which the minimum is searched by explicitly allowing for such cusps in the parametrization of the phases, we find that the solutions remain practically the same.

## 8.2 Illustration of the solutions

To illustrate various features of our numerical solutions, we freeze for a moment all the inputs and analyze the properties of the specific solution we then get.

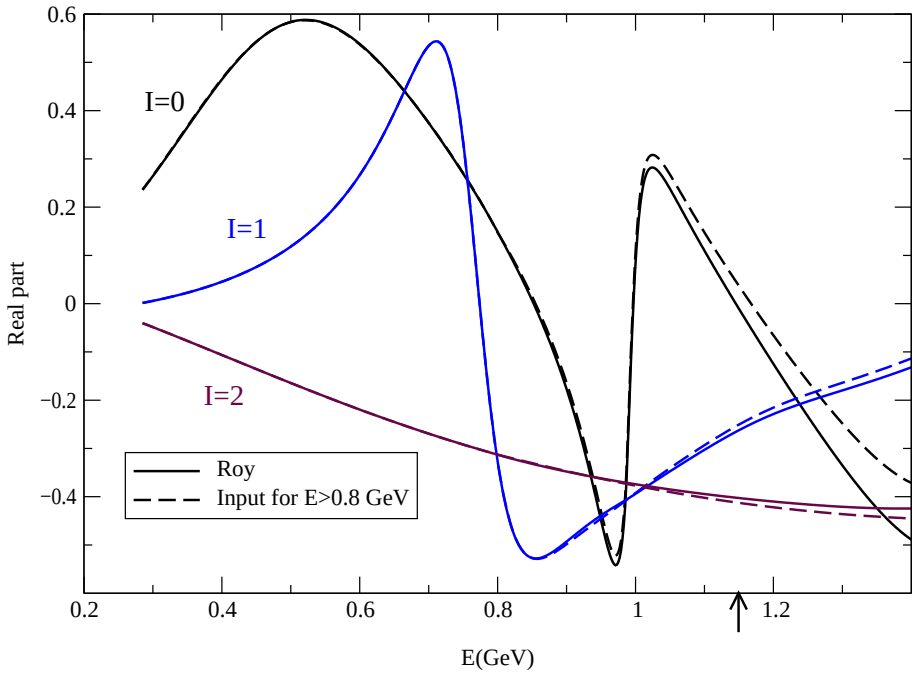


Figure 6: Numerical solution of the Roy equations for $a_0^0 = 0.225$, $a_0^2 = -0.0371$ (the value of $a_0^0$ corresponds to the center of the range considered while the one of $a_0^2$ results if the input used for $\mathrm{Im}\, t_0^2$ is taken from the central curve in fig. 5). The arrow indicates the limit of validity of the Roy equations.

The input for the imaginary parts above $s_0$ is the following: For the $I = 0$ wave, we use the parametrization labelled $K_1$ (Etkin) of Au et al. [55]. In the case of the $I = 1$ wave, we rely on the energy–dependent analysis of Hyams et al. [47], smoothly modified between $s_0$ and $4M_K^2$ to match the value $\delta_1^1(s_0) = 108.9°$. For the $I = 2$ wave, we take the central curve in fig. 5. The driving terms are specified in eq. (4.1). Moreover we fix $a_0^0 = 0.225$. With this input, the minimization leads to $a_0^2 = -0.0371$ and the Schenk parameters take the values listed in table 3, in units of $M_\pi$.
The plot in fig. 6 shows that the numerical solution is indeed very good: Below $s_0$, it is not possible to distinguish the two curves representing the right and left

| | $I = 0$ | $I = 1$ | $I = 2$ |
|---|---|---|---|
| $A_\ell^I$ | 0.225 | $3.63 \cdot 10^{-2}$ | $-3.71 \cdot 10^{-2}$ |
| $B_\ell^I$ | 0.246 | $1.34 \cdot 10^{-4}$ | $-8.55 \cdot 10^{-2}$ |
| $C_\ell^I$ | $-1.67 \cdot 10^{-2}$ | $-6.98 \cdot 10^{-5}$ | $-7.54 \cdot 10^{-3}$ |
| $D_\ell^I$ | $-6.40 \cdot 10^{-4}$ | $1.41 \cdot 10^{-6}$ | $1.99 \cdot 10^{-4}$ |
| $s_\ell^I$ | 36.7 | 30.7 | −11.9 |

Table 3: Schenk parameters of the solution shown in fig. 6.

hand sides of eq. (5.1). For this solution we found as a minimum $\Delta^2_{\rm Roy} = 2.1 \cdot 10^{-5}$, which corresponds to an average difference between the right and left hand sides of about $6 \cdot 10^{-4}$.

Having solved the Roy equations in the low–energy region, we now have a representation for the imaginary parts of the three lowest partial waves from threshold up to $s_2$. Since the driving terms account for all remaining contributions, we can then calculate the Roy representation for the real parts from threshold up to 1.15 GeV (full lines in fig.6). On the same plot, above $s_0$, we also show the real part of the partial wave representation that we used as an input for the imaginary parts (dashed lines). The comparison shows that the input we are using is well compatible with the Roy equations (we should stress at this point that in none of the phase–shift analyses which we are using as input the Roy equations have been used).

# 9 Universal band

As we have discussed in the preceding sections, for a given value of $a_0^0$ and fixed input, the Roy equations admit a solution without cusp only for a single value of $a_0^2$. By varying the input value of $a_0^0$, the Roy equations define a function $a_0^2 = F(a_0^0)$ that is known in the literature as the "universal curve" [44]. The experimental uncertainties in the input above 0.8 GeV convert this curve into a band. The universal band is the area in the $(a_0^0, a_0^2)$ plane that is allowed by the constraints given by the $\pi\pi$–scattering data above 0.8 GeV and the Roy equations. In this section we give a more precise definition of our universal band, and calculate it accordingly.

We first point out that the universal curve $a_0^2 = F(a_0^0)$ depends rather mildly on the input in the $I = 0$ and $I = 1$ channel (a more quantitative statement concerning this dependence is given below). For this reason, we only consider the uncertainties in the input for the $I = 2$ channel. The available data in this channel are shown in fig. 5, together with five different curves that we have used as input. For each one of these, we obtain a universal curve, which nearly represents a straight line in the $(a_0^0, a_0^2)$ plane. The resulting five lines are shown in fig. 7. The central one is well represented by the following second degree polynomial:

$$a_0^2 = -0.0849 + 0.232\, a_0^0 - 0.0865\, (a_0^0)^2 \quad . \tag{9.1}$$

The analogous representations for the top and bottom lines read:

$$\begin{aligned} a_0^2 &= -0.0774 + 0.240\, a_0^0 - 0.0881\, (a_0^0)^2 \quad , \\ a_0^2 &= -0.0922 + 0.225\, a_0^0 - 0.0847\, (a_0^0)^2 \quad . \end{aligned} \tag{9.2}$$

The region between these two solid lines is our universal band. It is difficult to make a precise statement in probabilistic terms of how unlikely it is that

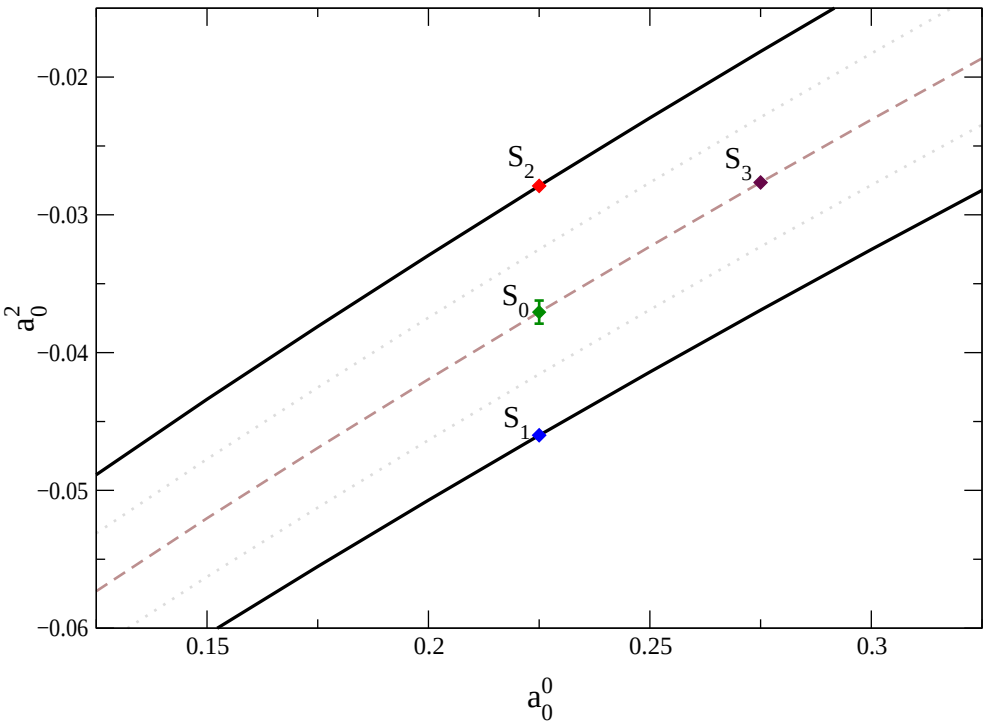


Figure 7: Universal band. The five lines correspond to the five different curves shown in fig. 5 (the top line, for instance, results if the input for $\mathrm{Im}\, t_0^2$ in the region above 0.8 GeV is taken from the top curve in that figure). $S_0$ marks our reference point: $a_0^2 = 0.225$, $a_0^2 = -0.0371$. The bar attached to it indicates the uncertainty in $a_0^2$ due to the one in the phase $\delta_0^0$ at the matching point – the most important remaining source of error if the input for $\mathrm{Im}\, t_0^2$ is held fixed.

the physical values of the two scattering lengths are outside this band. With our rather generous choice of the two extreme curves, we consider it fair to say that the experimental information above the matching point essentially excludes such values. In fact, we will argue below that the theoretical constraints arising from the consistency of the Roy equations above the matching point restrict the admissible region even further.

We now turn to the dependence of the universal curve $a_0^2 = F(a_0^0)$ on the input in the $I = 0$ and $I = 1$ channels, keeping the one for $I = 2$ fixed. Changes in the input above $2M_K$ are practically invisible at threshold: If we keep the phase shifts at the matching point fixed, the three different available inputs for the $I = 0$ and $I = 1$ channels yield values of $a_0^2$ that differ by less than one permille. The phase shifts at $s_0$ are the only relevant factor here. Moreover, for the value of $a_0^2$, $\delta_0^0(s_0)$ is much more important than $\delta_1^1(s_0)$: Shifts of $\delta_1^1(s_0)$ by $\pm 2^\circ$ change the value of $a_0^2$ roughly by a permille, but a change by $\pm 3.4^\circ$ in $\delta_0^0(s_0)$ induces a shift of $\Delta a_0^2 = \pm 8.4 \cdot 10^{-4}$, which amounts to two percent. Even so, this is much smaller than the width of the band, as can be seen in fig. 7.

We have also varied $\sqrt{s_0}$ within the bounds 0.78 and 0.86 GeV and found that the dependence of the relation $a_0^2 = F(a_0^0)$ on $s_0$ is rather weak. To exemplify, we mention that for the solution with $a_0^0 = 0.25$ at the center of the universal band, a shift from $\sqrt{s_0} = 0.8$ GeV to 0.85 GeV changes $a_0^2$ by $10^{-3}$.

# 10 Consistency

It takes a good balancing of the various terms occurring in the Roy equations for the partial waves not to violate the unitarity limit. In the case of the $S$-wave with $I = 0$, for instance, the contribution to $\mathrm{Re}\, t_0^0$ that arises from the subtraction term $k_0^0(s)$ is very large already at 1 GeV: The solution shown in fig. 6 corresponds to $a_0^0 = 0.225$ and $a_0^2 = -0.0371$, so that $k_0^0(s) = 2.7$ for $s = 1\,\mathrm{GeV}^2$. As the energy grows, the term increases and reaches $k_0^0(s_1) = 3.6$ at the upper end of the region where our equations are valid, $s_1 = 68\, M_\pi^2$. Unless the contributions from the dispersion integrals nearly compensate the subtraction term, the unitarity limit, $|\,\mathrm{Re}\, t_0^0\,| \leq (2\sigma)^{-1} \simeq \frac{1}{2}$ is violated. The example in fig. 6 demonstrates that we do find solutions for which such a cancellation takes place, with values of $a_0^0$, $a_0^2$ that are within the universal band.

It is striking that, above the matching point, this solution very closely follows the real part of the input. In a restricted sense, this is necessary for the solution to be acceptable physically: The solution is obtained by identifying the imaginary part above the matching point with the one obtained from a particular representation of the partial waves. The Roy equations then determine the real part of the amplitude in the region below $\sqrt{s_1} = 1.15\,\mathrm{GeV}$. If the result were very different from the real part of the particular representation used, we would have to conclude that this representation cannot properly describe the physics. This amounts to a consistency condition: Above the matching point, the Roy solution should not strongly deviate from the real part of the input. The condition can be met only if the cancellation discussed above takes place, but it is stronger. The example in fig. 6 demonstrates that there are solutions that obey the consistency condition remarkably well, indicating that our apparatus is indeed working properly.

We will discuss the consistency condition on a quantitative level below. Before entering this discussion, we briefly comment on a different aspect of our framework: the stability of the solutions. The behaviour below 0.8 GeV is not sensitive to the uncertainties in the input used for the imaginary parts above 1 GeV. We can modify that part of the input quite substantially, and without changing anything else (not even below $s_0$) still get a decent solution from threshold up to the limit of validity of our equations. Naturally, if we do not modify the Schenk parameters that define the phase below $s_0$, the Roy equations are not strictly obeyed, but the deviation from the true solution is quite small. The reason is that, if $s$ is small, the kernels $K_{\ell\ell'}^{II'}(s,s')$ strongly suppress the contributions from

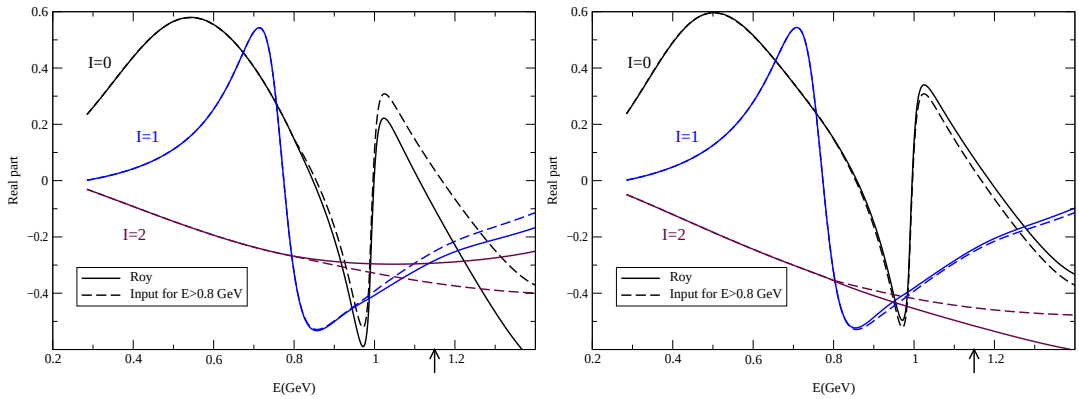


Figure 8: Solutions of the Roy equations for $a_0^0 = 0.225$ and two extreme values for $a_0^2$. The left figure corresponds to the point $S_2$ in fig.7, while the one on the right shows the solution for $S_1$. The arrows indicate the limit of validity of the Roy equations.

the region where $s'$ is large. The term $K_{00}^{00}(s,s')$, for instance, has the following expansion for $s' \gg s$:

$$K_{00}^{00}(s,s') = \frac{1}{9}\left\{11s^2 - 10s(4M_\pi^2) - (4M_\pi^2)^2\right\}\frac{1}{s'^3} + O\left(\frac{1}{s'^4}\right) \quad .$$

The interval above 1 GeV only generates very small contributions to the integrals on the r.h.s. of the Roy equations, if these are evaluated in the region below the matching point.

We now take up the consistency condition and first observe that, once a solution has a consistent behaviour above the matching point, reasonable changes in the input above 1 GeV lead to solutions that also obey the consistency condition: It looks as if the Roy equations were almost trivially satisfied, behaving like an identity for $E > 1$ GeV. Is this consistent behaviour automatic, or does it depend crucially on part of the input ?

The answer to this question can be found in fig. 8, where we show two solutions obtained with the same value of $a_0^0$ as in fig. 6, but different inputs for $\mathrm{Im}\, t_0^2$: The solution on the left is obtained by using the top curve in fig. 5 instead of the central one ($a_0^2 = -0.0279$ instead of $a_0^2 = -0.0371$). The solution on the right corresponds to the bottom curve in fig. 5, where $a_0^2 = -0.0460$. The figure clearly shows that the consistent picture which we have at the center of the universal band is almost completely lost if we go to the upper border of this band: It is by no means trivial that we at all find solutions for which the output is consistent with the input.

The fact that the peaks and valleys seen in the solutions mimic those in the input can be understood on the basis of analyticity alone: The curvature above the matching point arises from the behaviour of the imaginary parts there. The

relevant term is the one from the principal value integral,

$$\mathrm{Re}\, t(s) = \frac{1}{\pi} \int\!\!\!\!\!\!-_{4M_\pi^2}^{s_2} ds' \, \frac{\mathrm{Im}\, t(s')}{s'-s} + r(s) \quad .$$

The remainder, $r(s)$ contains the contributions associated with the subtraction polynomial, the left hand cut, the higher partial waves, as well as the asymptotic region. On the interval $s_0 < s < s_1$, it varies only slowly and is well approximated by a first order polynomial in $s$.

The representations of the partial wave amplitudes that we are using as an input are specified in terms of simple functions. In the vicinity of the region where we are comparing their real parts with the Roy solutions, these are analytic in $s$, except for the cut along the positive real axis. Hence they also admit an approximate representation of the above form – the contributions from distant singularities are well approximated by a first order polynomial. Disregarding the interpolation needed to match the representation with the prescribed value of the phase at $s_0$, their imaginary parts coincide with the one of the corresponding Roy solution above the matching point. The small differences occurring in the interpolation region and below the matching point do not generate an important difference in the curvature. We conclude that the difference between the Roy solution and the real part of the input must be linear in $s$, to a good approximation. Moreover, within the accuracy to which our solutions obey the Roy equations, the two expressions agree at the matching point, by construction. Accordingly, the relation can be written in the form

$$\mathrm{Re}\, t(s)_{\,\mathrm{Roy}} = \mathrm{Re}\, t(s)_{\,\mathrm{input}} + (s-s_0)\,\beta \quad . \tag{10.1}$$

We have checked that this relation indeed holds to sufficient accuracy, for all three partial waves. This does not yet explain why the solution follows the real part of the input, but shows that it must do so up to a term linear in $s$ that vanishes at the matching point. In particular, if the difference between input and output is small at the upper end of validity of our equations, then analyticity ensures that the same is true in the entire region between the matching point and that energy (in this interval, $s$ varies by about a factor of two).

In view of the uncertainties attached to our input, we cannot require the Roy equations to be strictly satisfied also above the matching point. The band spanned by the two green lines in fig. 9 shows the region in the $(a_0^0, a_0^2)$ plane, where the solution for $\mathrm{Re}\, t_0^0(s)$ differs from the real part of the input by less than 0.05 (expressed in terms of the parameter $\beta$ in eq. (10.1), this amounts to $|\beta_0^0| < 0.07\,\mathrm{GeV}^{-2}$). Likewise, the band spanned by the two blue lines represents the region where $|\mathrm{Re}\, t_0^2(s)_{\mathrm{Roy}} - \mathrm{Re}\, t_0^2(s)_{\mathrm{input}}| < 0.05$, so that $|\beta_0^2| < 0.07\,\mathrm{GeV}^{-2}$. The corresponding band for the $P$-wave is much broader – in this channel, the consistency condition is rather weak and is met everywhere inside the universal band. We conclude that, in the lower half of the universal band, all three waves

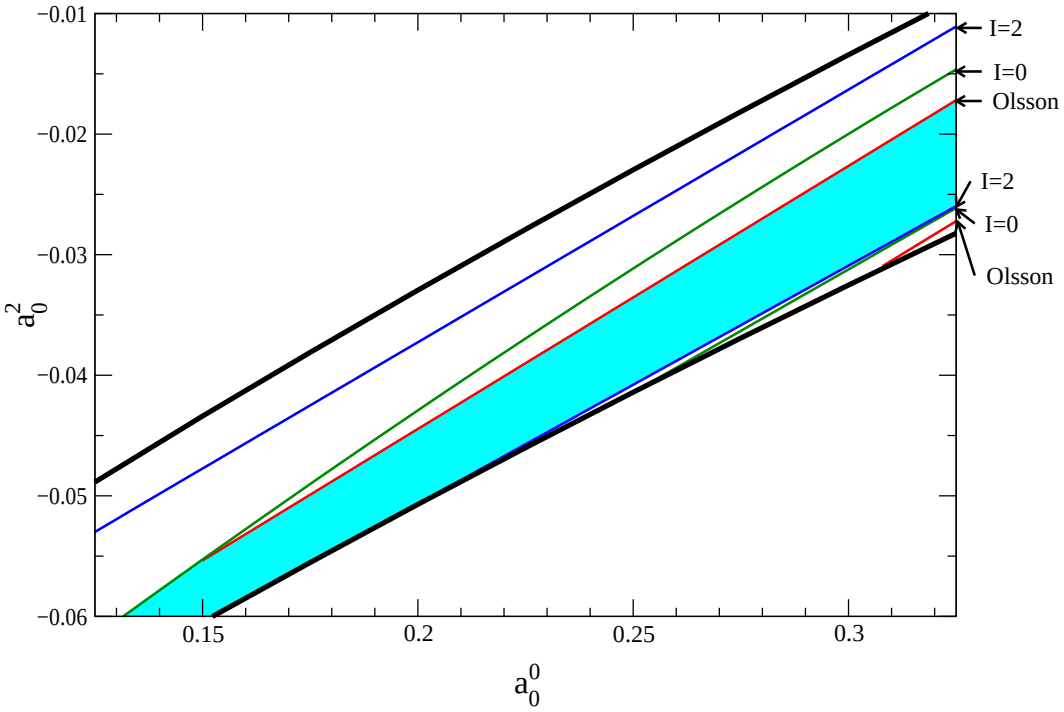


Figure 9: Regions inside which the consistency condition is met. The band between the two blue lines is for the condition in the $I = 2$ channel, whereas the one between the two green lines is for the $I = 0$ channel. The two red lines delimit the band inside which the Olsson sum rule is satisfied. The shaded area gives the intersection of the three bands.

show a consistent behaviour, while for the upper quarter of the band, this is not the case (the situation at the upper border is shown on the left in fig. 8).

It is not difficult to understand why the consistency condition is strongest for the $I = 0$ $S$-wave. In this connection, the most important term in the Roy equations is the one from the subtraction polynomial – the solution can satisfy the consistency condition only if the term proportional to $s$ is nearly cancelled by a linear growth of the remaining contributions. The term generates the contribution $(\beta_0^0, \beta_1^1, \beta_0^2) = (6, 1, -3) \times (2a_0^2 - 5a_0^2)/(72\, M_\pi^2)$ to the coefficients that describe the difference between output and input for the three lowest partial waves. The subtraction polynomial thus contributes twice as much to $\beta_0^0$ as to $\beta_0^2$, so that the consistency band for the $I = 2$ wave must be about twice as broad as the one for the $I = 0$ wave, while the one for the $P$-wave must roughly be six times broader. At the qualitative level, these features are indeed born out in the figure, but we stress that the term from the subtraction polynomial is not the only one that matters – those arising from the integrals also depend on the values of $a_0^0$ and $a_0^2$. The two green lines correspond to a variation in $a_0^2$ by about $\pm 0.004$. Increasing

$a_0^2$ by 0.004, the value of the subtraction term $k_0^2(s_1)$ decreases by 0.10. The fact that the lines correspond to a change in $\mathrm{Re}\, t_0^0(s_1)$ of only $\pm 0.05$ implies that the contributions from the integrals reduce the shift by a factor of 2. Also, if only the subtraction term were relevant, the consistency bands would be determined by the combination $2a_0^2 - 5a_0^2$ and thus have a slope of $\frac{2}{5}$. Actually, these bands are roughly parallel to the universal band, whose slope is positive, but smaller by about a factor of 2.

# 11 Olsson sum rule

In the Roy equations, the imaginary parts above the matching point and the two subtraction constants $a_0^0$, $a_0^2$ appear as independent quantities. The consistency condition interrelates the two in such a manner that the contributions from the integrals over the imaginary parts nearly cancel the one from the subtraction term. In fact, a relation of this type can be derived on general grounds.

The fixed-$t$ dispersion relation (2.4) contains two subtractions. In principle, one subtraction suffices, for the following reason. The $t$-channel $I = 1$ amplitude

$$T^{(1)}(s,t) \equiv \frac{1}{6}\left\{2\,T^0(s,t) + 3\,T^1(s,t) - 5\,T^2(s,t)\right\}$$

does not receive a Pomeron contribution and thus only grows in proportion to $s^{\alpha_\rho(t)}$ for $s \to \infty$. The dispersion relation (2.4), however, does contain terms that grow linearly with $s$. For the relation to be consistent with Regge asymptotics, the contribution from the subtraction term must cancel the one from the dispersion integral[6]. At $t = 0$, this condition reduces to the Olsson sum rule, which relates the subtraction constants to an integral over the imaginary parts [67]:

$$2\,a_0^0 - 5\,a_0^2 = \frac{M_\pi^2}{8\pi^2}\int_{4M_\pi^2}^\infty ds\,\frac{2\,\mathrm{Im}\,T^0(s,0) + 3\,\mathrm{Im}\,T^1(s,0) - 5\,\mathrm{Im}\,T^2(s,0)}{s\,(s-4M_\pi^2)}\,. \qquad (11.1)$$

It is well known that this sum rule converges only slowly – the contributions from the asymptotic region cannot be neglected. We split the integral into four pieces,

$$2\,a_0^0 - 5\,a_0^2 = O_{SP} + O_D + O_F + O_{as}\ .$$

The first term represents the contributions from the imaginary parts of the $S$- and $P$-waves in the region below 2 GeV, which are readily worked out, using our Roy solutions on the interval from threshold to 0.8 GeV and the input phase shifts on the remainder. The result is not very sensitive to the input used and is well approximated by a linear dependence on the scattering lengths,

$$O_{SP} = 0.483 \pm 0.011\ + 1.13\,(a_0^0 - 0.225) - 1.01\,(a_0^2 + 0.0371)\ .$$

[6] In the case of the $t$-channel amplitudes with $I = 0$ and $I = 2$, the fixed-$t$ dispersion relation (2.4) does ensure the proper asymptotic behaviour.

The remainder is closely related to the moments $I^I_n$ introduced in appendix B.1: here, we are concerned with the case $n = -1$. The term $O_D$ describes the contribution from the imaginary part of the $D$-waves, in the interval from threshold to 2 GeV. The relevant experimental information is discussed in appendix B.3, where we also explain how we estimate the uncertainties. The numerical result reads $O_D = 0.061 \pm 0.004$, including the small, negative contribution from the $I = 2$ $D$-wave. The bulk stems from the tensor meson $f_2(1275)$: In the narrow width approximation, this contribution amounts to 0.063. For the analogous contribution due to the $F$-wave, we obtain $O_F = 0.017 \pm 0.002$ (in narrow width approximation, the term generated by the $\rho_3(1690)$ yields 0.013). Those from the asymptotic region are dominated by the leading Regge trajectory – as noted above, the Pomeron does not contribute. Evaluating the asymptotic contributions with the formulae given in appendix B.4, we obtain $O_{as} = 0.102 \pm 0.017$. Collecting terms, this yields

$$2\,a_0^0 - 5\,a_0^2 = 0.663 \pm 0.021 + 1.13\,(a_0^0 - 0.225) - 1.01\,(a_0^2 + 0.0371) \quad . \tag{11.2}$$

The result corresponds to a band in the $(a_0^0, a_0^2)$ plane:

$$a_0^2 = -0.044 \pm 0.005 + 0.218\,(a_0^0 - 0.225) \quad . \tag{11.3}$$

The band is spanned by the two red lines shown in fig. 9. One of these nearly coincides with the lower border of the universal band, while the other runs near the center. The Olsson sum rule thus imposes roughly the same relation between $a_0^0$ and $a_0^2$ as the consistency condition. Note that the asymptotic contributions are numerically quite important here: The term $O_{as}$ amounts to a shift in $a_0^2$ of $-0.026 \pm 0.004$. The fact that – in the region where our solutions are internally consistent – the sum rule is indeed obeyed, represents a good check on our asymptotics.

The Olsson sum rule ensures the proper asymptotic behaviour of the amplitude only for $t = 0$. In order for the terms that grow linearly with $s$ to cancel also for $t \neq 0$, the imaginary part of the $P$-wave must obey an entire family of sum rules. The matter is discussed in detail in appendix C.1, where we demonstrate that one of these offers a further, rather sensitive test of our framework. The relationship between the Roy equations and those proposed by Chew and Mandelstam [68] is described in appendix C.2, where we also comment on the asymptotic behaviour of the dispersion integrals that occur on the r.h.s. of the Roy equations for the $S$- and $P$-waves.

# 12 Comparison with experimental data

In our framework, the only free parameter is $a_0^0$. Comparing our Roy equation solutions to data, we can determine the range of $a_0^0$ consistent with these, as well

as a corresponding range for $a_0^2$. This experimental determination of the two $S$-wave scattering lengths is the final scope of the present analysis and the main subject of the present section. Data on the $\pi\pi$ amplitude are available in a rather wide range of energies (we do not indicate the upper limit in energy when this exceeds 1.15 GeV, the limit of validity of our equations):

- $K_{e4}$ data for the combination $\delta_0^0 - \delta_1^1$ ($2M_\pi \leq E \leq 0.37$ GeV);
- ACM and Losty et al. data for $\delta_0^2$ ($0.35$ GeV $\leq E$);
- Data on the vector form factor – according to the discussion in section 7.3, these can safely be converted into values for $\delta_1^1$ in the region of the $\rho$ ($0.5 \leq E \leq 0.9$ GeV);
- CERN–Munich, and Berkeley data in the channels with $I = 0$ and $I = 1$ ($0.5$ GeV $\leq E$);

In the Roy equations, $a_0^0$ and $a_0^2$ exclusively enter through the subtraction polynomials, specified in eq. (1.2). Those relevant for the $S$-waves contain a constant contribution given by the scattering length and a term proportional to $(s - 4M_\pi^2) \times (2a_0^0 - 5a_0^2)$. In the $I = 0$ wave, that term is larger than $a_0^0$ from $E \sim 0.5$ GeV on. For the $I = 2$ wave, the linear term starts dominating over $a_0^2$ even earlier. Since $t_1^1(s)$ vanishes at threshold, the corresponding subtraction polynomial exclusively involves the linear term. This implies that, except in the vicinity of threshold, the behaviour of the solutions is sensitive only to the combination $2a_0^0 - 5a_0^2$ of scattering lengths – roughly the combination that characterizes the universal band. Accordingly, only data that reach down close to threshold give a direct handle to separately determine $a_0^0$ and $a_0^2$. In fact, only those coming from $K_{e4}$ decays meet this condition.

There is another threshold in energy that is obviously relevant for our approach: the matching point $s_0$. We will make a clear distinction between data points below $s_0$ and those at higher energies. The comparison to data above $s_0$ can hardly yield any information on the scattering lengths, because the behaviour of our solutions at those energies very strongly depends on the input used for the imaginary parts: The uncertainties in the experimental input completely cover the dependence of the solutions on the scattering lengths – we will discuss this in detail below. Instead, we analyze the requirement that the solution is consistent with the input for $s > s_0$, in the sense discussed in section 10. This condition turns out to be practically independent of the input used for the imaginary parts above $s_0$ and does therefore yield a meaningful constraint on $2a_0^0 - 5a_0^2$.

## 12.1 Data on $\delta_0^0 - \delta_1^1$ from $K_{e4}$, and on $\delta_0^2$ below 0.8 GeV

Let us first consider the $K_{e4}$ data. The comparison between our solutions and the high-statistic data of the Geneva–Saclay collaboration [69] is shown in fig. 10, for

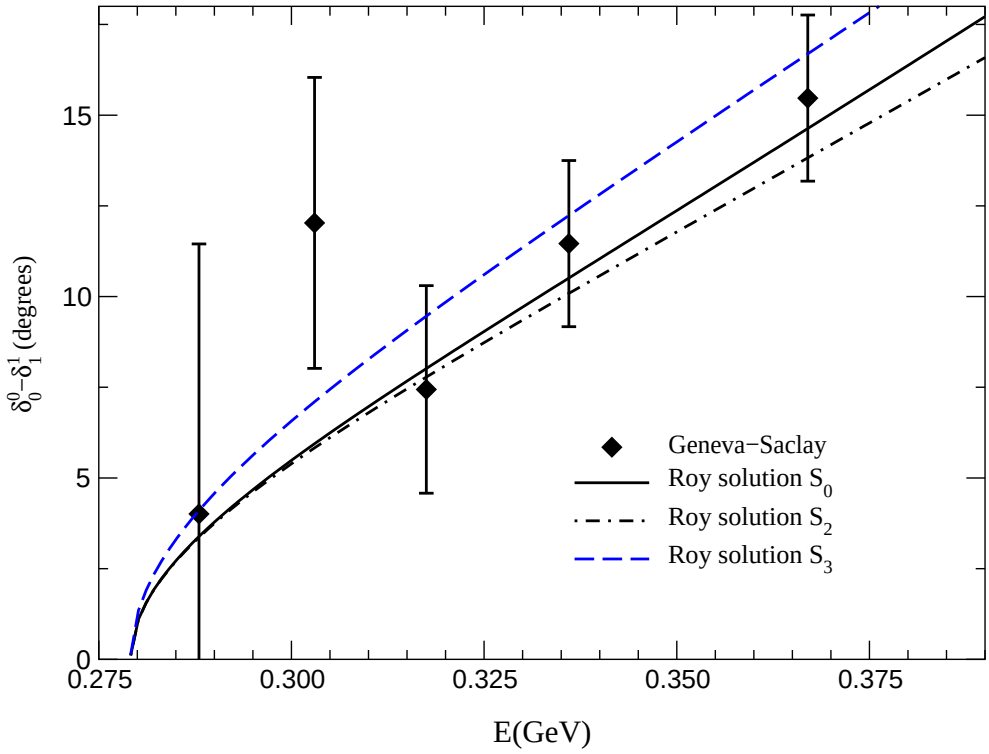


Figure 10: Comparison of our Roy solutions for different values of the scattering lengths with the data of the Geneva–Saclay collaboration, Rosselet et al. [69]. The full, dash-dotted and dashed lines correspond to the points $S_0$, $S_2$ and $S_3$ in fig. 7.

various values of the scattering lengths. The figure confirms the simple intuition that these data are mainly sensitive to $a_0^0$. In accordance with previous analyses [75], we find that they roughly constrain $a_0^0$ to the range between 0.18 and 0.3.

As for the low–energy data in the $I = 2$ channel, we should stress that this wave is quite strongly constrained once $\delta_0^2(s_0)$ is fixed. Because of the absence of any structures between threshold and 0.8 GeV, once we fix $\delta_0^2(s_0)$, the only freedom is in the way the phase approaches zero at threshold, i.e. in the value of $a_0^2$ – which depends on $a_0^0$. Fig. 11 shows that, at fixed $\delta_0^2(s_0)$, even a sizeable change in $a_0^0$ is barely visible in the $I = 2$ phase. The only important factor here is the value of the phase at the matching point: The comparison with the experimental data basically tells us which value of $\delta_0^2(s_0)$ is preferred.

A quantitative statement can be made in terms of $\chi^2$, and in principle we could calculate three different $\chi^2$-values, based on the three sets of data shown in fig. 5. Two of these, however, represent two different analyses of the same set of $\pi N \to \pi\pi N$ data. Their difference is a clear sign of the presence of sizeable systematic errors. We have estimated the latter using the difference, point by point, between the two analyses A and B of ref. [53], and added this in

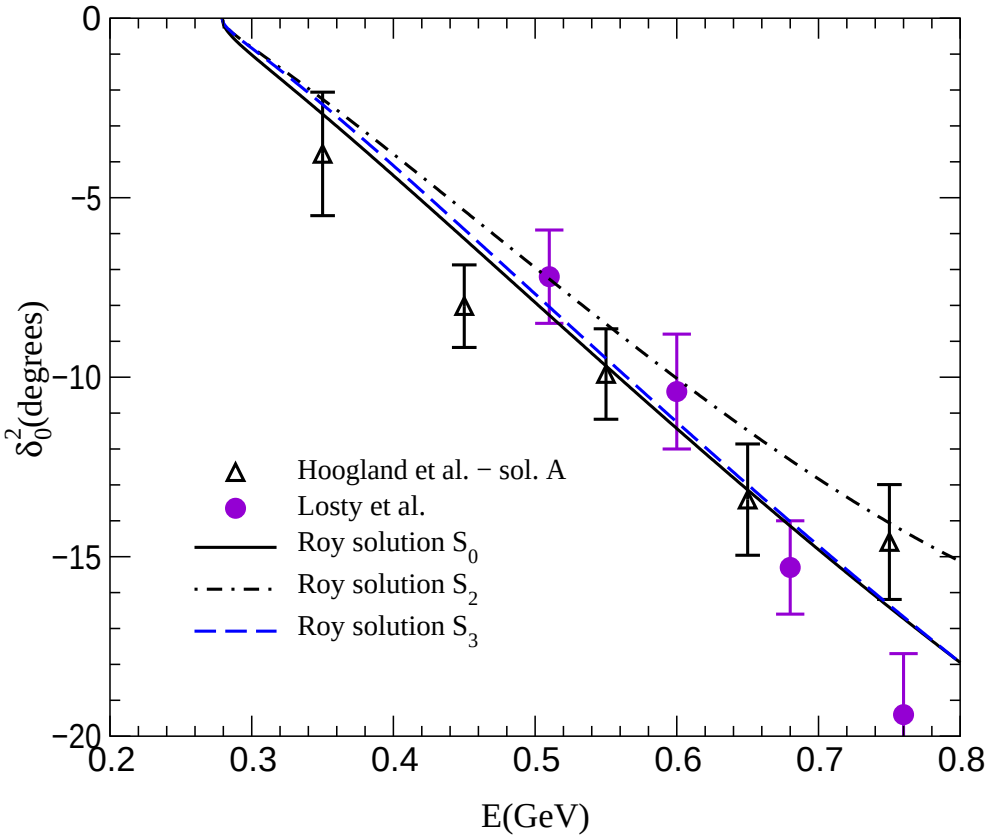


Figure 11: Comparison of our Roy solutions with the data on $\delta_0^2$ obtained by the ACM collaboration [53] and by Losty et al. [51]. The full, dash-dotted and dashed lines correspond to the points $S_0$, $S_2$ and $S_3$ in fig. 7.

quadrature to the statistical errors. As reference we have used the ACM(A) set of data, but have checked that interchanging it with the one of Losty et al. does not give significantly different results. The corresponding $\chi^2$, combined with the one obtained from the $K_{e4}$ data, has a minimum $\chi^2_{min} = 5.1$ (with 8 d.o.f.) at $a_0^0 = 0.242$, $a_0^2 = -0.0357$. The contour corresponding to 68% confidence level ($\chi^2 = \chi^2_{min} + 2.3$) is shown in fig. 12: The range $0.18 < a_0^0 < 0.3$ is dictated by the $K_{e4}$ data, whereas the $I = 2$ data exclude the upper border of the band.

## 12.2 The $\rho$ resonance.

The input used at the matching point implies that the $P$-wave phase shift must pass through 90° somewhere between threshold and 0.8 GeV – the Roy equations determine the place where this happens and how rapidly the phase must grow with the energy there. The solutions turn out to be very stiff: Varying the values of $a_0^0$ and $a_0^2$ within the universal band, and also varying the input for the imaginary parts above 0.8 GeV within the experimental uncertainties, we obtain

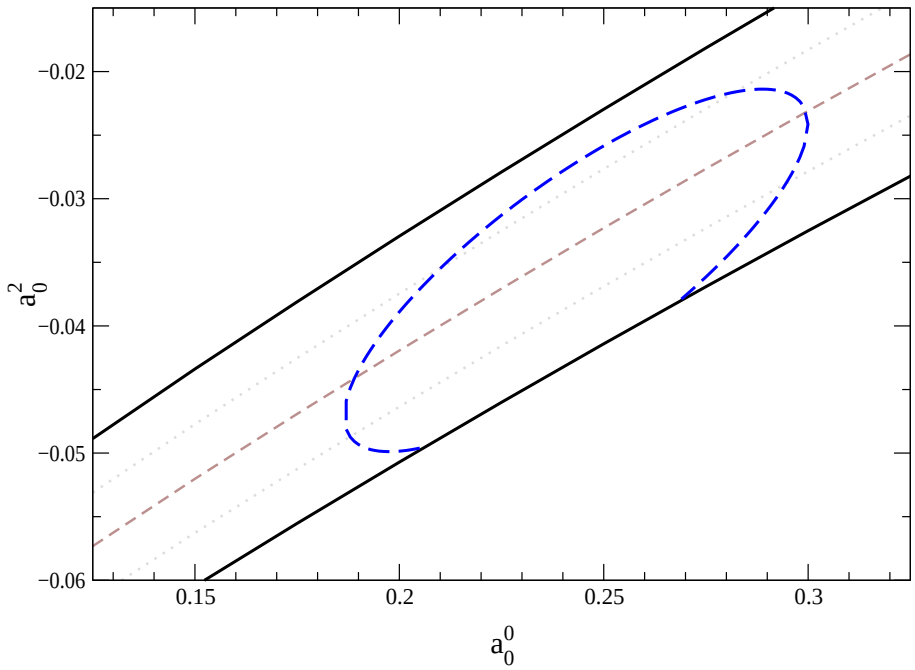


Figure 12: Range selected by the data below 0.8 GeV. The dashed line represents the 68% C.L. contour obtained by combining the Geneva–Saclay data on $K_{e4}$ decay with those from ACM(A) on $\delta_0^2$.

the narrow band of solutions shown in fig. 13.

In this figure, the energy range only extends to 0.82 GeV, for the following reason: Our solutions move along the Argand circle only below the matching point. At higher energies, the real part of the partial wave calculated from the Roy equations does not exactly match the imaginary part used as an input: unless we correct the latter, the elasticity $\eta_1^1$ differs from unity, already before the inelastic channels start making a significant contribution. If the consistency condition is met well, the departure from unity is small, but it can become as large as 5% if we go to the extreme of the consistency region shown in fig.9. This means that it does not make much sense to extract the value of the phase without adjusting the imaginary part. The proper way to do this is to extend the interval on which the Roy equations are solved, but we did not carry this out.

In the region $0.7\,\text{GeV} < 0.82\,\text{GeV}$, the result closely follows the data of the CERN-Munich collaboration. Below 0.7 GeV, however, the data are in conflict with the outcome of our analysis: The five lowest data points are outside the range allowed by the Roy equations, a problem noted already in ref. [6]. In our opinion, we are using a generous estimate of the uncertainties to be attached to our input. Note, in particular, that at those energies, the driving terms barely contribute. We conclude that the discrepancy between our result and the CERN-Munich phase shift analysis occurring on the left wing of the $\rho$ is likely to be

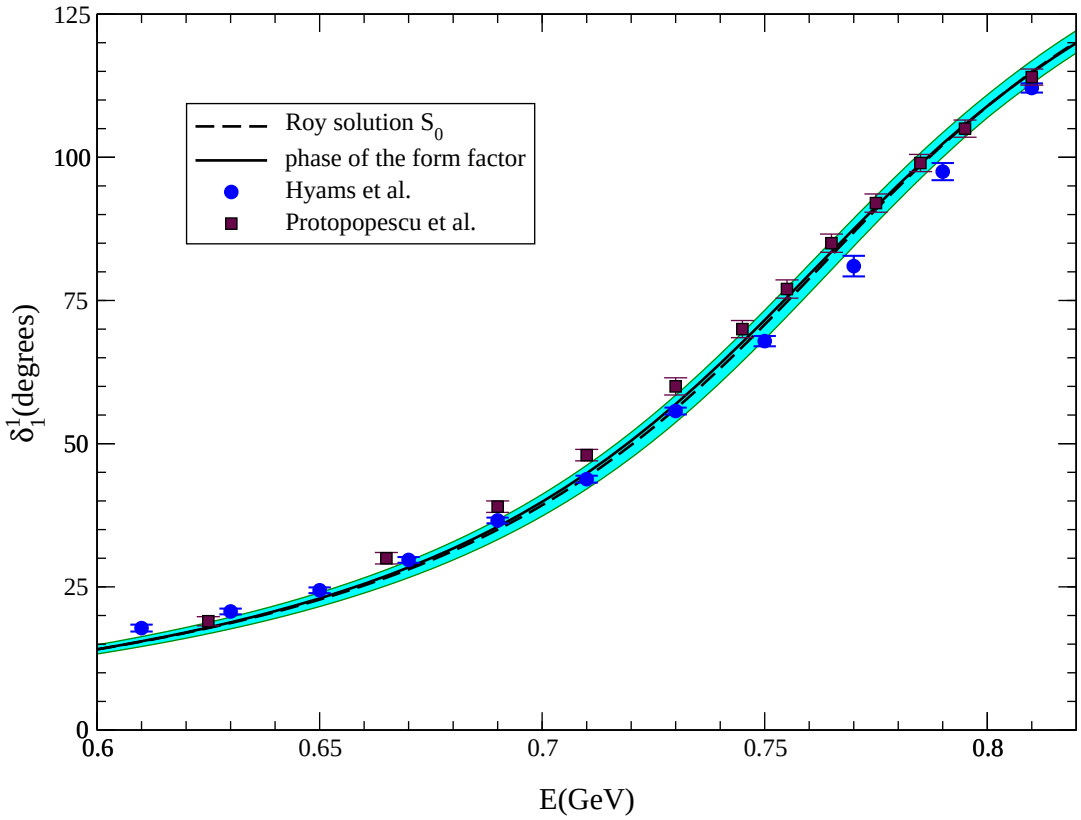


Figure 13: P-wave phase shift. The band shows the result of our analysis, obtained by varying the input within its uncertainties, while the data points indicate the phase shift measured in the process $\pi N \to \pi\pi N$ by the CERN-Munich collaboration. The full line represents the phase of the vector form factor (Gounaris-Sakurai fit of ref. [64]).

attributed to an underestimate of the experimental errors. As discussed below, the comparison with the $e^+e^-$ and $\tau$ decay data corroborates this conclusion.

Concerning the resonance parameters, we first give the ranges of mass and width that follow if, in the vicinity of the resonance, the phase shift is approximated by a Breit-Wigner formula[7]

$$e^{2\,i\,\delta_1^1(s)} = \frac{M_\rho^2 + i\,\Gamma_\rho M_\rho - s}{M_\rho^2 - i\,\Gamma_\rho M_\rho - s} \quad , \qquad \mathrm{tg}\,\delta_1^1(s) = \frac{\Gamma_\rho M_\rho}{M_\rho^2 - s} \quad .$$

In this approximation, the mass of the resonance is the real value of the energy where the phase passes through 90° and the width may be determined from the value of the slope $d\delta_1^1/ds$ at resonance. The solutions contained in the band shown

[7]The difference between $M_\rho^2 \pm i\,M_\rho\Gamma_\rho$ and $(M_\rho \pm \frac{i}{2}\,\Gamma_\rho)^2$ is beyond the accuracy of that approximation. The second is obtained from the first with the substitution $M_\rho^2 \to M_\rho^2 - \frac{1}{4}\,\Gamma_\rho^2$, $M_\rho\Gamma_\rho \to M_\rho\Gamma_\rho$, which increases the value of $M_\rho$ by about 4 MeV.

in the figure correspond to the range $M_\rho = 774 \pm 3\,\mathrm{MeV}$ and $\Gamma_\rho = 145 \pm 7\,\mathrm{MeV}$, to be compared with the average values obtained by the Particle Data Group, $M_\rho = 770.0 \pm 0.8\,\mathrm{MeV}$, $\Gamma_\rho = 150.7 \pm 1.1\,\mathrm{MeV}$ [70].

The only process independent property of the resonance is the position of the corresponding pole – the above numbers specify this position only approximately. To determine it more accurately, we first observe that the Roy equations yield a representation of the partial wave $t_1^1(s)$ on the first sheet, in terms of the imaginary parts along the real axis. The first sheet contains both a right and a left hand cut. We need to analytically continue the function from the upper rim of the right hand cut into the lower half plane (second sheet). The difference between the values obtained in this manner and those found by evaluating the Roy representation in the lower half plane is given by the analytic continuation of the imaginary part,

$$\mathrm{Im}\, t_1^1(s) = \frac{1}{\sigma(s)}\, \sin^2\delta_1^1(s) \quad .$$

On the first sheet, $t_1^1(s)$ does not have singularities. Hence a pole can only arise from the continuation of the imaginary part. Indeed, the function $\sin^2\delta_1^1(s)$ contains the term $\exp 2\,i\,\delta_1^1(s)$, which has a pole below the real axis. The position is readily worked out with the explicit, algebraic parametrization of the phase that we are using. The result illustrates an observation made long ago [71, 72, 73]: The pole mass is lower than the energy at which the phase goes through $90^\circ$, by about 10 MeV: For the band shown in the figure, the pole position varies in the range

$$M_\rho = 762.5 \pm 2\,\mathrm{MeV} \quad , \qquad \Gamma_\rho = 142 \pm 7\,\mathrm{MeV} \quad .$$

The $e^+e^-$ and $\tau$ data neatly confirm the conclusion reached above: The phase of the form factor is in perfect agreement with the behaviour of the $P$-wave that follows from the Roy equations, but differs from the data of the CERN-Munich phase shift analysis, particularly below 0.7 GeV. In our opinion, the information obtained about the behaviour on the left wing of the resonance on the basis of the reactions $e^+e^- \to \pi^+\pi^-$ and $\tau \to \pi^-\pi^0\nu$ is more reliable than the one obtained from $\pi N \to \pi\pi N$. The fact that the Roy equations are in good agreement with the $e^+e^-$ and $\tau$ data is very encouraging.

In view of the clean determination of the $P$-wave phase shift through $e^+e^-$ and $\tau$ experiments, we find it instructive to draw fixed $\chi^2$-contours in the $(a_0^0, a_0^2)$ plane. To do so, we first need to attach an error bar to the curve representing the phase shift. In section 7.4, we estimated the uncertainty in $\delta_1^1(s_0)$ at $\pm 2^\circ$ or $\pm 2\%$. As we go down in energy, the relative precision of the determination of the phase decreases: A generous estimate of the uncertainty at $\sqrt{s} = 0.5$ GeV is 10% or $\pm 0.6^\circ$. A smooth interpolation between these two values is our estimate of the experimental error bar (below that energy, the $e^+e^-$ and $\tau$ data become

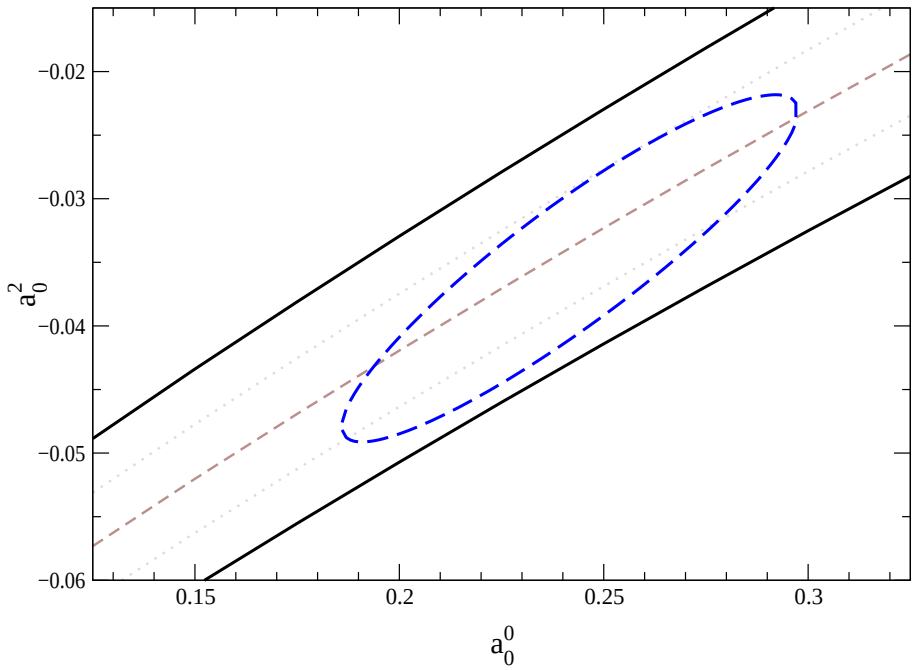


Figure 14: 68% C.L. contour obtained by combining all relevant low energy data: $K_{e4}$ decay, ACM(A) data on $\delta_0^2$ below 0.8 GeV and results for $\delta_1^1$ extracted from the $e^+e^-$ and $\tau$ data on the pion form factor.

scarce and have sizeable uncertainties). To construct the $\chi^2$ we have compared our solutions to the experimentally determined phase shift at five points between 0.5 and 0.75 GeV. Combining this $\chi^2$ with those from the data on $K_{e4}$ decays and on $\delta_0^2$ below 0.8 GeV, we obtain the 68% C.L. area drawn in fig. 14. The minimum of the $\chi^2$ is now 5.4 (with 13 d.o.f.). The position of the minimum is barely shifted: It now occurs at $a_0^0 = 0.240$, $a_0^2 = -0.0356$. In other words, at the place where the $\chi^2$ of the $K_{e4}$ data on $\delta_0^0 - \delta_1^1$ and those on $\delta_0^2$ had a minimum, the $\chi^2$ relative to the data on the form factor is practically zero and also has a minimum. In view of the fact that the uncertainties in $\delta_1^1$ are very small, this is quite remarkable. The data on the $P$-wave do not change the position of the minimum, but shrink the ellipse along the width of the universal band. As expected, they do not reduce the range of allowed values of $a_0^0$.

## 12.3 Data on the $I = 0$ $S$-wave below 0.8 GeV

In fig. 15 we compare the $S$-wave obtained from our Roy equation solutions with the available data: CERN-Munich [47] and Berkeley [48]. The band shown is a representation of the uncertainties in the solution, which have two main sources: the uncertainty in $\delta_0^0(s_0)$ and the one in $\delta_0^2(s_0)$ (width of the universal band). The central curve shows our reference solution $a_0^0 = 0.225$, $a_0^2 = -0.0371$. The uncertainties indicated do not account for the changes occurring if the value

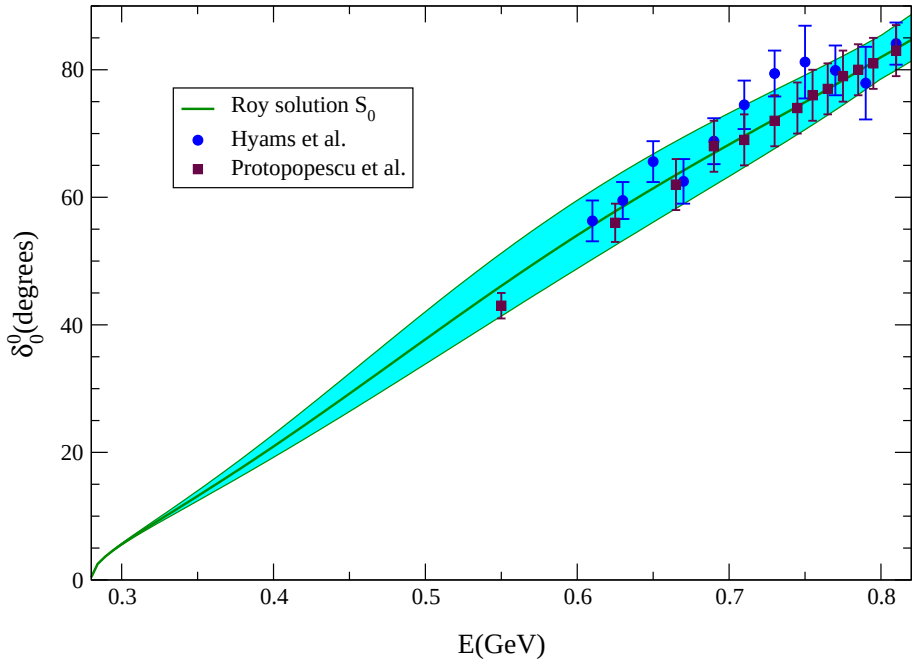


Figure 15: Comparison between the Roy solution for the $S$-wave and the phase shift analyses of the CERN-Munich (circles) and Berkeley (squares) collaborations. The band shows the uncertainties in the Roy solution, which are dominated by those in $a_0^0$ and $a_0^2$.

$a_0^0 = 0.225$ is modified. Changing this value within reasonable bounds, however, brings the solution out of the band only below 0.4 GeV, already far below the first data point. The figure shows good agreement with the data, especially so for the Berkeley data set. The CERN-Munich data set shows a certain structure, which does not occur in our solutions – in view of the uncertainties in the data, this difference does not represent a problem.

Despite the positive picture which emerges from the comparison, we refrain from using these data to draw confidence–level contours in the $(a_0^0, a_0^2)$ plane. The $S$-wave phase shifts have been extracted simultaneously with the $P$-wave. As discussed in the preceding section, these are affected by systematic errors which are at least as large as the statistical ones. The same must be true for the data in the $I = 0$ channel, so that a quantitative comparison with the Roy solutions is barely significant.

## 12.4 Data above 0.8 GeV

The Roy equations are valid up to $\sqrt{s_1} = 1.15$ GeV. In fig. 16, we show three different solutions for the $I = 0$ and $I = 1$ partial waves, in the region above the matching point. They are obtained by using three different inputs for the imaginary parts (note that the curves represent our solutions, not the real parts

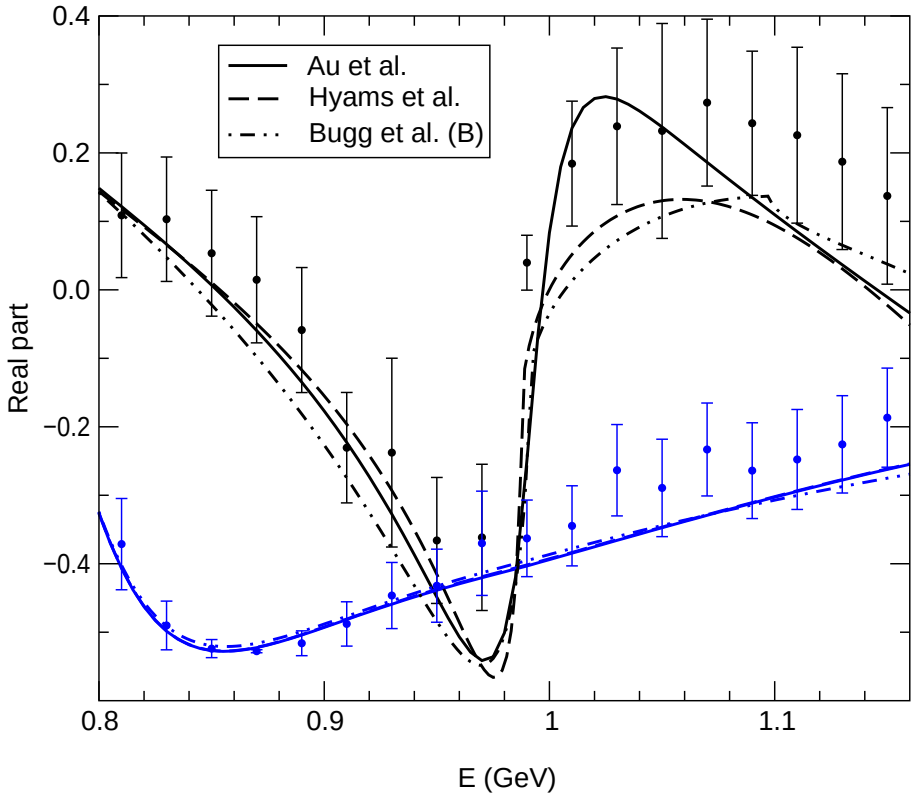


Figure 16: Behaviour of the solutions above the matching point. The curves show the solutions obtained with three different inputs for the imaginary parts. The data points are taken from the energy independent analysis of the CERN-Munich data [47]. The $I = 0$ $S$-wave is shown in black, the $I = 1$ $P$-wave in blue.

of the input). The figure shows that the differences are substantial, especially in the $S$-wave, despite the fact that, below $\sqrt{s_0} = 0.8\,\mathrm{GeV}$, the three solutions are practically identical, for all three waves. Evidently, above the matching point, the Roy solutions are very sensitive to the input used for the imaginary parts.

It is not difficult to understand why that is so. As discussed in detail in section 10, the solutions follow the real parts of the representation that is used as input (see fig. 6 for the case of Au et al. – in the other two cases, the picture is similar). The real parts of the three representations differ considerably. Moreover, all of these are systematically lower than the "data points" in fig. 16, which show the result of an energy independent analysis of the CERN-Munich data [47]. In view of this, it is not surprising that the three Roy solutions are quite different and that they are also systematically lower than the data points.

We conclude that a comparison of the Roy solutions with the data in the region above the matching point does not yield reliable information about the values of the two $S$-wave scattering lengths and we do therefore not show confidence–level

contours relative to data above 0.8 GeV.

# 13 Allowed range for $a_0^0$ and $a_0^2$

The above discussion has made clear that we can rely only on two rather solid sources of experimental information to determine the two $S$-wave scattering lengths: the data on $K_{e4}$ and those on the $P$-wave in the $\rho$ region. The former determine a range of allowed values for $a_0^0$ while the latter yield a range for the combination $2a_0^0 - 5a_0^2$. The consistency condition and the Olsson sum rule impose further constraints. Figure 17 summarizes our findings: We have superimposed the ellipse of fig. 14 with the lines that delimit the consistency bands for the two $S$-waves, as well as those relevant for the Olsson sum rule. The allowed range for $a_0^0$ and $a_0^2$ is the intersection of the ellipse with the band where the Olsson sum rule is obeyed within the estimated errors. In that region, the solutions also satisfy the consistency condition.

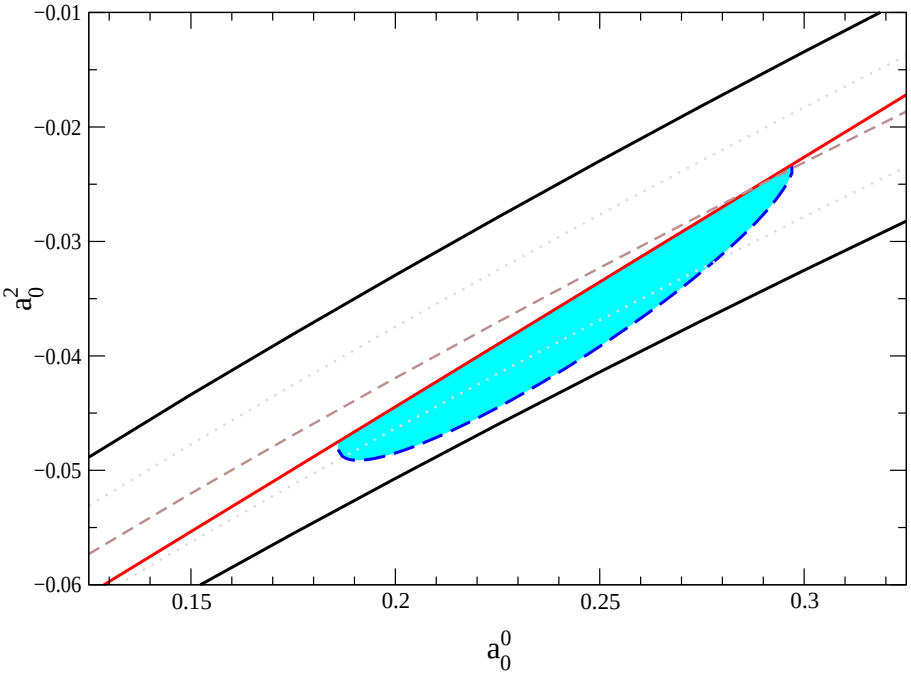


Figure 17: Intersection of the ellipse in fig. 14 (68% C.L. relative to the data on $K_{e4}$ decay, on $\delta_0^2$ and on the form factor) with the bands allowed by the consistency condition in all the three channels and by the Olsson sum rule.

We find it quite remarkable that the data on the shape of the $\rho$ resonance, the consistency condition and the Olsson sum rule all show a preference for the lower part of the universal band. This gives us confidence that our conclusion on which region in the $(a_0^0, a_0^2)$ plane is allowed by the present experimental information is

rather solid. Once the new data on $K_{e4}$ decays will become available, the allowed range in $a_0^0$ will become much narrower, and we will have a very small ellipse. The prospects of making a real precision test of the predictions for the two $S$-wave scattering lengths in the near future, appear to be very good, in particular also in view of the pionium experiment under way at CERN [29].

The $\pi N \to \pi\pi N$ data do provide essential information concerning the input of our calculations, but, as discussed in sections 12.3 and 12.4, they do not impose a firm constraint on the scattering lengths (incidentally, these data also prefer the lower half of the universal band). This is unfortunate, because the power of the Roy equations (unitarity, crossing symmetry and analyticity) is that of connecting regions of very different energy scales. The behaviour of the two $S$-waves in the immediate vicinity of threshold is determined by the scattering lengths. In the combination $2a_0^0 - 5a_0^2$, these also determine the linear growth of the subtraction polynomial: As we discussed in detail in section 10, the large contribution from the polynomial must be compensated to a high degree of accuracy by the dispersive integrals. We therefore expect that a reanalysis of the $\pi N \to \pi\pi N$ data based on the Roy equations would lead to a rather stringent constraint on the allowed region, as it would make full use of the information contained in these data – in our opinion, the existing phase shift analyses are a comparatively poor substitute.

# 14 Threshold parameters

## 14.1 $S$- and $P$-waves

As shown in ref. [74], the effective ranges of the $S$- and $P$-waves and the $P$-wave scattering length can be expressed in the form of sum rules, involving integrals over the imaginary parts of the scattering amplitude and the combination $2a_0^0 - 5a_0^2$ of $S$-wave scattering lengths. The sum rules may be derived from the Roy representation by expanding the r.h.s. of eq. (5.1) in $q^2$ and reading off the coefficients according to eq. (2.3). In the case of the $S$-wave effective ranges, the expansion can be interchanged with the integration over the imaginary parts only after removing the threshold singularity. This can be done by supplementing the integrand with a term proportional to the derivative

$$\frac{d}{ds}\,\frac{1}{\sqrt{s(s-4\,M_\pi^2)}} = -\frac{h(s)}{\{s(s-4\,M_\pi^2)\}^2}\quad,\quad h(s) = (s-2M_\pi^2)\sqrt{s(s-4M_\pi^2)}\quad.$$

In this notation, the sum rules may be written in the form:

$$\begin{aligned} b_0^0 = {} & \frac{1}{3M_\pi^2}\,(2a_0^0 - 5a_0^2) + \frac{16}{3\pi}\int_{4M_\pi^2}^{s_2} \frac{ds}{\{s(s-4M_\pi^2)\}^2}\,\Big\{4M_\pi^2(s-M_\pi^2)\,\mathrm{Im}\,t_0^0(s) \\ & - 9M_\pi^2(s-4M_\pi^2)\,\mathrm{Im}\,t_1^1(s) + 5M_\pi^2(s-4M_\pi^2)\,\mathrm{Im}\,t_0^2(s) - \tfrac{3}{2}(a_0^0)^2\,h(s)\Big\} \end{aligned}$$

$$-\frac{8}{\pi}\int_{s_2}^{\infty}\frac{ds}{\{s(s-4M_\pi^2)\}^2}\,(a_0^0)^2\,h(s)+b_{0\,d}^0\quad, \tag{14.1}$$

$$\begin{aligned}
b_0^2 = &-\frac{1}{6M_\pi^2}\,(2a_0^0-5a_0^2)+\frac{8}{3\pi}\int_{4M_\pi^2}^{s_2}\frac{ds}{\{s(s-4M_\pi^2)\}^2}\Big\{2M_\pi^2(s-4M_\pi^2)\,\mathrm{Im}\,t_0^0(s)\\
&+9M_\pi^2(s-4M_\pi^2)\,\mathrm{Im}\,t_1^1(s)+M_\pi^2(7s-4M_\pi^2)\,\mathrm{Im}\,t_0^2(s)-3(a_0^2)^2\,h(s)\Big\}\\
&-\frac{8}{\pi}\int_{s_2}^{\infty}\frac{ds}{\{s(s-4M_\pi^2)\}^2}\,(a_0^2)^2\,h(s)+b_{0\,d}^2\quad,\\
a_1^1 = &\frac{1}{18M_\pi^2}\,(2a_0^0-5a_0^2)+\frac{8M_\pi^2}{9\pi}\int_{4M_\pi^2}^{s_2}\frac{ds}{\{s(s-4M_\pi^2)\}^2}\Big\{-2(s-4M_\pi^2)\,\mathrm{Im}\,t_0^0(s)\\
&+9(3s-4M_\pi^2)\,\mathrm{Im}\,t_1^1(s)+5(s-4M_\pi^2)\,\mathrm{Im}\,t_0^2(s)\Big\}+a_{1\,d}^1\quad,\\
b_1^1 = &\frac{8}{9\pi}\int_{4M_\pi^2}^{s_2}\frac{ds}{\{s(s-4M_\pi^2)\}^3}\Big\{-2(s-4M_\pi^2)^3\,\mathrm{Im}\,t_0^0(s)+9\Big(3\,s^3-12\,s^2M_\pi^2\\
&+48\,sM_\pi^4-64M_\pi^6\Big)\,\mathrm{Im}\,t_1^1(s)+5(s-4M_\pi^2)^3\,\mathrm{Im}\,t_0^2(s)\Big\}+b_{1\,d}^1\,.
\end{aligned}$$

The integrals only involve the imaginary parts of the $S$- and $P$-waves and are cut off at $s=s_2$. The contributions from higher energies, as well as those from the imaginary parts of the partial waves with $\ell=2,3,\ldots$ are contained in the constants $b_{0\,d}^0$, $b_{0\,d}^2$, $a_{1\,d}^1$, $b_{1\,d}^1$. By construction, these represent derivatives of the driving terms at threshold,

$$d_0^0(s)=q^2b_{0\,d}^0+O(q^4)\,,\quad d_1^1(s)=q^2a_{1\,d}^1+q^4b_{1\,d}^1+O(q^6)\,,\quad d_0^2(s)=q^2b_{0\,d}^2+O(q^4)\,.$$

The numerical values obtained within our framework are given in the upper half of table 4, where we also show the numbers quoted in the compilation of Nagels et al. [75], which are based on the analysis of Basdevant, Froggatt and Petersen [6]. In accordance with the literature, we use pion mass units. Since the relevant physical scale is of the order of 1 GeV, the numerical values rapidly decrease with the dimension of the quantity listed. The columns A – E indicate the following contributions to the total[8]:

A. Contribution from the subtraction term $\propto 2a_0^2-5a_0^2$.

B. Imaginary parts of the $S$- and $P$-waves on the interval $4\,M_\pi^2<s<s_0$. This contribution is evaluated with the Roy solutions described in the text.

C. Imaginary parts of the $S$- and $P$-waves in the range $s_0<s<s_2$. Here, we are relying on the experimental information, discussed in section 7.

D. Imaginary parts of the higher partial waves in the range $4\,M_\pi^2<s<s_2$. These are calculated in the same manner as for the driving terms of the $S$- and $P$-waves (see appendix B.3).

[8]The numbers given for the total include the tiny additional contributions to $b_0^0$ and $b_0^2$ that arise from the integrals over $h(s)(a_0^0)^2$ and $h(s)(a_0^2)^2$ in the interval $s_2<s<\infty$. Numerically, these amount to $\delta b_0^0=-6.3\cdot10^{-4}\,M_\pi^{-2}$ and $\delta b_0^2=-1.7\cdot10^{-5}\,M_\pi^{-2}$.

| | A | B | C | D | E | total | $\Delta_1$ | $\Delta_2$ | ref.[75] | units |
|---|---|---|---|---|---|---|---|---|---|---|
| $b_0^0$ | 2.12 | .45 | −.03 | .02 | .00 | 2.56 | ±.02 | $^{+.28}_{-.12}$ | $2.5 \pm 0.3$ | $10^{-1} M_\pi^{-2}$ |
| $b_0^2$ | −1.06 | .26 | .02 | .01 | .00 | −.77 | ±.003 | $^{+.03}_{-.07}$ | $-.82 \pm .08$ | $10^{-1} M_\pi^{-2}$ |
| $a_1^1$ | 3.53 | −.03 | .13 | −.01 | .01 | 3.63 | ±.02 | $^{+.29}_{-.11}$ | $3.8 \pm 0.2$ | $10^{-2} M_\pi^{-2}$ |
| $b_1^1$ | — | 4.05 | 1.39 | −.07 | .08 | 5.45 | ±.13 | $^{+.35}_{-.44}$ | | $10^{-3} M_\pi^{-4}$ |
| $a_2^0$ | — | 1.29 | .28 | .07 | .03 | 1.67 | ±.01 | $^{+.15}_{-.06}$ | $1.7 \pm .3$ | $10^{-3} M_\pi^{-4}$ |
| $b_2^0$ | — | −3.48 | −.04 | .25 | .02 | −3.25 | ±.07 | $^{+.34}_{-.87}$ | | $10^{-4} M_\pi^{-6}$ |
| $a_2^2$ | — | 1.67 | −.51 | .35 | .02 | 1.53 | ±.07 | $^{+1.1}_{-.45}$ | $1.3 \pm 3$ | $10^{-4} M_\pi^{-4}$ |
| $b_2^2$ | — | −3.10 | −.09 | .06 | .02 | −3.11 | ±.07 | $^{+.41}_{-.95}$ | | $10^{-4} M_\pi^{-6}$ |
| $a_3^1$ | — | 5.11 | .26 | .05 | .01 | 5.43 | ±.1 | $^{+1.6}_{-.72}$ | $6 \pm 2$ | $10^{-5} M_\pi^{-6}$ |
| $b_3^1$ | — | −3.96 | −.01 | .01 | .01 | −3.95 | ±.08 | $^{+.89}_{-1.9}$ | | $10^{-5} M_\pi^{-8}$ |

Table 4: Threshold parameters of the $S$-, $P$-, $D$- and $F$-waves. The significance of the entries in columns A–E is specified in the text. The column $\Delta_1$ indicates the uncertainty due to the error bars in the experimental input at and above 0.8 GeV, whereas $\Delta_2$ shows the shifts occurring if $a_0^0$ and $a_0^2$ are varied within the ellipse of fig. 14, according to eqs. (14.2) and (14.4).

E. Asymptotic contributions, $s > s_2$. These are evaluated with the representation given in appendix B.4.

For the reasons discussed earlier, we use $\sqrt{s_0} = 0.8\,\mathrm{GeV}$, $\sqrt{s_2} = 2\,\mathrm{GeV}$. The values quoted in columns A and B are obtained with our reference solution, $a_0^0 = 0.225$, $a_0^2 = -0.0371$, which corresponds to the point $S_0$ in fig. 7.

The table shows that the result for $b_0^0$, $b_0^2$, $a_1^1$, $b_1^1$ is dominated by the contributions from the subtraction term and from the imaginary parts of the $S$- and $P$-waves. The higher partial waves and the asymptotic region only yield tiny corrections. The sum D+E represents the contribution from the driving terms. In the evaluation of these terms, which is discussed in detail in appendix B.5, we have constrained the polynomial fit with the relevant derivatives at threshold, so that the numerical values of the four constants $b_{0\,d}^0$, $b_{0\,d}^2$, $a_{1\,d}^1$, $b_{1\,d}^1$ are correctly reproduced by the corresponding terms in the representation (4.1).

The uncertainty given in column $\Delta_1$ of table 4 only accounts for the noise seen in our evaluation for the specific values $a_0^0 = 0.225$, $a_0^2 = -0.0371$ (errors in columns B–E added up quadratically). The sensitivity to these two parameters

is well represented by linear relations of the form[9]

$$\begin{aligned} b_0^0 &= \phantom{-}2.56 \times 10^{-1} M_\pi^{-2} \, \{ 1 + \phantom{0}3.2 \, \Delta a_0^0 - 12.7 \Delta a_0^2 \} \, , \\ b_2^0 &= -0.77 \times 10^{-1} M_\pi^{-2} \, \{ 1 + 2.5 \, \Delta a_0^0 - \phantom{1}7.6 \, \Delta a_0^2 \} \, , \\ a_1^1 &= \phantom{-}3.63 \times 10^{-2} M_\pi^{-2} \, \{ 1 + 2.3 \, \Delta a_0^0 - \phantom{1}7.8 \, \Delta a_0^2 \} \, , \\ b_1^1 &= \phantom{-}5.45 \times 10^{-3} M_\pi^{-4} \, \{ 1 + 0.1 \, \Delta a_0^0 - \phantom{1}5.7 \, \Delta a_0^2 \} \, , \end{aligned} \tag{14.2}$$

with $\Delta a_0^0 = a_0^0 - 0.225$, $\Delta a_0^2 = a_0^2 + 0.0371$. Using this representation, the $1\sigma$ ellipse of fig. 14 can be translated into $1\sigma$ ranges for the various quantities listed in the table – these are shown in column $\Delta_2$ (since our reference point is not at the center of the ellipse, the ranges are asymmetric).

The table neatly demonstrates that the two $S$-wave scattering lengths are the essential low energy parameters – the uncertainty in the result is due almost exclusively to the one in $a_0^0$, $a_0^2$. This is to be expected on general grounds [76]: The integrals occurring in the above sum rules are rapidly convergent, so that only the behaviour of the partial waves in the threshold region matters. The uncertainties in the input used for the imaginary parts above the matching point only enter indirectly, through their effect on the $S$- and $P$-waves in the threshold region. We did not expect, however, that the effect would be as small as indicated in the table and add a few comments concerning this remarkable finding.

In order to document the statement that the uncertainties which we are attaching to the phenomenological input of our calculation (behaviour of the imaginary parts above the matching point, elasticity, driving terms) only have a minute effect on the result for the threshold parameters, we find it best to give the numerical size of this effect (column $\Delta_1$ of the table). We repeat that the numbers quoted there merely indicate the noise seen in our evaluation – we do not claim to describe the scattering amplitude to that accuracy. Isospin breaking, for instance, cannot be neglected at that level of precision.

The reason why the threshold parameters are insensitive to the uncertainties of our input is the following. As discussed in detail in sections 6–9, the solutions of the Roy equations in general exhibit a cusp at the matching point. If the imaginary parts above 0.8 GeV and the value of $a_0^0$ are specified, there is a solution with physically acceptable behaviour in the vicinity of the matching point only if the parameter $a_0^2$ is chosen properly. In other words, there is a strong correlation between the behaviour of the imaginary parts and the parameters $a_0^0$, $a_0^2$. As we are selecting a specific value for these parameters, we are in effect subjecting the imaginary parts to a constraint. For this reason, the uncertainties in the input can barely be seen in the output for the threshold parameters – the main effect is hidden in $a_0^0$, $a_0^2$. The correlation just described originates in the fact that one

[9] For $0.15 \leq a_0^0 \leq 0.30$ the representation holds inside the universal band to better than 4%. Similar relations also follow directly from the representation of the $S$- and $P$-waves given in appendix D, but since the threshold region does not carry particular weight when solving the Roy equations, these do not have the same accuracy.

of the two subtraction constants is superfluous: The combination $2\,a_0^0 - 5\,a_0^2$ may be represented as a convergent dispersion integral over the imaginary part of the amplitude.

The correlation is illustrated by the lines in fig. 7, which correspond to the specific parametrization of the input used for the imaginary part of the $I = 2$ $S$-wave shown in fig. 5. As there is very little experimental information about the energy dependence of this partial wave, we have worked out the change in the Roy solutions that occurs if this energy dependence is modified above the matching point. The result for the threshold parameters turns out to be practically unaffected. Also, we have varied the driving terms within the uncertainties given in section 4. Again, the response in the threshold parameters can barely be seen.

## 14.2 $D$- and $F$-waves

Similar sum rules also hold for the threshold parameters of the higher partial waves. The contributions from the imaginary parts of the $S$- and $P$-waves are obtained by expanding the kernels occurring in the Roy equations for the $D$- and $F$-waves around threshold. We write the result in the form

$$
\begin{aligned}
a_2^0 &= \frac{16}{45\pi}\int_{4M_\pi^2}^{s_2}\frac{ds}{s^3\,(s-4M_\pi^2)}\,\Big\{(s-4M_\pi^2)\,\mathrm{Im}\,t_0^0(s)+9(s+4M_\pi^2)\,\mathrm{Im}\,t_1^1(s)\\
&\qquad +5(s-4M_\pi^2)\,\mathrm{Im}\,t_0^2(s)\Big\}+a_{2\,d}^0\ ,\\
b_2^0 &= -\frac{32}{15\,\pi}\int_{4M_\pi^2}^{s_2}\frac{ds}{s^4\,(s-4M_\pi^2)}\,\Big\{(s-4M_\pi^2)\,\mathrm{Im}\,t_0^0(s)-3(s-12M_\pi^2)\,\mathrm{Im}\,t_1^1(s)\\
&\qquad +5(s-4M_\pi^2)\,\mathrm{Im}\,t_0^2(s)\Big\}+b_{2\,d}^0\ ,\\
a_2^2 &= \frac{8}{45\pi}\int_{4M_\pi^2}^{s_2}\frac{ds}{s^3\,(s-4M_\pi^2)}\,\Big\{2(s-4M_\pi^2)\,\mathrm{Im}\,t_0^0(s)-9(s+4M_\pi^2)\,\mathrm{Im}\,t_1^1(s)\\
&\qquad +(s-4M_\pi^2)\,\mathrm{Im}\,t_0^2(s)\Big\}+a_{2\,d}^2\ ,\qquad (14.3)\\
b_2^2 &= -\frac{16}{15\,\pi}\int_{4M_\pi^2}^{s_2}\frac{ds}{s^4\,(s-4M_\pi^2)}\,\Big\{2(s-4M_\pi^2)\,\mathrm{Im}\,t_0^0(s)+3(s-12M_\pi^2)\,\mathrm{Im}\,t_1^1(s)\\
&\qquad +(s-4M_\pi^2)\,\mathrm{Im}\,t_0^2(s)\Big\}+b_{2\,d}^2\ ,\\
a_3^1 &= \frac{16}{105\pi}\int_{4M_\pi^2}^{s_2}\frac{ds}{s^4\,(s-4M_\pi^2)}\,\Big\{2(s-4M_\pi^2)\,\mathrm{Im}\,t_0^0(s)+9(s+4M_\pi^2)\,\mathrm{Im}\,t_1^1(s)\\
&\qquad -5(s-4M_\pi^2)\,\mathrm{Im}\,t_0^2(s)\Big\}+a_{3\,d}^1\ ,\\
b_3^1 &= -\frac{128}{105\,\pi}\int_{4M_\pi^2}^{s_2}\frac{ds}{s^5\,(s-4M_\pi^2)}\,\Big\{2(s-4M_\pi^2)\,\mathrm{Im}\,t_0^0(s)+36M_\pi^2\,\mathrm{Im}\,t_1^1(s)\\
&\qquad -5(s-4M_\pi^2)\,\mathrm{Im}\,t_0^2(s)\Big\}+b_{3\,d}^1\ ,
\end{aligned}
$$

where $a^0_{2\,d}$, $b^0_{2\,d}$, ... contain the contributions from $s > s_2$ as well as those from the higher partial waves. The evaluation of these contributions, however, meets with problems that we need to discuss in some detail.

First, we note that the definition of the driving terms in eq. (3.2) is suitable only for the analysis of the $S$- and $P$-waves. For $\ell \geq 2$, the functions $d^I_\ell(s)$ contain a branch cut at threshold, so that these quantities are complex. In order to solve the Roy equations for the $D$-waves, for instance, the contributions generated by their imaginary parts need to be isolated, using a different decomposition of the right hand side of these equations. As far as the scattering lengths and effective ranges are concerned, however, only the values of the functions $d^I_\ell(s)$ and their first derivatives at threshold are needed, which are real.

A more subtle problem arises from the fact that the explicit form of the kernels occurring in the Roy equations for the higher partial waves depends on the choice of the partial wave projection. As discussed in detail in ref. [77], the definition (A.4) – which we used in our analysis of the $S$- and $P$-waves – does not automatically ensure that the threshold behaviour of the partial waves with $\ell \geq 3$ starts with the power $q^{2\ell}$. The problem arises from the fact that the solution of the Roy equations leads to a crossing symmetric scattering amplitude only if the imaginary parts of the higher partial waves satisfy sum rules such as the one in eq. (B.8). In particular, the expansion of the $F$–wave in powers of $q$ in general starts with

$$\mathrm{Re}\, t^1_3(s) = x^1_3\, q^4 + a^1_3\, q^6 + b^1_3\, q^8 + \ldots$$

For the fictitious term $x^1_3$ to be absent, the imaginary parts of the higher partial waves must obey a sum rule. In fact, we have written down the relevant sum rule already: equation (B.8). The derivation given in section B.2 shows that this constraint ensures crossing symmetry of the terms occurring in the expansion of the scattering amplitude around threshold, up to and including contributions of $O(q^4)$. The threshold expansion of the partial waves with $\ell \geq 3$ thus only starts at $O(q^6)$ if this condition holds – in particular $x^1_3$ then vanishes. The sum rule that allows us to pin down the asymptotic contributions to the driving terms for the $S$- and $P$-waves thus at the same time also ensures the proper threshold behaviour of the $F$–waves. The absence of a term of $O(q^6)$ in the $G$-waves leads to a new constraint, which could be derived in the same manner, etc. Note that the contributions from the imaginary parts of the $S$- and $P$-waves are manifestly crossing symmetric – the constraints imposed by crossing symmetry exclusively concern the higher waves[10].

The $F$-wave scattering length occurs in the expansion of the amplitude around threshold among the contributions of $O(q^6)$, two powers of $q$ beyond the term just

[10]The family of sum rules discussed in appendix C.1 does not follow from crossing symmetry, but from an asymptotic condition that goes beyond the Roy equations. As shown there, those sum rules do tie the imaginary part of the $P$-wave to the higher partial waves.

discussed. In the numerical analysis, we thus need to make sure that the sum rule holds to high precision if we are to get a reliable value in this manner. For the effective range, the situation is even worse. This indicates that for the numerical analysis of the higher partial waves, the extension of the range of validity of the Roy equations achieved if the standard partial wave projection (A.2) is replaced by (A.3) generates considerable complications.

For the evaluation of the threshold parameters, this extension is not needed – we may use the partial wave projection (A.2), for which the problem discussed above does not occur. In particular, $x_3^1$ then automatically vanishes, so that the evaluation of the scattering lengths and effective ranges does not pose special numerical problems. To evaluate those from the asymptotic region, we expand the fixed-$t$ dispersion relation (2.4) in powers of $t$. The results obtained for $a_0^0 = 0.225$, $a_0^2 = -0.0371$ are listed in the lower half of table 4.

The dependence on the $S$-wave scattering lengths may again be represented (to better than 6% inside the universal band for $0.15 \le a_0^0 \le 0.30$) with a set of linear relations:

$$\begin{array}{ll}
a_2^0 = & 1.67 \times 10^{-3} M_\pi^{-4} \{ 1 + 2.6\, \Delta a_0^0 - 8.6\, \Delta a_0^2 \}, \\
b_2^0 = & -3.25 \times 10^{-4} M_\pi^{-6} \{ 1 + 6.6\, \Delta a_0^0 - 17\, \Delta a_0^2 \}, \\
a_2^2 = & 1.53 \times 10^{-4} M_\pi^{-4} \{ 1 + 14\, \Delta a_0^0 - 25\, \Delta a_0^2 \}, \\
b_2^2 = & -3.11 \times 10^{-4} M_\pi^{-6} \{ 1 + 6.2\, \Delta a_0^0 - 11\, \Delta a_0^2 \}, \\
a_3^1 = & 5.43 \times 10^{-5} M_\pi^{-6} \{ 1 + 5.5\, \Delta a_0^0 - 8\, \Delta a_0^2 \}, \\
b_3^1 = & -3.95 \times 10^{-5} M_\pi^{-8} \{ 1 + 8\, \Delta a_0^0 - 8\, \Delta a_0^2 \}.
\end{array} \tag{14.4}$$

The sensitivity is more pronounced here than in the case of the threshold parameters for the $S$- and $P$-waves. In particular, the linear representation for the $D$-wave scattering length $a_2^2$ only holds to a good approximation if $a_0^0$ and $a_0^2$ do not deviate too much from the central values.

# 15 Values of the phase shifts at $s = M_K^2$

A class of important physical processes where the $\pi\pi$ phase shifts play a relevant role is that of kaon decays. Let us recall, for instance, that the phase of $\varepsilon'$ is given by the value of $\delta_0^2 - \delta_0^0 + \frac{1}{2}\,\pi$ at $s = M_K^2$. In this section, we give numerical values for the three phase shifts at the kaon mass as they come out from our Roy equation analysis, and show the explicit dependence on the two $S$-wave scattering lengths. In this manner, an improved determination of the latter will immediately translate into a better knowledge of the phases at $s = M_K^2$.

The decays $K^0 \to \pi\pi$ and $K^+ \to \pi\pi$ concern slightly different values of the energy. In view of the fact that the CP-violating parameter $\varepsilon'$ manifests itself in the decays of the neutral kaons, we evaluate the phases at $s = M_{K^0}^2$. Note that, in addition to this difference in the masses, there are also isospin breaking effects in the relevant transition matrix elements. As far as the $\pi\pi$ phases are concerned,

| | Value at $s = M_{K^0}^2$ | $\Delta_1$ | $\Delta_2$ |
|---|---|---|---|
| $\delta_0^0$ | 37.3 | $\pm 1.4$ | $^{+4.3}_{-1.6}$ |
| $\delta_1^1$ | 5.5 | $\pm 0.1$ | $^{+.3}_{-.13}$ |
| $\delta_0^2$ | $-7.8$ | $\pm 0.04$ | $^{+.7}_{-.8}$ |
| $\delta_0^0 - \delta_0^2$ | 45.2 | $\pm 1.3$ | $^{+4.5}_{-1.6}$ |

Table 5: Values of the phase shifts at $s = M_{K^0}^2$ in degrees. The central value is obtained with our reference solution of the Roy equations, where $a_0^0 = 0.225$, $a_0^2 = -0.0371$. The column $\Delta_1$ indicates the uncertainty due to the error bars in the experimental input at and above 0.8 GeV, whereas $\Delta_2$ shows the shifts occurring if $a_0^0$ and $a_0^2$ are varied within the ellipse of fig. 14, according to eq. (15.1).

however, the isospin breaking effects due to $m_d - m_u$ are tiny, because $G$-parity implies that these only occur at order $(m_d - m_u)^2$.

As in the preceding section, we give values at the reference point $a_0^0 = 0.225$ and $a_0^2 = -0.0371$, and break down the errors into those due to the noise in our calculations and those due to the poorly known values of the two scattering lengths. The results are shown in table 5. Like for the threshold parameters, the two $S$-wave scattering lengths are the main source of uncertainty. In the present case, the errors due to the uncertainties in our experimental input at 0.8 GeV are not negligible, but they amount to at most 4%.

The dependence of the central values on the two scattering lengths is well described by the following polynomials:

$$\begin{aligned}
\delta_0^0(M_{K^0}^2) &= 37.3^\circ \left\{1 + 3.0\Delta a_0^0 - 8.5\Delta a_0^2\right\} , \\
\delta_1^1(M_{K^0}^2) &= 5.5^\circ \left\{1 + 1.7\Delta a_0^0 - 6.7\Delta a_0^2\right\} , \\
\delta_0^2(M_{K^0}^2) &= -7.8^\circ \left\{1 + 1.9\Delta a_0^0 - 13\Delta a_0^2\right\} , \\
\delta_0^0(M_{K^0}^2) - \delta_0^2(M_{K^0}^2) &= 45.2^\circ \left\{1 + 2.8\Delta a_0^0 - 9.4\Delta a_0^2\right\} .
\end{aligned} \tag{15.1}$$

Our results are in agreement with refs. [60, 78, 79], but are more accurate. In the foreseeable future, the two $S$-wave scattering lengths will be pinned down to good precision, so that the above formulae will fix the phases to within remarkably small uncertainties.

# 16 Comparison with earlier work

The Roy equations were used to obtain information on the $\pi\pi$ scattering amplitudes, already in the early seventies. Most of the work done since then either

follows the method of Pennington and Protopopescu [3, 4] or the one of Basdevant, Froggatt and Petersen [5, 6]. In the present section, we briefly compare these two approaches with ours. A review of the results obtained by means of the Roy equations is given in ref. [9].

To our knowledge, Pennington and Protopopescu [3] were the first to analyze $\pi\pi$ scattering data using Roy's equations. In principle, the approach of these authors is similar to ours. In our language, they fixed the matching point at $\sqrt{s_0} = 0.48$ GeV. As input data, they relied on the $\pi\pi$ production experiment of the Berkeley group [48], using the data of Baton et al. [45] for the $I = 2$ channel (at the time they performed the analysis, the high-energy, high-statistics CERN-Munich data [47] were not yet available). The Roy equations then allowed them to extrapolate the $S$- and $P$-wave phases of Protopopescu et al. [48] to the region below 0.48 GeV. Comparing the Roy-predicted real parts with the data (this corresponds to what we call consistency), they found that these constrain the two $S$-wave scattering lengths to the range $a_0^0 = 0.15 \pm 0.07$, $a_0^2 = -0.053 \pm 0.028$. In their subsequent work [4], they then used the Roy equations to solve the famous Up-Down ambiguity that occurs in the analysis of the $S$-wave.

The fact that, in their analysis, the matching point is taken below the mass of the $\rho$ has an interesting mathematical consequence: As discussed in section 6.3, the Roy equations do then not admit a solution for arbitrary values of $a_0^0$, $a_0^2$, even if cusps at the matching point are allowed for (the situation corresponds to row IV of table 1). To enforce a solution, one may for instance keep the input for the imaginary parts as it is, but tune the scattering length $a_0^2$. The result, however, in general contains strong cusps in the partial waves with $I = 0, 1$. These can only be removed if the input used for the imaginary parts above the matching point is also tuned – the situation is very different from the one encountered for our choice of the matching point.

Basdevant, Froggatt and Petersen [5, 6] constructed solutions of the Roy equations by considering several phase shift analyses and a broad range of $S$-wave scattering lengths. The method used by these authors is different from ours in that they relied on an analytic parametrization of the $S$- and $P$-waves from threshold up to $\sqrt{s_2} = \sqrt{110}\, M_\pi = 1.47\,\mathrm{GeV}$, the onset of the asymptotic region in their case. Some of the parameters occurring therein are determined from a fit to the data, some by minimizing the difference between the right and left hand sides of the Roy equations in the region below $\sqrt{s_0} = \sqrt{60}\, M_\pi = 1.08$ GeV. In this manner, they construct universal bands corresponding to the Berkeley [48], Saclay [45] and CERN-Munich phases as determined by Estabrooks et al. [50]. The individual bands are not very much broader than the shaded region in fig. 17, but they are quite different from one another: Crudely speaking, the Berkeley band is centered at the upper border of our universal band, while the one constructed with the CERN-Munich phases is centered at the lower border. The Saclay band runs outside the region where we can find acceptable solutions at all.

In order to compare their results with ours, we first note that, for the six explicit solutions given in table 5 of [6], the value of $a_0^0$ varies between $-0.06$ and 0.59. Only two of these correspond to values of the $S$-wave scattering lengths in the region considered in the present paper: $\mathrm{BKLY}_2$ and $\mathrm{SAC}_2$. For these two, the value of the $P$-wave phase shift at 0.8 GeV is 108.3° and 108.0°, respectively, remarkably close to the central value of the range allowed by the data on the form factor, eq. (7.2). Concerning the value of $\delta_0^0$ at 0.8 GeV, however, the two solutions differ significantly: While $\mathrm{BKLY}_2$ yields 79.7° and is thus within our range in eq. (7.4), the value 70.2° that corresponds to $\mathrm{SAC}_2$ is significantly lower. In our opinion, that solution is not consistent with the experimental information available today. In the interval from threshold to 0.8 GeV, our solution differs very little from $\mathrm{BKLY}_2$. Above this energy, the imaginary part of the $I = 0$ $S$-wave in $\mathrm{BKLY}_2$ is substantially smaller than the one we are using as an input. Nevertheless, the solutions are very similar at low energies, because the behaviour below the matching point is not sensitive to the input above 1 GeV.

# 17 Summary and conclusions

The Roy equations follow from general properties of the $\pi\pi$ scattering amplitude. We have set up a framework to solve these equations numerically. In the following, we summarize the main features of our approach and the results obtained with it, omitting details – even if these would be necessary to make the various statements watertight.

1. In our analysis, three energies $s_0 < s_1 < s_2$ play a special role:

$$\begin{array}{rclcrcl} \sqrt{s_0} & = & 0.8\,\mathrm{GeV} & , & s_0 & = & 32.9\,M_\pi^2 \\ \sqrt{s_1} & = & 1.15\,\mathrm{GeV} & , & s_1 & = & 68\,M_\pi^2 \\ \sqrt{s_2} & = & 2\,\mathrm{GeV} & , & s_2 & = & 205.3\,M_\pi^2 \end{array} .$$

We refer to the point $s_0$ as the matching point: At this energy, the region where we calculate the partial waves meets the one where we are relying on phenomenology. The point $s_1$ indicates the upper end of the interval on which the Roy equations are valid, while $s_2$ is the onset of the asymptotic region.

2. Given the strong dominance of the $S$- and $P$-waves, we solve the Roy equations only for these, and only on the interval $4M_\pi^2 < s < s_0$, that is on the lower half of their range of validity. In that region, the contributions generated by inelastic channels are negligibly small. There, we set $\eta_0^0(s) = \eta_1^1(s) = \eta_0^2(s) = 1$. In the interval from $s_0$ to $s_2$, we evaluate the imaginary parts with the available experimental information, whereas above $s_2$, we invoke a theoretical representation, based on Regge asymptotics. We demonstrate that crossing symmetry imposes a strong constraint on the asymptotic contributions, which reduces the corresponding uncertainties quite substantially – in most of our results, these are barely visible.

3. The Roy equations involve two subtraction constants, which may be identified with the two $S$-wave scattering lengths $a_0^0$, $a_0^2$. In principle, one subtraction would suffice: The Olsson sum rule relates the combination $2\,a_0^0 - 5\,a_0^2$ to an integral over the imaginary parts in the forward direction (or, in view of the optical theorem, over the total cross section). This imposes a correlation between the input used for the imaginary parts and the values of the $S$-wave scattering lengths, but using this constraint ab initio would lead to an unnecessary complication of our scheme. We instead treat the two subtraction constants as independent parameters. The consequences of the Olsson sum rule are discussed below.

4. Unitarity converts the Roy equations for the $S$- and $P$-waves into a set of three coupled integral equations for the corresponding phase shifts: The real part of the partial wave amplitudes is given by a sum of known contributions (subtraction polynomial, integrals over the region $s_0 < s < s_2$ and driving terms) and certain integrals over their imaginary parts, extending from threshold to $s_0$. Since unitarity relates the real and imaginary parts in a nonlinear manner, these equations are inherently nonlinear and cannot be solved explicitly.

5. Several mathematical properties of such integral equations are known, and are used as a test and a guide for our numerical work. In particular, the existence and uniqueness of the solution is guaranteed only if the matching point $s_0$ is taken in the region between the place where the $P$-wave phase shift goes through $90^\circ$ and the energy where the $I = 0$ $S$-wave does the same. As this range is quite narrow ($0.78\,\mathrm{GeV} < \sqrt{s_0} < 0.86\,\mathrm{GeV}$), there is little freedom in the choice of the matching point – we use $\sqrt{s_0} = 0.8$ GeV. According to table 1, the multiplicity index of the interval $0.86 < \sqrt{s_0} < 1\,\mathrm{GeV}$ is equal to 1. By way of example ($\sqrt{s_0} = 0.88$ GeV), we have verified that our framework indeed admits a one–parameter family of numerical solutions if the matching point is taken in that energy range.

6. A second consequence of the mathematical structure of the Roy equations is that, for a given input and for a random choice of the two subtraction constants, the solution has a cusp at $s_0$: In the vicinity of the matching point, the solution in general exhibits unphysical behaviour. The strength of the cusp is very sensitive to the value of $a_0^2$. In fact, we find that the cusp disappears in the noise of our calculation if that value is tuned properly. Treating the imaginary parts as known, the requirement that the solution is free of cusps at the matching point determines the value of $a_0^2$ as a function of $a_0^0$. This is how the universal curve of Martin, Morgan and Shaw manifests itself in our approach.

7. The input used for the imaginary parts above the matching point is subject to considerable uncertainties. In our framework, the values of the $S$- and $P$-wave phase shifts at the matching point represent the essential parameters in this regard. In order to pin these down, we first make use of the fact that the data on the pion form factor, obtained from the processes $e^+e^- \to \pi^+\pi^-$ and $\tau \to \pi^-\pi^0\nu_\tau$, very accurately determine the behaviour of the $P$-wave phase shift in the region of the $\rho$-resonance, thus constraining the value of $\delta_1^1(s_0)$ to a remarkably narrow

range. Next, we observe that the absolute phase of the $\pi\pi$ scattering amplitude drops out in the difference $\delta_1^1 - \delta_0^0$, so that one of the sources of systematic uncertainty is eliminated. Indeed, the phase shifts extracted from the reaction $\pi N \to \pi\pi N$ yield remarkably coherent values for this difference. Since the $P$-wave is known very accurately, this implies that $\delta_0^0(s_0)$ is also known rather well. The experimental information concerning $\delta_0^2$, on the other hand, is comparatively meagre. We vary it in the broad range shown in fig. 5.

8. The uncertainties in the experimental input for the imaginary parts and those in the driving terms turn the universal curve into a band in the $(a_0^0, a_0^2)$ plane, part of which is shown in fig. 7. Outside this "universal band", the Roy equations do not admit physically acceptable solutions that are consistent with what is known about the behaviour of the imaginary parts above the matching point.

9. One of the striking features of the solutions is that, above the matching point, they very closely follow the real part of the partial wave used as input for the imaginary part, once the value of $a_0^2$ is in the proper range. The phenomenon is discussed in detail in section 10, where we show that, in a certain sense, this property represents a necessary condition for the solution to be acceptable physically. The region where this consistency condition holds is shown in fig. 9: It roughly constrains the admissible values of $a_0^2$ to the lower half of the universal band.

10. As mentioned above, the Olsson sum rule relates the combination $2a_0^0 - 5a_0^2$ of scattering lengths to an integral over the imaginary parts of the amplitude. Evaluating the integral, we find that the sum rule is satisfied in the band spanned by the two red curves shown in fig. 9. The Olsson sum rule thus amounts to essentially the same constraint as the consistency condition. Presumably, the universal band is of the same origin: Physically acceptable solutions only exist if the subtraction constants are properly correlated with the imaginary parts. The shaded region in fig. 9 shows the domain where all of these conditions are satisfied. It is by no means built in from the start that the various requirements can simultaneously be met – in our opinion, the fact that this is the case represents a rather thorough check of our analysis.

11. The admissible region can be constrained further if use is made of experimental data below the matching point. At the moment there are two main sources of information on $\pi\pi$ scattering below 0.8 GeV: A few data points for the $I = 2$ $S$-wave phase shift – which to our knowledge will, unfortunately, not be improved in the foreseeable future – and a few data points on $\delta_0^0 - \delta_1^1$ very close to threshold, as measured in $K_{e4}$ decays. These data do provide an important constraint. We compare our solutions inside the universal band to both sets of data. As shown in fig. 12, the corresponding $\chi^2$ contours nicely fit inside the universal band. The net result for the allowed range of the parameters is shown in fig. 17, which summarizes our findings.

12. To our knowledge, the Roy equation analysis is the only method that

allows one to reliably translate low energy data on the scattering amplitude into values for the scattering lengths. As discussed above, the available data do correlate the value of $a_0^2$ with the one of $a_0^0$. Unfortunately, however, the value of $a_0^0$ as such is not strongly constrained: In agreement with earlier analyses, we find that these data are consistent with any value of $a_0^0$ in the range from 0.18 to 0.3.

13. The new experiments at Brookhaven [27] and at DAΦNE [28] will yield more precise information in the very near future. We expect that the analysis of the forthcoming results along the lines described in the present paper will reduce the error in $a_0^0$ by about a factor of three. Moreover, the pionic atom experiment under way at CERN [29] will allow a direct measurement of $|a_0^0 - a_0^2|$ and thus confine the region to the intersection of the corresponding, approximately vertical strip with the region shown in fig. 17.

14. The two subtraction constants $a_0^0$, $a_0^2$ are the essential parameters at low energies: If these were known, our method would allow us to calculate the $S$- and $P$-wave phase shifts below 0.8 GeV to an amazing degree of accuracy. The parameters $a_0^0$, $a_0^2$ act like a filter: If the solutions are sorted out according to the values of these parameters, the noise due to the uncertainties in our input practically disappears, because variations of that input require a corresponding variation, either in $a_0^0$ or in $a_0^2$ – otherwise, the behaviour of the solution near the matching point is unacceptable. A simple explicit representation for the $S$- and $P$-wave phase shifts as functions of the energy is given in appendix D. The representation explicitly displays the dependence on $a_0^0$, $a_0^2$.

15. We have also analyzed the implications for the scattering lengths of the $P$-, $D$- and $F$-waves, as well as for the various effective ranges. The fact that $a_0^0$ and $a_0^2$ are the essential low energy parameters manifests itself also here: If we change the input in the Roy equations within the uncertainties, but keep $a_0^0$ and $a_0^2$ constant, the values of the various threshold parameters vary only by tiny amounts, typically around one percent or less. The main source of uncertainty in the determination of the threshold parameters is by far the one attached to the $S$-wave scattering lengths.

16. If the energy approaches the matching point, the uncertainties in the experimental input, naturally, come more directly into play. Also, the uncertainties in the driving terms grow rather rapidly with the energy. At the kaon mass, however, these are still very small. We have analyzed the phase shifts at $E = M_K$ in detail, because these represent an important ingredient in the calculation for various decay modes of the $K$ mesons. The result shows that the uncertainties are dominated by those in $a_0^0$, $a_0^2$, also at that energy. We conclude that the future precision data on $K_{\ell_4}$-decay and on pionic atoms will translate, via the Roy equations, into a rather precise knowledge of the $\pi\pi$ scattering amplitude (not only the lowest three partial waves) in the entire low–energy region, extending quite far above threshold.

17. In the present paper, we followed the phenomenological path and avoided making use of chiral symmetry, in order not to bias the data analysis with the-

oretical prejudice. A famous low energy theorem [32] predicts the values of the two basic low energy parameters in terms of the pion decay constant. The prediction holds to leading order in an expansion in powers of the quark masses. The corrections arising from the higher order terms in the chiral expansion are now known to order $p^6$ (two loops) [40]. We plan to match the chiral perturbation theory representation of the scattering amplitude with the phenomenological one obtained in the present paper [80]. This should lead to a very sharp prediction for $a_0^0$ and $a_0^2$. The confrontation of the prediction with the forthcoming results of the precision measurements will subject chiral perturbation theory to a crucial test.


## Acknowledgements

We are indebted to W. Ochs, M. Pennington and G. Wanders for many discussions and remarks concerning various aspects of our work. Also, we wish to thank G. Ecker for providing us with his notes on the problem that were very useful at an early phase of this investigation. Moreover, we thank J. Bijnens, P. Büttiker, S. Eidelman, F. Jegerlehner, B. Loiseau, B. Moussallam, S. Pislak, A. Sarantsev, J. Stern and B. Zou for informative comments, in particular also for detailed information on data and phase shift analyses. This work was supported by the Swiss National Science Foundation, Contract No. 2000-55605.98, by TMR, BBW-Contract No. 97.0131 and EC-Contract No. ERBFMRX-CT980169 (EURODAΦNE).


# A Integral kernels

Crossing symmetry, $A(s,u,t) = A(s,t,u)$, implies that the isospin components $\vec{T} = (T^0, T^1, T^2)$ are subject to the constraints ($u \equiv 4M_\pi^2 - s - t$)

$$\begin{aligned} \vec{T}(s,u) &= C_{tu}\,\vec{T}(s,t)\,, \\ \vec{T}(t,s) &= C_{st}\,\vec{T}(s,t)\,, \\ \vec{T}(u,t) &= C_{su}\,\vec{T}(s,t)\,, \end{aligned}$$

where the crossing matrices $C_{tu} = C_{ut}$, $C_{su} = C_{us}$, $C_{st} = C_{ts}$ are given by

$$C_{tu} = \begin{pmatrix} 1 & 0 & 0 \\ 0 & -1 & 0 \\ 0 & 0 & 1 \end{pmatrix} \qquad C_{su} = \begin{pmatrix} \frac{1}{3} & -1 & \frac{5}{3} \\ -\frac{1}{3} & \frac{1}{2} & \frac{5}{6} \\ \frac{1}{3} & \frac{1}{2} & \frac{1}{6} \end{pmatrix} \qquad C_{st} = \begin{pmatrix} \frac{1}{3} & 1 & \frac{5}{3} \\ \frac{1}{3} & \frac{1}{2} & -\frac{5}{6} \\ \frac{1}{3} & -\frac{1}{2} & \frac{1}{6} \end{pmatrix}$$

Their products obey the relations

$$\begin{aligned} &(C_{tu})^2 = (C_{su})^2 = (C_{st})^2 = \mathbf{1}\,, \\ &C_{st}\,C_{tu} = C_{tu}\,C_{us} = C_{us}\,C_{st}\,, \qquad C_{su}\,C_{ut} = C_{ts}\,C_{su} = C_{ut}\,C_{ts}\,. \end{aligned}$$

The quantities $g_2(s,t,s')$, $g_3(s,t,s')$ occurring in the fixed-t dispersion relation (2.4) represent $3\times 3$ matrices built with $C_{st}$, $C_{tu}$ and $C_{su}$,

$$\begin{aligned} g_2(s,t,s') &= -\frac{t}{\pi\, s'\,(s'-4M_\pi^2)}\,(u\,C_{st}+s\,C_{st}\,C_{tu})\left(\frac{\mathbf{1}}{s'-t}+\frac{C_{su}}{s'-u_0}\right) \quad , \\ g_3(s,t,s') &= -\frac{s\,u}{\pi\, s'(s'-u_0)}\left(\frac{\mathbf{1}}{s'-s}+\frac{C_{su}}{s'-u}\right) \quad , \end{aligned} \tag{A.1}$$

where $u=4M_\pi^2-s-t$ and $u_0=4M_\pi^2-t$.

The straightforward partial wave projection of the amplitude reads

$$t_\ell^I(s)=\frac{1}{64\pi}\int_{-1}^1 dz P_\ell(z)\,T^I(s,t_z) \quad , \qquad t_z=\tfrac{1}{2}(4M_\pi^2-s)(1-z) \quad . \tag{A.2}$$

On account of crossing symmetry, the formula is equivalent to

$$t_\ell^I(s)=\frac{1}{32\pi}\int_0^1 dz P_\ell(z)\,T^I(s,t_z) \quad . \tag{A.3}$$

As pointed out by Roy [1], the second form of the projection is preferable in the present context, because it involves smaller values of $|t_z|$, so that the domain of convergence of the partial wave series for the imaginary parts on the r.h.s. of the fixed-$t$ dispersion relation (2.4) becomes larger: Whereas for the straightforward projection, the large Lehmann-Martin ellipse is mapped into $-4M_\pi^2<s<32M_\pi^2$, the one in eq. (A.3) corresponds to $-4M_\pi^2<s<60M_\pi^2$.

The kernels $K_{\ell\ell'}^{II'}(s,s')$ that occur in eq. (1.1) are different from zero only if both $I+\ell$ and $I'+\ell'$ are even. With the partial wave projection (A.3), the explicit expression becomes[11]

$$\begin{aligned} K_{\ell\ell'}^{II'}(s,s') &= (2\ell'+1)\int_0^1 dz\, P_\ell(z)\,K_{\ell'}(s,t_z,s')^{II'} \quad , \\ t_z &= \tfrac{1}{2}(4M_\pi^2-s)(1-z) \quad . \end{aligned} \tag{A.4}$$

The functions $K_{\ell'}(s,t,u)^{II'}$ are the matrix elements of

$$K_{\ell'}(s,t,s')=g_2(s,t,s')+g_3(s,t,s')\,P_{\ell'}\left(1+\frac{2t}{s'-4M_\pi^2}\right) \quad . \tag{A.5}$$

[11] Note that the fixed-$t$ dispersion relation (2.4) is not manifestly crossing symmetric – for $\ell'\geq 2$, the kernels do depend on the specific form used for the partial wave projection. In particular, the kernels occurring in the Roy equations for the waves with $\ell\geq 3$ are proportional to $(s-4M_\pi^2)^\ell$ only if the projection in eq. (A.2) is used – for the one we are using here, the proper behaviour of the solutions only results if the contributions from the imaginary parts of the different partial waves compensate one another near threshold (see section 14.2). For a detailed discussion of these issues we refer to [77].

The kernels contain the usual pole at $s = s'$, generating the right hand cut of the partial wave amplitudes, as well as a piece $\bar{K}^{II'}_{\ell\ell'}(s,s')$ that is analytic in $\mathrm{Re}\, s > 0$, but contains a logarithmic branch cut for $s \leq -(s' - 4M_\pi^2)$:

$$K^{II'}_{\ell\ell'}(s,s') = \frac{1}{\pi(s'-s)}\,\delta^{II'}\,\delta_{\ell\ell'} + \bar{K}^{II'}_{\ell\ell'}(s,s') \quad .$$

To illustrate the structure of the second term, we give the explicit expression for $I = I' = \ell = \ell' = 0$:

$$\bar{K}^{00}_{00}(s,s') = \frac{2}{3\,\pi\,(s-4M_\pi^2)}\,\ell n\!\left(\frac{s+s'-4M_\pi^2}{s'}\right) - \frac{2\,s+5\,s'-16M_\pi^2}{3\pi\,s'\,(s'-4M_\pi^2)} \quad .$$

We do not need to list other components – they may be generated from the above formulae by means of standard integration routines.

# B Background amplitude

## B.1 Expansion of the background for small momenta

The background amplitude only contains very weak singularities at low energies. At small values of the arguments, $A(s,t,u)_d$ thus represents a slowly varying function of $s,t,u$, which is adequately approximated by a polynomial. We may, for instance, consider the Taylor series expansion around the center of the Mandelstam triangle: Set $s_0 = \frac{4}{3}M_\pi^2, s = s_0 + x, t = s_0 - \frac{1}{2}(x-y)$, expand in powers of $x$ and $y$ and truncate the series. Alternatively, we may exploit the fact that, in view of the angular momentum barrier, the dispersion integral over the imaginary parts of the higher partial waves receives significant contributions only for $s' \gtrsim 1\,\mathrm{GeV}^2$. For small values of $s$ and $t$, we can therefore expand the kernels $g_2(s,t,s')$ and $g_3(s,t,s')$ in inverse powers of $s'$. The coefficients of this expansion are homogeneous polynomials of $s$, $t$ and $M_\pi^2$, which may be ordered with the standard chiral power counting. The corresponding expansion of the Legendre polynomial starts with

$$P_\ell\left(1 + \frac{2\,t}{s'-4M_\pi^2}\right) = 1 + \ell(\ell+1)\,\frac{t}{s'} + O\left(p^4\right) \quad .$$

Truncating the expansion at order $p^6$, the background amplitude becomes

$$\begin{aligned}\vec{T}(s,t)_d = -32\,\pi\,\Big\{&(t\,u\,C_{st} + s\,u\,C_{su} + s\,t\,C_{tu})\,(\mathbf{1}+C_{su})\,\vec{I}_0 \\ &+\{s^2\,t\,C_{tu} + u^2\,s\,C_{su} + t^2\,u\,C_{st} + (t^2\,s\,C_{tu} + s^2\,u\,C_{su} + u^2\,t\,C_{st})\,C_{su}\}\,\vec{I}_1 \\ &+s\,t\,u\,(\mathbf{1}+C_{su})\,\vec{H}\Big\} + O(p^8) \quad .\end{aligned} \tag{B.1}$$

The coefficients $\vec{I}_0$ and $\vec{I}_1$ represent moments[12] of the imaginary part at $t = 0$,

$$I_n^I = \frac{1}{32\,\pi^2} \int_{4M_\pi^2}^\infty \frac{ds\ \mathrm{Im}\, T^I(s,0)_d}{s^{n+2}(s-4M_\pi^2)} \quad . \tag{B.2}$$

In view of the optical theorem, these quantities are given by integrals over the total cross section, except that the contributions from the $S$- and $P$-waves below $s_2$ are to be removed. Equivalently, we may express these coefficients in terms of the imaginary parts of the partial waves:

$$I_n^I = \sum_{\ell=2}^\infty \frac{(2l+1)}{\pi} \int_{4M_\pi^2}^{s_2} \frac{ds\ \mathrm{Im}\, t_\ell^I(s)}{s^{n+2}(s-4M_\pi^2)} + \sum_{\ell=0}^\infty \frac{(2l+1)}{\pi} \int_{s_2}^\infty \frac{ds\ \mathrm{Im}\, t_\ell^I(s)}{s^{n+2}(s-4M_\pi^2)} \,. \tag{B.3}$$

Except for a contribution proportional to $I_1^1$, the last term in eq. (B.1) may be expressed in terms of the derivative of $\mathrm{Im}\,\vec{T}(s,t)_d$ with respect to $t$:

$$H^I = -2\, I_1^1\, \delta_1^I + \frac{1}{32\,\pi^2} \int_{4M_\pi^2}^\infty \frac{ds}{s^3}\, \frac{\partial\, \mathrm{Im}\, T^I(s,t)_d}{\partial t}\bigg|_{t=0} \quad . \tag{B.4}$$

Here, only the higher partial waves contribute:

$$H^I = \sum_{\ell=2}^\infty (2l+1)\{\ell(\ell+1) - 2\,\delta_1^I\}\, \frac{1}{\pi} \int_{4M_\pi^2}^\infty \frac{ds\ \mathrm{Im}\, t_\ell^I(s)}{s^3(s-4M_\pi^2)} \quad . \tag{B.5}$$

The expression is similar to the one for $I_1^I$, except that the sum over the angular momenta picks up a factor of $\ell(\ell+1)$, indicating that partial waves with higher values of $\ell$ are more significant here. Note that all of the above moments are positive.

## B.2 Constraints due to crossing symmetry

The expansion of the background amplitude starts at order $p^4$, with a manifestly crossing symmetric contribution determined by the moments $\vec{I}_0$. The term from $\vec{I}_1$ is also crossing symmetric, but the one proportional to $s\,t\,u$ violates the condition $\vec{T}(s,u)_d = C_{tu}\,\vec{T}(s,t)_d$, unless the $I = 1$ component of the vector $(\mathbf{1} + C_{su})\,\vec{H}$ vanishes, i.e.

$$2H^0 = 9H^1 + 5H^2 \quad . \tag{B.6}$$

This sum rule is both necessary and sufficient for the polynomial approximation to the background amplitude to be crossing symmetric up to and including contributions of order $p^6$.

[12] The factor $1/(s-4M_\pi^2)$ could also be expanded in inverse powers of $s$, but this would worsen the accuracy of the polynomial representation. Note that the same factor also occurs in the representation (3.6) for the contributions generated by the imaginary part of the $S$- and $P$-waves below $s_2$: The expansion of the functions $W^I(s)$ in powers of $s$ yields integrals of the same form. Hence the low energy expansion of the full amplitude can be expressed in terms of moments of this type.

The sum rule illustrates the well-known fact that crossing symmetry leads to stringent constraints on the imaginary parts of the partial waves with $\ell \geq 2$ (for a thorough discussion, see [81, 42]). Crossing symmetry implies for instance that $\mathrm{Im}\, t_2^0(s)$ can be different from zero only if some of the higher partial waves with $I = 1$ or $I = 2$ also possess an imaginary part – in marked contrast to the situation for the $S$- and $P$-waves, where crossing symmetry does not constrain the imaginary parts.

In the form given, the sum rule only holds up to corrections of order $M_\pi^2$. We may, however, establish an exact variant by expanding the $I = 1$ component of the relation $\vec{T}(s,u)_d = C_{tu}\vec{T}(s,t)_d$ around threshold, for instance in powers of $t$ and $u$. In order for the term of order $t\,u$ occurring in the expansion of the left hand side to agree with the corresponding term on the right hand side, the imaginary parts must obey the sum rule

$$\int_{4M_\pi^2}^\infty \frac{ds}{s^2\,(s-4M_\pi^2)}\,\Big\{2\,\mathrm{Im}\,\dot{T}^0(s,0) - 5\,\mathrm{Im}\,\dot{T}^2(s,0)\Big\} = \\ 3\int_{4M_\pi^2}^\infty \frac{ds\,(3\,s-4\,M_\pi^2)}{s^2\,(s-4M_\pi^2)^3}\,\Big\{(s-4\,M_\pi^2)\,\mathrm{Im}\,\dot{T}^1(s,0) - 2\,\mathrm{Im}\,T^1(s,0)\Big\}\quad , \quad \text{(B.7)}$$

where $\dot{T}^I(s,t)$ stands for the partial derivative of $T^I(s,t)$ with respect to $t$. Expressed in terms of the imaginary parts of the partial waves, the relation reads

$$\sum_{\ell=2,4,\,\ldots}(2\ell+1)\,\ell\,(\ell+1)\int_{4M_\pi^2}^\infty \frac{ds}{s^2\,(s-4M_\pi^2)^2}\,\{2\,\mathrm{Im}\,t_\ell^0(s) - 5\,\mathrm{Im}\,t_\ell^2(s)\} = \\ \sum_{\ell=3,5,\,\ldots}(2\ell+1)\,\{\ell\,(\ell+1)-2\}\int_{4M_\pi^2}^\infty \frac{ds\,(s-\frac{4}{3}M_\pi^2)}{s^2\,(s-4M_\pi^2)^3}\,9\,\mathrm{Im}\,t_\ell^1(s)\quad . \quad \text{(B.8)}$$

The approximate version (B.6) differs from this exact result only through terms of order $M_\pi^2$.

The constraints imposed by crossing symmetry show, in particular, that the concept of tensor meson dominance is subject to a limitation that does not occur in the case of vector dominance: The hypothesis that convergent dispersion integrals or sum rules are saturated by the contributions from a spin 2 resonance leads to coherent results only at leading order of the low energy expansion. The sum rule (B.7) demonstrates that the hypothesis in general fails: Crossing symmetry implies that singularities with $\ell \geq 2$ cannot be dealt with one by one.

Since the relation (B.6) ensures crossing symmetry, the above low energy expansion of the isospin components of the amplitude is equivalent to a manifestly crossing symmetric representation of the background amplitude:

$$A(s,t,u)_d = p_1 + p_2\,s + p_3\,s^2 + p_4\,(t-u)^2 + p_5\,s^3 + p_6\,s(t-u)^2 + O(p^8)\,. \quad \text{(B.9)}$$

By construction, $A(s,t,u)_d$ does not contribute to the $S$-wave scattering lengths. This condition fixes $p_1$ and $p_2$ in terms of the remaining coefficients:

$$p_1 = -16M_\pi^4\,p_4\,, \quad p_2 = 4M_\pi^2\,(-p_3 + p_4 - 4M_\pi^2\,p_5)\,, \quad \text{(B.10)}$$

The explicit expressions for the latter read

$$\begin{aligned}
p_3 &= \frac{8\,\pi}{3}\,(4I_0^0 - 9I_0^1 - I_0^2) + \frac{16\,\pi}{3}\,M_\pi^2\,(-8\,I_1^0 - 21\,I_1^1 + 11\,I_1^2 + 12\,H) \;\;, \\
p_4 &= 8\,\pi\,(I_0^1 + I_0^2) + 16\,\pi\,M_\pi^2\,(I_1^1 + I_1^2) \;\;, \\
p_5 &= \frac{4\,\pi}{3}\,(8\,I_1^0 + 9\,I_1^1 - 11\,I_1^2 - 6\,H) \;\;, \\
p_6 &= 4\,\pi(I_1^1 - 3\,I_1^2 + 2\,H) \;\;.
\end{aligned} \tag{B.11}$$

In view of the sum rule (B.6), only two of the components of $\vec{H}$ are independent. Moreover, the amplitude only involves a combination thereof:

$$H \equiv \tfrac{2}{5}(H^0 - 2H^1) = \tfrac{2}{9}\,(H^0 + 2H^2) = H^1 + H^2 \;\;. \tag{B.12}$$

The above formulae show that the leading background contribution is determined by the integrals $\vec{I}_0$, which yield

$$p_1 = O(M_\pi^4) \;\;, \quad p_2 = O(M_\pi^2) \;\;, \quad p_3 = O(1) \;\;, \quad p_4 = O(1) \;\;.$$

The contributions from $\vec{I}_1$ and $\vec{H}$ modify the result by corrections that are suppressed by one power of $M_\pi^2$ and, in addition, generate a polynomial of third degree in $s$, $t$, $u$, characterized by $p_5$ and $p_6$.

## B.3 Background generated by the higher partial waves

Next, we turn to the numerical evaluation of the integrals $\vec{I}_0$, $\vec{I}_1$, $\vec{H}$ and first consider the contributions from the imaginary parts of the partial waves with $\ell \geq 2$ in the region below 2 GeV. The integrals are dominated by the resonances, which generate peaks in the imaginary parts. In the vicinity of the peak, we may describe the phase shift with the Breit-Wigner formula

$$e^{2i\delta(s)} = \frac{M_r^2 + i\Gamma_r M_r - s}{M_r^2 - i\Gamma_r M_r - s} \;\;,$$

where $M_r$ and $\Gamma_r$ denote the mass and the width of the resonance, respectively. To account for inelasticity (decays into states other than $\pi\pi$), we multiply the corresponding expression for the imaginary part of the partial wave amplitude with the branching fraction $\Gamma_{r\to\pi\pi}/\Gamma_r$. This leads to

$$\mathrm{Im}\, t_{\ell_r}^{I_r}(s) = \sqrt{\frac{s}{s-4M_\pi^2}}\;\frac{\Gamma_{r\to\pi\pi}\Gamma_r M_r^2}{(s-M_r^2)^2 + \Gamma_r^2 M_r^2} \;\;,$$

where $I_r$ and $\ell_r$ denote the isospin and the spin of the resonance, respectively. In the narrow width approximation, the formula simplifies to

$$\mathrm{Im}\, t_{\ell_r}^{I_r}(s) = \pi\,\Gamma_{r\to\pi\pi} M_r (1 - 4M_\pi^2/M_r^2)^{-\frac{1}{2}}\delta(s - M_r^2) \;\;. \tag{B.13}$$

Only four of the states listed in the particle data booklet [70] below 2 GeV have spin $\ell \geq 2$ and carry the proper quantum numbers to be produced in $\pi\pi$ collisions: The spin 2 resonances $f_2(1275)$ and $f_2'(1525)$, the spin 3 state $\rho_3(1681)$ and the state $f_J(1710)$, whose spin is not firmly established, but must be even. There is no evidence for exotic states: $f_2, f_2'$ and $f_J$ are isoscalars, while the $\rho_3$ is an isovector.

Very likely, the lightest spin 4 state is the $f_4(2044)$: A linear $\rho(770) - f_2(1275) - \rho_3(1691)$ Regge trajectory calls for a spin 4 recurrence almost exactly there. At any rate, if the spin of the state $f_J(1710)$ were equal to 4 or even larger, it would sit above that trajectory and thus upset the standard Regge picture, which we will be making use of to estimate the asymptotic part of the driving terms. We take it for granted that $J = 0$ or 2 and conclude that only the $I = 0$ $D$-wave and the $F$-wave contain resonances below 2 GeV. In the following, we discuss the contributions generated by these states, comparing the result obtained from the narrow width formula with the one found on the basis of two different phase shift analyses.

The most important contribution arises from the tensor meson $f_2(1275)$. Inserting the values $M_{f_2} = 1275\,\mathrm{MeV}$, $\Gamma_{f_2\to\pi\pi} = 157\,\mathrm{MeV}$, the narrow width formula gives $I^0_{0\,f_2} = .25\,\mathrm{GeV}^{-4}$, $I^0_{1\,f_2} = .15\,\mathrm{GeV}^{-6}$, $H^0_{f_2} = .93\,\mathrm{GeV}^{-6}$, to be compared with the results obtained with the parametrizations of the $D$-wave in refs. [47] and [57], which yield

$$[47]: \; I^0_{0\,D} = .25\,\mathrm{GeV}^{-4}, \; I^0_{1\,D} = .18\,\mathrm{GeV}^{-6}, \; H^0_D = 1.10\,\mathrm{GeV}^{-6} \quad , \tag{B.14}$$

$$[57]: \; I^0_{0\,D} = .27\,\mathrm{GeV}^{-4}, \; I^0_{1\,D} = .19\,\mathrm{GeV}^{-6}, \; H^0_D = 1.17\,\mathrm{GeV}^{-6} \quad . \tag{B.15}$$

These numbers show that the contributions from the imaginary part of the $D$-wave are dominated by the $f_2(1275)$.

We add a few remarks concerning the detailed behaviour of $\mathrm{Im}\, t^0_2(s)$ and first note that the $f_2'(1525)$ mainly decays into $K\bar{K}$. In the present context, this state may be ignored, because the corresponding $\pi\pi$ partial width is tiny: $\Gamma_{f_2'\to\pi\pi} = .62 \pm .14\,\mathrm{MeV}$. The phase shift analysis of ref. [57] does contain a second resonance in the $D$-wave, which generates a small enhancement in the integrands on the r.h.s. of eqs. (B.3), (B.5) towards the upper end of the range of integration. The numerical result in eq. (B.15) includes the tiny contribution produced by this enhancement, but this effect only accounts for a small fraction of the difference in the values obtained with the two different phase shift analyses. The main reason for that difference is that the two representations of the $D$-wave in refs. [47, 57] do not agree very well on the left wing of the $f_2(1275)$. In the context of the present paper, these details are not essential – we use the difference between the two phase shift analysis as a measure for the uncertainties to be attached to the moments.

To estimate the significance of the remaining partial waves with $I = 0$, we consider the contribution generated by the $f_4(2044)$. This resonance also mostly

decays into states other than $\pi\pi$. The relevant partial width is $\Gamma_{f_4\to\pi\pi} = 35 \pm 4$MeV. The narrow width formula shows that the contribution from this state is very small: $I^0_{0\,f_4} = .009\,\mathrm{GeV}^{-4}$, $I^0_{1\,f_4} = .002\,\mathrm{GeV}^{-6}$, $H^0_{f_4} = .04\,\mathrm{GeV}^{-6}$. Moreover, the center of the peak is outside our range of integration – more than half of the contribution from this level is to be booked in the asymptotic part. We conclude that the imaginary parts of the partial waves with $\ell \geq 4$ only matter at energies above 2 GeV.

The $\rho_3(1681)$ shows up as a peak in the imaginary part of the $F$-wave. According to the particle data tables [70], it mainly decays into $4\pi$. The partial width of interest in our context is $\Gamma_{\rho_3\to\pi\pi} = 38 \pm 3\,\mathrm{MeV}$. Inserting this in the narrow width formula, we obtain $I^1_{0\,\rho_3} = .020\,\mathrm{GeV}^{-4}$, $I^1_{1\,\rho_3} = .007\,\mathrm{GeV}^{-6}$, $H^1_{\rho_3} = .07\,\mathrm{GeV}^{-6}$, to be compared with the values found by performing the numerical integration with the representations for the $F$-wave given in the two references quoted above:

$$[47]: \; I^1_{0\,F} = .028\,\mathrm{GeV}^{-4}\,,\; I^1_{1\,F} = .012\,\mathrm{GeV}^{-6}\,,\; H^1_F = .12\,\mathrm{GeV}^{-6}\;\;, \tag{B.16}$$

$$[57]: \; I^1_{0\,F} = .030\,\mathrm{GeV}^{-4}\,,\; I^1_{1\,F} = .016\,\mathrm{GeV}^{-6}\,,\; H^1_F = .16\,\mathrm{GeV}^{-6}\;\;. \tag{B.17}$$

In the present case, the narrow width formula only accounts for about half of the result: The region below the resonance is equally important. There, the difference between the two phase shift analyses is more pronounced than for the $D$-waves. Accordingly, the uncertainties in the $F$-wave contributions to the moments are larger.

The formula (B.13) predicts that the contribution generated by the imaginary part of the $I = 2$ waves vanishes, because that channel does not contain any resonances. According to Martin, Morgan and Shaw [82], the $D$-wave phase shift may be approximated as $\delta^2_2(s) \simeq -0.003\,(s/4M_\pi^2)\,(1-4M_\pi^2/s)^{\frac{5}{2}}$. The corresponding contributions to the moments are indeed very small: $I^2_0 = 0.005\,\mathrm{GeV}^{-4}$, $I^2_1 = 0.006\,\mathrm{GeV}^{-6}$, $H = 0.04\,\mathrm{GeV}^{-6}$. In the following, we assume that these estimates do hold to within a factor of two.

This completes our discussion of the contributions generated by the higher partial waves in the region below 2 GeV. The net result is that these are due almost exclusively to the $D$- and $F$-waves. The numerical results are listed in row L of table 6. For $I = 0, 1$, the values given rely on the phase shift analyses of refs. [47, 57], while the estimates for $I = 2$ correspond to the parametrization of ref. [82].

| | $I=0$ | | | $I=1$ | | | $I=2$ | | |
|---|---|---|---|---|---|---|---|---|---|
| | $I_0^0$ GeV$^{-4}$ | $I_1^0$ GeV$^{-6}$ | $H^0$ GeV$^{-6}$ | $I_0^1$ GeV$^{-4}$ | $I_1^1$ GeV$^{-6}$ | $H^1$ GeV$^{-6}$ | $I_0^2$ GeV$^{-4}$ | $I_1^2$ GeV$^{-6}$ | $H^2$ GeV$^{-6}$ |
| L | .26 | .19 | 1.13 | .029 | .014 | .14 | .005 | .006 | .04 |
| R | .03 | .004 | .11 | .018 | .003 | .07 | – | – | – |
| P | .01 | .001 | .04 | .010 | .001 | .04 | .010 | .001 | .04 |
| total | .30 | .19 | 1.28 | .058 | .018 | .24 | .015 | .007 | .08 |
| ± | .01 | .01 | .05 | .007 | .002 | .03 | .008 | .006 | .04 |

Table 6: Moments of the background amplitude. The rows L, R and P indicate the contributions from the region below 2 GeV, from the leading Regge trajectory and from the Pomeron, respectively. The last two rows show the result for the sum of these contributions and our estimate of the uncertainties, respectively.

## B.4 Asymptotic contributions

We now turn to the contributions from the high energy tail of the dispersion integrals. The asymptotic behaviour of the scattering amplitude may be analyzed in terms of Regge poles. A trajectory with isospin $I$ generates a contribution $\propto s^{\alpha(t)}$ to the $t$-channel isospin component $\mathrm{Im}\, T^{(I)}(s,t)$, which is defined by

$$\mathrm{Im}\, T^{(I)}(s,t) = \sum_{I'} C_{st}^{II'}\, \mathrm{Im}\, T^{I'}(s,t) \quad .$$

The asymptotic behaviour of the amplitude with $I_t = 1$ ($s \to \infty$, $t$ fixed) is governed by the $\rho$-trajectory,

$$\mathrm{Im}\, T^{(1)}(s,t) = \beta_\rho(t)\, s^{\alpha_\rho(t)} \quad .$$

The Pomeron dominates the high energy behaviour of the $I_t = 0$ amplitude. Together with the contribution from the $f$-trajectory, the Regge representation of this component reads

$$\mathrm{Im}\, T^{(0)}(s,t) = 3\, P(s,t) + \beta_f(t)\, s^{\alpha_f(t)} \quad .$$

In the absence of exotic trajectories, the component with $I_t = 2$ rapidly tends to zero when $s$ becomes large. The asymptotic behaviour of the $s$-channel isospin components thus takes the form

$$\begin{aligned}
\mathrm{Im}\, T^0(s,t) &= P(s,t) + \tfrac{1}{3}\beta_f(t)\, s^{\alpha_f(t)} + \beta_\rho(t)\, s^{\alpha_\rho(t)} + (t \leftrightarrow u) \quad , \\
\mathrm{Im}\, T^1(s,t) &= P(s,t) + \tfrac{1}{3}\beta_f(t)\, s^{\alpha_f(t)} + \tfrac{1}{2}\beta_\rho(t)\, s^{\alpha_\rho(t)} - (t \leftrightarrow u) \quad , \\
\mathrm{Im}\, T^2(s,t) &= P(s,t) + \tfrac{1}{3}\beta_f(t)\, s^{\alpha_f(t)} - \tfrac{1}{2}\beta_\rho(t)\, s^{\alpha_\rho(t)} + (t \leftrightarrow u) \quad .
\end{aligned} \tag{B.18}$$

If $t$ is kept fixed, the terms with $P(s,t)$ and $\beta(t)\, s^{\alpha(t)}$ dominate, generating a peak in the forward direction, while the analogous structure in the backward direction

(fixed $u$) is described by those with $P(s,u)$ and $\beta(u)\, s^{\alpha(u)}$. At fixed $t$, the crossed terms drop off very rapidly with $s$, so that their contribution disappears in the noise of the calculation and may just as well be dropped.

The Lovelace-Shapiro-Veneziano model [83, 84, 85] provides a very instructive framework for understanding the interplay of the asymptotic contributions with the resonance structures seen at low energies (see appendix E). In that model, the $\rho$- and $f$-trajectories are linear and exchange degenerate,

$$\alpha_\rho(t) = \alpha_f(t) = \alpha_0 + t\,\alpha_1 \quad . \tag{B.19}$$

We fix the intercept with the Adler zero, $\alpha(M_\pi^2) = \frac{1}{2}$, and choose the slope such that the spin 1 state on the leading trajectory occurs at the proper mass:

$$\alpha_1 = \tfrac{1}{2}\,(M_\rho^2 - M_\pi^2)^{-1} \quad , \qquad \alpha_0 = \tfrac{1}{2} - \alpha_1\, M_\pi^2 \quad . \tag{B.20}$$

The amplitude may be represented as a sum of narrow resonance contributions. Since the model does not contain exotic states, $\mathrm{Im}\, T^2(s,t)$ vanishes, so that the residues $\beta_f(t)$ and $\beta_\rho(t)$ are in the ratio 3:2. The explicit expression reads

$$\beta_\rho(t) = \tfrac{2}{3}\beta_f(t) = \frac{\pi\,\lambda\,(\alpha_1)^{\alpha(t)}}{\Gamma[\alpha(t)]} \quad . \tag{B.21}$$

Finally, we fix the overall normalization constant $\lambda$ such that the width of the $\rho$ agrees with what is observed. This requires

$$\lambda = 96\,\pi\,\Gamma_\rho\, M_\rho^2\,(M_\rho^2 - 4M_\pi^2)^{-\frac{3}{2}} \quad . \tag{B.22}$$

The model explicitly obeys crossing symmetry and yields a decent picture both for the masses and widths of the resonances occurring on the leading trajectory and for the qualitative properties of the Regge residues $\beta_\rho(t)$, $\beta_f(t)$. The main deficiency of the model is lack of unitarity: It does not contain a Pomeron term, so that the total cross section tends to zero at high energies. While the model yields quite decent values for the full widths, it does not account for the fact that the resonances often decay into states other than $\pi\pi$, particularly if the available phase space becomes large – in the model, the branching fraction $\Gamma_{r\to\pi\pi}/\Gamma_r$ is equal to 1. Consequently, the LSV-model overestimates the magnitude of the Regge residues – a significant fraction thereof should be transferred to the Pomeron term. For this reason, the model can only serve as a semi-quantitative guide.

As discussed in section B.2, crossing symmetry strongly correlates the asymptotic behaviour of the partial waves with their properties at low energy. In particular, the parameters occurring in the Regge representation of the scattering amplitude can be extracted from low energy phenomenology. For a review of these calculations, we refer to the article by Pennington [43]. The value obtained

for $\beta_\rho(0)$ is smaller[13] than what follows from eqs. (B.21), (B.22) by a factor of $0.6 \pm 0.1$. Also, while the formula (B.21) implies that the residue contains a zero at $t_0 = 2M_\pi^2 - M_\rho^2 = -0.55\,\mathrm{GeV}^2$ because $\alpha(t)$ vanishes there, the calculation of ref. [43] instead yields a zero at $t_0 = -0.44 \pm 0.05\,\mathrm{GeV}^2$. This confirms the remarks made above: The LSV-model describes the qualitative properties of the Regge residues quite decently, but overestimates their magnitude.

In the numerical evaluation, we use the linear $\rho$-trajectory specified above, $\alpha_\rho(t) = \alpha(t)$, and fix the corresponding residue with the results of ref. [43], which are adequately described by a modified version of the LSV-formula:

$$\beta_\rho(t) = \frac{\pi \lambda_1 \alpha_1^{\alpha(t)}}{\Gamma[\,(t-t_0)\,\alpha_1]} \quad , \qquad t_0 = -0.44\,\mathrm{GeV}^2 \quad , \qquad \lambda_1 = (.78 \pm .13)\,\lambda \quad . \tag{B.23}$$

We determine the properties of the $f$-trajectory with exchange degeneracy, i.e. set $\alpha_f(t) = \alpha(t)$ and $\beta_f(t) = \frac{3}{2}\beta_\rho(t)$. For the Pomeron, we use the representation

$$P(s,t) = \sigma\, s\, e^{\frac{1}{2}bt} \quad . \tag{B.24}$$

While the parameter $b = 8\,\mathrm{GeV}^{-2}$ [43] describes the width of the diffraction peak, the optical theorem implies that $\sigma$ represents the asymptotic value of the total $\pi\pi$ cross section. Evidently, the above parametrization can be adequate only in a limited range of energies: The cross section does not tend to a constant, but grows logarithmically. In the present context, however, the behaviour at very high energies is an academic issue, because the integrands of the moments rapidly fall off with $s$. What counts is that the above representation yields a decent approximation for c.m. energies in the range between 2 and 3 GeV. There, the terms generated by the $\rho$-$f$-trajectory are by no means negligible: The formula (B.18) shows that at 2 GeV (3 GeV), these terms by themselves generate a contribution to $\mathrm{Im}\,T^0(s,0)$ that corresponds to a total cross section of 21 mb (14 mb) – in the energy range relevant for the moments, the Pomeron term does not represent the dominating contribution to the total cross section. As discussed in detail in ref. [43], crossing symmetry leads to the estimate $\sigma = (6 \pm 5)\,\mathrm{mb}$. Although the error bar is large, the value is significantly smaller than what is indicated by the rule of thumb $\sigma_{tot}^{\pi\pi} \simeq \frac{2}{3}\,\sigma_{tot}^{\pi N} \simeq \frac{4}{9}\,\sigma_{tot}^{NN} \simeq 20\,\mathrm{mb}$.

Indeed, the sum rule (B.6) confirms this result. The numerical values obtained with the above representation for the contributions from the $\rho$-$f$-trajectory are indicated in row R of table 6. If the high energy tail is omitted altogether, the l.h.s. of the sum rule (B.6) becomes $(2H^0)_L = 2.3\,\mathrm{GeV}^{-6}$, while the r.h.s. amounts to $(9H^1 + 5H^2)_L = 1.5\,\mathrm{GeV}^{-6}$. Clearly, further contributions are required to bring the sum rule into equilibrium. The Regge terms do contribute more to the

[13] In ref. [43], the residue is written as $\beta_\rho(t) = \frac{16}{3}\pi\gamma_\rho(t)\,\alpha_1^{\alpha_\rho(t)-\frac{1}{2}}$. The result obtained for the value at $t = 0$ is $\gamma_\rho(0) = (0.6 \pm 0.1) M_\pi^{-1}$, to be compared with the number $\gamma_\rho(0) = 0.97\,M_\pi^{-1}$ that follows from eqs. (B.19)-(B.22).

right than to the left and reduce the discrepancy by a factor of two. Since the Pomeron affects the various isospin components almost equally, it contributes about 7 times more to the right than to the left. For the sum rule to be obeyed within the uncertainties of the remaining contributions, the value of $\sigma$ must be in the range $\sigma = (5 \pm 3)\,\mathrm{mb}$.

Let us compare our representation of the background with the model used for the asymptotic behaviour in the early literature. Assume that, above an energy of 1.5 GeV, the imaginary parts can be described by a Pomeron term with $\sigma_{tot} = 20\,\mathrm{mb}$ and a Regge term that corresponds to the leading trajectory of the LSV-model. The l.h.s. of the sum rule (B.6) then takes the value $2H^0 = 3.3$, while the r.h.s yields $9H^1 + 5H^2 = 6.1$ (to be compared with the value 2.6 obtained for either one of the two sides with our representation of the background). Evidently, the model is in conflict with crossing symmetry. In the region relevant for the driving term integrals, the LSV-model overestimates the Regge residues by about 40% [43] and the sum rule (B.6) then implies that the value $\sigma = 20\,\mathrm{mb}$ is too large by about a factor of 4.

We repeat that our calculation has no bearing on the asymptotic behaviour of the total cross section – we are merely observing that, unless the value of $\sigma$ is in the range $5 \pm 3\,\mathrm{mb}$, the representation used for the amplitude violates crossing symmetry. The row P indicates the contributions to the moments generated by the Pomeron if $\sigma$ is taken in the middle of this range. The net result of our calculation is contained in the last two rows of table 6, which list the outcome for the moments and for the error bars to be attached to these, respectively. For the quantity $H$ defined in eq. (B.12), we obtain

$$H = 0.32 \pm 0.02\,\mathrm{GeV}^{-6} \quad . \tag{B.25}$$

## B.5 Driving terms

The polynomial approximation for the background amplitude can be used to determine the low energy behaviour of the driving terms – it suffices to evaluate the partial wave projections of the polynomial $\vec{T}(s,t)_d$. The range of validity of the resulting representation for the driving terms, however, only extends to c.m. energies of about 0.6 GeV. For our numerical work, we need a representation that holds for higher energies.

The approximations for the imaginary parts discussed above yield the following representation of the driving terms:

$$\begin{aligned}
d_\ell^I(s) &= d_\ell^I(s)_L + d_\ell^I(s)_R + d_\ell^I(s)_P \quad , \\
d_\ell^I(s)_L &= \sum_{I'=0}^{2} \sum_{\ell'=2}^{3} \int_{4M_\pi^2}^{s_2} ds'\, K_{\ell\ell'}^{II'}(s,s')\, \mathrm{Im}\, t_{\ell'}^{I'}(s') \quad , \\
d_\ell^I(s)_H &= \frac{1}{32\,\pi} \int_0^1 dz P_\ell(z)\, T^I(s,t_z)_H \quad , \qquad H = R,P
\end{aligned}$$

$$\vec{T}(s,t)_H = \int_{s_2}^{\infty} ds' g_2(s,t,s') \cdot \mathrm{Im}\,\vec{T}(s',0)_H + \int_{s_2}^{\infty} ds' g_3(s,t,s') \cdot \mathrm{Im}\,\vec{T}(s',t)_H \ ,$$
$$\mathrm{Im}\,T^0(s,t)_R = \tfrac{3}{2}\,\beta_\rho(t)\,s^{\alpha(t)} + \tfrac{3}{2}\,\beta_\rho(u)\,s^{\alpha(u)} \ ,$$
$$\mathrm{Im}\,T^1(s,t)_R = \beta_\rho(t)\,s^{\alpha(t)} - \beta_\rho(u)\,s^{\alpha(u)} \ ,$$
$$\mathrm{Im}\,T^2(s,t)_R = 0 \ ,$$
$$\mathrm{Im}\,T^0(s,t)_P = \mathrm{Im}\,T^2(s,t)_P = P(s,t) + P(s,u) \ ,$$
$$\mathrm{Im}\,T^1(s,t)_P = P(s,t) - P(s,u) \ .$$

The result of the numerical evaluation of these integrals with the parameter values specified above is given in eq. (4.1).

We use the difference between the results for $d_0^0(s)_L$ and $d_1^1(s)_L$ obtained with the two phase shift analyses quoted above as a measure for the uncertainties in these quantities. In the case of the $I = 2$ $D$-wave, we assume that the Martin-Morgan-Shaw formula does describe the behaviour of the imaginary part to within a factor of 2. For the Regge-contributions, we use the error estimate $\gamma_\rho(0) = (0.6 \pm 0.1) M_\pi^{-1}$ given in ref. [43]. Finally, the uncertainties attached to the Pomeron term correspond to those in the value $\sigma = 5 \pm 3\,\mathrm{mb}$, obtained in section B.4. The result quoted in eq. (4.2) is obtained by adding the corresponding error bars quadratically and fitting the outcome with a polynomial.

There is a neat and rather thorough check of the above calculation. The driving terms represent the partial wave projections of the background amplitude. Since that amplitude must be crossing symmetric, we may equally well calculate the projections with the formula (A.2) instead of using (A.3) – the result should be the same. The modification of the partial wave projection changes the form of the kernels $K_{\ell\ell'}^{II'}(s,s')$ and the contributions from the imaginary parts of the higher partial waves below 2 GeV then change, quite substantially. The contributions from the asymptotic region, however, are also modified. In the sum, these changes indeed cancel out, to a remarkable degree of accuracy. This corroborates the claim that our description of the background is approximately crossing symmetric. Evidently, the sum rule (B.6) plays an important role here, as it correlates the magnitude of the asymptotic contributions with those from the low energy region.

# C Sum rules and asymptotic behaviour

## C.1 Sum rules for the $P$-wave

As discussed in section 11, the Olsson sum rule ensures the correct asymptotic behaviour of the $t$-channel $I = 1$ scattering amplitude $T^{(1)}(s,t)$ for $s \to \infty$, $t = 0$. The requirement that this amplitude has the proper high energy behaviour also for $t < 0$ implies a further constraint, which is readily derived from the fixed-$t$ dispersion relation (2.4). It suffices to evaluate the coefficient of the term that grows linearly with $s$ and to subtract the value at $t = 0$. The result involves the

following integrals over the imaginary parts of the amplitude ($t \leq 0$):

$$S(t) \equiv \int_{4M_\pi^2}^{\infty} ds\, \frac{2\,\mathrm{Im}\,\bar{T}^0(s,t) + 3\,\mathrm{Im}\,\bar{T}^1(s,t) - 5\,\mathrm{Im}\,\bar{T}^2(s,t)}{12\,s\,(s+t-4M_\pi^2)} - \int_{4M_\pi^2}^{\infty} ds\, \frac{(s-2M_\pi^2)\,\mathrm{Im}\,T^1(s,0)}{s\,(s-4M_\pi^2)\,(s-t)\,(s+t-4M_\pi^2)} \quad . \tag{C.1}$$

The barred quantities stand for $\mathrm{Im}\,\bar{T}^I(s,t) = \{\mathrm{Im}\,T^I(s,t) - \mathrm{Im}\,T^I(s,0)\}/t$. The amplitude $T^{(1)}(s,t)$ has the proper asymptotic behaviour only if $S(t)$ vanishes for space-like values of $t$. Since the $S$-waves drop out, the condition amounts to a family of sum rules that relate integrals over the imaginary part of the $P$-wave to the higher partial waves. For $t = 0$, for instance, the sum rule may be written in the form

$$\int_{4M_\pi^2}^{\infty} ds\, \frac{\mathrm{Im}\,t_1^1(s)}{s^2\,(s-4M_\pi^2)} = \sum_{\ell=2,4,\,\ldots} (2\ell+1)\,\ell\,(\ell+1) \int_{4M_\pi^2}^{\infty} ds\, \frac{2\,\mathrm{Im}\,t_\ell^0(s) - 5\,\mathrm{Im}\,t_\ell^2(s)}{18\,s\,(s-4M_\pi^2)^2} + \sum_{\ell=3,5,\,\ldots} (2\ell+1) \int_{4M_\pi^2}^{\infty} ds\, \frac{\{\ell(\ell+1)\,s - 4\,(s-2\,M_\pi^2)\}\,\mathrm{Im}\,t_\ell^1(s)}{6\,s^2\,(s-4M_\pi^2)^2} \quad . \tag{C.2}$$

The integrals over the individual partial waves converge more rapidly than in the case of the Olsson sum rule, but the factor $\ell(\ell+1)$ gives the higher partial waves more weight – in fact, the contributions from the asymptotic region are even more important here. The sum rule is of the same structure as the one that follows from crossing symmetry, eq. (B.7), but there are two differences: The integrals converge less rapidly by one power of $s$ and the $P$-wave does not drop out.

Since the sum rule (C.2) offers a good opportunity to check the representation used for the asymptotic region, we evaluate it explicitly with our input for the imaginary parts. We split the integration into one from threshold to $\sqrt{s_2} = 2\,\mathrm{GeV}$ and one over the asymptotic region, $s > s_2$ (compare appendix B). Denoting the low energy part of the integral over the $P$-wave by

$$S_P = \int_{4M_\pi^2}^{s_2} ds\, \frac{\mathrm{Im}\,t_1^1(s)}{s^2\,(s-4M_\pi^2)} \quad ,$$

we write the sum rule in the form

$$S_P = S_D + S_F + S_{as} \quad , \tag{C.3}$$

where $S_D$ and $S_F$ stand for the analogous integrals over the $D$- and $F$-waves. While the low energy contributions from the waves with $\ell \geq 4$ are neglected, their high energy tails are accounted for in the term $S_{as}$, which collects all contributions from the region above $s_2$.

The form (C.2) of the sum rule is suitable to calculate the contributions from the interval $4M_\pi^2 < s < s_2$. Numerically, we obtain

$$S_P = 1.93 \pm 0.08 \quad , \qquad S_D = 0.55 \pm 0.03 \quad , \qquad S_F = 0.13 \pm 0.01 \quad ,$$

in units of $\mathrm{GeV}^{-4}$. To evaluate the asymptotic contributions, we instead use the form (C.1): The term $S_{as}$ coincides with the expression $S(0)/48\pi$, except that the integration now only extends over the interval $s_2 < s < \infty$. Inserting the representation specified in appendix B.4, we find that the bulk stems from the leading Regge trajectory $(1.12 \pm 0.19)$. The Pomeron does not contribute to the first integral on the r.h.s. of eq. (C.1), because that integral is of the same isospin structure as the one occurring in the Olsson sum rule, but it does generate a small negative term via the second integral $(-0.02 \pm 0.01)$. The net result for the asymptotic contributions,

$$S_{as} = 1.10 \pm 0.19 \ ,$$

leads to $S_{D}+S_{F}+S_{as} = 1.77\pm0.19$. Within the errors, the outcome agrees with the numerical value $S_{P} = 1.93\pm0.08$ obtained for the l.h.s. of the sum rule (C.3). Note that more than half of the r.h.s. stems from the asymptotic region. We conclude that our asymptotic representation is valid within the estimated uncertainties, also for this sum rule, which converges more slowly than the moments considered in appendix B. Since the Olsson sum rule belongs to the same convergence class as the one above, we feel confident that our error estimates apply also in that case.

## C.2 Asymptotic behaviour of the Roy integrals

If the imaginary parts of the partial waves with $\ell > 1$ are discarded, the Roy equations become a closed system for the $S$- and $P$-waves. The explicit expressions for the kernels show that the dispersion integrals over the imaginary parts of these waves grow linearly with $s$, like the subtraction polynomials. Except for the contributions from the higher partial waves, the r.h.s. of the Roy equations for the $S$- and $P$-waves thus grows in proportion to $s$:

$$\begin{aligned}
&\mathrm{Re}\, t_0^0 \to \frac{\Sigma\, s}{12 M_\pi^2} \ , \qquad \mathrm{Re}\, t_1^1 \to \frac{\Sigma\, s}{72 M_\pi^2} \ , \qquad \mathrm{Re}\, t_0^2 \to -\frac{\Sigma\, s}{24 M_\pi^2} \ , \\
&\Sigma = 2\, a_0^0 - 5\, a_0^2 - \frac{4M_\pi^2}{\pi} \int_{4M_\pi^2}^\infty ds\, \frac{2\,\mathrm{Im}\, t_0^0(s) + 27\,\mathrm{Im}\, t_1^1(s) - 5\,\mathrm{Im}\, t_0^2(s)}{s\,(s-4M_\pi^2)} \ . \qquad \text{(C.4)}
\end{aligned}$$

So, if the coefficient $\Sigma$ vanishes, the contribution from the dispersion integrals cancels the one from the subtraction polynomial, simultaneously for all three partial waves [2, 82]. In fact, if the imaginary parts of the higher partial waves are dropped and if $\Sigma$ is set equal to zero, the Roy equations become identical to those proposed by Chew and Mandelstam [68] (see ref. [2] for a detailed discussion). The expression for $\Sigma$ resembles the Olsson sum rule, where the contributions from the $S$- and $P$-wave read

$$2\, a_0^0 - 5\, a_0^2 = \frac{4M_\pi^2}{\pi} \int_{4M_\pi^2}^\infty ds\, \frac{2\,\mathrm{Im}\, t_0^0(s) + 9\,\mathrm{Im}\, t_1^1(s) - 5\,\mathrm{Im}\, t_0^2(s)}{s\,(s-4M_\pi^2)} + \ldots$$

If only the $S$-waves are retained, the Olsson sum rule does imply that $\Sigma$ vanishes – evidently, this sum rule is closely related to the observation that the linearly rising contribution from the subtraction terms must cancel the one from the dispersion integrals (section 10). As is well-known, however, the coefficient of the $P$-wave term in $\Sigma$ differs from the one in the Olsson sum rule. The implications of this discrepancy for the Chew-Mandelstam framework are discussed in the references quoted above. The family of sum rules derived in appendix C.1 points in the same direction: The imaginary part of the $P$-wave is tied together with those of the higher partial waves – setting these equal to zero leads to inconsistencies [86].

For the above asymptotic formulae to apply at $E \sim 1\,\mathrm{GeV}$, two conditions would have to be met: (a) the contributions from the higher partial waves can be ignored at these energies and (b) the integrals over the imaginary parts of the $S$- and $P$-waves are dominated by the contributions from low energies. Unfortunately, neither of the two conditions is met. The solutions show a pronounced structure in the region above the matching point – evidently, we are not dealing with the asymptotic behaviour there. The numerical value of $\Sigma$ is negative: The integral in eq. (C.4) over-compensates the term $2a_0^0 - 5a_0^2$. We may lay the blame upon the contributions above the matching point – if the integral were cut off there, $\Sigma$ would approximately vanish.

The situation is quite different for the Olsson sum rule, which does not rely on low energy approximations but represents the exact version of the condition that must be obeyed by the two subtraction constants for the scattering amplitude to have the proper asymptotic behaviour. In that case, the coefficient of the $P$-wave is three times smaller – the region above the matching point plays an essential role in bringing the sum rule into balance. The numerical evaluation in section 11 shows that even those from the region above 2 GeV are significant. The rapid growth of the driving terms indicates that the higher partial waves become increasingly important as the energy rises – it is clear that the asymptotic behaviour of the partial wave amplitudes cannot be studied on the basis of the $S$- and $P$-wave contributions to the r.h.s of the Roy equations.

We conclude that, at the quantitative level, the above simple mechanism cannot explain why, for suitable values of $a_0^0$ and $a_0^2$, our solutions remain within the bounds set by unitarity. For an analysis of the behaviour above the matching point that neither discards the higher partial waves, nor relies on low energy dominance, we refer to sections 10 and 11.

# D Explicit numerical solutions

In this appendix, we make available our explicit numerical solutions of the Roy integral equations. We proceed as follows. For a few tens of pairs $(a_0^0, a_0^2)$ in the universal band (see fig. 7), we have constructed the three lowest partial waves at $2M_\pi \leq \sqrt{s} \leq 0.8$ GeV. As we explain in the main text, we parametrize the phase

| | $A_0^0$ | $B_0^0$ | $C_0^0$ | $D_0^0$ | $s_0^0$ |
|---|---|---|---|---|---|
| $z_1$ | .2250 | .2463 | $-.1665\cdot10^{-1}$ | $-.6403\cdot10^{-3}$ | $.3672\cdot10^{2}$ |
| $z_2$ | .2250 | .1985 | $.3283\cdot10^{-2}$ | $-.4136\cdot10^{-2}$ | $.1339\cdot10$ |
| $z_3$ | .0000 | .1289 | $.1142\cdot10^{-1}$ | $-.3699\cdot10^{-2}$ | .6504 |
| $z_4$ | .0000 | $.1426\cdot10^{-1}$ | $.1400\cdot10^{-1}$ | $-.3980\cdot10^{-2}$ | $-.3211\cdot10$ |
| $z_5$ | .0000 | $.8717\cdot10^{-2}$ | $.1613\cdot10^{-1}$ | $-.3152\cdot10^{-2}$ | $-.1396\cdot10$ |
| $z_6$ | .0000 | $.5058\cdot10^{-1}$ | $.3000\cdot10^{-1}$ | $-.7354\cdot10^{-2}$ | $-.4114\cdot10$ |
| $z_7$ | .0000 | $-.4266\cdot10^{-2}$ | $-.4045\cdot10^{-2}$ | $-.1212\cdot10^{-2}$ | $-.3447\cdot10$ |
| $z_8$ | .0000 | $-.4658\cdot10^{-2}$ | $.2110\cdot10^{-2}$ | $-.4544\cdot10^{-2}$ | $-.8428\cdot10$ |
| $z_9$ | .0000 | $-.5358\cdot10^{-2}$ | $.1095\cdot10^{-1}$ | $-.4558\cdot10^{-2}$ | $-.6350\cdot10$ |
| $z_{10}$ | .0000 | $-.2555\cdot10^{-2}$ | $.4249\cdot10^{-2}$ | $-.1271\cdot10^{-2}$ | $-.1486\cdot10$ |

| | $A_1^1$ | $B_1^1$ | $C_1^1$ | $D_1^1$ | $s_1^1$ |
|---|---|---|---|---|---|
| $z_1$ | $.3626\cdot10^{-1}$ | $.1337\cdot10^{-3}$ | $-.6976\cdot10^{-4}$ | $.1408\cdot10^{-5}$ | $.3074\cdot10^{2}$ |
| $z_2$ | $.1834\cdot10^{-1}$ | $-.2336\cdot10^{-2}$ | $.1965\cdot10^{-3}$ | $-.1974\cdot10^{-4}$ | $-.2459$ |
| $z_3$ | $.1081\cdot10^{-1}$ | $-.8563\cdot10^{-3}$ | $.3268\cdot10^{-4}$ | $-.8821\cdot10^{-5}$ | $-.1733$ |
| $z_4$ | $-.3195\cdot10^{-2}$ | $.1678\cdot10^{-3}$ | $.2173\cdot10^{-4}$ | $-.6047\cdot10^{-6}$ | $.6323\cdot10^{-1}$ |
| $z_5$ | $.1670\cdot10^{-3}$ | $.4147\cdot10^{-4}$ | $.3267\cdot10^{-5}$ | $-.1617\cdot10^{-5}$ | $-.1090\cdot10^{-2}$ |
| $z_6$ | $-.9543\cdot10^{-3}$ | $.8402\cdot10^{-4}$ | $.2059\cdot10^{-4}$ | $-.3125\cdot10^{-5}$ | $.2724\cdot10^{-1}$ |
| $z_7$ | $.5049\cdot10^{-3}$ | $-.9308\cdot10^{-4}$ | $.1070\cdot10^{-4}$ | $-.1257\cdot10^{-5}$ | $-.7218\cdot10^{-2}$ |
| $z_8$ | $.4595\cdot10^{-4}$ | $-.2755\cdot10^{-3}$ | $.5554\cdot10^{-4}$ | $-.4432\cdot10^{-5}$ | $.1483\cdot10^{-1}$ |
| $z_9$ | $-.9000\cdot10^{-4}$ | $-.2308\cdot10^{-3}$ | $.5307\cdot10^{-4}$ | $-.4415\cdot10^{-5}$ | $.1813\cdot10^{-1}$ |
| $z_{10}$ | $-.1198\cdot10^{-4}$ | $-.6120\cdot10^{-4}$ | $.1519\cdot10^{-4}$ | $-.1344\cdot10^{-5}$ | $.5016\cdot10^{-2}$ |

| | $A_0^2$ | $B_0^2$ | $C_0^2$ | $D_0^2$ | $s_0^2$ |
|---|---|---|---|---|---|
| $z_1$ | $-.3706\cdot10^{-1}$ | $-.8553\cdot10^{-1}$ | $-.7542\cdot10^{-2}$ | $.1987\cdot10^{-3}$ | $-.1192\cdot10^{2}$ |
| $z_2$ | .0000 | $-.1236\cdot10^{-1}$ | $.3466\cdot10^{-1}$ | $-.2524\cdot10^{-2}$ | $-.4040\cdot10^{2}$ |
| $z_3$ | $-.3706\cdot10^{-1}$ | $-.6673\cdot10^{-2}$ | $.2857\cdot10^{-1}$ | $-.1993\cdot10^{-2}$ | $-.3457\cdot10^{2}$ |
| $z_4$ | .0000 | $.4901\cdot10^{-2}$ | $.2674\cdot10^{-2}$ | $.1506\cdot10^{-2}$ | $-.9879\cdot10^{2}$ |
| $z_5$ | .0000 | $.2810\cdot10^{-1}$ | $.1477\cdot10^{-1}$ | $.2915\cdot10^{-3}$ | $-.9856\cdot10^{2}$ |
| $z_6$ | .0000 | $.4010\cdot10^{-1}$ | $.2458\cdot10^{-1}$ | $.1325\cdot10^{-2}$ | $-.2072\cdot10^{3}$ |
| $z_7$ | .0000 | $-.1663\cdot10^{-1}$ | $-.3030\cdot10^{-1}$ | $.8759\cdot10^{-3}$ | $-.1589\cdot10^{3}$ |
| $z_8$ | .0000 | $-.6784\cdot10^{-1}$ | $-.9512\cdot10^{-1}$ | $.4713\cdot10^{-2}$ | $-.5259\cdot10^{3}$ |
| $z_9$ | .0000 | $-.5429\cdot10^{-1}$ | $-.8744\cdot10^{-1}$ | $.5313\cdot10^{-2}$ | $-.5366\cdot10^{3}$ |
| $z_{10}$ | .0000 | $-.1178\cdot10^{-1}$ | $-.2535\cdot10^{-1}$ | $.1730\cdot10^{-2}$ | $-.1723\cdot10^{3}$ |

Table 7: Polynomial coefficients for Roy solutions.

shifts $\delta_\ell^I$ of the solutions in the manner proposed by Schenk [65],

$$\tan\delta_\ell^I = \sqrt{1-\frac{4M_\pi^2}{s}}\; q^{2\ell}\left\{A_\ell^I + B_\ell^I q^2 + C_\ell^I q^4 + D_\ell^I q^6\right\}\left(\frac{4M_\pi^2 - s_\ell^I}{s - s_\ell^I}\right) \quad , \qquad \text{(D.1)}$$

Each solution of the Roy equations corresponds to a specific value of the $3 \times 5$ coefficients in this expansion,

$$A_\ell^I = A_\ell^I(a_0^0, a_0^2),\; \ldots\; ,\; s_\ell^I = s_\ell^I(a_0^0, a_0^2)\; .$$

We approximate these by a polynomial of third degree in the scattering lengths $a_0^0$ and $a_0^2$. In terms of the variables

$$u = \frac{a_0^0}{p_0} - 1 \;\; , \;\; v = \frac{a_0^2}{p_2} - 1 \;\; , \;\; p_0 = 0.225 \;\; , \;\; p_2 = -0.03706 \;\; ,$$

the numerical representation for the coefficient $B_0^0$, for instance, reads

$$B_0^0 = z_1 + z_2\, u + z_3\, v + z_4\, u^2 + z_5\, v^2 + z_6\, u\, v + z_7\, u^3 + z_8\, u^2\, v + z_9\, u\, v^2 + z_{10}\, v^3 \;\; .$$

The $15 \times 10$ numbers $z_1, \ldots, z_{10}$ for the coefficients $A_0^0, B_0^0, \ldots, s_0^2$ are displayed in table 7, in units of $M_\pi^2$.

# E Lovelace-Shapiro-Veneziano model

In this appendix, we describe the model used to illustrate the basic properties of the Regge poles occurring in the asymptotic representation of the scattering amplitude [83, 84, 85]. In this model, the $\pi\pi$ scattering amplitude is taken to be of the form

$$A(s,t,u)_V = \lambda_1\, \Phi(\alpha_s, \alpha_t) + \lambda_1\, \Phi(\alpha_s, \alpha_u) + \lambda_2\, \Phi(\alpha_t, \alpha_u)\, ,$$

where $\Phi(\alpha, \beta)$ is closely related to the Beta-function,

$$\Phi(\alpha,\beta) = \frac{\Gamma(1-\alpha)\Gamma(1-\beta)}{\Gamma(1-\alpha-\beta)} \;\; .$$

and $\alpha_s$ represents a linear Regge trajectory,

$$\alpha_s = \alpha_0 + \alpha_1 s\, .$$

At fixed $t$, the function $\Phi(\alpha_s, \alpha_t)$ shows Regge behaviour when $s$ tends to infinity:

$$\Phi(\alpha_s, \alpha_t) \to (-\alpha_s)^{\alpha_t}\Gamma(1-\alpha_t)\, .$$

At the same time, the representation $(1-\alpha_t > 0)$

$$\begin{aligned}\Phi(\alpha_s,\alpha_t) &= (1-\alpha_s-\alpha_t)\,B(1-\alpha_s,1-\alpha_t) \\ &= (1-\alpha_s-\alpha_t)\,\left\{\frac{1}{1-\alpha_s}+\sum_{n=1}^{\infty}\frac{\alpha_t(\alpha_t+1)\cdots(\alpha_t+n-1)}{n!\,(n+1-\alpha_s)}\right\}\end{aligned} \tag{E.1}$$

shows that the amplitude may be expressed as a sum of narrow resonance contributions, with mass

$$M_n^2 = (\alpha_1)^{-1}(n-\alpha_0)\ , \qquad n=1,2,\ldots$$

The coupling constants $\lambda_1, \lambda_2$ may be chosen such that the amplitude does not contain resonances with $I=2$. For this condition to be satisfied, the corresponding $s$-channel isospin component

$$T^2(s,t)_V = 2\,\lambda_1\,\Phi(\alpha_t,\alpha_u) + (\lambda_1+\lambda_2)\,(\Phi(\alpha_s,\alpha_t)+\Phi(\alpha_s,\alpha_u))$$

should be free of poles in the physical region of the $s$-channel. This requires

$$\lambda_2 = -\lambda_1 \equiv \tfrac{1}{2}\lambda\,,$$

so that the amplitude takes the form

$$\begin{aligned}A(s,t,u)_V &= -\tfrac{1}{2}\lambda\,\{\Phi(\alpha_s,\alpha_t)+\Phi(\alpha_s,\alpha_u)-\Phi(\alpha_t,\alpha_u)\}\ , \\ T^0(s,t)_V &= -\tfrac{1}{2}\lambda\,\{3\,\Phi(\alpha_s,\alpha_t)+3\,\Phi(\alpha_s,\alpha_u)-\Phi(\alpha_t,\alpha_u)\}\ , \\ T^1(s,t)_V &= -\lambda\,\{\Phi(\alpha_s,\alpha_t)-\Phi(\alpha_s,\alpha_u)\}\ , \\ T^2(s,t)_V &= -\lambda\,\Phi(\alpha_t,\alpha_u)\ .\end{aligned} \tag{E.2}$$

In the chiral limit, where the Mandelstam triangle shrinks to the point $s=t=u=0$, the amplitude must contain an Adler zero there. Indeed, the factor $1-\alpha_s-\alpha_t$ generates such a zero if $\alpha_0=\frac{1}{2}$. Hence the deviation of $\alpha_0$ from $\frac{1}{2}$ must be of order $M_\pi^2$, so that $\alpha_s-\frac{1}{2}$ represents a quantity of order $p^2$. At leading order of the low energy expansion, the behaviour of the amplitude therefore represents the first term in the expansion around the point $\alpha_s=\alpha_t=\alpha_u=\frac{1}{2}$, which in view of $\Gamma(\frac{1}{2})=\sqrt{\pi}$ yields

$$A(s,t,u)_V = \pi\,\lambda\,(\alpha_s-\tfrac{1}{2}) + O(p^4)\,, \tag{E.3}$$

This does have the structure of the Weinberg formula, provided the intercept $\alpha_0$ is chosen such that $\alpha_s$ passes through the value $\frac{1}{2}$ at $s=M_\pi^2$, i.e. [84]

$$\alpha_0 = \tfrac{1}{2} - \alpha_1\,M_\pi^2\,.$$

The lowest levels of spin 1, 2, 3, 4 indeed occur on an approximately linear trajectory with this intercept: Fixing the value of the slope with $M_\rho$,

$$\alpha_1 = \tfrac{1}{2}\,(M_\rho^2 - M_\pi^2)^{-1}\,,$$

the model predicts

$$M_{f_2} = 1319\,(1275)\,\mathrm{MeV},\ M_{\rho_3} = 1699\,(1691)\,\mathrm{MeV},\ M_{f_4} = 2008\,(2044)\,\mathrm{MeV},$$

where the numbers in brackets are those in the data tables [70].

The representation (E.1) shows that for $s > 4\,M_\pi^2$, $t < 0$, the imaginary part of $\Phi(\alpha_s, \alpha_t)$ consists of a sequence of $\delta$-functions:

$$\begin{aligned}
\mathrm{Im}\,\Phi(\alpha_s, \alpha_t) &= -\pi \sum_{n=1}^{\infty} R_n(\alpha_t)\,\delta(\alpha_s - n)\ \ , \\
R_n(\alpha) &= \frac{\Gamma(\alpha_t + n)}{\Gamma(n)\Gamma(\alpha_t)} = \frac{1}{(n-1)!}\,\alpha_t\,(\alpha_t + 1)\,\cdots\,(\alpha_t + n - 1)\ \ .
\end{aligned}$$

For the imaginary part of the $s$-channel isospin components, we thus obtain

$$\begin{aligned}
\mathrm{Im}\,T^0(s,t)_V &= \frac{3\,\lambda\,\pi}{2\,\alpha_1} \sum_{n=1}^{\infty} \{R_n(\alpha_t) + R_n(\alpha_u)\}\,\delta(s - M_n^2)\ \ , \\
\mathrm{Im}\,T^1(s,t)_V &= \frac{\lambda\,\pi}{\alpha_1} \sum_{n=1}^{\infty} \{R_n(\alpha_t) - R_n(\alpha_u)\}\,\delta(s - M_n^2)\ \ , \\
\mathrm{Im}\,T^2(s,t)_V &= 0\,,
\end{aligned}$$

with $u = 4\,M_\pi^2 - t - M_n^2$.

We may then read off the imaginary parts of the partial wave amplitudes by decomposing the polynomial $R_n(\alpha)$ into a Legendre series:[14]

$$\begin{aligned}
R_n(\alpha_t) &= \sum_{\ell=0}^{n} (2\,\ell + 1)\,P_\ell\left(1 + \frac{2\,t}{M_n^2 - 4\,M_\pi^2}\right)\,r_{n\,\ell}\ \ , \\
\mathrm{Im}\,t_\ell^0(s)_V &= \frac{3\,\lambda}{64\,\alpha_1}\{1 + (-1)^\ell\} \sum_{n=\ell}^{\infty} r_{n\,\ell}\,\delta(s - M_n^2)\ \ , \\
\mathrm{Im}\,t_\ell^1(s)_V &= \frac{\lambda}{32\,\alpha_1}\{1 - (-1)^\ell\} \sum_{n=\ell}^{\infty} r_{n\,\ell}\,\delta(s - M_n^2)\ \ , \\
\mathrm{Im}\,t_\ell^2(s)_V &= 0\ \ .
\end{aligned}$$

On the leading trajectory, the coefficients are

$$r_{n\,n} = \frac{n}{2^n\,(2\,n+1)!!}\,\alpha_1^n\,(M_n^2 - 4\,M_\pi^2)^n\,.$$

Comparison with the narrow width formula (B.13) shows that the model predicts the width of the various levels as[15]

$$\Gamma_{n\,\ell}^{\pi\pi} = \frac{\lambda\,\omega^I\,r_{n\,\ell}}{32\,\pi\,\alpha_1\,M_n^2}(M_n^2 - 4\,M_\pi^2)^{\frac{1}{2}}\,, \tag{E.4}$$

[14] In the case of $t_0^0(s)$, the sum over $n$ only starts at $n = 1$.

[15] The formula reproduces the numerical results in Table I of ref. [85], if the parameter values are adapted accordingly ($\alpha_0 = 0.48$, $\alpha_1 = 0.9\,\mathrm{GeV}^{-2}$, $\Gamma_\rho = 112\,\mathrm{MeV}$, $M_\rho = 764\,\mathrm{MeV}$).

where $\omega^I$ depends on the isospin of the particle: $\omega^0 = 3$, $\omega^1 = 2$, $\omega^2 = 0$. In particular, the result for the width of the $\rho$ reads

$$\Gamma_\rho = \frac{\lambda}{96\,\pi\,M_\rho^2}\,(M_\rho^2 - 4\,M_\pi^2)^{\frac{3}{2}}\,. \tag{E.5}$$

Fixing the coupling constant with the experimental value $\Gamma_\rho = 151.2\,\mathrm{MeV}$, we obtain $\lambda/32\pi = 0.728$. The formula (E.4) then predicts

$$\Gamma_{f_2}^{\pi\pi} = 130\,(157)\,\mathrm{MeV}\,, \qquad \Gamma_{\rho_3}^{\pi\pi} = 51\,(51)\,\mathrm{MeV}\,, \qquad \Gamma_{f_4}^{\pi\pi} = 46\,(35)\,\mathrm{MeV}\,,$$

where the numbers in brackets are again taken from the data tables [70]. This shows that the model does yield a decent picture, not only for the masses but also for the widths of the particles on the leading trajectory.

In addition to the levels on the leading trajectory, the model, however, also contains plenty of daughters, with a rather strong coupling to the $\pi\pi$-channel. For the states on the first daughter trajectory, for instance, equation (E.4) yields $\Gamma_{10}^{\pi\pi} = 783\,\mathrm{MeV}$, $\Gamma_{21}^{\pi\pi} = 154\,\mathrm{MeV}$, $\Gamma_{32}^{\pi\pi} = 113\,\mathrm{MeV}$, $\Gamma_{43}^{\pi\pi} = 42\,\mathrm{MeV}$, etc. The scalar daughter of the $\rho$ is particularly fat.

It is clear that an amplitude that describes all of the levels as narrow resonances fails here. Unitarity implies the bound

$$\int_{4\,M_\pi^2}^{M^2} ds\,\mathrm{Im}\,t_0^0(s)\,\sqrt{1 - 4M_\pi^2/s} \leq M^2 - 4M_\pi^2\,.$$

This condition is violated for $M < 1.3\,\mathrm{GeV}$. Also, if the intercept of the leading trajectory is fixed with the Adler condition as above, the scalar daughter of the $f_2$ is a ghost: The formula (E.4) yields a negative decay width [85]. In this respect, the model is deficient – as witnessed by the life of even royal families, the decency of a mother does not ensure that her daughters behave.

The problem also shows up in the S-wave scattering lengths: Chiral symmetry relates the coefficient of the leading term in the low energy expansion (E.3) to the pion decay constant,

$$\pi\,\lambda\,\alpha_1 = \frac{1}{F_\pi^2}\quad. \tag{E.6}$$

If the coupling constant $\lambda$ is fixed such that the model yields the proper width for the $\rho$, the l.h.s. of this relation exceeds the r.h.s. by a factor of 1.7. Accordingly, the prediction of the model for $a_0^0$ exceeds the current algebra result by about this factor. In the vicinity of threshold, the behaviour of the amplitude is determined by the properties of the function $\phi(\alpha,\beta)$ for $\alpha \simeq \beta \simeq \frac{1}{2}$. There, the first term in the series (E.1) accounts for about two thirds of the sum. The spin 1 component of this term is due to $\rho$-exchange, while the spin 0 part arises from the scalar daughter of the $\rho$. By construction, the former does have the proper magnitude. The S-wave scattering lengths are too large because the scalar daughter of the $\rho$ is too fat.

As was noted from the start [85], the model is not unique. To arrive at a more realistic model, we could add extra terms that domesticate the daughters and leave the leading trajectory and the position of the Adler zero untouched. Note, however, that the number of states occurring in the Veneziano model corresponds to the degrees of freedom of a string, while the spectrum of bound states in QCD is the one of a local field theory, where the number of independent states grows much less rapidly with the mass. Modifications of the type just mentioned can at best provide a partial cure. In particular, these do not remove the main deficiency of the model, lack of unitarity.

# References


[1] S. M. Roy, Phys. Lett. **B36** (1971) 353.

[2] J. L. Basdevant, J. C. Le Guillou and H. Navelet, Nuovo Cim. **A7** (1972) 363.

[3] M.R. Pennington and S.D. Protopopescu, Phys. Rev. **D7** (1973) 1429.

[4] M.R. Pennington and S.D. Protopopescu, Phys. Rev. **D7** (1973) 2591.

[5] J. L. Basdevant, C. D. Froggatt and J. L. Petersen, Phys. Lett. **B41** (1972) 173; ibid. 178.

[6] J. L. Basdevant, C. D. Froggatt and J. L. Petersen, Nucl. Phys. **B72** (1974) 413.

[7] J. L. Petersen, Acta Phys. Austriaca Suppl. **13** (1974) 291; Yellow report CERN 77-04 (1977).

[8] C. D. Froggatt and J. L. Petersen, Nucl. Phys. **B91** (1975) 454; ibid. **B104** (1976) 186 (E); ibid. **B129** (1977) 89.

[9] D. Morgan and M.R. Pennington, in ref. [10], p. 193.

[10] L. Maiani, G. Pancheri and N. Paver, *The Second* DAΦNE *Physics Handbook* (INFN-LNF-Divisione Ricerca, SIS-Ufficio Publicazioni, Frascati, 1995).

[11] G. Mahoux, S. M. Roy and G. Wanders, Nucl. Phys. **B70** (1974) 297.

[12] B. Ananthanarayan, Phys. Rev. **D58** (1998) 036002 [hep-ph/9802338].

[13] G. Auberson and L. Epele, Nuovo Cim. **A25** (1975) 453.

[14] C. Pomponiu and G. Wanders, Nucl. Phys. **B103** (1976) 172.

[15] D. Atkinson and R. L. Warnock, Phys. Rev. **D16** (1977) 1948.

[16] D. Atkinson, T. P. Pool and H. Slim, J. Math. Phys. **18** (1977) 2407.

[17] L. Epele and G. Wanders, Phys. Lett. **B72** (1978) 390; Nucl. Phys. **B137** (1978) 521.

[18] T. P. Pool, Nuovo Cim. **A45** (1978) 207.

[19] A.C. Heemskerk, *Application of the N/D method to the Roy equations*, PhD thesis, University of Groningen, 1978.

[20] A. C. Heemskerk and T. P. Pool, Nuovo Cim. **A49** (1979) 393.

[21] C. Lovelace, Comm. Math. Phys. **4** (1967) 261.

[22] O. Brander, Comm. Math. Phys. **40** (1975) 97.

[23] P. Büttiker, *Comparison of Chiral Perturbation Theory with a Dispersive Analysis of $\pi\pi$ Scattering*, PhD thesis, Universität Bern, 1996;

B. Ananthanarayan and P. Büttiker, Phys. Rev. **D54** (1996) 1125 [hep-ph/9601285]; Phys. Rev. **D54** (1996) 5501 [hep-ph/9604217]; Phys. Lett. **B415** (1997) 402 [hep-ph/9707305] and in ref. [25], p. 370.

[24] O. O. Patarakin, V. N. Tikhonov and K. N. Mukhin, Nucl. Phys. **A598** (1996) 335;

O. O. Patarakin (for the CHAOS collaboration), in ref. [25], p. 376, and hep-ph/9711361; $\pi N$ Newsletter 13 (1997) 27;

M. Kermani *et al.* [CHAOS Collaboration], Phys. Rev. **C58** (1998) 3431.

[25] A.M. Bernstein, D. Drechsel and T. Walcher, editors, *Chiral Dynamics: Theory and Experiment*, Workshop held in Mainz, Germany, 1-5 Sept. 1997, Lecture Notes in Physics Vol. 513, Springer, 1997.

[26] J. Gasser, A. Rusetsky, and J. Schacher, Miniproceedings of the Workshop *HadAtom99*, held at the University of Bern, Oct. 14-15, 1999, [hep-ph/9911339].

[27] J. Lowe, in ref. [25], p. 375, and hep-ph/9711361; talk at *Workshop on Physics and Detectors for* DA$\Phi$NE, Frascati, Nov. 16-19, 1999, to appear in the Proceedings [http://wwwsis.lnf.infn.it/talkshow/dafne99.htm];

S. Pislak, in ref. [26], p. 25.

[28] P. de Simone, in ref. [26], p. 24.

[29] B. Adeva et al., Proposal to the SPSLC, CERN/SPSLC 95-1 (1995).

[30] J. Gasser and G. Wanders, Eur. Phys. J. **C10** (1999) 159 [hep-ph/9903443].

[31] G. Wanders, hep-ph/0005042.

[32] S. Weinberg, Phys. Rev. Lett. **17** (1966) 616.

[33] J. Gasser and H. Leutwyler, Phys. Lett. **B125** (1983) 325.

[34] N. H. Fuchs, H. Sazdjian and J. Stern, Phys. Lett. **B269** (1991) 183;

J. Stern, H. Sazdjian and N. H. Fuchs, Phys. Rev. **D47** (1993) 3814 [hep-ph/9301244];

M. Knecht and J. Stern, in ref. [10], p. 169, and references cited therein;

J. Stern, in ref. [25], p. 26, and hep-ph/9712438.

[35] J. Sá Borges, Nucl. Phys. **B51** (1973) 189; Phys. Lett. **B149** (1984) 21; ibid.**B262** (1991) 320; Phys. Lett. **B149** (1984) 21;

J. Sa Borges and F. R. Simao, Phys. Rev. **D53** (1996) 4806;

J. Sa Borges, J. Soares Barbosa and V. Oguri, Phys. Lett. **B393** (1997) 413;

J. Sa Borges, J. Soares Barbosa and M. D. Tonasse, Phys. Rev. **D57** (1998) 4108 [hep-ph/9707394].

[36] M. Knecht *et al.*, Nucl. Phys. **B457** (1995) 513 [hep-ph/9507319]; ibid. **B471** (1996) 445 [hep-ph/9512404].

[37] L. Girlanda *et al.*, Phys. Lett. **B409** (1997) 461 [hep-ph/9703448].

[38] M. G. Olsson, Phys. Lett. **B410** (1997) 311 [hep-ph/9703247].

[39] D. Počanić, in ref. [25], p. 352, and hep-ph/9801366; in *Proc. International Workshop on Hadronic Atoms and Positronium in the Standard Model*, Dubna, Russia, edited by M. A. Ivanov *et al.*, p. 33, 1998, and hep-ph/9809455.

[40] J. Bijnens *et al.*, Phys. Lett. **B374** (1996) 210 [hep-ph/9511397]; Nucl. Phys. **B508** (1997) 263 [hep-ph/9707291]; ibid. **B517** (1998) 639 (E).

[41] A. Martin, Nuovo Cim. **42** (1966) 930; ibid. **44** (1966) 1219; *Scattering Theory: Unitarity, Analyticity and Crossing*, Lecture Notes in Physics, vol. 3, Springer-Verlag, Berlin-Heidelberg-New York, 1969.

[42] S. M. Roy, Helv. Phys. Acta **63** (1990) 627.

[43] M. R. Pennington, Annals Phys. **92** (1975) 164.

[44] D. Morgan and G. Shaw, Nucl. Phys. **B10** (1969) 261; Phys. Rev. **D2** (1970) 520.

[45] J.P. Baton *et al.*, Phys. Lett. **B25** (1967) 419; Nucl. Phys. **B3** (1967) 349; Phys. Lett. **B33** (1970) 525; ibid. 528.

[46] W. Ochs, *Die Bestimmung von $\pi\pi$-Streuphasen auf der Grundlage einer Amplitudenanalyse der Reaktion* $\pi^-\mathrm{p}\to\pi^-\pi^+\mathrm{n}$ *bei* 17 GeV/c *Primärimpuls*, PhD thesis, Ludwig-Maximilians-Universität, München, 1973.

[47] B. Hyams *et al.*, Nucl. Phys. **B64** (1973) 134.

[48] S. D. Protopopescu *et al.*, Phys. Rev. **D7** (1973) 1279.

[49] G. Grayer *et al.*, Nucl.Phys. **B75** (1974) 189.

[50] P. Estabrooks and A. D. Martin, Nucl. Phys. **B79** (1974) 301.

[51] M. J. Losty *et al.*, Nucl. Phys. **B69** (1974) 185.

[52] B. Hyams et al., Nucl. Phys. **B100** (1975) 205.

[53] W. Hoogland *et al.*, Nucl. Phys. **B126** (1977) 109.

[54] H. Becker *et al.* [CERN-Cracow-Munich Collaboration], Nucl. Phys. **B150** (1979) 301.

[55] K. L. Au, D. Morgan and M. R. Pennington, Phys. Rev. **D35** (1987) 1633.

[56] B. S. Zou and D. V. Bugg, Phys. Rev. **D48** (1993) 3948; ibid. **D50** (1994) 591;

V. V. Anisovich, D. V. Bugg, A. V. Sarantsev and B. S. Zou, Phys. Rev. **D50** (1994) 1972; ibid. 4412.

[57] D. V. Bugg, B. S. Zou and A. V. Sarantsev, Nucl. Phys. **B471** (1996) 59. We thank B.S. Zou and A.V. Sarantsev for providing us with the corresponding Fortran codes.

[58] R. Kaminski, L. Lesniak and K. Rybicki, Z. Phys. **C74** (1997) 79 [hep-ph/9606362];

R. Kaminski, L. Lesniak and B. Loiseau, Eur. Phys. J. **C9** (1999) 141 [hep-ph/9810386];

R. Kaminski, L. Lesniak and K. Rybicki, Acta Phys. Polon. **B31** (2000) 895 [hep-ph/9912354].

[59] J.Gunter *et al.* [E852 Collaboration], hep-ex/0001038.

[60] W. Ochs, $\pi N$ Newslett. **3** (1991) 25.

[61] S. Eidelman and F. Jegerlehner, Z. Phys. **C67** (1995) 585 [hep-ph/9502298].

[62] R. Barate *et al.* [ALEPH Collaboration], Z. Phys. **C76** (1997) 15.

[63] L. Łukaszuk, Phys. Lett. **B47** (1973) 51.

[64] S. Anderson *et al.* [CLEO Collaboration], hep-ex/9910046.

[65] A. Schenk, Nucl. Phys. **B363** (1991) 97.

[66] The NAG library, The Numerical Algorithms Group Ltd, Oxford UK.

[67] M. G. Olsson, Phys. Rev. **162** (1967) 1338.

[68] G. F. Chew and S. Mandelstam, Phys. Rev. **119** (1960) 467.

[69] L. Rosselet *et al.*, Phys. Rev. **D15** (1977) 574.

[70] C. Caso *et al.* [Particle Data Group], Eur. Phys. J. **C3** (1998) 1.

[71] J. Pišút and M. Roos, Nucl. Phys. **B6** (1968) 325.

[72] C. B. Lang and A. Mas-Parareda, Phys. Rev. **D19** (1979) 956.

[73] J. Bohacik and H. Kuhnelt, Phys. Rev. **D21** (1980) 1342.

[74] G. Wanders, Helv. Phys. Acta **39** (1966) 228.

[75] M. M. Nagels *et al.*, Nucl. Phys. **B147** (1979) 189.

[76] H. Leutwyler, Nucl. Phys. **A623** (1997) 169C [hep-ph/9709406].

[77] D. Atkinson and T. P. Pool, Nucl. Phys. **B81** (1974) 502.

[78] J. F. Donoghue, C. Ramirez and G. Valencia, Phys. Rev. **D38** (1988) 2195.

[79] J. Gasser and U. G. Meissner, Phys. Lett. **B258** (1991) 219.

[80] G. Colangelo, J. Gasser and H. Leutwyler, work in progress.

[81] G. Wanders, *Springer Tracts in Modern Physics* 57 (1971) 22.

[82] B.R. Martin, D. Morgan and G. Shaw, *Pion-Pion Interactions in Particle Physics* (Academic Press, London, 1976).

[83] G. Veneziano, Nuovo Cim. **57** (1968) 190.

[84] C. Lovelace, Phys. Lett. **B28** (1968) 264.

[85] J. A. Shapiro, Phys. Rev. **179** (1969) 1345.

[86] C. Lovelace, Nuovo Cim. **21** (1961) 305.